# EFFECTS OF STRESS, PORE PRESSURE, AND PORE FLUIDS ON BULK STRAIN, VELOCITY, AND PERMEABILITY IN ROCKS

by

**Karl B. Coyner**

B.S., University of Arizona

(1977)

SUBMITTED TO THE DEPARTMENT OF EARTH, ATMOSPHERIC, AND PLANETARY SCIENCES IN PARTIAL FULFILLMENT OF THE REQUIREMENTS FOR THE DEGREE OF

DOCTOR OF PHILOSOPHY

at the



September 6, 1984

Signature of Author ..... Karl B. Coyner
Department of Earth, Atmospheric, and Planetary Sciences
September 1984

Certified by ..... M. Nafi Toksoz
Thesis Advisor

Accepted by ..... Theodore R. Madden
Theodore R. Madden
Chairman
Departmental Committee on Graduate Students

# EFFECTS OF STRESS, PORE PRESSURE, AND PORE FLUIDS ON BULK STRAIN, VELOCITY, AND PERMEABILITY IN ROCKS

by

**Karl B. Coyner**

Submitted to the Department of Earth, Atmospheric and Planetary Sciences
on September 6, 1984, in partial fulfillment of the requirements
for the degree of Doctor of Philosophy.

## ABSTRACT

This thesis examines the response of various physical properties of rocks to hydrostatic confining pressure and pore fluid pressure. The physical properties include static strain, permeability, and ultrasonic velocities, and experimental data are presented in connection with all three. In addition, velocities for both dry and fluid- saturated samples are presented and various models are tested to see how well they predict saturated velocities from dry.

The static strain response of porous solids to combinations of confining stress and pore pressure is investigated both theoretically and experimentally. The theoretical analysis is a synopsis of linear elasticity relations for porous media taken mainly from Biot (1941), Gassmann (1951), Biot and Willis (1956), and Geertsma (1957). Experimental strain measurements on a suite of rocks as a function of hydrostatic confining stress and pore pressure are presented. Equilibrium strain at any combination of confining stress and pore pressure is predicted on the basis of 1) the zero pore pressure or drained, jacketed, stress-strain relation, and 2) the unjacketed stress-strain relation. Although an "effective stress law" for bulk strain (Nur and Byerlee, 1971; Garg and Nur, 1972; Carroll, 1979) can be formulated by associating terms in the basic elasticity relations, the prediction of strain proceeds more directly from the aforementioned two sets of measurements. Unjacketed strain measurements with a confining pressure fluid are emphasized as a means of directly measuring the intrinsic strains of aggregate minerals in rocks and for calculating the intrinsic bulk moduli. A technique is outlined for experimentally obtaining pore volume or porosity as a function of confining pressure from unjacketed and jacketed strain data. An argument is made, based on the linear elasticity analysis for strain response, that the difference between external stress and internal pore pressure, often called the effective stress or effective pressure if external stresses are uniform, predicts many physical properties exclusive of bulk strain because of 1) the large intrinsic moduli of minerals, and 2) the definition of a stress as a force per unit area is maintained during deformation because of the small strains normally encountered in consolidated rocks and sediments. Jacketed and unjacketed stress-strain data, jacketed and unjacketed bulk moduli, and porosity calculations, all as a function of confining pressure, are presented for a suite of igneous, metamorphic, and sedimentary rocks.

The permeability of rocks to combinations of confining pressure and pore pressure is investigated. Simple elasticity considerations, which exclude

irreversible effects such as hysteresis, indicate that differential pressure, the difference between confining and pore pressure, should determine permeability in homogeneous porous materials in which the solid phase has a bulk modulus of typical rock-forming minerals. Experimental measurements of permeability for a sample of Chelmsford granite at two different pore pressures support this conclusion since the differential pressure determines permeability to within experimental error. Also investigated is the anomalously high pore pressure dependence of permeability in Berea sandstone as previously observed by Zoback and Byerlee (1975) with a light machine oil and by Walls and Nur (1979) with distilled water. The effect is observed with a 50,000 ppm NaCl solution, but only on the first cycle of variation in pore and confining pressures. Further cycles result in reduction and perhaps disappearance of the effect. Permeability measurements with distilled water as the pore fluid indicate substantial reduction due to mechanical blockage of fluid pathways as measured and interpreted by Khilar and Fogler (1983). Interpretation of permeability measurements and pore pressure effects are complicated by the presence of natural hydrocarbons in Berea sandstone and by its water sensitivity.

The dependence of P- and S-wave velocities on the combined influence of pore and confining pressures is investigated. Simple considerations of rock elasticity similar to those in the permeability analysis indicate that differential pressure, the difference between confining pressure and pore pressure, should determine velocity in the absence of effects due to pore fluid properties and hysteresis. Measured P- and S-wave velocities in granites, sandstones, and a limestone were made as a function of pore and confining pressures systematically varied so as to avoid hysteresis. Pore fluids used include nitrogen gas, benzene, and water. Experimental velocities indicate that the variation of pore fluid bulk modulus and density at different pore pressures often cause small (several per cent or less) but systematic deviations of velocities from being determined by the differential pressure. In measurements where variations in pore fluid properties are not important, as in fluid-saturated S-wave velocities or fluid-saturated P-wave velocities in one sandstone measured with water, or where the variation in pore fluid properties can be easily accounted for, as in the nitrogen-saturated S-wave velocities in the porous sedimentary rocks, there is evidence that the shear and bulk moduli are being determined by differential pressure. In general, however, the determination of velocities by differential pressure can only be considered an approximation, although probably a good one in water-saturated rocks.

Measurements of ultrasonic (1 Mhz) P- and S-wave velocities for a suite of rocks including sandstones, limestone, granitic rocks, and a metamorphic dolomite are presented. Measurements were made on vacuum-dry (20 $\mu$m Hg) and benzene-saturated (100 bars pore pressure) samples for all of the rocks, and also water-saturated (100 bars pore pressure) for most of the samples. Measurements were made at ambient laboratory temperatures. The effects of water at reducing shear moduli for a number of the rocks at higher confining pressures are noted. For this reason benzene-saturated measurements were made. Dry versus saturated measurements indicate that both shear and bulk moduli increase upon saturation in all rocks except for the limestone. The increase is greatest for the bulk moduli and the greatest at lower confining pressures for both bulk and shear moduli. In all of the low porosity rocks (granites, dolomite) and in the lowest porosity sandstone (9.5%) the saturated S-wave velocities are higher than dry. For the higher porosity sandstones the saturated S-wave velocities are higher than dry at low pressures and cross over at higher pressures as the effect of density supersedes the effects of saturation

on the shear modulus. Velocity data are compared with various models. The Gassmann equation for saturated effective bulk modulus does not predict saturated P-wave velocities for either low porosity granitic rocks or higher porosity sedimentary rocks. Predicted velocities are consistently low even if the saturated shear modulus is used. Using the fluid density to predict saturated S-wave velocities cannot account for the higher saturated shear moduli. The effects of pore fluid inertia on velocities as treated by Biot (1956a,b) appear to be negligible for the sandstones and perhaps nonexistent for the Bedford limestone as saturated S-velocities are predicted exactly from dry with the saturated bulk density. The increase of saturated over dry shear moduli is consistent with the crack models of Budiansky and O'Connell (1974) and Kuster and Toksöz (1974). Although velocity data can be interpreted on the basis of these crack models it is not the purpose here to judge whether or not they are appropriate for all rocks, only to note the consistency between observations and these models as constructed. The Budiansky and O'Connell model with isolated cracks fits dry and saturated velocities for two of the low porosity rocks (Westerly granite and Webatuck dolomite) with low crack densities. Dry and saturated P- and S-wave velocities for Westerly granite are consistent with the model of Kuster and Toksöz for a spectrum of ellipsoidal pore shapes, as implemented by Cheng (1978), particularly with regards to the higher saturated shear moduli.

Thesis Supervisor: M. Nafi Toksöz
Title: Professor of Geophysics

## ACKNOWLEDGEMENTS

Prof. Nafi Toksöz supported me for a number of years during the time I developed the topics addressed in this thesis and the experimental equipment necessary for their solution. Prof. Brace started me in rock mechanics and kindly allowed me space in the 7th floor laboratory. Arthur Cheng of ERL provided me with the computer programs used to analyze the strain data and assisted in the preparation of Chapter 2. Mark Willis provided the plotting software used in most of the data plots. Jock Hirst gave me free reign in the 7th floor machine shop during the time I spent building and developing the equipment. Stephen Gildea of ERL assisted me in linking the data acquisition system to the HP1000. Tien-Wien Lo assisted me generally about the lab in the past year and helped in collecting part of the strain data used in Chapter 2.

I would like to thank my father for instilling in me a sense of how things work and my mother for usually making me put them back together again. Mary Karish has encouraged me over the past year to do my best and has been rewarded with my extended periods of lucubration.

# TABLE OF CONTENTS

# CHAPTER 1

# INTRODUCTION

The main question addressed by this thesis is the effectiveness of pore pressure versus confining pressure in determining the physical properties of rocks. In the earth, because of rock porosity and fluids to fill that porosity, the overall stress field has two components: a frame or lithostatic stress transmitted at grain to grain contacts and, secondly, a hydrostatic pore pressure. Lithostatic stresses can have both magnitude and direction while pore pressure is necessarily hydrostatic if in equilibrium. These two components can be simulated in the rock mechanics laboratory with jacketed rock samples subjected to external stresses together with independent internal pore pressure. Many geophysical properties of rocks, whether in the earth or for samples in the laboratory, will depend on both. Only a uniform external stress, or a confining pressure, in addition to pore pressure, are used in the experimental measurements of this thesis. Differential pressure is defined as the difference between confining pressure and pore pressure.

How confining stress and pore pressure determine physical properties is commonly associated with the term "effective stress". Sometimes this phrase is referred to as a law or as a principle, but really it is only a definition by Terzaghi (1923), who observed that the difference between uniaxial stress and pore pressure, or the effective stress, determines uniaxial strain and the shear stress at failure in muds and soils. Over the years effective stress has been applied to rocks, other materials, and to various other physical properties to the extent that it has become established as something more than a definition. Whether or

not it should apply to bulk strain, permeability, and velocities in rocks is one purpose for this thesis.

Chapter 2 examines the strain response of porous materials to combinations of confining pressure and pore pressure. If the strain response is understood then the dependence of other physical properties on stress and pore pressure can be interpreted. It is shown how Biot's early consolidation work (Biot ,1941) fundamentally established the stress-strain relations for linear porous solids, which essentially eclipsed effective stress as a concept with any true physical meaning, such as being related somehow to "effective" stresses at grain contacts. Chapter 2 contains a fair amount of experimental strain data collected for the purpose of evaluating whether or not there is an "effective stress law" for bulk strain. It is shown that even though the linear elasticity relations can be reformulated, and an "effective stress" defined, there is no fundamental intrinsic meaning to the definition. For a nonlinear solid, such as most rocks, the strain at any combination of confining pressure and pore pressure is predictable from the drained, jacketed stress- strain relation and the unjacketed stress-strain relation. From the former relation the jacketed bulk modulus can be calculated as a function of confining pressure; from the latter the unjacketed bulk modulus can be calculated, and this is also a measure of the intrinsic bulk modulus of the aggregate minerals. Subtraction of the unjacketed strain from the jacketed strain gives the pore volume strain or the porosity as a function of confining pressure. These stress-strain relations, calculated moduli, and porosity relations are given for a suite of igneous, metamorphic, and sedimentary rocks.

Chapter 3 investigates the permeability of rocks to combinations of confining and pore pressures. Linear elasticity relations taken from Chapter 2 indicate that differential pressure should determine permeability because the intrinsic moduli of typical rock-forming minerals are so large. Experimental

not it should apply to bulk strain, permeability, and velocities in rocks is one purpose for this thesis.

Chapter 2 examines the strain response of porous materials to combinations of confining pressure and pore pressure. If the strain response is understood then the dependence of other physical properties on stress and pore pressure can be interpreted. It is shown how Biot's early consolidation work (Biot ,1941) fundamentally established the stress-strain relations for linear porous solids, which essentially eclipsed effective stress as a concept with any true physical meaning, such as being related somehow to "effective" stresses at grain contacts. Chapter 2 contains a fair amount of experimental strain data collected for the purpose of evaluating whether or not there is an "effective stress law" for bulk strain. It is shown that even though the linear elasticity relations can be reformulated, and an "effective stress" defined, there is no fundamental intrinsic meaning to the definition. For a nonlinear solid, such as most rocks, the strain at any combination of confining pressure and pore pressure is predictable from the drained, jacketed stress- strain relation and the unjacketed stress-strain relation. From the former relation the jacketed bulk modulus can be calculated as a function of confining pressure; from the latter the unjacketed bulk modulus can be calculated, and this is also a measure of the intrinsic bulk modulus of the aggregate minerals. Subtraction of the unjacketed strain from the jacketed strain gives the pore volume strain or the porosity as a function of confining pressure. These stress-strain relations, calculated moduli, and porosity relations are given for a suite of igneous, metamorphic, and sedimentary rocks.

Chapter 3 investigates the permeability of rocks to combinations of confining and pore pressures. Linear elasticity relations taken from Chapter 2 indicate that differential pressure should determine permeability because the intrinsic moduli of typical rock-forming minerals are so large. Experimental

permeability measurements of two rocks, the Chelmsford granite and Berea sandstone, are used to test this conclusion. For Chelmsford granite the results indicate that differential pressure determines permeability when care is taken to avoid the introduction of hysteresis into the measurements. For Berea sandstone the anomalous behavior of pore pressure having a greater effect than confining pressure is investigated. This was previously observed by Zoback and Byerlee (1975) and by Walls and Nur (1979) and interpreted as a result of compliant clays lining the pore walls of a quartz grain framework. The anomalous effect is observed with a 50,000 ppm NaCl solution but only clearly on the first cycle of confining and pore pressures. Therefore, the effect may only be a transient. Permeability measurements and interpretation of the pore pressure effect are, however, severely complicated by the presence of natural hydrocarbons and the water sensitivity of Berea sandstone. The water sensitivity results in a large drop in permeability when the saline solution is purged and replaced with distilled water.

In a manner similar to Chapter 3, Chapter 4 investigates the effects of pore pressure and confining pressure on P- and S- wave velocities. The common assumption is that differential pressure determines velocities but this is rather confused in the experimental literature. A simple elasticity argument similar to that for permeability in Chapter 3 is made to indicate why differential pressure should determine velocities in the absence of hysteresis and pore fluid effects. Experimental measurements of P- and S-velocities as a function of confining pressure and pore pressure for a number of rocks are presented. Although made somewhat difficult by the sensitivity of velocities to pore fluid properties, which change as a function of pore pressure, the experimental results indicate that differential pressure does indeed determine velocity. Observed deviations are caused by pore fluid properties such as fluid compressibility and density which

change as a function of pressure. These effects of pore fluid properties are somewhat maximized by the choice of pore fluids for most of the measurements: benzene and nitrogen gas. For velocity measurements, as opposed to permeability measurements, the effects of pore fluid properties are not easily isolated.

Chapter 5 presents a collection of vacuum- dry and benzene-saturated P- and S-velocities measured as a function of confining pressure for a suite of 9 rocks. In addition, for 5 of the rocks water-saturated measurements are also made after thorough drying to remove the benzene. By using benzene as opposed to water a set of dry and saturated velocities are obtained which depend on rock composition, pore structure, and fluid properties. The effects of water at reducing the saturated shear modulus, which becomes particularly evident at higher confining pressures, are avoided by using benzene. Dry and saturated velocities are more comparable with benzene as the pore fluid because the calculated dry moduli are applicable to the saturated rock frame. The most significant result in the velocity data is the observation that saturated shear moduli are larger than dry for all of the rocks tested exclusive of the Bedford limestone, which represents a nearly linear solid. In that rock the dry and saturated shear moduli appear to be the same. For low porosity rocks (3 granitic rocks and 1 dolomite) saturated shear velocities are consistently higher than in the dry case. The increase of saturated over dry P-wave velocities and bulk moduli are always larger than for the S-wave velocities and shear moduli. These observations are consistent with the idea that rocks contain small discontinuous cracks whose shapes strongly increase the saturated moduli over the dry state. The final portion of Chapter 5 attempts to understand and model the differences between dry and saturated data with Gassman's equation (1951), Biot (1956a,b) inertial effects, and the ellipsoidal pore models of Budiansky and O'Connell

(1974) and Kuster and Toksöz (1974).

Chapter 6 is a summary of conclusions from all of the previous chapters.

# CHAPTER 2

# STATIC DEFORMATION OF FLUID-SATURATED ROCKS

## INTRODUCTION

A remarkable variety of geological processes and geophysical properties as we know them would not exist on earth without water. Because rocks and sediments are porous in the crust, at least down to the brittle-ductile transition, water may freely exist as a separate fluid phase at depth. Where lithosphere is subducted water may be carried to even greater depths. As a result of water, or more accurately aqueous solutions in the crust there are phenomena as diverse as hydrothermal ore deposits, the lowering of solidus temperatures in basaltic magmas, diagenesis, substantial current flow through rock, and acoustic attenuation. Even hydrocarbons and organically-derived gas are possible only because of the water which sustained the original plant life.

The pressure in fluids at depth may be a significant factor in some processes. Pressure in the fluid phase can be generated by gravity, stress waves, tectonic stress, heat, and chemical or electrical potentials. A simple model for an ideal earth is a column of interconnected pore space filled with water in which pore pressure increases with depth proportional to density and the gravitational constant. There are obvious important exceptions, mostly because of the time scales involved. On one hand, some deep mines in crystalline rock are dry and pore pressure is insignificant. In developing sedimentary basins, on the other hand, rapid sedimentation and burial combined with heat and low permeability

leads to overpressurized pore fluids. On a shorter time scale, the instantaneous compressibility for an acoustic stress wave in rock may create local pressure gradients in the fluid phase because of pore shape. Another example of the importance of pore pressure is in the interpretation of earthquakes and overthrust faulting as complex reactions between regional stress fields and temporal and spatial variations in pore fluid pressure. Several instances have been documented of earthquakes being turned on and off by high-pressure fluid injection in wells.

Because of rock porosity, fluids to fill that porosity, and sources of fluid pressure, the overall mechanical response of rocks and sediments with fluids is determined by a two-component stress system. An overall frame or confining stress is transmitted through grain-to-grain contacts and may vary as a function of direction. The second stress component is pore pressure. Fortunately, fluid cannot support shear except over small distances. In low-frequency or static situations pore pressure is therefore hydrostatic.

A logical analysis of the mechanical response of rocks and sediments would treat confining stress and pore pressure as independent variables. There is, however, a simplifying functional relation generally known as "effective stress". Historically, Terzaghi (1923, 1925) showed in laboratory experiments that uniaxial consolidation and strength of fully-saturated soils is governed by the simple difference between normal stress and pore pressure. This difference became known as the "effective stress", and was identified as the controlling parameter in these types of deformation studies.

Over the years this simple observation has been extended and applied to cover the deformation of rocks and other porous materials besides soils. In addition, other physical properties studied in the laboratory, such as fracture

strength and frictional resistance, acoustic velocities and attenuation, electrical resistivity, and permeability, have been associated with effective stress. Brace (1972) reviewed a number of these properties as they depend on cavity shape and noted that to the depth at which interconnected cavities exist there is a possible influence of pore pressure on physical properties. As a term, effective stress is often used as a synonym for differential pressure, again the simple difference between confining pressure and pore pressure.

The main purpose of this study is to investigate the equilibrium or static strain response of rocks to a combination of confining stress and pore pressure. This is the key to understanding what effective stress means because changes in other physical properties, such as velocity and permeability, can be interpreted and modelled if elastic deformation is described. The first section of this paper is a review of the linear elastic material description of porous solids as initially developed by Biot (1941) for analysis of the three-dimensional consolidation of soils. The analysis is carried out in fair detail because, as will be shown in the second section, what has been proposed as an "effective stress law" for bulk strain (Nur and Byerlee, 1971; Garg and Nur, 1973; Carroll, 1979) can be seen as an extension of the linear elastic description. The third section uses some graphical examples to clarify the points.

While there has been much effort at measuring and interpreting the stress-strain relations for dry or drained earth materials, there have only been a few previous experimental efforts aimed toward an understanding of the combined role of pore pressure and confining stress on static strain in rocks (Van der Knapp, 1959; Nur and Byerlee, 1971). A major effort of this paper is to present experimental static strain data for a suite of rocks including sandstones, granites, and limestone, where both pore pressure and confining stress are systematically varied. In the fifth, sixth, seventh, and eighth sections of this

paper the experimental test and results are discussed. Inert nitrogen is used as the pore fluid and confining stress is uniform confining pressure. Strain is measured with strain gages attached directly to rock samples. The experimental strain data agrees with the predictions of linear elasticity theory or the proposed effective stress laws for bulk strain (Nur and Byerlee, 1972; Garg and Nur, 1973; Carroll, 1979) when nonlinear behavior of the samples is incrementalized over many steps that are each nearly linear. This is possible through the power of the computer in collecting finely digitized experimental stress-strain data. The prediction of strain at any combination of pore and confining pressures, however, proceeds more directly from the jacketed and unjacketed stress-strain data without the need of calculating bulk moduli.

Jacketed and unjacketed stress-strain relations and corresponding moduli are presented and calculated for a suite of rocks. The eigth section of this paper points out how pore volume and porosity can be calculated quite accurately as a function of confining stress from jacketed and unjacketed stress-strain measurements. The unjacketed strain test, which has been neglected in recent years, is emphasized as a direct measurement of the intrinsic bulk modulus.

## LINEAR ELASTICITY OF FLUID-SATURATED POROUS MEDIA

Consider a homogeneous and isotropic porous solid. The following analysis is of a sample element large enough so that the porosity distribution doesn't interfere with the homogeneity assumption. For this sample element stress is defined as total force per unit area and strain is defined as relative displacement between points in the solid phase. Assume that the pores are empty. The strain tensor as a function of stress for this sample element is

$$\varepsilon_{ij} = \frac{1}{2G}(\sigma_{ij} - \frac{1}{3}\sigma_{kk}\delta_{ij}) + \frac{1}{9K}(\sigma_{kk}\delta_{ij}), \qquad (2\text{-}1)$$

where $\varepsilon_{ij}$ is strain, $\sigma_{ij}$ is deviatoric stress, $\sigma_{kk}$ is hydrostatic stress, and $\delta_{ij}$ is the Kronecker's delta. The elastic bulk modulus is $K$ and shear modulus is $G$. Strains are considered infinitesimal so that solid translation and rotational terms are not used. Repeated indices indicate summation. In this form the stress tensor is decomposed into two parts, the left term in parenthesis representing deviatoric stress and the right term representing pure hydrostatic stress. The deviatoric stress changes the shape and strain is a function of the shear modulus; the hydrostatic stress changes the volume and strain is a function of the bulk modulus.

Alternatively, the tensor expression can be expressed with the Poisson's ratio $\nu$ of the porous solid. The identity for an isotropic material is

$$K = \frac{2G(1+\nu)}{3(1-2\nu)},$$

and

$$\varepsilon_{ij} = \frac{1}{2G}(\sigma_{ij} - \frac{1}{3}\sigma_{kk}\delta_{ij}) + \frac{\nu}{2G(1+\nu)}(\sigma_{kk}\delta_{ij}). \qquad (2\text{-}2)$$

Now consider the effect of a pore fluid at an equilibrium pressure of value $p$ introduced throughout the pore space. No bulk shear strain will occur because fluid pressure is hydrostatic and the porous solid is isotropic. The result of pore pressure is a pure volumetric strain, equal in all directions. An additional term is added to the stress-strain relation so that the complete expression becomes

$$\varepsilon_{ij} = \frac{1}{2G}(\sigma_{ij} - \frac{1}{3}\sigma_{kk}\delta_{ij}) + \frac{1}{9K}(\sigma_{kk}\delta_{ij}) + \frac{1}{3H}p\,\delta_{ij} \qquad (2\text{-}3)$$

Pore pressure $p$ is positive and the sign of the additional term is positive so that bulk strain decreases with an increase in $p$. The convention used in this analysis

is that compression is negative. The constant $H$ was introduced by Biot (1941) and is simply defined as the ratio between bulk volume strain and pore pressure change $p$ with external stress constant. Biot (1941) and Biot and Willis (1957) suggested appropriate experimental tests for the determination of $H$. Bulk modulus $K$ is measured with either the pores empty of fluid or else at constant pore pressure, i.e., a drained test.

As can be seen from the form of Eq. (2-3) the constant $H$ is a modulus similar to the bulk and shear moduli. The constant $H$ can, however, be defined in terms of bulk modulus $K$ and solid matrix modulus $K_s$ of the solid phase with the additional assumption that the solid phase is homogeneous and isotropic. This assumption was used by Gassmann (1951) and later Geertsma (1957). A short derivation follows.

For the sample element under consideration if there is only a hydrostatic confining pressure, such that $\sigma_{ij} = -\sigma\delta_{ij}$, and a pore pressure of value $p$, the expression for bulk strain $\varepsilon$ from Eq. (2-3) becomes

$$\varepsilon = -\left(\frac{1}{K}\sigma - \frac{1}{H}p\right). \tag{2-4}$$

The overall stress field can be decomposed into two stress states, individually analyzed, and the resulting strains summed by virtue of the overall linearity assumption. In Fig. 2-1 the decomposed stress states are schematically shown. Stress state (1) is an equal and uniform internal and external hydrostatic stress $p$. The normal stress over every boundary between pore and matrix is uniquely defined as $p$. An important point is that homogeneity requires that the porosity cannot split the sample, either because the sample element is too small or else because of a fracture. Since the solid phase is homogeneous and isotropic, with bulk modulus $K_s$, the result is a pure volumetric strain

$$\varepsilon_1 = -\frac{1}{K_s}p. \tag{2-5}$$

Stress state (2) is an external hydrostatic stress $\sigma - p$ with constant pore pressure and the resulting volumetric strain is

$$\varepsilon_2 = -\frac{1}{K}(\sigma - p) \tag{2-6}$$

Summation of the two volume strains gives

$$\varepsilon_1 + \varepsilon_2 = -\frac{1}{K}\sigma - \left(\frac{1}{K_s} - \frac{1}{K}\right)p. \tag{2-7}$$

Comparison with Eq. (2-4) reveals that

$$\frac{1}{H} = \frac{1}{K} - \frac{1}{K_s}. \tag{2-8}$$

The stress-strain relation in Eq. (2-3) can therefore be written as

$$\varepsilon_{ij} = \frac{1}{2G}\left(\sigma_{ij} - \frac{1}{3}\sigma_{kk}\delta_{ij}\right) + \frac{1}{9K}(\sigma_{kk}\delta_{ij}) + \frac{1}{3}\left(\frac{1}{K} - \frac{1}{K_s}\right)p\,\delta_{ij} \tag{2-9}$$

This is the overall stress-strain relation for a linear, isotropic, macro- and micro-homogeneous porous solid when pore fluid pressure is an additional state variable.

Solving Eq.(2-9) with respect to stresses gives the relation

$$\sigma_{ij} = (K - \frac{2}{3}G)\delta_{ij}\varepsilon_{kk} + 2G\varepsilon_{ij} - \zeta p\,\delta_{ij}, \tag{2-10}$$

where

$$\zeta = 1 - \frac{K}{K_s}. \tag{2-11}$$

This is perhaps the simplest expression and can be found in Biot (1941, 1962) and

Rice (1980). The first coefficient in parentheses can be identified with the Lamé parameter $\lambda$. The material constant $\zeta$ was called $\alpha$ by Biot (1941 and later) and by Nur and Byerlee (1971). If microhomogeneity and isotropy are assumed the equivalence in Eq. (2-11) is exactly correct. Otherwise, $\zeta$ is a material constant to be determined, and appropriate experimental tests are given by Biot (1941) and by Biot and Willis (1957). The quantity of fluid expelled during a jacketed compression test divided by bulk volumetric strain furnishes the value of $\zeta$. This will be discussed in a later section.

To this point the assumption has been that pore pressure remains constant during external static deformation, as for a drained experiment or an open system. To complete the static linear description the fluid mass must be included with stress, strain, and pore pressure as fundamental state variables. Biot (1941) defined the response of fluid volume in the pores to stress and pore pressure as $\Theta$, the increment of fluid volume per unit volume of porous solid. The expression for $\Theta$ is

$$\Theta = \frac{1}{3H_1}(\sigma_{kk}) + \frac{1}{R}p, \qquad (2\text{-}12)$$

where $H_1$ and $R$ are material constants. For constant confining stress the volume of fluid displaced into the pores of a unit volume is calculated with $\frac{1}{R}$.

Through the definition of a strain potential energy for the porous solid it can be shown that $H_1 = H$, the constant in Eq. (2-8). The argument used by Biot (1941, 1973) is that $\sigma_{ij}d\varepsilon ij + pdv_p$, $v_p$ being the pore fluid volume, is an exact differential, and there is a thermodynamic argument for why this is true (Biot, 1973). For the present purpose, however, the important result from his energy argument is the reciprocity between the response of pore volume $v_p$ to hydrostatic confining stress $\sigma$ and bulk volume response $V_b$ to pore pressure $p$.

This can be expressed as

$$\left[\frac{\partial V_b}{\partial p}\right]_\sigma = -\left[\frac{\partial v_p}{\partial \sigma}\right]_p. \tag{2-13}$$

Love (1944) also gives several forms of the reciprocity theorem for elasticity. Gassmann (1951) and Geertsma (1957) also use reciprocity in their derivations.

Reciprocity can be used to show that $H_1 = H$. If the porosity is fully connected and fully saturated with pore fluid the increment of fluid content $\Theta$ in Eq. (2-12) can be identified with change in pore volume normalized to bulk volume. The equivalent to Eq. (2-12) is

$$\frac{1}{V_b} dv_p = \frac{1}{V_b}\left[\frac{\partial v_p}{\partial \sigma}\right]_p d\sigma + \frac{1}{V_b}\left[\frac{\partial v_p}{\partial p}\right]_\sigma dp \tag{2-14}$$

If the porous solid is completely immersed in fluid with pressure $p$ bulk volumetric strain is given by $1/K_s$. If the external pressure $p$ is removed such that only pore pressure $p$ remains, the overall porous solid will expand by an amount inversely proportional to bulk modulus $K$. Summing these two stages gives the partial derivative of bulk volume to pore pressure with constant confining pressure

$$\frac{1}{V_b}\left[\frac{\partial V_b}{\partial p}\right]_\sigma = \left[\frac{1}{K} - \frac{1}{K_s}\right]. \tag{2-15}$$

The same result can be seen in Eq. (2-7) if confining stress $\sigma$ is set equal to zero. By reciprocity, Eq. (2-13), the partial derivative of pore volume to hydrostatic confining stress is given by

$$\frac{1}{V_b}\left[\frac{\partial v_p}{\partial \sigma}\right]_p = -\left[\frac{1}{K} - \frac{1}{K_s}\right]. \tag{2-16}$$

With the matrix solid homogeneity and isotropy assumption the equivalence of Eq. (2-8) holds, and substitution of Eq. (2-16) into Eq. (2-14) gives

$$\frac{1}{V_b}dv_p = \frac{1}{H}d\sigma + \frac{1}{V_b}\left[\frac{\partial v_p}{\partial p}\right]_\sigma dp. \tag{2-17}$$

Comparison with Eq. (2-12) indicates that $H_1 = H$ and that

$$\frac{1}{R} = \frac{1}{V_b}\left[\frac{\partial v_p}{\partial p}\right]_\sigma, \tag{2-18}$$

and now it will be shown that $R$ can be expressed as a function of porosity, bulk modulus, and solid matrix bulk modulus.

The change in pore volume with pore pressure can be equated to change in bulk volume $V_b$ and solid matrix volume $v_s$ by

$$\frac{1}{V_b}\left[\frac{\partial v_p}{\partial p}\right]_\sigma = \frac{1}{V_b}\left[\frac{\partial V_b}{\partial p}\right]_\sigma - \frac{1}{V_b}\left[\frac{\partial v_s}{\partial p}\right]_\sigma. \tag{2-19}$$

Bulk volume and pore volume are related to solid matrix volume $v_s$ through the porosity $\varphi$ such that

$$V_b = \frac{v_s}{1-\varphi}$$

$$v_p = \frac{\varphi}{1-\varphi}v_s. \tag{2-20}$$

Substitution of Eqs. (2-20) into the reciprocity theorem, Eq. (2-13), gives

$$\left[\frac{\partial v_s}{\partial p}\right]_\sigma = -\varphi\left[\frac{\partial v_s}{\partial \sigma}\right]_p. \tag{2-21}$$

On the righthand side of Eq. (2-21) the differential for solid volume $v_s$ is the difference between the differential for bulk volume, equal to $1/K$, and the

differential for pore volume, Eq. (2-16). Therefore

$$\frac{1}{V_b}\left(\frac{\partial v_s}{\partial p}\right)_\sigma = \varphi\left(\frac{1}{K_s}\right), \tag{2-22}$$

and substitution of this with Eq. (2-15) into Eq. (2-19) gives

$$\frac{1}{V_b}\left(\frac{\partial v_p}{\partial p}\right)_\sigma = \frac{1}{K} - (1+\varphi)\left(\frac{1}{K_s}\right). \tag{2-23}$$

Consequently, if the matrix solid is homogeneous and isotropic, the Biot constant $R$, referring to Eq. (2-18) and (2-23), can be identified as

$$\frac{1}{R} = \frac{1}{K} - (1+\varphi)\left(\frac{1}{K_s}\right), \tag{2-24}$$

which is also given by Geertsma (1957). Therefore the increment of fluid volume $\Theta$ of Biot(1941) can be expressed as a change in pore volume

$$\frac{1}{V_b}(\Delta v_p) = \frac{1}{V_b}\left(\frac{1}{K} - \frac{1}{K_s}\right)\frac{\sigma_{kk}}{3} + \frac{1}{V_b}\left(\frac{1}{K} - \frac{1}{K_s}\right)p - \frac{\varphi}{K_s}p, \tag{2-25}$$

or, equating pore volume with fluid volume $v_f$, a change in fluid volume

$$\Delta v_f = \left(\frac{1}{K} - \frac{1}{K_s}\right)\frac{\sigma_{kk}}{3} + \left(\frac{1}{K} - \frac{1}{K_s}\right)p - \frac{v_f}{K_s}p, \tag{2-26}$$

where $v_f$ is the fluid volume in the unstressed state. Eq. (2-26) can be found in Rice and Cleary (1976, their Eq. (2-2)).

Following Rice and Cleary (1976), the variation in fluid mass $\Delta m_f$ in response to pore pressure and confining stress may be expressed in a linear expansion of $m_f = \rho_f v_f$ to give

$$\Delta m_f = \Delta\rho_f v_f + \rho_f \Delta v_f, \tag{2-27}$$

where $\Delta m_f$ is variation in fluid mass, $\Delta\rho_f$ is variation in fluid density, $\Delta v_f$ is variation in fluid volume, and $v_f$ and $\rho_f$ are fluid volume and fluid density in the reference state. Using the identity of the fluid bulk modulus $K_f$,

$$K_f = \frac{\rho_f p}{\Delta\rho_f}, \tag{2-28}$$

the substitution of Eq. (2-28) and Eq. (2-26) into Eq. (2-27) gives

$$\Delta m_f = \rho_f \frac{v_f}{K_f} p + \rho_f \left[\frac{1}{K} - \frac{1}{K_s}\right]\left[\frac{\sigma_{kk}}{3} - p\right] + \rho_f \frac{v_f}{K_s} p. \tag{2-29}$$

This is the equation for fluid mass variation with stress and pore pressure when the solid matrix modulus can be locally associated with $K_s$ at every point in the solid. Together with Eq. (2-10) and Darcy's fluid flow equation a full set of constitutive relations are achieved for linear, isotropic, homogeneous, porous solids, with fully compressible constituents. Coupled with equilibrium conditions and compatibility conditions the full field equations, including diffusivity, can be generated (Rice and Cleary, 1976; Rice, 1980).

A crucial assumption in these derivations is that of solid matrix homogeneity and isotropy. This is also part of the reason why there are so many different symbols and material constants in various treatments. The assumptions can be distinguished by considering a macrohomogeneous and macroisotropic versus a microhomogeneous and microisotropic porous solid. Macrohomogeneity is fundamentally necessary for the analysis of stress and pressure on a sample element of the porous solid. Macroisotropy has been assumed but is not necessary, and the extension to various symmetries was done by Biot (1956). The key issue is microhomogeneity and microisotropy. If the solid matrix is everywhere microhomogeneous and microisotropic, and the porosity is fully

interconnected, then the solid matrix bulk modulus $K_s$ can be used in all of the previous equations. Geologic materials, however, are far short of that ideal. Many different minerals exist in rocks and sediments and each mineral type is usually elastically anisotropic. A quick look at Birch's compilation in Clark (1966) shows that mineral elastic constants may vary by over 100%. The resolution of this fact to theory is by the definition of an equivalent homogeneous porous solid with equivalent solid matrix bulk modulus $K_s'$. This is a representative statistical average of all the different moduli of the individual minerals. It can be calculated as a Voigt-Reuss-Hill average (Brace, 1965) or else measured directly in an unjacketed stress-strain measurement. A collection of $K_s'$ values for some rocks can be found in Birch's compilation in Clark (1966, Table 7-13). The experimental section of this paper will present many more.

The use of $K_s'$ in place of $K_s$ in Eqs. (2-25), (2-26), and (2-29) is not, however, totally correct. The $K_s$ in the last term of those equations can be traced to the variation in pore volume with constant differential pressure (Biot, 1973; Brown and Korringa, 1975). Brown and Korringa (1975) define the compressibility

$$\kappa_\varphi = -\frac{1}{v_\varphi}\left(\frac{\partial v_\varphi}{\partial p}\right)_{p_d}, \tag{2-30}$$

where $v_\varphi$ is pore volume, $p$ is pore pressure, and $p_d$ is differential pressure, $\sigma$ - $p$. If the solid matrix is microhomogeneous and microisotropic the compressibility $\kappa_\varphi$ equals $1/K_s$, and the variation in pore volume $v_\varphi$ is equivalent to stress state (1) in Eq.(2-6). Biot(1973) also distinguished the compressibility $C_m$ and Rice and Cleary (1976) distinguished the modulus $K_s''(= 1/\kappa_\varphi)$.

Using these two constants, $K_s'$ and $K_s''$, Eqs. (2-10), (2-11), and (2-29), the constitutive relations, are rewritten

$$\sigma_{ij} = (K - \frac{2}{3}G)\delta_{ij}\varepsilon_{kk} + 2G\varepsilon_{ij} - \zeta p\,\delta_{ij}, \tag{2-31}$$

$$\zeta = 1 - \frac{K}{K_s'}, \tag{2-32}$$

$$\Delta m_f = \rho_f \frac{v_f}{K_f} p + \rho_f \left(\frac{1}{K} - \frac{1}{K_s'}\right)\left(\frac{\sigma_{kk}}{3} + p\right) - \rho_f \frac{v_f}{K_s''} p. \tag{2-33}$$

The significance of $K_s'$ and $K_s''$ is that they are material constants that, when experimentally measured, remove the homogeneity and isotropy requirement on the solid matrix. Equivalently, the $H$ and $R$ constants of Biot (1941) could be used. It may be noted that the analysis with $K_s'$ and $K_s''$ and Biot's analysis using $H$ and $R$ are far more general, therefore, than the analysis of Gassmann (1951) and Geertsma (1957), both of whom specialize to the case of a homogeneous and isotropic matrix of modulus $K_s$. Biot almost certainly realized this in 1941, but what must be remembered is that Biot's original application was soils. In a partially saturated, clay dominated soil the parameters such as porosity, matrix modulus, and pore fluid modulus are almost impossible to define and measure. By sticking to $H$ and $R$ Biot 1) defined measurable constants ($H$ and $R$), 2) did not have to assume microhomogeneity and microisotropy, and 3) avoided any mention of porosity, so that the discussion and confusion with Terzaghi's "effective porosity" was avoided altogether.

Several other useful relations between bulk volume, pore volume, and porosity can be derived with the equations. For this purpose assume $K_s = K_s' = K_s''$. From Eq. (2-16) the differential of pore volume strain with hydrostatic confining stress $\sigma$ was given by

$$\frac{1}{V_b}\left(\frac{\partial v_p}{\partial \sigma}\right)_p = -\left(\frac{1}{K} - \frac{1}{K_s}\right). \tag{2-16}$$

The variation in porosity $\varphi$ with hydrostatic confining stress $\sigma$ can then be calculated from the expression

$$\left[\frac{\partial\varphi}{\partial\sigma}\right]_p = \frac{\partial(v_p / V_b)}{\partial\sigma} = \frac{1}{V_b}\frac{\partial v_p}{\partial_\sigma} - \frac{v_p}{V_b^2}\frac{\partial V_b}{\partial\sigma}. \tag{2-34}$$

The first term on the left is given by Eq. (2-16), and the second term on the right includes the definition of bulk modulus $K$ and porosity $\varphi$. Eq. (2-34) can therefore be expressed as

$$\left[\frac{\partial\varphi}{\partial\sigma}\right]_p = -\left[\frac{1}{K} - \frac{1}{K_s}\right] + \frac{v_p}{V_b}\left[\frac{1}{K}\right]$$

$$= -\frac{(1-\varphi)}{K} + \frac{1}{K_s}. \tag{2-35}$$

This means that porosity variation with external confining stress $\sigma$ can be calculated from $\varphi$, $K$, and $K_s$ ($=K_s'$). If porosity is very low and $K << K_s$, such as with crack-dominated solids at low pressure, the porosity can be ignored and

$$\left[\frac{\partial\varphi}{\partial\sigma}\right]_p = -\left[\frac{1}{K} - \frac{1}{K_s}\right]. \tag{2-36}$$

This is the expression given by Walsh (1965). The expression in Eq. (2-35) is, however, more general.

## EFFECTIVE STRESS

The modern idea of an effective stress in fluid-saturated porous media apparently originated with Karl Terzaghi, who is generally regarded as the father of soil mechanics. For soils and muds the consideration of a pore fluid phase and possible pore pressure is obviously fundamental to the definition of materials and to the understanding of mechanical properties. From Terzaghi's experimental studies on the uniaxial consolidation and shear strength of fully-saturated soils (1923, 1925) he concluded that the controlling parameter for these properties was the simple difference between normal stress $\sigma$ and pore

fluid pressure $p$

$$\langle\sigma\rangle = \sigma - p. \tag{2-37}$$

In his relation $\sigma$ is an external frame stress such as that applied to a sample in the laboratory by a deformation platen. It is positive in compression. Pore pressure $p$ is kept constant during the application of normal stress, perhaps controlled through holes in the deformation platen and a low strain rate, and hence this is the definition of a drained test. The parameter $\langle\sigma\rangle$ became known as the effective stress and determined deformation and strength in these types of experiments. This was adequate for fully saturated soils as was experimentally shown by numerous subsequent studies. For partially saturated soils Bishop (1955) suggested a relation for effective stress of the form

$$\langle\sigma\rangle = \sigma - p_1 + x(p_1 - p_2), \tag{2-38}$$

where $p_1$ is pore fluid gas pressure, $p_2$ is pore fluid water pressure, and $x$ is a coefficient depending on the degree of saturation. In partially saturated soils gas and water pressure may be different due to surface tension and this relation attempts to account for this variation.

Apparently there was much disagreement over why and how Terzaghi's effective stress relation worked. The term "effective" to some minds references a micromechanical concept of how an external confining stress is distributed between grain contacts and pore fluid pressure, resulting in an intergranular "effective" stress between grains. For an isotropic aggregate the forces from fluid and solid across a given grain contact can be calculated quite simply (Skempton, 1960). If $a$ is the area of solid particles per unit area of aggregate, the fluid forces on the plane sum to $(1-a)p$, where $p$ is pore pressure. hence the intergranular stress $\sigma_g$ is

$$\sigma_g = \sigma - (1-a)p, \tag{2-39}$$

where $\sigma$ is the normal external stress. One minus the area of the solid over area of aggregate, however, is also a definition of porosity $\varphi$, and so

$$\sigma_g = \sigma - \varphi p. \tag{2-40}$$

If intergranular stress $\sigma_g$ is equated with effective stress $<\sigma>$ the resulting expression is a function of porosity.

Terzaghi envisioned soils as individual plates and grains of solid material separated by springs that compressed during compaction. Terzaghi reasoned and argued that the simple differential pressure $\sigma$ - $p$ could not determine deformation in the limit of zero porosity. The simple intergranular stress hypothesis above agrees with this. As the porosity goes to zero the effect of pore pressure goes to zero. In the other direction, however, soils and muds in his experiments that deform according to $\sigma$ - $p$ did not have 100% porosity. Terzaghi suggested that because individual particles have surface roughness there is actually an "effective porosity" for intergranular stress that for soils was approximately equal to 1.

Biot (1935, 1941) established the physics of three dimensional consolidation. In his work he totally discarded effective stress and instead treated external stress and pore fluid pressure as independent variables. Stress was defined as total force per unit area of a representative homogeneous element and not separated between solid and fluid. The micromechanics of particle surfaces in contact were implicitly contained in the overall bulk and shear moduli and in the phenomenological constants $H$ and $R$. Time effects in consolidation were included with Darcy's law. The linear elasticity of porous media presented in the previous section is the Biot formulation for consolidation. For muds and soils the

bulk modulus is much greater than the intrinsic bulk modulus and the Biot stress-strain relation becomes equal to the Terzaghi relation.

In subsequent redevelopments of Biot's consolidation equations by Gassmann (1951) and Geertsma (1957) more readily defined physical parameters such as intrinsic bulk modulus ($K_s$), pore fluid modulus ($K_f$), and porosity ($\varphi$) were introduced in place of the original $H$ and $R$ constants of Biot. These too have been used in the previous section. It is significant to note, however, that effective stress was not referenced although the concept continued to be extensively used in the soil mechanics literature (Skempton, 1960; Süklje, 1969). Hubbert and Rubey (1959) argued for the Terzaghi relation as a general principle for stress in the crust.

When it became apparent that pore fluid injection could cause earthquakes (Healy *et al.*, 1968) or that pore pressure could be responsible for temporal velocity variations and aftershocks associated with earthquakes (Nur, 1971; Nur and Booker, 1972; Booker, 1974), pore pressure effects and effective stress were revived in a major way. For the most part effective stress was used as a synonym for differential pressure (Brace, 1972). In some cases, however, it gained additional status as the "law of effective stress" (Brace and Martin, 1968; Nur and Byerlee, 1971; Garg and Nur, 1973), the "effective stress concept" (Carroll, 1979), or as any of a number of "effective pressure laws" (Robin, 1973).

The mechanics of rock response to pore pressure and confining stress at small strains is well described by the linear elasticity of porous media in the first section. What is generally called effective stress or effective stress "laws" can be explained from the descriptions of the first section. Here it will be shown how the "effective stress law" for bulk strain (Nur and Byerlee, 1971; Garg and Nur, 1973; Carroll, 1979) and pore volume strain (Robin, 1973) are formulated from the

linear elasticity analysis.

It is possible to regroup terms in the stress-strain relationship (Eq. 2-10) so that stress and pore pressure are combined as an "effective stress." This was done by Nur and Byerlee (1971), Garg and Nur (1973), and Carroll (1979). Nur and Byerlee (1971) actually started out with Eq. (2-10) and derived $\zeta$ (their $\alpha$) in Eq. (2-11) along the same lines as Gassmann (1951) and Geertsma (1957). Eq. (2-10) from the first section can be regrouped as

$$\sigma_{ij} + \zeta p \delta_{ij} = (K - \frac{2}{3}G)\delta_{ij}\varepsilon_{kk} + 2G\varepsilon_{ij}$$

$$\zeta = 1 - \frac{K}{K_s} \qquad (2\text{-}41)$$

The combination of stress and pore pressure on the left Nur and Byerlee (1971) termed "effective stress" $<\sigma_{ij}>$ so that

$$<\sigma_{ij}> = (K - \frac{2}{3}G)\delta_{ij}\varepsilon_{kk} + 2G\varepsilon_{ij}$$

$$<\sigma_{ij}> = \sigma_{ij} + \zeta p \delta_{ij}. \qquad (2\text{-}42)$$

Therefore $<\sigma_{ij}>$ describes strain as a function of hydrostatic confining stress and pore pressure $p$ as if there were no pore pressure. Rice and Cleary (1976) also use this definition in their development. Nur and Byerlee (1971) applied Eq. (2-10) to the specific case of a microhomogeneous and microisotropic linear solid and hence $\frac{1}{H} = \frac{1}{K} - \frac{1}{K_s}$.

The Nur and Byerlee (1971) and Garg and Nur (1973) definition of effective stress is an association of the confining stress and pore pressure in Eq. (2-10). Absolute strain could however be predicted directly from Eq. (2-10). This is made clear in the section with graphical examples and in the experimental test.

Biot (1962a) referenced "effective stress" ($\sigma'$) as the simple difference

$$\sigma'_{ij} = \sigma_{ij} + \delta_{ij} p, \tag{2-43}$$

the portion of the total stress in excess of local pore pressure $p$. With this definition, the stress-strain relation Eq. (2-10) becomes

$$\sigma'_{ij} - (1-\zeta)\delta_{ij} p = (K - \frac{2}{3}G)\delta_{ij}\varepsilon_{kk} + 2G\varepsilon_{ij}, \tag{2-44}$$

obviously quite different from the Nur and Byerlee (1971) definition.

The Nur and Byerlee (1971) definition of effective stress is strictly valid only for an isotropic, linear, homogeneous, porous solid. Bulk isotropy is required because the bulk modulus $K$ and intrinsic bulk modulus $K_s$ are used in Eq. (2-11). Carroll (1979) analyzed the general anisotropic case although Biot (1955, 1956) had extended his consolidation equations to general anisotropy some years earlier. The same derivation as that of Nur and Byerlee (1971) was followed except that the bulk modulus $K$ was replaced by a tensor of elastic moduli $M_{ijkl}$ and the intrinsic bulk modulus $K_s$ was replaced by a tensor of elastic compliances $C^s_{ijkk}$. The effective stress for deformation of an anisotropic solid then becomes

$$<\sigma_{ij}> = \sigma_{ij} + p(\delta_{ij} - M_{ijkl} C^s_{klmm}). \tag{2-45}$$

Comparing this expression with the Nur and Byerlee (1971) definition of effective stress,

$$<\sigma_{ij}> = \sigma_{ij} + p(1 - \frac{K}{K_s})\delta_{ij}, \tag{2-46}$$

anisotropy in either the solid matrix or overall porous solid means a different effective stress in different directions. Of course Eq. (2-10) could be formulated

with tensor moduli and this was done by Biot (1955, 1956) although without the succinctness of tensor notations. The question of anisotropy will be further addressed and clarified in the graphical examples.

Linear elasticity equations in the first section describe both bulk strain and pore volume strain in response to pore pressure and confining stress. As Nur and Byerlee (1973) defined an "effective stress law" for bulk strain so too Robin (1973) defined an "effective stress law" for pore volume strain. From Eq. (2-16) of the first section the variation in pore volume $\Delta v_p$ about some reference state at constant pore pressure normalized to pore volume is given by

$$\frac{\Delta v_p}{v_p} = -\frac{1}{\varphi}\left(\frac{1}{K} - \frac{1}{K_s}\right)\sigma. \tag{2-47}$$

The variation in response to a combination of confining stress and pore pressure is derived from Eq. (2-25) of the first section and is given by

$$\frac{\Delta v_p}{v_p} = -\frac{1}{\varphi}\left(\frac{1}{K} - \frac{1}{K_s}\right)(\sigma - p) - \frac{1}{K_s}p. \tag{2-48}$$

This equation can be expanded to

$$\frac{\Delta v_p}{v_p} = -\frac{1}{\varphi}\left[\frac{K_s - K}{K_s K}\right]\left[\sigma - p + \frac{\varphi K}{K_s - K}p\right]. \tag{2-49}$$

Comparison of this last equation with Eq. (2-48) gives an "effective stress" for pore volume strain

$$<\sigma> = \sigma - \left[1 - \frac{\varphi K}{(K_s - K)}\right]p. \tag{2-50}$$

Substitution of reasonable moduli and porosities for rocks shows that the coefficient in brackets is nearly 1, or that

$$\langle\sigma\rangle = \sigma - p. \tag{2-37}$$

The reason Eq. 2-50 develops the way it does is because the change in pore volume is normalized to pore volume. If it were normalized to bulk volume instead, the porosity change of the porous medium is described, and if the change in porosity rather than pore volume is described by an "effective stress law" the last equation is exact.

## GRAPHICAL EXAMPLES

A few graphical examples with synthetic data will clarify most of the points and concepts made in the previous sections. Various plots shown in Fig. 2-2 are stress-strain relations for different idealized porous materials. On these plots the vertical axis is hydrostatic confining stress and the horizontal axis is strain.

In Fig. 2-2a the stress-strain relation for a perfectly linear, isotropic, homogeneous, porous solid is shown. Although the strain axis may be linear or volumetric strain, assume for this discussion that it is volumetric strain. The steeper of the two solid lines extending out from the origin, labelled U, is the stress-strain relation for the solid matrix material. If the porous solid is micro-homogeneous and micro-isotropic the inverse slope of this line is $K_s$, the solid matrix or intrinsic bulk modulus. If these attributes only apply on a macroscopic scale then the slope is $K_s'$, the solid matrix bulk modulus of an equivalent homogeneous material. The strain measured in an unjacketed stress-strain test, where confining pressure fluid freely infiltrates the pores, would follow line U.

The shallower solid line in Fig. 2-2a, labelled J, is the jacketed stress-strain relation with the pores empty or at least drained of pressure. The inverse slope is $K$, the jacketed bulk modulus, which includes features of pore closure in addition to solid matrix strain.

The upper solid line in Fig. 2-2a which is parallel to the jacketed stress-strain line represents the jacketed stress-strain relation for the porous solid with constant pore pressure of level $p$. Since pore pressure cannot be greater than confining pressure the origin for this line is at hydrostatic confining pressure $p$. At this point pore pressure equals confining pressure and the overall solid, as well as porosity and solid matrix, has experienced volumetric strain $p/K_s$. Assume that confining pressure $\sigma$ combined with pore pressure $p$ results in bulk volumetric strain $\varepsilon$. The stress field may be decomposed into two steps because of linearity. The first step is an equal internal and external pressure $p$ that results in strain $p/K_s$. The second step is an external pressure $\sigma - p$ with constant pore pressure that results in a strain $(\sigma - p)/K$. Total strain is the sum of these two steps:

$$\frac{(\sigma - p)}{K} + \frac{p}{K_s} = \varepsilon, \tag{2-51}$$

or

$$\sigma - (1 - \frac{K}{K_s})p = K\varepsilon \tag{2-52}$$

$$\zeta = 1 - \frac{K}{K_s}. \tag{2-11}$$

This is Eq. (2-10) of the first section for the case of hydrostatic confining pressure and a completely homogeneous and isotropic porous solid.

The "effective stress law" or "concept" of Nur and Byerlee (1971), Garg and Nur (1973), Robin (1973), and Carroll (1979), is to describe the strain at confining stress $\sigma$ and pore pressure $p$ in terms of the same strain at zero pore pressure. Their effective stress is the left term in Eq. 2-52. In Fig. 2-2a the dashed line down from the point $\sigma$, $\varepsilon$ to the zero pore pressure relation line J and from there across to the stress axis graphically defines the effective stress or pressure. This is simply a matter of definition and the effective pressure so defined has no

intrinsic physical meaning. Since $K$ and $K_s$ are both constants the coefficient 1 - $K/K_s$ is constant with pressure.

The plot in Fig. 2-2b shows what happens when the pore space is structurally anisotropic. The solid matrix remains, on the average, isotropic, and so the single steeper solid line is solid matrix strain. The horizontal axis is linear strain, however, to show the anisotropy in 2 directions represented by the pair of shallower solid lines. For an anisotropic rock the effective stress will be different depending on direction. Linear strain at a confining stress $\sigma$ and pore pressure $p$ will, if related to the strain with zero pore pressure, correspond to two different "effective pressures" $\sigma'$ and $\sigma''$. This is indicated by the dashed lines in Fig. 2-2b. If the matrix solid is also anisotropic the lack of uniqueness in defining a single effective stress is further exacerbated because solid matrix strain will also vary with direction. In the experimental test problems with anisotropy in the samples were avoided by using bulk strain. Even if effective stress were calculated for linear strain, anisotropy is not a major problem in the samples studied. At low pressures modulus anisotropy is greatest, but since $K<<K_s$, the coefficient $\zeta$ is not that sensitive to sizable differences in $K$.

The plot in Fig. 2-2c is more representative of a real rock and the main points for the entire chapter including the real experimental data are contained here. The horizontal axis is volumetric strain. The matrix solid stress-strain relation is nearly linear; any nonlinearity would be caused by occluded porosity, crystal defects, or inhomogeneity. The jacketed stress-strain relation with zero pore pressure starts out nonlinear because of the nonlinear nature of pore and crack closure. At high confining pressures those pore features responsible for most of the nonlinear strain have been removed. The inverse slope of the stress-strain relation at high pressure is the bulk modulus of a nearly linear porous solid with a certain amount of porosity, not of the solid matrix which is

still given by the straight line.

The stress-strain relation at constant pore pressure $p$ is the zero pore pressure curve with the origin relocated along the solid matrix stress- strain relation at hydrostatic confining pressure $p$. Bulk volumetric strain at confining pressure $\sigma$ and pore pressure $p$ is a sum of solid matrix strain $p/K_s$ and zero pore pressure strain at confining pressure $\sigma$ - $p$. The bulk modulus $K$ is a function of differential pressure $\sigma$ - $p$. Consequently, the coefficient $\zeta$ is a function of differential pressure.

The effective stress $\sigma'$ for hydrostatic confining pressure $\sigma$ and pore pressure $p$ is graphically calculated in Fig. 2-2c. It can be seen that the definition reduces the effect of pore pressure by coming down to a strain level higher on the zero pore pressure curve than that at $\sigma$ - $p$. At higher pressures the slopes approach that of the solid matrix and the effect of pore pressure is further reduced. This simply reflects a decrease in the value of coefficient $\zeta$. For rocks the solid matrix strain is an appreciable part of overall strain and the effective stress calculated is larger than differential pressure. For muds and soils bulk strain is much larger than solid matrix strain, $\zeta$ is nearly equal to 1, and the effective stress definition approximates differential stress. Essentially, the effective stress definition above for rocks obscures the solid matrix strain by reducing the effect of pore pressure. If the vertical axis is instead the solid matrix stress-strain relation in Fig. 2-2c, then differential pressure determines strain.

In Fig. 2-2d the relation between unjacketed and jacketed bulk volume strain, and pore volume strain, is graphically depicted for a nonlinear rock with finite strain. The vertical axis is confining pressure and the horizontal axis is volumetric strain. At constant pore pressure the bulk volume stress-strain

relation is given by the curve labelled $V_b$. Solid matrix volume strain is measured in an unjacketed stress-strain test and is the straight solid line labelled $v_s$. Because rocks in general behave as a semilinear material (Biot, 1973) the nonlinear bulk strain can be continuously broken down into pore volume strain and linear solid volume strain. The difference between bulk volume strain and solid matrix volume strain is pore volume strain, the middle curve labelled $v_p$ in Fig. 2-2d. All strains are normalized to overall bulk volume. With bulk and solid matrix volume strain measured directly, the decrease in pore volume and hence porosity with confining pressure can be calculated quite accurately with finely incrementalized data points and the relation expressed in Eq. 2-35 which relates the change in porosity with confining pressure, porosity, and jacketed and unjacketed bulk moduli. In practice, however, the porosities are so small, particularly for the igneous and metamorphic rocks, that the initial porosity can be assumed to be zero, and Eq. 2-36 holds. The result is that the decrease in porosity at any confining pressure is directly calculated by subtracting the unjacketed from jacketed strain, and this porosity decrease can be referenced to the initial porosity.

This is similar reasoning as followed by Walsh (1965) in his technique for calculating the porosity of low-porosity rocks. Reference is made to the unjacketed stress-strain measurement but in practice (Brace, 1965; Brace *et al.*, 1966) the emphasis was on measuring the tangent to the high pressure jacketed stress- strain relation to obtain crack porosity. In the technique outlined in the previous paragraph for the calculation of porosity as a function of confining pressure it is not necessary to either 1) go to high pressures to achieve a semi-linear stress-strain slope, or 2) estimate the zero-pressure intercept from a tangent drawn to the high pressure stress-strain relation. The tangent is measured directly in the unjacketed measurement and, along with the jacketed

data, gives two direct measurements from which porosity decrease is readily calculated. This procedure does not, however, ease the calculation of crack porosity because for this a tangent must still be drawn, be it on the strain or the porosity relation as a function of confining pressure.

## EXPERIMENTAL TEST

Rocks, sediments, and soils fall far short of the ideal porous solids described in the elasticity analysis. Rocks are normally not very homogeneous, isotropic, or linear, and strain amplitudes are often larger than infinitesimal. It should be of general interest, then, to investigate whether the equations fit real materials such as rocks. In the experiments to be described the bulk strain of a suite of rock samples was measured as a function of systematically cycled hydrostatic confining stress and internal gas pore pressure. For each sample, jacketed and unjacketed bulk moduli were calculated and the stress-strain measurements were compared with that predicted by the equations in the analysis. Additional measurements of jacketed and unjacketed strain were then made for a number of other rock samples.

The linear description in the first section originated with Biot (1941). Since that time there have apparently been only two relevant experimental stress-strain studies on rocks, where pore pressure was a variable in addition to confining stress. These are by Van der Knaap (1959) and by Nur and Byerlee (1971). Although he reports that experiments were run on a number of sandstones and limestones, Van der Knaap (1959) only gives data for a sample of Belait sandstone ($\varphi$=15%). He established experimentally the essential features of the analysis given in the first section and in the graphical examples. First, the stress-strain curve measured for this rock at a constant pore pressure of about 1 kbar was predicted from the zero pore pressure curve by using the intrinsic

bulk modulus measured in an unjacketed stress-strain test. Without a jacket the confining pressure fluid fills the porosity of the sample and the resultant strain can be identified with an average modulus of the solid phase. The prediction corresponds to Fig. 2-2c in the graphical examples, where the zero pore pressure curve slides up the straight line of the intrinsic solid modulus to a point equal to pore pressure p.

The second feature of the analysis established experimentally by Van der Knaap (1959) is the division of bulk strain between pore volume strain and solid matrix volume strain. According to the linear elastic description the solid matrix volume strain should be inversely proportional to the intrinsic solid bulk modulus. For Belait sandstone Van der Knaap measured bulk strain as a function of increasing confining stress and, simultaneously, pore fluid expelled from the pore space at constant pore pressure. The difference between these two had to be the amount of solid matrix strain. This measured difference agreed with the predicted calculation based on the intrinsic solid bulk modulus.

Nur and Byerlee (1971) measured bulk strain on a sample of Weber sandstone ($\varphi$=9.5%, this paper) at various unspecified combinations of pore pressure and confining stress. Although their aim was to test an "effective stress law" for bulk strain, the prediction of strain with pore pressure with their "effective stress" indicates that the incrementalized linear elasticity description works. This is because the true source of their "effective stress" is the Biot linearized elasticity equations as shown in the first section. Garg and Nur (1973), however, working with the same data set on Weber sandstone, replot "effective stress" versus strain and show a negative discrepancy between predicted and measured strain. They suggest that the data includes a time effect due to slow pore fluid diffusion, but why this did not show up in the earlier work is not clear. Nur and Byerlee (1971) do mention that up to 12 hours

between data points was necessary for equilibration.

These two studies, then, are apparently the only ones to investigate the combined influence of pore pressure and confining pressure on strain. The conclusion is that not enough experiments on this fundamental issue have been made. Also lacking are experiments with pore pressure and confining pressure on rocks of extreme micro-inhomogeneity and micro-anisotropy, such as crystalline granites.

Data can be found in the literature, however, which can be used in the equations. Fatt (1959) measured and calculated for Boise sandstone jacketed and unjacketed bulk modulus, porosity, and the coefficient $\zeta$ at several confining pressures. These values, in addition to shear modulus and fluid compressibility, fix the properties necessary for predicting the static elastic response. A major emphasis in experimental studies has been the stress-strain response of jacketed samples that are dry or, if saturated, at constant pore pressure (Adams and Williamson, 1923; Zisman, 1933; Carpenter and Spencer, 1940; Hughes and Cook, 1953; Fatt, 1958; Brace, 1965; Simmons *et al.*, 1974). These kind of data provide the jacketed bulk modulus, and values have been compiled by Birch (Clark, 1966, Table 7-13). The important observation in these studies is the functional nonlinearity between stress and strain caused by local changes in contact area and asperity closure, especially at low stress. Because of nonlinearity the static moduli are a function of stress. Whether or not the static moduli are a function of differential stress, $\sigma - p$, is a question addressed in this experimental study.

In addition to the jacketed bulk modulus K the unjacketed bulk modulus $K_s'$ is required. Experimental stress-strain measurement of an unjacketed sample, where confining pressure fluid penetrates the pores, is a direct measure of an

average intrinsic modulus of the solid matrix. This is a measurement emphasized in this experimental study. Values for a number of rocks have been compiled by Birch (Clark, 1966, Table 7-13), but most of the data is quite old and there is a great deal of scatter in the measurements. The largest proportion of unjacketed moduli in Birch's compilation come from Zisman (1933). Instrumentation and techniques have seemingly improved since that time. Nur and Byerlee (1971) report a value of 0.454 Mbar for Westerly granite which has been cited (Rice and Cleary, 1976) but which is somewhat lower than Voigt-Reuss averages (Brace, 1965; Siegfried and Simmons, 1978) and other measurements by Knopoff (1954), Adams and Williamson (1923), and this study, which indicate values between 0.49 and 0.56 Mbar. Unjacketed bulk moduli for a number of rocks are measured and tabulated in this experimental section.

An alternative to the direct measurement of intrinsic solid modulus is to calculate a Voigt-Reuss-Hill average from modal analysis and individual mineral moduli. This was done by Brace (1965). This calculation assumes that individual mineral moduli from other sources are appropriate and that microanisotropy is random.

Several points are clear in the previous experimental efforts with pore fluids and pore pressure. Nur and Byerlee (1971) had a serious problem with time-dependent effects because it took so long (~12 hours) for strain to equilibrate. Also clear from the experimental results of Mann and Fatt (1960) and Wyllie *et al.* (1958) is that liquids, particularly water, increased strain levels in the sandstones studied. Presumably, there is a chemical-physical interaction of pore fluid with matrix that increases elastic compliance. Todd (1973), however, reports agreement of static compressibilities in a dry and water-saturated sample of Fairfax diabase.

In order to accurately assess the elasticity relations and to avoid the deleterious effects of liquid pore fluids on strain, the decision was made early in this study to use nitrogen gas as the pore fluid. The three favorable aspects of gas are: 1) no interaction between pore fluid and rock matrix, 2) high compressibility, so that when pore volume is strained from confining stress the change in pore pressure is minimal, and 3) low viscosity, so that pore pressure equilibrates rapidly throughout the pore space and with the external nitrogen gas reservoir. Nitrogen gas was chosen because of readily available 6000 psi cylinders. Regulated pressures to that level were then possible without the need of a pump.

The basic experimental method was to measure bulk strain on jacketed samples of rock subjected to systematic cycles of confining pressure and pore fluid pressure. Rock strain was measured with strain gages attached directly to the rock surface, leads from which were brought out through the jacketing material. Confining pressure to 1 kbar was generated on the jacketed samples in a pressure vessel. A small high-pressure fitting penetrated the sample jacket and associated tubing brought nitrogen gas pore pressure up to 350 bars from an external gas reservoir.

For the measurement of unjacketed bulk modulus jackets were removed from the samples and kerosene confining pressure fluid penetrated the pores. Strain was measured to 1 kbar pressure.

With stress-strain data from jacketed measurements at zero pore pressure and unjacketed strain measurements, bulk modulus and intrinsic bulk modulus could be calculated. The theory of the first section could then be used to predict and compare with strain measurements at various pore pressures. In the following paragraphs the experimental test is broken down into discussions of

rock samples, instrumentation, procedure, and data reduction.

Strain measurements were made on the suite of sandstones, granites, limestones, marbles, and dolomites listed in Table 1. The listing includes dry bulk density, average grain size, porosity, and an average intrinsic bulk modulus $K_s$ measured for each of the samples. Dry bulk density was measured on vacuum-dried, precisely ground cylindrical cores. Average grain diameter was estimated from hand specimen and thin sections and is accurate to ±10%. Porosity was determined by comparison of vacuum-dry and water- or benzene-saturated weighings and values reported are accurate to about ±0.1% as determined by repeated measurements.

The average intrinsic bulk modulus $K_s$ reported for each of the samples in Table 1 was calculated from unjacketed stress-strain measurements on each of the samples. These values will be refered to and discussed in later sections of this chapter.

Stress-strain relations for the first seven samples in Table 1 were measured as a function of systematically varied confining and nitrogen pore fluid pressures. After the measurement and interpretation of bulk strain as a function of confining pressure and pore pressure was evident and understood, additional jacketed and unjacketed stress-strain data was collected for the remaining 11 samples in Table 1. The experimental apparatus was fully automated for controlling both increasing and decreasing pressure and data collection and so these additional experiments required only the effort of sample preparation, gage attachment, and setup in the pressure vessel.

Almost all of the rocks in Table 1 constitute part of a standard set of rocks previously studied by various investigators in the rock mechanics literature. In terms of the major point made in this paper, the behavior of rock strain in

response to pore and confining pressure relative to the definition of effective pressure, the exact identity of these rocks is unnecessary. The linear elastic description describes any porous solid. Nonetheless, more detailed lithologic and thin-section petrographic descriptions are given in Appendix B for the samples in Table 1.

Rock samples were of two types. Large 3" diameter by 2" long finely finished cores were prepared for the jacketed measurements with pore pressure. Small blocks, usually about 1" square by 1/2" thick were prepared for the unjacketed measurements so as to preserve the larger cores from kerosene contamination. The small blocks were first measured jacketed and then unjacketed. Therefore, multiple data sets could be compared from different samples of the same rock.

Rock samples were cored from various larger blocks of rock using a water-cooled diamond core drill. Samples were finished to a nominal 2" long by 3" diameter size with diamond-wheel cylindrical and surface finish grinders. Small block samples were cut to dimension with a diamond saw. Samples were flushed with water and acetone and then saturated in acetone by pulling a vacuum on the sample while submerged in an acetone-filled beaker. Samples were kept saturated for at least 24 hours and then vacuum dried (20 $\mu$m Hg) at 60 degrees C for at least 24 hours.

Strain gages were applied directly to the finished surfaces of the samples. For the core samples three strain gages (BLH FAE-50-S6E) were attached in three mutually perpendicular directions on the cylindrical surface, one axially and two circumferentially. For the block samples normally two gages, sometimes three, were attached in mutually perpendicular directions. If bedding or a rift plane were present gages were oriented according to the planar feature. The general area on the sample where a gage was to be attached was always sanded

with 400 grit sandpaper. For all of the samples with appreciable porosity the rock surface was first filled with a viscous epoxy (BLH EPY 150) to prevent gage collapse into the pores under pressure. This epoxy, when dry, was sanded until the minerals were uniformly exposed, finishing with 400 grit paper. This procedure was found to be much easier when the epoxy was colored with a red dye. After surface preparation gages were applied with epoxy (EPY 150) and clamped to the samples with teflon sheets, sections of 3 inch thin-wall brass tubing, and hose clamps.

In Fig. 2-3 is a diagram of the jacketed sample arrangement within the pressure vessel apparatus. Pore pressure in the sample is controlled through a stainless steel fitting which penetrates the jacket. High pressure tubing from the fitting through the closure plug to outside of the vessel goes to either a vacuum pump or a regulated nitrogen gas tank. The sample jacket contains two layers. First is a polyurethane sheet that is slit around the gages for lead attachment. After clean #22 copper wire is soldered to the gages the entire assembly of fitting, sample, and jacket is potted with an air-drying liquid polyurethane compound (Flexane, Devcon Corp.). The polyurethane sheet prevents the compound from entering the pores of the sample. Stress-strain tests on jacketed and unjacketed nonporous aluminum and lucite indicated no interference from the jacket on strain measurements.

A 3-wire lead system was used between the sample strain gages and the bridge completion network. Each gage had an individual bridge conditioning module (Analog Devices 2B30K) with one half of the bridge completed by shared 120 ohm resistors (Vishay 0.01%) A common shunt resistor on one of the shared resistors allowed for simultaneous calibration of all of the strain gages. The bridge conditioning modules output connects to the HP 3497A data acquisition/control unit and from there to the HP 1000 computer.

The pressure vessel apparatus in Fig. 2-3 is capable of subjecting samples up to 15 inches long and almost 3.5 inches in diameter to hydrostatic confining pressures up to 4 kbar. In these experiments. however, the samples were much smaller and pressures never exceeded 1.2 kbar. The confining pressure fluid is kerosene pumped up to pressure by an air-driven Haskell pump. Air to the pump and air to an air-operated high pressure relief valve is controlled by individual solenoid valves. These solenoid valves are in turn controlled by relays on a board in the HP 3497A data acquisition/control unit. Confining pressure and pore pressure are monitored by pressure transducers whose signals are conditioned with Analog Devices 2B31K modules and then fed into the HP 3497A data acquisition/control unit. This device is in turn controlled by the HP 1000 computer. Software developed on the computer controlled the cycling of confining fluid pressure and the collection of data from the strain gages and pressure transducers.

The procedure for a typical stress-strain measurement with pore pressure is now described. The jacketed sample arrangement with leads attached was located within the pressure vessel and a 20 bar confining pressure was applied. Allowing the sample to stay at zero pressure for lengths of time without this pressure made it susceptible to leaks. A vacuum (20 $\mu$m Hg) was pulled on the sample for no less than 24 hours. Several slow cycles of confining pressure were then automatically applied up to the maximum desired confining pressure in order to get a repeatable stress-strain curve. This was determined by the collected data and was usually achieved after 3 cycles. For the sandstones it was found that strain, after initially decreasing at a given pressure over the first few cycles, increased with additional cycles. The maximum confining pressure for the sandstones was 1000 bars, for the granites 1200 bars, and for the limestone 750 bars. Hysteresis and repeatability of the vacuum stress-strain curves was

usually less than 10 microstrain ($10 \times 10^{-6}$ inch/inch of sample).

After cycling to obtain a repeatable vacuum stress-strain curve the measurements with pore pressure could begin. For most of the rock samples confining pressure was cycled with constant nitrogen gas pore pressures of 50, 100, 150, 200, 250, and 300 bars. The procedure was to alternately raise confining pressure and pore pressure until confining pressure was about 5 bars above the desired pore pressure. Equilibrium was assumed when strain readings leveled off at a stable value. For the sandstones and limestone this took about 15 minutes and for the granites about 30 minutes. After the system equilibrated, the confining presure was cycled up with strain and pressure measurements recorded every 10 bars at a stress rate of about 5 bars/minute. Pore pressure was maintained at a constant level by periodic adjustments with the regulator or released via a valve. After reaching the desired maximum, confining pressure was reduced with measurements recorded every 25 bars. Pore pressure was then slowly released, confining pressure was reduced to 20 bars, and the overall system was allowed to equilibrate for 6 to 24 hours before the next cycle. For most of the samples multiple cycles were run with the same pore pressure.

Initially, the unjacketed bulk modulus, or the intrinsic bulk modulus, was calculated from the different pore pressure strain measurements at constant differential pressure. If differential pressure is kept constant as the absolute magnitudes vary, the strain undergone by the sample is a measure of the intrinsic bulk modulus $K_s'$. The data for this calculation were limited by the number of runs with different pore pressures and the results were not precise. To accurately fix the solid matrix modulus $K_s'$ unjacketed stress-strain measurements were made on smaller "block" samples. Two or three gages attached to these block samples were oriented in directions similar to the larger cores. The first step for these samples was a set of jacketed stress-strain cycles.

The samples were fully encapsulated and suspended in the pressure vessel without the pore pressure fitting. These measurements were compared with the measurements on the larger cores for repeatability. The jacket was then snipped off, the sample saturated with kerosene, again placed in the pressure vessel, and unjacketed cycles of stress-strain were measured to 1 kbar. With the system automated these cycles were slowed down to ensure that pore pressure equalled confining pressure. Typically one cycle took about 10 hours. Permeability, however, does not change with pressure in this measurement.

One drawback of the strain gage technique is that once attached, the gage cannot be calibrated except electronically by the gage factor assigned by the manufacturer ($G.F. = \frac{\Delta R/R}{\Delta L/L} \approx 2.00$). From the strain gage to the computer the system is exceedingly accurate and calibration is based on the gage factor. Ambient temperature and electronic fluctuation result in at most a ± 5 microstrain drift over a 10 hour period. The real question is how well the resistance change of the gage reflects true bulk strain in the rock. Points to consider in answering this question include: 1) filling the pores with epoxy probably stiffens the rock directly below the gage, 2) the epoxy layer between gage and rock surface absorbs some of the true strain, 3) repeatability of the measured stress-strain relation at a particular point on the rock between different gages, and 4) repeatability of the measured stress-strain relation in the same orientation for different samples of the same rock.

During the course of this study approximately 165 strain gages were attached to 35 rocks and standards. Perhaps the best estimate of error is gained in that process. Point 1 in the list above is perhaps not that serious. Jacketed data on some of the sandstones in this study compares favorably with that of Fatt (1958) and Mann and Fatt (1960). They measured some of the same rocks

with an external cantilever-type device. For the unjacketed measurements the calculated bulk modulus for some of the clean sandstones is nearly that of quartz, so the epoxy in the pore space does not seriously interfere with that measurement. Point 2 above was studied by Brace (1964) and is termed the "pressure effect." All of the data in this study have been corrected for pressure effect by adding 0.06 microstrain per bar of confining pressure.

Points 3 and 4 in the list above are addressed from the standpoint of having made so many measurements. For almost all of the rocks at least 2 samples were measured jacketed. For Westerly granite, Chelmsford granite, and Berea sandstone 4 samples were measured. About 10% of the gages applied resulted in questionable data. This was indicated by 1) strongly negative hysteresis strain in jacketed tests or 2) failure to agree with other gages in the same orientation. For the few jacketed tests where good gages were replaced the subsequent measured strains were repeatable to about ± 1%. For the different samples of Westerly and Chelmsford the jacketed absolute linear strains at 1 kbar compared to within ± 40 microstrain at levels of 1000-2500 microstrain.

In the unjacketed tests the intrinsic solid strain was quite reproducible. For samples of Westerly granite, Bedford limestone, and Berea sandstone linear strain was repeatable to within 2%.

Jacketed and unjacketed bulk moduli and the coefficient $\zeta$ (Eq. 2-11) were calculated as a function of confining pressure from the jacketed and unjacketed digitized strain data for samples of each of the rocks. Both types of linear strain data were initially corrected for pressure effect as mentioned previously and then summed in the three gage directions for each sample. For samples with only two strain gages either an average was taken for the third direction or else an appropriate doubling of one gage was used to calculate bulk strain. Strain

data were taken from the increasing pressure portion of normally the third or fourth confining pressure cycle.

A Chebyshev polynomial was globally fit to the strain data as a function of pressure with a least squares algorithm previously developed by Cheng and Johnston (1981). The differentiated polynomial yielded bulk moduli at each pressure where strain data were collected. Therefore, in the plots of moduli and the coefficient $\zeta$ in the next section each of the points in the plots correspond to acquired strain data. For the jacketed data a 5th to 7th order was normally used while a 3rd order polynomial was used for the unjacketed data. The choice of polynomial order reflects a judgement between reading too much detail into the data versus too little. The unjacketed strain data normally deviated only slightly from a linear function with confining pressure. A differentiated 2nd-order polynomial yields a linear change (increasing) in bulk modulus with pressure while a differentiated 4th-order polynomial oftens yields complex positive and negative deviations beyond consistent interpretation. Therefore a 3rd-order polynomial for the unjacketed strain data reflects a compromise as faithful to the original strain data as deemed reasonable. Similarly, polynomials of order less than 5 were usually not able to account fully for the nonlinearity of jacketed strains with pressure. Decision of what order polynomial to use were made interactively with the computer. In a sense some of the subjectivity in this procedure does not differ that substantially from the graphical technique of Brace (1965), who visually smoothed strain data and calculated moduli with the aid of a ruler to draw tangents. Somewhat in the other extreme is the method of Siegfried and Simmons (1978) who computationally differentiated a local quadratic function fitted to a limited number of adjacent data points (5 or 7).

The unjacketed stress-strain data and the calculated unjacketed bulk moduli as a function of confining pressure reflect some difficulties with the strain

gage technique, particularly at pressures less than about 200 bars. A portion of the nonlinearity in the stress-strain relation at these low pressures is due to the epoxy bond between gage and prepared material surface. This nonlinearity in the present data tends to be overemphasized at times in the third-order polynomials used to calculate the unjacketed bulk moduli. For the jacketed bulk moduli, on the other hand, this effect is reduced because for most of the rocks the stress-strain relation is highly nonlinear at low pressures and higher order polynomials are used. For the unjacketed bulk moduli an average value was calculated in addition to that which is plotted in the figures, and these average values are tabulated for the different rocks in Table 1. These average values were used for plotting the $\zeta$ coefficient as a function of confining pressure in the data and plots to be discussed. One of the benefits of the DSA technique (Simmons et al., 1974) is that artifacts such as this are removed when data from the sample gage and fused silica reference gage are subtracted.

Details in the curves of unjacketed or intrinsic bulk moduli as a function of confining pressure should not be over-interpreted. The amount the intrinsic bulk moduli increase with pressure is probably a maximum. For the average intrinsic bulk moduli in Table 1 probable error is approximately ±0.2 Mb. In the plots of intrinsic bulk moduli versus pressure the error at any pressure may extend from the points as plotted to the average value as given in Table 1. At pressures below 200 to 300 bars the intrinsic moduli as plotted are minimums. The absolute error of the jacketed bulk moduli for a particular strain data set is approximately ±0.15 Mb at pressures below about 200 bars and somewhat less, about ±0.1 Mb, in the middle part of the pressure range. Because the curve-fitting and differentiation suffers most towards the ends of the range of data, at high pressure also the error falls to about ±0.15 Mb. Representative error bars are shown in Fig. 2-15 for Westerly granite and Fig. 2-11 for Weber sandstone.

During the course of measuring rocks two different synthetic materials were measured. These were fused silica (GE125) and aluminum (T2024), which was not heat-treated. Bulk moduli calculated from the stress-strain data are 0.385 Mb for the fused silica and 0.735 Mb for the aluminum. The value for aluminum is similar to the 0.744 Mbar value reported by Bridgman (1923, p. 166) and the 0.752 Mbar value reported by Brace (1965).

## EXPERIMENTAL RESULTS

There are several aspects to the experimental strain data collected in this study. In this section the results of strain collected as a function of confining and pore pressure will be discussed. In succeeding sections the jacketed and unjacketed bulk moduli and then the coefficient $\zeta$ and porosity are discussed.

Volume microstrain versus pressure plots for the seven rocks systematically studied with pore pressure are shown in Figs. 2-4 through 2-10. There is a dichotomous interpretation for the data and the two interpretations define the axes differently as will be discussed. The solid black curve in each plot, however, is the measured zero pore pressure (vacuum) volumetric strain versus confining pressure. Volumetric strain is the sum of strains from three mutually perpendicular gages on each rock sample. The squarish symbols in these plots are the strain measurements with different pore pressures, i.e., 50, 100, etc., bars. There is no need to distinguish absolute values of pore pressure in the symbols because there are no systematic trends beyond the interpretations given. The immediate conclusion from the profusion of data points on top of the solid black line is that bulk strain in the tests with pore pressure is understood and very predictable.

The first interpretation of the data in Figs. 2-4 through 2-10 is with the "effective stress law" for bulk strain of Nur and Byerlee (1971), Garg and Nur

(1973), and Carroll (1979). For this interpretation the vertical axis is effective pressure and is defined by

$$\langle\sigma\rangle = \sigma - \zeta p \tag{2-53}$$

$$\zeta = 1 - \frac{K}{K_s'}, \tag{2-54}$$

where $\langle\sigma\rangle$ is effective pressure, $\sigma$ is confining pressure, $p$ is pore pressure, $K$ is bulk modulus, and $K_s'$ is solid matrix bulk modulus. The horizontal axis is volumetric microstrain and the origin is at zero pressure. From the zero pore pressure stress-strain data and unjacketed stress-strain data shown in Figs. 2-19 though 2-25 the two moduli and the coefficient $\zeta$ were calculated as a function of pressure. For each of the rocks these values are plotted in Figs. 2-11 through 2-17. For each data point of volume microstrain measured with pore pressure and confining pressure the effective pressure was calculated with the above equation. In calculating effective stress the moduli at a pore and confining pressure were taken as a function of the simple difference between pore and confining pressure. The square symbols in Figs. 2-4 through 2-10 represent calculated effective pressure versus volume microstrain. Agreement is excellent, regardless of rock-type. This means that bulk strain at any combination of pore and confining pressure is predictable from the zero pore pressure data and unjacketed data. Strain in the Weber sandstone with pore pressure that was investigated by Nur and Byerlee (1971) and Garg and Nur (1973) is predicted exactly in Fig. 2-4 for all pore pressures. Strain in the granites and in the limestone is also predicted exactly with the definition of effective pressure.

The coefficient $\zeta$ decreases with increasing confining pressure according to the plots in Figs. 2-11 through 2-17. Since $K_s'$ is nearly constant with pressure, $\zeta$ decreases with increasing pressure in a manner that reflects the increase in $K$. In Fig. 2-18 the value of $\zeta$ between zero and 1 kbar pressure is summarized for

(1973), and Carroll (1979). For this interpretation the vertical axis is effective pressure and is defined by

$$\langle\sigma\rangle = \sigma - \zeta p \tag{2-53}$$

$$\zeta = 1 - \frac{K}{K_s'}, \tag{2-54}$$

where $\langle\sigma\rangle$ is effective pressure, $\sigma$ is confining pressure, $p$ is pore pressure, $K$ is bulk modulus, and $K_s'$ is solid matrix bulk modulus. The horizontal axis is volumetric microstrain and the origin is at zero pressure. From the zero pore pressure stress-strain data and unjacketed stress-strain data shown in Figs. 2-19 though 2-25 the two moduli and the coefficient $\zeta$ were calculated as a function of pressure. For each of the rocks these values are plotted in Figs. 2-11 through 2-17. For each data point of volume microstrain measured with pore pressure and confining pressure the effective pressure was calculated with the above equation. In calculating effective stress the moduli at a pore and confining pressure were taken as a function of the simple difference between pore and confining pressure. The square symbols in Figs. 2-4 through 2-10 represent calculated effective pressure versus volume microstrain. Agreement is excellent, regardless of rock-type. This means that bulk strain at any combination of pore and confining pressure is predictable from the zero pore pressure data and unjacketed data. Strain in the Weber sandstone with pore pressure that was investigated by Nur and Byerlee (1971) and Garg and Nur (1973) is predicted exactly in Fig. 2-4 for all pore pressures. Strain in the granites and in the limestone is also predicted exactly with the definition of effective pressure.

The coefficient $\zeta$ decreases with increasing confining pressure according to the plots in Figs. 2-11 through 2-17. Since $K_s'$ is nearly constant with pressure, $\zeta$ decreases with increasing pressure in a manner that reflects the increase in $K$. In Fig. 2-18 the value of $\zeta$ between zero and 1 kbar pressure is summarized for

the seven rocks studied in detail. The largest value of $\zeta$ is at low confining pressure since bulk modulus $K$ is lowest relative to solid matrix bulk modulus $K_s$. Of the three sandstones studied Navajo had the stiffest response, and the value of $\zeta$ never reaches above 0.75. For the other two sandstones, Berea and Weber, $\zeta$ almost reaches 1 at low pressure. At high pressure $\zeta$ for these sandstones is around 0.5, Bedford limestone has very little nonlinear strain, few crack like pore structures, and $\zeta$ decreases very little with pressure. The greatest range of $\zeta$ is for the three granites. At low pressure, Chelmsford granite $\zeta$ is nearly 1; at high pressure it decreases to about 0.25.

In these data the effective stress law for bulk strain of Nur and Byerlee (1971), Garg and Nur (1973), and Carroll (1979) has been shown experimentally correct for a large variety of rocks. As shown in the second section effective stress is an extension of Biot's linearized elasticity equation. There is a far easier means of predicting the strain without calculating moduli or effective stress. This is a second interpretation of the data in Figs. 2-4 through 2-10. If $\Phi_j$ is the drained and jacketed stress-strain response of the porous solid and $\Phi_u$ is the unjacketed stress-strain response, the strain $\varepsilon$ at any combination of pore pressure $p$ and hydrostatic confining stress $\sigma$ is

$$\varepsilon = \Phi_j(\sigma - p) + \Phi_u(p). \tag{2-55}$$

Total strain is simply a sum of the drained and jacketed response at the differential pressure plus the unjacketed response at the pore pressure. Conceptually the overall stress field has been decomposed into an equal internal and external pressure $p$ and an external pressure $\sigma - p$. For this interpretation the vertical axis in Figs. 2-4 through 2-10 is now differential pressure and the horizontal axis is the drained, jacketed response to differential pressure. The origin of the plots is $\Phi_u(p)$, which varies as a function of pore pressure, and in

this interpretation is being subtracted out. There is no need to replot the data in Figs. 2-4 through 2-10 because agreement is still excellent.

The main result is that bulk strain in response to pore and confining pressure is understood and predictable from the drained, jacketed and unjacketed stress-strain relation. For this purpose the "effective stress" of Nur and Byerlee (1971), Garg and Nur (1973), and Carroll (1979) is a rather redundant calculation. The data necessary to calculate effective stress can be used directly to predict strain with pore pressure.

A fundamental aspect of the data is the duplication of the drained, constant pore pressure stress-strain function regardless of pore pressure. Particularly for the granites studied there is severe microinhomogeneity and microanisotropy of mineral grains. The linear compressibility of quartz along the $c$ axis is 0.718 $Mb^{-1}$; perpendicular to the $c$ axis it is 0.995 $Mb^{-1}$ (Birch, Table 7-12, in Clark, 1966). The linear compressibility of orthoclase is much more anisotropic: along the $a$ axis 1.013 $Mb^{-1}$; along the $c$ axis 0.468 $Mb^{-1}$. Microcline is a solid solution of orthoclase and albite and is a common phase in the granites studied. With these different mineral grains adjacent, cracks develop due to mechanical anisotropy as well as thermal expansion anisotropy during cooling (Nur, 1969). In the application of pore pressure and confining pressure in the laboratory the process is conceptualized as two stages. First an equal internal and external pressure at the value of the pore pressure, then an external pressure equal to the differential pressure. The application of an equal internal and external pressure necessarily causes shear stresses and grain boundary reorganization where minerals with different compressibilities meet. For example, where the $c$ axis of orthoclase lies parallel to the $c$ axis of quartz the application of 1 kbar pore and confining pressure during an unjacketed test will result in 468 microstrain in orthoclase and 995 microstrain in the quartz. If a small crack

separates the two minerals surface topographies will shift relative to each other. When confining pressure is then applied at constant pore pressure of 1 kbar the nonlinear aspect of strain as the crack closes may be different than when pore pressure is zero. Whether there is more strain or less strain is not predictable as that is a function of an exact description of topography. The order in which stresses are introduced will also be a factor. In the data collected on granites with pore pressure no measurable consistent trend in bulk strain was detected with increasing pore pressure. Therefore the conclusion is that microanisotropy and microinhomogeneity do not seriously affect the nonlinear constant pore pressure strain response after an initial pore and confining pressure are placed on the rock.

## JACKETED AND UNJACKETED BULK MODULI

Jacketed and unjacketed bulk moduli calculated from the respective strain data as a function of confining pressure are discussed in this section. For the first seven rocks in Table 1 these moduli are found in Figs. 2-11 through 2-17. For the rest of the rocks in Table 1 the moduli are plotted in Appendix A, the "b" plots of Figs. A-1 through A-11.

Jacketed bulk moduli and strain reflect the nonlinearity of stress-strain relations for most rocks. This nonlinearity is interpreted as due to closure of small discontinuities or cracks within the rock (Adams and Williamson, 1923; Zisman, 1933; Brace, 1965). The discontinuities may be modelled as simple geometric, usually ellipsoidal, shapes (Eshelby, 1957; Walsh, 1965; Wu, 1966; Korringa *et al.*, 1979). With this type of model a distribution of different pore shapes can be generated based on crack aspect ratios closing at different pressures (Siegfried and Simmons, 1978). Alternatively, the discontinuities may be modelled as free surfaces between which Hertzian contacts exist (Walsh and

Grosenbaugh, 1979). In addition, more porous sedimentary rocks may be modelled as assemblages of spheres connected by Hertzian contacts (Fatt, 1958; Duffy and Mindlin, 1957). Unjacketed bulk moduli, on the other hand, reflect an average of the intrinsic bulk moduli for the individual aggregate minerals. Both moduli can be compared with previous measurements on the same or similar rocks.

20 years ago Brace (1965) measured stress-strain relations and calculated linear compressibilities as a function of hydrostatic stress for a suite of low-porosity rocks which included samples of Westerly granite, Vermont marble, Blair dolomite, and Webatuck dolomite. His bulk compressibilities, found by summing linear compressibilities, can be inverted for bulk moduli and compared with the present data set. Both the Blair and Webatuck dolomite samples were taken from the same block of rock. The Westerly granite and Vermont marble samples, however, are from different sources.

The technique of Brace (1965) used strain gages expoxied to a copper jacket previously seated onto the sample with pressure, whereas the present technique, as well as that of Simmons and coworkers (Simmons *et al.*, 1974; Siegfried and Simmons, 1978), epoxies the strain gages directly to the sample. Both Brace's strain data and the data in this study were corrected for pressure effect on the strain gages. In Simmon's technique strain of a fused silica reference is subtracted from the measured rock strain to remove pressure effect along with thermal effects. Linear compressibilities were calculated by Brace from visual estimation of the tangent to recorded stress-strain relations. Bulk moduli in the present study are the derivatives of a Chebyshev polynomial globally fit to the stress-strain data.

Inverted bulk compressibilities from Brace (1965) are represented by stars in the plots of bulk moduli as a function of confining pressure for Westerly granite (Fig. 2-15), Vermont marble (Fig. A-2b), Blair dolomite (Fig. A-4b), and Webatuck dolomite (Fig. A-5b). Agreement is good for the Vermont marble and Blair dolomite values. Brace's calculations of bulk moduli for Blair dolomite at 0, 500, and 1000 bars are systematically higher by about 0.01 Mb but this is only slightly more than 1% of absolute value. Agreement for the Vermont marble data is surprizing considering the dramatic increase in moduli with pressure, from less than 0.03 Mb at zero pressure up to 0.70 Mb at 1 Kbar. The higher value of 0.12 Mb at zero pressure reported by Brace reflects either a lower compliance for his sample or else difficulties in measuring the tangent to the stress-strain relation.

Bulk moduli calculated for the Webatuck dolomite sample in this study are lower than those calculated by Brace (1965). The greatest difference is at 200 bars pressure where Brace's value of 0.53 Mb is substantially higher than the 0.32 Mb calculated here. There is agreement at zero pressure, about 0.03 versus 0.05 Mb from Brace, and at higher pressures values tend to converge. At 1Kbar pressure Brace records a value of 0.84 Mb versus 0.80 Mb in the present data. Most of the difference is perhaps accounted for by the lack of a 3rd strain gage when sample strain was measured in this study (Fig. A-5a). Webatuck dolomite is a metamorphic dolomite and foliation is evident in hand specimen. Anisotropy, however, is apparently parallel with the foliation in addition to across the foliation, both in microcrack structure and dolomite grain orientation (Fig. A-5a). The jacketed stress-strain data records anisotropy of microcrack structure in addition to mineral orientation. Brace's linear compressibility data in 3 directions varies up to 11% from the mean at zero pressure and up to 22% from the mean at 9 Kbar. At low pressures the differences mainly reflect microcrack

anisotropy. At high pressures, where the effects of microcracks on compressibility are minimized, the persistent differences indicate a preferred mineral orientation. The unjacketed strain data is beneficial in directly measuring anisotropy due to mineral orientation. Similar anisotropy is evident in the unjacketed strain data for the marbles (Yule, Vermont).

In this study 2 samples of Westerly granite from each of 2 blocks were measured. One block, obtained from Brace's laboratory and labelled "Avner" , was red-colored and similar to most of the samples found about his laboratory. Another block, obtained from the Bonner Monument Co. in Westerly, R.I., was a blue-colored variety. These different varieties of Westerly granite are well known to the workers at the Bonner Monument Co. Mineralogies in the different varieties appear to be the same, the red westerly granite being tinted red by reddish microcline. Measured bulk density for the blue variety is higher than for the red (Table 1). Bulk moduli calculated from stress-strain data for samples from both of these rocks are consistently higher than those reported by Brace (1965). In Fig. 2-15 the calculations for red Westerly granite are plotted and Brace's values are represented by stars. Brace's values are systematically lower by about 0.04 to 0.05 Mb from zero up to the highest pressure measured, 1 Kbar. Possible explanations include natural variation in the microcrack populations in different sources of Westerly granite or the possibile use of samples in other studies which introduced additional compliant porosity. It was noted at the Bonner Monument Co. that room-size boulders of the rock are processed. If blocks of this size are blasted and perhaps dropped in the procedure a fair degree of artificial cracks are possibly shock- induced. Some of the material, rejected for this very reason, may find its may into the laboratory via the tailings pile. Squeezing a sample in a machine chuck or vise can also introduce cracks.

Stress-strain data and calculated values of jacketed and unjacketed bulk moduli for samples of red and blue Westerly granite are found in Figs. 2-23 and 2-15 for the red and Figs. A-11a and A-11b for the blue. Samples(2) from the red Westerly granite consistently had higher levels of jacketed and unjacketed strain at a given pressure and also tended to be more anisotropic in jacketed strain measurements. Jacketed bulk moduli for the blue Westerly granite (Fig. A-11b) are uniformly higher by about 0.015 Mb at any given pressure. The unjacketed intrinsic bulk moduli are higher by a lesser amount, 0.01 Mb or less, although this difference is less than the accuracy in the measurement and calculation. A possible explanation for the higher compliance of the red Westerly granite is that it represents a wetter and later stage in the emplacement of dikes into the host rocks, somewhat like a pegmatite, and perhaps a remobilized form of blue Westerly granite. Consequently, the red Westerly granite contains more cracks and more compliant mineralogy from the exsolution and cooling effects of water.

The unjacketed bulk moduli calculated from an average slope for the unjacketed stress-strain data are about 0.56 Mb for the two types of Westerly granite. Similar values were also measured and calculated for samples of Chelmsford granite, Barre granite, which has a mineral content nearly the same as Westerly granite (Appendix B), and Henderson augen gneiss (Table 1). These values, surprisingly similar, appear to be somewhat higher than expected from calculations of the Voigt-Reuss average intrinsic moduli based on mineralogy. Brace (1965) calculated Voigt and Reuss bulk moduli of 0.488 Mb and 0.474 Mb, respectively, at zero pressure based on his modal percentages and mineral bulk moduli. Because of the dependence of mineral moduli on pressure, although slight in comparison to that of the overall aggregate, the respective moduli rise to 0.503 Mb and 0.488 Mb at 2 Kbar. Siegfried and Simmons (1978), using the mineral composition of their sample of Westerly granite, calculate Voigt and

Reuss bounds of 0.510 Mb and 0.531 Mb, respectively. All of these calculations give lower results than the 0.56 Mb values measured in this study. Other measurements of unjacketed bulk moduli also differ substantially. Nur and Byerlee (1971) measured for a sample of Westerly granite an average value of 0.45 Mb over 2.5 kbar. As reported in Birch (1966), other measured unenclosed bulk moduli of Westerly granite include a value of 0.513 Mb at 1 bar by Adams and Williamson (1923) and values of 0.472 Mb at 2 kbar and 0.549 Mb at 10 kbar by Knopoff (1953).

The average intrinsic bulk moduli calculated for the granitic rocks tend to be on the high side of these other measurements. The reason is not entirely clear but the data appear to be interpreted properly as a similar average value is arrived at for all of the granitic rocks. The increase of intrinsic bulk moduli with pressure has several causes: 1) nonlinearity inherent in the strain gage technique due to the finite thickness of the epoxy bond between gage and substrate, 2) the increase in moduli of crystalline minerals with pressure, or 3) occluded porosity within minerals in the form of compliant shapes.

Todd (1973) and Todd *et al.* (1973) report linear compressibilities for a sample of Chelmsford granite in three mutually perpendicular directions oriented according to the preferred planes of cracks in this sample. Compressibilities at several pressures have been summed and inverted for bulk moduli and are plotted in Fig. 2-16 as asterisks. Agreement between the data sets is fair. At zero pressure the slightly higher value in Todd's data probably reflects the difficulty in measuring the tangent to the stress-strain data.

Garg and Nur (1973) calculated bulk modulus as a function of confining pressure for Weber sandstone by taking the derivative of a simple cubic polynomial fit to the stress-strain data. The data, from Nur and Byerlee (1971),

was apparently measured in a single direction with an external ram. Bulk moduli values at several pressures from the polynomial relation of Garg and Nur (1973) are plotted as asterisks in Fig. 2-11. Bulk moduli calculated from data for the experiments in this study are significantly lower, particularly at zero pressure. The sample in this study was obtained from Byerlee's lab and presumably is from the same core. Part of the discrepancy between data sets may be due to the anisotropy in Weber sandstone. In this study jacketed strain was measured in three directions. Strain measured perpendicular to bedding was about 50% larger than that parallel to bedding (Fig. 2-19) and this anisotropy may not be included in the bulk moduli calculated by Garg and Nur (1973). At approximately 1 kbar pressure bulk strain in this study is about 10,800 microstrain whereas in the data of Garg and Nur it is only about 5,800 microstrain. In addition, at low pressures the higher bulk moduli are a reflection of the numerical procedure. A cubic polynomial, globally fit to the stress-strain data, cannot account for the severe nonlinearity in strain at low pressures. When differentiated the resulting moduli will tend to be high.

King (1969), as part of a study of the ratio between static and dynamic moduli in sandstones, measured lateral and axial strain in large samples of Berea sandstone with a strain gage technique similar to the one in this study. His calculated bulk moduli at several pressures agree almost exactly with those measured in this study (Fig. 2-12). In addition, Simmons *et al.* (1982) report static bulk compressibilities at several pressures for three samples of Berea sandstone. The averages of the three samples, multiplied by 3 and inverted, give bulk moduli values plotted as the circles in Fig. 2-12, in very close agreement with the calculations in this study and those of King (1969).

## $\zeta$ AND POROSITY

The material constant $\zeta$ introduced in the stress-strain analysis of linear porous solids is quite useful for visualizing the experimentally measured strain response of rocks. In this discussion the symbol $\zeta$ is used, as in recent derivations (Rice and Cleary, 1976; Garg and Nur, 1973; Rice, 1980), although in Biot's work (1941,1961) and in Nur and Byerlee's formulation (1971) the symbol $\alpha$ is used. Biot (1941) and Biot and Willis (1957) pointed out that $\zeta$ (their $\alpha$) is the ratio between pore volume strain and bulk volume strain in a drained, jacketed test, and that the lower limit of $\zeta$ is the porosity $\varphi$ and the upper limit is 1.

This identity and the bounds can be easily derived for a linear porous solid with a homogeneous and isotropic solid matrix. For such a material $\zeta$ can be associated with bulk modulus $K$ and intrinsic bulk modulus $K_s$ in the following relation:

$$\zeta = 1 - \frac{K}{K_s}. \tag{2-11}$$

Bulk strain for the solid in response to hydrostatic confining pressure $\sigma$ at constant pore pressure is given by

$$\frac{1}{V_b}\left(\frac{\partial V_b}{\partial \sigma}\right)_p = \frac{1}{K}. \tag{2-56}$$

Pore volume strain for the solid is given by

$$\frac{1}{V_b}\left(\frac{\partial v_p}{\partial \sigma}\right)_p = \frac{1}{K} - \frac{1}{K_s}. \tag{2-16}$$

The ratio of these two expressions gives the stated result,

$$\left(\frac{\partial v_p}{\partial V_b}\right)_p = 1 - \frac{K}{K_s}, \tag{2-57}$$

which is $\zeta$.

The numerical value of $\zeta$ is bounded by $\varphi \leq \zeta \leq 1$. First, as can be seen from the expression for $\zeta$, the value must be positive but cannot be greater than 1 since $K \leq K_s$ is always true. The lower limit may be obtained from Eq. (2-35) which describes the porosity response to confining pressure

$$\left[\frac{\partial \varphi}{\partial \sigma}\right]_p = \frac{(1-\varphi)}{K} - \frac{1}{K_s}. \tag{2-35}$$

Multiplying through by K gives

$$K\left[\frac{\partial \varphi}{\partial \sigma}\right]_p = -\varphi + \left[1 - \frac{K}{K_s}\right]. \tag{2-58}$$

The expression in parentheses on the right is $\zeta$. The left side of the equation, representing the porosity change as a function of pressure multiplied by the positive bulk modulus, cannot be negative with increasing $\sigma$. Therefore $\zeta \geq \varphi$.

The significance of the coefficient $\zeta$ is that it represents the ratio of pore volume to bulk volume strain in a jacketed, drained test. For laboratory studies of rock properties measured as a function of confining stress the source of information on physical dimension is given by rock strain. The bulk strain of rocks under pressure, an easily measured quantity, is a combination of solid matrix strain in addition to pore volume strain. Pore volume strain is the desired quantity, and the coefficient $\zeta$ bridges bulk strain data to pore volume strain. The numerical value is a direct indication of pore volume response to pressure with one assumption. This interpretation of $\zeta$ is only strictly true for fully homogeneous and isotropic solids. The experimental evidence of Van der Knapp (1959) indicates that, at least for the sandstone studied, this assumption is not too severe, as his directly measured bulk volume and pore volume strains were related by the measured intrinsic bulk modulus.

The value of $\zeta$ can, therefore, be interpreted in a manner quite different than as the pore pressure coefficient in the effective stress law for bulk strain. It represents the fraction of bulk volume strain which goes into pore volume strain. Since it is calculated from the intrinsic and jacketed bulk moduli it also represents how close the jacketed bulk modulus is to the intrinsic. For materials which are very compliant, such as a cracked granite at low pressure, the jacketed bulk modulus is much lower the the intrinsic bulk moduli of the constituent grains, and $\zeta$ approaches the value 1. At very high pressures most of the compliant porosity is closed and $\zeta$ approaches the value of the porosity, or nearly the value 0. Therefore the value of $\zeta$ summarizes in a single number the difference between the jacketed and intrinsic moduli. In all of the plots of bulk moduli versus pressure $\zeta$ as a function of pressure is also plotted. These are Figs. 2-11 through 2-17 for the first seven rocks in Table 1 and Figures A-1b through A-11b, the 'b' plots, in Appendix A for the other rocks. The scale for $\zeta$ is always from 0 to 1 and is found along the right vertical axis in these plots. Fig. 2-18 is a summary plot of the range of $\zeta$ values between zero and 1 kbar confining pressure for the seven rocks studied with pore pressure. In the calculation of $\zeta$ as a function of pressure the average value of intrinsic bulk modulus found in Table 1 for the various samples was used.

Almost the entire range of $\zeta$ values possible, from 1 down to the porosity, which is nearly 0 for some of the rocks, can be found for the samples studied. Since the intrinsic bulk modulus is approximately constant with pressure the $\zeta$ versus pressure curves essentially mirror the curves of jacketed bulk modulus versus pressure. For the Berea, Weber, and Kayenta sandstones, the Chelmsford granite, the Cedar City diorite, the Webatuck dolomite, and the Yule and Vermont marbles, the value of $\zeta$ approaches 1 at low pressure, indicating that almost all of the measured bulk strain is pore volume strain. Because of cracks or highly

compliant point contacts the pore spaces in these rocks are easily strained at low pressure. For most soils and muds $\zeta$ is also indistinguishable from 1, and for this reason Terzaghi (1923) concluded that the effective stress law for strain was the difference between load and pore pressure. For most of the low porosity rocks at high pressure the greatest portion of bulk strain is in the deformation of the matrix minerals, so that the value of $\zeta$ is low. For Westerly granite at 1 kbar confining pressure $\zeta$ is approaching a fairly constant value of about 0.22, indicating that 22% of external bulk strain is being absorbed by the pore space.

The lower limit of $\zeta$, the porosity, is approached in the Vermont marble (Fig. A-2b) at 1 kbar pressure and in the Blair dolomite (Fig. A-4b) essentially at any pressure. Initial porosity of Vermont marble is approximately 0.5% and that of Blair dolomite probably close to zero. Therefore the lower bound of $\zeta$ is approached, or probably equalled in the case of Blair dolomite. This means that all of the bulk strain is mineral matrix strain. Whatever porosity remains must be nearly spherical. Both the unjacketed and jacketed strain versus pressure data of Blair dolomite are the same (within a few microstrain) and, if unjacketed bulk modulus were allowed to vary with pressure, the values of $\zeta$ at pressures less than 500 bars seen in Fig. A-4b would drop to 0. The low $\zeta$ values are simply reflecting the approach of jacketed bulk modulus to unjacketed intrinsic bulk modulus. For Vermont marble, composed of nearly pure calcite, at 1 kbar the jacketed bulk modulus is 0.70 Mb, just shy of the average bulk modulus of calcite (0.72 Mb). The measurements of Yule marble, also nearly pure calcite, should have a similar behavior as those of Vermont marble, although the measured intrinsic bulk modulus came out high (0.76 Mb) and therefore $\zeta$ values are correspondingly higher. Anisotropy in the Yule marble is apparently more complicated than in the Vermont marble sample studied, as determined by repeated measurements.

Rocks with negligible nonlinear strain, as for the samples of Bedford and Solenhofen limestone (Figs. 2-22 and A-1a), have a nearly constant, small range of $\zeta$ values (Figs. 2-14 and A-1b). For Bedford limestone this is about 0.6, meaning that about 60% of the bulk strain measured is a pore volume strain. For Solenhofen limestone the bulk modulus is approximately twice that of Bedford limestone and $\zeta$ values range slightly over 0.3. Therefore the pore volume in Bedford limestone is approximately twice as compliant as that in Solenhofen for a given increment in confining pressure. Of course the same could be interpreted from the measured bulk moduli directly because in this case the intrinsic bulk moduli are nearly the same (calcite). The usefulness of $\zeta$ is more apparent in comparing rocks with different mineralogies since it essentially normalizes the bulk modulus to the intrinsic bulk modulus of the constituent minerals.

Values of $\zeta$ for the sandstones measured, the Weber, Navajo, Berea, Kayenta, Boise, and Pottsville, are generally between 1 and 0.5 over the range of confining pressure from 0 to 1 kbar. The Weber, Berea, and Kayenta sandstones all have extremely low bulk moduli near zero pressure and so $\zeta$ approaches the value 1.

The numerical value of $\zeta$ calculated as a function of confining pressure can be used to calculate pore volume strain and hence porosity as a function of pressure from bulk strain. A more direct technique subtracts the digitized unjacketed stress-strain data from the jacketed stress-strain data since they represent bulk and matrix volume strains. This procedure was described at the end of the section entitled "Graphical Examples". Also noted there is the similarity to the crack porosity of Walsh (1965). The strain arrived at upon subtraction is the pore volume strain, and since it is normalized to bulk volume it is the porosity reduction at any given pressure.

For all of the rocks in Table 1 porosity versus confining pressure has been calculated using this procedure. For the seven rocks studied with pore pressure the results are plotted in Figs. 2-26 through 2-32. For the remaining rocks the results are plotted in Appendix A, the "c" plots, Figs. A-1c through A-11c. The scales on all of the plots are the same for easy comparison. Initial porosities for these samples were calculated from dry and saturated weighings of the large cores and are recorded in Table 1. Accuracy of the initial porosity is not critical for calculating the porosity decrease with confining pressure, and the porosity curves can therefore be shifted up and down the porosity axis. The porosity versus confining pressure relation for any sample is as accurate as the difference between the two sets of strain data. Probable error in these plots is therefore approximately ±0.01 absolute porosity. These porosity data derived from the strain data are much more accurate than could be obtained by directly measuring fluid expelled from the rock under pressure.

The amount porosity decreases with pressure in these plots is essentially a reflection of how much strain the various rocks have experienced under pressure. The highly-porous sandstones (Weber, Navajo, Berea, Kayenta, Boise, and Pottsville) show the most rapid and largest decreases in porosity, excluding the Cedar City quartz diorite. Of these, the Berea porosity (initial $\rho$=17.8%) decreases the most between 0 and 1 kbar, by slightly more than 0.8%. The Navajo (initial $\rho$=11.8%) decreases the least, by about 0.24%. The amount porosity decreases with pressure, however, does not correlate with porosity. Pottsville sandstone only has an initial porosity of 2.9%, but decreases by 0.47% at 1 kbar, while Boise sandstone, with the largest initial porosity of 26.7%, decreases by only slightly more, 0.55%. The porosity decrease with pressure is reflecting the combined influence of the number of pores and their compliance due to pore shape. This is also reflected in the bulk modulus, but the porosity relation is an

integrated form of how the bulk modulus is changing over the entire pressure range. The usefulness of this porosity data is that modelling of various physical properties, particularly acoustic, requires some specification of pore shape and densities as a function of pressure. The porosity gives these types of calculations some link with actual pore strain.

Bedford limestone and Solenhofen limestone, both almost linear porous solids, show a nearly linear decrease in porosity with pressure, the Bedford limestone decreasing by about twice the rate of Solenhofen.

The two marbles, Yule and Vermont, and the Webatuck dolomite are all similar in that the porosity decrease with pressure levels off after about 200 to 300 bars, and is the essentially the same for all three. Those pore shapes which give rise to the tremendous increase in bulk moduli with pressure do contribute to the decrease in porosity at lower pressures.

Cedar City quartz diorite is an exception to the other rocks in that it is highly weathered and fragile. Porosity decrease with pressure is by far the largest, from 8.0% down to nearly 6.8% by 500 bars pressure.

The three granitic rocks, Westerly, Barre, and Chelmsford, and the Henderson augen gneiss represent an fairly large spectrum in how rapidly the porosities decrease with pressure. Henderson augen gneiss porosity only decreases 0.05% between 0 and 1 kbar, and almost all of this occurs by about 350 bars. The porosity decrease of the three granites is greatest for the Chelmsford, from 1.1% down to 0.75% at 1 kbar, intermediate for the Barre, from 0.7% down to 0.48% at 1 kbar, and least for the Westerly, from 0.8% down to 0.7% at 1 kbar. After about 500 bars the rate of porosity decrease with pressure for the Chelmsford and Barre are nearly the same. None of these rocks begin to approach zero porosity at 1 kbar. Brace (1965) distinguished the persistent high

pressure porosity as the pore porosity, or that fraction of the porosity which might be considered as nearly spherical and very stiff.

Brace *et al.* (1965) calculated crack porosity versus confining pressure for several granites and a quartzite using a graphical technique based on the linear elasticity analysis from Walsh (1965). A favorable comparison between their calculation and the present one for red Westerly granite is shown in Fig. 2-30. The comparison assumes that initial porosity is exactly 0.8% for both samples although this value could be shifted up and down without changing the result. Brace *et al.* (1965) report crack porosities at several pressures between 0.05 and 4 Kbar confining pressure. The difference between crack porosity at any pressure and that initially present at zero pressure (in this case 50 bars) is a measure of how much the porosity has decreased as a function of pressure. The difference between 1 Kbar ($0.32 \times 10^{-3}$) and 50 bars ($1.43 \times 10^{-3}$) is $1.11 \times 10^{-3}$, meaning that porosity decreased by approximately 0.11% between 50 bars and 1 Kbar confining pressure. This corresponds quite well with the approximately 0.10% porosity decrease between zero pressure and 1 Kbar shown in Fig. 2-30. Additional values reported by Brace *et al.* (1965) for pressures less than 1 Kbar also agree very closely. Again, the distinction between the two techniques is that the difference between jacketed and unjacketed strain is based on directly measured quantities while the crack porosity determination depends on visualizing the tangent to jacketed stress-strain data at high pressure. In the Westerly granite data of Brace *et al.* (1965) this tangent was accurately visualized.

## GENERAL DISCUSSION

The theoretical development of linear elasticity and the experimental test of bulk strain clearly indicate that effective stress is an unnecessary definition in

the description of bulk deformation of intact rocks where pore pressure and confining stress are variables. With the drained, jacketed stress-strain relation and the unjacketed stress-strain relation measured, deformation behavior at any combination of confining stress and pore pressure is completely described. To calculate the "effective stress law" for bulk strain of Nur and Byerlee (1971), Garg and Nur (1973), and Carroll (1979) is not necessary to predict strain with pore pressure.

The observation remains, however, that differential stress, or pressure, adequately describes various physical properties of rocks measured in the laboratory with pore pressure in addition to confining stress. These properties include acoustic velocities, both P- and S-wave (Gardner *et al.*, 1965; Chapter 4, this thesis) fluid permeability (Knutson and Bohor, 1963; Brace *et al.*, 1968; Chapter 3, this thesis) pore phase electrical resistivity (Coyner, unpublished results), and fracture strength (Robinson, 1959; Handin *et al.*, 1963; Brace and Martin, 1968). These observations, that pore pressure is equally "effective" as confining stress in laboratory measurements, have been associated with Terzaghi's effective stress relation (Brace, 1972). Terzaghi, however, introduced the concept to describe deformation and failure in muds and soils. The question to be answered is why these other physical properties should be described by the same relationship, especially since bulk strain is clearly not.

In this paper the linear static theory of Biot for fluid-saturated porous solids has been developed and applied to the bulk and pore volume deformation of rocks. Even though linearity and infinitesimal strain are fundamental assumptions, aspects of the analysis can be applied to the physical properties listed above. This is in spite of the fact that these properties may vary in a highly nonlinear fashion with stress. The purpose here is not to model this nonlinearity with pore closure models, but to explain the strain response to a

combination of stress and pore pressure which would lead to the Terzaghi relation.

The linear analysis of the first section allows for the decomposition of stresses given in Eqs.(5) and (6) and shown in Fig. 2-1. From the viewpoint of this decomposition the effect of a pore pressure $p$ and a confining stress $\sigma$ on other physical properties can be addressed. The argument is similar for all of the properties listed above exclusive of bulk strain. Recall that the two-step decomposition is an equal and uniform internal and external stress equal to pore pressure $p$ and an external stress of value $\sigma-p$. This decomposition, in fact, mimics a possible laboratory procedure in testing for a pore pressure effect.

The first step in the analysis ideally reduces every linear dimension by an amount inversely proportional to the intrinsic bulk modulus of the solid phase. For rocks, which are composed of various anisotropic minerals and perhaps a fraction of occluded porosity, this statement is only an approximation. This statement is exactly true for a microhomogeneous and microisotropic porous solid with fully interconnected porosity. Given this assumption, there is an equal fractional decrease in solid and pore phases. Therefore, the porosity, the aspect ratios of all the cracks and pores, and the relative orientation of all cracks and pores, all remain constant. For silicate and salt-like crystalline structures the intrinsic modulus is quite large, about 0.37 Mb for quartz and larger for other silicates and ionic solids. This means that an equal external and internal pressure of 1 kbar reduces linear dimensions by approximately 0.1%. A crack 10.0 microns in diameter becomes 9.99 microns in diameter.

The effect on physical properties of this first step is negligible. Since porosity remains constant electrical resistivity does not change if Archie's Law holds. Fluid permeability, even though quite sensitive to 3-dimensional pore

shape, should not decrease measurably when pore dimensions decrease by 0.1%. Acoustic velocity does not change because aspect ratios are constant and the bulk density increase is negligible. Fracture strength does not change because crack and pore orientation has not changed and the amount of strain is so small that the stress definition as a force per unit area changes negligibly.

The second step in the analysis, the application of external pressure $\sigma - p$, is what causes the asperities to close and pore surfaces to come into contact. The differential stress, $\sigma - p$, is then seen as the "effective" stress because it determines the deformation of pores that leads to a change in the physical properties. Because of the inherent stiffness of minerals that make up rocks and sediments and the hydrostatic pressure of pore fluid the differential stress or the "effective stress" describes the response of physical properties. The Terzaghi relation has the status of a very good approximation.

There is a general usefulness for measuring the static strain of rocks. A laboratory technique for investigating rock properties has been the measurement of properties such as velocity, attenuation, resistivity, and permeability, as the rock sample is subjected to confining stress. As the cracks and pores close the properties may change dramatically. The reason these tests are useful is that the mineralogy of the phases remains constant, so that variable is removed. Properties are measured and can be modelled with cracks or ellipsoids of various shape that shrink and change in number with pressure. An appeal to what is actually happening to the rock under stress must go to strain measurements because they provide dimensional information. In the previous section it was shown how subtraction of unjacketed stress-strain data from jacketed stress-strain data gives pore volume deformation as a function of confining stress. This result should be useful in modelling the physical properties of these rocks.

The other point to emphasize here is the unjacketed stress-strain test. This test gives a direct measurement of solid matrix modulus averaged over many elastically anisotropic composite grains in various orientations. The measurement is useful for two reasons. One, as was previously discussed, pore volume strain as a function of confining stress can be calculated. Two, the intrinsic solid matrix modulus is necessary in most velocity modelling as well as in deformation modelling. For rocks, if there is little occluded porosity or crystal defects, the static calculation of intrinsic bulk matrix modulus from unjacketed stress-strain data can be directly used in velocity modelling. The static and dynamic modulus should be nearly the same for the solid phase. For the overall bulk rock dynamic modulus can be much larger than static modulus (Cheng and Johnston, 1981).

## CONCLUSIONS

(1) The static bulk strain of rocks in response to a combination of confining pressure and pore presure is predictable and understood by the linear elastic description of porous media. Strain at any combination of hydrostatic confining stress and pore pressure can be predicted from 1) the drained stress-strain response of the porous solid, and 2) the unjacketed stress-strain response.

(2) The lack of microhomogeneity and microisotropy does not measurably influence the drained bulk stress-strain relation with an initial pore pressure. Experimental observations show the zero pore pressure stress-strain response is followed in a rock with pore pressure $p$, the only difference being a constant shift in pressure and strain $p/K_s'$ due to the intrinsic modulus $K_s'$ of the rock. Silicate minerals are so stiff that grain boundary shear due to pore pressure has a minimal effect on the

subsequent nonlinear strain response to confining stress.

(3) The differential pressure $\sigma$ - $p$ will generally determine those physical properties exclusive of bulk strain which are strongly influenced by the presence of cracks and pores, i.e., velocity, attenuation, permeability, resistivity, and fracture strength. The reason is because of the large intrinsic modulus of crystalline minerals and the small bulk strains of rock in response to stress.

(4) The "effective stress law" for strain proposed by Nur and Byerlee (1971), Garg and Nur (1973), Robin (1973), and Carroll (1979) is simply a reformulation of the Biot linearized description of fluid-saturated porous media. Effective stress so defined for intact materials entails no fundamental description of micromechanic distribution of stress between grains in intact rock. The prediction of bulk strain at any combination of confining and pore pressure proceeds directly from the measurements listed under poin 1.

(5) The coefficient $\zeta$ was initially introduced by Biot (1941, his $\alpha$) and is a fairly useful material constant. Experimentally determined, $\zeta$ equals the ratio of change in pore volume to change in bulk volume at constant pore pressure. This coefficient, in addition to bulk modulus and shear modulus, complete the constitutive equation for drained response. The coefficient $\zeta$ can be calculated from the bulk modulus K and the matrix solid bulk modulus $K_s$ by the relation

$$\zeta = 1 - \frac{K}{K_s}$$

The moduli can be incrementalized with stress to account for nonlinearity in stress-strain. The value of $\zeta$ is theoretically $\varphi \leq \zeta \leq 1$ for a solid of porosity $\varphi$.

(6) Assuming that semilinearity (Biot, 1973) is generally true for rocks, the porosity or pore volume change with confining stress can be calculated from the initial porosity and carefully measured jacketed and unjacketed stress-strain relations. Porosity versus confining pressure has been calculated for the rocks listed in Table 1. The results show that porosity change with confining stress to 1 kbar is largest for the sandstones, least for the low porosity granites, marbles, and dolomite.

(7) A large volume of jacketed and unjacketed static stress-strain data for a number of rocks has been presented. Bulk moduli and intrinsic bulk moduli have been calculated for these rocks as a function of confining stress. The intrinsic bulk modulus $K_s'$ from unjacketed stress-strain tests has been emphasized as a simply measured parameter, the value of which is quite useful in modelling studies. The moduli substantially add to the available data on static elastic response of rocks.

**Table 1: Rock Samples in this Study**

| Rock | Density ($g / cm^3$) | Grain Size ($mm$) | Porosity (%) | $K_s$ ($Mb$) |
|---|---|---|---|---|
| Berea Sandstone | 2.197 | 0.1 | 17.8 | 0.39 |
| Navajo Sandstone | 2.316 | 0.15 | 11.8 | 0.36 |
| Weber Sandstone | 2.392 | 0.05 | 9.5 | 0.385 |
| Bedford Limestone | 2.360 | 0.75 | 11.9 | 0.65 |
| Westerly Granite (red) | 2.620 | 0.75 | 0.8 | 0.56 |
| Chelmsford Granite | 2.606 | 1.5 | 1.1 | 0.56 |
| Barre Granite | 2.635 | 3. | 0.7 | 0.56 |
| Solenhofen Limestone | 2.607 | 0.01 | 4.7 | 0.72 |
| Vermont Marble | 2.695 | 0.2 | 0.5 | 0.715 |
| Yule Marble | 2.698 | 0.5 | 0.5 | 0.75 |
| Blair Dolomite | 2.837 | 0.05 | 0.05 | 0.81 |
| Webatuck Dolomite | 2.846 | 0.45 | 0.5 | 0.97 |
| Henderson Augen Gneiss | 2.738 | 1.5 | 0.8 | 0.57 |
| Pottsville Sandstone | 2.542 | 0.2 | 2.9 | 0.39 |
| Boise Sandstone | 1.996 | 0.2 | 26.7 | 0.36 |
| Kayenta Sandstone | 2.017 | 0.15 | 23.1 | 0.33 |
| Cedar City Diorite | 2.300 | 1. | 8.0 | 0.32 |
| Westerly Granite (blue) | 2.641 | 0.75 | 0.8 | 0.56 |

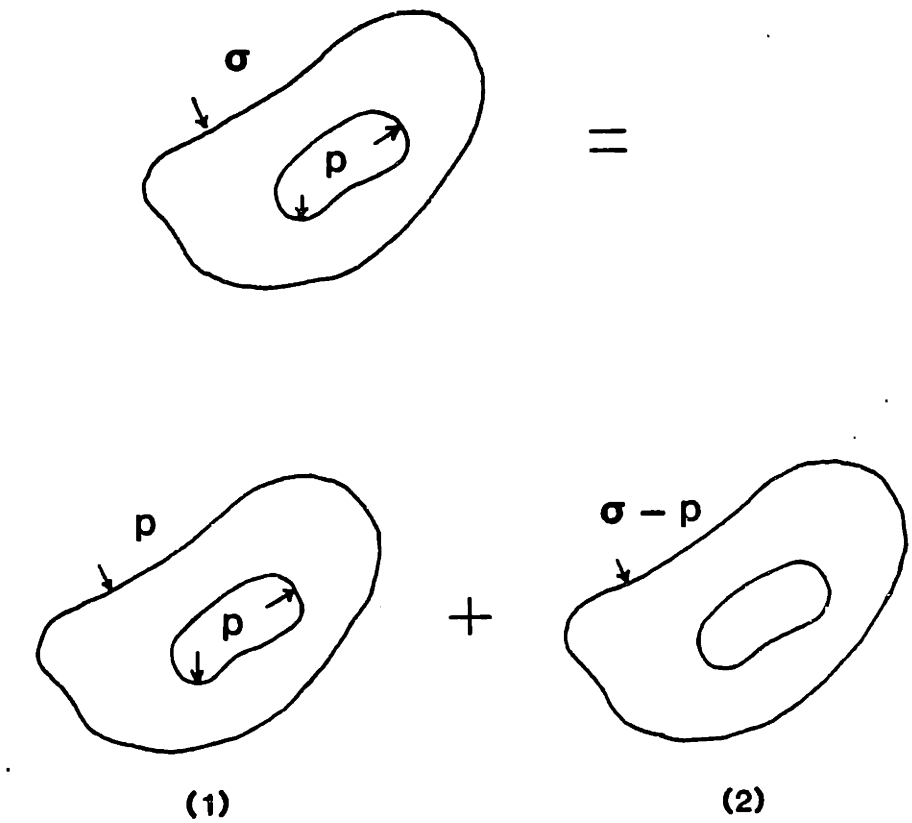


Figure 2-1. Stress field decomposition for porous solid (rock) with hydrostatic confining stress $\sigma$ and pore pressure $p$. Stress state (1) is an equal internal and external stress $p$ ; stress state (2) is an external stress $\sigma$ - $p$.

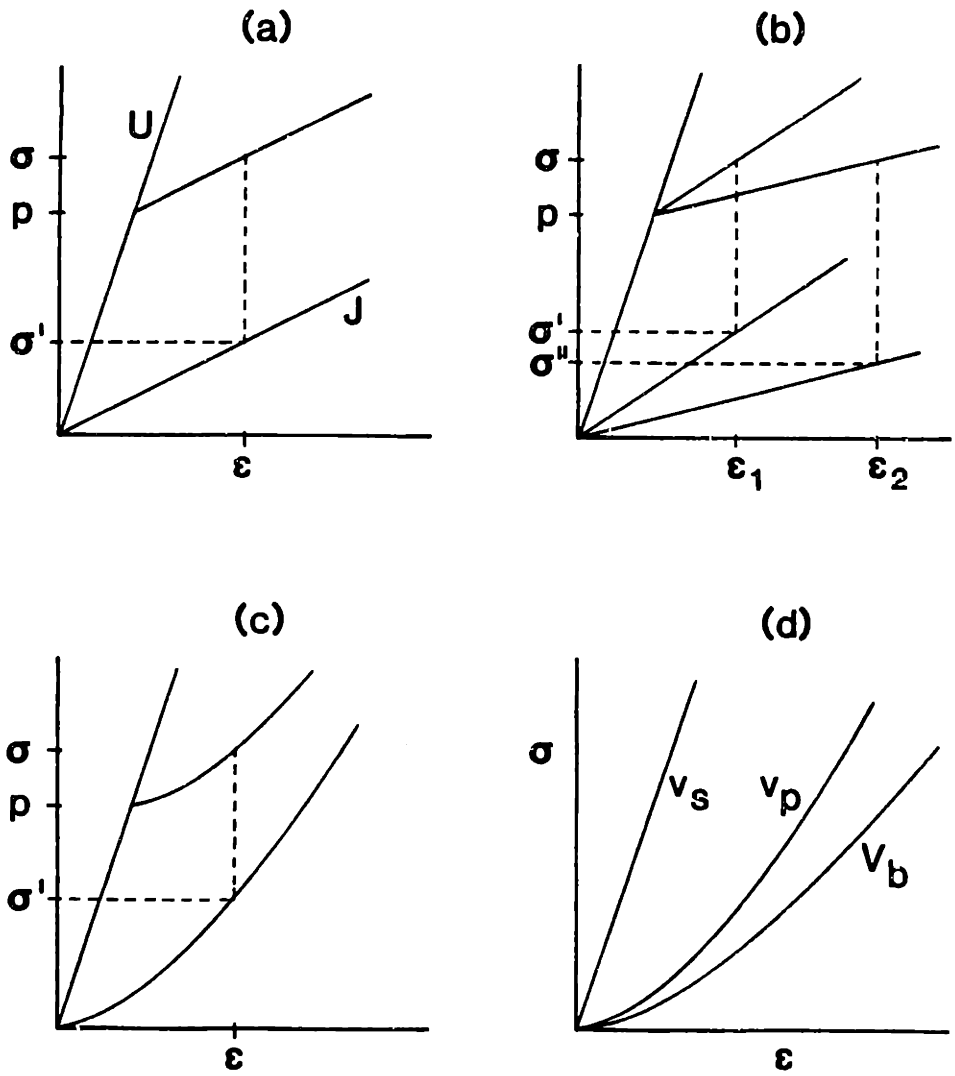


Figure 2-2. Static stress-strain relations with synthetic data. In (a), (b), and (c), the upper parallel relation is with pore pressure $p$. (a) linear, isotropic, porous solid. Jacketed strain with zero pore pressure is line J and unjacketed strain is line U ; effective stress $\sigma'$ defined at stress $\sigma$ and pore pressure $p$. (b) linear, anisotropic, porous solid. Note nonuniqueness of effective stress definition for two directions. (c) nonlinear solid (rock). Note how effective stress $\sigma'$ for strain $\varepsilon$ obscures solid matrix strain due to pore pressure $p$ by making pore pressure appear less "effective." (d) bulk strain as a sum of pore volume strain and solid matrix strain based on semilinear behavior. Pore volume strain and hence porosity as a function of confining stress can be calculated from bulk strain (jacketed data) and solid matrix strain (unjacketed data).

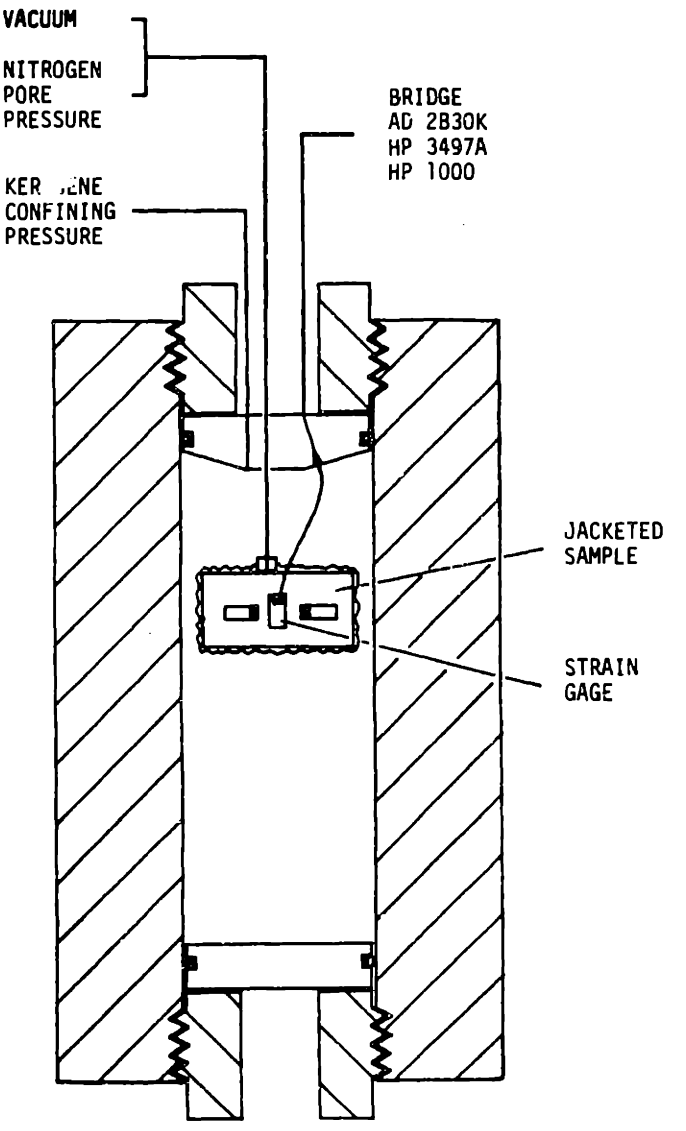


Figure 2-3. High pressure experimental apparatus for strain measurements with jacketed sample sujected to hydrostatic confining pressure and nitrogen pore pressure. Sample with strain gages is shown loaded inside of the pressure vessel.

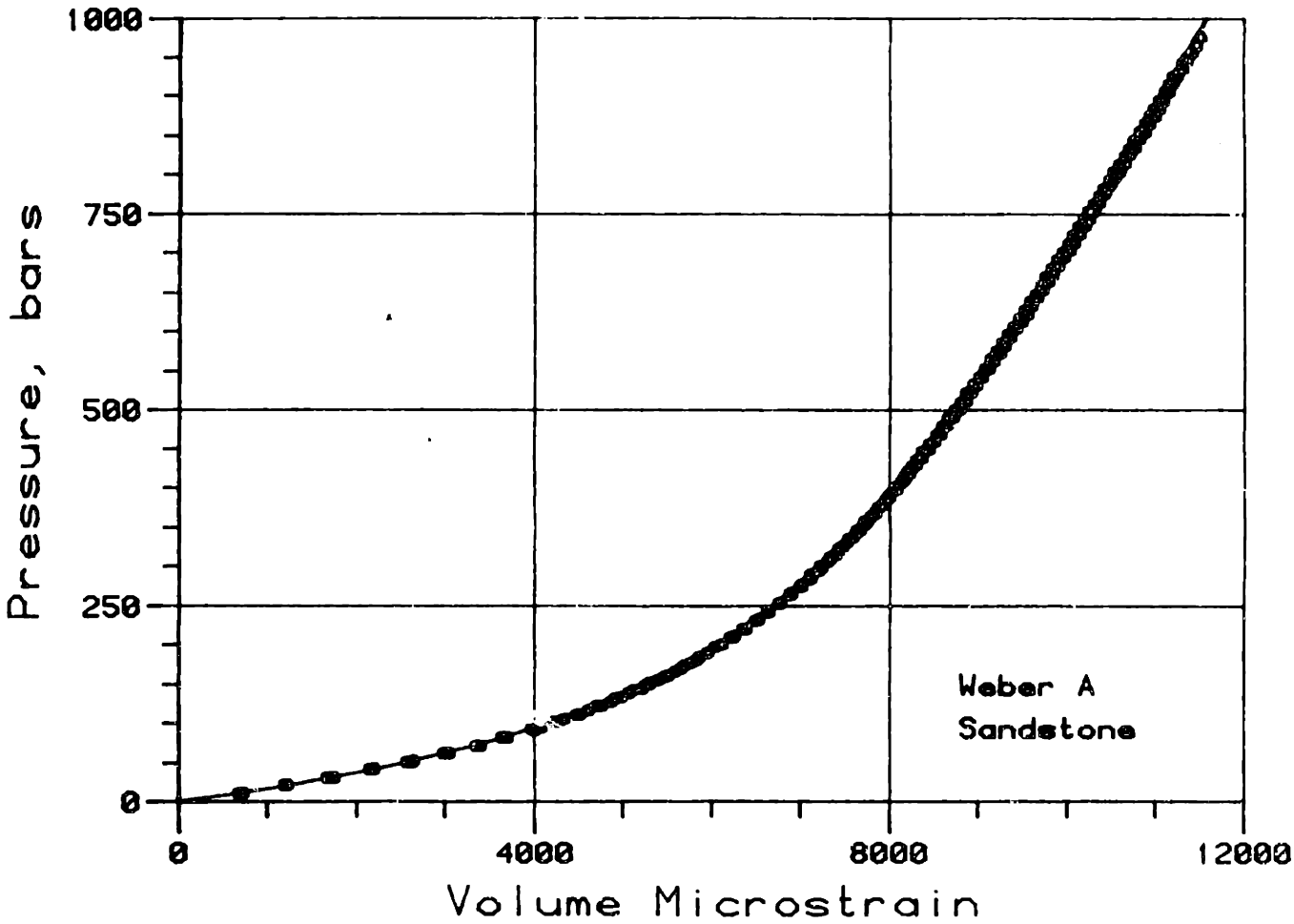


Figure 2-4. Volumetric strain versus confining pressure for Weber sandstone. Solid line is vacuum dry stress-strain relation. Squarish symbols are volumetric strains measured at various pore pressures and are predicted by 1) displacing the zero pore pressure curve along the solid matrix stress- strain relation or 2) calculating the "effective stress." In the first case the pressure axis is differential pressure and the strain axis origin is unjacketed sample strain at each pore pressure; in the second case the pressure axis is effective pressure and the strain axis is absolute strain from zero confining pressure.

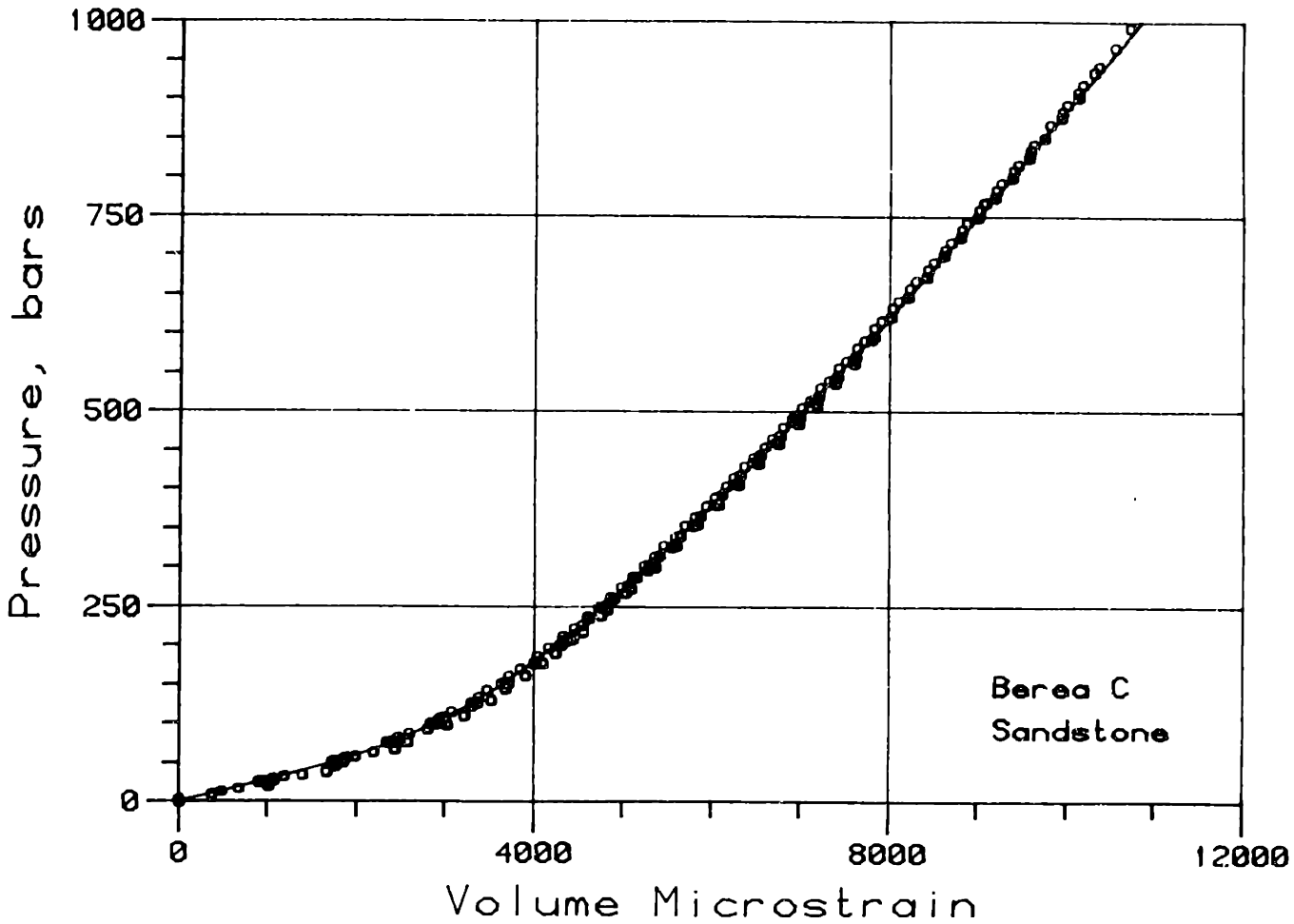


Figure 2-5. Volumetric strain versus confining pressure for Berea sandstone. Solid line is vacuum dry stress-strain relation. Square symbols are volumetric strains measured at various pore pressures.

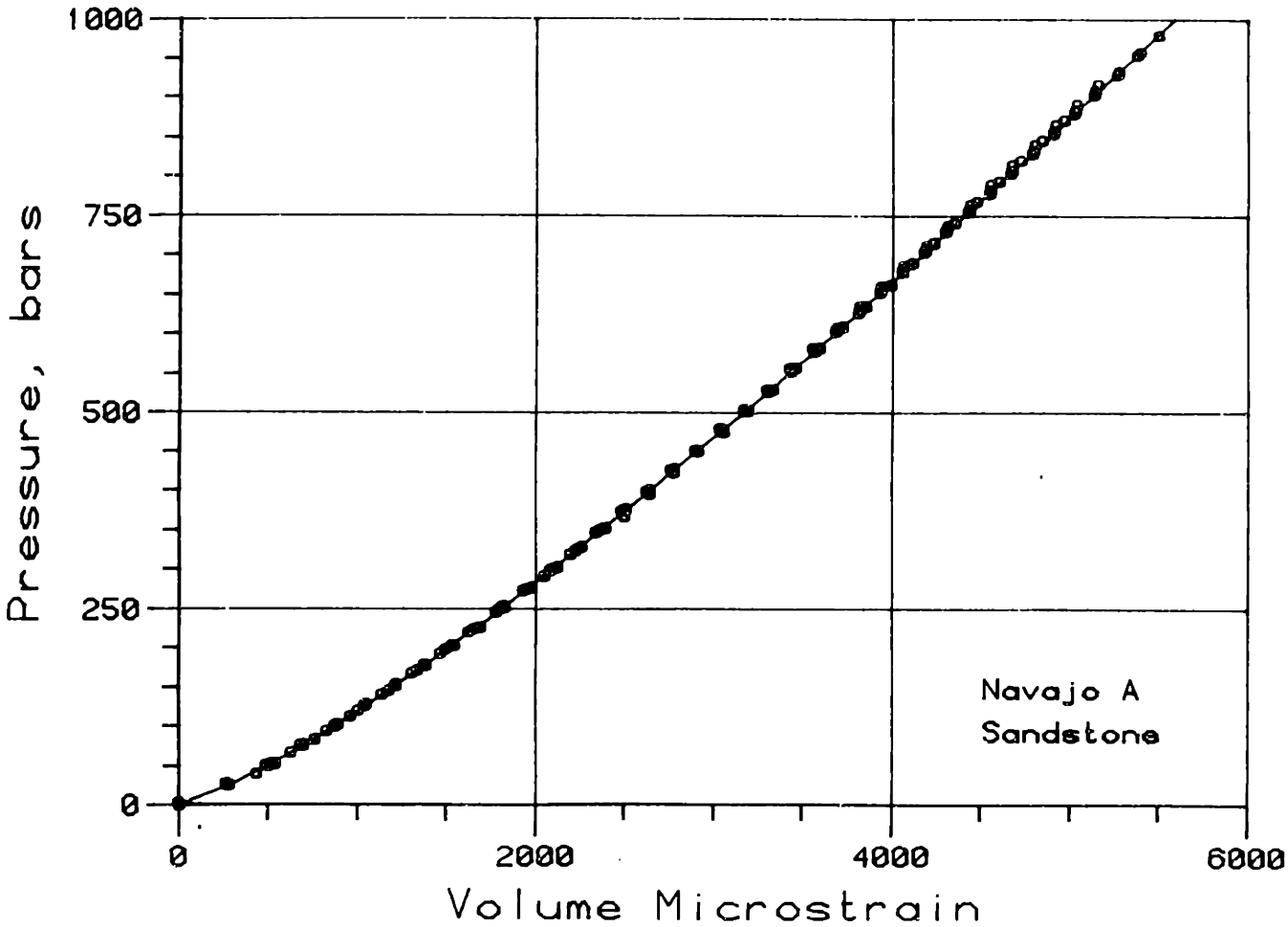


Figure 2-6. Volumetric strain versus confining pressure for Navajo sandstone. Solid line is vacuum dry stress-strain relation. Square symbols are volumetric strains measured at various pore pressures.

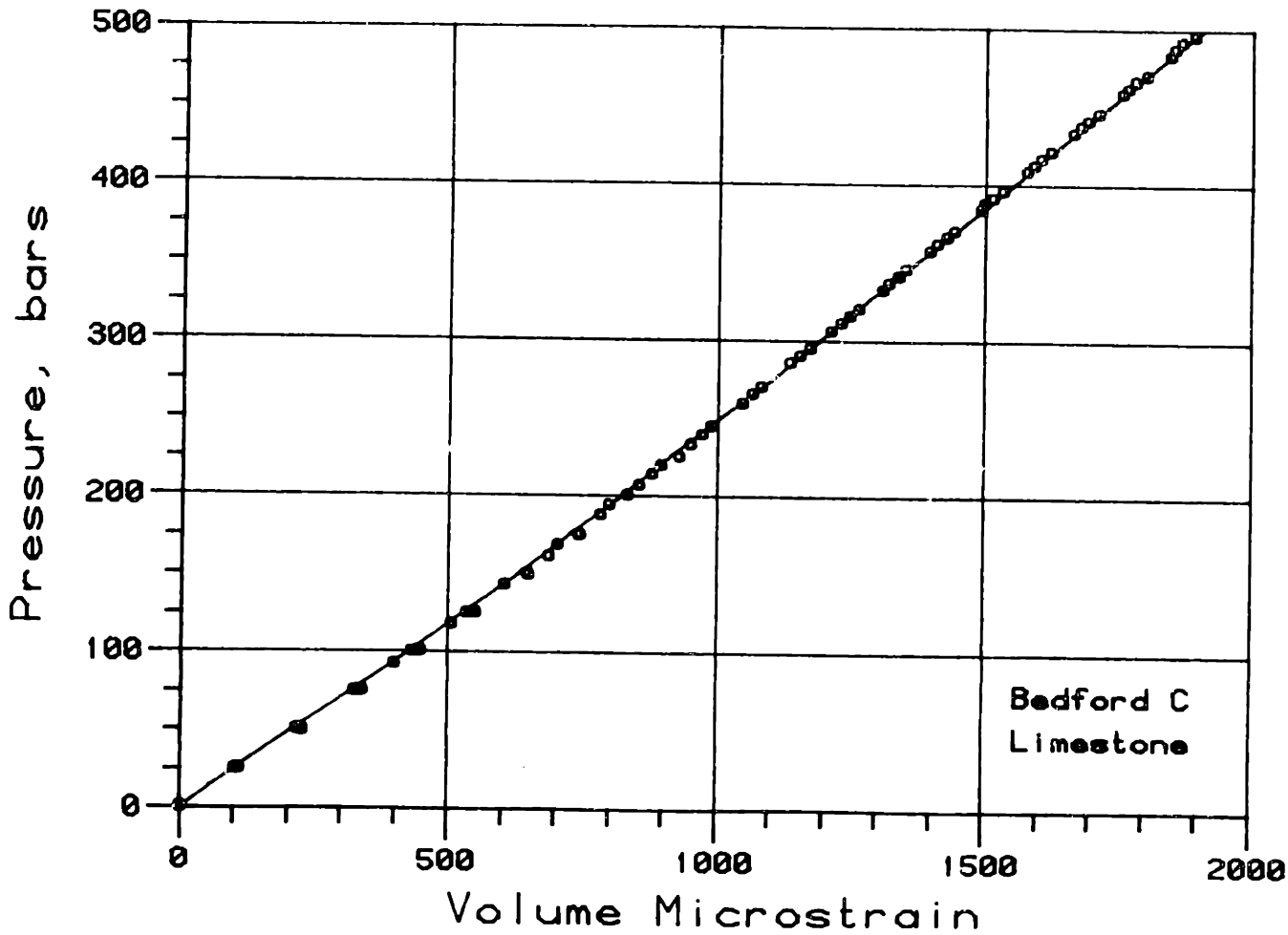


Figure 2-7. Volumetric strain versus confining pressure for Bedford limestone. Solid line is vacuum dry stress-strain relation. Square symbols are volumetric strains measured at various pore pressures.

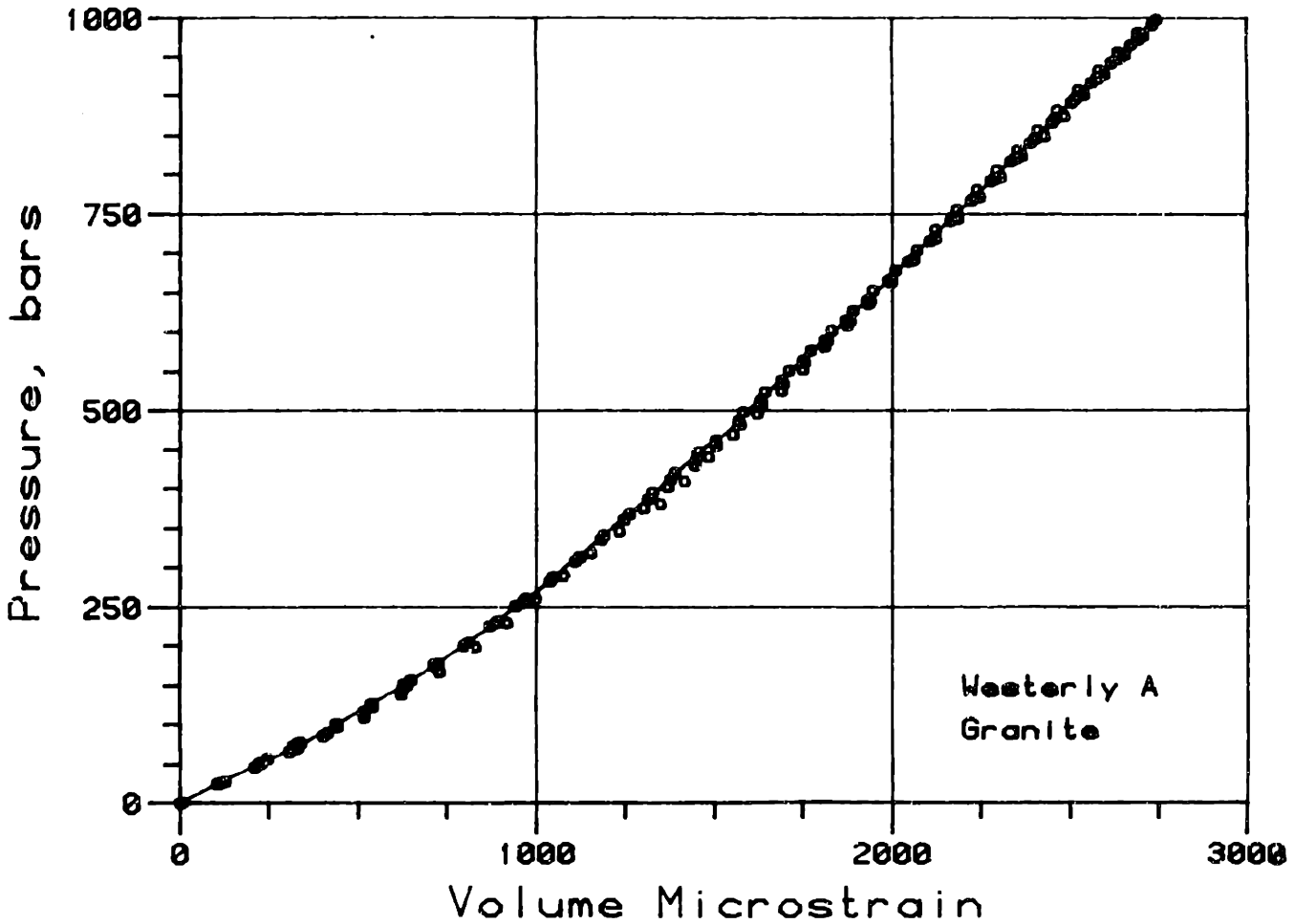


Figure 2-8. Volumetric strain versus confining pressure for Westerly granite. Solid line is vacuum dry stress-strain relation. Square symbols are volumetric strains measured at various pore pressures.

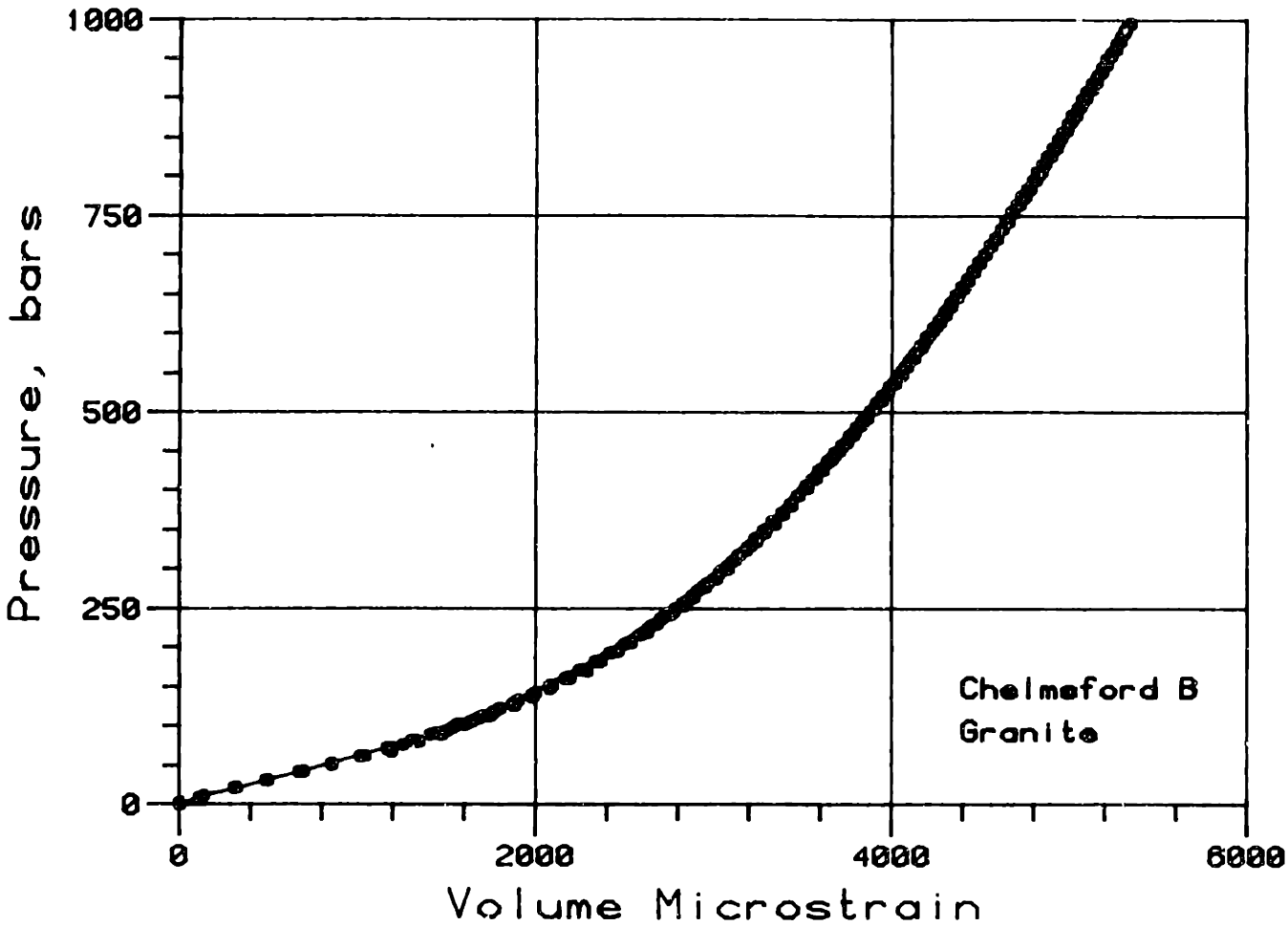


Figure 2-9. Volumetric strain versus confining pressure for Chelmsford granite. Solid line is vacuum dry stress-strain relation. Square symbols are volumetric strains measured at various pore pressures.

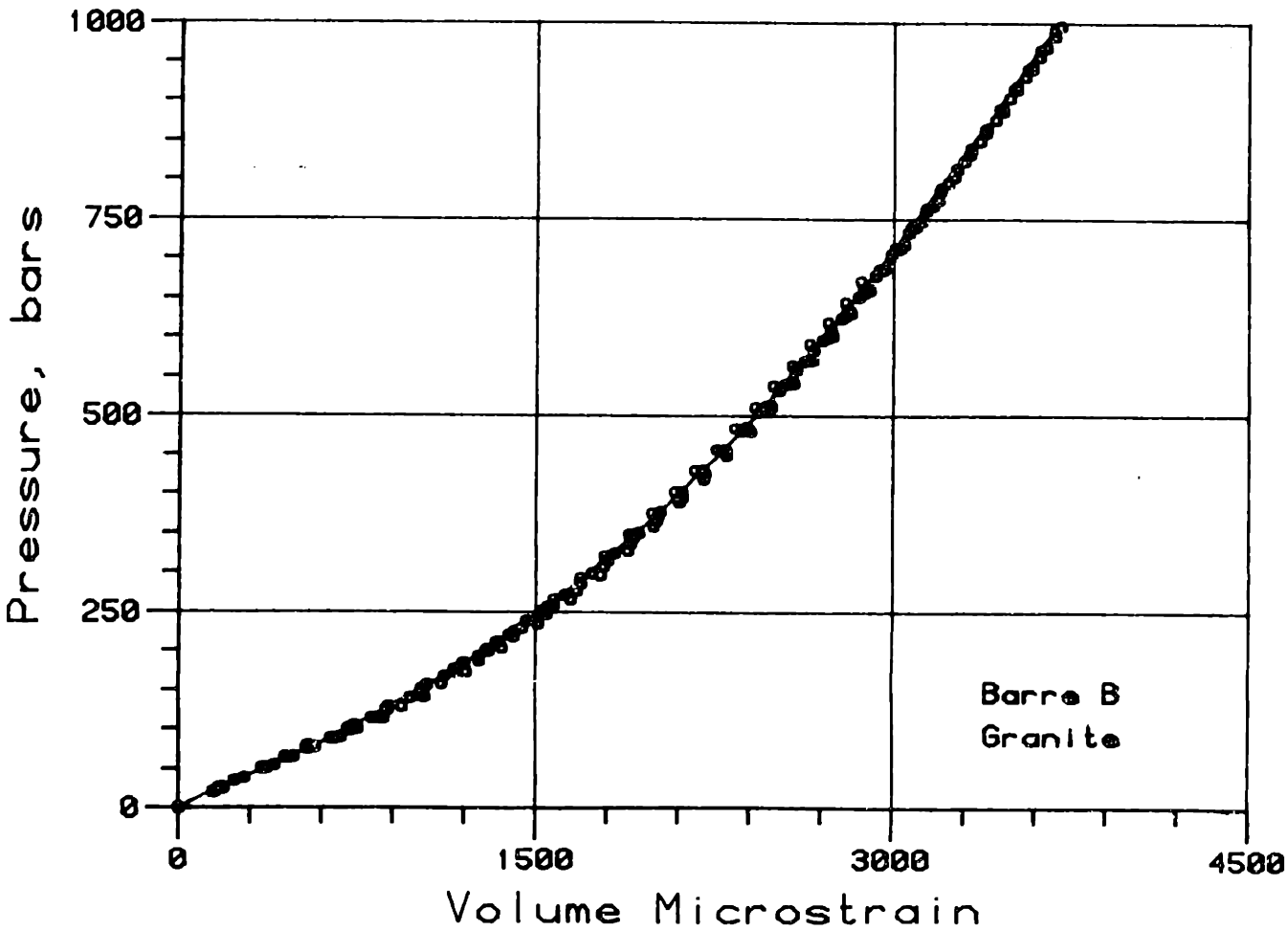


Figure 2-10. Volumetric strain versus confining pressure for Barre granite. Solid line is vacuum dry stress-strain relation. Square symbols are volumetric strains measured at various pore pressures.

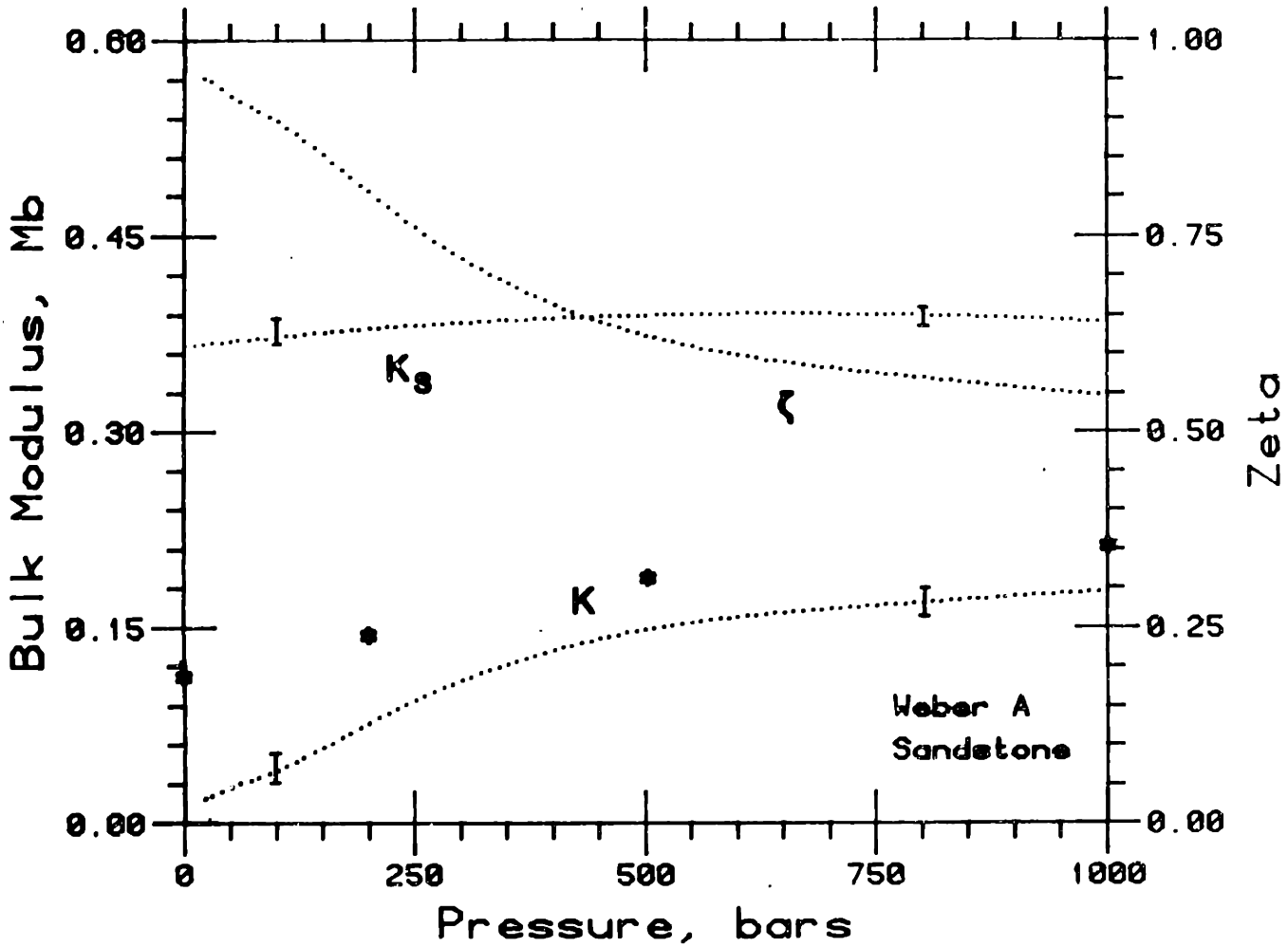


Figure 2-11. Jacketed bulk modulus $K$, unjacketed bulk modulus $K_s$, and $\zeta$ as a function of hydrostatic confining pressure for Weber sandstone. Bars represent probable error. Asterisks represent bulk moduli reported by Garg and Nur (1973).

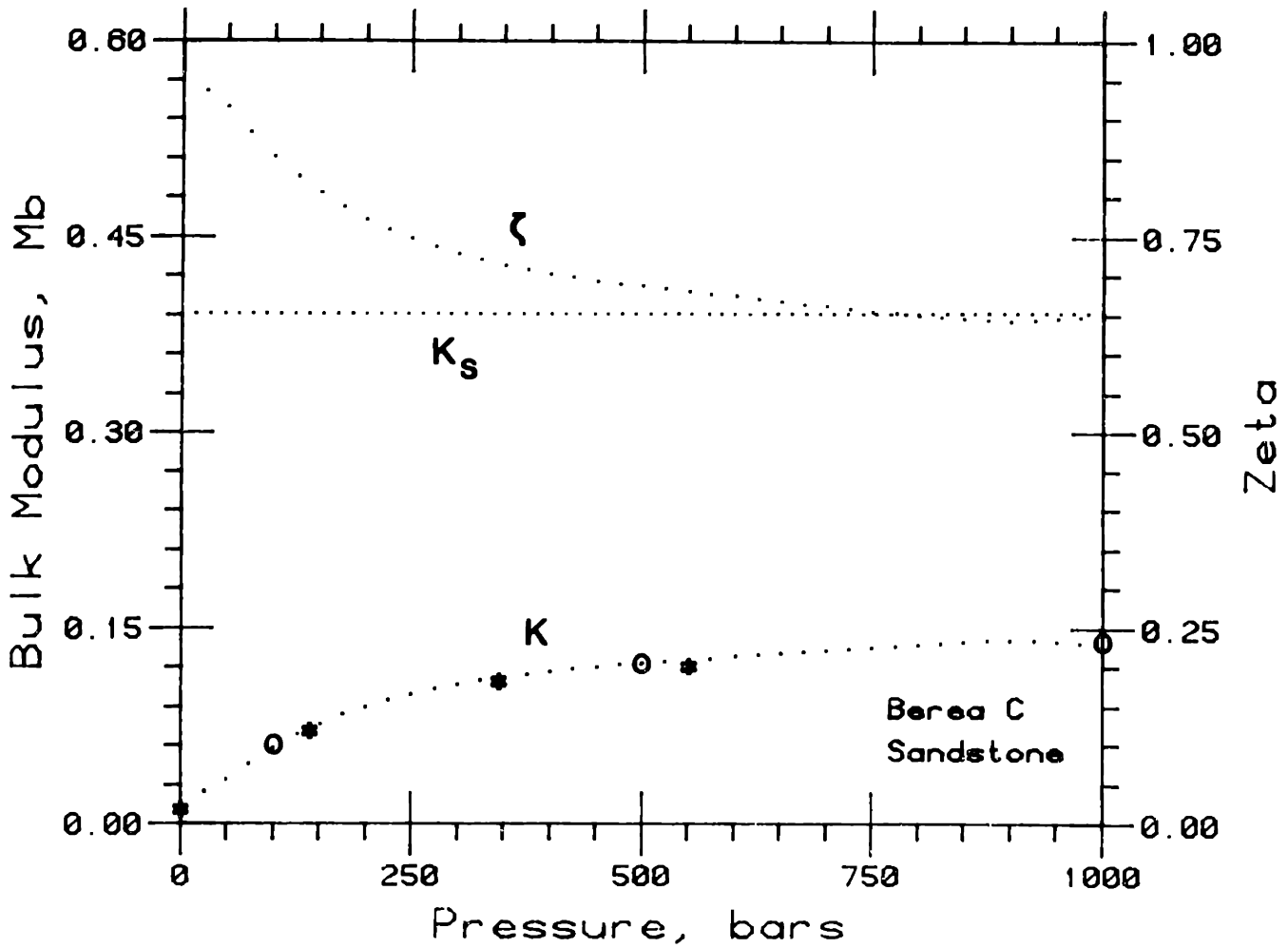


Figure 2-12. Jacketed bulk modulus $K$, unjacketed bulk modulus $K_s$, and $\zeta$ as a function of hydrostatic confining pressure for Berea sandstone. Asterisks represent bulk moduli reported by King (1969). Circles represent bulk moduli reported by Simmons *et al.* (1982).

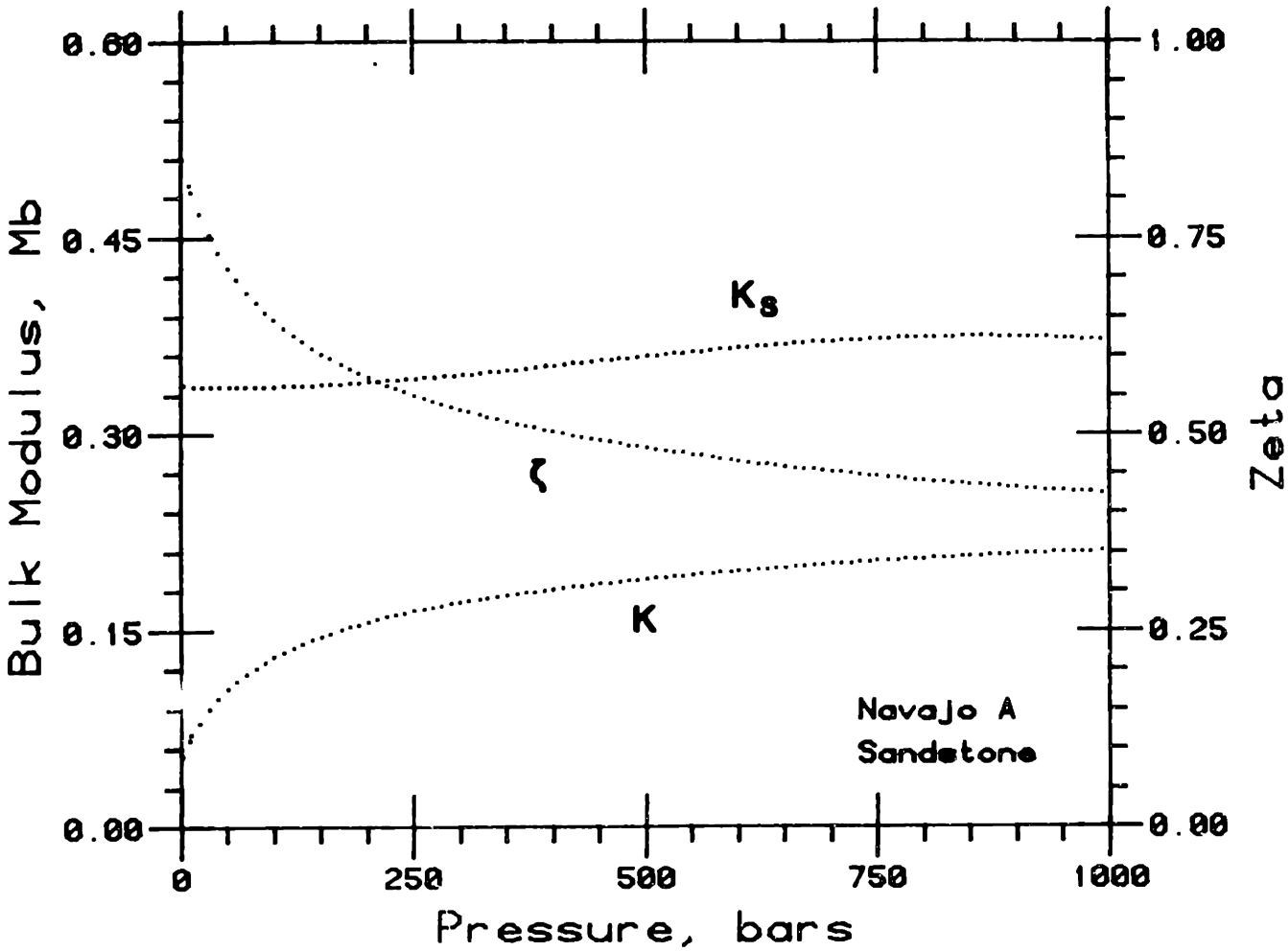


Figure 2-13. Jacketed bulk modulus $K$, unjacketed bulk modulus $K_s$, and $\zeta$ as a function of hydrostatic confining pressure for Navajo sandstone.

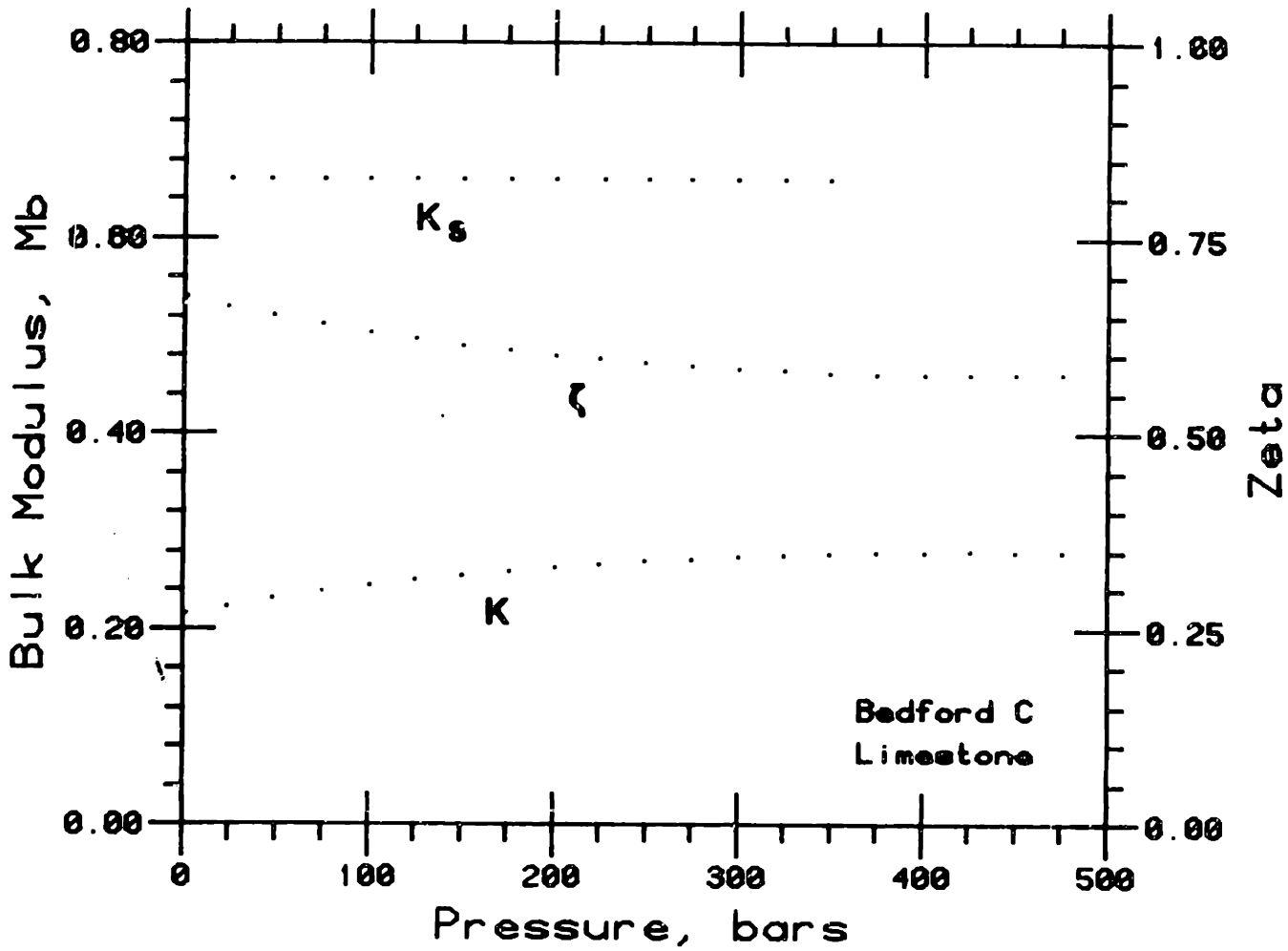


Figure 2-14. Jacketed bulk modulus $K$, unjacketed bulk modulus $K_s$, and $\zeta$ as a function of hydrostatic confining pressure for Bedford limestone.

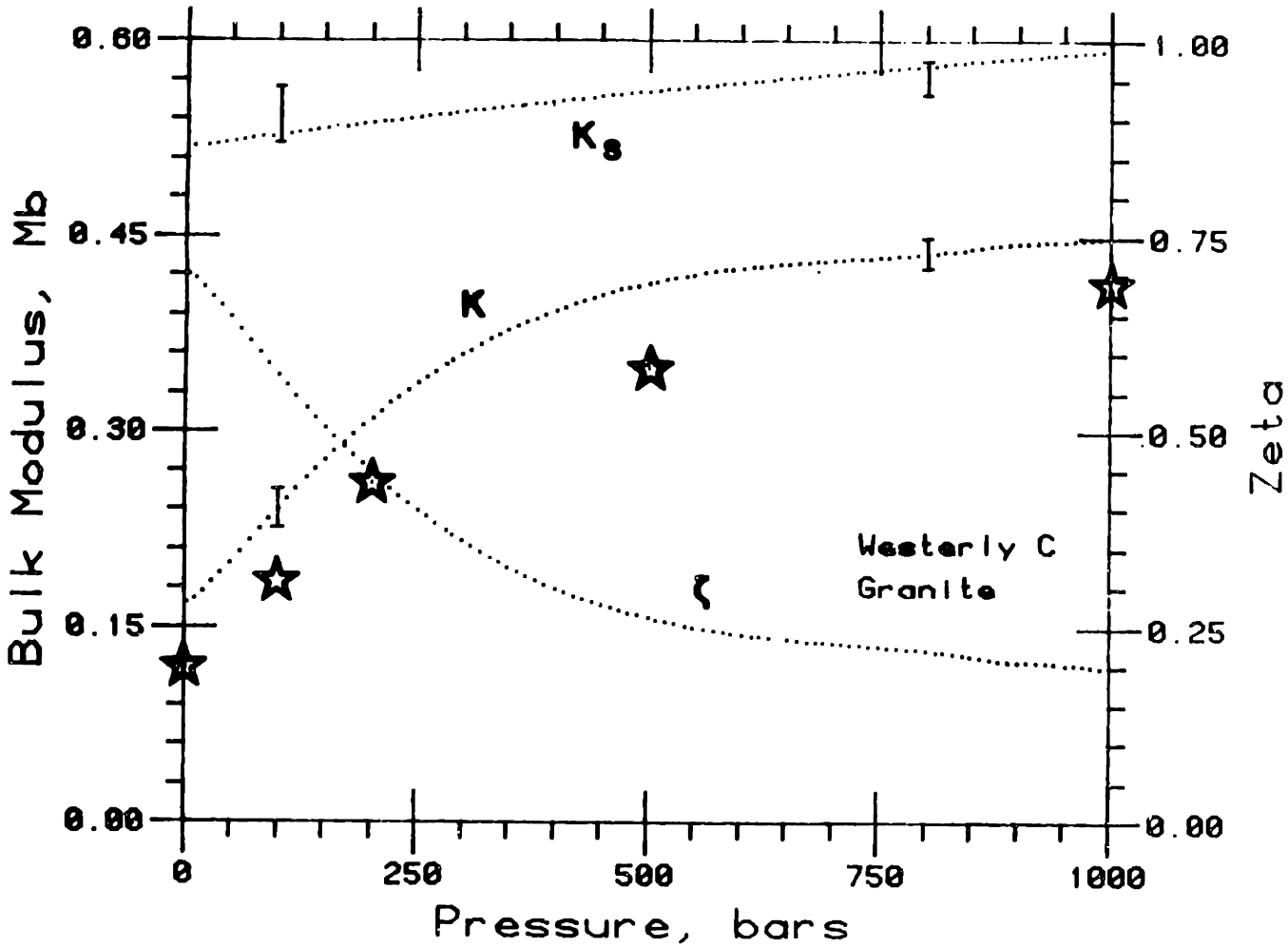


Figure 2-15. Jacketed bulk modulus $K$, unjacketed bulk modulus $K_s$, and $\zeta$ as a function of hydrostatic confining pressure for Westerly granite (red). Bars represent probable error. Stars represent bulk moduli reported by Brace (1965).

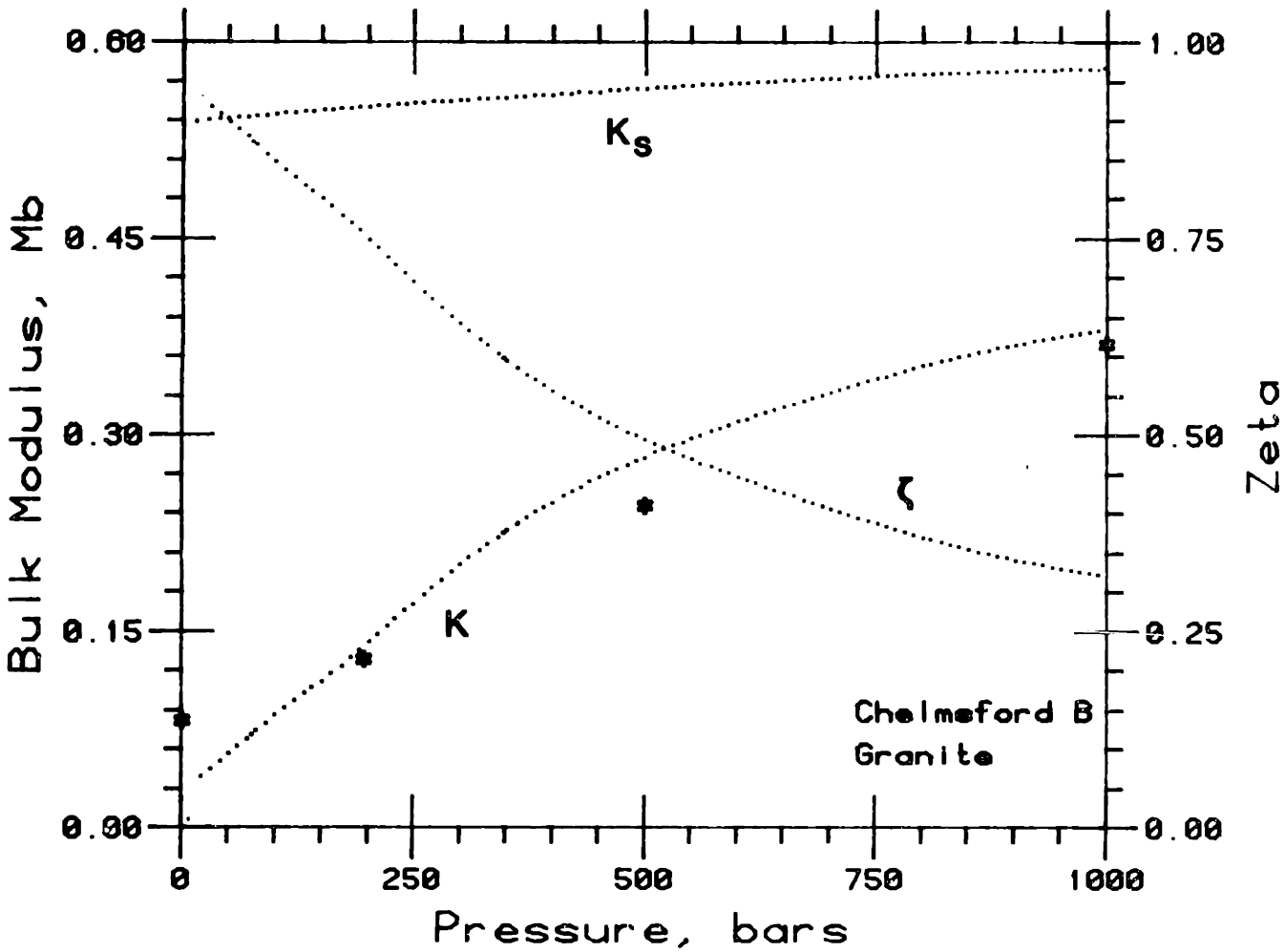


Figure 2-16. Jacketed bulk modulus $K$, unjacketed bulk modulus $K_s$, and $\zeta$ as a function of hydrostatic confining pressure for Chelmsford granite. Asterisks represent bulk moduli reported by Todd (1973).

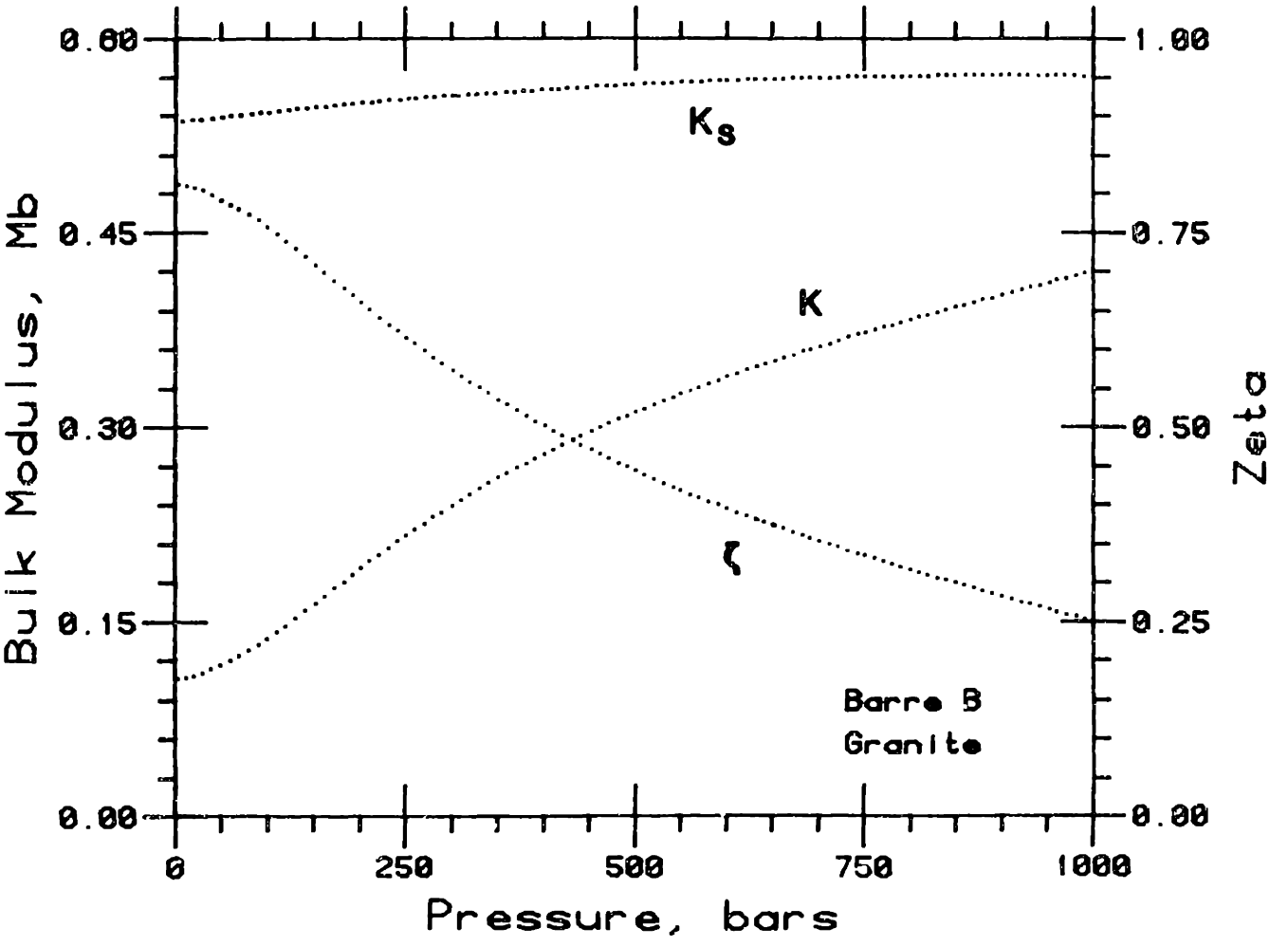


Figure 2-17. Jacketed bulk modulus $K$, unjacketed bulk modulus $K_s$, and $\zeta$ as a function of hydrostatic confining pressure for Barre granite.

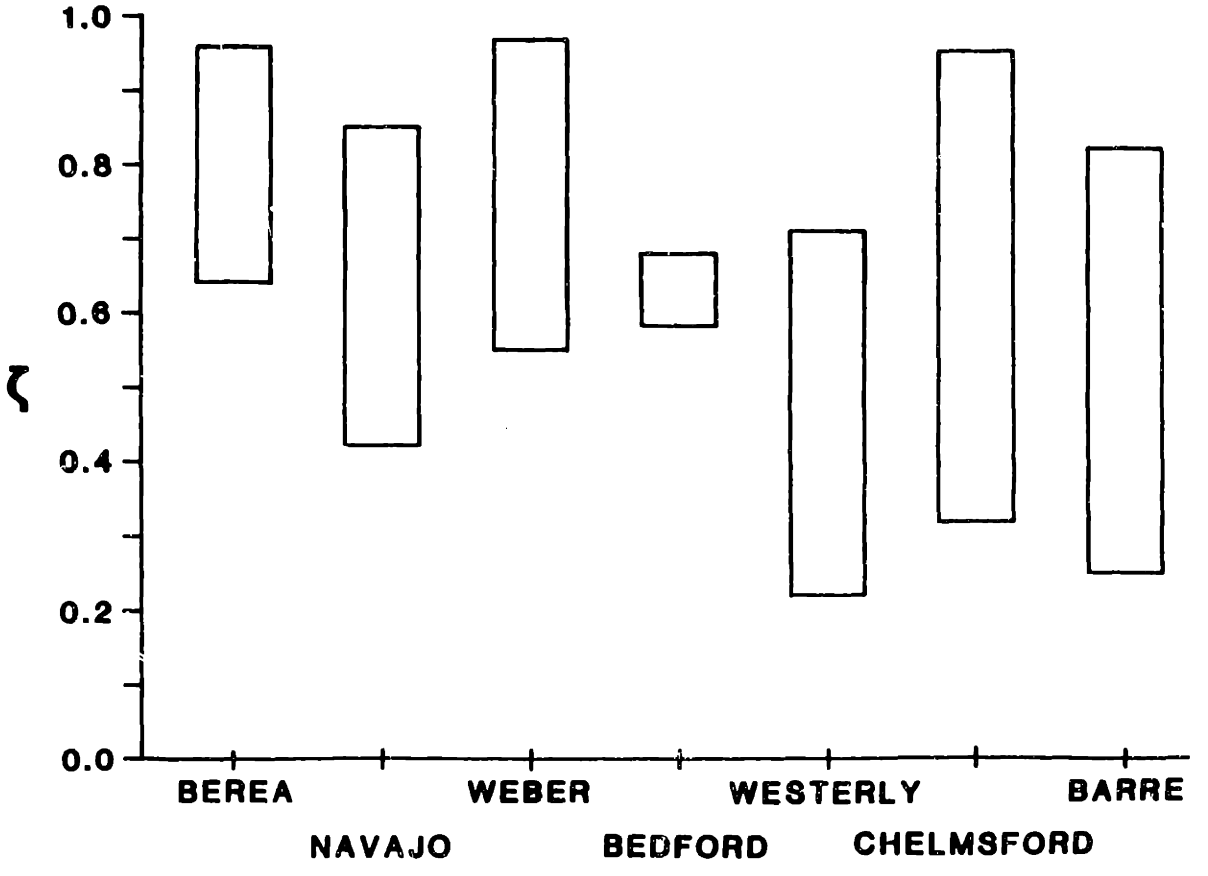


Figure 2-18. Summary plot of range of $\zeta$ values between 0 - 1 kbar confining pressure for seven rocks.

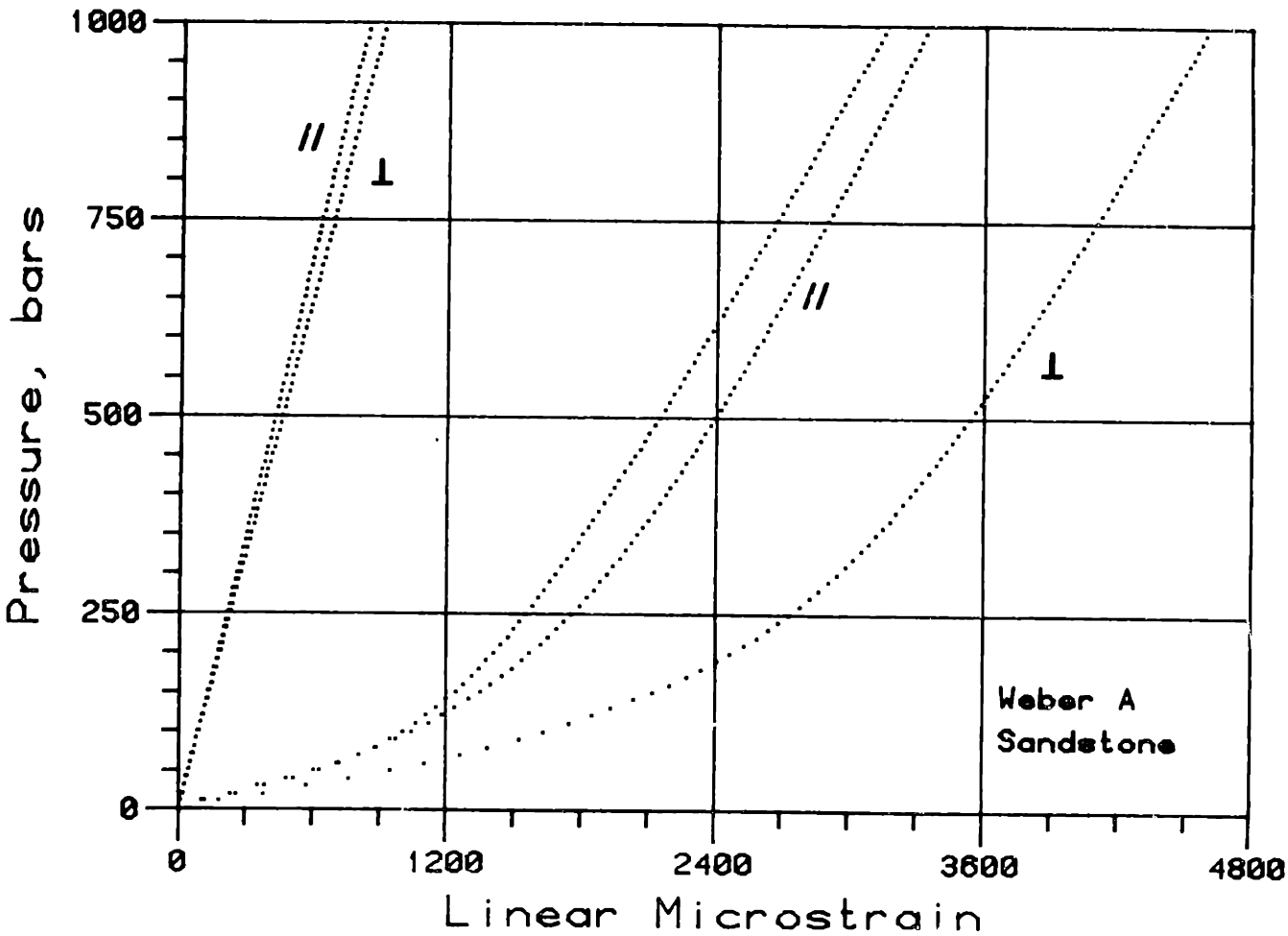


Figure 2-19. Linear strain versus confining pressure for Weber sandstone. The highly nonlinear curves to the right are jacketed strain; the nearly linear lines to the left are unjacketed strain. Symbols correspond to measurements oriented parallel and perpendicular to bedding.

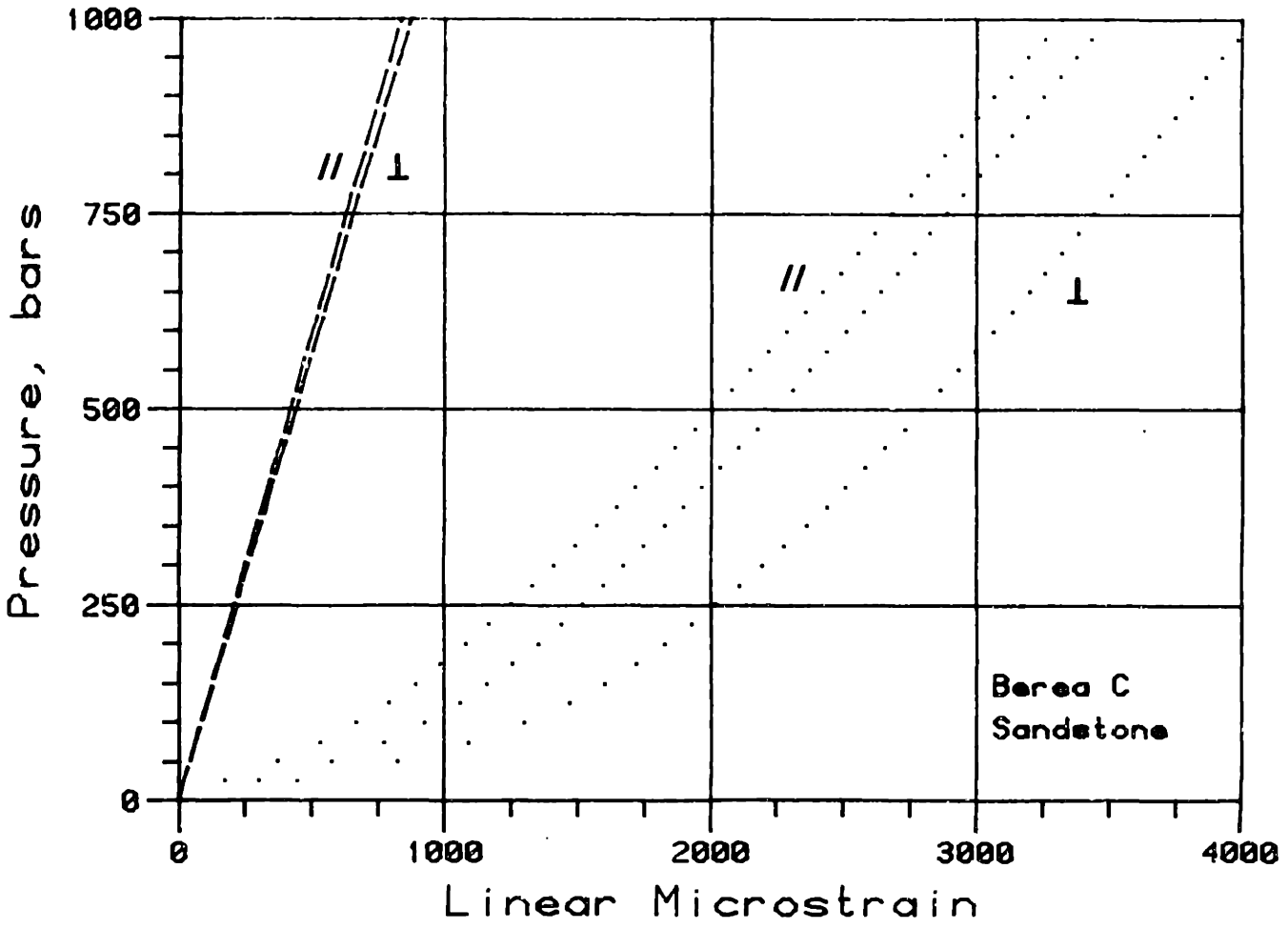


Figure 2-20. Unjacketed and jacketed linear stress-strain measurements for Berea sandstone. Symbols correspond to measurements oriented parallel and perpendicular to bedding.

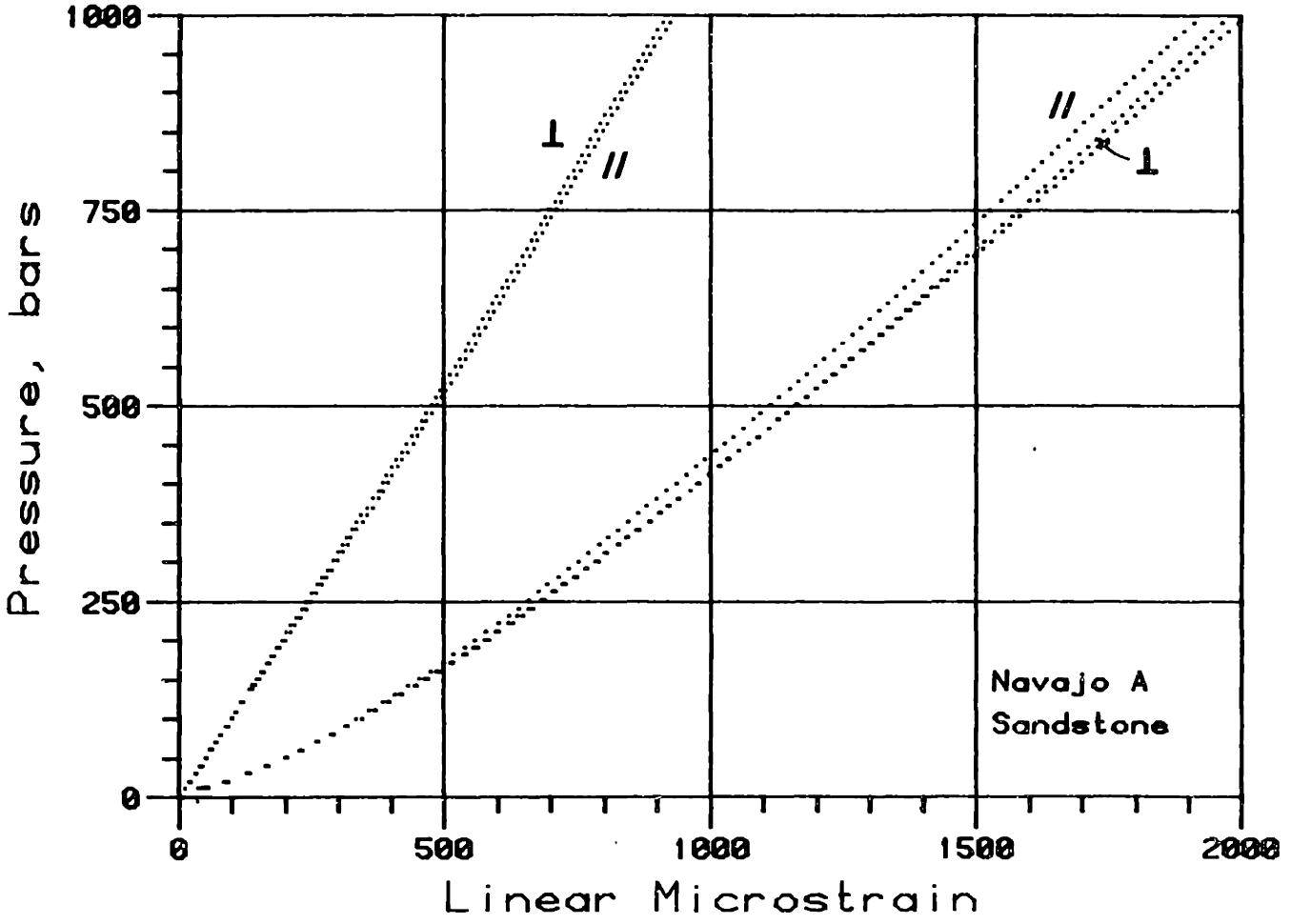


Figure 2-21. Unjacketed and jacketed linear stress-strain measurements for Navajo sandstone. Symbols correspond to measurements oriented parallel and perpendicular to bedding.

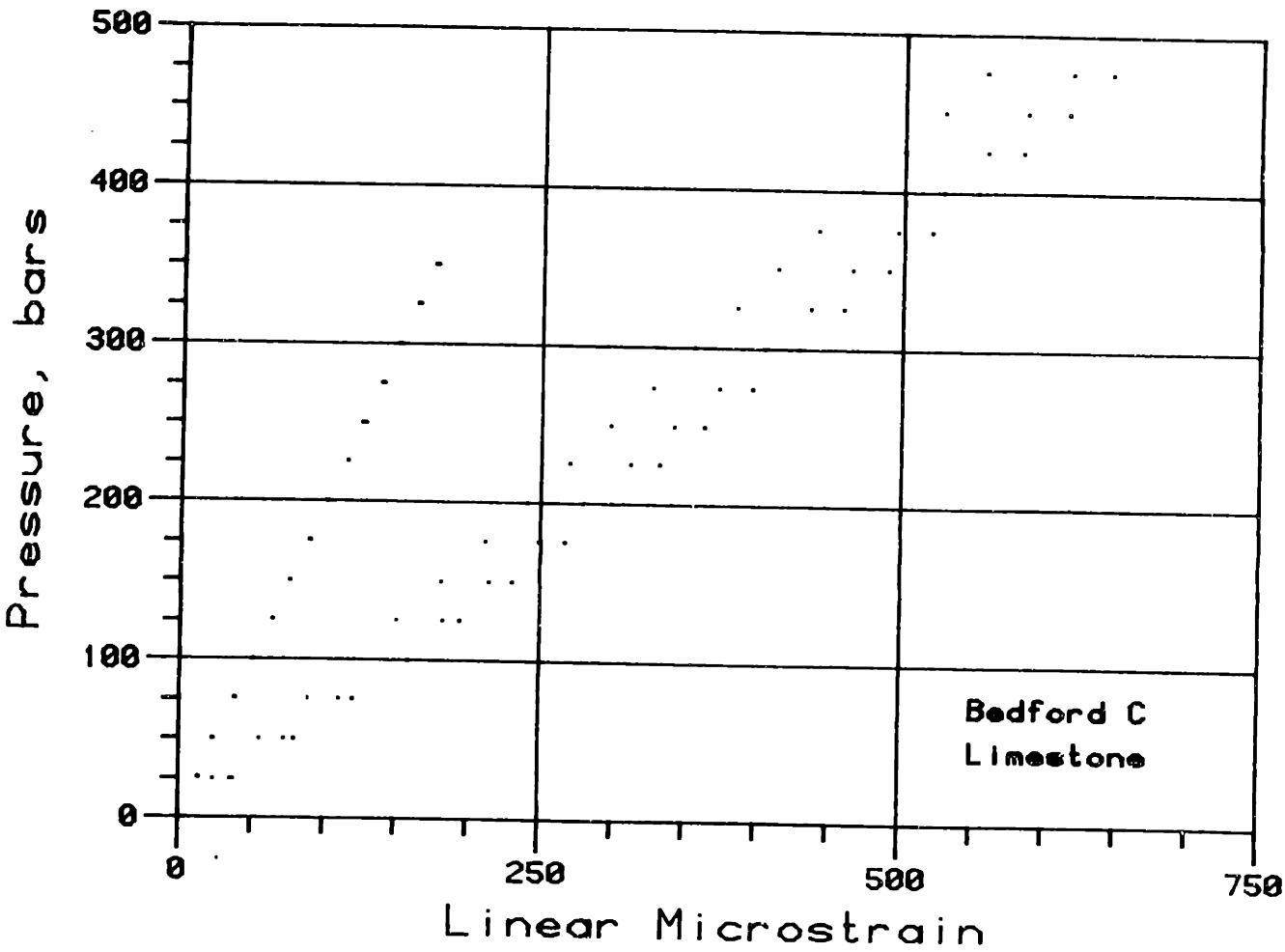


Figure 2-22. Unjacketed and jacketed linear stress-strain measurements for Bedford limestone.

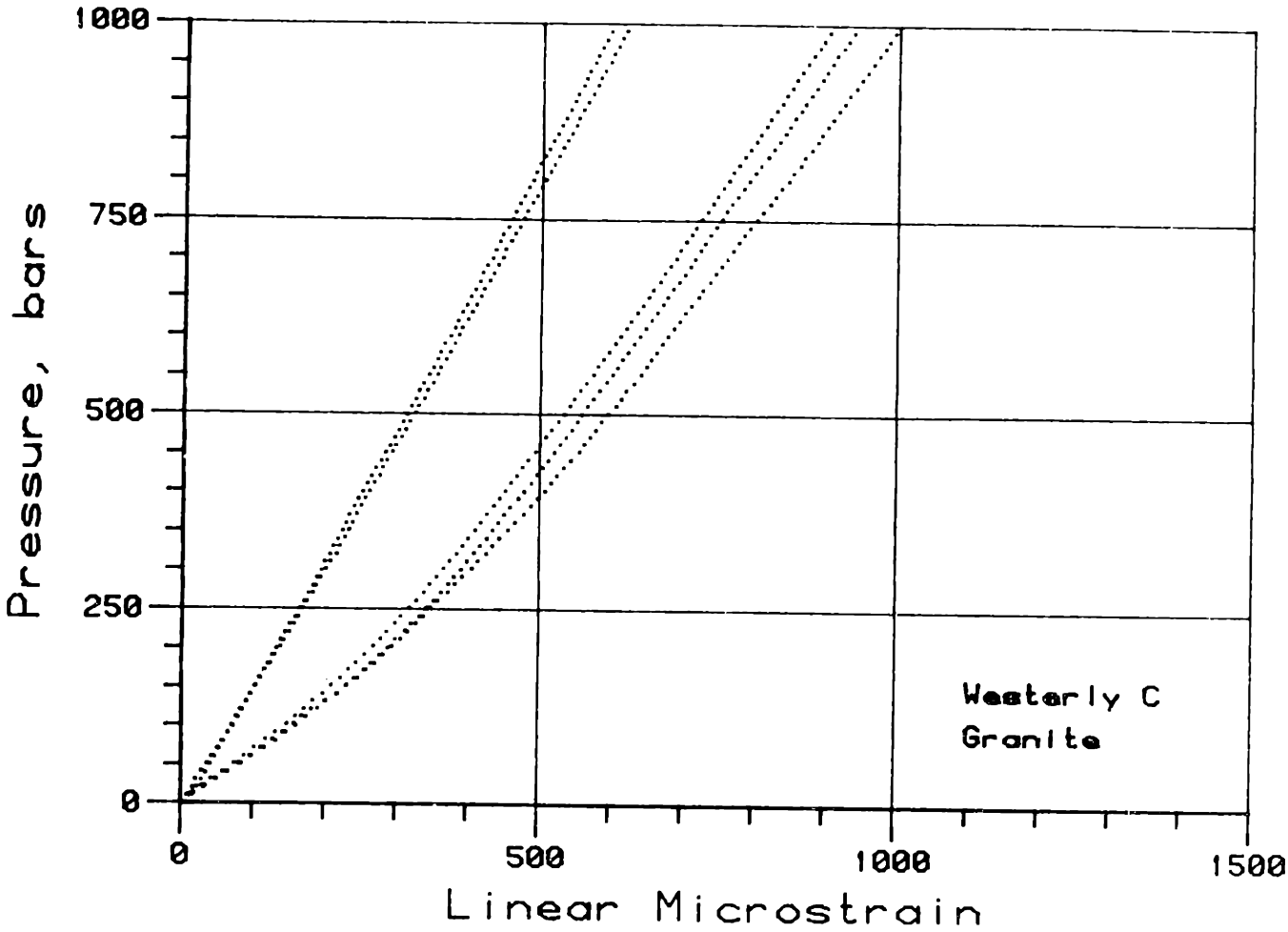


Figure 2-23. Unjacketed and jacketed linear stress-strain measurements for Westerly granite (red).

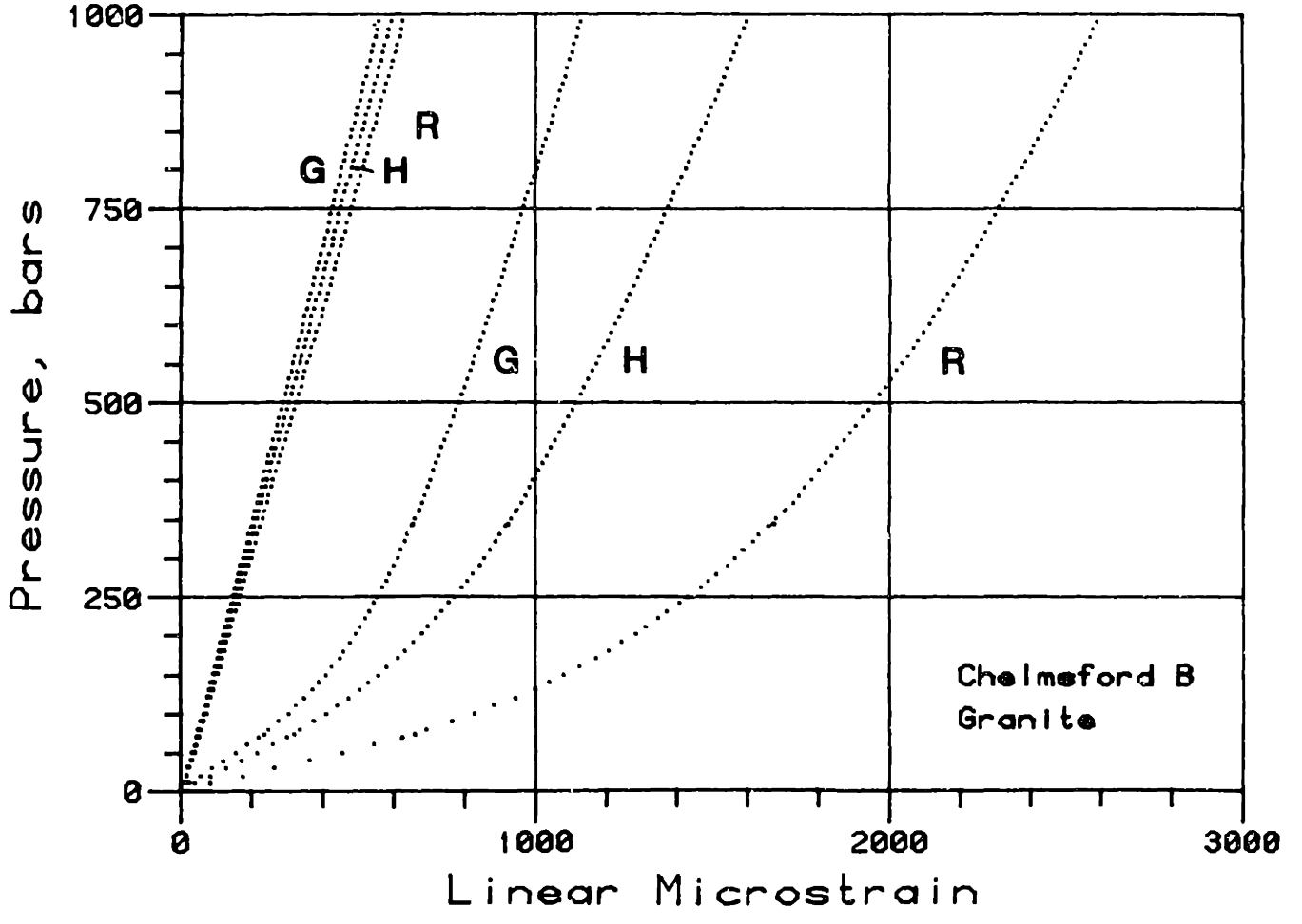


Figure 2-24. Unjacketed and jacketed linear stress-strain measurements for Chelmsford granite. Curves labelled G, H, and R correspond to measurements perpendicular to grain, headgrain, and rift planes identified in the quarry samples.

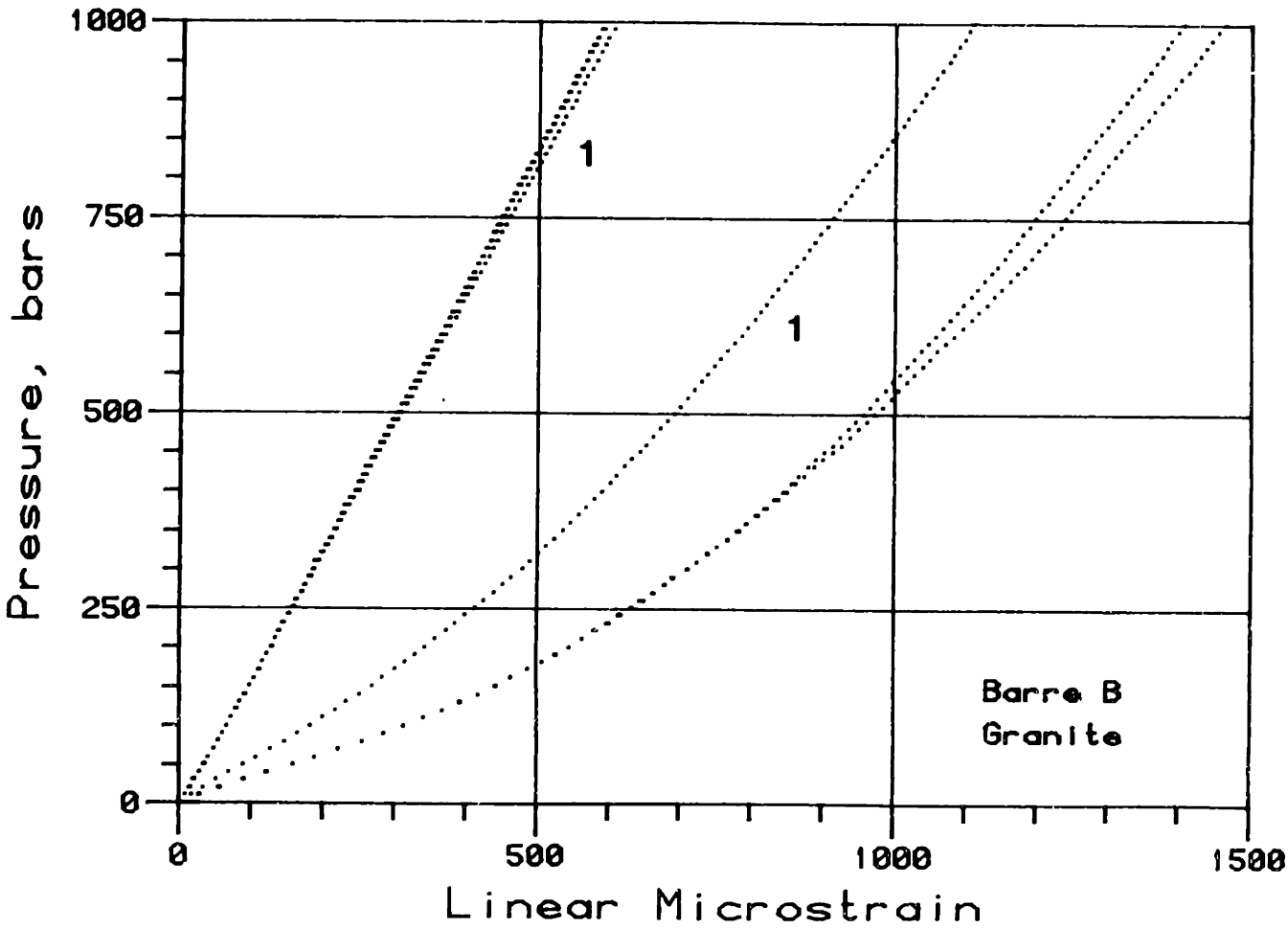


Figure 2-25. Unjacketed and jacketed linear stress-strain measurments for Barre granite. Curves labelled 1 correspond to same orientation.

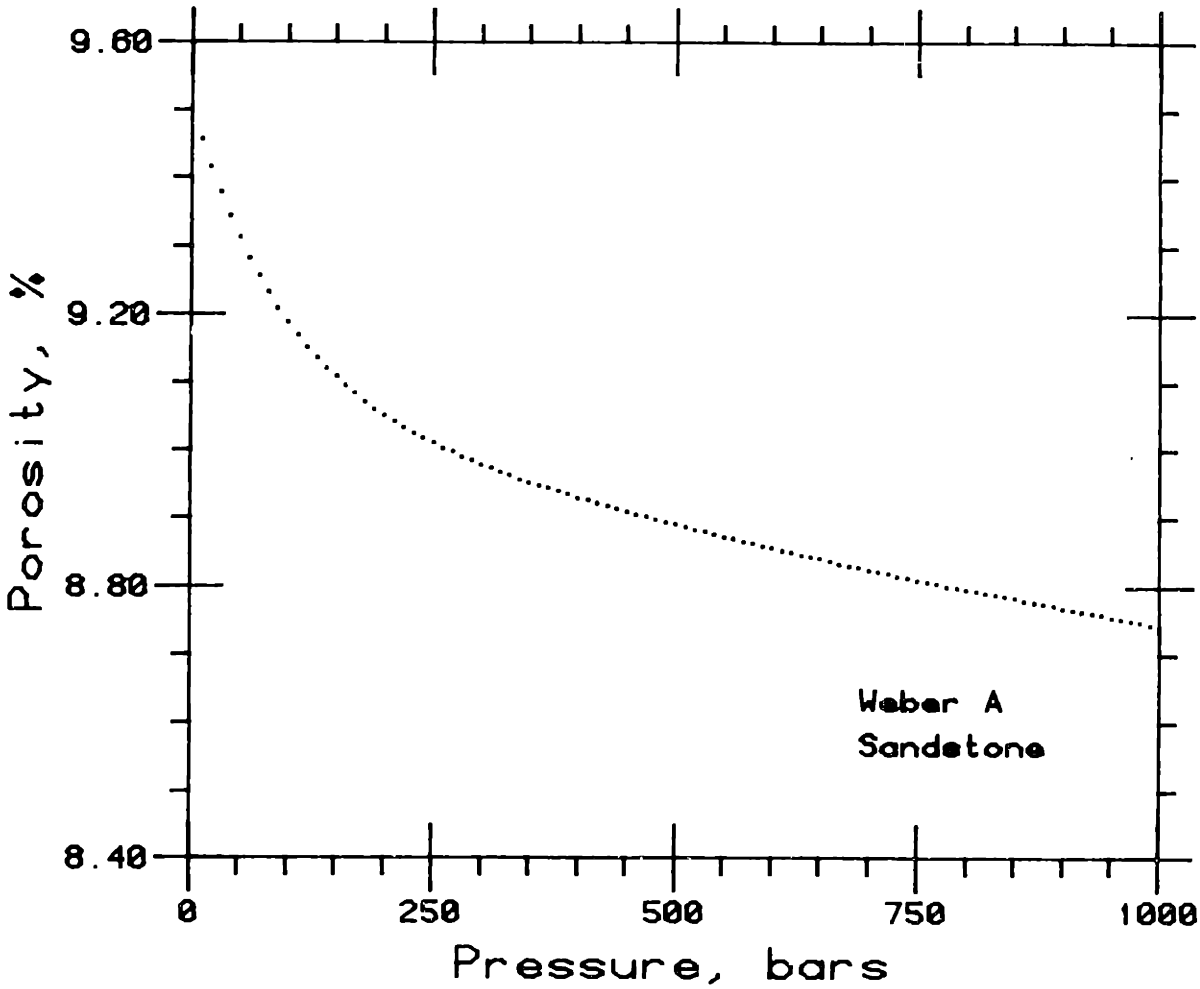


Figure 2-26. Porosity versus confining pressure for Weber sandstone calculated from unjacketed and jacketed stress-strain measurements.

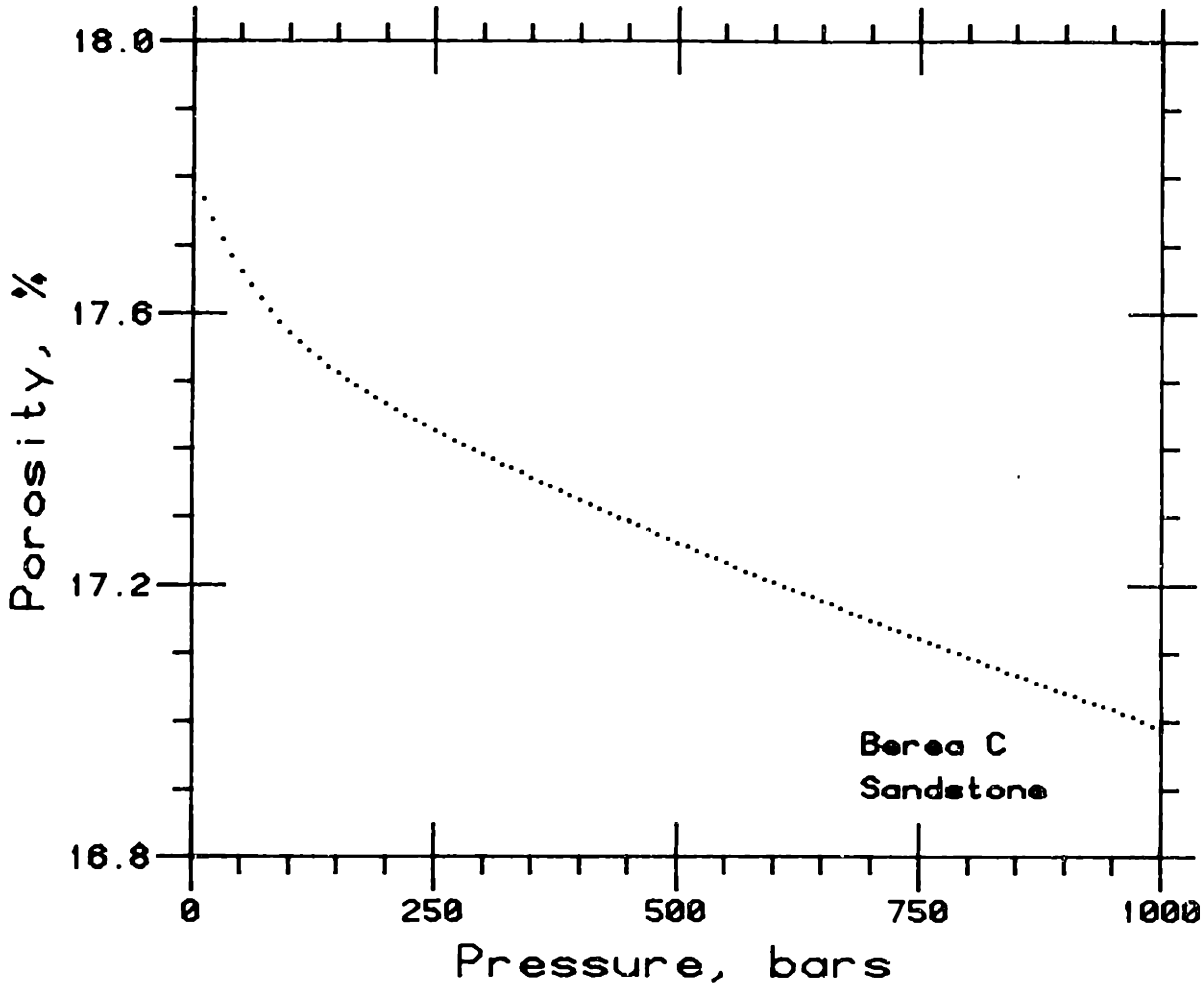


Figure 2-27. Porosity versus confining pressure for Berea sandstone calculated from unjacketed and jacketed stress-strain measurements.

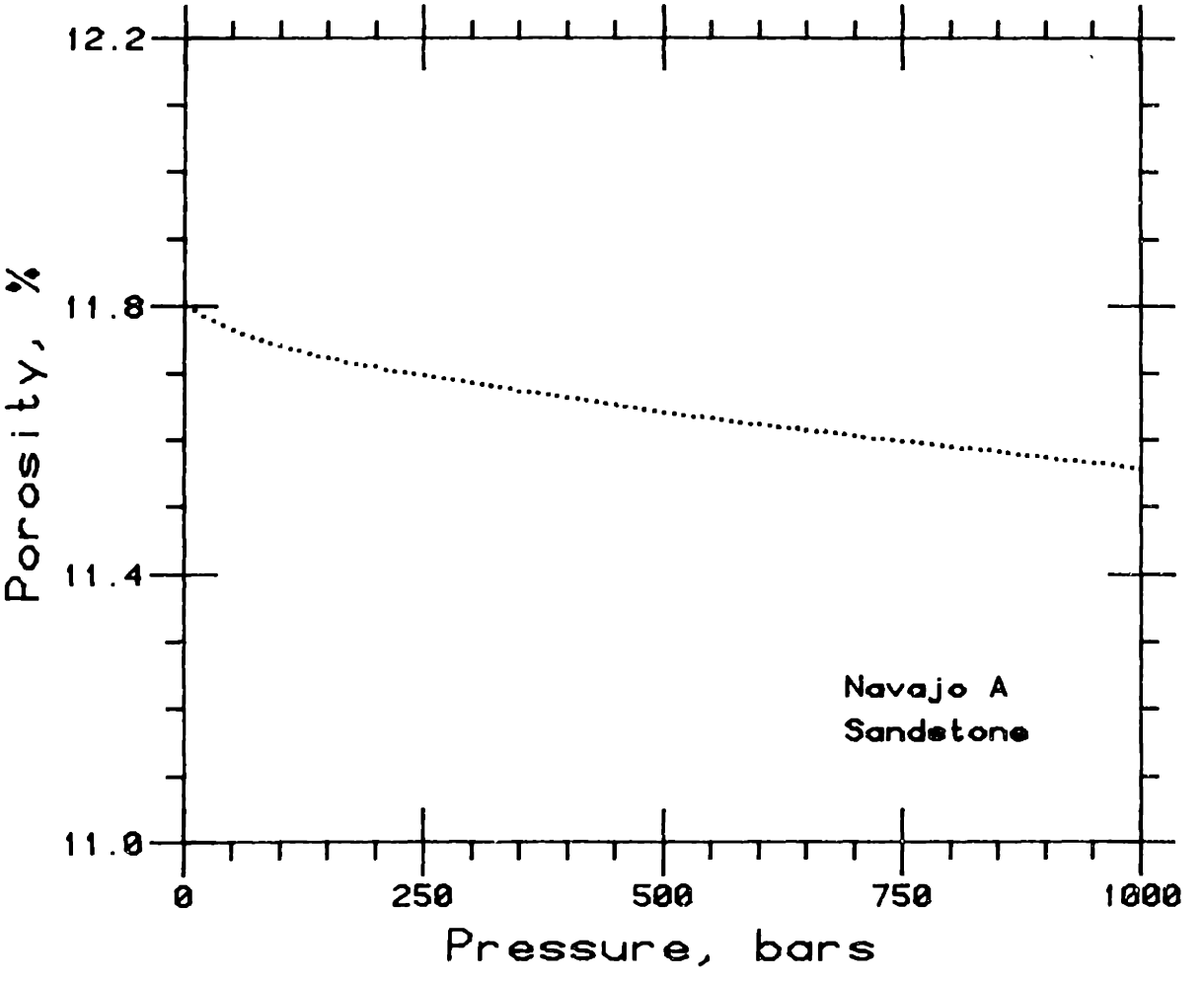


Figure 2-28. Porosity versus confining pressure for Navajo sandstone calculated from unjacketed and jacketed stress-strain measurements.

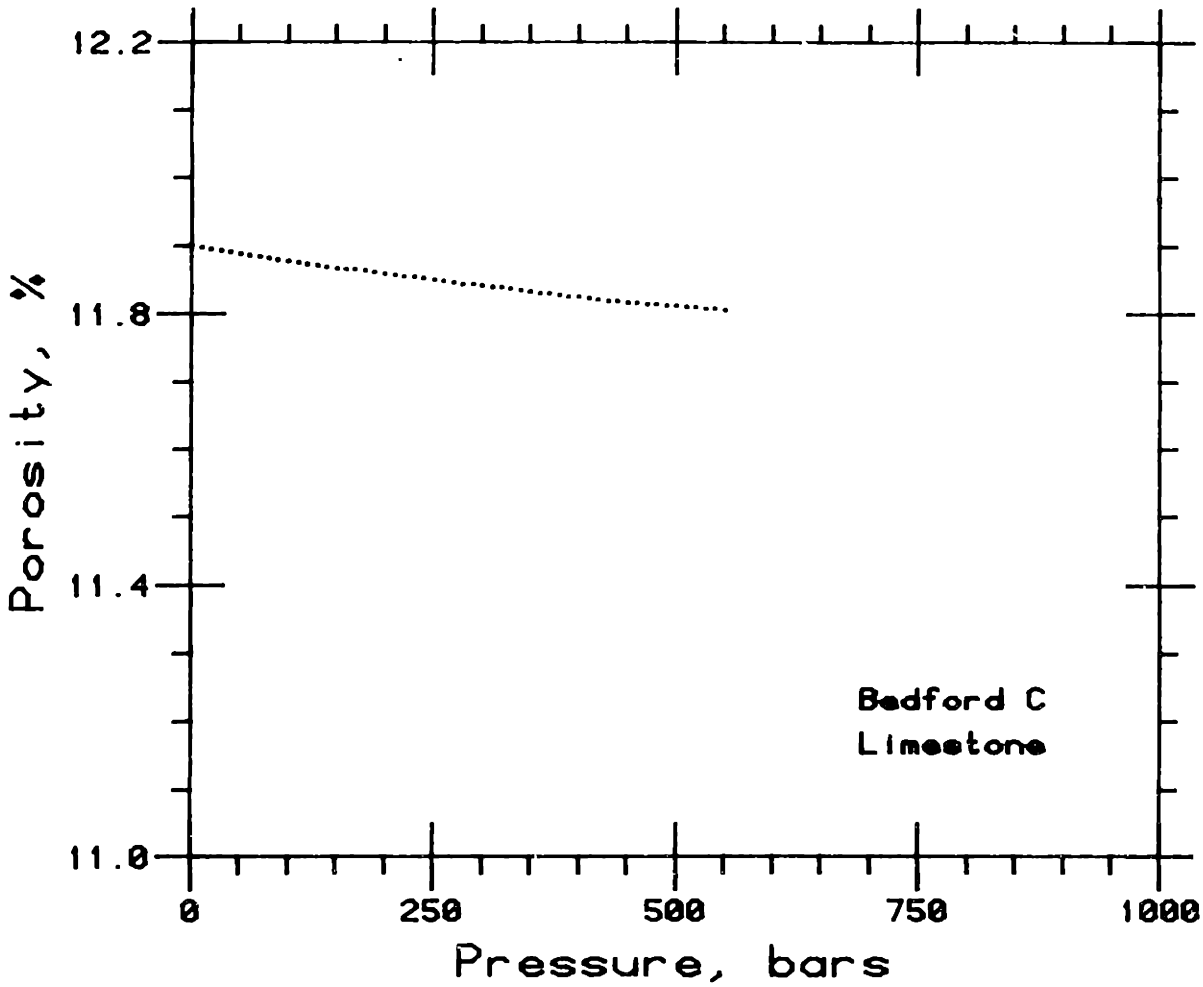


Figure 2-29. Porosity versus confining pressure for Bedford limestone calculated from unjacketed and jacketed stress-strain measurements.

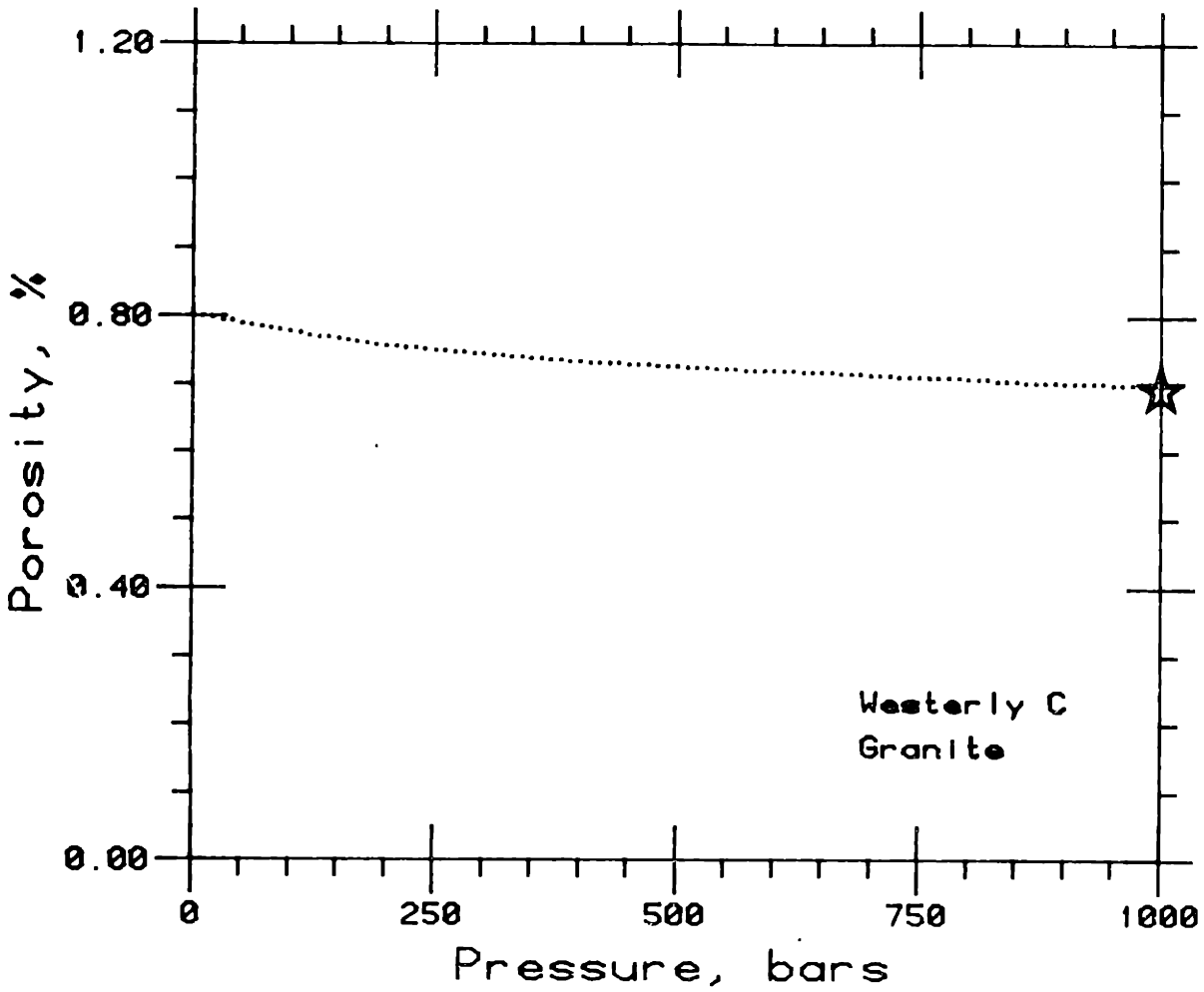


Figure 2-30. Porosity versus confining pressure for Westerly granite (red) calculated from unjacketed and jacketed stress-strain measurements. Star symbol represents value reported by Brace *et al.* (1965).

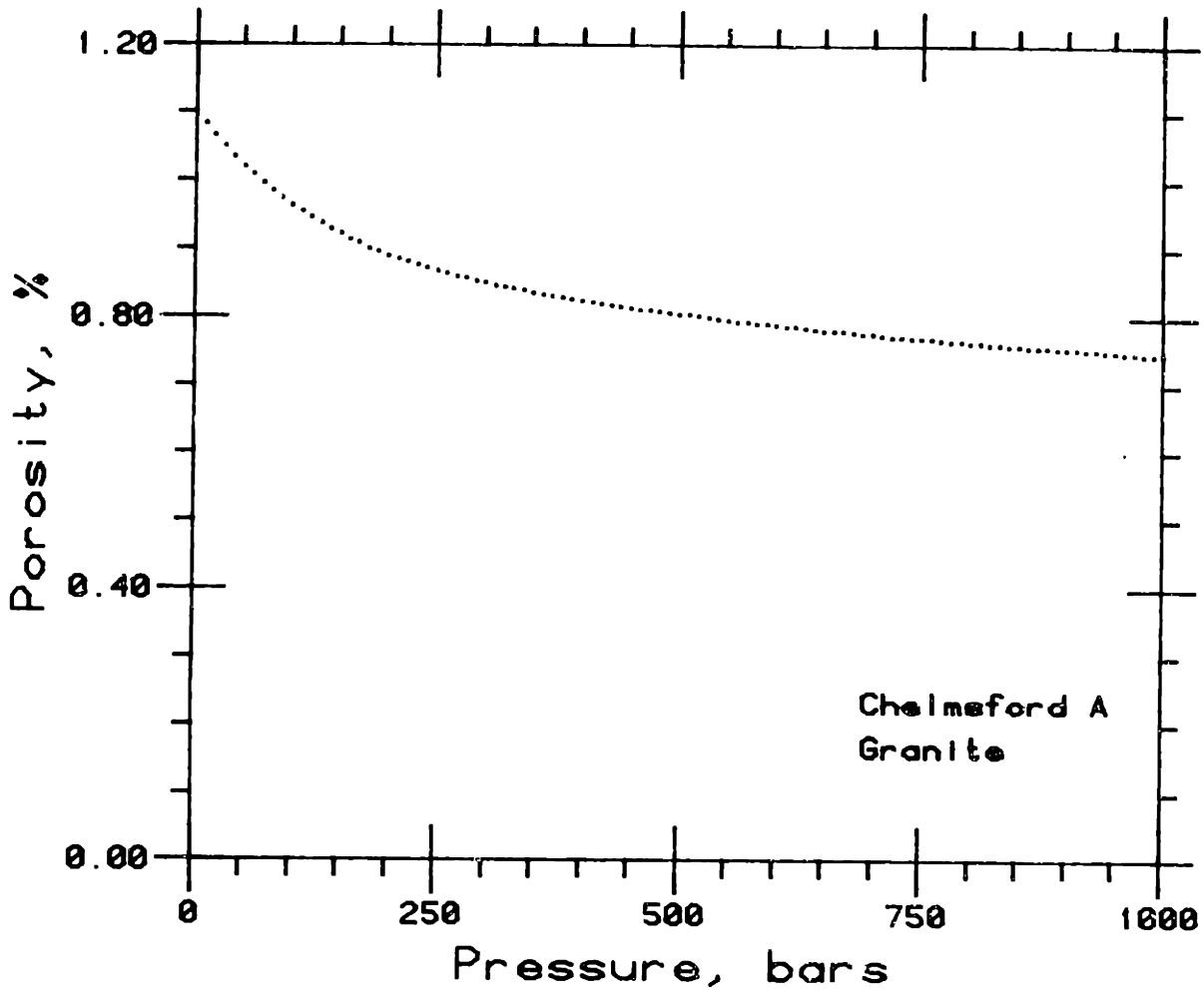


Figure 2-31. Porosity versus confining pressure for Chelmsford granite calculated from unjacketed and jacketed stress-strain measurements.

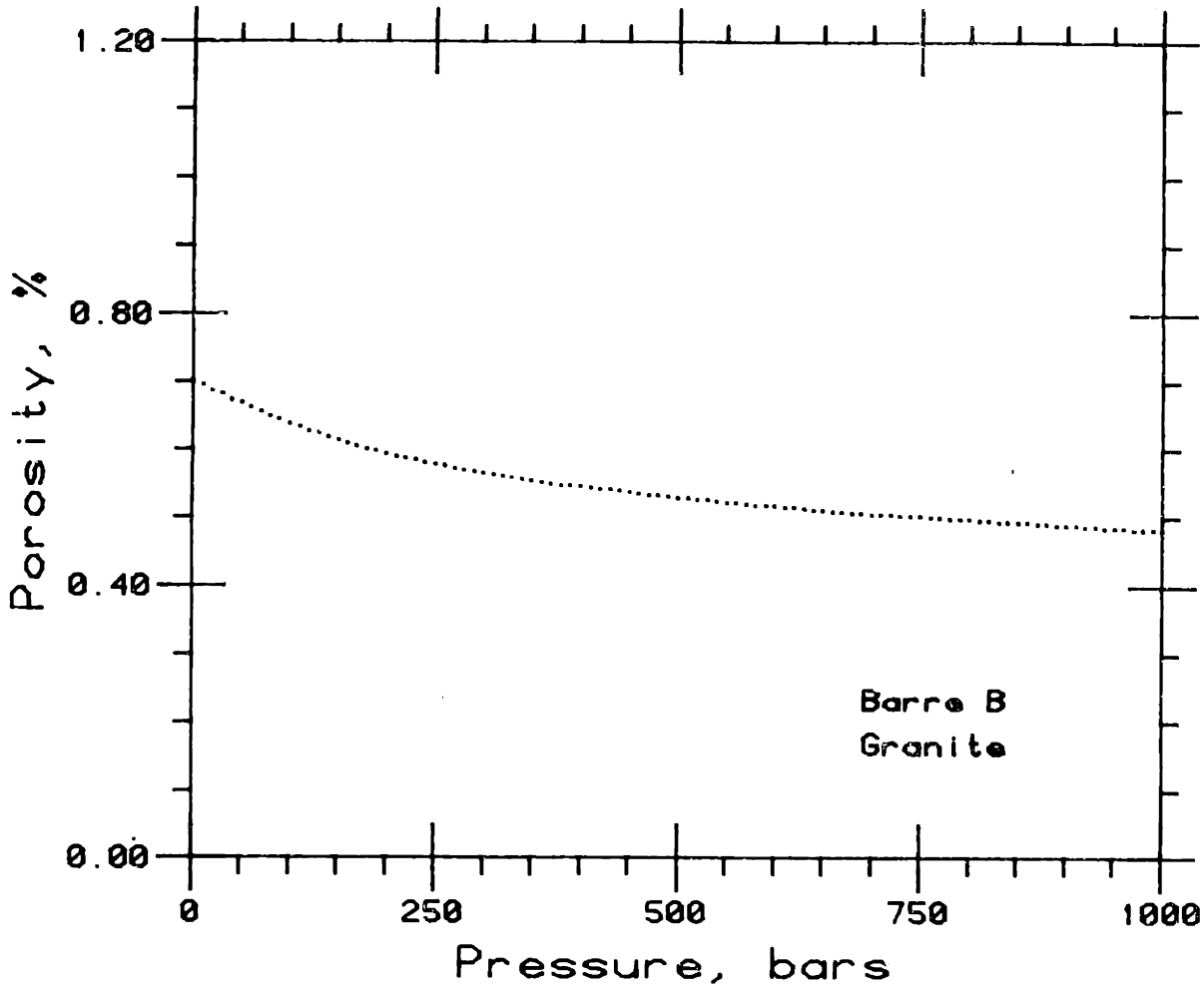


Figure 2-32. Porosity versus confining pressure for Barre granite calculated from unjacketed and jacketed stress-strain measurements.

# CHAPTER 3

# THE EFFECT OF CONFINING PRESSURE AND PORE PRESSURE ON PERMEABILITY IN SEVERAL ROCKS

## INTRODUCTION

The fluid permeability of rocks and sediments is a crucial parameter in many geological processes and reservoir engineering procedures. Permeability values vary over many orders of magnitude (see Brace, 1981, for a compilation) and are often poorly constrained *in-situ* because of the presence of joints and fractures. Prediction of permeability from other physical properties such as electrical resistivity (Brace, 1977; Walsh and Brace, 1984) or borehole tube waves (Beydoun *et al.*, 1984) is a significant goal because the direct measurement or estimation of permeability in the earth is difficult.

Some aspects of those pore features controlling permeability can be identified by understanding how permeability of rocks and sediments responds to stress in the laboratory. Confining pressure decreases the permeability of rocks and sediments. For intact granites the functional dependence can be dramatic. An increase in confining pressure to 1 kbar reduces the permeabilities of some granites by orders of magnitude (Brace, 1968; Coyner *et al.*, 1979). In these rocks the effect of confining pressure is to close narrow, low aspect ratio pores which figure prominently in the interconnected porosity which determines permeability. For porous sandstones the dependence of permeability on confining pressure is normally found to be much smaller. For Berea sandstone

permeability decreases by only a few millidarcies between 0 and 800 bars confining pressure. Pore and crack closure mechanics at grain contacts, which give rise to large changes in velocity and attenuation, contribute little to the larger pores which determine permeability in porous sandstones. This poses a dilemma in attempting to predict bulk permeability from acoustic data.

An important aspect of rock permeability is its dependence on the combined influence of both confining pressure and pore pressure. This dependence is necessary to understand because at depth pore pressure can be a significant variable and is the force which causes fluids to flow. Simple elasticity considerations presented in the analysis section of this paper suggest that the simple differential pressure, $\sigma - p$, where $\sigma$ is confining pressure and $p$ is pore pressure, should approximate permeability in most intact rocks. This has been previously suggested and experimentally observed (Knutson and Bohor, 1963; Brace *et al.*, 1968; Vairogs, 1971).

Some recent laboratory measurements of permeability in several sandstones, however, indicate an anomalous behavior with regards to pore pressure. Experiments by Zoback and Byerlee (1975), Walls and Nur (1979), and Riepe *et al.* (1983), where both pore pressure and confining pressure were varied, indicate that a relation of the form $\sigma - np$, with $n > 1$, governs permeability in some sandstones.

Zoback (1975) and Zoback and Byerlee (1975) measured permeability of Berea sandstone as pore pressure and confining pressure were systematically varied. The pore fluid was a fairly viscous lubricating oil. The results of their work are reproduced in Fig. 3-1 for flow normal (top) and parallel (bottom) to apparent bedding in the sandstone. Plotted is permeability versus differential pressure. Data points along each of the dashed lines represent different pore

pressures, from 35 to 200 bars, such that the top dashed line represents the change in permeability with constant pore pressure (200 bars) as confining pressure was increased from about 300 to 900 bars. The decrease in permeability is exceedingly small, amounting to only a few millidarcies decrease over this confining pressure range.

The key observation in this data is that all of the dashed lines do not fall on top of each other. This would be the case if the simple differential pressure governed permeability. At a constant differential pressure permeability increases as pore pressure increases. The observation is not explained by hysteresis as measurements made as pore pressure was increased agreed with those when pore pressure was decreased.

An explanation for this phenomenon in Berea sandstone was first proposed by Zoback and Byerlee (1975). A conceptual model for the pore network in this sandstone is shown in Fig. 3-2. They suggested that a phase of higher compressibility than the quartz grain framework lining the pores of these sandstones is preferentially compressed in response to pore pressure quite independently of confining pressure which is carried at the grain-to-grain contacts. For the highly compressible phase they suggested clays and various accessory minerals. Since permeability is so sensitive to absolute dimension the compression of these clays would lead to higher permeabilities at higher pore pressures. This is in contrast to the effect of a similar increase in confining pressure, which would only slightly decrease porosity, and consequently cause a minimal decrease in permeability. Therefore the effect of pore pressure is greater than confining pressure. An empirical fit of the permeability data to an equation of the form $\sigma - np$ led to a linear relationship with $n \approx 4.0$.

Zoback (1975) and Zoback and Byerlee (1975) also measured permeability of Berea sandstone parallel to apparent bedding in a similar fashion and the results are shown in the lower plot of Fig. 3-1. They observed that permeability was much higher, varying from nearly 200 mD at 0 bars down to about 130 mD at 800 bars differential pressure. The pore pressure effect noted perpendicular to bedding was almost negligible given the scatter of data, so that $n \approx 1$.

Walls and Nur (1979) measured this pore pressure effect for Berea and several additional sandstones and noted that the magnitude of the effect correlated somewhat with percentage clay content. They felt that the larger the clay content, the larger the effect. They measured the permeability of seven sandstones with distilled water as the pore fluid. Pore pressure was varied between 20 and 300 bars and confining pressure between 50 and 600 bars. Their results are shown in Fig. 3-3. The upper plot is permeability normalized to that measured at zero confining pressure (presumably benchtop). Permeability at zero pressure is given in the legend next to abbreviated names. The abbreviations correspond to the sandstone names given in the lower of the two plots in Fig. 3-3. For all of the data points in the upper plot of Fig. 3-3 the differential pressure is 50 bars. If the simple differential pressure governs permeability the data points would fall along the dashed line at $k/k_0 = 1.0$, as they nearly do for the synthetic $Al_2O_3$ and the St. Peters sandstone. For the other sandstones normalized permeability data points fall above this line, indicating that pore pressure has a relatively greater effect than confining pressure in determining permeability. Normalized permeability versus confining pressure at a constant pore pressure (20 bars) is shown in the lower plot of Fig. 3-3.

Walls and Nur (1979) explained their observations using the conceptual model of Zoback and Byerlee (1975). As can be seen in the data of Fig. 3-3 the

effect is surprisingly linear with pressure. They fit a linear equation of the form $\sigma - np$ to the data and plotted the $n$ versus volume clay content, not distinguishing between different types of clays, and concluded, that greater clay content correlated with larger values of $n$.

Riepe *et al.* (1983) investigated pressure effects in about 15 sandstones, mainly well-consolidated rocks with low permeabilities (<1mD). They used dry, inert gas, nitrogen or helium, as the pore fluid to avoid interaction with the rock matrix. A large portion of their data concerns corrections for inertial and slip effects (Klinkenberg and Forchheimer effects) in order to arrive at the true permeability as a function of confining pressure and pore pressure. For one sandstone, described as a red, arcosic, Upper Carboniferous rock with about 5% clay minerals, they note an anomalous pore pressure effect on permeability. They calculate $n = 1.4 - 2.7$ in the relation $\sigma - np$, so that again pore pressure has a greater effect than confining pressure in determining permeability. Closer examination of their data for this rock, however, indicates that a Klinkenberg-effect was possibly present at low pore pressures and so their conclusion, as they themselves indicated, must be considered preliminary.

The observed pore pressure effect in sandstones and the correlation with clay content by Walls and Nur (1979) could perhaps have significant implications for geologic systems where fluid flows through rocks with clay. The mechanisms of oil and gas migration out of source rocks, for instance, would be enhanced by the increase in permeability due to pore pressure during thermal maturation. Fluid injection in wells and the production of hydrocarbons would also be enhanced by increasing the pore pressure. Faulting and earthquake-related phenomena associated with pore pressures along fault zones rich in clayey gouge and permeability data for such gouges (Morrow and Byerlee, 1984) would perhaps be interpreted differently if permeability increased with pore pressure in the

gouge.

Both the pore structures and distribution of clay and other secondary minerals in sandstones have been studied using electron microscopy by Simmons *et al.* (1982). These show great variability from on sandstone to another and complicate the comparison of measurements from one sample to another.

An additional aspect of these observations is the increased difficulty of predicting permeability in the earth if permeability values in rocks with clay are a function of both confining pressure as well as pore pressure. The interpretation of physical properties in the earth is aided by the general observation that differential or effective pressure determines values (Brace, 1972).

This paper examines the effect of pore pressure and confining pressure on permeability. Simple considerations of rock elasticity in response to confining pressure and pore pressure are used to show that differential pressure should determine permeability in rocks composed of silicates and other minerals of equally high intrinsic moduli. Experimental permeability data for two rocks, the Chelmsford granite and Berea sandstone, are presented and discussed. The observation is made that at least for the Berea sandstone the pore pressure effect is complicated by the presence in this rock of residual oil of natural origin, perhaps intimately associated with clays.

## ELASTICITY CONSIDERATIONS

A simple static linear elasticity analysis of pore volume and bulk volume strain indicates that the differential pressure, $\sigma - p$, should approximately determine the permeability of most intact rocks when both confining pressure $\sigma$ and pore pressure $p$ are variable. Assuming a functional relation or a set of

measured data for permeability as a function of confining pressure at constant pore pressure is assumed as a starting point, the question is how that functional relation or data will differ at some other pore pressure. Even though the data may vary in a highly nonlinear manner with pressure, the analysis indicates that because typical rock-forming minerals are so stiff and behave as a nearly linear solid the pore pressure can be viewed as a "neutral" pressure and the difference between pore and confining pressure as an "effective" pressure.

The analysis assumes that changes of pore fluid properties (compressibility, viscosity) in response to pore pressure are normalized through the calculation of permeability. In addition, experimental realities such as hysteresis of permeability measurements during pressure cycling are not dealt with. The strain analysis is describing pore and bulk volume strain of a linear, homogeneous solid under reversible conditions and with infinitesimal strain.

At any given combination of pore pressure $p$ and confining pressure $\sigma$ the strain response of a linear porous solid can be calculated by decomposing the stress field into two components. The first component is a uniform pressure $p$ both inside the pores and on the outside boundary of the sample. The second component is an external confining pressure $\sigma$ - $p$ on the entire outside boundary of the sample element, not distinguishing between pore and solid volumes.

The first component results in a uniform strain over every linear dimension, including pore space and solid, if the matrix material is homogeneous and isotropic. Isotropy of the overall solid as determined by the geometrical arrangement of pores is not necessary. The amount of strain is determined by the intrinsic bulk modulus $K_s$ of the matrix material. Because strain is uniform over every linear dimension the fractional decrease of pore volume and bulk

volume is the same and porosity, therefore, remains constant. Since it is the absolute dimension of pores which determines permeability, however, it is necessary to consider the intrinsic moduli of silicates. For $\alpha$-quartz this is about 0.37 Mb, and assume for the moment that quartz is perfectly isotropic. For a porous solid composed solely of this quartz an equal external and internal pressure of 1 kbar results in a reduction of about 0.1% over every linear dimension, calculated by inverting 0.37 Mb, dividing by three, and multiplying by 1 kbar. A crack 1 micron in diameter becomes 0.999 microns in diameter, and a crack 10 microns in diameter becomes 9.99 microns in diameter, independent of porosity. Even though permeability is strongly dependent on 3-dimensional pore dimensions the effect of 0.1% strain should be negligible because it is so small.

The second component of stress, $\sigma - p$, results in pore and crack closure in addition to solid matrix strain. Bulk strain is described by bulk modulus $K$. This second component of stress, the differential pressure, is what causes the permeability to change, and so it is seen as the "effective pressure". There is, however, no fundamental law which says that differential pressure should determine permeability. This is only an approximation because the moduli of silicates and other rock-forming minerals are so high.

There are several reasons and possible exceptions for why differential pressure may not determine permeability. Essentially, these revolve around the assumption of matrix homogeneity and matrix isotropy. If these conditions are not met there will be diverse contrasts of linear moduli within the porous aggregate and the uniform strain condition, which resulted from an equal external and internal pressure as discussed above, will not hold. Shear strains will occur wherever there is a contrast in linear moduli, and these shear strains could open (or close) cracks and pores such that bulk permeability changes. In realistic rocks the mineralogy is not homogeneous and isotropic. Linear moduli

volume is the same and porosity, therefore, remains constant. Since it is the absolute dimension of pores which determines permeability, however, it is necessary to consider the intrinsic moduli of silicates. For $\alpha$-quartz this is about 0.37 Mb, and assume for the moment that quartz is perfectly isotropic. For a porous solid composed solely of this quartz an equal external and internal pressure of 1 kbar results in a reduction of about 0.1% over every linear dimension, calculated by inverting 0.37 Mb, dividing by three, and multiplying by 1 kbar. A crack 1 micron in diameter becomes 0.999 microns in diameter, and a crack 10 microns in diameter becomes 9.99 microns in diameter, independent of porosity. Even though permeability is strongly dependent on 3-dimensional pore dimensions the effect of 0.1% strain should be negligible because it is so small.

The second component of stress, $\sigma$ - $p$, results in pore and crack closure in addition to solid matrix strain. Bulk strain is described by bulk modulus $K$. This second component of stress, the differential pressure, is what causes the permeability to change, and so it is seen as the "effective pressure". There is, however, no fundamental law which says that differential pressure should determine permeability. This is only an approximation because the moduli of silicates and other rock-forming minerals are so high.

There are several reasons and possible exceptions for why differential pressure may not determine permeability. Essentially, these revolve around the assumption of matrix homogeneity and matrix isotropy. If these conditions are not met there will be diverse contrasts of linear moduli within the porous aggregate and the uniform strain condition, which resulted from an equal external and internal pressure as discussed above, will not hold. Shear strains will occur wherever there is a contrast in linear moduli, and these shear strains could open (or close) cracks and pores such that bulk permeability changes. In realistic rocks the mineralogy is not homogeneous and isotropic. Linear moduli

in the minerals of a granite may vary by over 100%. In addition, moduli may be lower for grains with substantial occluded porosity, which is perhaps the case for the plagioclase grains full of micropores noted by Montgomery and Brace (1974). More compliant phases preferentially located may seriously violate the uniform strain conclusion above. This is the essence of the compressible clay model proposed by Zoback and Byerlee (1975) for the sandstones, that a hidden secondary phase exists in the pore spaces. External bulk strain due to an equal internal and external pressure, such as for an unjacketed stress-strain experiment, would be smaller than internal pore strain in response to the pressure. Consequently, permeability would be larger at the higher pore pressures.

The possibility of matrix inhomogeneity and anisotropy were included in the static linear elasticity treatment by Biot (1973), Brown and Korringa (1975), and Rice and Cleary (1976) by the definition of a new compressibility (using the $\kappa_\varphi$ notation of Brown and Korringa, 1975):

$$\kappa_\varphi = -\frac{1}{v_\varphi}\left(\frac{\partial v_\varphi}{\partial p}\right)_{p_d},$$

where $v_\varphi$ is pore volume, $p$ is pore pressure, and $p_d$ is differential pressure, $\sigma - p$. This defines the compressibility of the pore volume, normalized to itself, as a function of pressure at constant differential pressure. Referring back to the first component of stress in the previous analysis it was stated that, for a perfectly homogeneous and isotropic matrix, the amount of strain would be determined by the intrinsic modulus $K_s$. Therefore, the compressibility $\kappa_\varphi$ would equal $1/K_s$ if this were true. Otherwise, $\kappa_\varphi$ represents how pore volume changes in response to constant differential pressure because of matrix inhomogeneity and matrix anisotropy. Brown and Korringa (1975) consider several possibilities for both a random inhomogeneous aggregate and a preferentially located

compliant phase. If there is a compliant phase within the sandstones this would mean $\kappa_\phi < 1/K_s$, but to actually measure this directly by monitoring pore volume and bulk volume changes would be difficult. Permeability is a much more sensitive indication. Similarly, in the next section the permeability of a granite is tested to find out if differential pressure determines permeability. If it does not one must conclude that $\kappa_\phi \neq 1/K_s$ or else that some other experimental artifacts, such as hysteresis, are present.

Since clays have been used to explain the observations of anomalous pore pressure dependence in sandstones it is worthwhile to consider the elastic response of clays. Clay aggregates are very compressible under some conditions; individual clay particles are silicates and have similar intrinsic bulk moduli. In a compression test on soils when the pore fluid is allowed to escape, as in a drained and jacketed test, measured compressibility and strain will be very large. In a compression test where the source of stress is pore pressure, and the sample under test is unjacketed, the overall bulk strain is very small, inverse to the intrinsic bulk modulus of the solid phase. This is true if the pore fluid is fully equilibrated throughout the clay aggregate. The Zoback and Byerlee model for clays lining the pore spaces of a sandstone is the equivalent of an "unjacketed" test, if the pore fluid freely infiltrates the pore phase. The result of an increase in pore pressure is not to compress the clays in the manner of a jacketed compression test, but to reduce the size of the clay aggregate proportional to the intrinsic compressibility.

This point is summed up in a table of intrinsic ($C_s$) to bulk (C) compressibility ratios for various geologic materials taken from Skempton (1960) and shown in Fig. 3-4. Values of $C_s$ are all about the same for rocks, soils, and muds dominated by silicates. Bulk compressibility values for soils and muds are much larger because of the loose distribution of silicate particles in these

materials. If the source of stress in either rock or clays is pore pressure, the overall bulk strain and pore volume strain will be about the same.

Because the intrinsic bulk moduli are similar between clays and granites, one would predict that the permeability through both materials should be determined by differential pressure, even though the porosity of both are so different. In the next section experimental evidence for this is presented for a granite. Such evidence also exists for pure clays at high pressures. Morin (1982) measured the permeabilities of unconsolidated sediments and clays as a function of pore pressure. His data are reproduced in Fig. 3-5. The permeability data (coefficient of permeability) in this plot was collected by passing seawater through slugs of ocean-bottom clays that were contained in a stainless steel sleeve. Permeability was measured versus changes in hydrostatic pressure $p$ in an unjacketed test as the steel sleeve only held the muds together in a cylinder. As can be seen from Fig. 3-5 permeability change with pressure is very small for the oozes, smectite, and illite, particularly when looking at the actual data points instead of the drawn line. The lack of significant and consistent pressure dependence in the permeability data of Fig. 3-5 indicates that fully saturated clays are not compressible in response to pore pressure in a manner which increases permeability. The experimental setup of a steel cyclinder holding the clays in these experiments essentially mimics a similar situation as in the clayey sandstones, where instead of steel there are quartz grains. In addition to the negligible permeability change there was no measurable strain of the clay slug as the pore pressure was changed (Morin, personal communication), again indicating that the overall strain was the strain of each individual silicate or calcite mineral in response to pore pressure. The measurement of this strain was below the resolution of the experimental system in this case.

## LABORATORY OBSERVATIONS - CHELMSFORD GRANITE

The permeability of a sample of Chelmsford granite was measured as a function of systematically varied confining and pore pressure for the purpose of testing whether or not differential pressure determined permeability. Coyner *et al.* (1979) measured the permeabilities of several granites as a function of confining pressure at constant pore pressure and found that the permeability of Chelmsford granite, parallel to the rift direction, was comparitively high and also decreased dramatically with increasing confining pressure. Because of the large range of permeability as a function of pressure this granite would be quite sensitive to deviations from the differential pressure. It also is inhomogeneous with an abundant divergence of mineral phases, as described in Appendix B of this thesis. Therefore, in addition, Chelmsford granite is a good choice with which to test whether or not contrasting linear moduli for the different minerals will affect permeability at constant differential pressure.

The permeability test of Chelmsford granite was based on the transient technique of Brace *et al.* (1968). Nitrogen was used as the pore fluid in the experiments for three reasons: 1) low viscosity, vastly decreasing the time needed for a permeability transient test from hours to minutes, 2) large compressibility, so that pore pressure equilibration after a confining pressure or pore pressure change was rapid, and 3) no pore fluid/solid chemical interactions.

A diagram of the experimental arrangement is shown in Fig. 3-6. The precisely ground, cylindrical Chelmsford granite core was 7.5 cm in diameter and 5 cm long, acetone washed and vacuum dried at 60 degrees C several times. The sample was located between two cylindrical titanium holders and jacketed with a polyurethane compound. Radial and concentric grooves on the titanium faces

distributed pore fluid across the ends of the sample. Pore fluid tubing from the lower titanium holder connected to a lower reservoir and one port of a differential pressure transducer. Tubing exiting through the top of the pressure vessel went to a small reservoir, a regulated nitrogen pressure tank, and a vacuum pump. Hydrostatic confining pressure was generated by pumped kerosene. Pore pressure came from the regulated nitrogen gas tank.

The experimental procedure was designed to avoid hysteresis in the measurements introduced by systematics in the cycling of pore and confining pressures. Similar procedures can be found in Chapters 2 and 4 for strain and velocity measurements. The cardinal rule in comparing measurements at different levels of pore and confining pressures, differential pressure being constant, is not to subject the rock sample to an immediately previous higher differential pressure than the one at which the comparison is being made. To do so will result in permeability values which are a function of the previously higher differential pressure in addition to the present differential pressure. For example, consider a sample which gives a repeatable set of permeability measurements as a function of cycled confining pressure. Some hysteresis will occur as confining pressure is lowered, resulting in lower permeability values, how much lower being determined by the rate at which pressure is lowered in addition to characteristics of the rock. For a granite the important characteristics are the number, interconnectedness, and inelasticity of the cracks through which pressure in the pore fluid is transported. At zero pressure assume that enough time is allowed for the pore system to fully recover from the pressure history and that another cycle will give repeatable measurements. If confining pressure is cycled upward with pore pressure at 1 bar the permeability measured at 501 bars will correspond to a measurement at a differential pressure of 500 bars. If a permeability measurement is desired at a similar

differential pressure, but with pore pressure at 300 bars, the order in which pore and confining pressures are applied will affect the measurement. Starting from zero for both pressures, if confining pressure is first raised to 800 bars, followed by pore pressure to 300 bars, there will have been a previously higher differential pressure of 800 bars applied to the sample when confining pressure was initially raised. The subsequent introduction of pore pressure to 300 bars will not fully restore porosity to that present when the confining pressure was 501 bars and the pore pressure 1 bar because of hysteresis. The permeability measured will be lower. If, on the other hand, starting from zero pressure, confining and pore pressures are simultaneously raised to 300 bars, after which confining pressure is raised to 800 bars, the sample will never have experienced a differential pressure in excess of 500 bars. By analogy the sample is placed fully equilibrated into an ocean of pore fluid at a depth corresponding to 300 bars, after which the porosity is isolated and confining pressure is raised to 800 bars while pore pressure remains constant. Following this procedure avoids the systematic introduction of hysteresis into the measurements, and comparison of the permeabilities at the two levels of pressures, where differential pressure remains constant, should exclude effects due to hysteresis. This is the ideal which was strived for in these experiments.

Similar observations of cycled confining and pore pressures and the introduction of hysteresis into velocity measurements may be found in the data of Banthia *et al.* (1964) as discussed and interpreted by Gardner *et al.* (1965). In velocity measurements the nature of pore strain hysteresis is such that velocities are higher as pressure is removed as opposed to lower permeabilities.

Before the actual permeability experiment, confining pressure was cycled up to 1 kbar 3 times. A vacuum of 20 $\mu$m Hg was pulled throughout the pore fluid tubing system and sample for 2 days while confining pressure was kept at about

15 bars. Confining pressure and pore pressure were alternately raised in approximately 30 bar increments to a confining pressure of 102 bars and a nitrogen pore pressure of 100 bars. Confining pressure was then incrementalized in steps upward to a maximum 1000 bars while pore pressure was maintained at 100 bars. At each step permeability was measured by the transient technique. A small pulse of nitrogen pressure, about 2-3 bars above ambient, was introduced at one end of the sample with a valve and nitrogen tank regulator at time zero for the measurement. The decay of pressure across the sample with time was monitored with the differential pressure transducer and recorded on a strip chart recorder.

This procedure was repeated for a pore pressure of 300 bars nitrogen after letting the sample set at 15 bars confining pressure and vacuum pore pressure for about 24 hours after the experiment at 100 bars pore pressure. Confining pressure was raised to 302 bars and pore pressure to 300 bars, incrementally raising each in steps so as to prevent the differential pressure from exceeding 30 bars. Permeability measurements with the transient technique were made at confining pressure increments chosen to give differential pressures equal to those in the 100 bar measurements.

Each measurement of pressure decay across the sample was plotted logarithmically with time. Linearity of the plots was excellent. Permeability was calculated from the slopes of these plots according to the solution for one-dimensional transient flow through a cylinder (Brace *et al.*, 1968):

$$k = \left(\frac{\alpha \mu L}{A}\right)\left(\frac{1}{\beta V_1} + \frac{1}{\beta V_2}\right)^{-1}$$

where $k$ is permeability, $\alpha$ is the decay slope from the plot, $\mu$ is fluid viscosity, $\beta$ is fluid compressibility, $V_1$ and $V_2$ are reservoir volumes at each end of the

sample, $A$ is cross-sectional area of the sample, and $L$ is length of the sample. The products $\beta V_1$ and $\beta V_2$ were measured directly with a screw-piston pressure generator in the reservoirs leading to each end of the sample with a solid aluminum sample loaded as the core.

All of the values necessary for the permeability calculation are accurate to within ±1%. Sample dimensions, decay slope, and the products $\beta V$ were directly measured with at least this accuracy. Nitrogen viscosity was taken from Stephens and Lucas (1979) and is accurate to ±1%. The temperature dependence of nitrogen viscosity is less than 1% over the several degrees that laboratory temperature varied about ambient. The calculated permeability values are accurate to approximately ±3% given the accuracy of the various parameters, or about the size of the symbols used in the plot of data.

The permeability data from these experiments are plotted in Fig. 3-7. Permeability is plotted on a logarithmic scale versus differential pressure for the two different pore pressures, 100 bars (open squares) and 300 bars (crosses). All data are taken from the increasing confining pressure cycle.

Clearly the permeability data are adequately following a differential pressure relation of the form $\sigma$ - $p$. At low differential pressures, less than 100 bars, the data have some scatter. This was found in several repeated experiments at the two pore pressures and reflect natural fluxuations in the measured permeabilities during different pressure cycles. There was not any systematic deviation for measurements at a given pore pressure, as indicated by the alternating values at 50 and 100 bars differential pressure in Fig. 3-7. Several reasons for the deviations include 1)flow of gas between the sample and jacket, 2) very rapid decay times, less than 30 seconds at 300 bars, probably include a thermal decay in addition to the fluid flow, and 3) hysteresis in crack

geometry from experiment to experiment. Permeability is dropping dramatically in the first few hundred bars of confining pressure as the interconnected cracks that dominate the nonlinear elastic response of low porosity crystalline granites (Brace, 1965) close. At differential pressures above 100 bars the data points practically fall on top of each other and there is no consistent trend within experimental error of any variation at the different pore pressures. From this data the conclusion is that differential pressure indeed determines permeability as can best be determined over the pressure range considered. The Chelmsford granite is an example of a rock where homogeneity and anisotropy of individual phases is large and yet there is no apparent deviation of measured permeabilities from the differential pressure. The elasticity analysis argues the same point, that the intrinsic moduli of minerals are so large that the differential pressure should determine permeability. The compressibility $k_\phi$ of Brown and Korringa (1975) is evidently not that different from $1/K_s$ to have a measurable effect on permeability in this rock over the pressure range studied.

## LABORATORY OBSERVATIONS - BEREA SANDSTONE

Two sets of permeability experiments were carried out on two core samples of Berea sandstone, both perpendicular to bedding, and both prepared from blocks collected at the Buckeye quarry near South Amherst, Ohio. The purpose was to investigate the pore pressure effect for this sandstone previously reported by Zoback and Byerlee (1975) and by Walls and Nur (1979). As became clear in the experiments this effect is quite small, difficult to measure, and perhaps transitory over several cycles of pressure. In addition, the water sensitivity of the Berea sandstone (Khilar and Fogler, 1983) and the presence of hydrocarbons complicates the permeability behavior. The first set of experiments to be described were made on a core freshly extracted from a block without any

vacuum drying or flushing. The second set, which actually preceded the first experiments in time, were on a core which was repeatedly flushed with acetone and benzene solvents and dried in a vacuum chamber with heat in order to remove hydrocarbons.

Because Berea sandstone is much more permeable than the granite previously discussed a constant flow technique was used to measure permeability. The experimental arrangement for this technique utilized various accessory equpiment included in the basic high pressure design shown schematically in Fig. 3-6. The cylindrical sample, porous spacer discs, and titanium endpieces were jacketed and located in the pressure vessel as previously with the granite. A high pressure, double-headed, positive displacement, metering pump was used to circulate the pore fluid in a continuous loop through the sample. Bladder accumulators were used to dampen out pulses created by the strokes of the metering pump. A differential pressure transducer was used to continuously monitor the pore pressure difference between the ends of the sample. Output of the transducer was recorded with a strip chart recorder. Flow rate was determined by the stroke length and shaft diameters on the metering pump. Permeability was calculated according to Darcy's law.

The experimental procedure was as follows. The jacketed sample assembly was located in the pressure vessel and cycled three times to 600 bars. A vacuum was pulled throughout the pore fluid system, including the rock, for about 24 hours while confining pressure was held at about 15 bars. De-aired pore fluid, either the salt solution, distilled water, or kerosene, was then introduced from a reservoir connected near the base of the system, near the metering pump, and the pore fluid system including sample was saturated to the highest point where the vacuum was being pulled. The entire pore fluid system was flushed and

cleaned with suitable solvents between experiments with the water solutions and the kerosene. Confining pressure was raised to about 80 bars with the Haskell pump and pore pressure was raised to 50 bars with the flow to the metering pump arranged so that pore fluid from a pore fluid reservoir could be pumped up to pressure. When 50 bars of pore fluid pressure was reached the valves associated with the metering pump were switched so as to cut off the reservoir supply and to establish the continuous loop circulation. Stroke lengths on both heads of the pump were adjusted for an even flow with a pore pressure gradient of about 1 to 4 bars across the sample. Usually it was not necessary to adjust stroke length or to stop the pump. Confining pressure was incrementally raised to a maximum differential pressure of 600 bars for the experiments with kerosene, 400 bars for the experiments with water and salt solutions. Since permeability decreases only slightly with increasing differential pressure and the objective was to test for an increase in permeability at constant differential pressure it was not necessary to measure at higher confining pressures. At each step in confining pressure permeability was inversely proportional to the differential pressure transducer output. A reasonably constant pressure differential was reached in about 10 minutes after changing confining pressure, except for the measurements related to water sensitivity to be discussed. Essentially the only activity during the measurements at constant pore pressure was a raising and lowering of confining pressure. Pumping rate and pore pressure remained constant and changes in differential pressure reflected changes in permeability.

Confining pressure was raised up to the maximum differential pressure desired and then lowered again. These cycles of confining pressure at each pore pressure were repeated at least 3 times to judge hysteresis and reproducibility of the data. After the cycles of confining pressure for the 50 bar pore pressure

measurements the confining pressure was kept slightly above 100 bars while the pore pressure was raised to 100 bars. Pore pressure was increased simply by adding nitrogen gas from a regulated tank to the gas side of the bladder accumulators. This could be done while the metering pump continued to circulate pore fluid. The cycle of confining pressure was repeated and permeability measured for the same set of differential pressures as with the 50 bar measurements. In a similar manner this procedure was repeated for pore pressures of 150, 200, and 250 bars. In the following discussion this entire measurement process, including all of the individual cycles of confining pressure at constant pore pressure, *e* all of the measurements at different pore pressures, will be referred to as a "cycle." Each cycle required about 20 hours to complete. After each cycle the pore pressure was released to zero and the confining pressure left at about 15 bars for at least 12 hours. Before the next cycle a vacuum was pulled on the pore fluid to remove any air which might have infiltrated the pore fluid system.

The first set of experiments involved a single Berea sandstone core for which permeability was alternately measured with 50,000 ppm NaCl solution, distilled water, and then the saline solution again. Measurements with the saline solution as a function of systematically varied confining and pore pressure were made first, following the described procedure. Over the first cycle of pressures the pore pressure effect, an increase in permeability at higher pore pressures with constant differential pressure, was observed. These data are shown in Fig. 3-8 where measured permeability in milli-Darcys is plotted versus differential pressure at the various pore pressures from 50 bars up to 250 bars. The approximate error in these measurements is ±2 mD, due to small irreproducibilities and hysteresis in the calculated permeabilities as confining pressure was raised and lowered. Hysteresis typically resulted in calculated

permeabilities drifting downward by about 2 mD over the time confining pressure was cycled at constant pore pressure. The reported permeabilities represent an average of two measurements which tends to negate this hysteresis for measurements at any given pore pressure.

As can be seen in the data of Fig. 3-8 the decrease in permeability with increasing differential pressure at any given pore pressure is about 8 mD or less between 0 and 500 bars differential pressure. At any constant differential pressure, however, the permeability increases as the pore pressure increases. This is the effect previously observed by Zoback and Byerlee (1975) and by Walls and Nur (1979). The increase in permeability is fairly linear with increasing pore pressure except between the 200 and 250 bar pore pressure measurements, which are closer together than any of the other sets of adjacent pore pressure data. At a differential pressure of 300 bars, for example, the permeability increases by about 12 mD between the measurement at 50 bars pore pressure and 200 bars pore pressure. This correlates quite well with the approximately 11 mD increase measured by Zoback and Byerlee (1975) shown in Fig. 3-1. This is somewhat larger than the 8 mD increase measured by Walls and Nur (1979) over a 200 bar pore pressure range at a differential pressure of 50 bars which can be seen in Fig. 3-3.

As defined, one cycle refers all of the variations in pressure required to cover all of the increments in pore pressure. After the first cycle, the observed increase in permeability at constant differential pressure decreased. In Fig. 3-9 is shown the data for the second complete cycle. There is still an increase in permeabilities at a constant differential pressure, but the effect is much reduced. The data at 250 bars pore pressure are consistently higher than data at the other pore pressures, and the data at 200 just barely so, but within experimental error the values at lower pore pressures are following the

differential pressure as nearly as can be determined. The third cycle, shown in Fig. 3-10, has more deviation that is basically on the level of irreproducibility of the data. The 50 bar pore pressure values are lower than the rest, but the 100 bar values are the highest, while the rest fall in between. This scatter is about the error limits on the data, and although there may be an effect, it is much smaller than that initially observed in the first cycle data (Fig. 3-8), and cannot be clearly discerned.

After these three cycles were completed the saline solution was replaced with fresh distilled water. The data reflected the water sensitivity of Berea sandstone as investigated by Khilar and Fogler (1983). Distilled water from the supply reservoir was pumped through the sample, still under a confining pressure of about 50 bars, to purge the sample of the saline solution. Approximately 5 liters of distilled water were pumped through the core. Subsequently, the intention was to make permeability measurements with distilled water at the various pore and confining pressures. Immediately, however, it was found that the permeability was drastically reduced to levels on the order of 3 to 5 milli-Darcys. The differential pore pressure measured across the sample ends drifted upwards, or towards decreasing permeabilities, over periods of time on the order of hours and was very sensitive to stops and starts of the metering pump. Difficulties in getting reproducible measurements as a function of constant differential pressure at different levels of pressures were so great as to be inconclusive. At one point the sample was removed from the pressure vessel, dried at about 60 degrees C, rejacketed and replaced in the vessel with the same flow direction as before. It was found that permeabilities had not changed significantly and drifted in the range of 3 to 5 mD. If there is a dependence of permeability on distilled water pore pressure it is less than 2 mD over the range of pore pressures from 50 to 250 bars, which is about the

experimental error shown in Fig. 3-10.

After measurements with distilled water the pore fluid was purged and replaced with the saline solution once again. Permeabilities rose to between 12 and 15 mD, drifting with time, but not as much as with the distilled water measurements, and continued to be sensitive to stops and starts of the circulating flow. In order to obtain consistent results the cycling of confining pressure at constant pore pressure was stopped and measurements were made only at a constant differential pressure of 50 bars with a modified procedure. After measuring at 50 bars pore pressure and 100 bars confining pressure the two pressures were incrementally raised in 25 bar steps upwards to 100 bars pore pressure and 150 bars confining pressure as the metering pump continued to circulate pore fluid. The strategy was to minimize as much as possible any "shock" to the system perhaps caused by rapidly changing pressures or stopping and starting the metering pump. The observed pore pressure differential settled to a constant value relatively rapidly, within 5 minutes, but about 30 minutes was allowed before the measurement was considered completed. The procedure of slowly incrementing pressures and measuring the pore pressure differential across the sample at a differential pressure of 50 bars was continued up until 200 bars pore pressure, 250 bars confining pressure. The permeabilities calculated at each of the pore pressures for a constant differential pressure of 50 bars are: 13.4 mD at 50 bars, 13.5 mD at 100 bars, 13.7 mD at 150 bars, and 13.8 mD at 200 bars, all accurate to about ±0.15 mD. There is a trend towards higher permeabilities at the higher pore pressures but it is exceedingly small and borders on the negligible.

The difficulties with the distilled water permeability measurements and the differences between permeabilities measured with distilled water and saline solution reflect the water sensitivity of Berea sandstone. Jones and Owens (1979)

noted that this water sensitivity meant that permeabilities measured with brine would be 50% less than those measured with gas, and that those measured with distilled water would be 99% less. Khilar and Fogler (1983) fully investigated this behavior for Berea sandstone for different salinities, flow rates, directions of flow, and thicknesses of core samples. They found that rapid drops in permeabilities occurred at NaCl concentrations less than about 4000 ppm. The large drop in permeability upon introduction of distilled water, which they term "water shock", could be partially restored by replacing the fluid with saline solution and resversing the flow direction. The physical model they developed is that clay particles go into suspension in the lower salinity and distilled water pore fluids and mechanically block narrower pore throats, reducing permeability. Reversal of flow with distilled water unblocks these throats but continued reverse flow causes the same particles to block pore throats in the opposite direction. Reversed flow with highly saline solution, however, allows the clays to flocculate and attach to the pore wall, thereby restoring for the most part the initial permeability.

In addition to the water sensitivity, an aspect of Berea sandstone which complicates the measurement and interpretation of permeabilities is the presence of small quantities of natural hydrocarbons in the pore space. These hydrocarbons possibly contribute to the observed pore pressure effect. Preliminary benchtop flow tests with a simple gravity feed system using water and acetone pore fluids revealed that acetone initially exiting from Berea samples had a deep reddish-brown color. The color disappeared within several repeated flushings with an amount of acetone equal to approximately 2 to 3 pore volumes of the Berea core. Cores of Berea sandstone prepared from samples collected at the Buckeye quarry in South Amherst, Ohio, those supplied by Chevron Oil Company, and a block from J. Byerlee's lab at the U.S.G.S., all gave

the same result: a reddish- brown elutant during initial acetone flush. Distillation and evaporation of the acetone elutant left an oily, sticky reddish-brown residue.

A gas chromatography analysis of the residue indicated that hydrocarbon was being flushed from the sandstone. In Fig. 3-11 is shown a gas chromatogram of the residue dissolved in pentane made over the temperature range from 50 to 220 degrees C. The labelled peaks in the chromatogram correspond to different normal- paraffins extending from $n$-$C_{10}$ up to $n$-$C_{18}$. These were identified by making chromatograms of pure dodecane and octodecane. This analysis is not intended to be a thorough characterization of the hydrocarbon content of Berea sandstone and should not be interpreted as such. It does indicate, however, that the substance dissolved and flushed with acetone from the core samples was indeed a hydrocarbon.

The source of this hydrocarbon is probably the Ohio shale of Devonian age which stratigraphically underlies the Berea sandstone in Ohio. Newberry (1860), in one of the early works on petroleum geochemistry, described the production of oil from the Berea near Mecca, Ohio, and suggested that thermal metamorphism of the underlying organic-rich black shale was the source for the oil. A generalized stratigraphic column for Ohio is shown in Fig. 3-12. Note that the Berea sandstone is Upper Mississippian in age and that it occurs directly above the Ohio shale. To this day the Berea sandstone is one of the principal producers of oil and gas in the state of Ohio. An extensive geological investigation of the Berea sandstone and adjacent units is given in Pepper *et al.* (1954). An interesting photo in that paper (Fig. 19) shows a roadside outcrop of Berea sandstone, the basal 10 inches of which reportedly contains oil. In the area of the Buckeye quarry in South Amherst, Ohio, the Berea sandstone is a deltaic channel sandstone deposited from an ancient river which was carving

into the underlying shale. The organic-rich facies of the Devonian shale in the western half of the Appalachian basin in Ohio contain 5 - 15% volume percent organic material (Schmoker, 1980). Although through geologic time the shale has never been buried deeply enough for temperatures to reach that level necessary for substantial oil generation the shale is probably old enough to have sourced some oil in addition to gas.

It is worth noting from the data of Walls and Nur (1979) that the strongest pore pressure effect was measured in the Bandera, Berea, and Massillon sandstones. All of these rocks are from known oil-producing strata. The Massillon sandstone is from a quarry in Glenmont, Ohio, is probably Mississippian and syngenetic with the Berea, and is in any case above the same Devonian shale as is the Berea. The Bandera sandstone is from the Pennsylvanian Marmaton Group in southeast Kansas and is part of a thick section of oil and gas-producing formations.

Flushing the core samples with acetone had a measurable effect on the porosities of Berea sandstone. This indicates that the hydrocarbon either occupies or blocks a portion of the pore space in the sandstone when water is introduced as a saturant. This is if the effect of acetone on the mixed illite-kaolinite is not to rearrange the saturable pore space within the clays. clays In Table 1 is a list of measured porosities both before and after acetone flushing for a number of Berea sandstone samples including ones collected at the quarry as well as from J. Byerlee's U.S.G.S. laboratory (H & I) and from Chevron Oil Field Research Company (G). Porosity was measured by comparing vacuum-dry and water-saturated weighings of precisely ground cores nominally 7.62 cm in diameter by 5.08 cm long. Repeated weighings of dry and saturated samples indicated that porosity was precise to about 0.1%. The first column of porosities are those measured after initial preparation and the second column those

measured after repeated acetone flushes. The average measured porosity for all samples increased from 17.07% to 17.91% after the acetone flushings and, in addition, became more uniform. Either a fraction of the pore space is occupied by the oil or, more likely, the water-saturant is prevented from entering a proportion of the porosity blocked by the hydrocarbon. Dry weighings with a precision of ±0.05 g indicated that the weight of material flushed from the samples amounted to less than 0.1 g per 7.62 cm diameter by 5.08 cm long core.

Permeability measurements as a function of confining pressure and pore pressure were made on a Berea sample perpendicular to bedding which had been repeatedly flushed with acetone and dried to remove the hydrocarbons. In addition, the sample was soaked and flushed with benzene at pore pressures up to 300 bars in the pressure vessel in order to ensure that all hydrocarbons were removed. Kerosene was used as the pore fluid in these measurements to avoid the problem with water sensitivity. The viscosity of kerosene at atmospheric pressure is taken as 2.3 centi- Poise (Chemical Engineers Handbook, 1978). The initially described procedure of cycling confining pressure up and down for each of the pore pressures was followed.

The permeability data from these experiments are plotted in Fig. 3-13 versus differential pressure. All of the data points are from measurements collected on the increasing portion of the confining pressure cycle. The different symbols correspond to the various pore pressures at which permeabilities were measured. Because the dependence with pressure of the viscosity of kerosene is not well-constrained the error limits on this data are dominated by this uncertainty. Although the absolute value of viscosity is not important, the increase in viscosity with pressure is, and the increase of 0.003 Poise per bar is an approximate average for the different components which make up kerosene. The error bar shown in Fig. 3-13 covers the range from 0.002 up to 0.004, and the

corresponding permeabilities could fall, systematically, either higher or lower at constant differential pressure within these error bars. Nonetheless, if there are any increases or decreases they are very small, on the order of 2 mD or less, and certainly not as large as reported in Fig. 3-8. The dependence on differential pressure at constant pore pressure is small as seen in the previous data with saline solution. The absolute values of permeability, about 20 to 23 mD, are lower than those measured previously with the saline solution but the repeated cycles of flushing and drying have probably caused partial blockage of pore throats and therefore reduced permeability. More importantly, the increase in permeability with pore pressure at constant differential pressure is not seen. For this sample of Berea sandstone, flushed clear of hydrocarbons, differential pressure determines permeability as can best be determined to within experimental error.

It must be emphasized that the increase in permeability with pore pressure at constant differential pressure was only clearly observed over the first cycle of pressures. Subsequent cycles did not show the pore pressure effect to be clearly present, and therefore it may only be a transient effect.

There are several possibilities for a compliant secondary phase. It may be trapped gases, hydrocarbons, poorly understood clay structures, or any combination of these. The gases may be due to incomplete initial saturation of the porosity or else natural gases associated with the hydrocarbons. Certainly the presence of a small amount of gas, trapped within a combination of the clay and hydrocarbon phases, would result in a highly compliant mixture. Incomplete initial saturation is possible given the incredibly complex habits of clays in sandstones (Simmons *et al.*, 1982; Heaviside *et al.*, 1983), which could probably trap gases in some conditions. Zoback and Byerlee (1975) used a fairly viscous lubricating oil (about 20 centi-Poise at atmospheric pressure) in their measurements, and since the oil would not wet the surfaces of silicates the

possibility that saturation was incomplete must be considered. Difficulties in saturation would correlate with lower permeabilities and higher clay content and it is noted that in the data of Walls and Nur (1979) the largest pore pressure effect was measured in the least permeable sandstone with the highest clay content (Bandera sandstone).

Conceivably the hydrocarbon itself could be compliant enough to give rise to the observed pore pressure effect. Since the effect nearly disappeared in the measurements with saline solution on the fresh Berea core before removing the hydrocarbons, however, it may be that the hydrocarbons themselves are not the cause. Gases associated with the hydrocarbons could be the cause. The Berea is exposed at the surface and subject to water-washing and microbial degradation, both of which produce gas (Hunt, 1982). In addition, the Devonian shales produce gas which is probably intermixed with the hydrocarbons. The clays in Berea are authigenic (Tosoya and Nur, 1983) and there has probably been extensive fluid flow through the formation through geologic time. The Berea sandstone is sandwiched between two fairly impermeable shale formations and extends over a widespread area. As these adjacent shales compacted and expulsed fluids, perhaps including oil and gas, the migrating fluids could be partly responsible for the feldspar to clay reactions. Therefore it is possible that oil and gas migration was combined with the formation of the authigenic clays and that the two are intermixed. A formation similar to the Berea but buried deeper is the Strawn formation in Texas where similar reactions occur at present at depth (Land and Dutton, 1978).

Given the transient observation of the effect in this study it is possible that the first cycle of pressures essentially "squeezed" the compliant structures to the point that they were no longer compliant. The trapped gases may have been freed to dissolve into the pore fluid. A complex mixture of hydrocarbons and

clays may have been permanently strained such that its compliance was reduced or at least ceased to be important in later permeability measurements.

The mechanism by which the compliant phase causes the pore pressure effect is a function of its preferential location in the pore space. Because of the high compressibility in response to pore pressure either the absolute size of pores increases or else constricted pore throats which are immiscible to the pore fluid at low pressures are able to pass fluid at higher pressures.

An additional concern is the effect of a solvent like acetone on the clays when used to flush the hydrocarbons. The effect of various solvents on permeability of clays was studied experimentally by Mesri and Olsen (1971). The permeability of clays is a function of fluid-solid chemistry and kinetics. Dielectric constant of the pore fluid influences permeability of bulk clay samples because of flocculation and peptization. The large dielectric constant of a polar saturant such as water tends to satisfy surface charges on individual clays and and to disperse clay aggregates (peptization), forming many small flow channels and resulting in a relatively low permeability. In the experiments of Khilar and Fogler (1983) the dispersion of clays within a grain framework resulted in the blockage and constriction of flow passages. A nonpolar fluid with minimal dielectric constant, such as benzene, causes aggregates to form and results in a few relatively larger pore channels through which fluids flow and permeability is higher. The dielectric constant of acetone is about half that of water and so the effect on permeability would be somewhere between the effect due to distilled water and benzene. Permeability in these experiments, however, was not measured with acetone. Acetone (and benzene) were only used to flush samples free of hydrocarbons. Whether the clays particles rearrange themselves into the same structure after the acetone is driven off is not clear.

It must be emphasized that the pore pressure effect was observed with saline solution in this study, with lubricating oil by Zoback and Byerlee (1975), and with distilled water by Walls and Nur (1979). These different fluids represent end-members of the interaction effects with clays mentioned previously. That the pore pressure effect is recorded for the different pore fluids indicates that fluid-clay matrix interactions are not the dominating factor. In the measurements of Riepe *et al.* (1983) they used nitrogen as a pore fluid and consequently there is no fluid/solid chemistry at all although the fact that the samples are vacuum dry may perhaps have altered the clay morphology.

Since the pore pressure effect was only observed as a transient the experimental evidence in this study can only be considered tentative. Further experiments could be done on the Berea and Bandera sandstones since the effect has been observed to be strongest in these two rocks. Experiments with distilled water, however, would have to isolate the effects of water sensitivity from any observed effect of increasing pore pressure. Since the decrease in permeability with confining pressure is fairly small and complicates the procedure the recommended experimental design and procedure is to do an unjacketed test along the lines of that by Morin (1982), such that differential pressure remains at zero.

## CONCLUSIONS

Differential pressure, confining pressure minus pore pressure, should determine permeability in most intact geologic materials when the solid phase is composed of silicates or other minerals with equally high moduli. The elasticity considerations indicate that pore volume strain is very small when pore and confining pressures change equally and probably has a negligible influence on permeability. Hence, differential pressure should determine permeability. There

are, however, several possible exceptions. In the practical measurement of permeability there will be some hysteresis due to uneven pressure cycling and the irreversible strain response of pore space characteristic to the particular rock or structure. Hysteresis was specifically avoided in the experimental measurements in this paper in order to test for other effects. Exceptions could also occur when a highly compliant phase occupies preferred sites within the porous structure such that it is shielded from confining pressure carried at the grain to grain contacts or across any other type of porous discontinuity. A preferred site is one which will affect bulk permeability as the compliant phase responds to pore pressure. Alternatively, a very stiff phase could occupy a preferred site in a compliant framework. The compliant phase could be hydrocarbons, mineral waxes, other organic materials, trapped gases, or a mineral grain with a large amount of occluded porosity in the form of compliant shapes.

Another possible exception could be caused by large contrasts of linear moduli either because of anisotropy within a single phase or else because of an inhomogeneous mixture of multiple phases. In the experimental nitrogen permeability measurements of Chelmsford granite it was found that, at least between the two sets of data at 100 bars and 300 bars pore pressure, differential pressure determined the permeability of a rock which is very sensitive to pressure. Since the mineralogy and corresponding moduli of Chelmsford granite are quite diverse and anisotropic it is concluded that, at least over the pressure range studied, inhomogeneity and anisotropy are not significant enough to cause measured permeabilities to deviate from being determined by the differential pressure.

The anomalous pore pressure dependence of permeability in Berea sandstone observed by Zoback and Byerlee (1975) with oil and by Walls and Nur

(1979) with distilled water was also initially observed in measurements with a highly saline (50,000 ppm) NaCl solution. By the third cycle of variation of confining and pore pressures, however, the effect diminished and disappeared, and differential pressure determined permeability. The effect probably results from an isolated compliant phase within the pore space of the sandstone as suggested by Zoback and Byerlee (1975). Measurement of the effect and identification of the compliant phase is complicated by: 1) the water sensitivity of Berea sandstone and, 2) the presence of naturally occurring hydrocarbons in all samples of Berea sandstone collected for this study. The compliant phase may be the hydrocarbons themselves, trapped gases, either associated with the hydrocarbons *in-situ* or else caused by incomplete saturation in the laboratory, or mixtures of clay particles, hydrocarbons, and gases. The pore pressure effect on absolute permeability pales in comparison to the water sensitivity of Berea sandstone noted in the experiments with NaCl solution and distilled water and more thoroughly treated by Khilar and Fogler (1983).

**Table 1: Berea Sandstone Porosity**

| Sample | Initial $\varphi$ | After Acetone Flush |
|---|---|---|
| A | 16.94 | 17.66 |
| B | 17.27 | 17.75 |
| C | 17.21 | 17.83 |
| D | 16.46 | 17.84 |
| E | 17.61 | 18.03 |
| F | 16.75 | 18.02 |
| G | 16.95 | 17.83 |
| H | 17.14 | 18.17 |
| I | 17.32 | 18.10 |

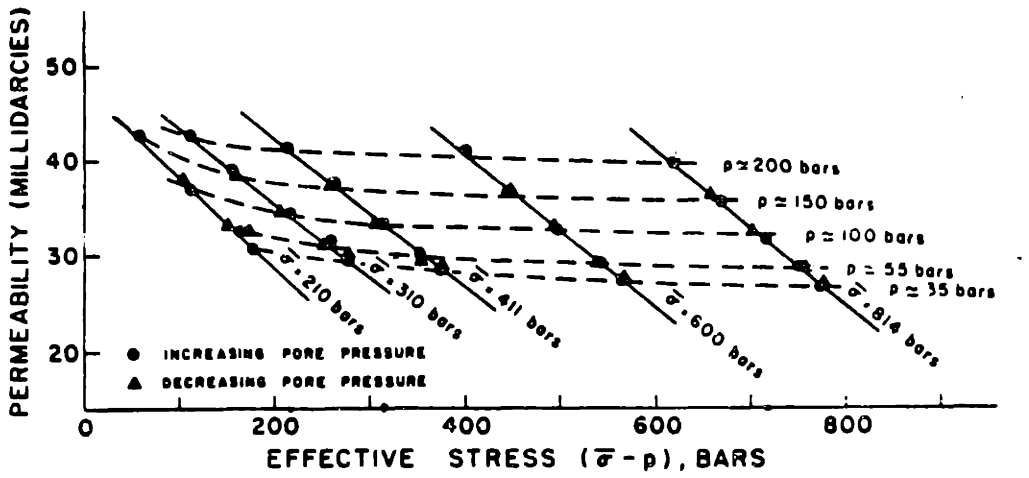


Permeability as function of effective stress ($\bar{\sigma}$ - p). Solid lines indicate equal confining pressure. Dashed lines indicate approximately equal pore pressure. Berea Sandstone; flow normal to bedding planes.

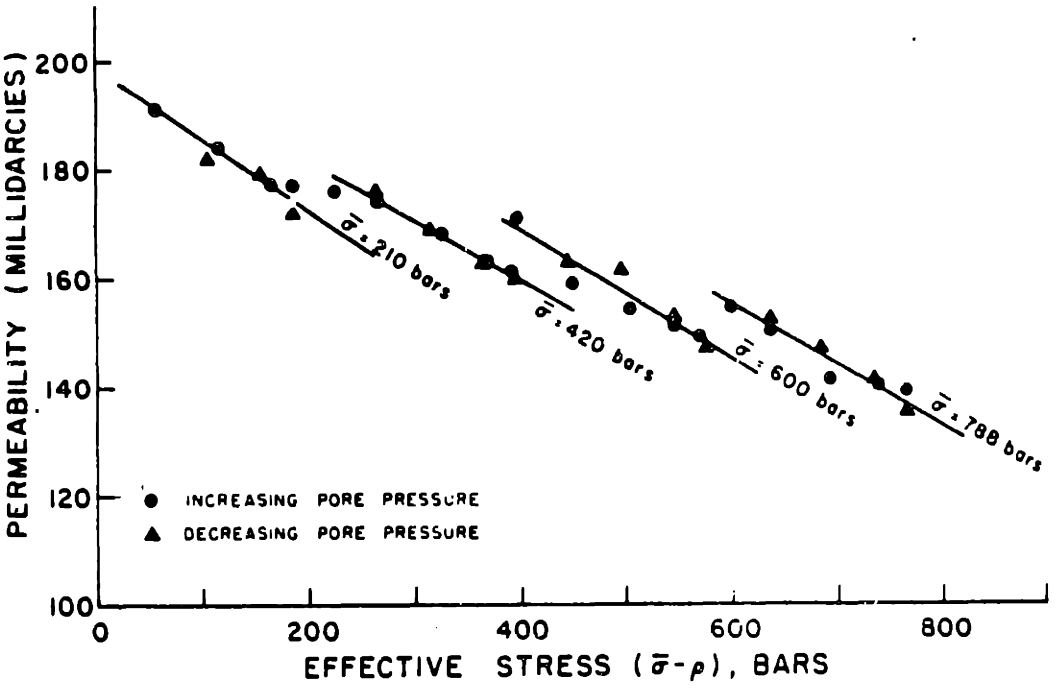


Permeability as function of effective stress ($\bar{\sigma}$ - p). Solid lines indicate equal confining pressure. Berea Sandstone; flow parallel with bedding planes

Figure 3-1. Anomalous pore pressure dependence for permeability of Berea sandstone measured perpendicular to bedding (top) and parallel with bedding (bottom) by Zoback and Byerlee (1975).

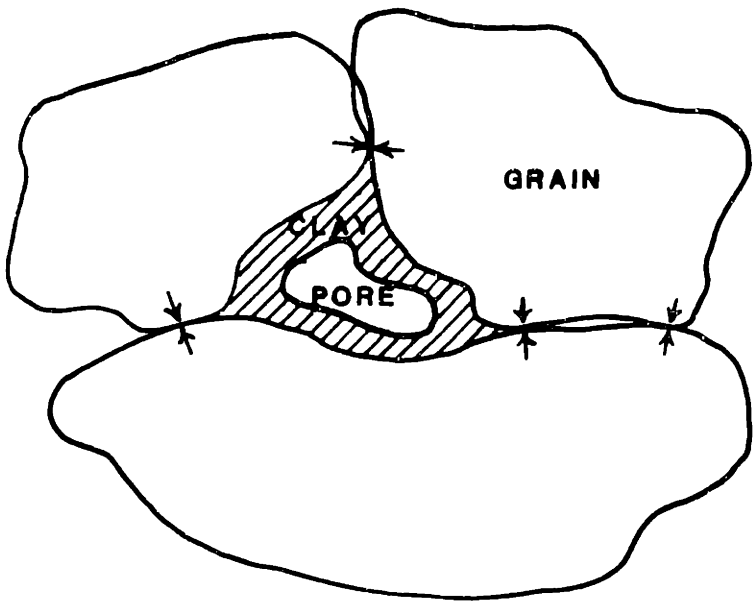


Figure 3-2. Conceptual model of pore space and rigid quartz grain frame proposed by Zoback and Byerlee (1975) to explain anomalous pore pressure dependence of permeability. The highly compressible pore filling material was suggested to be clay and accessory minerals; in this paper it is suggested that it might also include natural hydrocarbons or gases.

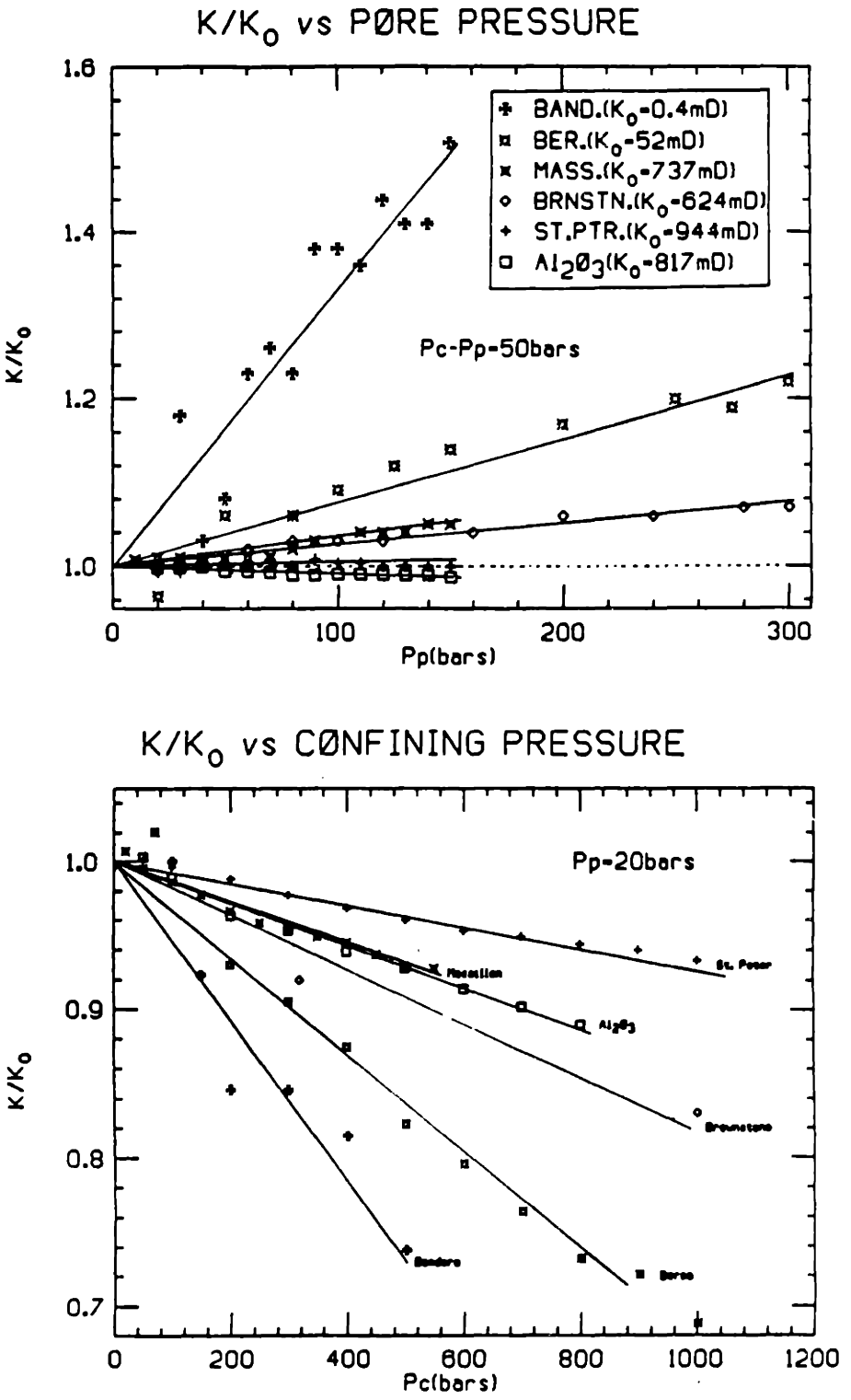


Figure 3-3. Data from Walls and Nur (1979) showing anomalous pore pressure dependence for a number of sandstones. The upper plot is permeability normalized to a value measured at zero pressure versus pore pressure for a number of sandstones and alundum with constant differential pressure (50 bars). The lower plot is permeability versus differential pressure at a constant pore pressure (20 bars).

**Compressibility Values for Soil, Rock, and Concrete**

| Material | Compressibility* per kN m$^2$ × $10^{-6}$ | | |
|---|---|---|---|
| | C | $C_s$ | $C_s/C$ |
| Quartzitic Sandstone | 0.059 | 0.027 | 0.46 |
| Quincy Granite (30 m deep) | 0.076 | 0.019 | 0.25 |
| Vermont marble | 0.18 | 0.014 | 0.08 |
| Concrete (approx.) | 0.20 | 0.025 | 0.12 |
| Dense sand | 18 | 0.028 | 0.0015 |
| Loose sand | 92 | 0.028 | 0.0003 |
| London clay (over cons.) | 75 | 0.020 | 0.00025 |
| Gosport clay (normally cons.) | 600 | 0.020 | 0.00003 |

* Compressibilities at $p$ = 98 kN m$^2$ (1 kgf/cm$^2$); Water $C_w$ = 0.49 × $10^{-6}$ per kN/m$^2$ (48 × $10^{-6}$ per kgf cm$^2$).
After Skempton (1960).

Figure 3-4. Table from Skempton (1960) showing the intrinsic or unjacketed compressibility $C_s$, the jacketed compresibility $C$, and the ratio of the two for various rocks ands soils. Note the similarity of intrinsic compressibilities for granite and clays. The unjacketed strain response of clay and granite would be nearly the same as indicated by the similarity of intrinsic compressibilities; the jacketed strain, however, would be much larger for the clay as shown by the value of $C$.

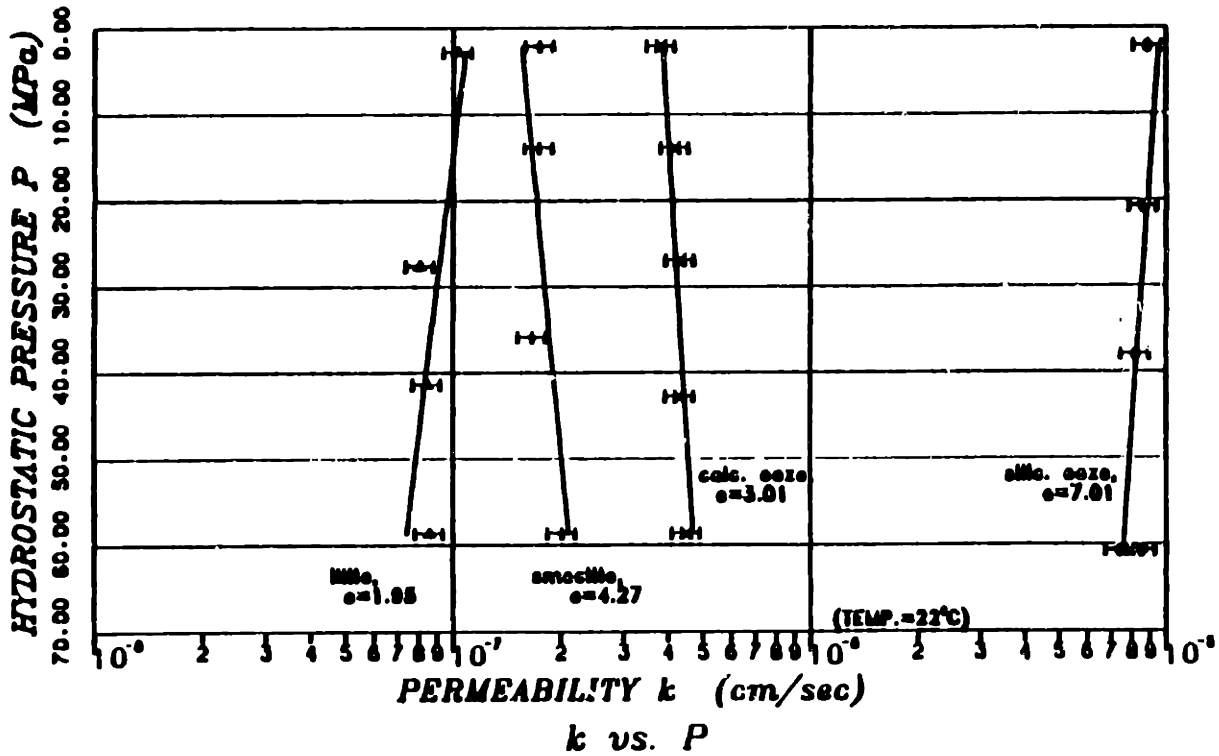


Figure 3-5. Coefficient of permeability of various clays and oozes measured as a function of pore pressure with seawater (from Morin, 1982).

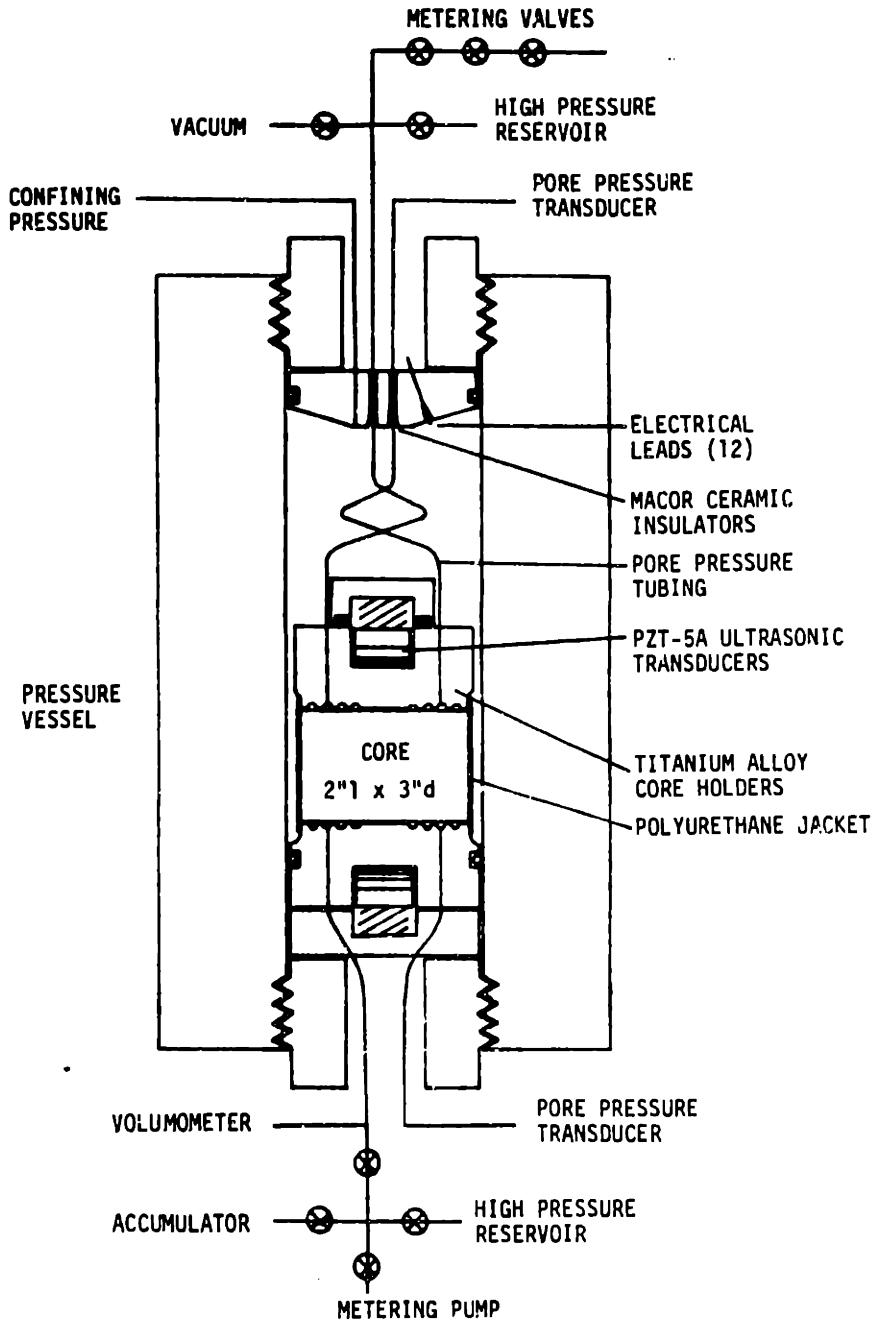


Figure 3-6. Experimental apparatus used to measure the permeability of Berea sandstone and Chelmsford granite as a function of confining pressure and pore pressure. Different arrangements of accesory equipment were used for transient tests and constant flow tests.

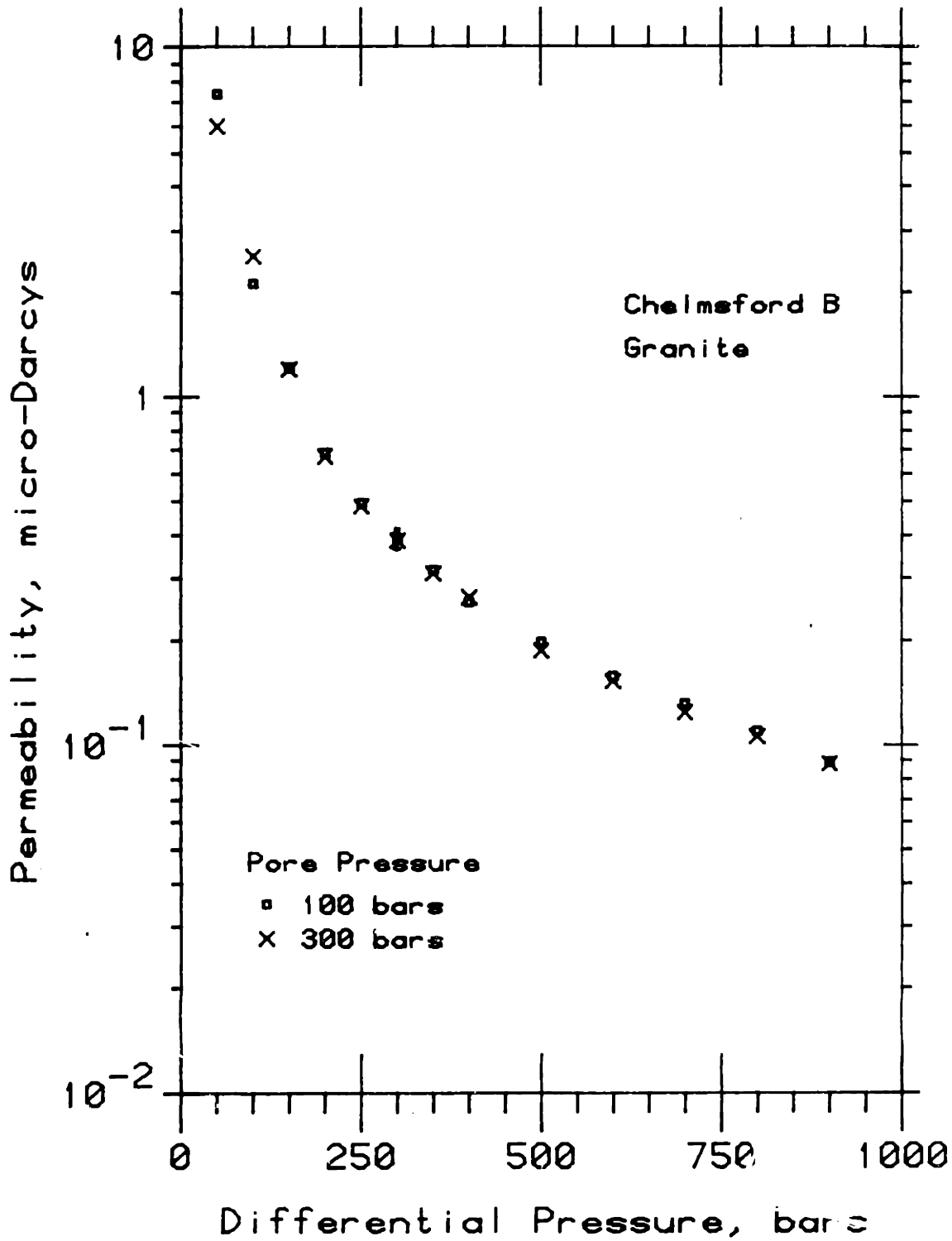


Figure 3-7. Permeability of Chelmsford granite as a function of differential pressure at nitrogen pore pressures of 100 and 300 bars. Length of bar indicates probable error.

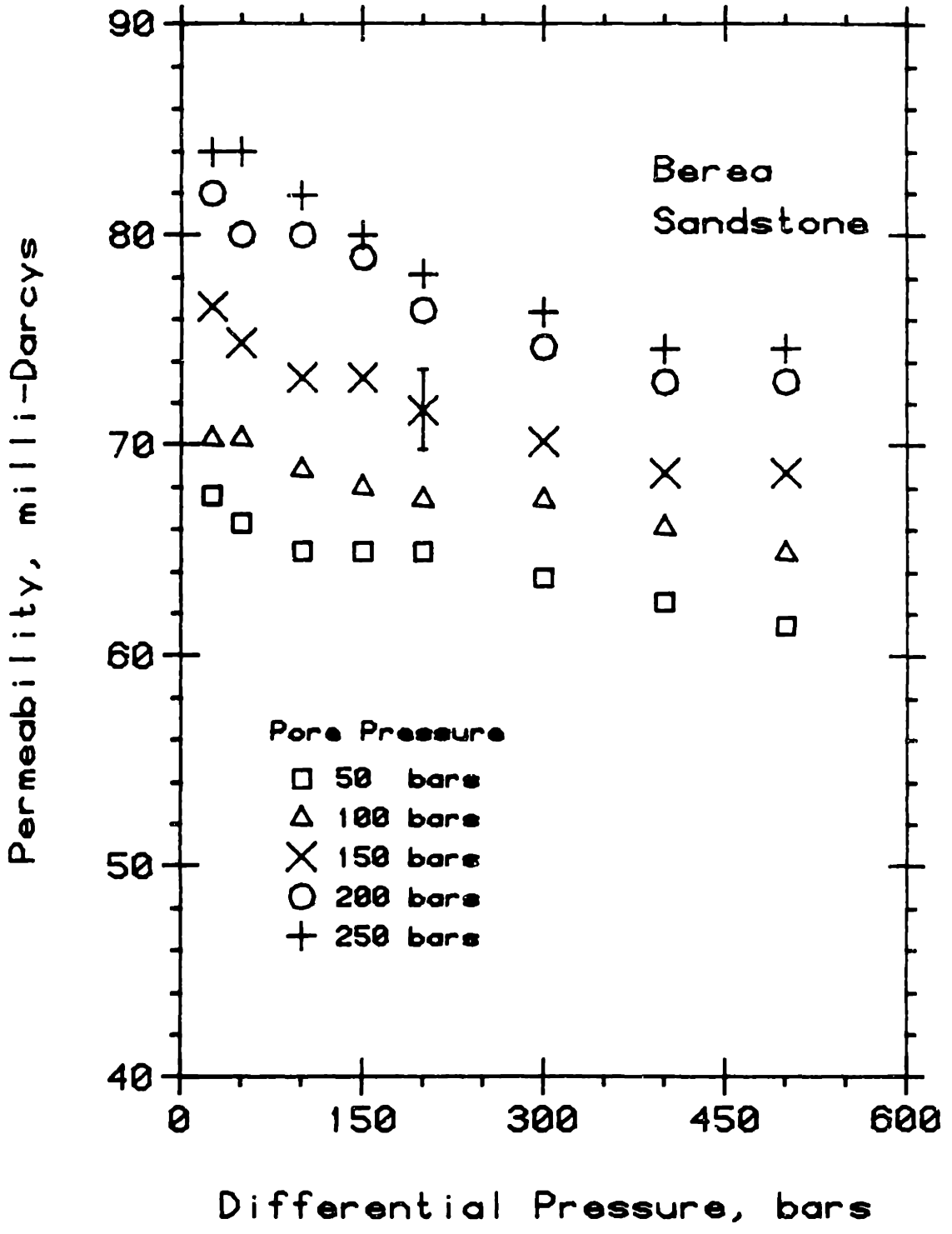


Figure 3-8. Permeability of Berea sandstone sample measured with saline solution (50,000 ppm NaCl) as a function of differential pressure at various pore pressures. Values are from the first cycle of variations of pore and confining pressures. Length of bar indicates probable error.

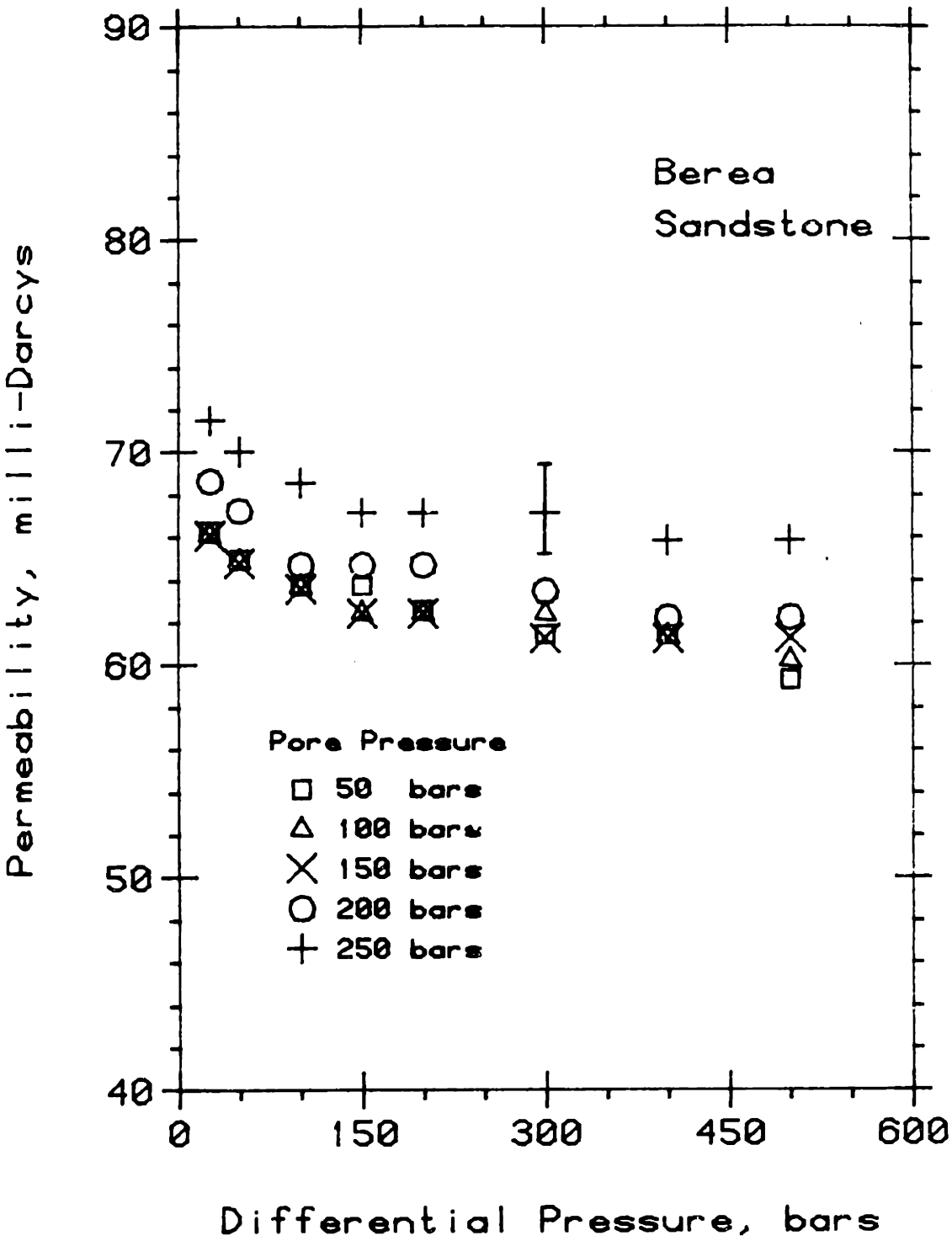


Figure 3-9. Permeability of Berea sandstone sample as a function of differential pressure at various saline solution pore pressures. Values are from the second cycle of variations of pore and confining pressures. Length of bar indicates probable error.

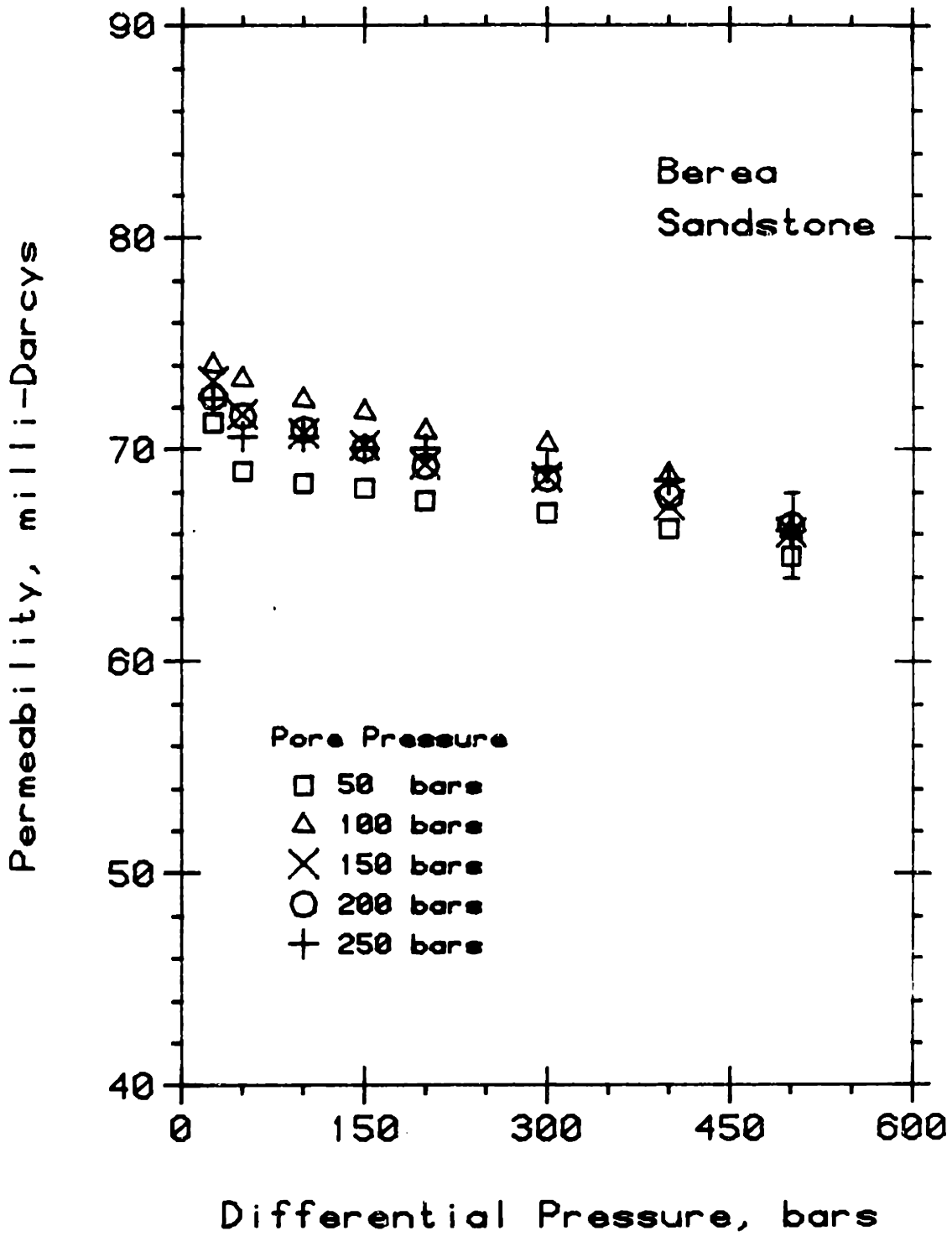


Figure 3-10. Permeability of Berea sandstone sample as a function of differential pressure at various saline solution pore pressures. Values are from the third cycle of variations of pore and confining pressures. Length of bar indicates probable error.

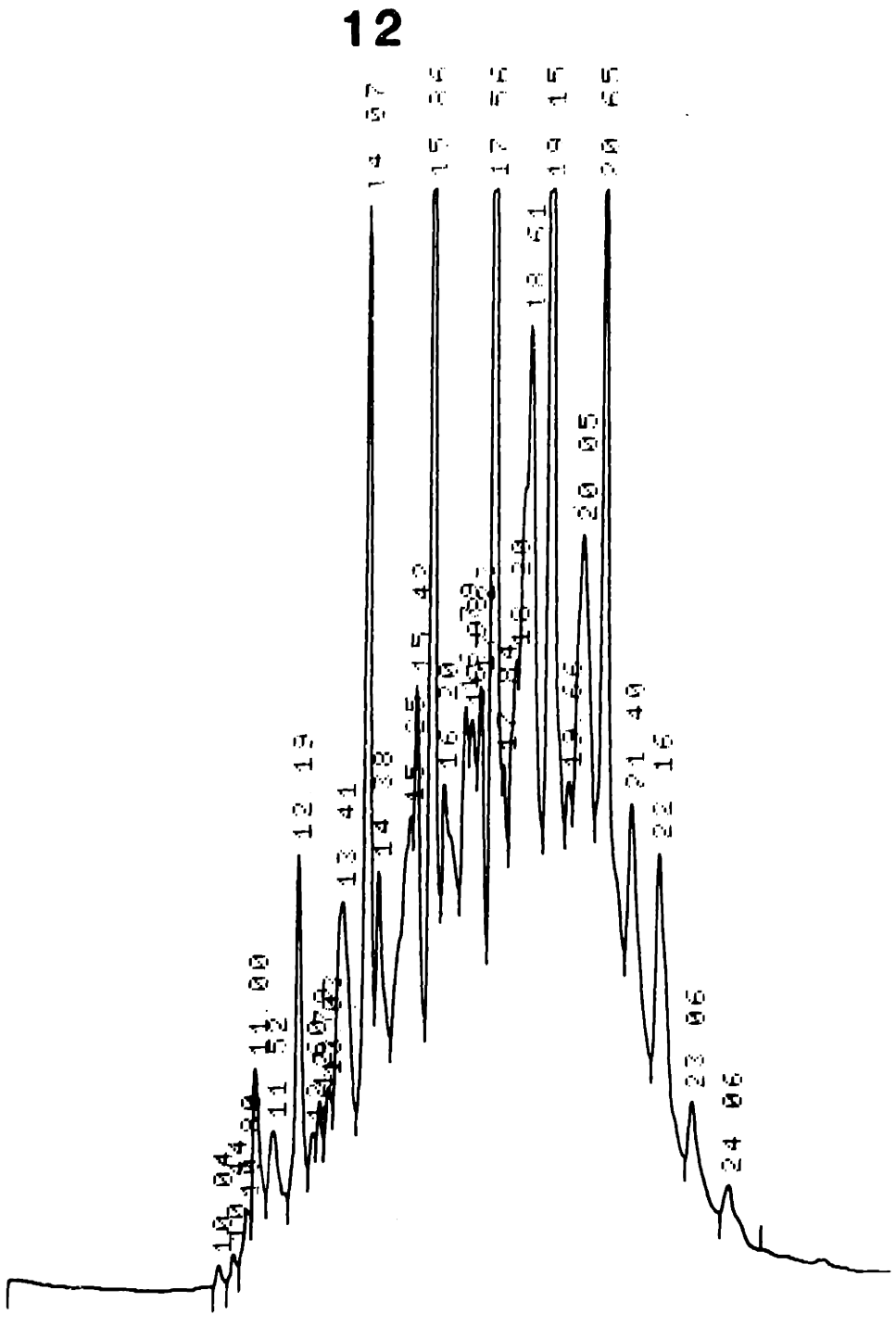


Figure 3-11. Gas chromatogram of hydrocarbon extracted with acetone from all samples of Berea sandstone. The peak labelled "12" is $C_{12}$ or dodecane. The regularly spaced peaks are the *n*-paraffins extending from $C_{10}$ at the left up to $C_{18}$ at the right.

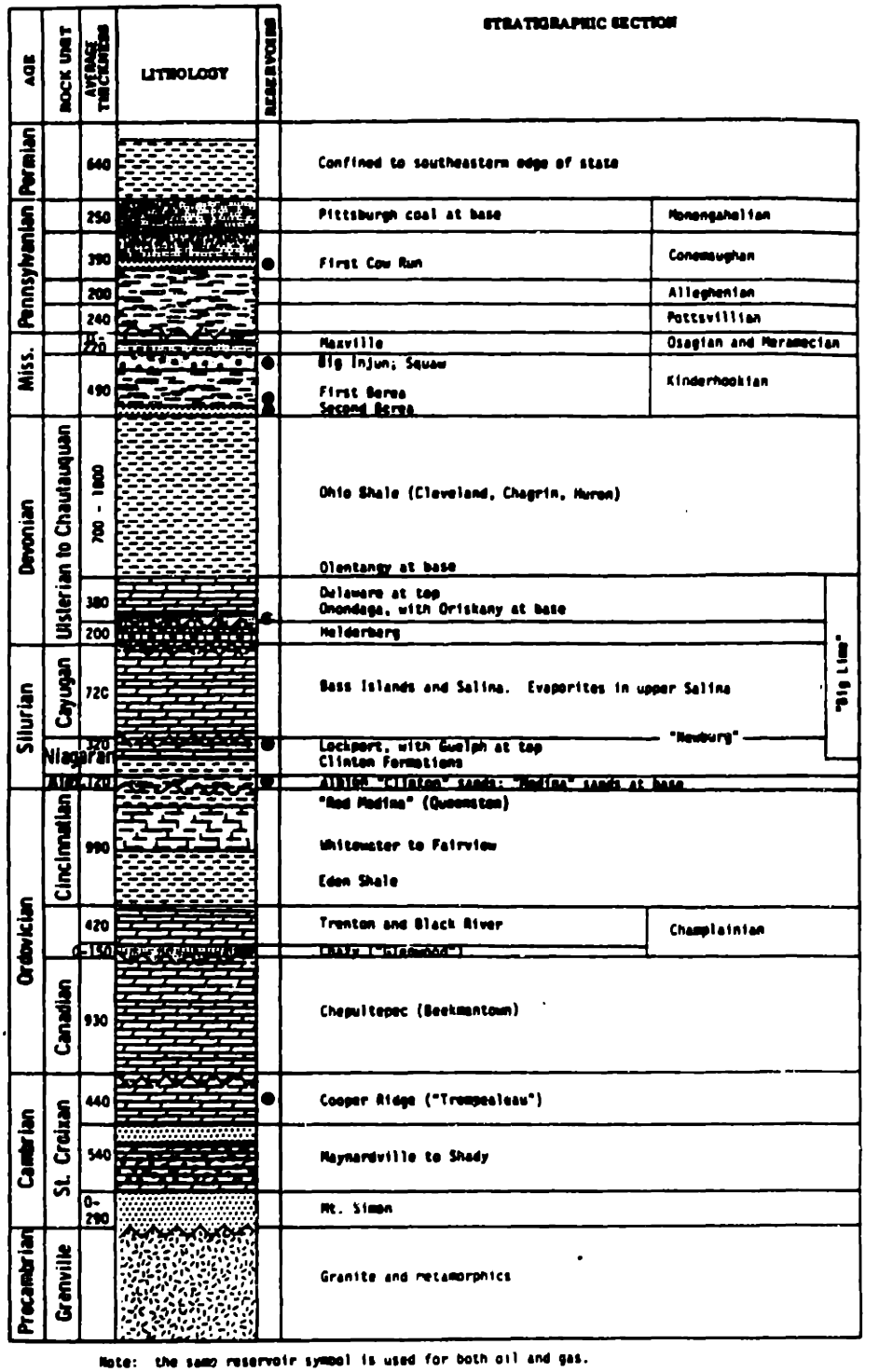


Figure 3-12. Stratigraphic column in Ohio showing the location of Berea sandstone directly above the organic-rich Ohio shale. Berea sandstone is a major producer of oil and gas in Ohio and the source rock is probably the Ohio shale.

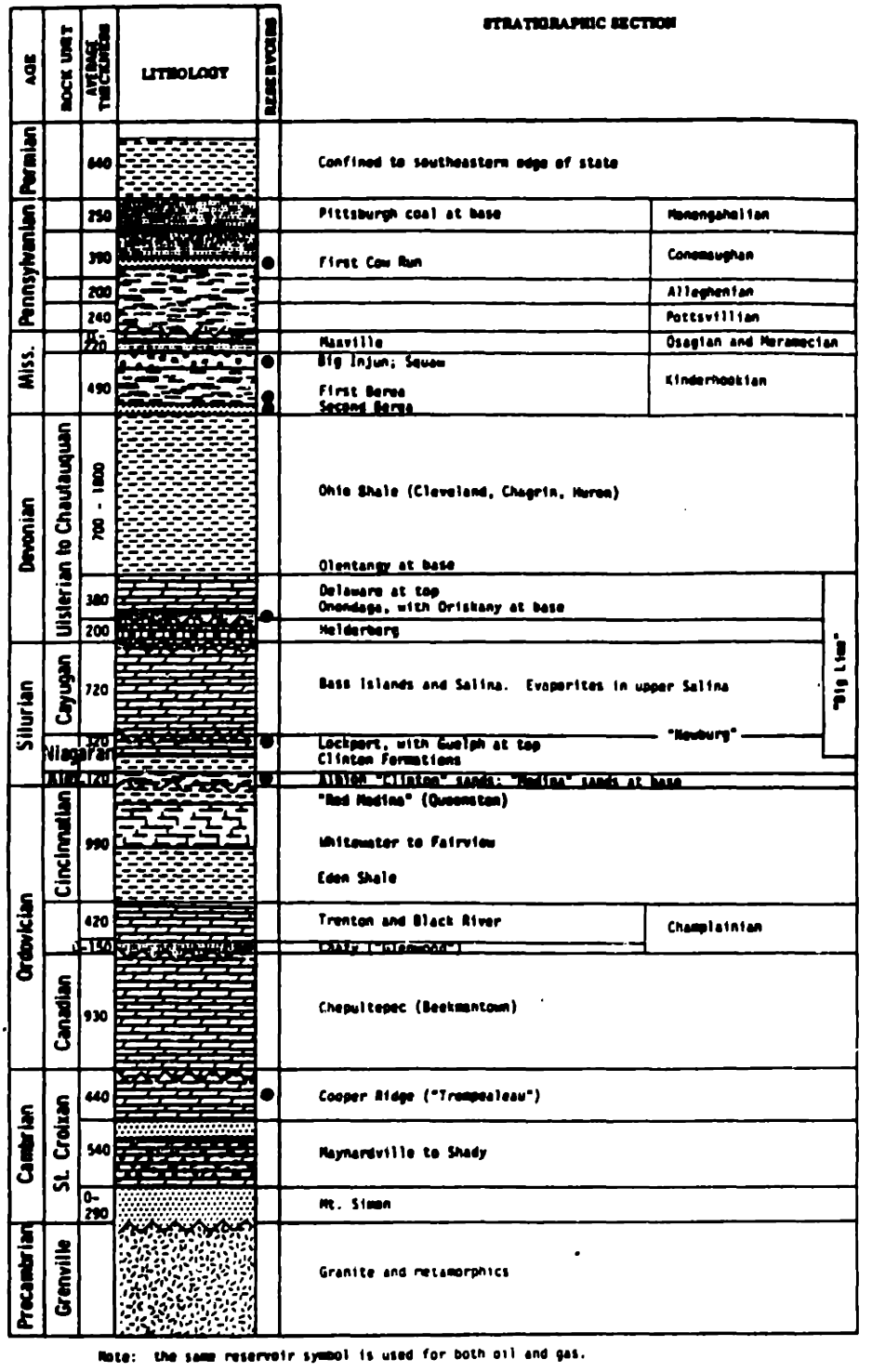


Figure 3-12. Stratigraphic column in Ohio showing the location of Berea sandstone directly above the organic-rich Ohio shale. Berea sandstone is a major producer of oil and gas in Ohio and the source rock is probably the Ohio shale.

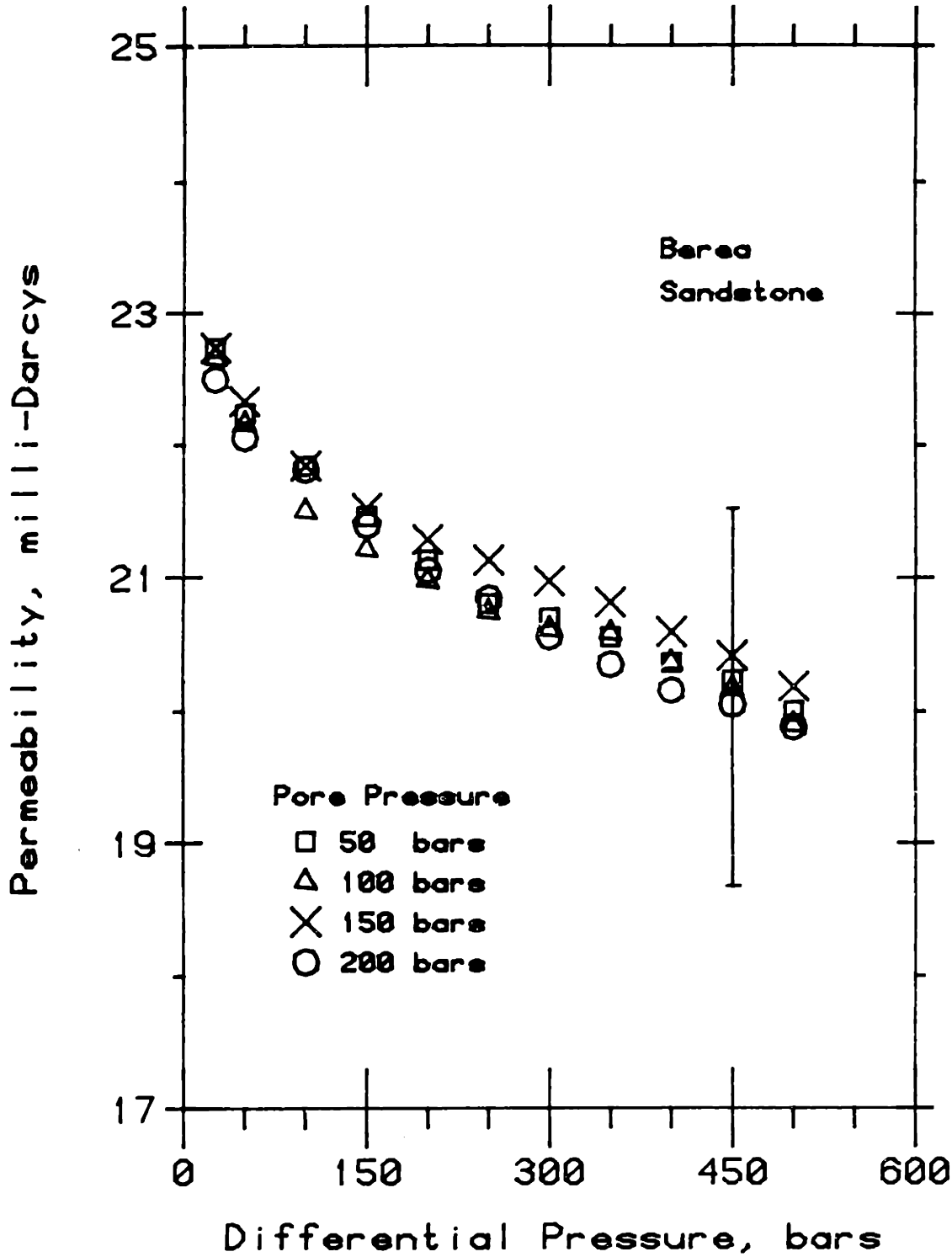


Figure 3-13. Permeability of Berea sandstone sample measured with kerosene as a function of differential pressure for various pore pressures. Sample was previously flushed with acetone and benzene to remove hydrocarbons. Different sample from the one for which data is shown in Figs. 3-8 through 3-10. Length of bar indicates probable error.

# CHAPTER 4

# THE EFFECT OF CONFINING PRESSURE AND PORE PRESSURE ON ULTRASONIC VELOCITIES IN ROCKS

## INTRODUCTION

A common assumption in the interpretation of measured acoustic velocities and attenuation in fluid saturated rocks is that the simple difference between external confining pressure and pore fluid pressure governs these properties. This difference is commonly referred to as either the "effective pressure" or else as the "differential pressure". Effective pressure recalls the original identification by Terzaghi (1924, 1944) of the difference between normal stress and pore pressure as the "effective stress" in determining the uniaxial strength and strain of soils. The extension of effective pressure to rocks and various physical properties was reviewed by Brace (1972). Differential pressure refers to the numerical difference between confining pressure and pore pressure. As long as the external stress condition is understood to be uniform, or hydrostatic, confusion with triaxial stress systems is avoided by use of the term "pressure". In this paper a uniform external stress, or a confining pressure, is being considered. Regardless of the terminology employed, the literature on acoustic properties of rocks and sediments is fairly unclear as to what extent an increase in pore pressure subtracts from an increase in confining pressure. When observed, experimental deviations of velocities from the differential pressure are fairly small, on the order of several percent or less of absolute value. Empirical fits of laboratory velocity data, however, to equations of the form $\sigma - np$, where $\sigma$

is confining pressure, $p$ pore pressure, and $n$ a coefficient, may result in the value of $n$ being substantially less than 1. Therefore it appears that pore pressure is less effective than confining pressure in determining acoustic velocities.

The purpose of this chapter is to review pertinent elasticity theory and to present experimental data specifically collected to investigate the adherence to differential pressure of P- and S-wave velocities. Static elasticity considerations of ideal linear, homogeneous, and isotropic porous solids (Biot, 1941, 1961) as well as the behavior of natural rocks (Chapter 2, this thesis) indicate that differential pressure determines the nature of porosity as it influences bulk modulus. Velocities, therefore, should indeed be determined by differential pressure. Experimental P- and S-wave velocities measured as a function of systematically varied confining and pore pressure for sandstones, limestone, and low porosity granitic rocks indicate a more complex relationship. These data, collected so as to minimize hysteresis, are interpreted to follow the differential pressure when the variations in pore fluid density and bulk modulus with pore pressure are not affecting measured velocities. In many of the measurements, however, systematic shifts of the velocities from the differential pressure occur because of the influence of changing pore fluid properties.

The exact relation between external confining and pore fluid pressures in the determination of acoustic properties is important for both the extrapolation of acoustic measurements and also to laboratory procedure. Jones and Nur (1984) extrapolate laboratory P-wave velocity measurements of fault zone materials to different *in-situ* conditions in the earth using an empirical relation which combines the static strain response as described in Chapter 2 of this thesis with the measured velocities as a function of confining pressure. Therefore a question is raised as to how velocities are extrapolated to different

pore and confining pressures.

In laboratory measurements of rock properties the precise control of pore pressure in addition to confining pressure can require a fair amount of additional effort and equipment. For the routine measurement of core properties and for the acoustic characterization of rocks in general this additional effort may be unnecessary if it can be shown why and to what extent the differential pressure determines velocities. One common solution for dealing with confining pressure versus pore pressure is to keep the pore pressure at a constant fraction of confining pressure, about 0.465, thereby simulating a differential pressure gradient with depth on the basis of density contrast between water and silicate solid. This procedure may be desirable if the purpose is to recreate exact *in-situ* conditions in the earth because, even if differential pressure should determine velocities, the bulk modulus and density of even a relatively incompressible fluid such as water will increase with pore pressure and perhaps have a measurable effect on velocities. If the purpose, on the other hand, is simply to characterize dry versus saturated acoustic properties it is probably more desirable to keep pore pressure and hence pore fluid properties constant. At worst, if samples are incompletely saturated at low pore pressures, an increase in pore pressure with differential pressure constant may dramatically increase P-wave velocity simply because of the increase in fluid bulk modulus. Another possible consequence of varying both confining pressure and pore pressure is that the sequence in which they are varied may systematically introduce hysteresis into the acoustic measurements.

A clear indication of whether or not the simple differential pressure, determines acoustic properties in rocks cannot be concluded from the previous published work on this topic. Hicks and Berry (1956) showed for two sandstone cores that compressional velocity was not a function of differential pressure. At

low differential pressures (dp = 2000, 1000, 0 psi) their data suggests that confining pressure has a greater effect than pore pressure on the order of 5%. At higher pressures, however, exact differential pressure determined velocity. They cite the work of Brandt (1955), who formulated a velocity function for randomly packed, non-spherical particles that depended on $\sigma - np$, where $\sigma$ is confining pressure, $p$ is pore pressure, and $n$ accounted for the manner in which the particles touched and varied in value from 0 to 1. Brandt (1955) found the value $n=0.87$ in an experiment. Wyllie *et al.* (1958) reported data on Berea sandstone and Citronelle sandstone which indicated that differential pressure did indeed govern velocity and that deviations, such as observed by Hicks and Berry (1956), could be explained by saturation difficulties with an oil-wet sandstone, particularly at low pressures. Banthia *et al.* (1964) report shear wave velocities that are a function of $\sigma - np$, where $n = 1 - K_s / K$ and $K_s$ and $K$ are the matrix compressibility and bulk compressibility, respectively. The definition of the coefficient $n$, however, comes from the linear description of bulk strain (Biot, 1941, 1961), which includes the strain of the intrinsic matrix solid as well as the overall bulk solid. This will be discussed in the next section. Gardner *et al.* (1965) show how this data includes a hysteresis effect and that velocity should be a function of differential pressure when a cyclic stress state has been impressed on the sample. Gardner *et al.* (1965) also discuss a simple linear elastic treatment of elastic moduli and density as a function of pore and confining pressure, concluding that the differential pressure should determine velocity. King (1966), however, measured P- and S-velocities in nitrogen and brine-saturated Berea sandstone that decreased by several percent as confining pressure was increased while differential pressure remained constant. The decrease was larger for the nitrogen than the brine-saturated rock, and the decrease was larger at lower differential pressure than at higher differential pressure. King (1966) suggested that the reduction in the nitrogen-saturated

case was due to bulk density increases caused by the increase in nitrogen density with pressure, and that the differential pressure determined velocity. Desai *et al.* (1969) found for 2 sandstones that compressional velocity depends on both pore and confining pressure while shear velocity depends only on the differential pressure. Finally, Gardner *et al.* (1974) presented P-wave velocity data for a water-saturated sandstone which indicated that differential pressure did indeed determine velocity.

For low porosity rocks the work of Nur and Simmons (1969) and Todd and Simmons (1972) both indicate that confining pressure is more effective than pore pressure in determining P-wave velocities. Nur and Simmons (1969) found for a sealed, saturated sample of Casco granite that shear and compressional velocity increased linearly by about 8% between 0 and 4 kbar, and that the slope of velocity versus pressure nearly equalled the slope of velocity versus pressure for a jacketed sample at confining pressures exceeding about 1.5 kbar. The experimental design, however, did not permit direct control of pore pressure as the saturated sample was simply sealed at room pressure. Incomplete saturation would lead to crack closure with confining pressure and velocities would go up because confining pressure did not equal pore pressure. In a thorough study Todd and Simmons (1972) measured compressional velocity in Chelmsford granite and Trigg limestone as pore pressure (water) and confining pressure were systematically varied to 1050 bars and 2000 bars, respectively. They found that velocity was described by a function of the form $\sigma - np$, $n < 1$. An empirical fit of the data for Chelmsford granite resulted in $n$ increasing from 0.50 at 100 bars pore pressure to 0.85 at 1050 bars pore pressure; for Trigg limestone the values were similar. Even though the calculated $n$ appear to change substantially the overall effect is quite small, less than 2.5% of the measured velocty, whereas overall precision of 1% is stated for the velocities.

In summary, the available experimental evidence reveals some subtle and interesting differences over whether or not the differential pressure determines acoustic velocity. Although observed deviations are quite small, on the order of several percent over 1 kbar, this uncertainty over whether there is a deviation or not impedes the normal progression of theory and experiment. In the experimental apparatus developed during the course of this study the resolution available in the measurements increased dramatically. Therefore this paper investigates how confining and pore pressures combine to determine velocities, initially with a simple elasticity analysis and, secondarily, with experimental velocity data.

## ELASTICITY ANALYSIS

This section contains a static linear elasticity analysis of pore volume and bulk volume strain in response to hydrostatic confining stress and pore fluid pressure. The purpose is to show why differential pressure, $\sigma - p$, should determine P- and S-wave velocities for most intact rocks, and also to indicate those situations where there may be exceptions. The analysis differs little from that of Gardner *et al.* (1965) and is intended to exclude effects due to hysteresis during pressure cycling and effects due to variation of pore fluid properties (density, fluid bulk modulus) as a function of pore fluid pressure. As will become apparent in the experimental section the effects on velocities due to variation of pore fluid properties with pressure are measurable. Although this is a static analysis and the velocity measurements dynamic, the static response of a porous solid indicates that pore shape, such as measured by an aspect ratio, is independent of pore pressure and confining stress at constant differential pressure. Therefore the conclusion is that velocities should not change because of pore structure considerations.

The stress-strain relation for a linear, isotropic, and homogeneous fluid-infiltrated porous solid is (Biot, 1941, 1962; Chapter 2 of this thesis)

$$\sigma_{ij} + (1-\frac{K}{K_s})p\,\delta_{ij} = (K-\frac{2}{3}G)\delta_{ij}\varepsilon_{kk} + 2G\varepsilon_{ij}, \tag{4-1}$$

where $\sigma_{ij}$ is stress, $p$ pore pressure, $G$ shear modulus, $K$ bulk modulus of the drained porous solid, $K_s$ intrinsic bulk modulus of the matrix solid, $\varepsilon_{kk}$ volumetric strain, and $\varepsilon_{ij}$ strain. If stress is hydrostatic there is no shear strain, and if volumetric strain is taken to be negative in positive compression, this relation can be restated as

$$\sigma - (1-\frac{K}{K_s})p = -K\varepsilon \tag{4-2}$$

This relation indicates that pore pressure will be less effective than confining pressure in determining bulk volumetric strain (Chapter 2), which includes matrix strain in addition to pore volume strain. It is the pore volume strain of crack and pore closure, however, which will determine physical properties such as velocities under confining pressure and not the matrix strain. Rearrangement of terms leads to

$$\frac{1}{K}(\sigma - p) + \frac{1}{K_s}p = -\varepsilon. \tag{4-3}$$

In this form the components of volumetric strain due to pore pressure and differential pressure can be isolated. Volumetric bulk strain of a linear, homogeneous porous solid at a given pore pressure and confining pressure can be analyzed in two steps. The first step is an equal internal and external pressure of value $p$, which results in a uniform volumetric strain $p/K_s$ and is given in the second term in the above expression. The second step is an external pressure $\sigma - p$ at constant pore pressure and results in a volumetric strain

$(\sigma-p)/K$ given in the first term in the above expression.

The effect of the first step on velocities is negligible. A uniform strain in every linear dimension does not change any of those pore features responsible for the bulk and shear moduli, either static or dynamic. The aspect ratios of every crack and pore do not change. Because strain is uniform over very linear dimension the fractional decrease of pore volume and bulk volume is the same and therefore porosity remains constant. There is an increase in density, but this is extremely small. If the intrinsic bulk modulus of silicates results in a strain of 0.1% of bulk dimension at a pressure of 1 kbar then the corresponding density increases by a similar percentage and the effect on velocities is negligible. Since the minerals which make up the matrix of the rocks studied behave as a reasonable linear solid, such that there is minimal occluded porosity which is compliant in an unjacketed stress-strain test (Chapter 2), this analysis is also applicable to nonlinear solids such as most rocks.

It is the second step in the analysis which results in pore closure of the sort which leads to a change in measured velocities. An external pressure $\sigma-p$ will close cracks and bring asperities into contact. Although the analysis is limited to infinitesimal strain the processes by which cracks and pores close can be incrementalized and the conclusion is the same.

## LABORATORY APPARATUS AND PROCEDURE

The simple results from the elasticity analysis section predict a negligible change in pore structure with constant differential pressure in the absence of effects due to microhomogeneity and anisotropy. The published experimental velocity data, however, particularly compressional velocity in low porosity rocks, support the contention that pore pressure is not as "effective" as confining

pressure. It was felt that additional laboratory acoustic measurements would clear up this discrepancy. The experiments described in this section involved measurement of shear and compressional velocities on cores systematically subjected to hydrostatic confining pressures to 1300 bars and pore pressures to 300 bars. As an experimental strategy the pore fluid of choice was nitrogen gas. The argument for gas, as pointed out by Todd (1973), is that dry P-wave velocities, particularly in granites filled with microcracks, span a much greater range as a function of differential pressure than the equivalent water saturated rock. Consequently, the nitrogen saturated rock is more suitable for a test of the differential pressure relation because of the increased sensitivity of velocities to pressure. Other favorable properties of gas include the low viscosity and high compressibility, which means that pore pressure equilibrates rapidly after changing either confining or pore fluid pressure. The problem with nitrogen gas, as was quickly found out, is that the change in density and compressibility of the gas between 0 and 300 bars was appreciable enough to affect the measured travel times. Measurements were also made with benzene as the pore fluid, chosen because the solubility of gases in benzene is high and chemical interaction with silicate minerals is low. Even with benzene, however, the increase in bulk modulus with pore pressure showed up in the P-velocity measurements for some of the rocks. For Berea sandstone additional measurements were made with distilled water as the pore fluid to contrast with the bezene saturated values.

The experimental arrangement is shown schematically in Fig. 4-1 and 4-2. Fig. 4-1 shows the high pressure apparatus with a sample loaded. Fig. 4-2 is a block diagram of the electronic equipment used to collect the ultrasonic acoustic measurements. Briefly, the principle features of the apparatus are: 1) large 7.5 cm diameter by 5 cm long samples, 2) independent hydrostatic

confining pressure and pore fluid pressure or vacuum, 3) isolation of ceramic transducers from the pressure media, 4) selection of P- and two mutually perpendicular S-waves at any given time for velocity and Q measurement, 5) computer control of the experiment.

Acoustic measurements were made on cylindrical cores 7.5 cm in diameter by 5 cm long. Samples were located between 2 titanium platens and jacketed with a multiple layered jacket of teflon (for benzene measurements), polyurethane sheet, and air-drying polyurethane liquid (Devcon Flexane). Two ports on each titanium transducer allow for the introduction of pore fluid pressure independent of confining pressure. Hydrostatic confining pressure is applied with kerosene pressurized by an air-driven Haskell pump. Pore fluid pressure is generated via a pressure generator or a positive displacement pump in the case of liquid or straight from a regulated high pressure nitrogen gas cylinder in the tests with nitrogen. Pressures are measured by pressure transducers wired to the HP3497A data acquisition and control unit. Solenoid air valves actuated by the HP3497A unit control air lines to the Haskell pump and to a metering pressure relief valve for the control of confining pressure.

Each titanium endpiece houses a multiply stacked, PZT ceramic composite transducer similar to that used by Johnston (1980). In each stack are two 1 Mhz, 2.5 cm diameter shear discs oriented 90 degrees to each other and a similar compressional wave disc. The overall pair of titanium endpieces are oriented for the shear wave polarization and the three sets of signals, two shear and one compressional, are sequentially generated and measured at any given time. Approximately 1.8 cm of titanium alloy is between the ceramic transducer and the end of the sample. The face of each titanium endpiece is coupled to the sample ends with a perforated (0.00254 cm) silver sheet. A steel cap with pressure-excluding electrical feedthroughs seals the ceramic transducer from

confining pressure fluid for the titanium endpiece located internally within the pressure vessel. The other titanium endpiece is the end plug for the pressure vessel and consequently the ceramic crystals are located externally. Neither pair of ceramic crystals is therefore subjected to the pressure media. Zero travel time, or time of flight with no sample present, was determined by measuring travel times through aluminum standards of thicknesses 1.27, 2.54, 3.81, 5.08, and 6.35 cm, and extrapolating back to zero thickness. There is a slight dependence of this zero travel time on pressure which was included in the data reduction. For the P-wave this time is approximately 7.54 $\mu$s, for the first S-wave 13.65 $\mu$s, and for the second S-wave 12.45 $\mu$s.

The electronics used to generate and receive the acoustic signals are shown in Fig. 4-2. A Panametrics 5055PR both generates the excitation pulse to the source transducer and receives the transmitted wave from the receiver transducer. It amplifies (usually 0 or +10 dB) and filters (0.3 Mhz high pass) the received signal. Electronic circuits and coaxial switches direct excitation pulses and signals of compressional and both shear waves to appropriate transducers. These circuits are controlled by the HP3497A unit. Output from the Panametrics is fed directly into the HP1980B oscilloscope which digitizes the signal at 100 Mhz, 10 bits, and sends it to the HP1000 computer for travel time pick, attenuation analysis, and a permanent record. Travel time was determined by a threshold voltage 2.5% of the overall peak-to-peak voltage of the amplified and filtered signal. The picking algorithm resulted in travel-time measurements repeatable to ± 10 nanoseconds for both P- and S-waves and this translates into an overall accuracy of ±0.15% at worst for the calculated velocities. Velocities were corrected for changes in sample length as measured by strain gages. This level of precision was verified by the duplication of measured travel times in repetetive cycles of confining pressure as well as by separate experiments where

the same rock sample was removed from the vessel and the jacketing procedure and measurements repeated.

An examples of waveforms collected from a sample of Navajo sandstone at 100 bars confining pressure and 100 bars benzene pore pressure is shown in Fig. 4-3. The signals are very clear. The excitation pulse is 180 volts, amplification is -10 dB, and there is a 0.3 Mhz high pass filter on these signals. The top trace is the P wave, the lower two traces the two S waves. The apparent time offset in the shear wave arrivals in due to the additional thickness of the second shear wave crystal the first shear wave has to go through. This effect, of course, is subtracted out in the zero travel time calibrations and in fact could be removed totally by rotating the titanium endpieces by 90 degrees. Note that the transducer design allow for direct measurement of shear wave anisotropy in 2 perpendicular directions in addition to the P wave. Anisotropy measurements are, however, not the purpose of this paper.

The samples chosen for these experiments included holocrystalline granitic rocks, sandstones, and a limestone. Table 1 lists all of the samples studied along with measured dry bulk densities, grain size estimated from hand specimen and thin section, and measured porosities from a comparison of dry and saturated weighings. Appendix B contains descriptions of these samples from hand specimen and thin section analysis.

Samples were extracted from larger blocks using a water-cooled diamond drill and ground with diamond wheel cylindrical and surface grinders to a nominal 7.5 cm diameter and 5 cm length with a parallelism tolerance of 0.0005 cm. During the experiments the end flatness of these large samples was discovered to be very important for coupling. Samples were washed and flushed with water and acetone and then saturated in acetone under a vacuum several

times for periods of 24 hours with vacuum drying at 20 $\mu$m Hg and 60 degrees C for periods up to 48 hours. Sample ends were lightly sanded and cleaned prior to jacketing. A benchtop jig held the sample between the two titanium endpieces for jacketing and orientation of sample directions with shear wave polarizations. Accuracy of shear wave polarization was approximately 0.1 degree. Jacketing of samples required 3 layers. The first layer closest to the sample was a thin teflon sheet to isolate pore fluids like benzene from the succeeding 2 jacketing materials. The second layer was a polyurethane sheet sealed with tetrahydrofuran and wire clamped around the titanium endpieces. Over the entire polyurethane sheet, wire clamps, and directly adjacent titanium a layer of air- drying polyurethane compound (Devcon Flexane) was applied to complete the jacketing procedure.

The experimental procedure for the measurement of velocities was designed to avoid or at least minimize the type of measurement hysteresis noted by Gardner *et al.* (1965). The jacketed sample and transducer assembly was placed into the pressure vessel and confining pressure was initially raised to about 20 bars. Pore pressure tubing connections were completed and a 20 $\mu$m Hg vacuum was pulled throughout all the pore fluid tubing to be used in the experiment as well as the sample under pressure. Confining pressure was then cycled three times at the rate of 10 bars every 2 minutes up to the maximum for the experiment. For all samples except the Bedford limestone this was 1000 bars; for the Bedford limestone the maximum confining pressure was held to 600 bars to minimize grain crushing. After cycling, the confining pressure was held at 20 bars for about 12 hours with a constant 20 micron vacuum pulled on the pore pressure system and sample. Measurements were made at room temperature which varied from 18 to 23 degrees C.

The first set of velocity measurements were made on the sample under vacuum. P- and S-wave travel times and waveforms were recorded as the confining pressure was raised in steps up to the maximum.

For measurements with pore fluids confining pressure and pore pressure were alternately raised such that the differential pressure never exceeded more than 50 bars. When the desired pore pressure was reached the system was allowed to equilibrate for no less than 2 hours before measurements proceeded with increasing confining pressure while the pore pressure was maintained at the constant desired value. This procedure alleviated the inclusion of hysteresis contained in the measurements of Banthia *et al.* (1964) as interpreted by Gardner *et al.* (1965). By alternating confining and pore pressures in 50 bar steps hysteresis is relegated to measurements below 50 bars differential pressure. This is because strain associated with asperity closure and surface contact is determined by differential pressure, as indicated in the elasticity analysis. When confining pressure is raised first the introduction of pore pressure does not fully reopen closed asperities commensurate with that expected from the calculated differential pressure. Velocities will be higher. This effect becomes more significant as the magnitudes of pressure increments increase. The procedure of Banthia *et al.* (1964), where the full confining pressure was first applied before the pore pressure was raised from zero, resulted in higher velocity measurements at higher levels of pressure, differential pressure being constant, because of this systematic introduction of hysteresis in the procedure. Ideally both confining and pore pressure would first be raised uniformly to the pore pressure, and then the confining pressure alone would be raised to the desired differential pressure. The procedure followed in these experiments approximated this ideal. By analogy the unjacketed rock sample is immersed fully equilibrated into an ocean of pore fluid down to a depth

equal to the pore pressure, after which only the external pressure is cycled.

After a cycle of confining pressure was completed the confining pressure was held a few bars above the pore pressure and each slowly reduced to zero pressure. Confining pressure was then slowly cycled up to about 100 bars and then again released down to about 15 bars. The system was allowed to sit at this pressure for no less than 6 hours after which the next level of pore pressure measurements (100, 200, or 300 bars) were made. Initial velocity measurements over the first 100 bars confining pressure were compared over the period of time required for all of the runs to check for longer term drifts in the zero pore pressure velocities. Such drifts were small, indicating that the procedure and amount of time between cycles of measurements was sufficient to remove hysteresis.

The time needed for pore pressure to equilibrate after a variation in either confining pressure or pore pressure depended on the rock sample. Both ends of the sample were accessed by the pore fluid system to allow rapid equilibration. For the high permeability sandstones and limestone pore fluid pressures equilibrated almost immediately; the time between different data points on a confining pressure cycle was at least 10 minutes however because of the time needed to record the various waveforms and travel times. For the granite samples, measurements with nitrogen gas as the pore fluid also equilibrated within 10 minutes. When benzene was the pore fluid, however, substantially greater time was required for the pore fluid pressure to equilibrate. Westerly granite is lower in permeability than the Chelmsford granite parallel to the rift (Coyner *et al.* , 1979) and consequently required more time to equilibrate. At low differential pressures, less than 250 bars, 10 to 30 minutes were required as evidenced in part by strain measurements as well as by changing amplitudes of the signals with time. At higher pressures longer periods were allowed, up to 4

hours at 1 kbar. At the high pressures terminal velocities are reached and the amount of change with time is very small.

## EXPERIMENTAL RESULTS - PORE PRESSURE

Plots of measured P- and S-wave velocities for the samples studied with systematic variations in pore pressure and confining pressure are shown in Figs. 4-4 through 4-17. Velocities are plotted versus differential pressure, the difference between hydrostatic confining pressure and pore pressure. Values are exclusively from the increasing portion of the confining pressure cycle. The various symbols on each plot represent different pore pressures from vacuum up to 300 bars and are identified in the key on each plot. The nitrogen pore pressures at 0 bars are actually a vacuum. With this data the dependence of P- and S-wave velocities on differential pressure will be examined and discussed for the different rock types represented. Figs. 4-4 through 4-7 are P- and S-wave velocities for Westerly and Chelmsford granite with nitrogen and benzene pore fluids. The propagation direction in the Chelmsford granite is perpendicular to the grain direction and the sense of shear is across the rift. Figs. 4-8 and 4-9 are P- and S-wave velocities for Bedford limestone with nitrogen and benzene pore fluids. Figs. 4-10 through 4-12 are P- and S-wave velocities for Navajo sandstone with the benzene and nitrogen S-wave velocities plotted separately for clarity. Figs. 4-13 through 4-17 are plots of velocities for Berea sandstone. The benzene and nitrogen S-wave velocities are plotted separately in Figs. 4-14 and 4-15 for clarity. Figs. 4-16 and 4-17 are P- and S-wave velocities for another sample of Berea sandstone measured with distilled water.

Cursory examination of these plots reveals many examples where velocities do not strictly follow the differential pressure. The deviations are usually fairly small, on the order of several percent or less, but also systematic. Most of these

deviations can be interpreted by a consideration of the variation in density and bulk modulus of the pore fluids with pore pressure. These properties are tabulated in Table 2 for nitrogen, benzene, and water at temperatures near ambient. Nitrogen gas density increases substantially with pressure, up to 0.299 g/cc at 300 bars. This decreases the velocities of the higher porosity limestone and sandstones at higher pore pressures. The bulk modulus of nitrogen with pressure increases by nearly 250% between 100 and 300 bars, and thereby increases the P-velocities of the granites and, to a lesser extent, the S-velocities of one of the granites (Chelmsford). Benzene is about twice as compressible as water and increases in bulk modulus with pressure such that P-velocities in the sedimentary rocks saturated with benzene increase at the higher pore pressures at constant differential pressure. The Chelmsford granite sample P-wave velocities are also slightly sensitive to the higher benzene bulk modulus. The bulk modulus of water, nearly twice that of benzene, does not increase as much with pressure and so, at least for the Berea sandstone sample measured, the differential pressure determines velocities. In the following paragraphs the data in these plots is discussed in detail with the point of view that if the pore fluid properties (bulk modulus, density) were constant with pressure the velocities would follow the differential pressure. The strongest evidence for this is found in the benzene saturated S-wave velocity data in the higher porosity limestone and sandstones, from the benzene saturated S-wave velocities in the granites, and from the water saturated P- and S-wave velocities in the Berea sandstone.

The Westerly granite P- and S-wave velocities in Figs. 4-4 and 4-5 and the Chelmsford granite P- and S-wave velocities in Figs. 4-6 and 4-7 are somewhat complementary although the range in velocities for Chelmsford granite as a function of confining pressure as well as the difference between dry and saturated velocities are much greater. As will be discussed in Chapter 5, this is a

reflection of a higher concentration of compliant cracks, or a larger degree of crack porosity (Walsh, 1965), in the Chelmsford granite. The P-wave velocities for the nitrogen saturated measurements for Westerly and Chelmsford both show the effect of increasing nitrogen bulk modulus with increasing pore pressure, such that velocities at a given differential pressure are higher at higher pore pressures. Deviation from differential pressure is most pronounced at low differential pressure where the effects of cracks and pore fluid saturation are greatest. After approximately 300 bars most of the compliant cracks in these samples are closed, the increase in velocity upon saturation is much reduced, and the effects of small increases in nitrogen bulk modulus are negligible.

The benzene saturated P-wave velocities for the Westerly granite sample are constant at constant differential pressures except for the zero pore pressure (actually 1 bar atmospheric) measurements. Although the saturation technique for the jacketed sample in the pressure vessel is quite thorough, in these measurements, which are some of the first made in this study, the effect of incomplete saturation on the P-wave velocities at 1 bar is apparent. At the higher benzene pore pressures of 100, 200, and 300 bars all of the velocities are the same at any given differential pressure and this indicates that differential pressure does indeed determine velocity. This observation of incomplete saturation is emphasized to show the benefit of using pore pressure in measurements to ensure complete saturation.

For the Chelmsford granite sample the increase in benzene saturated velocities over the nitrogen saturated velocities is quite large and the range of velocites as a function of differential pressure is also large, correlating with the much greater crack porosity in this granite relative to the Westerly granite sample. The result is that the benzene saturated P-wave velocities at constant differential pressure increase slightly with higher pore pressure as the benzene

bulk modulus is increasing. Measurements were mainly made at pore pressures of 100 and 300 bars with several additional points at zero pore pressure. Below a differential pressure of about 250 bars the P-wave velocities are systematically higher at a pore pressure of 300 bars by about 0.3-0.6%. This velocity increase did not show up in the Westerly granite data because of the reduced sensitivity to fluid bulk modulus in this sample.

This data can be compared with that of Todd (1973) and Todd and Simmons (1972) which was also collected on a sample of Chelmsford granite for the purpose of determining the relation between confining pressure, pore pressure, and P-wave velocities with water as the pore fluid. They found that the scatter in their data was reduced if the data were fit to an equation of the form $\sigma - np$, $n$ varying from 0.50 at a pore pressure $p$ of 100 bars, 0.75 at 300 bars; and up to 0.85 at 1050 bars. This emphasizes the large variation possible in values of $n$ when the magnitude of deviations from differential pressure are small, in this case 3-4%. At a differential pressure of 200 bars they measured the P-wave velocity at 100 bars water pore pressure to be 5.732 km/s and at 300 bars pore pressure to be 5.780 km/s, or an increase of about 0.8%. In the present measurements with benzene the velocities at comparable pressures are 5.667 km/s and 5.698 km/s, respectively, representing an increase of about 0.5%. According to Table 2 the bulk modulus of water increases from 22.2 Kbar to 23.8 Kbar, about 7%, between 100 and 300 bars; the bulk modulus of benzene at comparable pressures increases from 12.1 Kbar to 13.9 Kbar, about 14%. Unfortunately the sense of percentage increase is backwards: the larger change in benzene bulk modulus should correlate with a larger increase in benzene saturated velocities at the two pore pressures but the reverse is true. Perhaps too much is being expected from the two sets of data in comparing them at this level. Nonetheless, there is reasonable expectation that the increases in P-wave

velocity can be explained by the increases in pore fluid moduli. More intensive modelling of the velocity data with crack distributions and the inclusion of pore fluid properties would probably indicate the sensitivity of P-wave velocities to fluid bulk moduli on this small scale. Such modelling procedures are available (Cheng *et al.*, 1976; Cheng, 1978).

A positive indication of the that differential pressure determines velocities in the absence of pore fluid changes with pore pressure can be found in the S-wave velocity data for these two granites. The shear modulus is less sensitive to the fluid bulk modulus and since the density variations are negligible the S-wave velocities are more reliably interpreted. The strongest evidence is seen in the nitrogen and benzene saturated S-wave velocities for Westerly granite as shown in Fig. 4-5. The nitrogen saturated velocities closely follow the differential pressure over the entire range of velocities as a function of differential pressure. In addition, except for some scatter at low pressure, the benzene saturated velocities also follow the differential pressure. The Chelmsford granite S-wave velocities for the nitrogen saturations show some sensitivity to nitrogen pressure, increasing with pore pressure at low differential pressures, but there is a very large increase in velocities upon benzene saturation in this rock. The increase in nitrogen bulk modulus with pore pressure is therefore slightly increasing the shear modulus and this is recorded in the S-wave velocities as well as in the P-wave velocities for this rock. After about 250 bars differential pressure the velocties are all measured to be the same value. The benzene saturated data for the Chelmsford granite follow the differential pressure almost exactly over the entire pressure range.

The Bedford limestone is a good choice for studying the velocity response to combined pore fluid and confining pressures because, as is shown by the stress-strain measurements in Chapter 2, the rock is nearly an ideal linear, porous

solid. The range in velocities with differential pressure is comparitively small in relation to the other samples and, as is demonstrated in Chapter 5, the liquid saturated S-wave velocities are predicted exactly from the dry vacuum velocities on the basis of the liquid saturant contribution to bulk density. Therefore at least the effect of density increase with nitrogen pore pressure can be easily accounted for in the velocities at constant differential pressure.

In Fig. 4-8 and 4-9 are plotted the P- and S-wave velocities for nitrogen and benzene saturated Bedford limestone at the various pore pressures. The nitrogen saturated P- and S-wave velocities are lower at higher pore pressures because of the increase in nitrogen density. The benzene saturated P-wave velocities are higher at higher pore pressures because of the higher fluid bulk modulus. The best evidence for velocity following the differential pressure is seen in the benzene saturated S-wave velocities, values for which at the different pore pressures are exactly the same.

The decrease in velocities for the nitrogen saturated Bedford limestone sample are clearly interpreted to be a result of density increase due to the nitrogen. At 300 bars confining pressure the vacuum dry P- and S-wave velocities are 4.662 km/s and 2.629 km/s, respectively. The measured dry bulk density is 2.360 g/cc and the porosity is 11.9%. From Table 2 the density of nitrogen gas at 100 bars and 300 bars is .299 and .113 g/cc, respectively. According to the expressions for P- and S-wave velocities in a perfect linear elastic solid the velocities vary inversely with the square root of bulk density if the shear and bulk moduli are constant. Assuming they are constant, the predicted P- and S-wave velocities at 300 bars differential pressure, 100 bars pore pressure, are 4.649 and 2.622 km/s, respectively. This compares favorably with the measured P- and S-wave velocities of 4.644 and 4.623 km/s. At 300 bars differential pressure, 300 bars pore pressure, the predicted P- and S-wave

velocities are 4.627 and 2.609 km/s, respectively, comparing favorable with the measured values of 4.636 and 2.614 km/s, respectively. Therefore the conclusion is that differences in the nitrogen saturated velocities at constant differential pressure are attributable to density variations in the nitrogen.

The increase in P-wave velocities of benzene-saturated Bedford limestone at constant differential pressured are interpreted to be the result of increases in the bulk modulus of the benzene at higher pore pressures. In Chapter 5 the P-wave velocities of this sample with dry vacuum, benzene, and water pore fluids show that the benzene measurements fall about halfway between the dry and water saturated measurements. The benzene measurements at pore pressures of 200 and 300 bars in Fig. 4-8 are systematically higher because of the increase in fluid bulk modulus. The measurements at 0 bars pore pressure are lowest because of the lowest bulk modulus and, perhaps, in addition to incomplete saturation.

For the two sandstones, Navajo and Berea, the strongest evidence that differential pressure determines velocities comes from the measurements of S-wave velocities with benzene saturation shown in Figs. 4-12 and 4-15 in addition to the water saturated P- and S-wave velocity measurements of a second Berea sandstone sample in Figs. 4-16 and 4-17. In these plots velocities exactly follow the differential pressure because the sensitivity of the shear modulus in these sandstones to the range of benzene and water fluid bulk modulus over the various pore pressures is negligible. For the water saturated Berea sandstone the smaller percentage increase in fluid bulk modulus relative to the benzene results in the P-wave velocities in Fig. 4-17 exactly following the differential pressure. The P-wave velocities in Figs. 4-10 and 4-13 show both the effects of increasing fluid bulk modulus for the benzene measurements and the increasing density for the nitrogen measurements as a function of pore pressure. For the

Navajo sandstone the P-wave velocities almost uniformly increase with pore pressure when the saturant is benzene. The measurements at 0 bars are probably a little low because of incomplete saturation. In the nitrogen measurements for Navajo there seems to be some cancellation of the density increase with the increase of fluid bulk modulus with increasing pore pressures.

Calculations similar to those for the Bedford limestone indicate that the increase in nitrogen density accounts for the decrease in S-wave velocities for the Navajo and Berea sandstones at higher pore pressures, differential pressure remaining constant.

In addition to the benzene saturated velocity measurements of Berea sandstone, water saturated measurements were made, but on a different sample. These were done in order to contrast pore pressure effects of benzene saturated with water saturated measurements. The P- and S-wave velocities are shown in Figs. 4-16 and 4-17 as a function of differential pressure at various distilled water pore pressures. In both instances the measured velocities exactly follow the differential pressure. These results correspond to water saturated sandstone S-wave velocity measurements by Gardner *et al.* (1965) and P-wave velocities by Gardner *et al.* (1974), both data sets which followed the differential pressure. For the water saturated Berea sandstone the differential pressure determines velocities over the pore pressure range considered because the bulk modulus of the fluid is not changing enough to affect velocities.

## DISCUSSION

From the elasticity analysis and from the experimental measurements of velocities when changes of pore fluid properties were not important it is concluded that differential pressure determines velocities. Even when pore fluid

properties are important the magnitudes of the deviations are small, on the order of several percent or less of the absolute values.

Velocity data fit to equations of the form $\sigma - np$ will possibly include effects due to hysteresis as noted by Gardner *et al.* (1965) as well as effects due to changes in pore fluid properties as noted by Todd and Simmons (1973) and previously discussed. The coefficient $n$ in this expression should ideally be equal to 1 if hysteresis and changes in pore fluid properties are subtracted. In the experimental measurements a great deal of care was taken to avoid hysteresis.

Similarly, the extrapolation of laboratory or field acoustic data to different pore and confining pressures should ideally follow the differential pressure. This will also be true if the external stress condition is triaxial as long as the magnitudes of differences between principle stress directions and pore pressure are constant. Excluded in such an extrapolation are effects due to irreversible hysteresis and changes in pore fluid properties.

Changes in pore fluid properties with pore pressure are somewhat maximized in the experiments in this chapter because nitrogen gas and benzene are used to avoid irreversible interactions between pore fluid and matrix. Because benzene is nearly twice as compressible as water the effects of pore fluid bulk modulus increasing with pore pressure are more apparent with the benzene. Between 100 and 300 bars the bulk modulus of water (Table 2) increases by 7% while that of benzene increases by nearly 14%. The results with Berea sandstone indicate that with water, over the pore pressure range studied, the effect of varying bulk modulus on P- and S-wave velocities is negligible. Over much larger ranges of pore pressure, however, bulk modulus changes may contribute to differences in velocity, particularly P-wave. Todd and Simmons (1973) measured small (several percent) increases in P-wave velocity for

Chelmsford granite at a constant differential pressure which in part may be attributed to increases in water bulk modulus.

Although the purpose of the experimental measurements is to indicate how the velocities react to differential pressure, an additional observation concerning the amplitudes of the signals was noted. For the measurements with benzene and water saturations the amplitudes followed the differential pressure with a precision of approximately ±2%, and therefore it is concluded that acoustic attentuation over the ranges of pore fluid pressures encountered is a function of the differential pressure. For the measurements with nitrogen gas, however, it was noted that at progressively higher pore pressures, differential pressure being constant, the amplitudes of the signals decreased by up to 30% between vacuum and measurements at 300 bars pore pressure. The reason this is noted is because there is an intriging possibility for studying the attenuation mechanism in these rocks with this effect. The purpose here is simply to note this observation; it may possibly an experimental artifact which requires further investigation.

In terms of laboratory procedure it was concluded from these experiments that measurements with pore pressure should probably keep the pore pressure constant. This depends somewhat on the purpose of the experiment, however. Spencer (1979) and Johnston (1980) took the approach of keeping pore pressure at a constant fraction (0.465) of confining pressure, therebye simulating an assumed pressure gradient with depth based on the average density constrast of rock silicate minerals with fully saturated porosity. Unless the purpose is to exactly duplicate an assumed stress condition in the earth a more reasonable procedure for the measurement of acoustic properties is to keep the pore pressure at a constant value while the confining pressure or external stress is varied, obviously at values above the pore pressure. From these experiments it

was noted that even with care in the saturation of samples with vacuum there is probably trapped gases in the pore phase which lower the P-wave velocity. This was particularly true for the Westerly granite measurements with 1 bar benzene pore pressure. It is suggested that a pore pressure of 100 bars is more than sufficient to ensure complete saturation. Therefore a valid procedure to characterize saturated velocities in rocks is to alternately raise confining and pore fluid pressure to 100 bars in small increments and then to cycle confining pressure while maintaining pore fluid pressure at 100 bars.

## CONCLUSIONS

Differential pressure, confining pressure minus pore pressure, determines P- and S-wave velocities in most intact geologic materials exclusive of varying pore fluid properties, incomplete saturation effects, and hysteresis. The simple consideration of uniform strain when pore pressure equals confining pressure indicates that since pore shape does not change the velocities should not change. Therefore the confining pressure in excess of pore pressure, the differential pressure, determines velocities. Severe anisotropy of intrinsic mineral grains or a large occluded porosity phase which is compliant might cause exceptions although in the velocity measurements on granites this did not appear to be a measurable effect.

The experimental measurements of P- and S-wave velocities as a function of confining and pore pressure indicate that differential pressure determines velocities for both low porosity granitic rocks as well as higher porosity limestone and sandstones. This is after consideration of the variation in pore fluid properties (fluid bulk modulus, density) and how they change with pressure. The substantial increase in density for nitrogen with increasing pore pressure lowers velocities in the higher porosity rocks while the increase in fluid bulk modulus

increases P-wave velocities in the low porosity granites. The strongest evidence for differential pressure determining velocities in the absence of pore fluid effects comes from the S-wave velocities.

As a general laboratory procedure pore pressure in a liquid insures that residual gas in the pore space is dissolved in the pore fluid. For the purpose of measuring velocities and attenuation in dry and saturated conditions the best procedure is to keep pore pressure in the saturated measurements at a constant value, and 100 bars is probably a fairly good choice.

**Table 1: Rock Samples in this Study**

| Rock | Density (g/cc) | Grain Size (mm) | Porosity % |
|---|---|---|---|
| Westerly Granite (blue) | 2.641 | 0.75 | 0.8 |
| Chelmsford Granite | 2.606 | 1.5 | 1.1 |
| Bedford Limestone | 2.360 | 0.75 | 11.9 |
| Navajo Sandstone | 2.316 | 0.15 | 11.8 |
| Berea Sandstone | 2.197 | 0.1 | 17.8 |

**Table 2: Pore Fluid Properties At 20-22 ° C**

| Fluid | Pressure (bars) | Density (g/cc) | Bulk Modulus (Kbar) |
|---|---|---|---|
| Nitrogen | 100 | .113 | .100 |
| " | 200 | .215 | .211 |
| " | 300 | .299 | .343 |
| Benzene | 5 | .87 | 11.2 |
| " | 100 | .88 | 12.1 |
| " | 200 | .89 | 13.0 |
| " | 300 | .89 | 13.9 |
| Water | 10 | 0.999 | 20.4 |
| " | 100 | 1.0 | 22.4 |
| " | 200 | 1.01 | 23.2 |
| " | 300 | 1.01 | 24.0 |

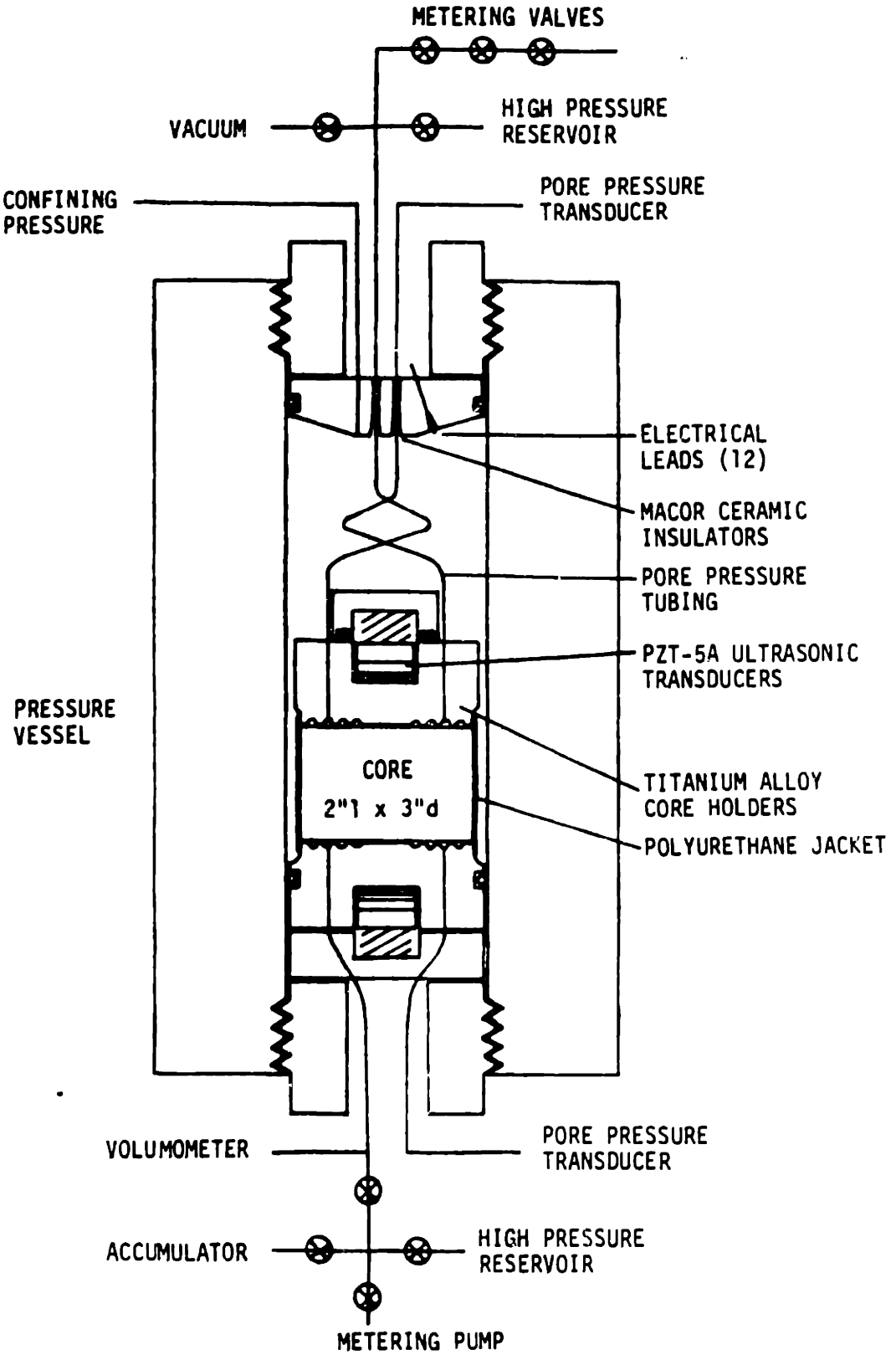


Figure 4-1. High pressure experimental apparatus for the measurement of P- and S-wave velocities. Hydrostatic confining pressure and pore fluid pressure are independently controlled.

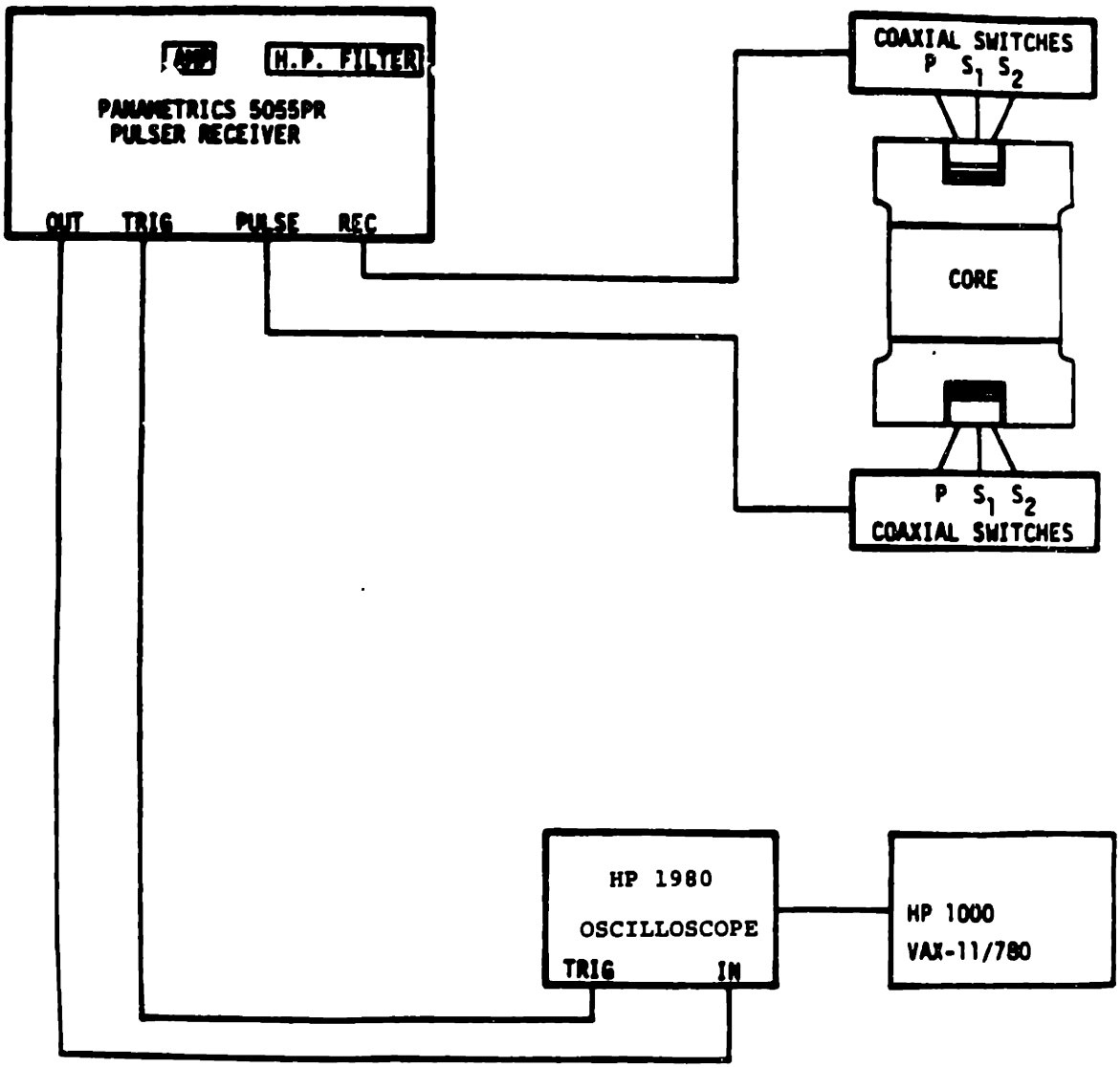


Figure 4-2. Block diagram of sample with transducer heads and electronics used to measure ultrasonic velocities and to record waveforms.

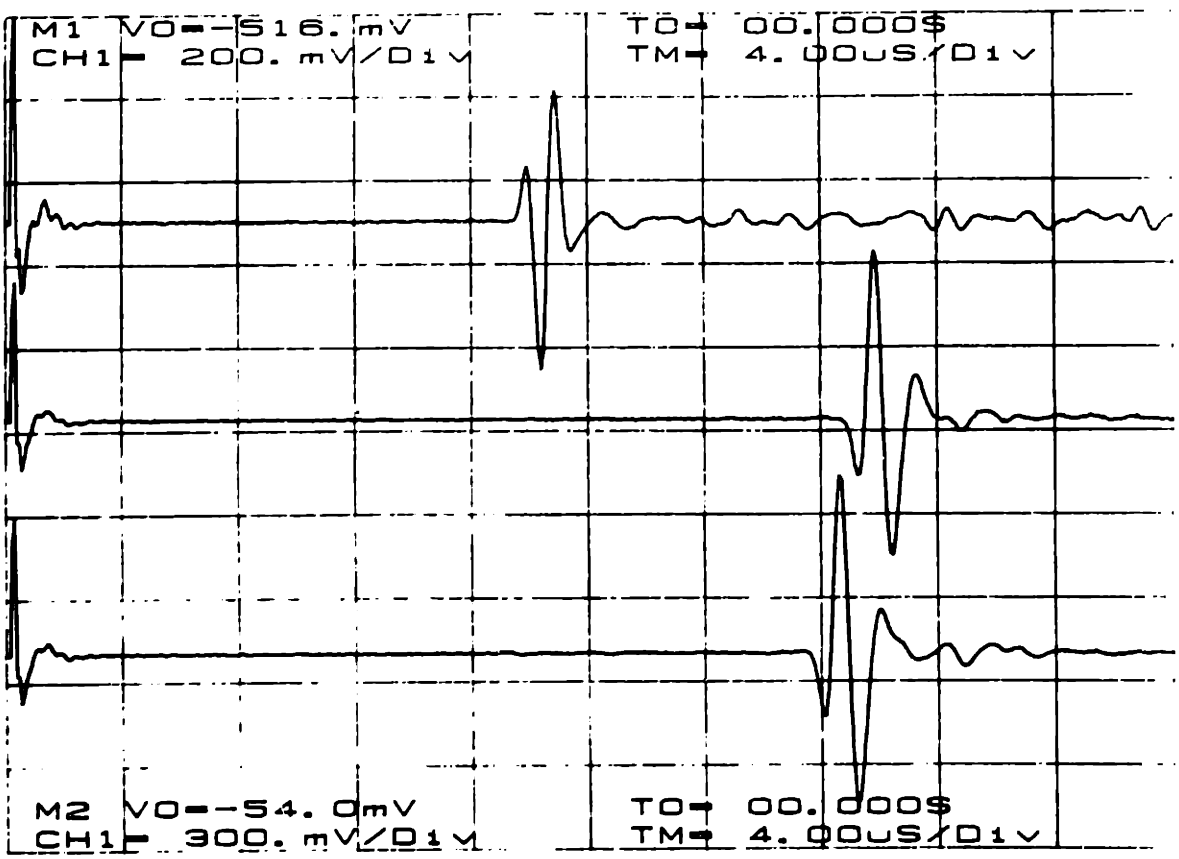


Figure 4-3. Examples of ultrasonic waveforms sequentially measured through a 5 cm thick core of Navajo sandstone at 1000 bars confining pressure. Top trace is P-wave and lower 2 traces are S-waves oriented at 90 degrees to each other. Signals are attenuated by -10 dB. The vertical voltage scale is 200 mv/div for the P-wave and 300 mv/div for the S-wave signals. Time is horizontal (4 $\mu$s/div) and the lefthand edge of the plot is the zero time at which the source is excited. Delay time introduced by the titanium transducer assemblies is approximately 7.54 $\mu$s for the P-wave, 13.7 $\mu$s for the middle S-wave, and 12.45 $\mu$s for the lower S-wave. S-wave arrival times are offset in the mechanical transducer design to isolate crosstalk.

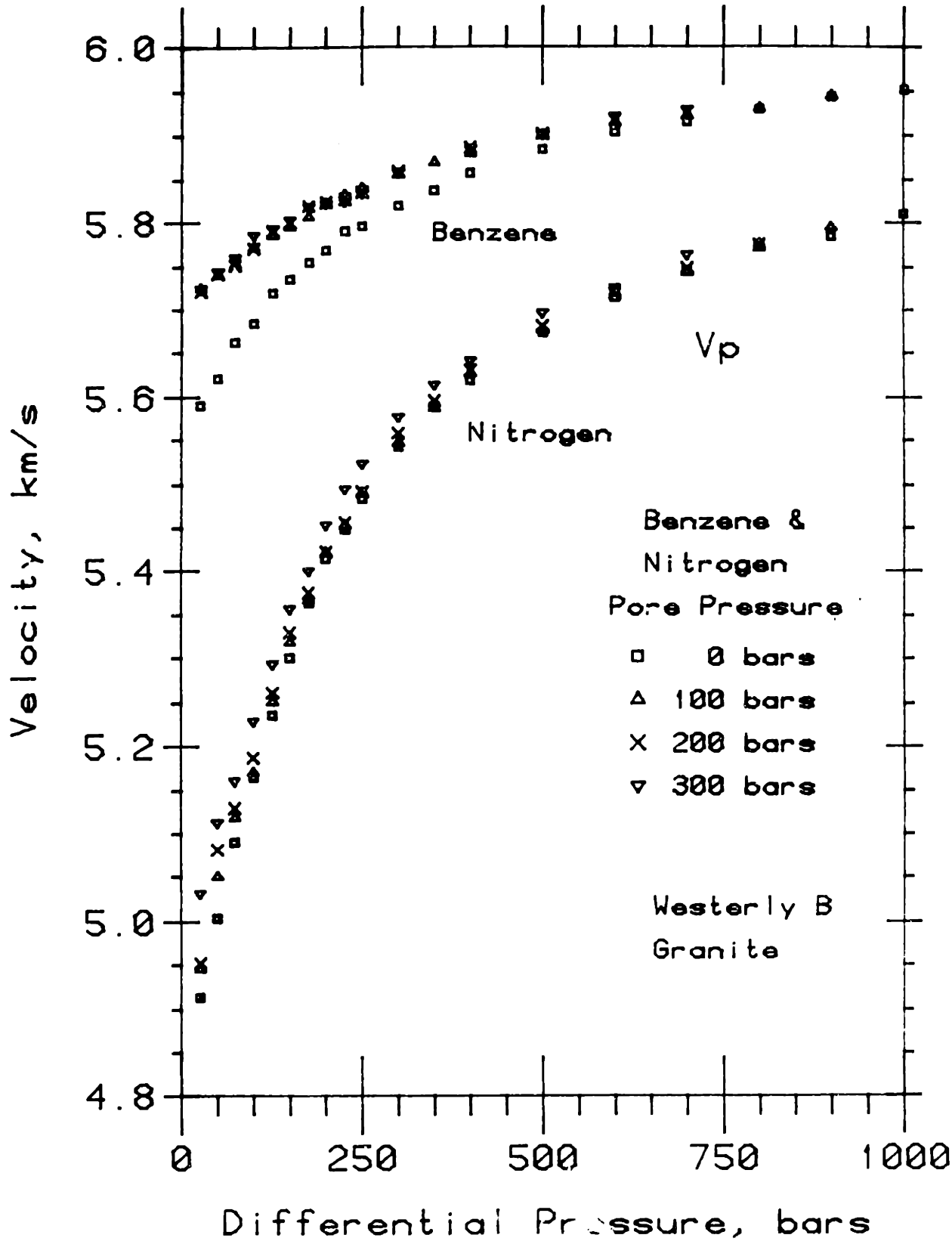


Figure 4-4. P-wave velocities versus differential pressure for Westerly granite at various benzene and nitrogen pore pressures.

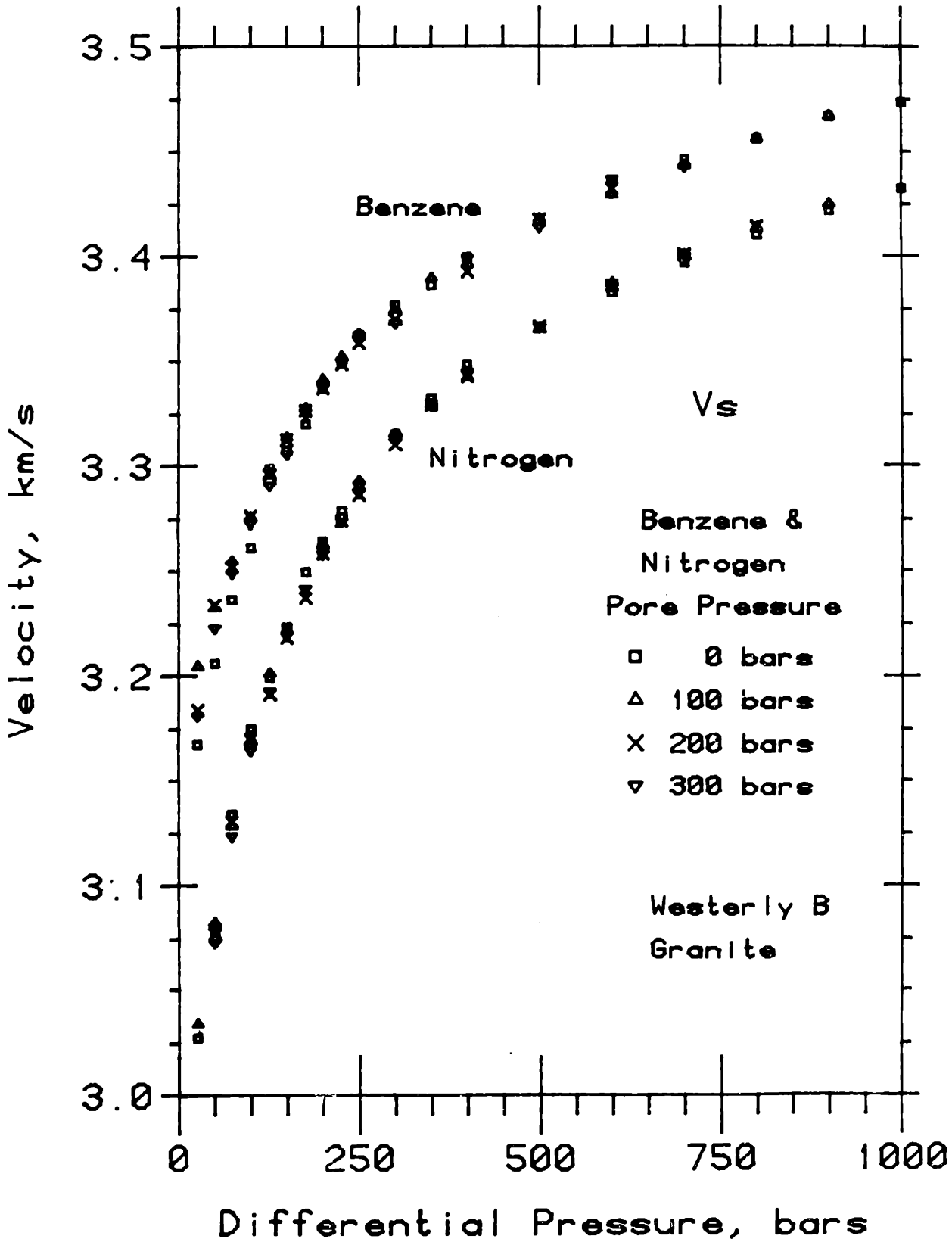


Figure 4-5. S-wave velocities versus differential pressure for Westerly granite at various benzene and nitrogen pore pressures.

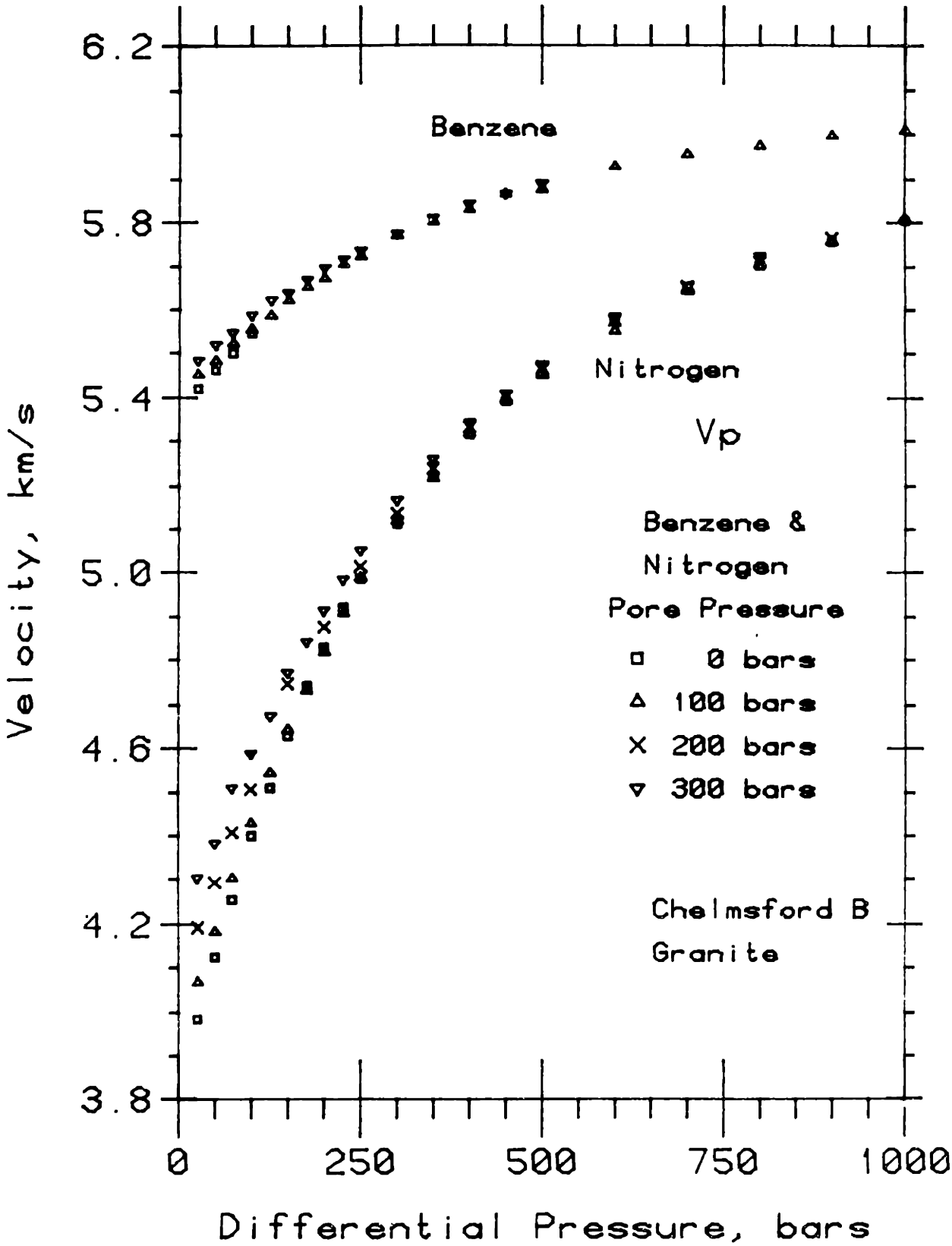


Figure 4-6. P-wave velocities versus differential pressure for Chelmsford granite at various benzene and nitrogen pore pressures.

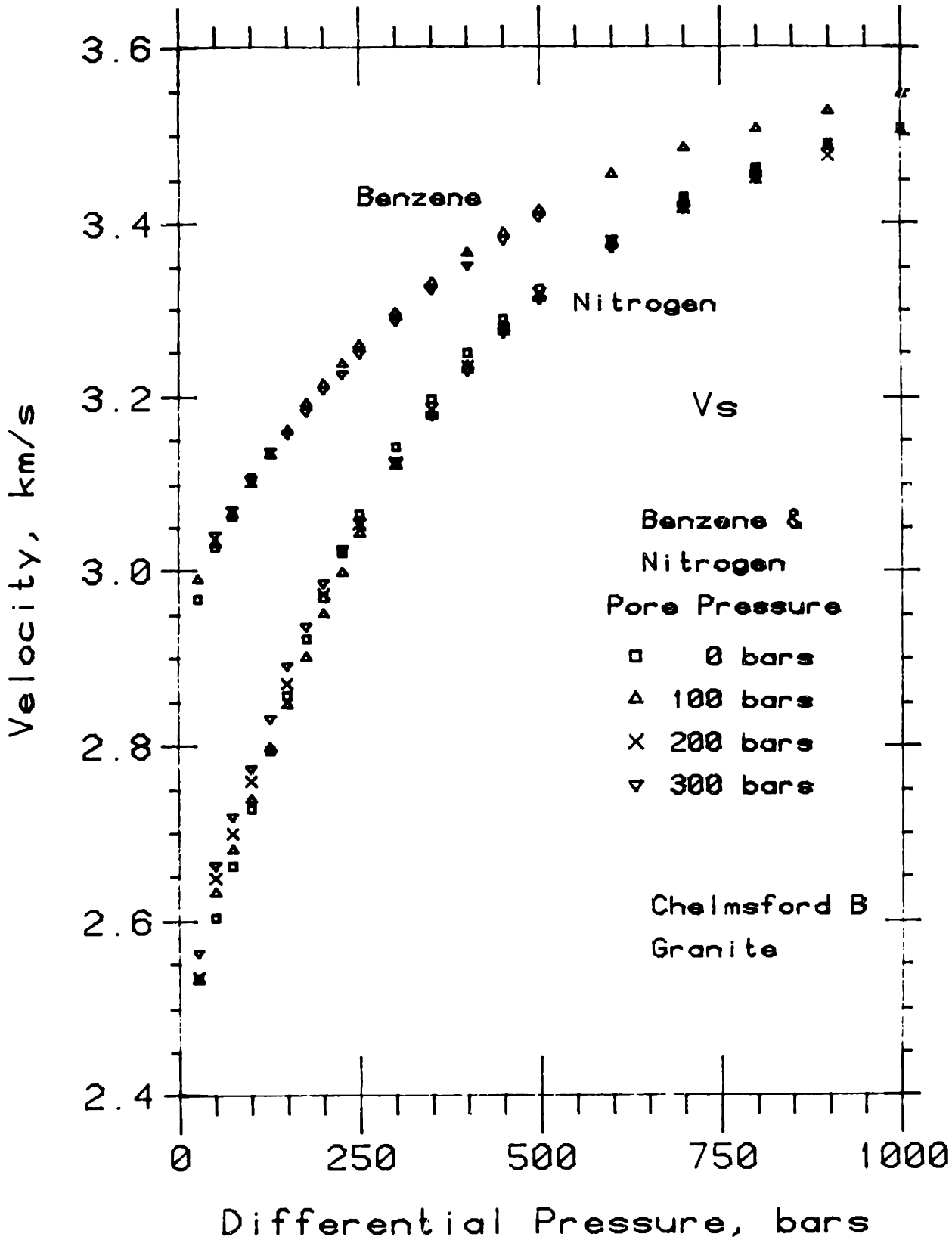


Figure 4-7. S-wave velocities versus differential pressure for Chelmsford granite at various benzene and nitrogen pore pressures.

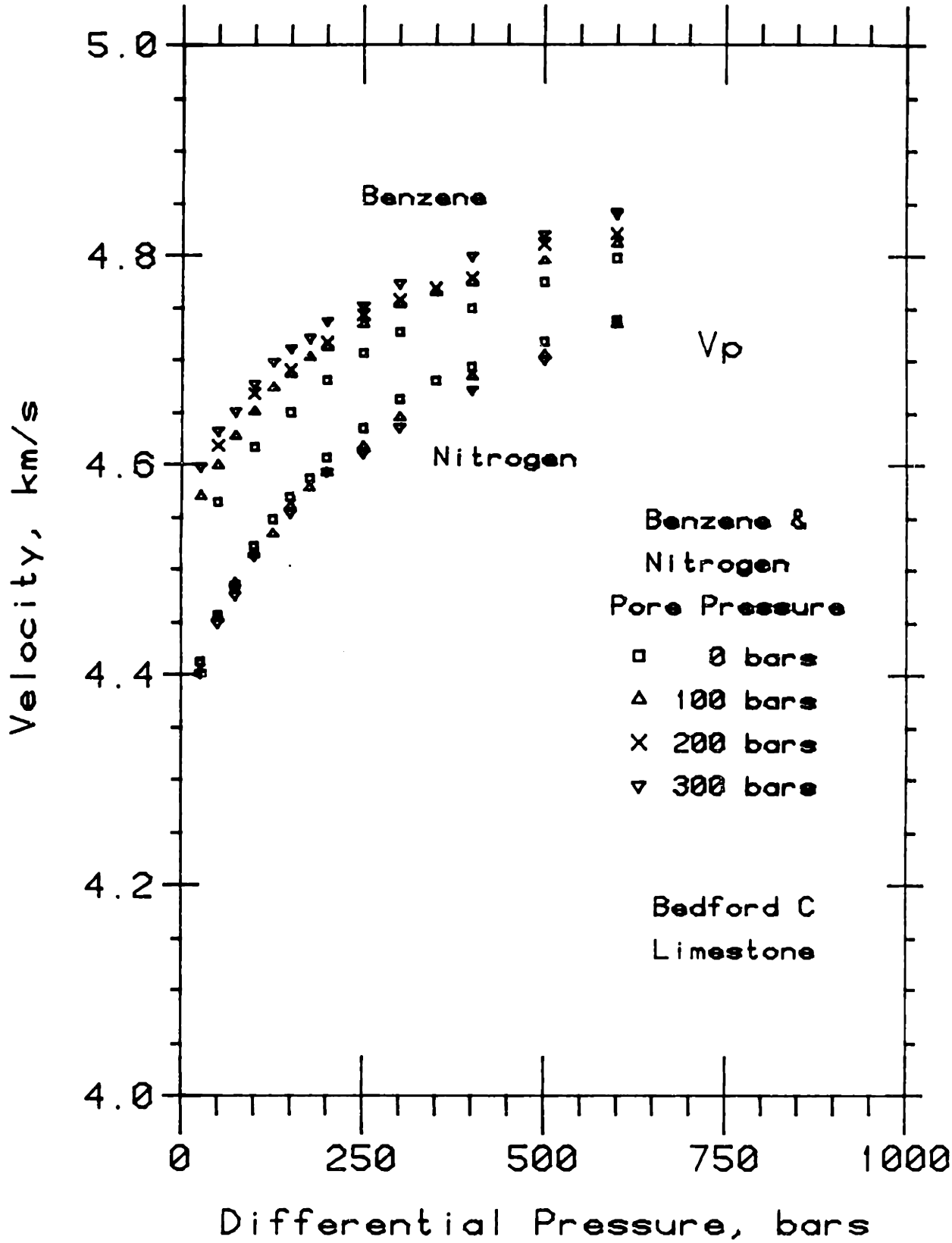


Figure 4-8. P-wave velocities versus differential pressure for Bedford limestone at various benzene and nitrogen pore pressures.

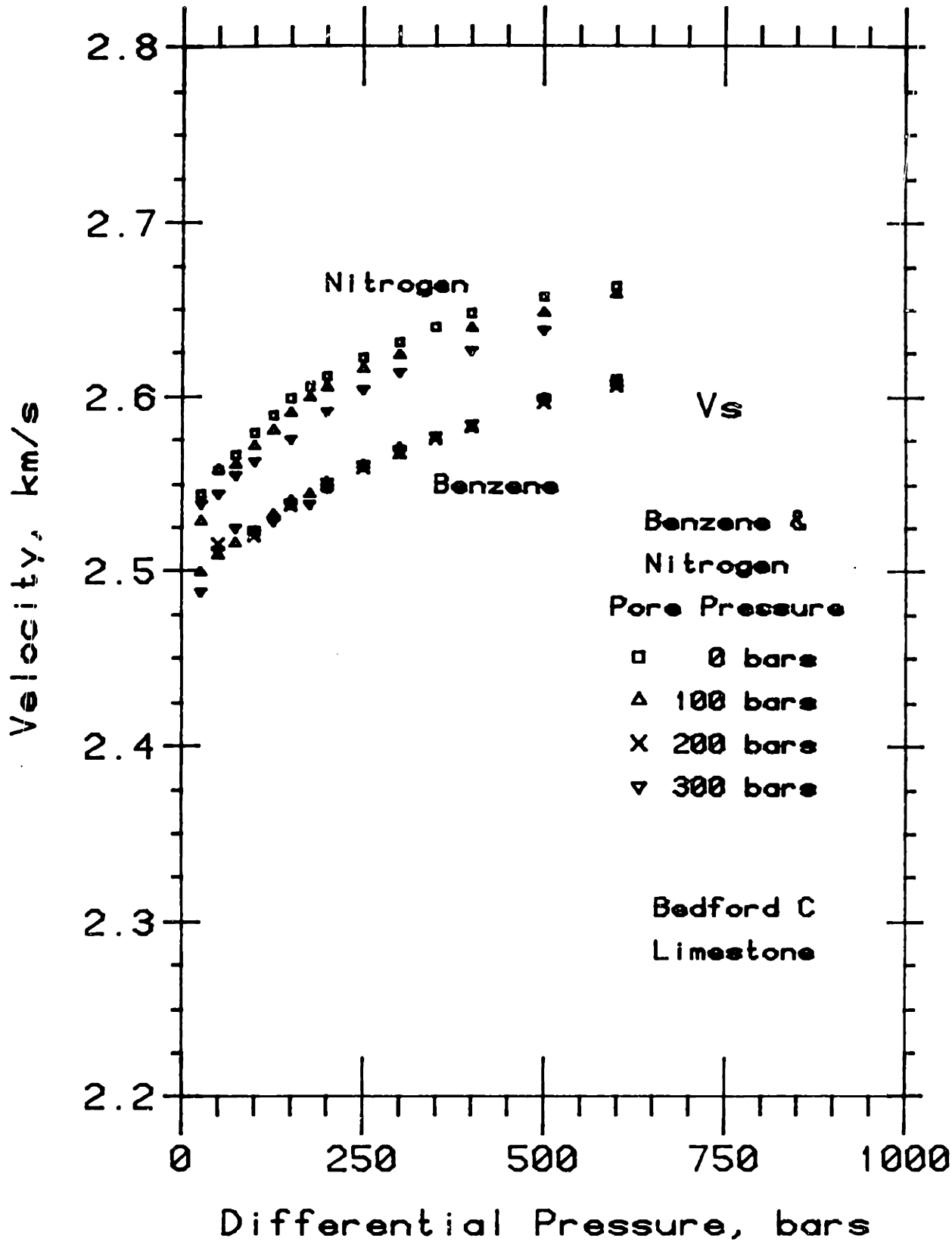


Figure 4-9. S-wave velocities versus differential pressure for Bedford limestone at various benzene and nitrogen pore pressures.

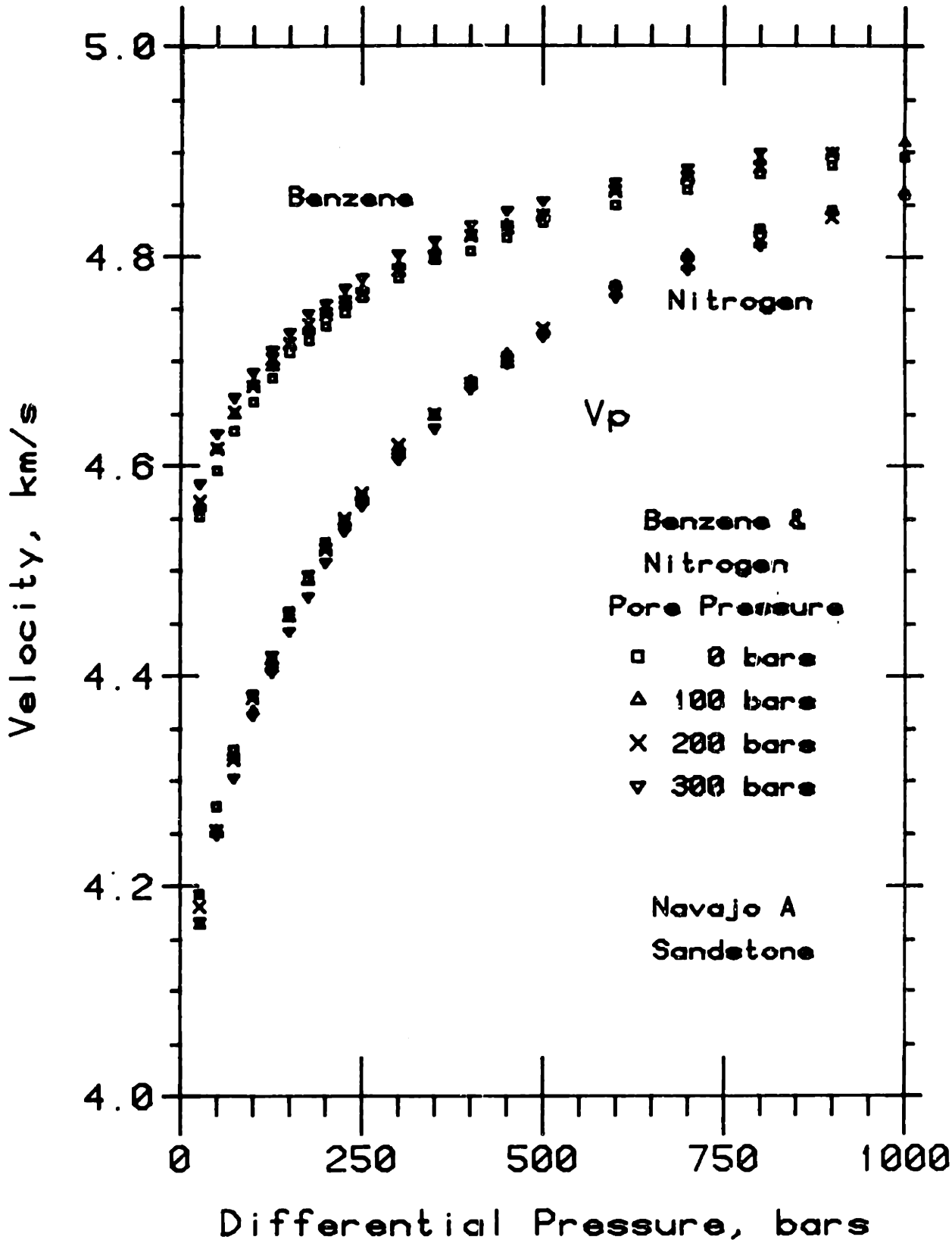


Figure 4-10. P-wave velocities versus differential pressure for Navajo sandstone at various benzene and nitrogen pore pressures.

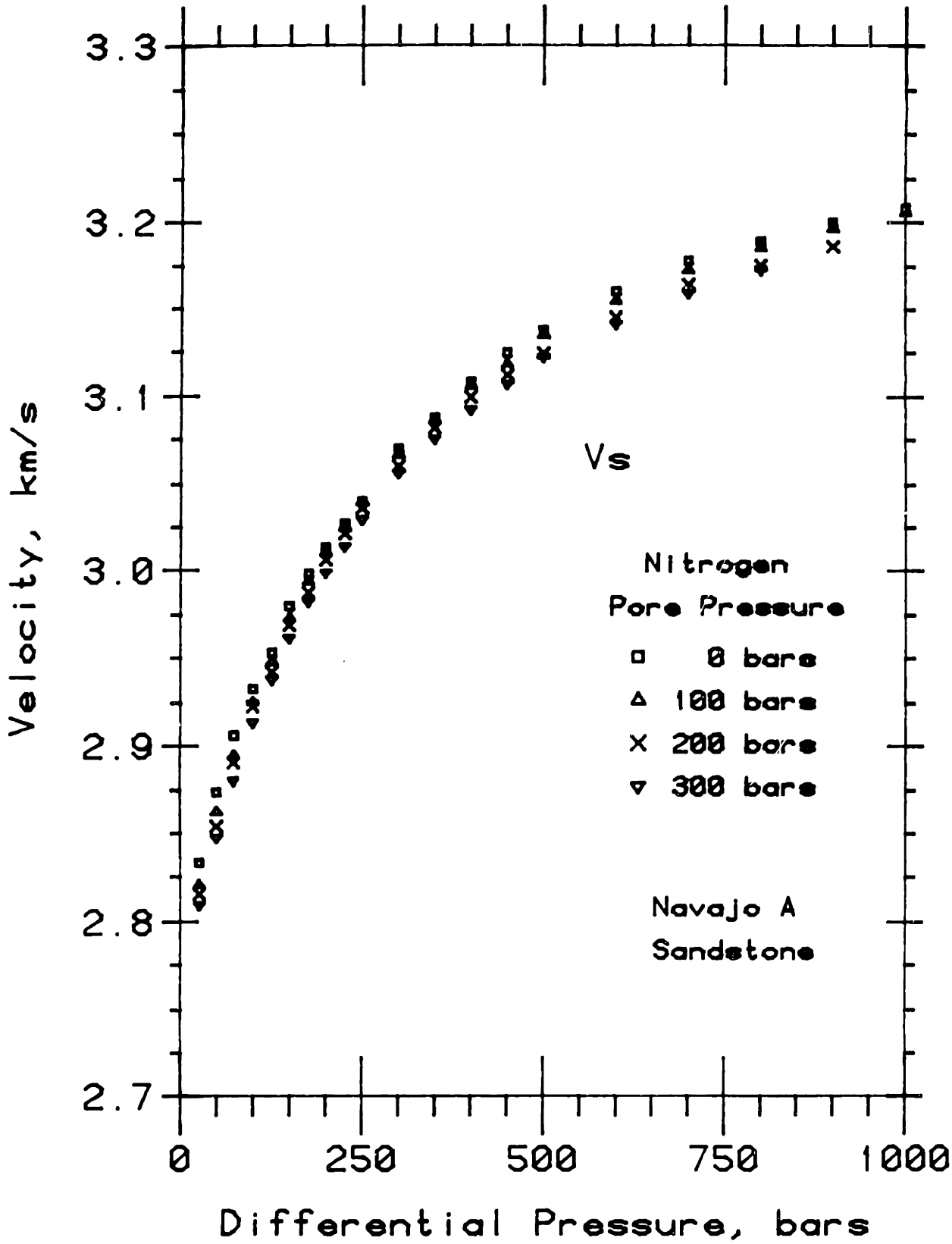


Figure 4-11. S-wave velocities versus differential pressure for Navajo sandstone at various nitrogen pore pressures.

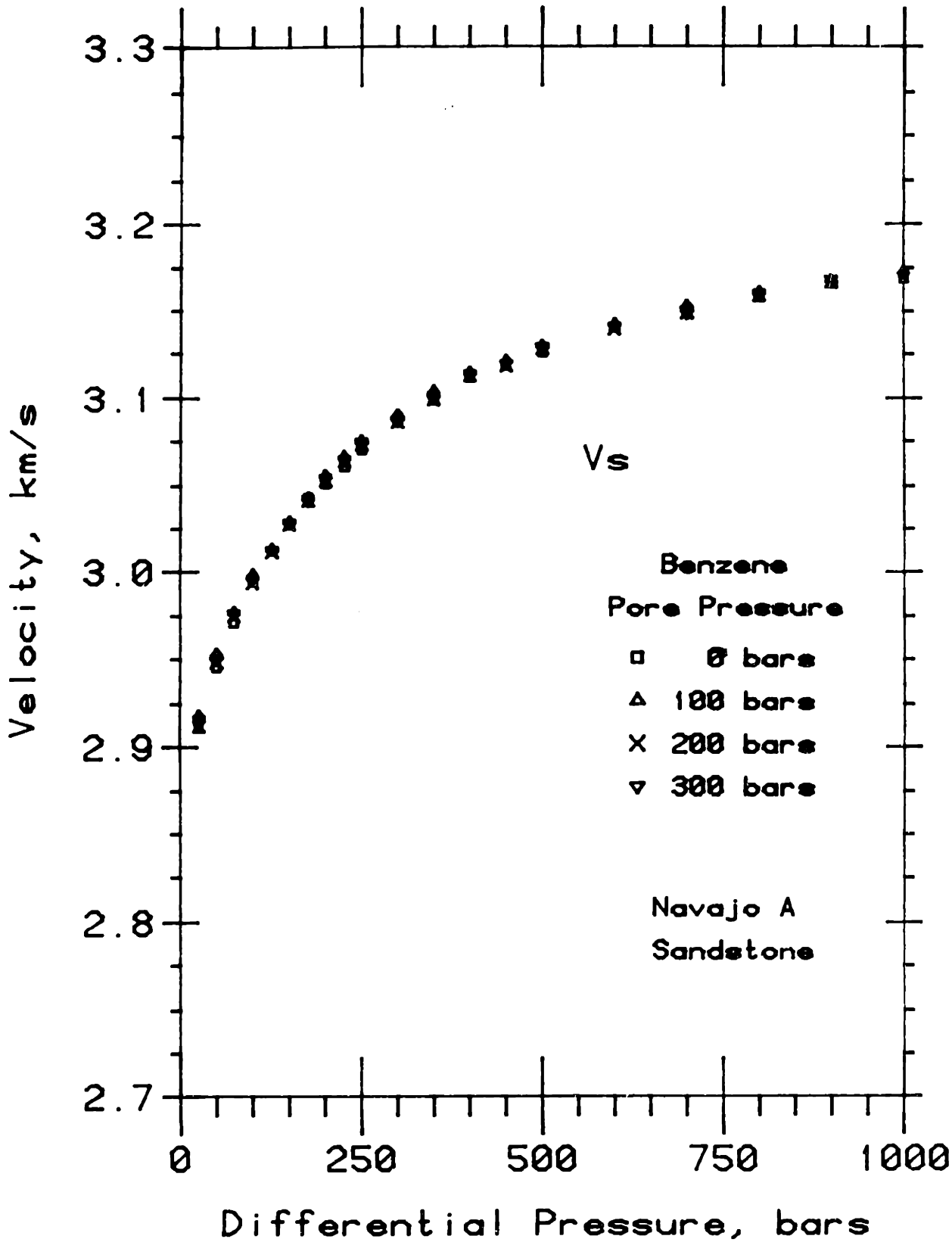


Figure 4-12. S-wave velocities versus differential pressure for Navajo sandstone at various benzene pore pressures.

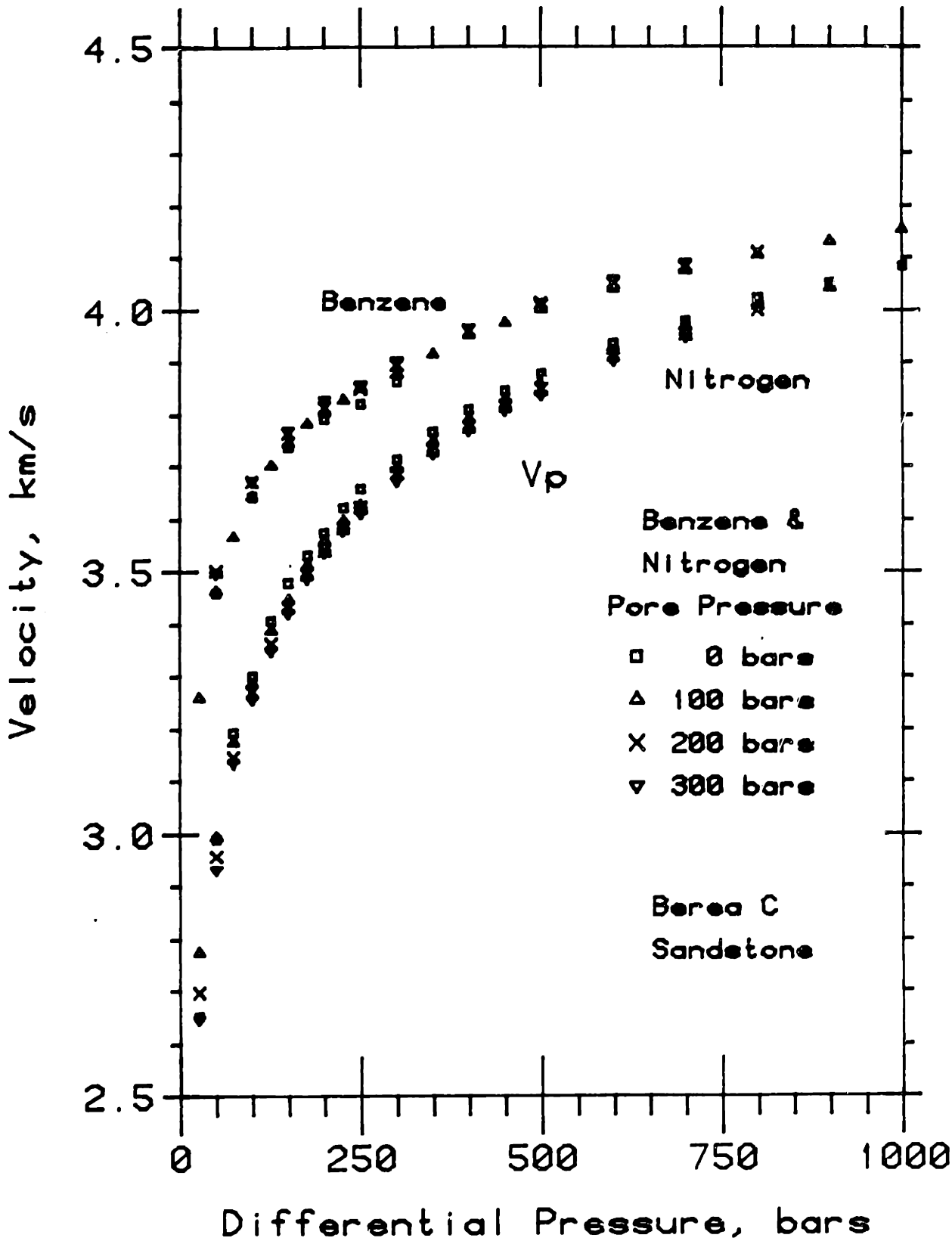


Figure 4-13. P-wave velocities versus differential pressure for Berea sandstone at various benzene and nitrogen pore pressures.

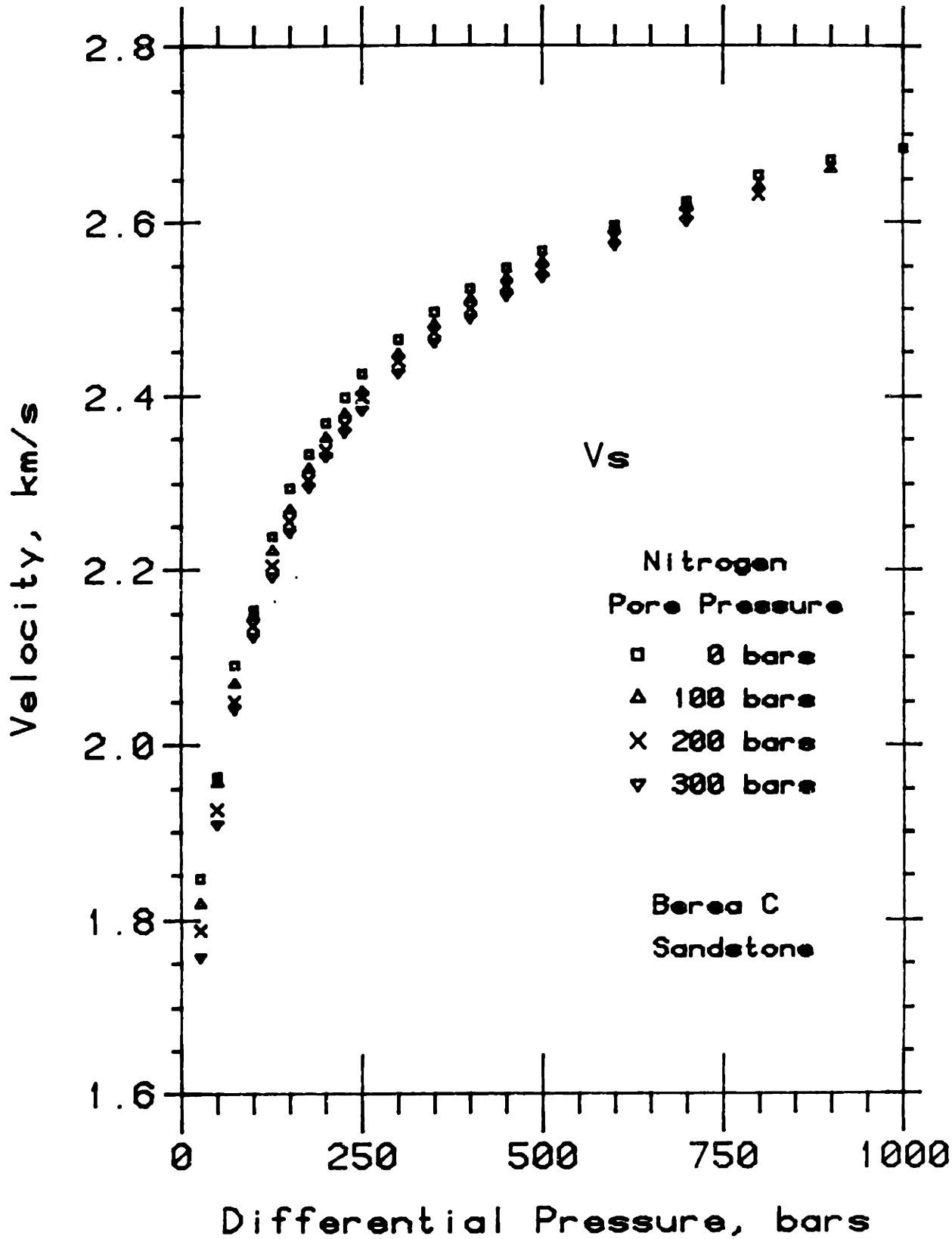


Figure 4-14. S-wave velocities versus differential pressure for Berea sandstone at various nitrogen pore pressures.

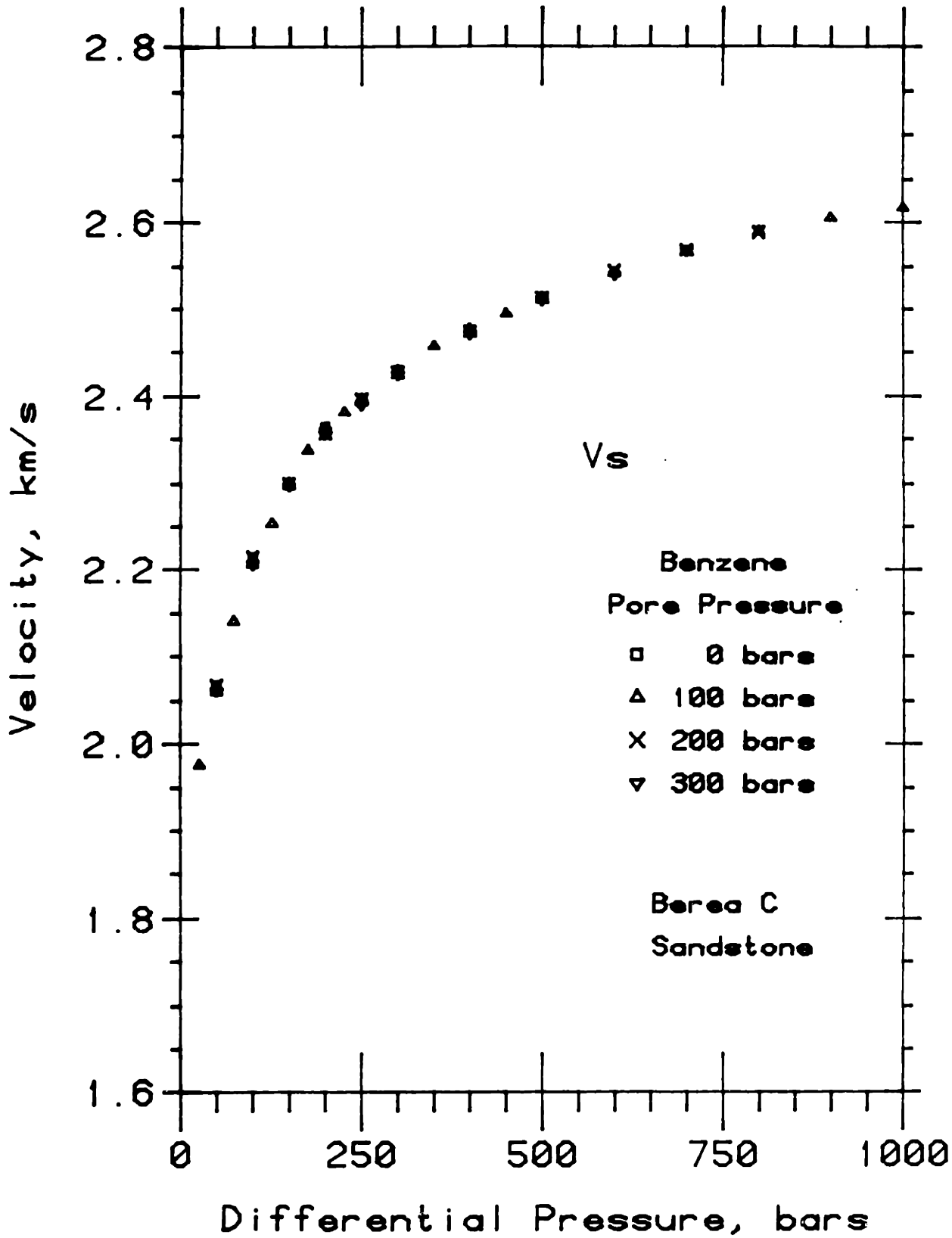


Figure 4-15. S-wave velocities versus differential pressure for Berea sandstone at various benzene pore pressures.

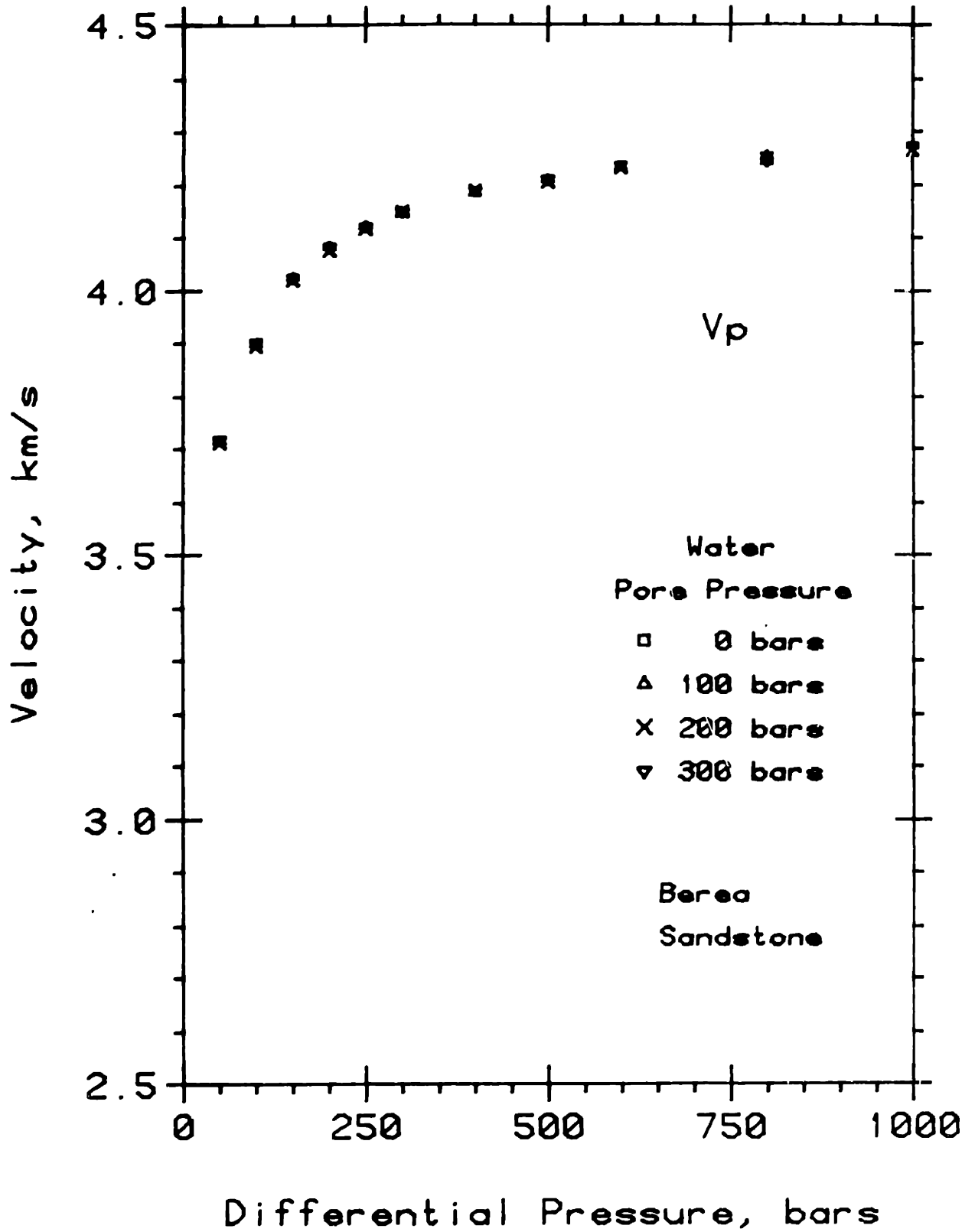


Figure 4-16. P-wave velocities versus differential pressure for Berea sandstone at various water pore pressures.

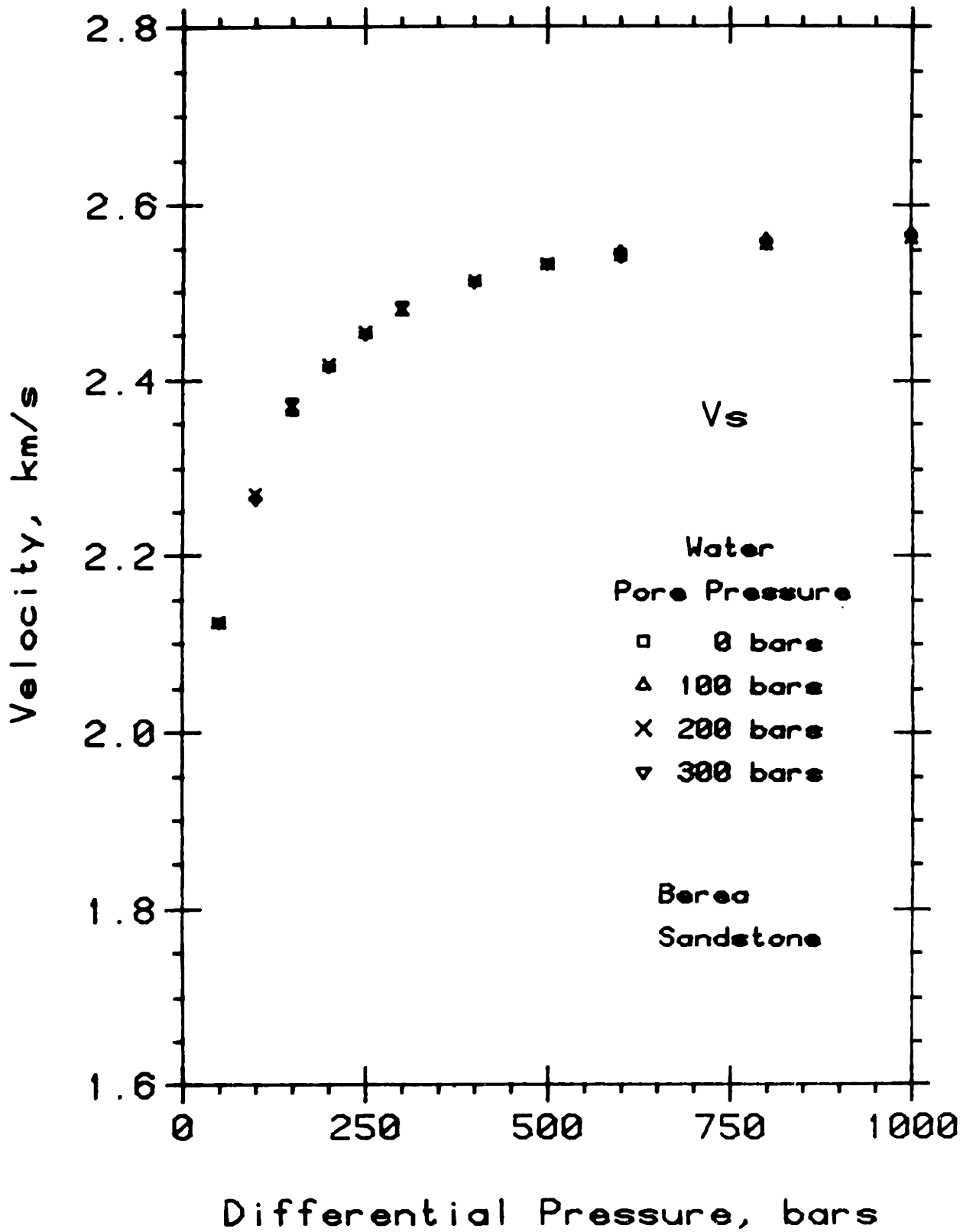


**Figure 4-17.** S-wave velocities versus differential pressure for Berea sandstone at various water pore pressures.

# CHAPTER 5

# THE EFFECTS OF CONFINING PRESSURE AND FLUID SATURATION ON ULTRASONIC VELOCITIES IN ROCKS

## INTRODUCTION

P- and S-wave acoustic velocities and attenuations in rocks depend on the mineralogy and nature of porosity peculiar to the rock, pore fluid properties, degree of saturation, frequency, and strain amplitude. The majority of these factors have been identified and can be isolated with laboratory experiments. In the laboratory acoustic properties may be measured as a function of stress, therebye changing the structural parameters while keeping mineralogy constant, and as a function of saturation, changing overall acoustic response by changing the nature of the pore fluid saturant. The effect of fluid saturation on measured P- and S-wave ultrasonic velocities in rocks are considered in this chapter.

Laboratory acoustic measurements of rock samples provide an ideal means for identifying the effects of pore fluids as well as for testing models of velocity and attenuation. The seminal experimental works of Wyllie *et al.* (1956), King (1966), and Nur and Simmons (1969) explored the effects of saturation and pressure on velocities. King (1966) measured ultrasonic P- and S-wave velocities of a suite of sandstone samples as a function of confining pressure for vacuum dry, water-, and kerosene-saturations. P-wave velocities increased upon saturation while the behavior of S-wave velocities were less regular, for some sandstones slightly higher than dry at low pressures while crossing over to lower

velocities at higher pressures. King (1966) interpreted the low pressure result as due to "relaxation effects" and also noted several instances where water saturated S-wave velocities were lower than the kerosene saturated velocities, indicating an effect of water on softening the quartz grain contacts. Nur (1969) and Nur and Simmons (1969) measured dry and water saturated P- and S-wave velocities for a suite of low porosity rocks. Their measurements clearly indicated a large increase of P-wave velocities upon water saturation while changes in S-wave velocities were much smaller and less regular. This was interpreted as an increase in bulk modulus for the saturated rock as narrow crack-like pores became much less compliant when filled with fluid. They concluded that the effect of saturation on S-wave velocity and the shear modulus was negligible.

Since these experimental studies several newer theories of the effect of cracks and ellipsoidal inclusions on acoustic properties have been developed, principally Kuster and Toksöz (1974) and Budiansky and O'Connell (1974). Both theories predict that the shear modulus and hence shear velocity should be larger upon saturation in porous solids where low aspect ratio, crack-like pores dominate.

This chapter presents a collection of "dry" and "saturated" ultrasonic P- and S-wave velocities which were measured specifically to investigate the effects of saturation and to check the validity of these crack models, in particular with regards to the higher saturated S-wave velocities in low porosity crystalline rocks. The definition of "dry" is a 20 $\mu$m Hg vacuum continuously applied to the sample for at least 24 hours before and as measurements were taken. The definition of "saturated" is benzene at 100 bars introduced through the pore pressure system into the sample under vacuum. Additional measurements with distilled water at 100 bars are also shown for most of the samples.

Benzene was chosen as the pore fluid in these measurements to reduce the deleterious effects of water, particularly in the higher porosity rocks at high confining pressures. An example of what happens when water versus benzene is added at these high pressures is shown in Fig. 5-1. Plotted is a set of stress-strain relations for a vacuum dry, water saturated, and benzene saturated sample of Berea sandstone. The introduction of water into the sample under pressure "softens" the rock so that linear strain increases, due to fluid interaction with the quartz grains or interstitial cements. Note that the three curves are pretty much parallel after a few hundred bars, so that the nature of porosity at low pressures are at least partially modified in the rock over the whole pressure range. This effect of water on static strain is contrasted with the presence of benzene as the pore fluid, which has little effect on strain except for a slight increase. Wyllie *et al.* (1958) also report similar effects for a sample of Berea sandstone saturated alternately with dry air, oil, silicone fluid, and water. Maximum strain was measured with water as the pore fluid; minimum strain was measured for the dry sample. Significantly, the silicone measurements were nearly as high as those with water, indicating that perhaps the solubility or wetting properties are not as important as the lubricating properties of the pore fluid. Similar strain measurements of dry and water saturated samples were made by Mann and Fatt (1960) for a number of sandstones. They too observed the large increase of water-saturated strain.

The effect of water is not simply static but is translated into dynamic measurements of velocities also. For many of the samples measurements of dry, benzene and water saturated velocities were made, and comparison of the different saturants will be made. This effort is reminiscient of King (1966), who compared dry, kerosene, and water saturations as a function of pressure for a number of sandstones. The most obvious effect of water saturation in his

measurements and in the present measurements was to severly reduce saturated S-wave velocities at high pressure. The softening mainly results in a lowering of the dry shear modulus.

Models of how rock matrix and pore shapes determine velocities often rely on a comparison of two endmembers, dry and completely saturated. In this paper the saturated case is a benzene saturated condition so as to minimize as much as possible the interaction of the saturating fluid with the matrix and fine-scale porosity. Obviously this removes these measurements from the realm of reality in terms of the earth, but that is not the purpose here. The purpose, which occupies the second half of this chapter, is a comparison of the dry and saturated velocities with models from which the prediction of saturated velocities can be made. All of these models rely on moduli measurements taken on the dry sample being isolated and applicable to the saturated measurements in combination with saturating fluid properties. Therefore the most valid analysis of these models with laboratory data is made

The laboratory apparatus and procedures used in the measurement of velocities as a function of saturation and pressure were described in Chapter 4 of this thesis. Briefly, the principle features of the apparatus are: 1) large 7.5 cm diameter by 5 cm long samples, 2) independent hydrostatic confining pressure and pore fluid pressure or vacuum, 3) isolation of ceramic transducers from the pressure media, 4) selection of P- and two mutually perpendicular S-waves at any given time for velocity and Q measurement, 5) computer control of the experiment. The center frequencies of the waveforms are approximately 800 - 900 kHz. Temperatures were laboratory ambient, about 18 to 23 ° C.

Travel time was determined by a threshold voltage 2.5% of the overall peak-to-peak voltage of the amplified and filtered digitized signal. The accuracy of the

measured travel-time is approximately ±15 ns. Lengths of samples were initially measured and corrected for shortening under pressure from strain measurements. The overall accuracy of calculated velocities is about ±0.2%.

The samples in this study are tabulated in Table 1. The sample suite includes holocrystalline granitic rocks, sandstones, a metamorphic dolomite, and a limestone. Also included in Table 1 are dry bulk densities and porosities for each of the samples calculated from dry and water- or benzene-saturated weighings. Appendix B contains a description of these rocks from hand specimen and thin section analysis. Stress-strain measurements and static moduli calculations for these samples can be found in Chapter 2.

After cycling the confining pressure was held at 20 bars for about 12 hours with constant 20 $\mu$m Hg vacuum applied to the pore pressure system and sample before acoustic data was collected. Vacuum dry measurements were made first as a function of confining pressure. After completing the cycle the system was allowed to rest at a pressure of about 10 bars for no less than 12 hours. Confining pressure and then pore pressure were raised to 100 bars pressure and the confining pressure cycled to the highest pressure while pore pressure was maintained at 100 bars.

Benzene saturated measurements always preceded water saturated measurements. After the benzene measurements samples were removed from the pressure vessel and thoroughly dried under vacuum at 80 ° C. Samples for which measurements with water were carried out were then rejacketed and the entire procedure repeated with water instead of benzene as the pore fluid.

## EXPERIMENTAL RESULTS

The experimental measurements of dry and saturated P- and S-wave velocities are presented in two separate sets. In the first set, Figs. 5-2 through 5-13, are plots of the vacuum dry (open squares) and benzene-saturated (solid squares) P- and S-wave velocities versus differential confining pressure for the 9 rocks listed in Table 1. Three of the plots, Figs. 5-4, 5-6, and 5-9, record the measured anisotropy of S-wave velocities for the samples of Barre granite, Chelmsford granite, and Bedford limestone. The saturated data was collected with benzene at a constant pore pressure of 100 bars to ensure complete saturation. All of the velocities are calculated from data collected as the confining pressure was increased. The velocity scales for each of the four low-porosity rocks and for the five higher-porosity rocks are the same for ease of comparison.

The second set of data, Figs. 5-14 through 5-23, are plots of the vacuum dry (open squares), benzene saturated (solid squares), and water saturated (solid squares as labelled in each plot) P- and S-wave velocities versus differential confining pressure for five of the samples. These include the Westerly granite, Bedford limestone, Weber sandstone, Berea sandstone, and Kayenta sandstone samples. In these plots the P- and S-wave velocities for each sample are shown in successive plots. The benzene saturated velocities are repeated from the data shown in Figures 5-2 through 5-13.

For the 5 samples which were measured dry, benzene-, and water-saturated, dynamic bulk and shear moduli have been calculated as a function of differential confining pressure. These are plotted in Figs. 5-24 through 5-33. Isotropy has been assumed in these calculations. Bulk and shear moduli for each of the samples are shown in successive plots.

The general features to be observed and discussed are the effects of pressure, saturation, and different types of pore fluids. Confining pressure increases both P- and S-wave velocities. This is interpreted to be a result of crack and pore closure. Pressure may completely close a crack or, probably more often the case, simply force rough surfaces into contact. Either process results in a more efficient transmission of stress through the rock and higher velocities. The rate of change in velocity with pressure is more rapid at low pressure as the more compliant cracks close. For most of the rocks the most dramatic increases in velocities have occurred by about 500 bars.

Saturation of rock porosity with liquids may either decrease or increase P- and S-wave velocities depending on the pressure and fluid type. In every instance P-wave velocities increase upon fluid saturation. For the low porosity crack-dominated rocks S-wave velocities also increase, and for the higher porosity sandstones S-wave velocities increase at low pressures but fall below dry at high pressures. The pore fluid saturants, benzene and water, show significant differences in there effect on velocities which are not interpretable based on fluid bulk modulus and density. The water saturant decreases the overall shear modulus, particularly at high pressures, so that S-wave velocities, in particular, are reduced. In the following paragraphs the effects of saturation, pore fluid type, and confining pressure are discussed for the low porosity granites, the dolomite, the limestone, and the sandstones.

Perhaps the most significant result in this velocity data is for the 3 granitic rocks, the Westerly, Barre, and Chelmsford, and for the Webatuck dolomite. Nur (1969) and Nur and Simmons (1969) measured dry and water-saturated velocities for all of these rocks except the Chelmsford. Their major conclusion was that P-velocities increase greatly upon water-saturation because of the large increase in effective bulk modulus with water in the cracks. For shear velocities they

measured a less regular behavior. Generally for confining pressures less than about 200 bars they found that water saturated S-wave velocities were higher than dry, but that at higher confining pressures saturated velocities fell below their dry measurements. They concluded that saturation had a nil effect on shear modulus. The data shown for the 3 granitic rocks and the dolomite support their conclusion for P-wave velocities but alter their conclusion for S-wave velocities. Clearly and consistently the saturated shear velocities are higher than the dry. Since the density increase for these rocks is negligible the saturated shear modulus in addition to the bulk modulus are both higher than in the dry case.

Velocity data for the Westerly granite sample (Figs. 5-2, 5-14, and 5-15) and the bulk and shear moduli as a function of differential pressure (Figs. 5-24 and 5-25) can be discussed in terms of saturation, the effect of different pore fluids, and compared with the data of Nur (1969). Compared with the other low porosity rocks the effects of saturation and confining pressure are the smallest for this rock. Both P- and S-wave velocities increase upon saturation with benzene and water, S-wave velocities only slightly, P-wave velocities much more. Compared with the data of Nur (1969), the dry velocities are nearly the same. The water saturated P-wave velocities of Nur (1969) at confining pressures below about 500 bars are systematically lower than in the present data (Fig. 5-14). This is perhaps due to incomplete saturation as noted in Chapter 4. As pore pressure was not controlled at a level above atmospheric a slight concentration of undissolved gas in the water would reduce fluid bulk modulus and lead to lower P-wave velocities. In the present measurements of P-wave velocities with benzene and water as the pore fluid saturants (Fig. 5-14) the higher bulk modulus of water (22.4 Kbar, Table 2) results in a higher velocity as compared with the benzene, which has a fluid bulk modulus of about half that of water (12.1

Kbar, Table 2). This is apparent in the bulk moduli calculated for the dry and two pore fluid saturations and shown in Fig. 5-24. The dry bulk modulus increases with pressure quite dramatically over the first 500 bars as small cracks close with pressure and transmit the acoustic stress wave more efficiently. Upon saturation the relatively incompressible pore fluids greatly diminish the compressibilities of cracks and the bulk modulus increases. In the data for Westerly granite there is probably some difficulty with the benzene saturated data at very low pressures (less than 150 bars). Above this pressure the difference between the bulk modulus with the two different fluids is relatively constant, the water saturated bulk modulus higher than the benzene because of the higher fluid bulk modulus for water.

The S-wave velocities for Westerly granite (Fig 5-15) and calculated shear moduli (Fig. 5-25) indicate both the increase due to saturation and also a possible effect of the water similar to that which will be noted in the sandstones. Nur's (1969) data showed that water saturated S-wave velocities fell below dry at pressures between 100 and 150 bars and systematically stayed there at higher pressures. This observation cannot be explained in terms of fluid bulk modulus or density; the porosity is not high enough for density to decrease velocities, as will be shown in the modelling section with Gassmann's equation. The benzene data in Fig. 5-15 shows that shear modulus and velocities are consistently higher than dry, and comparison of the different data sets for low porosity rocks indicates that the larger the crack porosity, the larger the increase in S-wave velocities above dry. It might also be concluded that the higher the bulk modulus of the saturating fluid, the higher the saturated S-wave velocities should be. The water data in Fig. 5-15 is higher at lower pressures (less than about 200 bars) but falls below the benzene data at higher pressures, dropping nearly to the dry velocities at 1 Kbar differential pressure. This is clearly seen in

the calculated shear moduli for the different fluid saturations in Fig. 5-25. Apparently the water is reducing the overall shear modulus by interacting with the matrix in the same manner as will be noted for the sandstones. Perhaps the data of Nur (1969) is recording a similar effect. For the low porosity rocks only Westerly was measured with water and only with one experiment. This result should be considered preliminary.

The velocity data for Barre granite (Figs. 5-3, 5-4) indicates that the effect of confining pressure and fluid saturation is intermediate between that on Chelmsford granite and Westerly granite. Benzene saturated P- and S-wave velocities are higher than dry by an amount intermediate between the other two granites. The terminal S-wave velocities at high pressures are almost the same for Westerly and Barre granite; the mineralogical modal analysis for theses two rocks are fairly similar (Appendix B) and at high pressure, when the effects of differing crack porosity are lessened, the velocities of the two converge. Dry P-wave velocities are less for the Barre, however, and saturated P-wave velocities are nearly the same at high pressure. The measured anisotropy in the two S-wave arrivals (Fig. 5-4) is interesting from the point of view of the effect of saturation. The difference between the directions of shear is reduced with the introduction of benzene.

The velocity data for Chelmsford granite (Figs. 5-5, 5-6) contains the most sizable effects of saturation on S-wave velocities. As will be presently discussed, Chelmsford also has the highest amount of crack porosity of the rocks studied. For the three granites the P-wave velocities increase the greatest upon saturation. The S-wave velocity anisotropy recorded in Fig. 5-6 indicates that both dry and saturated velocities with sense of shear across the rift direction are lower than the S-wave velocities across the headgrain, the propagation direction being perpendicular to the grain plane. Shear velocities in the same directions

on a dry sample of Chelmsford granite measured by Todd (1973) are somewhat different. At a confining pressure below about 700 bars the velocities across the rift were lower, in agreement with the present data. At higher confining pressures, however the data of Todd (1973) shows that S-wave velocities across the rift become higher than those across the headgrain. This was interpreted by Todd (1973) as an indication of crack-dominated moduli at lower pressures and mineral-dominated moduli (orientation of mica grains) at higher pressures.

The velocity data for Webatuck dolomite (Fig. 5-7) are consistent with the previous discussions of crack-dominated moduli and the effects of saturation and pressures. P- and S-wave velocities are higher with saturation, the P-wave velocities increasing the most in comparison to the other low porosity granites. At pressures above about 400 bars dry and saturated S-wave velocities converge, the saturated only slightly higher than dry. Terminal velocities at high pressure for the dolomite are higher than the granites because of the high bulk and shear modulus of the mineral dolomite. Nur (1969) measured dry and water saturated velocities from the same block. Similar behavior was observed for the P-wave velocities, but for the S-wave velocities he observed the same values between dry and saturated at pressures less than about 300 bars and higher dry values at higher pressures. This difference between the data of Nur (1969) and the present data is perhaps explained by the effect of water on the solubility of dolomite.

The effect on velocities with saturation correlates with crack porosity (Walsh, 1965) as was previously pointed out for P-waves by Nur (1969) and Nur and Simmons (1969). The correlation is somewhat confused however by the severe anisotropy in the Barre and particularly in the Chelmsford granite. Crack porosity is measured by referring back to the porosity versus pressure plots for these rocks in Chapter 2. The original definition and technique for measuring

crack porosity (Walsh, 1965) was intended merely to calculate porosity in cracked solids from volumetric stress-strain curves. In Chapter 2 it was shown how the subtraction of unjacketed from jacketed stress-strain data gives porosity as a function of pressure. Here those porosity curves are referred to. The idea is to fit a linear line to the porosity function at high pressure and then extrapolate back to zero pressure. Differences between that line and the measured porosity can be interpreted as due to the effect of cracks and called crack porosity. This is if the nonlinear aspect of stress-strain data is interpreted as due to the effect of cracks. The data in Chapter 2 was not really collected at high enough pressures to achieve a linear slope but an estimate of crack porosity sufficient for the present purpose can be obtained by taking the porosity decrease between zero and 1 kbar pressure. For Westerly granite this decrease is 0.08%, for Barre granite 0.22%, for Chelmsford granite 0.35%, and for the Webatuck dolomite 0.17%. This is actually a nice distribution of rocks except for the anisotropy. Looking at the Westerly velocity data it is seen that the lowest crack porosity correlates with the lowest jump in saturated P- and S-wave velocities over dry. Another correlation is with the rate of change of velocities with pressure which for Westerly, and particularly for the saturated P- and S-velocities, is lowest compared to the other low porosity rocks. The jump in saturated shear velocities is greatest for Chelmsford, which has the largest crack porosity, and intermediate for Barre granite. The differences between dry and saturated P-wave velocity are just about the same at zero pressure and so do not correlate with crack porosity. To emphasize again however these rocks are quite anisotropic in velocity, particularly the dry, at low pressure. The Webatuck dolomite also differs in that the P-wave velocity increase upon saturation is the greatest but the estimated crack porosity is 2nd lowest.

The Bedford limestone velocities (Figs. 5-8, 5-9, 5-19,5-17) are quite unique. In the pressure vessel the sample was never subjected to confining pressures higher than 600 bars in order to minimize the severe matrix damage noted by Johnston (1980) and seen in the data of Nur (1969). The stress-strain relation for this rock (Chapter 2) is nearly linear and consequently there is little or no natural crack porosity. The The effect of benzene and water saturation is to uniformly lower the shear velocities (Fig. 5-17). In Fig. 5-27 the shear modulus versus pressure is nearly the same for dry, benzene- and water saturations, ane the saturated velocities are therefore predicted on the basis of bulk density alone. In other words, this is the only rock measured where the dry and saturated shear moduli are apparently equal. There must be a few lower aspect ratio pores however, because the P-wave velocities show some pressure dependence and saturated P-velocities are higher then dry, the water saturated values being the highest. The bulk moduli in Fig. 5-16 indicate a uniform increase in water saturated moduli above the benzene saturated ones. A small but consistent anisotropy in the S-wave velocities is recorded in Fig. 5-9 for dry and benzene saturations. The lower velocities are perpendicular to bedding which is probably a result of groundwater dissolution/reprecipitation of the calcite. Nur (1969) measured velocities of Bedford limestone at much higher pressures and over many more cycles, a procedure which introduces irreversible grain crushing and hysteresis in velocities and attenuation (Johnston, 1980). In the present measurements confining pressure was kept low, less than 600 bars, to avoid these effects. Interestingly, the grain crushing introduces a population of cracks which are almost undetectable in the saturated P-wave velocity measurements. The dry P-wave velocity data of Nur (1969) shows tremendous increases with confining pressure, from under 3 km/s at pressures near 0 up to nearly 4.4 km/s at 1 kbar, while the present data shows only slight pressure sensitivity. Saturated velocities, however, are nearly the same in the two sets of

data, indicating that the presence of fluid in the pore space essentially "heals" the introduced cracks. The same, however, cannot be said for the S-wave velocities because in the data set of Nur (1969) there is the same pressure sensitivity and little difference between dry and saturated values.

The four sandstones, Weber, Navajo, Berea, and Kayenta, in order of increasing porosity, present an interesting spectrum of dry versus saturated velocities which contrast the effects of cracks and pores versus bulk density. Dry and benzene P- and S-wave velocities for the four are plotted in Figs. 5-10 through 5-13. Dry, benzene, and water saturated velocities are plotted in Figs. 5-18 through 5-23 for the Weber, Berea, and Kayenta samples. The important points to be made concern the effects of saturation versus the different saturants. To varying degrees the water saturated velocities, particularly the shear, indicate that water has a softening effect, especially at high pressure, relative to the benzene. This is clearly indicated in the calculated bulk and shear moduli plotted in Figs. 5-28 through 5-33. Bulk moduli for the different sandstones are higher for the water saturations because of the higher fluid bulk modulus for water, and the interpretation is consistent for all samples. Shear moduli, on the other hand, indicate that at low pressure water saturated shear moduli are higher than dry and the benzene saturated ones. As pressure is increased the water saturated shear moduli fall below the benzene shear moduli and then the dry moduli at high pressures. The effect of water is to reduce the shear moduli, particularly at high pressure, in a manner which is not readily explained on the basis of fluid modulus and density. Similar behavior for a number of sandstones can be found in the data of King (1966), who compared dry, kerosene, and water saturated P- and S-wave velocities for a number of sandstones.

For the benzene saturated S-wave velocities the Navajo, Berea, and Kayenta samples all show a crossing-over of dry and saturated at confining pressures between 200-500 bars. This is interpreted as a transition between crack-dominated velocities at low pressure, where saturated S-wave velocities are higher than dry, to more spherical pore-dominated velocities at higher pressures, where the larger saturated bulk density finally pulls the S-wave velocities below the dry. This same effect is seen in the sandstone data of King (1966) for the dry and kerosene-saturated velocities. When the saturant is water the shear modulus drops and saturated S-wave velocities fall well below the dry and inert fluid-saturated values. Water saturated P-wave velocities for the Weber and Kayenta sandstones show a similar effect of crossing below the benzene saturated values at high pressure. According the fluid bulk modulii, water being nearly twice that of benzene (Table 2), the water saturated P-wave velocities should always be higher than the benzene saturated velocities in the absence of the small density contrast.

The Weber sandstone benzene saturated S-wave velocities (Figs. 5-10, 5-19) fall well above dry at all pressures. This is an extremely fine-grained sandstone and probably should be called a siltstone. The stress-strain relation (Chapter 2) is very non-linear and if a crack porosity is assigned to this rock it would be about 0.5% at zero pressure. The saturated velocities show the largest increase of all sandstones measured. All of these observations point to the fact that this rock has substantial quantities of cracks. If cracks were to be assigned to each grain boundary this rock would probably have the highest concentration of the four sandstones. Weber is also sensitive to water as the pore fluid. Water saturated S-wave velocities are initially higher than benzene saturated values at confining pressures less than about 350 bars. At higher pressures the effects of water on the silicate frame shear modulus become important and the velocities

drop below the dry measurements above 700 bars differential pressure. The P-wave velocities are not as sensitive, and at pressures above 600 bars the water saturated measurements fall below the benzene saturated values.

The Navajo sandstone has the highest velocities of the four sandstones and the least dependence on pressure (Fig. 5-11). This rock also has the stiffest stress- strain relation and lowest crack porosity (≈0.8%). This is an extremely well-silicified rock and is from the White member of the Navajo formation as contrasted with the Red member, which was studied by Johnston (1980). In comparison, the P- and S-wave velocities in the present data set are both higher. The water saturated S-wave velocities of Johnston (1980) are lower than dry at all pressures while in the present data set the benzene saturated velocities are higher below about 500 bars and lower at higher pressures. Presumably, water saturated velocities for the particular sample studied here would be lower than those with benzene at the higher pressures.

The Berea sandstone velocity data (Figs. 5-12, 5-20, 5-21) and Kayenta sandstone data (Figs. 5-13, 5-22, 5-23) show similar pressure and saturation dependence with the Kayenta sample having slightly lower velocities and more sensitivity to the water saturant. Both rocks, and particularly the Kayenta, show a very rapid falloff in velocities below about 200 bars. The Kayenta sandstone is a very friable rock, coarser grained than the Berea, higher in porosity, and not as well cemented. Therefore to minimize cracks induced by the cycling of pressure the Kayenta sample was not subjected to pressures above 700 bars.

King (1966) and Johnston (1980) both measured velocities in samples of Berea sandstone. King's data included the dry, kerosene, and water saturated conditions for a sample of Berea with somewhat higher porosity, 20.5%, and lower density, 2.14 g/cc, as contrasted with the 17.8% porosity and 2.194 g/cc density

measured for the sample used in this study. The reported porosity for the sample studied by Johnston (1980) is approximately 16%. All of the dry data sets agree to within 5-10%, with Johnston's data slightly faster, particularly at low confining pressures. King's data for kerosene saturated Berea agress quite well with the present benzene saturated data. Benzene saturated P-wave velocities are higher than dry and S-wave velocities are higher than dry at low pressures (less than 300 bars for King's data; 250 bars for the present data), crossing over to being lower at higher pressures. The water saturated P-wave velocities also agree, with the values only slightly dropping below the benzene or kerosene values at the highest pressures (700 bars for King's data; 1000 bars for the present data). In the water saturated S-wave velocity data of both King and Johnston, however, the values are well below the dry and kerosene saturated values. In the present data set (Fig. 5-21), at pressures below about 250 bars, the water saturated velocities are higher than both the dry and benzene saturated values; above 250 bars the water saturated values fall below the benzene values. Part of this may be due to cycling. In the present data set the procedure did not include any cycles of confining pressure after the water was introduced. There is a tendency for velocities, particularly shear, to drop with successive cycles when water is the pore fluid.

The Kayenta sandstone velocity measurements with water as a pore fluid show a fair degree of sensitivity relative to the benzene measurements. At pressures below about 75 bars the water saturated S-wave velocities are higher than those with benzene. Above that pressure the water saturated measurements do not increase as fast as either the benzene or dry measurements, and above 150 bars fall well below the dry and benzene saturated measurements. For the P-wave velocities water saturated values fall below the benzene values above 200 bars and almost drop to the dry measurements at the

maximum differential pressure of 700 bars.

In the following sections various models of acoustic propagation are examined. The emphasis is on the effect of fluid saturation and, particularly, the observed increases of S-wave velocities. The benzene measurements are used in the modelling procedures because of the apparent difficulties in rationalizing water saturated measurements on the basis of only fluid bulk modulus and density properties.

## GASSMANN EQUATION

The Gassmann equation is a static calculation of the effective bulk modulus for a fluid-saturated porous solid considered as a closed system. The volumetric stress-strain response of a sample element is calculated with the condition that no fluid mass is allowed to cross the sample boundary as it is strained by a uniform external stress. For a compressive stress the pore pressure builds up and the response is stiffer than if the system were open and pore fluid were allowed to freely flow out of the strained,interconnected pore volume. The stress-strain behavior for the closed system may be associated with the "undrained" condition in reference to soil mechanics. Calculation of the undrained bulk modulus proceeds directly from the consolidation equations of Biot (1941), and Biot called the modulus the "instantaneous compressibility". The contribution of Gassmann (1951) was to specialize the linear static description to the case of a fully homogeneous and isotropic porous solid, consider the open and closed system response, and to apply the result to acoustic wave propagation. With the assumption of complete homogeneity and isotropy of the solid matrix the Biot material parameters can be replaced with the following four: the intrinsic bulk modulus $K_s$ of the matrix, the overall bulk modulus $K$, the fluid bulk modulus $K_f$ of the fluid filling the pores, and the

porosity $\varphi$. Pore pressure causes no bulk shear in linear elasticity and so the shear modulus is unaffected by whether the system is open or closed. Consequently the dry and saturated shear moduli are equal. Pore pressure is assumed to equilibrate throughout the interconnected porosity.

The constitutive equations for a linear, isotropic, and homogeneous fluid-saturated porous solid are (Chapter 2)

$$\sigma_{ij} = (K - \frac{2}{3}G)\delta_{ij}\varepsilon_{kk} + 2G\varepsilon_{ij} - \zeta p\,\delta_{ij}, \tag{5-1}$$

$$\zeta = 1 - \frac{K}{K_s}, \tag{5-2}$$

$$\Delta m_f = \rho_f \frac{v_f}{K_f} p + \rho_f \left[\frac{1}{K} - \frac{1}{K_s}\right]\left[\frac{\sigma_{kk}}{3} + p\right] - \rho_f \frac{v_f}{K_s} p. \tag{5-3}$$

where $\sigma_{ij}$ is stress, $p$ pore pressure, $G$ shear modulus, $\varepsilon_{kk}$ volumetric strain, $\varepsilon_{ij}$ strain, $m_f$ fluid mass, $\rho_f$ pore fluid density, $v_f$ pore fluid volume, and the other constants are as described in the previous paragraph. For the calculation of undrained bulk modulus $\Delta m_f = 0$ and Eq. 5-3 gives a relation between hydrostatic confining stress and pore pressure. Pore fluid volume is associated with porosity and fluid density drops out. This relation is substituted into the first equation for pore fluid pressure. Stress is assumed hydrostatic so the shear modulus and shear strains drop out. The result is an expression relating hydrostatic stress and volumetric strain. The modulus in this relation is the undrained or effective bulk modulus $K^*$ which, after algebraic manipulation, is related to the three bulk moduli and porosity in the expression

$$K^* = K + \frac{(K_s - K)^2}{K_s - K + \varphi(K_s / K_f)(K_s - K_f)} \tag{5-4}$$

This is the Gassmann equation for effective static bulk modulus of a sealed porous solid. A refinement by Brown and Korringa (1975) removed the

requirement for microhomogeneity and microisotropy by defining an additional modulus which has been discussed in Chapter 2. The above expression is used in the absence of experimental evidence indicating that this additional modulus differs from $K_s$ and neglecting the effect of pore hydrocarbons shown in Chapter 3.

The shear modulus is unaffected by pore fluid pressure so the effective shear modulus $G^*$ for the closed system is unchanged from the open system and

$$G^* = G \tag{5-5}$$

The application of these static results to dynamic acoustic velocities comes from the identification of the effective bulk and shear moduli with the moduli in the solutions to the wave equation in a linear isotropic media. For P- and S-wave velocities these are

$$V_p = \left[ \frac{K^* + \frac{4}{3}G^*}{\rho} \right]^{\frac{1}{2}} \tag{5-6}$$

$$V_s = \left[ \frac{G^*}{\rho} \right]^{\frac{1}{2}} \tag{5-7}$$

where $\rho$ is bulk density. From dry velocities and measured density the "drained" bulk modulus $K$ and shear modulus $G$ are calculated. Static moduli, although the model is based on a static calculation, cannot be used because of the larger dynamic versus static moduli found for rocks with cracks (Zisman, 1933; Simmons and Brace, 1965; Cheng and Johnston, 1981). The use of the Gassmann equation is limited simply to predicting saturated velocities from dry by calculating the effective bulk moduli together with a new bulk density computed from porosity and fluid density. Computing the effective bulk modulus $K^*$ requires that the fluid bulk modulus $K_f$, the measured porosity $\varphi$, and the

intrinsic bulk modulus $K_s$. The intrinsic bulk modulus can be estimated from mineralogy or else measured in an unjacketed stress-strain test (Chapter 2).

Benzene-saturated P- and S-wave velocities have been predicted with Gassman's equation from the dry velocities for the data on samples of Westerly and Chelmsford granite, Navajo, Berea, Kayenta, and Weber sandstone, and Bedford limestone. The intrinsic bulk moduli $K_s$, densities, and initial porosities were taken from Table 1 at the end of Chapter 2. In addition, the change in porosity and density with confining pressure were accounted for in the present calculations. Pore fluid properties of the benzene and water are given in Table 2. The results are shown in Figs. 5-34 through 5-48. Each figure is either the P- or S-wave dry and benzene or water-saturated (solid squares) velocities versus confining pressure. For the plots with P-wave velocities the dashed line is the predicted saturated P-wave velocity from the dry velocity moduli using Gassmann's equation for the effective bulk modulus, the dry shear modulus, and the saturated density computed from dry density and fluid density. Two separate plots of predicted and measured P-wave velocities have been prepared for water- and benzene-saturated velocities of the Berea, Kayenta, and Weber sandstones. In addition, in the plots for these three sandstones the P-wave velocities predicted from the dry shear moduli (curve A) are distinguished from those predicted from the saturated shear moduli (curve B). For the plots with S-wave velocities the dashed line is the predicted saturated velocity from the dry shear modulus and the saturated density. In the following paragraphs this data is discussed and references to the Gassmann equation predictions are intended to apply to both saturated P- and S- wave velocities although in a strict sense the Gassmann equation is only the calculation of the closed system effective bulk modulus.

In Figs. 5-34 and 5-35 the P- and S-wave velocities for Westerly granite and the P-velocities for Chelmsford granite are shown. Since bulk density increases almost negligibly upon saturation in these low porosity (≈1%) rocks the predicted saturated shear velocity is nearly unchanged from the dry case. As shown in Fig. 5-35 the saturated velocities are higher than the dry for Westerly granite, and this is the case for all of the low porosity rocks. The saturated shear modulus is consistently larger than the dry for all of the low porosity rocks.

In Figs. 5-34 and 5-36 the P-velocities for Westerly and Chelmsford granite show that the predicted saturated velocities make up little more than half of the difference between measured dry and saturated velocities. If instead of the dry shear modulus the saturated shear modulus is used in predicting P-wave velocity the dashed line moves up, but not substantially.

In Figs. 5-37 through 5-46 are shown the P- and S-wave velocities for Navajo, Berea, Kayenta, and Weber sandstones with the dashed Gassmann equation predictions. For these sandstones, with porosities ranging from 9.6-22.3%, the saturated densities become important in the predicted velocities. Since at low pressure for all three sandstones the saturated shear velocities as measured are higher than dry the prediction based on saturated density is in the wrong direction. At high pressure, when the effects of cracks are reduced, the predicted and measured saturated velocities are lower than dry and tend to converge. At 1 kbar pressure the Berea predicted S-wave velocity is nearest to the measured although still slighly lower.

The water- and benzene-saturated P-wave velocities predicted for the 4 sandstones always underestimate those which are measured. In Fig. 5-37 are shown the dry and benzene-saturated P-wave velocities for Navajo sandstone. The lowest dashed curve is the predicted velocities based on an intrinsic bulk

modulus $K_s$ of 0.36 Mb, which was measured in the unjacketed stress-strain experiment in Chapter 2. Predicted P-wave velocities are much lower than those measured, and at high pressures the saturated bulk density actually pulls the predicted velocities below the measured dry ones. The two other curves are for higher intrinsic bulk moduli, 0.5 and 0.6 Mb, and are included here to indicate the sensitivity of the Gassmann prediction to the value used for $K_s$. There may be some confusion between static and dynamic moduli and and what value to use for $K_s$. For single crystals, or materials without cracks, such as metals, static and dynamic moduli are essentially equivalent relative to rocks. In the Gassmann equation it is the intrinsic crack-free bulk modulus which is desired, and that measured in the unjacketed stress- strain test is just that. For Navajo sandstone the measured $K_s$ is 0.36 Mb, slightly lower than pure quartz because of the extensive secondary silica cementation, and this is also what the dynamic value should be.

In Fig. 5-39 the dry and benzene-saturated saturated P-wave velocities and predictions are plotted for Berea sandstone. An equivalent plot for water-saturated velocities is Fig. 5-40. In these plots there are two dashed curves representing different possibilities for applying Gassmann's equation to predict the saturated velocities. Curve A uses the dry bulk and shear moduli. For the benzene saturated velocities curve A is far below those measured. For the water saturated velocities it does better, and at high pressure actually reaches the measurements, but this is probably because the P-wave velocites with water are lower than expected because of the effect of water on lowering the shear modulus. Curve B uses the dry bulk modulus but the saturated shear moduli. This modified application of Gassmann's equation simply accepts the fact that saturated shear moduli are much higher than dry and will be used in predicting the P-wave velocities. Curve B does somewhat better at predicting saturated

velocities, particularly those with water, but still underestimates the measured values.

In Figs. 5-42 and 5-43 are equivalent plots for the Kayenta sandstone, and in Figs. 5-45 and 5-46 are equivalent plots for the Weber sandstone. As can be seen in all of these plots the Gassmann equation predicts velocities which are consistently low. Using the saturated shear moduli improves the predicted P-wave velocities, particularly for the Weber sandstone, but there are still large underestimations. For the water saturated Kayenta sandstone (Fig. 5-43) and Weber sandstone (Fig. 5-46), as was the case for Berea sandstone (Fig. 5-40), the B curves tend to fall below the A curves at high pressure. This is because the water saturated shear moduli are lower than the benzene saturated ones.

The only success of Gassmann's equation in predicting saturated velocities is for the S-wave velocities of Bedford limestone as shown in Fig. 5-48. Really this is only the prediction of saturated shear velocity on the basis of increased saturated density. The Gassmann equation for effective bulk modulus and hence saturated P-wave velocity underestimates the measured difference by more than half as shown in Fig. 5-47. Accurate prediction of saturated shear velocity for the Bedford limestone is actually a significant result as will be discussed in the next section on Biot inertial effects.

In conclusion, however,the Gassmann equation for effective satutated bulk modulus and the equating of dry and saturated shear modulus severely underestimates the effect of saturation. Saturated P- and S-wave velocities predicted from dry are consequently lower than measured in all rocks studied except for S-wave velocity in the Bedford limestone.

## BIOT (1956a,b) INERTIAL EFFECTS

One of the objections to the Gassmann equations for saturated velocities is the neglect of pore fluid inertia. The earlier work of Biot on acoustic propagation is a formulation of the static consolidation equations with the inclusion of inertia terms. This is an improvement over the earlier Gassmann equations in that one aspect of dynamic wave propagation, the inertia of the pore fluid relative to the motion of the matrix frame, is accounted for. Essentially the displacements of bulk frame and the pore fluid relative to the bulk frame are separately described by dynamic equations. The applicability is limited to solids with fairly uniform porosity, and the interaction of stress waves with what Biot (1962) would come to call "hidden coordinates" such as cracks is discounted.

As a function of frequency the treatment contrasts viscosity of the fluid phase versus inertia of the fluid phase. At low frequency (1956a) the viscosity of the pore fluid is assumed to maintain Poiseulle flow in response to pressure gradients due to stress waves. At high frequency (1956b) the inertia of pore fluid exceeds consideration of fluid viscosity and viscous shear is limited to a narrow zone at the boundary of the pore space. The two frequency ranges are separated by a critical frequency. The breakdown of Poiseulle flow above the critical frequency is determined by friction due to oscillatory motion at pore boundaries and so pore shape is a factor in addition to fluid viscosity and density. For the present measurements of ultrasonic velocities centered around 1 Mhz the range of application is the high frequency analysis. This maximizes the effect of pore fluid inertia on velocities.

Above the critical frequency but below the frequency at which scattering becomes important the solutions to the dynamic equations for fluid and solid for group velocities become

$$V_s = \left[\frac{G}{(1-\varphi)\rho_s + \varphi\rho_f - (1/\alpha)\varphi\rho_f}\right]^{\frac{1}{2}} \tag{5-8}$$

$$V_p = \left[\frac{P\rho_{22} + R\rho_{11} - 2Q\rho_{12} + \left[(P\rho_{22} + R\rho_{11} - 2Q\rho_{12})^2 - 4(\rho_{11}\rho_{22} - \rho_{12}^2)(PR - Q^2)\right]^{\frac{1}{2}}}{2(\rho_{11}\rho_{22} - \rho_{12}^2)}\right]^{\frac{1}{2}} \tag{5-9}$$

where

$$P = \frac{(1-\varphi)(1-\varphi-K/K_s)K_s + \varphi K_s K/K_f}{1-\varphi-(K/K_s)+\varphi(K_s/K_f)} + \frac{4}{3}G \tag{5-10a}$$

$$Q = \frac{(1-\varphi-K/K_s)\varphi K_s}{1-\varphi-(K/K_s)+\varphi(K_s/K_f)} \tag{5-10b}$$

$$R = \frac{\varphi^2 K_s}{1-\varphi-(K/K_s)+\varphi(K_s/K_f)} \tag{5-10c}$$

The symbols for the moduli are as previously defined and the bulk modulus $K$ and shear modulus $G$ are for the drained or dry porous solid. The density terms $\rho_{11}$, $\rho_{12}$, and $\rho_{22}$ are defined as

$$\rho_{11} + \rho_{12} = (1-\varphi)\rho_s \tag{5-11a}$$

$$\rho_{22} + \rho_{12} = \varphi\rho_f \tag{5-11b}$$

$$\rho_{12} = (1-\alpha)\varphi\rho_f . \tag{5-11c}$$

The density of the solid matrix is $\rho_s$ and that of the fluid $\rho_f$. The density or mass coefficient $\rho_{12}$ measures the inertial coupling or force on the pore fluid as the solid frame is accelerated. A nondimensional coefficient $\alpha$ of value greater than 1 represents an average geometry of the pore space as it affects inertial coupling. If $\alpha=\infty$, such as for a very tortuous and narrow pore geometry, the solid and fluid mover together and the equations for velocities reduce to Gassmann's equations. This is most clearly evident in the expression for shear velocity as the first two terms in the denominator are saturated bulk density. As coupling decreases the effect of pore fluid mass on bulk density is reduced and wave velocities increase.

Application of the inertial effects to the present measurements is best seen in the expression for shear velocity and by consideration of the requirement for uniform porosity. Shear modulus is unaffected by the presence of pore fluid. Apparent mass of the porous solid is reduced by pore fluid inertia as the surrounding frame oscillates and is determined by the geometrical factor $\alpha$. If coupling is negligible, such that $\alpha \approx 1$, the density term in the denominator is the bulk density of the saturated and drained or dry porous solid. The shear velocity in this case is the drained or dry shear velocity. At best the inertial effect can raise the saturated shear velocity up to the dry velocity, but not above.

Clearly the consideration of pore fluid inertia in the low porosity rocks ( 3 granitic rocks plus Webatuck dolomite ) has a negligible effect on velocity. Aside from the small fluid mass in the saturated condition, these rocks fail the requirement for uniform porosity. Since at all pressures the saturated shear velocities are higher than dry the fluid inertia is not determining the difference between dry and saturated velocities.

A significant indication of whether pore fluid inertia is important in the higher porosity rocks is given by the shear wave velocities for Bedford limestone ( $\varphi$ = 11.9 % ). As was shown in the previous section the uniformly lower saturated shear wave velocities for this rock are very accurately predicted form the effect of bulk density. Of the rocks studied Bedford limestone stands unique as a nearly perfect linear elastic solid. This is indicated by the nearly linear stress-strain relation shown in Chapter 2. The interpretation is that this rock has little or no crack porosity and that the dry and saturated shear moduli are almost equal. Relaxation effects due to pore fluids trapped in small pores is minimal. In terms of the ellipsoidal crack models to be discussed in later sections the porosity of Bedford limestone is nearly spherical. The significant result here in terms of inertial considerations is that the geometrical coupling

parameter $\alpha$ must be quite large for this rock based on the saturated S-wave velocities. If the S-wave velocity is accurate to 0.5% a minimum value of $\alpha$ is 3 and quite likely is somewhat larger. The strong indication in the S-wave velocity data is not only that inertial effects are small but perhaps nearly nonexistent.

For the sandstones an examination of the experimental dry and saturated velocities at high pressure ($\approx$ 1 kbar ) indicates a possible contribution of inertia to the saturated velocities. This is very speculative and done only to estimate a minimum value of $\alpha$. The assumption is that at high pressure the effects of cracks and narrow pore spaces are negated and since porosity does not decrease substantially the inertial effects over the entire pressure range may be surmised. This also assumes that those pore features which change with pressure do not affect the $\alpha$ parameter. At high pressures three of the four sandstones ( Berea, Navajo, and Kayenta ) have saturated S-wave velocites which drop below the dry velocities. For the Weber sandstone this does not occur and the following technique does not apply. When saturated and dry shear velocities are increasing uniformly and by a small amount at high pressure the implication of assuming minimal crack effects means the difference represents the effect of density only. To the extent that measured S-velocities fall above those predicted by saturated bulk density ( Gassmann's equation ) is an indication of inertial effects. The geometrical parameter $\alpha$ is adjusted in the expression for saturated S-wave velocity to agree with measured velocities at high pressure.

Berea sandstone probably offers the best data set of the sandstones from which to evaluate inertial coupling and the geometrical parameter $\alpha$. In Fig. 5-50 the vacuum-dry and benzene-saturated S-wave velocities are plotted from 0 to 1 kbar differential confining pressure. The dashed line is the Gassmann prediction if the saturated shear modulus were the same as dry and if coupling of fluid to solid matrix were perfect ( $\alpha=\infty$ ). If at high confining pressures ( 700 - 1000 bars

) the difference between the dashed line and measured saturated S-wave velocities is interpreted to represent inertial coupling the parameter $\alpha$ is calculated to be about 4.4 from the shear velocity expression. This is an absolute minimum because the measured an predicted S-wave velocities are tending to converge at higher pressures. At 1 kbar cracks of aspect ratio 0.001 are closing and it is quite likely that a good proportion of the difference between measured and predicted velocities are due to crack effects.

Nevertheless, in Figs. 5-49 and 5-50 are plotted the predicted saturated P- and S-wave velocities for Berea sandstone with a coupling factor of 4.4. Essentially the predicted and measured S-wave velocities at the highest pressures are pinned together and the effects propagated over the whole pressure range for P- and S-waves. Johnston (1980) did the same thing in evaluating the contribution of inertial effects to the attenuation. The results are not striking in terms of predicting saturated P- and S-wave velocities. Obviously the higher saturated S-wave velocities at low pressures are not predicted. The only benefit to the predicted P-wave velocities is to at least raise them slightly above the dry velocities at high pressure.

Similarly, in Figs. 5-51 and 5-52 the predicted velocities for Navajo sandstone are plotted based on a coupling of $\alpha = 2.1$. Because this $\alpha$ is smaller the effects on predicted velocities are more substantial over the Gassmann predictions relative to the Berea sandstone. Even when the inertial effects are vastly overestimated, as is the case here, the only benefit for the predicted P-wave velocities is to raise them almost to the measured dry velocities at high pressure.

The conclusion is that inertial effects of the pore fluid on velocities are negligible based on the Biot analysis. The coupling parameters calculated for

Berea and Navajo sandstones are absolute minimums. Saturated S-wave velocities for the Bedford limestone indicate that inertial effects are perhaps almost nonexistent in these measurements. Certainly Gassmann's equations are not failing for this ultrasonic data because of inertial effects.

## BUDIANSKY AND O'CONNELL CRACK MODEL

An analysis of the effect cracks have on the acoustic properties of solids has been advanced by Budiansky and O'Connell (1974) and O'Connell and Budiansky (1976,1978). The effective moduli are calculated for a solid with very thin, randomly oriented ellipsoidal cracks by estimating the potential energy change due to each cracks as introduced into the stressed, cracked solid. The distinction of using the cracked solid as opposed to the uncracked solid in the energy calculation is one possible application of the self-consistent assumption (Korringa *et al.*, 1979), and probably results in an overestimation of crack effects at large crack densities (Bruner, 1976). By referencing the potential energy change to the ultimately fully cracked body, as represented by the Poisson's ratio of the fully cracked body, the density of cracks possible is extended beyond that of earlier static analyses (Eshelby, 1957; Wu, 1966; Walsh, 1969), which apply to dilute concentrations of cracks. Crack count is indexed by a crack density parameter $\varepsilon$ which for $N$ circular cracks of radius $a$ per unit volume of solid is given by

$$\varepsilon = N\langle a^3 \rangle \tag{5-12}$$

Crack density may increase with the self-consistent approximation until the rock apparently falls apart when sufficient numbers of cracks intersect, and this value is $\varepsilon = 9/16$, according to a circular crack of radius $\approx$0.8 per unit volume.

The solutions of Budiansky and O'Connell (1974) for the shear and bulk moduli of cracked solids are posed as ratios of the cracked solid to the uncracked solid. For dry,circular cracks the crack density $\varepsilon$ as a function of intrinsic Poisson's ratio of the uncracked solid $\nu$ and that of the cracked solid $\bar{\nu}$ is given by

$$\varepsilon=\left(\frac{45}{16}\right)\frac{(\nu-\bar{\nu})(2-\bar{\nu})}{(1-\bar{\nu}^2)(10\nu-3\nu\bar{\nu}-\bar{\nu})} \tag{5-13}$$

The corresponding ratios of bulk modulus $\bar{K}$ and shear modulus $\bar{G}$ to the moduli of the uncracked solid $K$ and $G$ are given by

$$\frac{\bar{K}}{K}=1-\frac{16}{9}\left[\frac{1-\bar{\nu}^2}{1-2\bar{\nu}}\right]\varepsilon \tag{5-14}$$

$$\frac{\bar{G}}{G}=1-\frac{32}{45}\frac{(1-\bar{\nu})(5-\bar{\nu})}{(2-\bar{\nu})}\varepsilon \tag{5-15}$$

For saturated, circular cracks which are isolated such that no fluid is allowed to flow out of the cracks the crack density $\varepsilon$ in terms of the Poisson ratios is given by

$$\varepsilon=\frac{45}{32}\frac{(\bar{\nu}-\nu)(2-\bar{\nu})}{(1-\bar{\nu}^2)(1-2\nu)} \tag{5-16}$$

The corresponding ratios of bulk modulus $\bar{K}$ and shear modulus $\bar{G}$ in this saturated, isolated case to the moduli of the uncracked solid are given by

$$\frac{\bar{K}}{K}=1 \tag{5-17}$$

$$\frac{\bar{G}}{G}=1-\frac{32}{15}\left[\frac{1-\bar{\nu}}{2-\bar{\nu}}\right]\varepsilon \tag{5-18}$$

To evaluate the formulations in terms of measured P- and S-wave velocities the expressions for effective moduli can be expressed in terms of ratios of velocities of the cracked solid ($\overline{V_p}$, $\overline{V_s}$) to those of the uncracked solid ($V_p$, $V_s$). These are given by

$$\frac{\overline{V_s}}{V_s} = \left[\frac{\overline{G}}{G}\right]^{\frac{1}{2}} \tag{5-19}$$

$$\frac{\overline{V_p}}{V_p} = \left[\frac{(1-\overline{\nu})(1+\nu)}{(1+\overline{\nu})(1-\nu)}\frac{\overline{K}}{K}\right]^{\frac{1}{2}} \tag{5-20}$$

$$\frac{\overline{V_p}/\overline{V_s}}{V_p/V_s} = \left[\frac{(1-\overline{\nu})(1-2\nu)}{(1-2\overline{\nu})(1-\nu)}\right]^{\frac{1}{2}} \tag{5-21}$$

The wave velocity ratios are shown in Fig. 5-53 as a function of the crack density paramter $\varepsilon$. This plot is taken from O'Connell and Budiansky (1977) and separates out a number of different cases treated in that paper for the degree to which saturated cracks communicate. The saturated isolated case is for fluid-saturated cracks between which fluid does not flow during passage of a stress wave. The saturated isobaric case describes a situation where fluid equilibrates throughout all of the cracks to an equilibrium pressure such that there is extensive fluid flow. The familiar ring to this model is that it is essentially a restatement of the Gassmann equation in the static calculation of effective bulk modulus for a fluid-infiltrated porous solid. In terms of the model predictions the most relevent result to the present data is for the S-wave velocities which are in the upper right portion of the plot. For a given crack density the saturated S-wave velocity is higher than the dry for the saturated isolated case. For the saturated isobaric case the saturated S-wave velocities are the same as dry, as they were in the section covering the Gassmann equation. The shear velocities measured for the 3 granitic rocks and the Webatuck dolomite are higher than the dry and so the indication is that the saturated cracks are following the

saturated isolated case. O'Connell and Budiansky (1977) concluded that at ultrasonic frequencies based on the data of Nur and Simmons (1969) the data agreed with the saturated isobaric case because the saturation did not have substantial effect on the shear modulus.

O'Connell and Budiansky (1974, 1977) advocate a plot of the ratio $(\bar{V}_p / \bar{V}_s)/(V_p / V_s)$ versus $\bar{V}_s / V_s$ as a means with which to evaluate experimental data in terms of their crack model and the crack density parameter $\varepsilon$. In Figs. 5-54 through 5-57 this type of plot has been prepared from the measured dry and benzene saturated velocities of Westerly granite (Fig. 5-54), Barre granite (Fig. 5-55), Webatuck dolomite (Fig. 5-56), and Weber sandstone (Fig. 5-57). The solid and open squares are the measured velocities plotted as the appropriate ratios and the dashed lines are the predicted dry (lower dashed line) and fully saturated (upper dashed line) ratios as calculated from the above equations for dry and saturated isolated circular cracks. The intrinsic velocities $V_p$ and $V_s$ were taken as the highest velocities measured at 1 kbar which for the granites, dolomite, and Weber sandstone were benzene saturated velocities. The fit is quite good for the Westerly granite and Webatuck dolomite. The fit for the Barre granite is not so good for the dry velocities but it must be emphasized that this rock is quite anisotropic. The fit is poor for the Weber sandstone but this could be expected because the highly porous sandstones are not the cracked solids for which the model is intended. Similar plots for the Westerly granite and Webatuck dolomite can be found in O'Connell and Budiansky (1976) using the data of Nur and Simmons (1969). The fit with the present data is far better, mainly because the saturated shear velocities in the present data are higher than dry.

The main point to be made in regards to this crack model and the measured velocities has to do with the conclusion by O'Connell and Budiansky (1977) that the ultrasonic data follows the saturated isobaric case as treated by them. This

conclusion was mainly based on the data of Nur and Simmons (1969) which had indicated that saturated shear modulus did not differ substantially from dry. In the present data the saturated shear modulus clearly and consistently is higher than the dry, indicating that instead of the isobaric case it is the saturated isolated case which is being followed.

The plot of ratios as in the above figures does not distinguish between the isobaric and isolated cases, however. To evaluate more fully to what extent both P-wave and S-wave velocities were following the saturated isolated case the measured dry and saturated velocities were modelled with the above equations for dry and saturated circular cracks. There are several ways to do this and the technique chosen here is only one possibility. From the maximum velocities measured, which were benzene-saturated at 1 kbar pressure, the intrinsic Poisson's ratio $\nu$ was calculated. For each set of dry velocities at the various pressures from 0 to 1 kbar pressure the dry crack density was calculated from the Poisson's ratio in the equation relating crack density to Poisson's ratio. This crack density was assumed applicable to the saturated measurements and used to predict the saturated velocities with the above equations for saturated shear and bulk modulus. From these crack densities and the shear and bulk moduli as a function of pressure both the dry and saturated isolated P- and S-wave velocities were predicted as a function of pressure. This modelling procedure was applied to the two rocks which gave the best fit in the ratio plot, Westerly granite and the Webatuck dolomite. The results are shown in Figs. 5-58 and 5-59 for the Westerly granite and Figs. 5-60 and 5-61 for the Webatuck dolomite. The predicted dry and saturated velocites are remarkably close to those measured. The fit is best for the Webatuck dolomite and this is probably because at high pressure almost all of the cracks do actually close, resulting in the saturated and dry S-wave velocities coming together.

In addition, modelling results of the dry and benzene-saturated Barre granite velocity data are shown in Figs. 5-62 and 5-63. The S-wave velocities for each saturation were averaged between the two mutually perpendicular directions. The fits are not nearly as good as with the other two rocks, particularly for the S-wave velocities. Either the procedure works fortuitously for the Webatuck and Westerly data, does not apply to the Barre granite because of its high crack density, or else the anisotropy of Barre is not fully accounted for.

The crack densities versus pressure for the three rocks are plotted in Figs. 5-64. At pressures less than 100 bars there probably is some difficulty with the Westerly velocities which resutls in the bend in the curve. If the main trend is extrapolated to zero pressure the crack density obtained is about 0.2, which is the lower end of the range reported by Hadley (1976), 0.2 to 0.3, as reported by Budiansky and O'Connell (1977). The larger crack densities of Webatuck dolomite and Barre granite at pressures less than about 250 bars is clearly evident. Crack density at zero pressure is up around 0.4, which is one crack of greater than unit diameter per unit volume. Thus these rocks, according to the model, are extensively cracked.

In summary, the Budiansky and O'Connell self-consistent model for cracks does fit the data much better than any data previously available. The best agreement is obtained for the Westerly granite and Webatuck dolomite. The most significant aspect of the present data in terms of the model is to alter the conclusion of O'Connell and Budiansky (1977) in regards to the saturated and dry shear modulus being equal. Instead of the saturated isobaric case fitting the data and the conclusion of extensive fluid flow in the low porosity rocks causing attenuation, it now appears that this new data is more consistent with the saturated isolated case. This does not totally preclude fluid flow,

however,because there is an entire spectrum of combinations between these two endmembers.

## KUSTER - TOKSOZ CRACK AND PORE MODEL

Kuster and Toksöz (1974) obtained formula for the dynamic effective moduli of a two-phase medium with ellipsoidal inclusions by evaluating the scattered displacements of long wavelength plane waves from single inclusions embedded in an infinite matrix. Concentration, shapes, and properties of the inclusions (bulk modulus, shear modulus, density) determine the displacements and summation over all inclusions leads to a description of effective moduli for the bulk material. The experimental dry and saturated P- and S-wave are consistent with several aspects of this model, first and foremost with regards to the larger saturated shear moduli in the low porosity rocks. Secondly, since the model allows for a spectrum of pore shapes from very thin cracks up to spherical pores, the measured velocities of higher porosity rocks can be interpreted.

A quite useful demonstration of the effects pore shape and fluid saturation have on measured velocities as predicted by this model was given by a calculation of an idealized porous solid in Toksöz *et al.* (1976) and reproduced in Fig. 5-65. This plot is of P- and S-wave velocities normalized to the velocity of the solid matrix as a function of porosity. For various singular sets of aspect ratios the theoretically derived effective moduli can be used to calculate velocities at different concentrations, which can be equated with porosity. There are three main observations to be made from this plot, all of which correlate with various observations in the measured velocities which will follow. First, lower aspect ratio pores or cracks have a greater influence in decreasing velocities than the more spherical pores. Secondly, saturating fluids affect P-wave velocities more than the S-wave velocities relative to dry because of the higher sensitivity of

bulk modulus to saturation. Third, saturation has the greatest effect on the lower aspect ratio pores, increasing both velocities except for the more spherical pores.

What has been lacking for this model is clear experimental data supporting the predicted effect of saturation on S-wave velocities. The present data tends to resolve this need. First consider the velocities for the three granitic rocks and Webatuck dolomite. According to Walsh (1965) if the compliant porosity in these rocks is modelled as penny-shaped cracks the closure pressure is approximately $\alpha E_0$, where $\alpha$ is aspect ratio and $E_0$ the Young's modulus of the solid. As a rule of thumb for silicate rocks this means that at 1 kbar confining pressure cracks of aspect ratio 0.001 are closing. For most of the rocks measured in this study the differences between dry and saturated velocities are substantially reduced by 1 kbar, and the conclusion therefore is that cracks of this aspect ratio or lower are dominating the observed pressure and saturation dependence. In Fig. 5-65 the model predicts that for aspect ratios of 0.1 and less the saturated S-wave velocities should be higher than dry. All of the saturated S-wave velocities in the low porosity rocks are higher than dry, and the difference between dry and saturated is greater at low pressure where the lower aspect ratio pores are present.

The Bedford limestone S-wave velocity data would be modelled with pores of aspect ratio between 0.1 and 1.0. Although it was shown previously that saturated S-wave velocities were predicted directly from the saturated density, there must be at least some crack-like pores to give the pressure dependence of velocities and to increase the saturated P-wave velocities.

For the four sandstones studied the surprising result is the extent to which fine cracks dominate the velocities at low pressure as indicated by the higher

saturated S-wave velocities. The increase in shear modulus more than cancels out the increase in density upon saturation. The comparison of dry and saturated velocities in these rocks is, as was pointed out in the introduction, benefited greatly by the use of benzene as a pore fluid. In the modelling of sandstone data by Cheng (1978) the saturated matrix shear modulus invariably had to be lowered to fit both the saturated P- and S-wave velocities in the sandstones studied. The explanation that matrix clays are softening with the introduction of water is not entirely correct because quartz or amorphous silica will become more deformable with water. In any event, the challenge with this present data set is to model these higher porosity rocks with ellipsoidal shapes such that the saturated matrix shear modulus does not have to be changed from the dry. In addition, the unjacketed strain measurements from Chapter 2 provide the intrinsic matrix bulk modulus so that it does not have to be guessed at from mineral averages or else from high pressure jacketed strain measurements.

A quite interesting result from the modelling efforts of Cheng (1978) relevent to the present data is reproduced in Fig. 5-66. The data set is from Nur and Simmons (1969). The lines are the result of inversion schemes where the entire set of dry and saturated data was inverted with pressure to arrive at a spectrum of ellipsoidal pore shapes which close with pressure. Two observations can be made in comparison with the data on Westerly granite in Figs. 5-2, 5-14, and 5-15. First, the low pressure saturated P-wave velocity data in Figs. 5-2 and 5-14 fits the modelled P-velocties much better. Second, looking closely at the S-wave velocity modelled lines, it is seen that the saturated S-wave velocities are always higher than the dry, in agreement with the saturated Westerly data in Figs. 5-2 and 5-15.

# CONCLUSIONS

Fundamental acoustic measurements of velocities and attenuation as a function of confining pressure and fluid saturation for the purpose of comparing the purely mechanical effects of "dry" and "saturated" conditions are best served by avoiding water as the pore fluid. The water saturated measurements reflect an interaction between water and mineral matrix, reducing in particular the shear modulus of the sandstones at high pressures, and therefore add an additional parameter in the interpretation of dry and saturated velocities.

The measurements of vacuum dry and benzene saturated P- and S-wave velocities as a function of confining pressure indicate the ubiquitous presence of crack-like pores in determining the velocities of all the rocks studied with the exception of Bedford limestone. Crack-like pores filled with fluid increase both the bulk and shear modulus of the saturated rock. For the low porosity granites and dolomite the results are higher P- and S-wave velocities upon saturation. The greater the nonlinearity in the static stress- strain relation, the greater the interpreted crack porosity, and the greater the jump in saturated velocities over dry. The significant result in the present data is a clear and consistent increase in saturated S-wave velocities and shear modulus for all of the rocks upon saturation excluding the Bedford sandstone.

Gassmann's equation for the calculation of effective bulk modulus of the saturated rock fails to predict the measured saturated P-wave velocities from the dry. The equating of dry and saturated shear modulus and the prediction of saturated S-wave velocities on the basis of saturated density also fails except for the Bedford limestone, the saturated velocity of which is quite accurately predicted because it has little crack-like porosity.

The inertial effects of pore fluid at high frequency as treated by Biot (1956a,b) have a negligible influence on saturated velocities in the higher porosity rocks. Strong evidence for this is given by the prediction of saturated S-velocities in the Bedford limestone solely on the basis of saturated versus dry density. In the sandstones at high confining pressures, when the effects of cracks are minimized, the inertial effects could be evaluated. In the measurements presented confining pressure was never high enough to meet this criteria but carrying through the analysis indicated that absolute minimum values of the geometrical parameter $\alpha$ would be 4.4 for the Berea sandstone and 2.1 for the Navajo sandstone.

The observed higher saturated velocities, both P-wave and S-wave, in the low porosity rocks (3 granitic rocks and Webatuck dolomite) agree with the predictions of the Budiansky and O'Connell crack model. This is especially true of the higher saturated S-wave velocities relative to the dry. The conclusion of O'Connell and Budiansky (1977), that fluid flow between cracks is supported by laboratory observation of no effect of saturation on shear modulus, must be revised in light of the present data on some of the same rocks. Saturated shear moduli in the low porosity rocks are clearly and consistently higher than the dry. In terms of the various cases considered by O'Connell and Budiansky (1977) the observed dry and saturated velocities agree best with the saturated isolated analysis, not the saturated isobaric case as was concluded by them.

The observed higher saturated P- and S-wave velocities agree with the model of Kuster and Toksöz. The measured saturated P- and S-wave velocities for Westerly granite agree very well with the velocities predicted by Cheng (1978). Modelling of the velocity data presented in this thesis will proceed in the future.

**Table 1: Rock Samples in this Study**

| Rock | Density (g/cc) | Grain Size (mm) | Porosity % |
|---|---|---|---|
| Westerly Granite (blue) | 2.641 | 0.75 | 0.8 |
| Barre Granite | 2.635 | 3 | 0.7 |
| Chelmsford Granite | 2.606 | 1.5 | 1.1 |
| Webatuck Dolomite | 2.846 | 0.45 | 0.5 |
| Bedford Limestone | 2.360 | 0.75 | 11.9 |
| Weber Sandstone | 2.392 | 0.05 | 9.5 |
| Navajo Sandstone | 2.316 | 0.15 | 11.8 |
| Berea Sandstone | 2.197 | 0.1 | 17.8 |
| Kayenta Sandstone | 2.017 | 0.15 | 22.2 |

**Table 2: Pore Fluid Properties At 20-22 ° C**

| Fluid | Pressure (bars) | Density (g/cc) | Bulk Modulus (Kbar) |
|---|---|---|---|
| Benzene | 100 | .88 | 12.1 |
| Water | 100 | 1.00 | 22.4 |

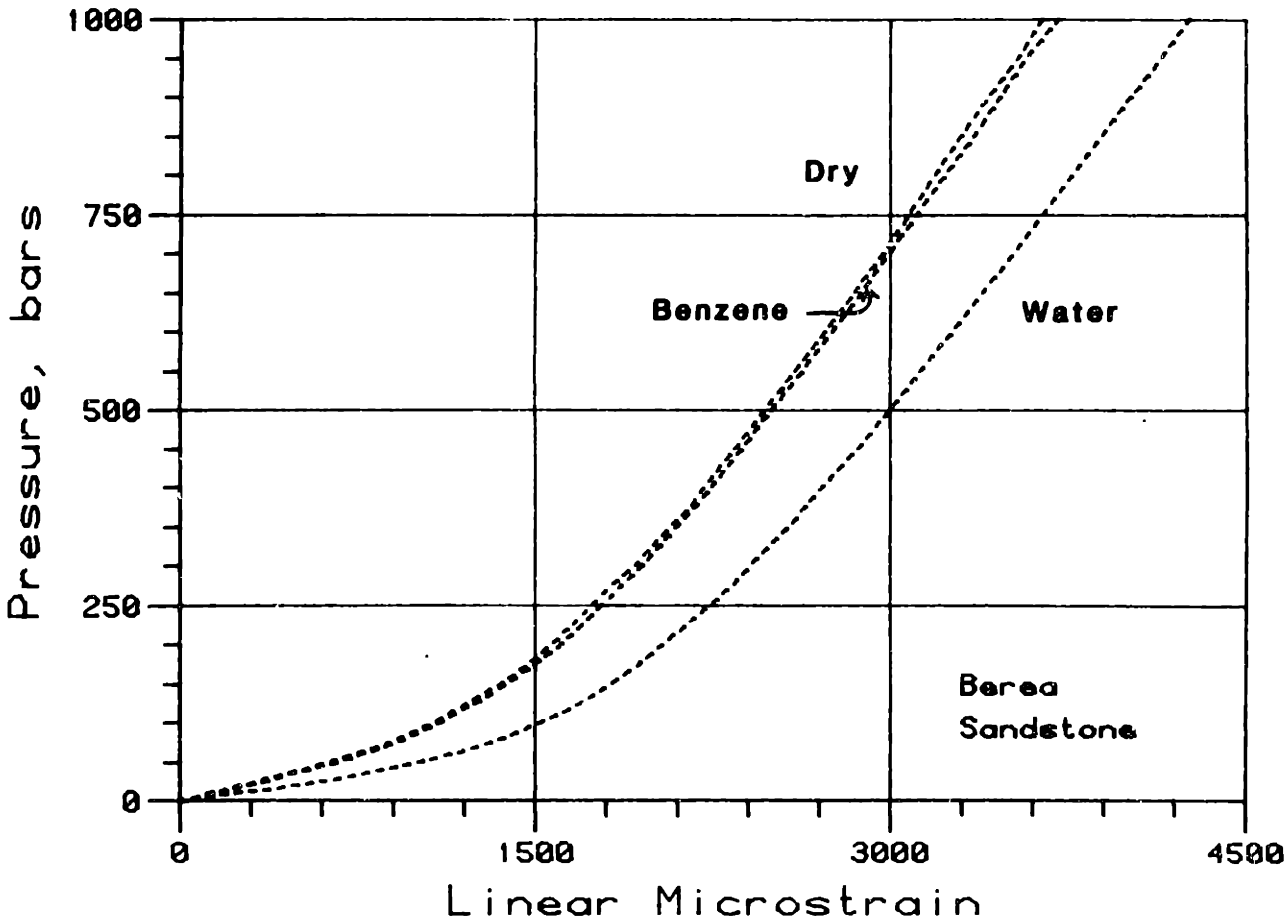


Figure 5-1. Vacuum dry, water saturated, and benzene saturated stress-strain relations for a sample of Berea sandstone. Saturated pore pressures are 1 bar (drained to atmospheric pressure).

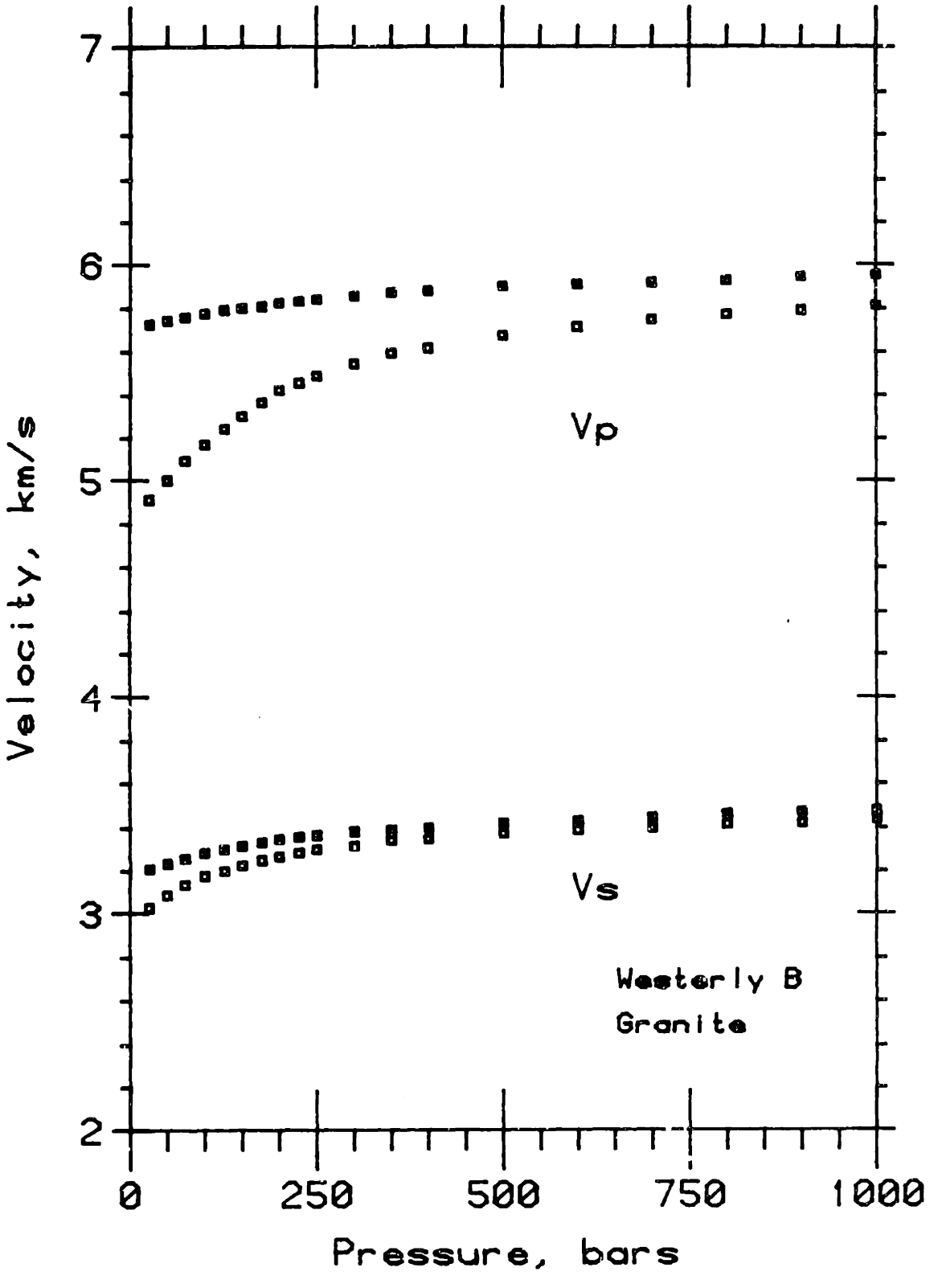


Figure 5-2. P- and S-wave velocities for Westerly granite versus differential pressure for dry (open squares; 20 $\mu$m Hg vacuum) and benzene (solid squares; 100 bars pore pressure) saturations.

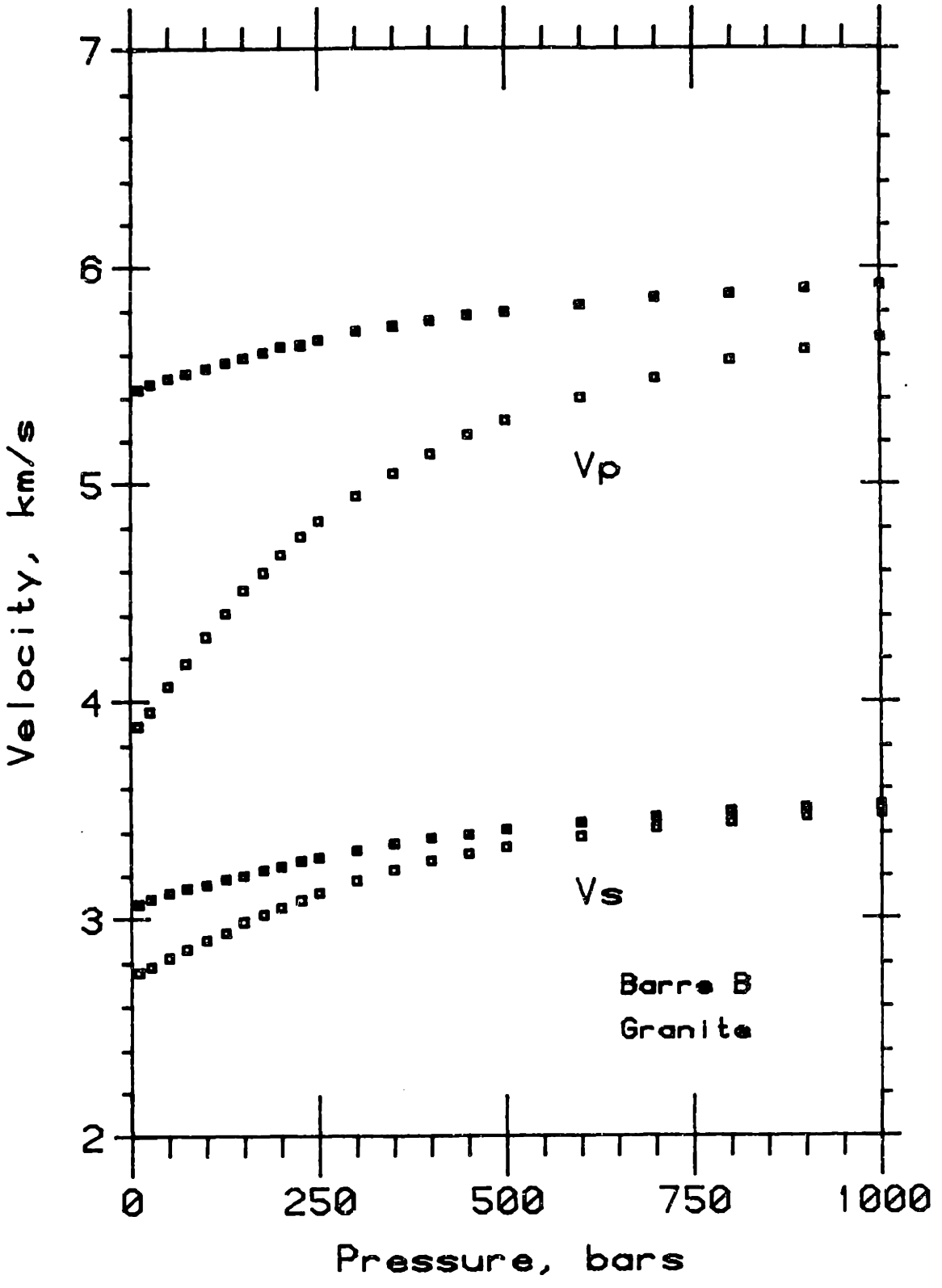


Figure 5-3. P- and S-wave velocities for Barre granite versus differential pressure for dry (open squares; 20 $\mu$m Hg vacuum) and benzene (solid squares; 100 bars pore pressure) saturations.

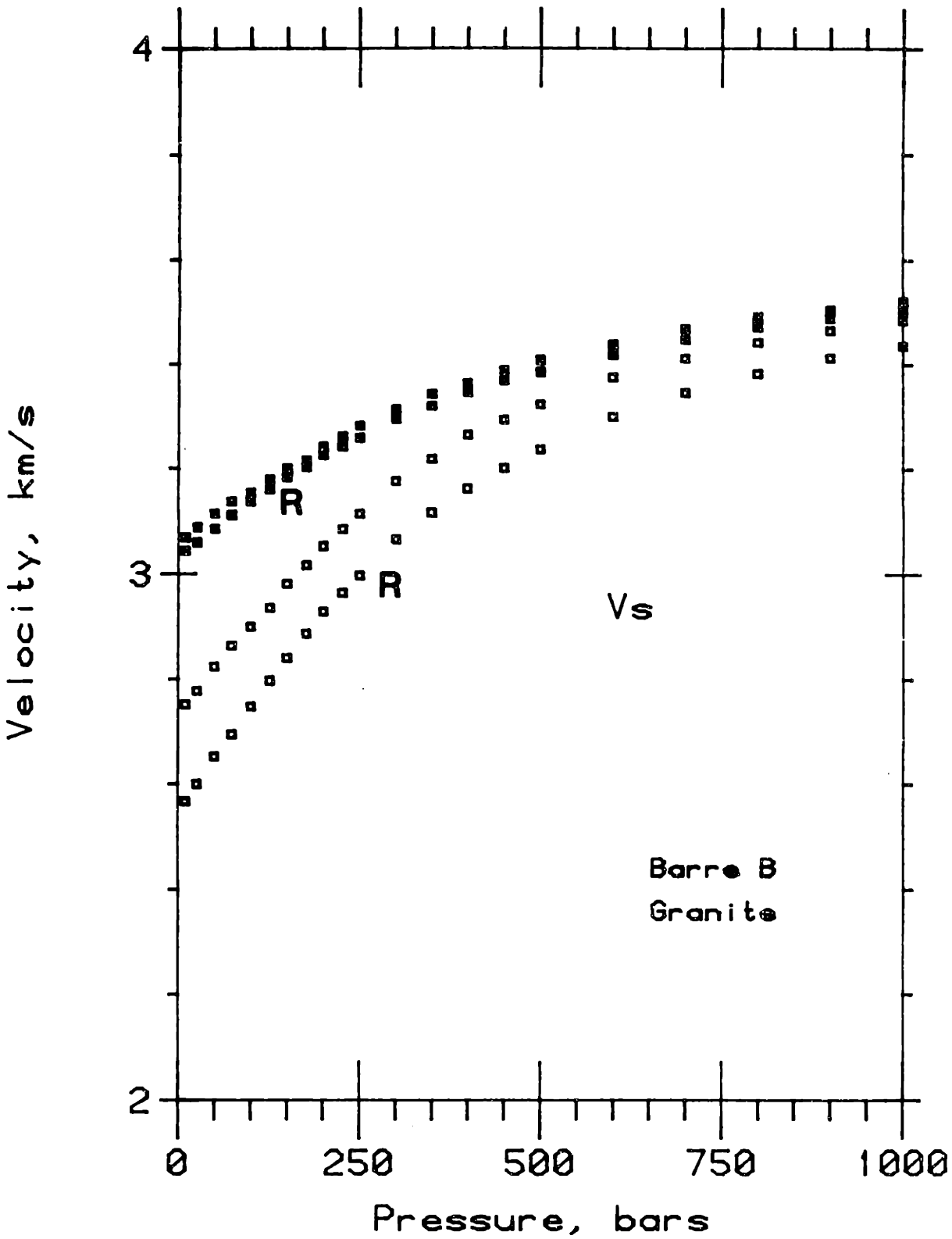


Figure 5-4. S-wave velocities in two directions for Barre granite versus differential pressure for dry (open squares; 20 $\mu$m Hg vacuum) and benzene (solid squares; 100 bars pore pressure) saturations. Propagation direction perpendicular to major rift plane. Sense of shear for lower set of dry and saturated velocities, labelled "R", is perpendicular to a second major rift plane used in the quarry in splitting the rock; second set is perpendicular to the hard direction.

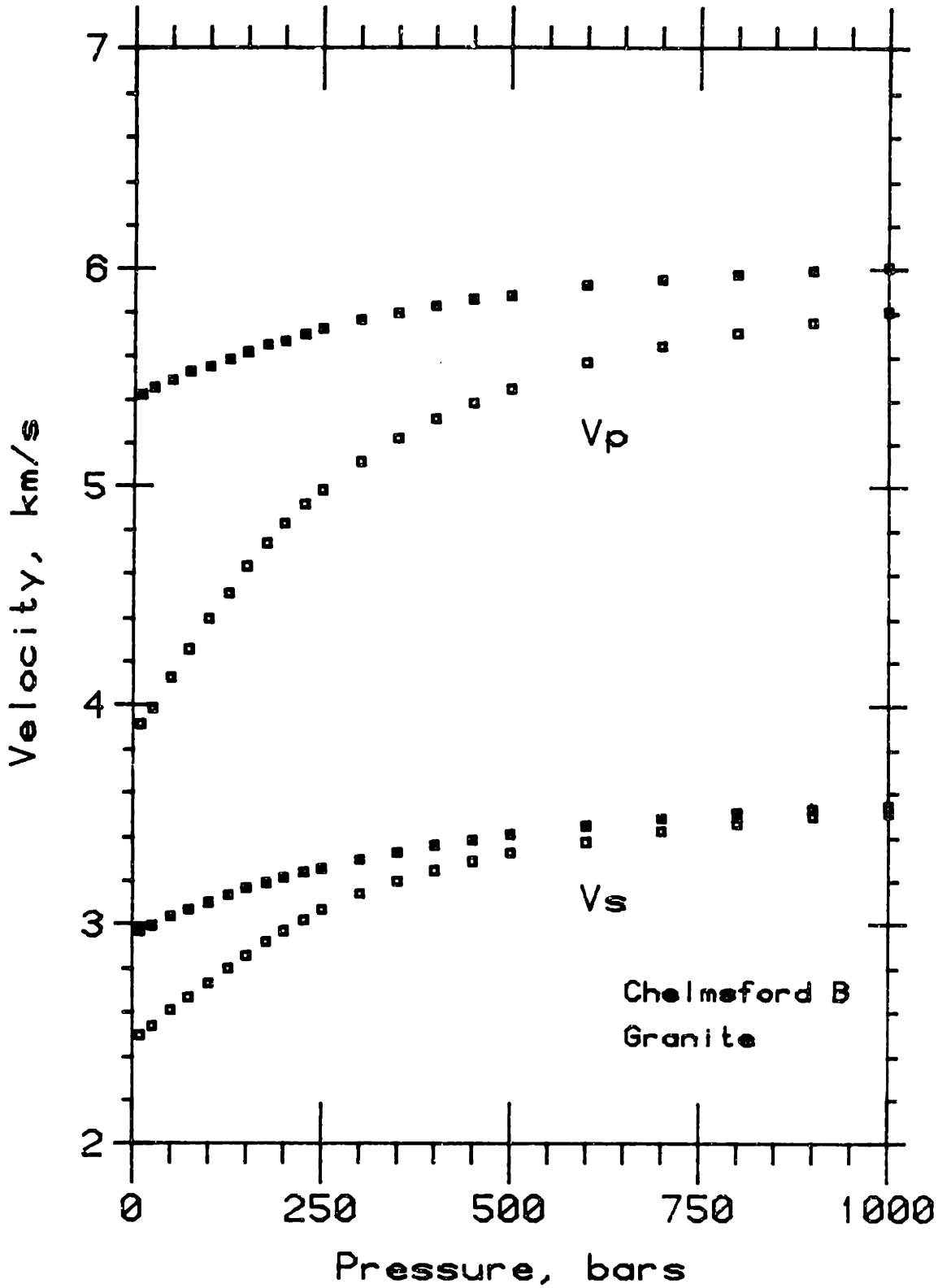


Figure 5-5. P- and S-wave velocities for Chelmsford granite versus differential pressure for dry (open squares; 20 $\mu$m Hg vacuum) and benzene (solid squares; 100 bars pore pressure) saturations. Propagation direction perpendicular to grain plane in the quarry terminalogy. Sense of shear for S-wave velocities is perpendicular to headgrain plane.

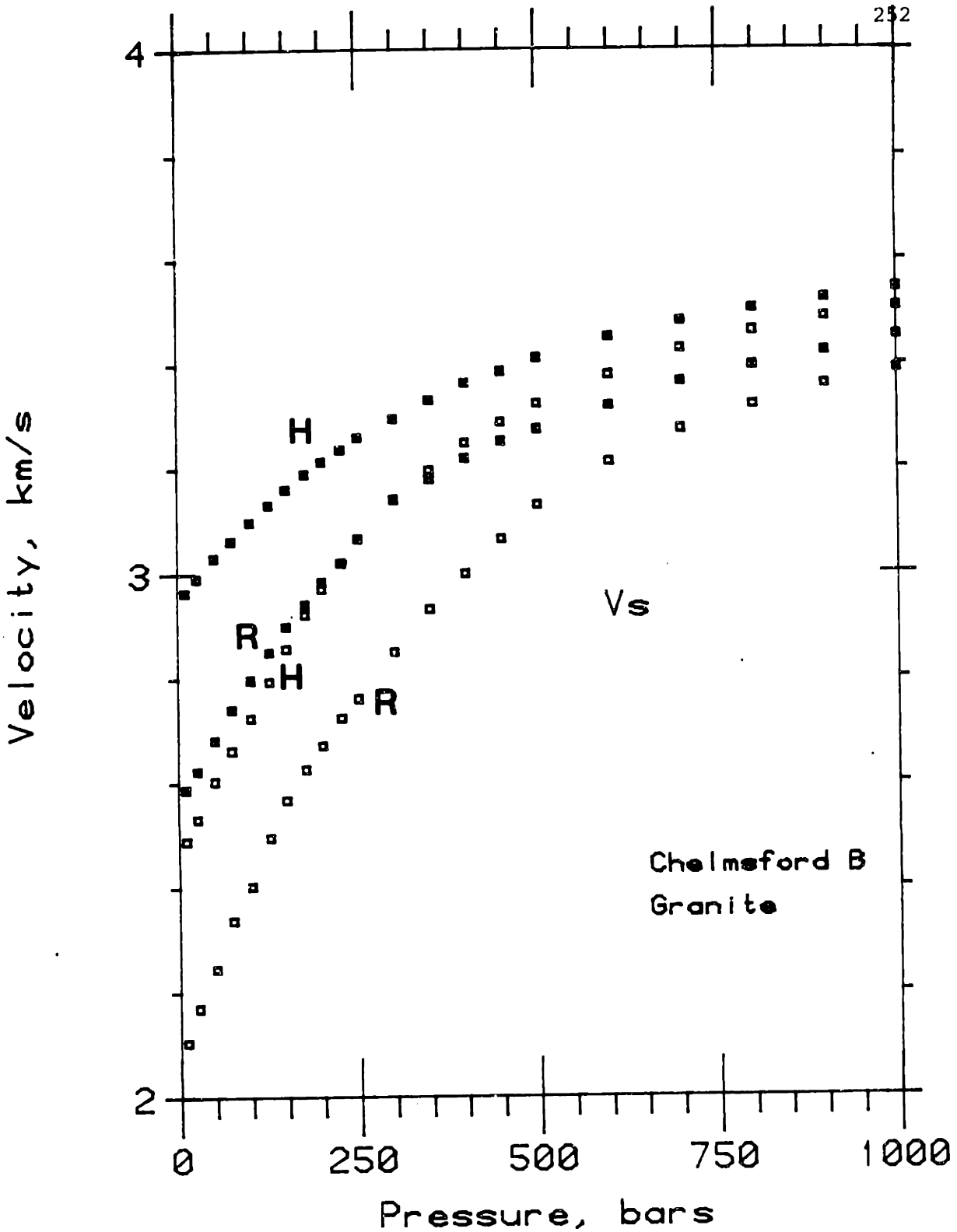


Figure 5-6. S-wave velocities in two directions for Chelmsford granite versus differential pressure for dry (open squares; 20 $\mu$m Hg vacuum) and benzene (solid squares; 100 bars pore pressure) saturations. Propagation direction perpendicular to grain plane. Sense of shear for lower set of dry and saturated velocities, labelled "R", is perpendicular to the rift plane used in the quarry; upper set, labelled "H", is perpendicular to the headgrain plane.

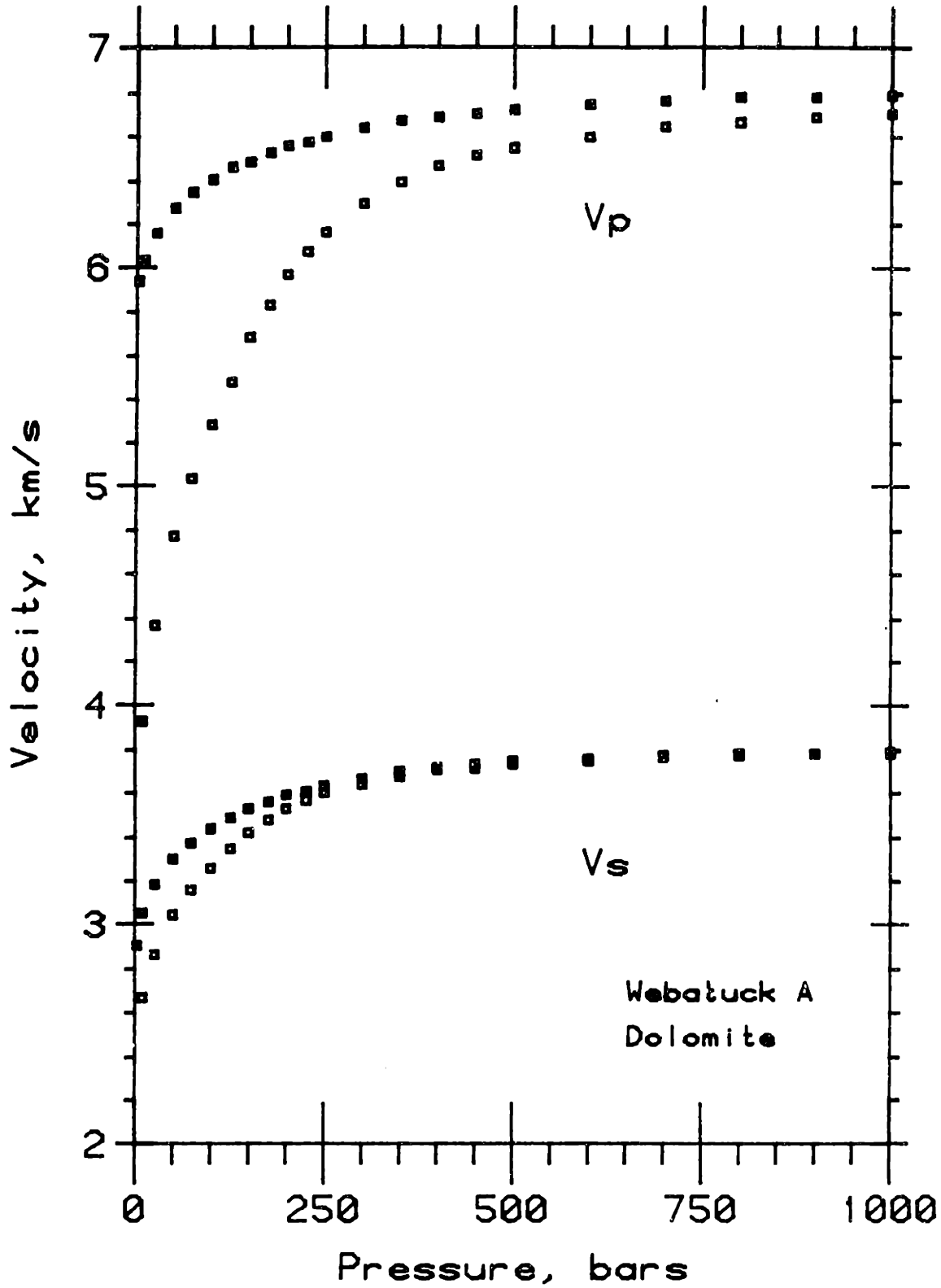


Figure 5-7. P- and S-wave velocities for Webatuck dolomite versus differential pressure for dry (open squares; 20 $\mu$m Hg vacuum) and benzene (solid squares; 100 bars pore pressure) saturations. Propagation direction perpendicular to foliation direction.

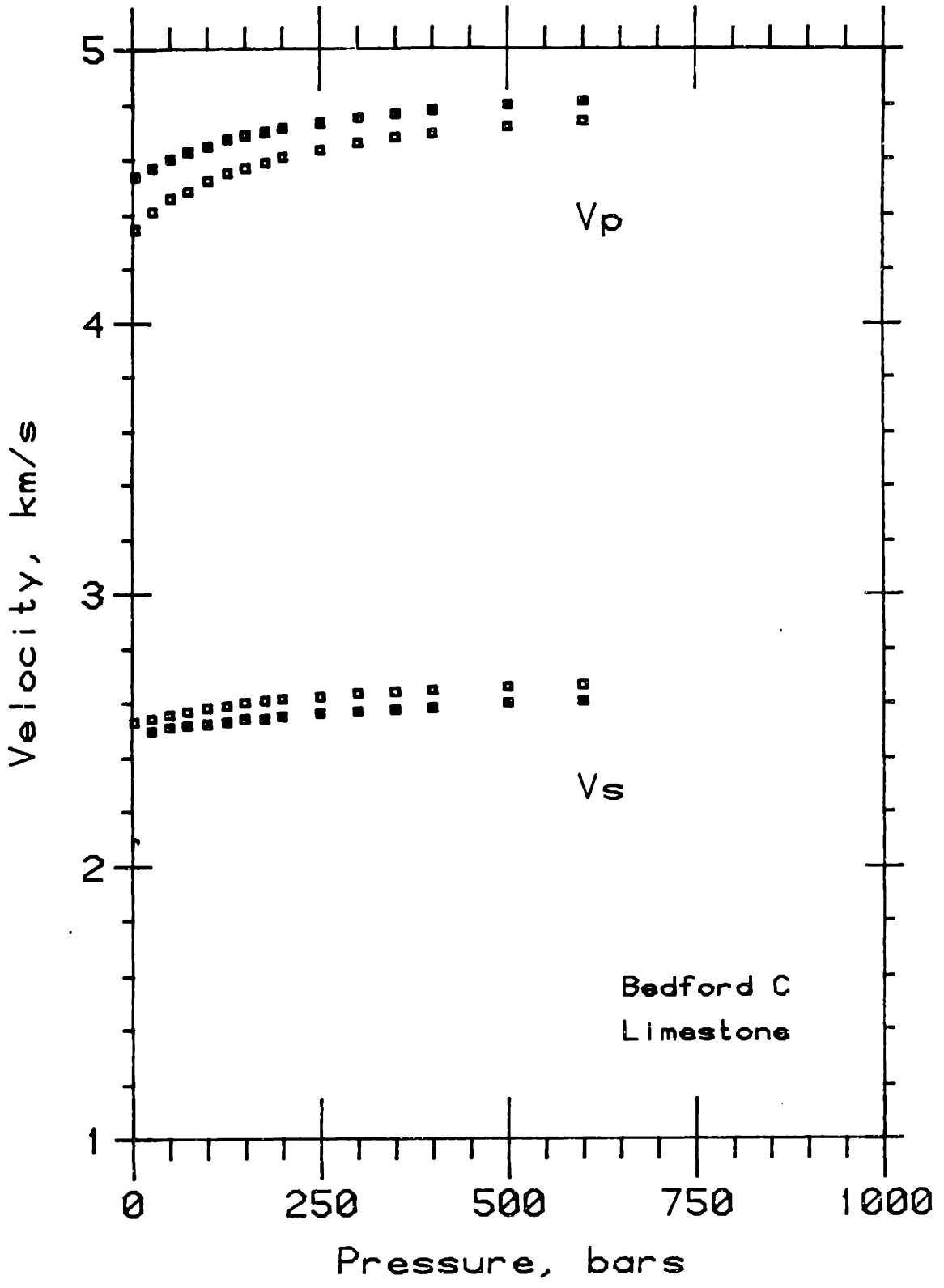


Figure 5-8. P- and S-wave velocities for Bedford limestone versus differential pressure for dry (open squares; 20 $\mu$m Hg vacuum) and benzene (solid squares; 100 bars pore pressure) saturations. Propagation direction parallel with bedding.

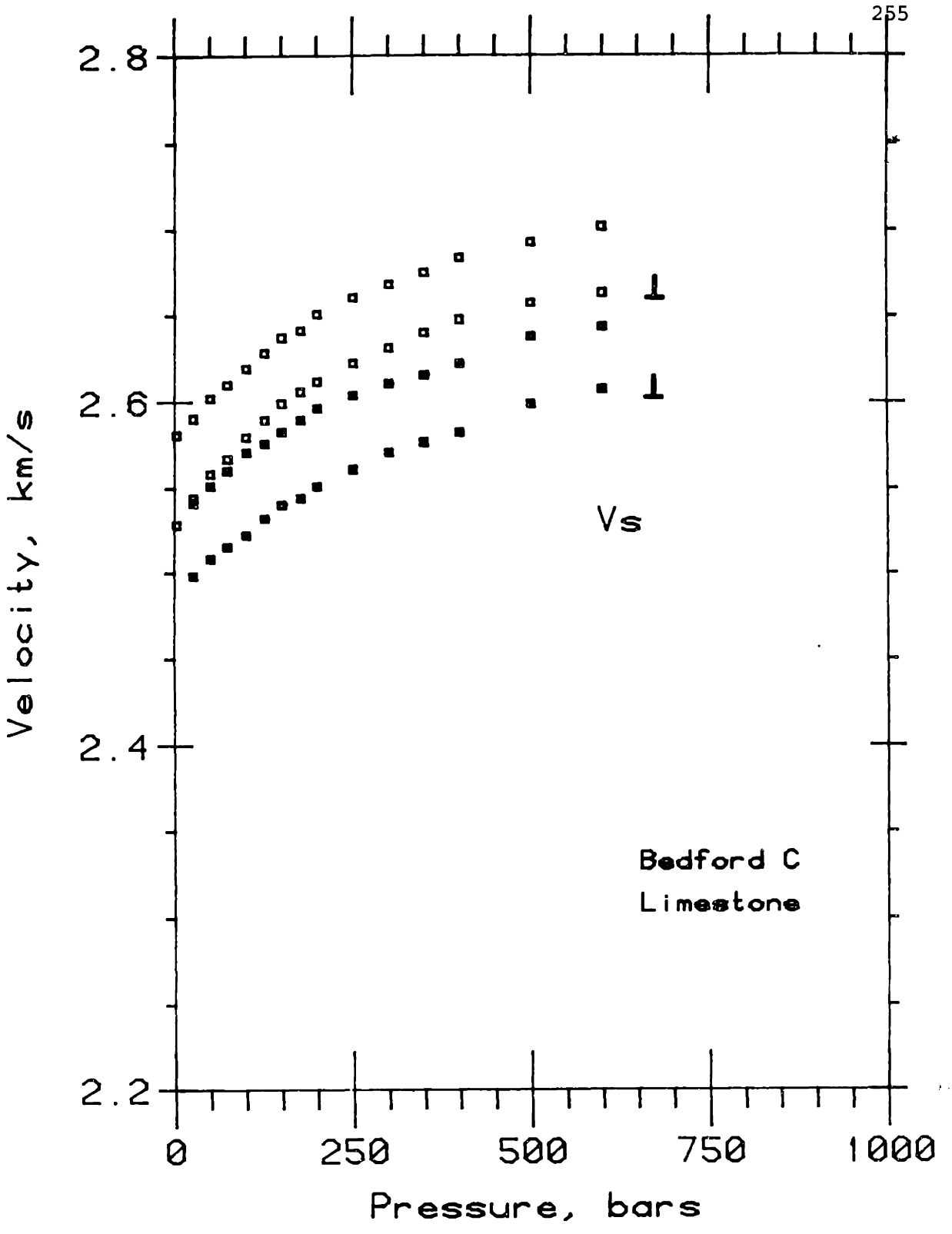


Figure 5-9. S-wave velocities in two directions for Bedford limestone versus differential pressure for dry (open squares; 20 $\mu$m Hg vacuum) and benzene (solid squares; 100 bars pore pressure) saturations. Propagation direction parallel with bedding. Sense of shear for labelled set of velocities perpendicular to bedding.

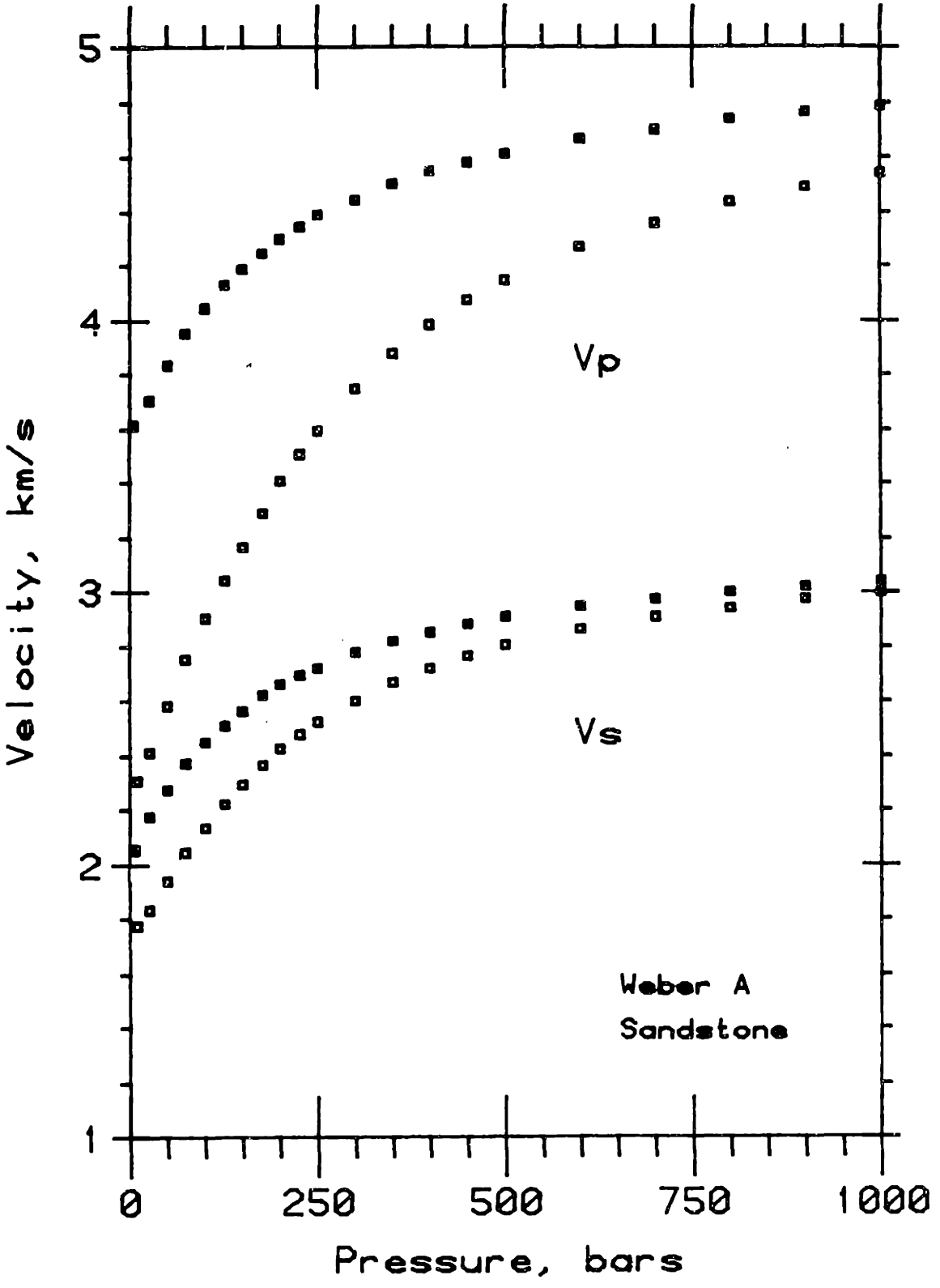


Figure 5-10. P- and S-wave velocities for Weber sandstone versus differential pressure for dry (open squares; 20 $\mu$m Hg vacuum) and benzene (solid squares; 100 bars pore pressure) saturations. Propagation direction perpendicular to bedding.

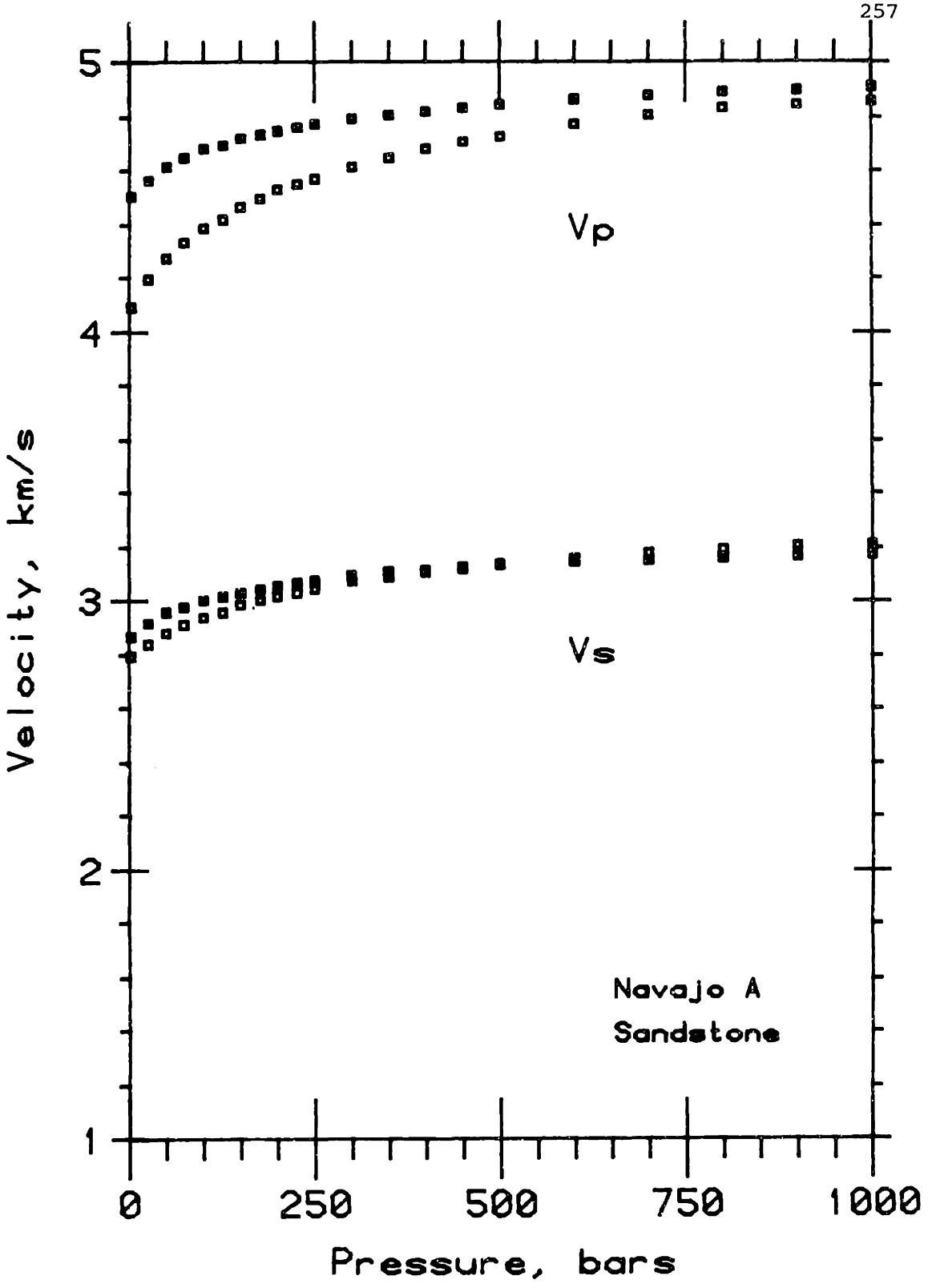


Figure 5-11. P- and S-wave velocities for Navajo sandstone versus differential pressure for dry (open squares; 20 $\mu$m Hg vacuum) and benzene (solid squares; 100 bars pore pressure) saturations. Propagation direction perpendicular to bedding.

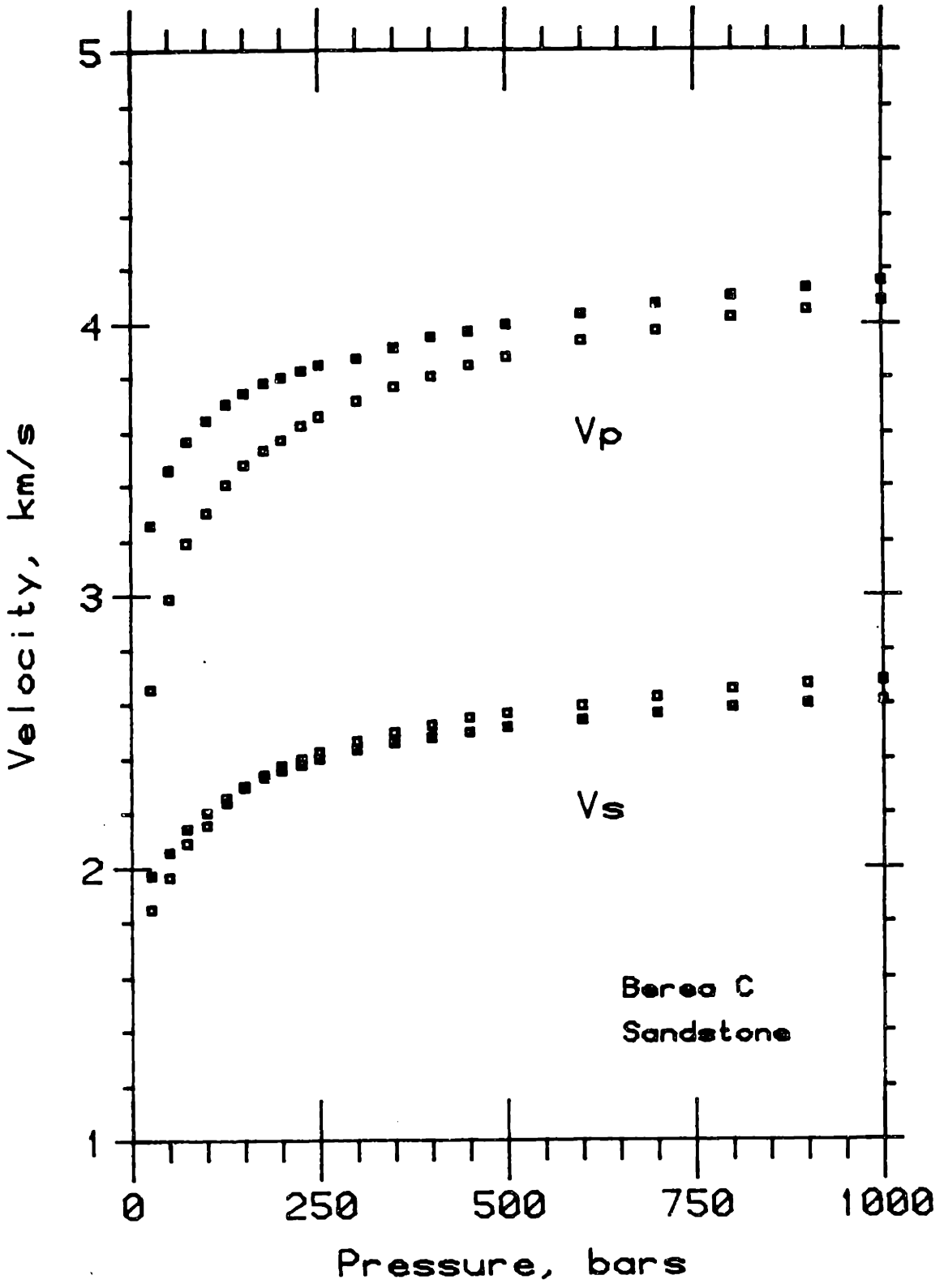


Figure 5-12. P- and S-wave velocities for Berea sandstone versus differential pressure for dry (open squares; 20 $\mu$m Hg vacuum) and benzene (solid squares; 100 bars pore pressure) saturations. Propagation direction parallel with bedding; there is minimal S-wave velocity anisotropy.

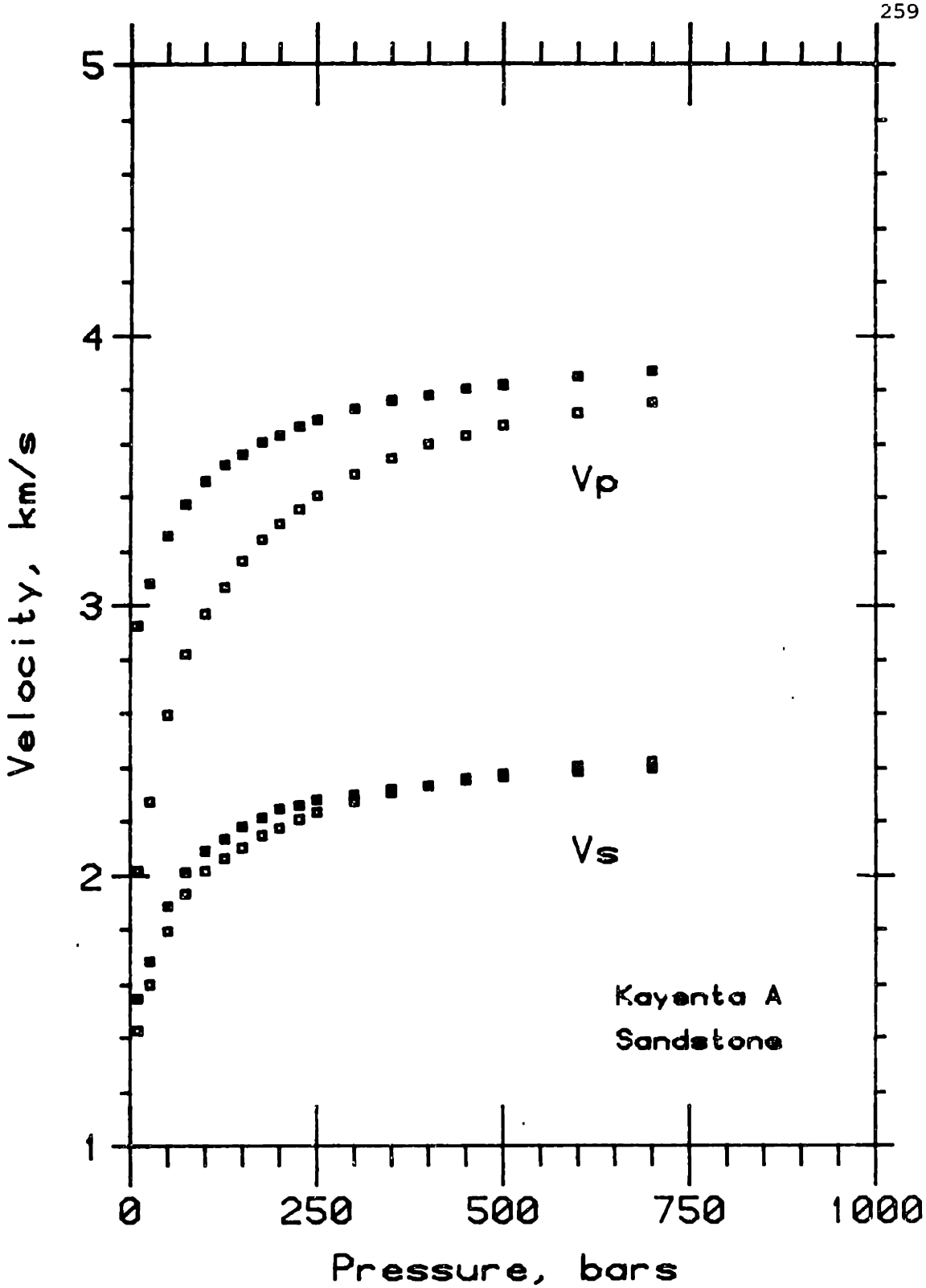


Figure 5-13. P- and S-wave velocities for Kayenta sandstone versus differential pressure for dry (open squares; 20 $\mu$m Hg vacuum) and benzene (solid squares; 100 bars pore pressure) saturations. Propagation direction perpendicular to bedding.

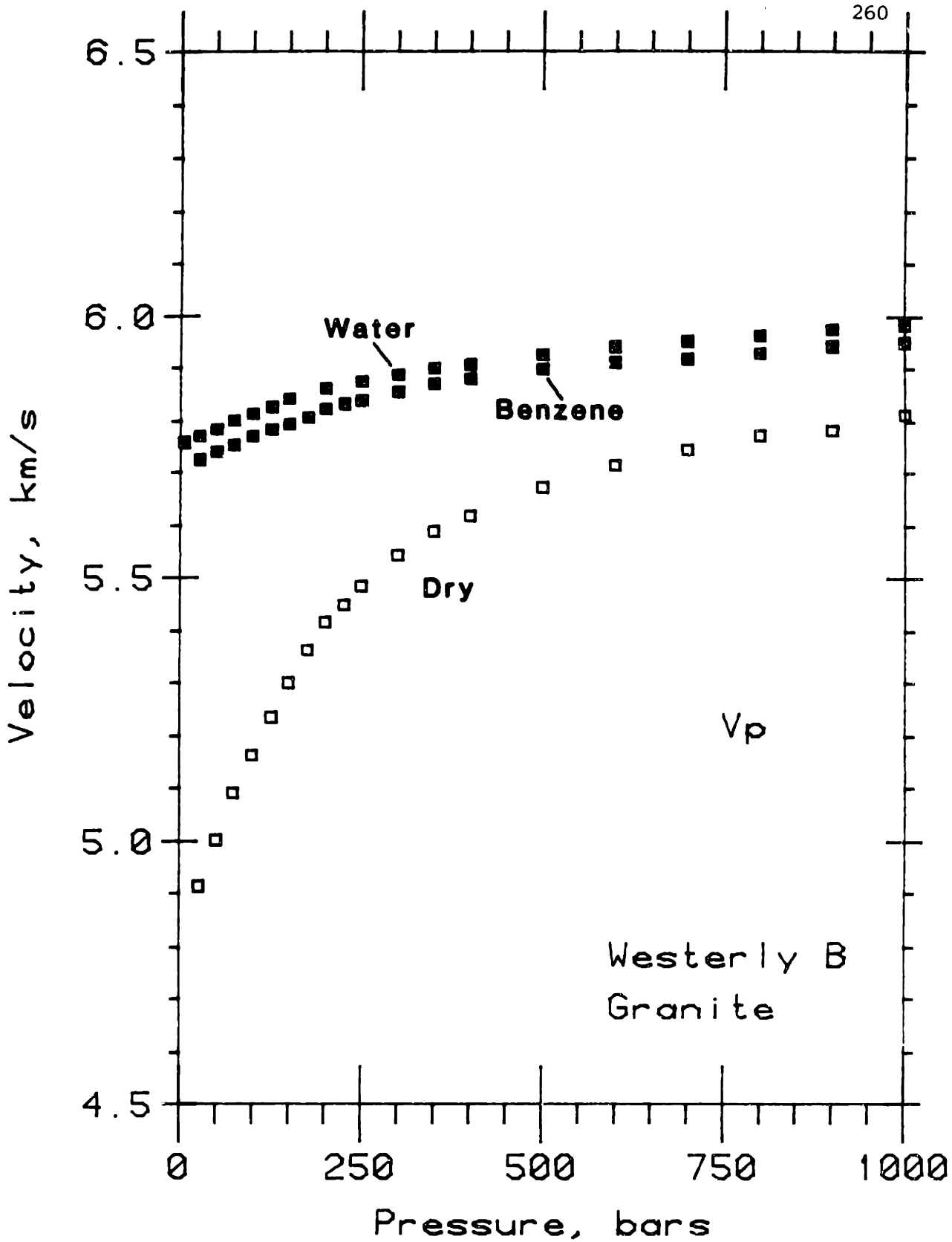


Figure 5-14. P-wave velocities for Westerly granite versus differential pressure for dry (open squares; 20 $\mu$m Hg vacuum), benzene (labelled solid squares; 100 bars pore pressure), and distilled water (labelled solid squares; 100 bars pore pressure) saturations.

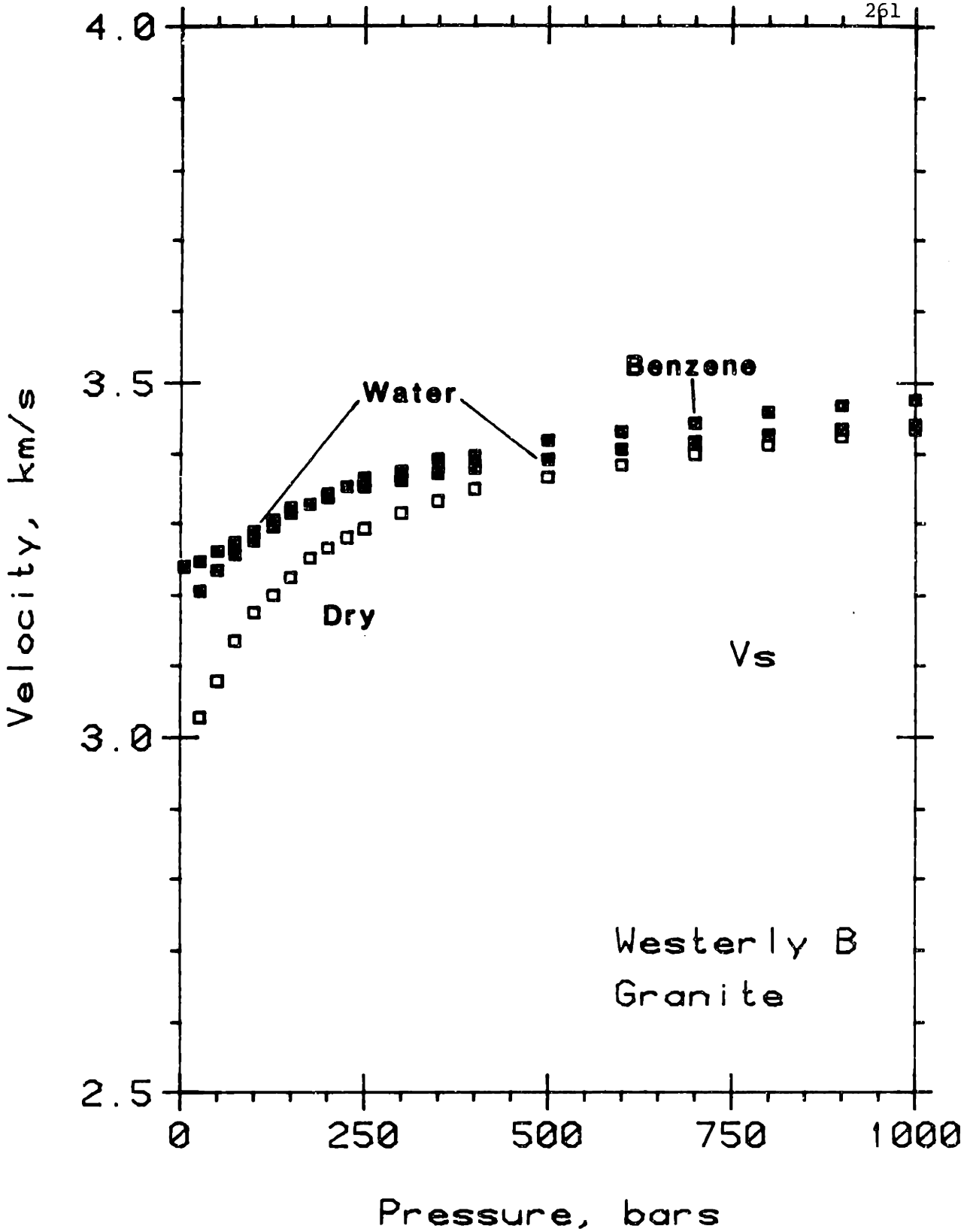


Figure 5-15. S-wave velocities for Westerly granite versus differential pressure for dry (open squares; 20 $\mu$m Hg vacuum), benzene (labelled solid squares; 100 bars pore pressure), and distilled water (labelled solid squares; 100 bars pore pressure) saturations.

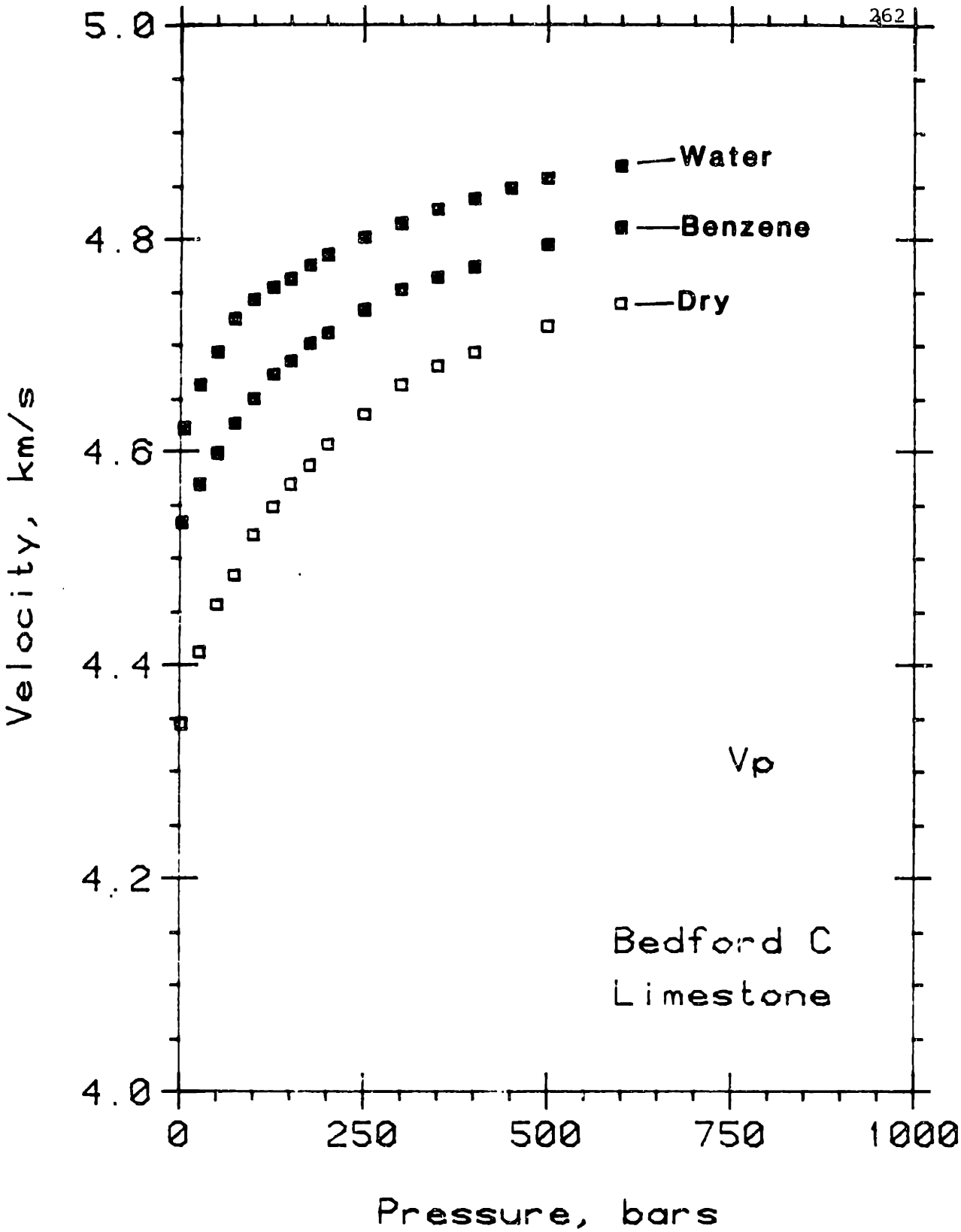


Figure 5-16. P-wave velocities for Bedford limestone versus differential pressure for dry (open squares; 20 $\mu$m Hg vacuum), benzene (labelled solid squares; 100 bars pore pressure), and distilled water (labelled solid squares; 100 bars pore pressure) saturations. Propagation direction parallel with bedding.

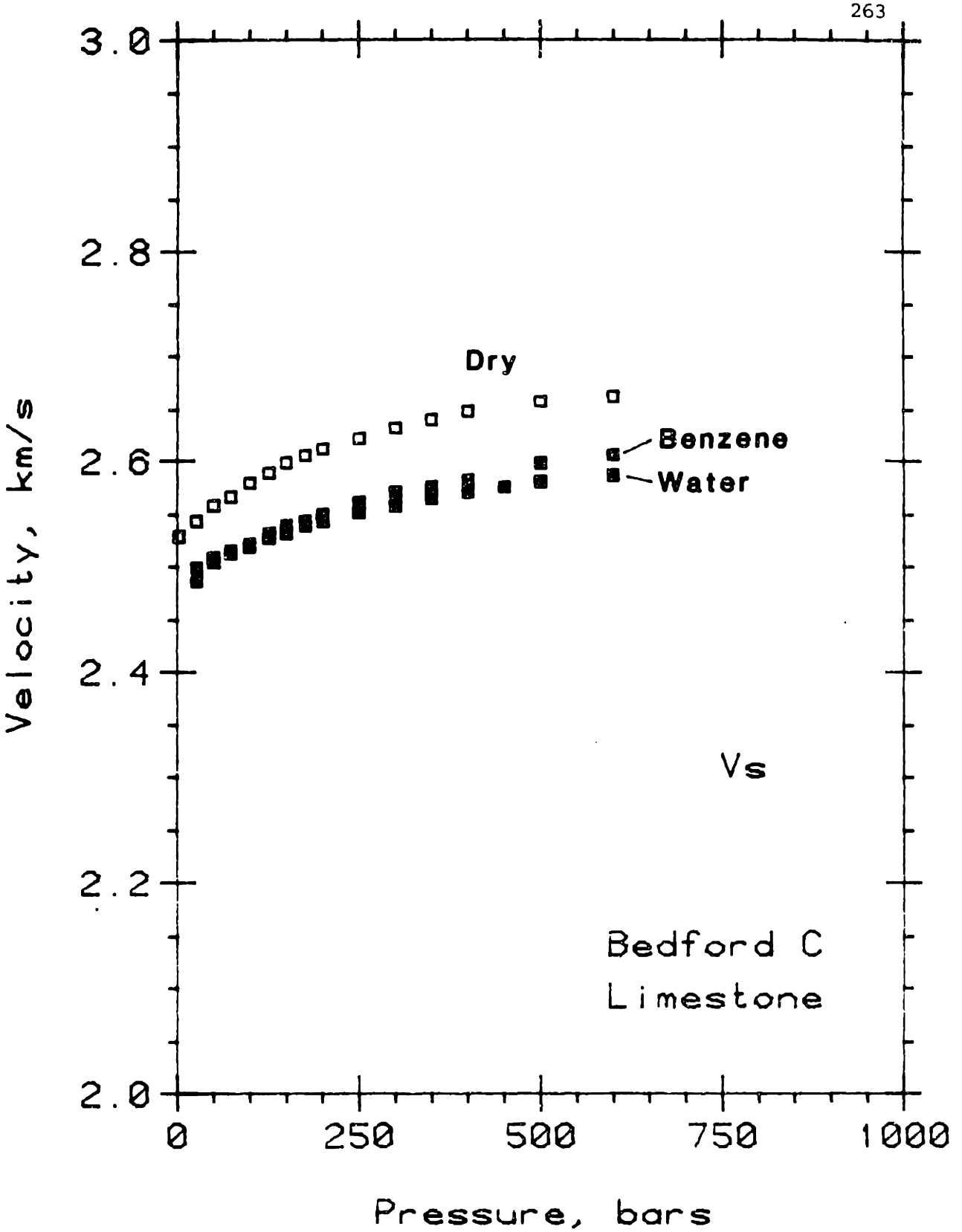


Figure 5-17. S-wave velocities for Bedford limestone versus differential pressure for dry (open squares; 20 $\mu$m Hg vacuum), benzene (labelled solid squares; 100 bars pore pressure), and distilled water (labelled solid squares; 100 bars pore pressure) saturations. Propagation direction parallel with bedding; sense of shear perpendicular to bedding.

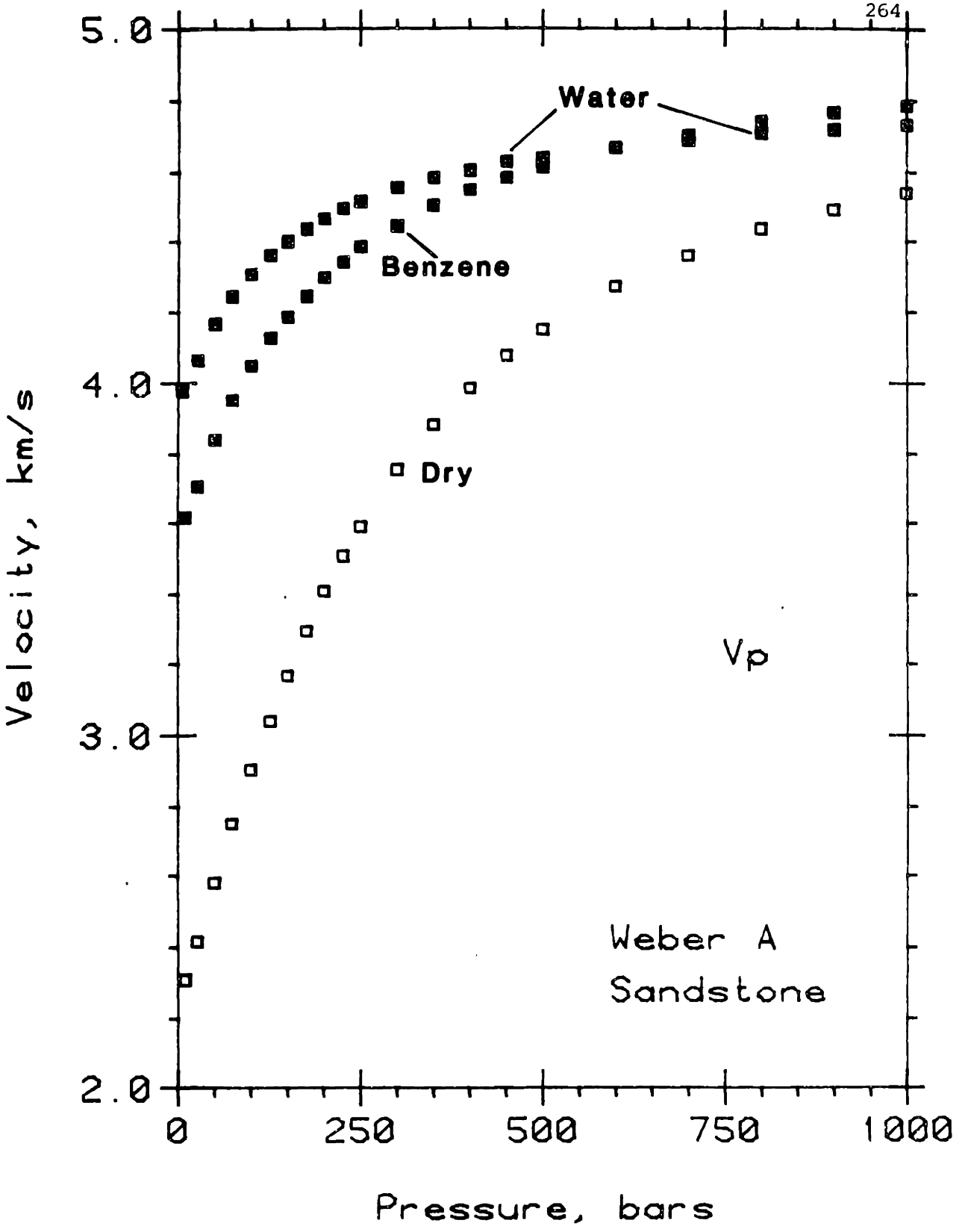


Figure 5-18. P-wave velocities for Weber sandstone versus differential pressure for dry (open squares; 20 $\mu$m Hg vacuum), benzene (labelled solid squares; 100 bars pore pressure), and distilled water (labelled solid squares; 100 bars pore pressure) saturations. Propagation direction perpendicular to bedding.

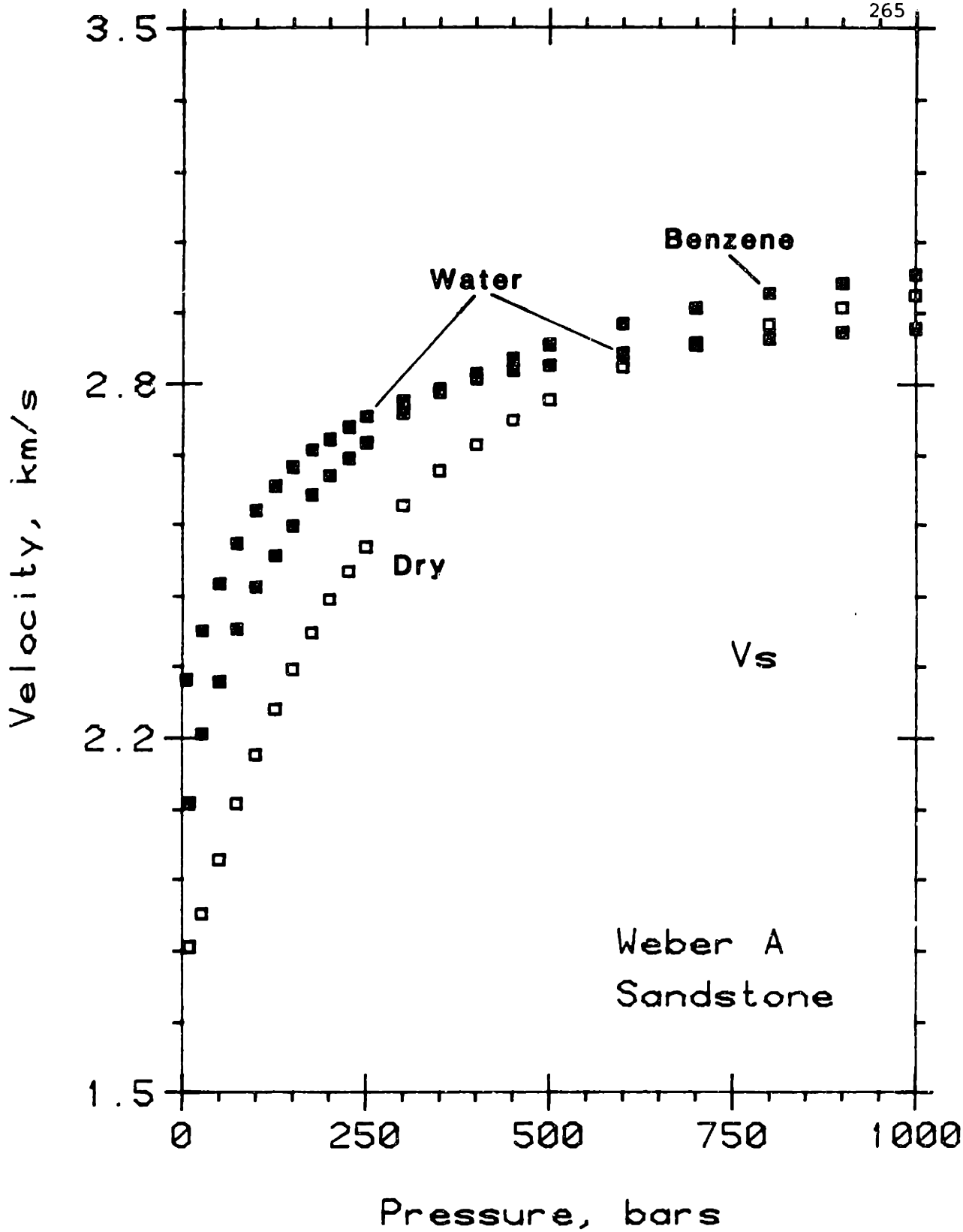


Figure 5-19. S-wave velocities for Weber sandstone versus differential pressure for dry (open squares; 20 $\mu$m Hg vacuum), benzene (labelled solid squares; 100 bars pore pressure), and distilled water (labelled solid squares; 100 bars pore pressure) saturations. Propagation direction perpendicular to bedding.

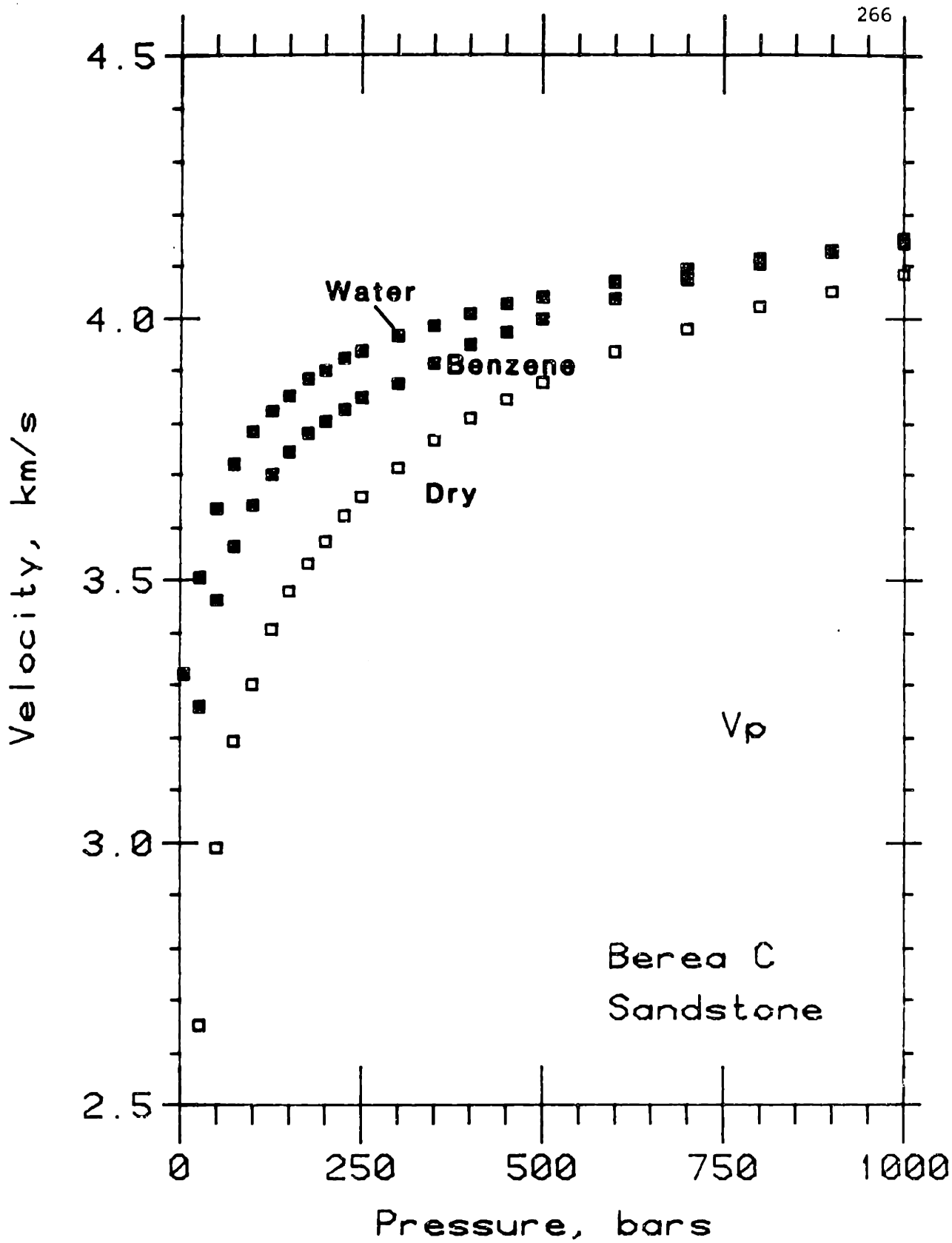


Figure 5-20. P-wave velocities for Berea sandstone versus differential pressure for dry (open squares; 20 $\mu$m Hg vacuum), benzene (labelled solid squares; 100 bars pore pressure), and distilled water (labelled solid squares; 100 bars pore pressure) saturations. Propagation direction parallel to bedding.

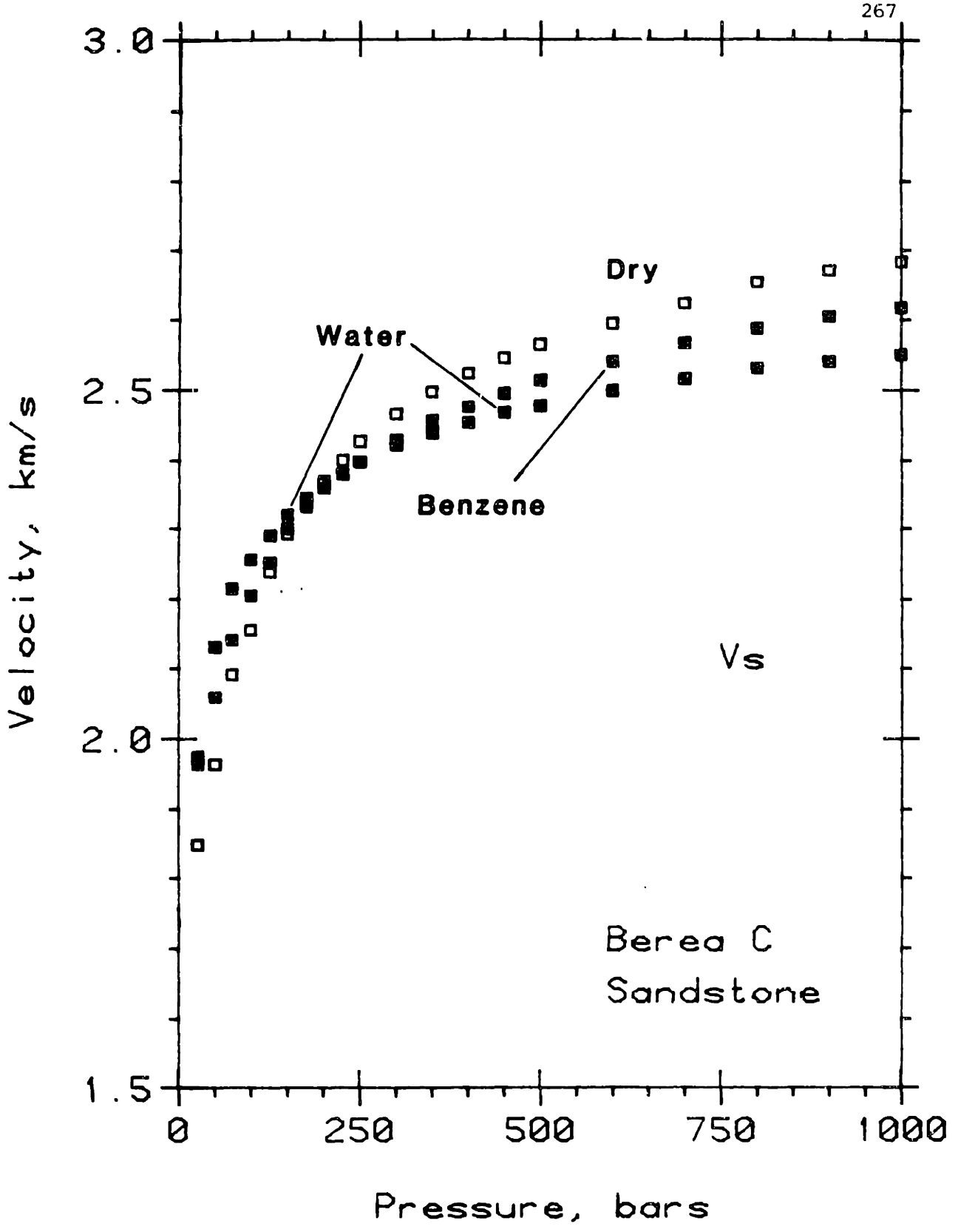


Figure 5-21. S-wave velocities for Berea sandstone versus differential pressure for dry (open squares; 20 $\mu$m Hg vacuum), benzene (labelled solid squares; 100 bars pore pressure), and distilled water (labelled solid squares; 100 bars pore pressure) saturations. Propagation direction parallel with bedding.

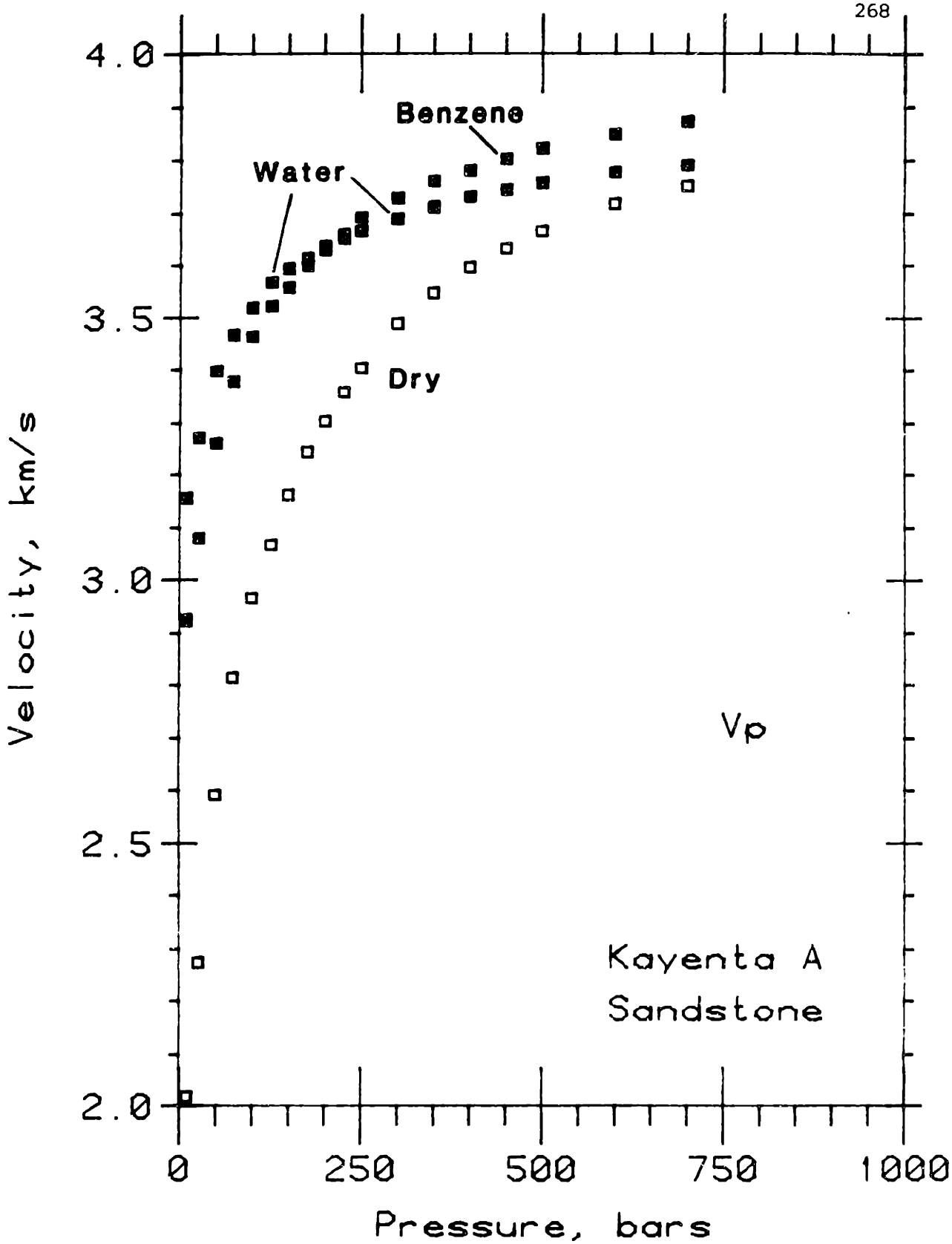


Figure 5-22. P-wave velocities for Kayenta sandstone versus differential pressure for dry (open squares; 20 $\mu$m Hg vacuum), benzene (labelled solid squares; 100 bars pore pressure), and distilled water (labelled solid squares; 100 bars pore pressure) saturations. Propagation direction perpendicular to bedding.

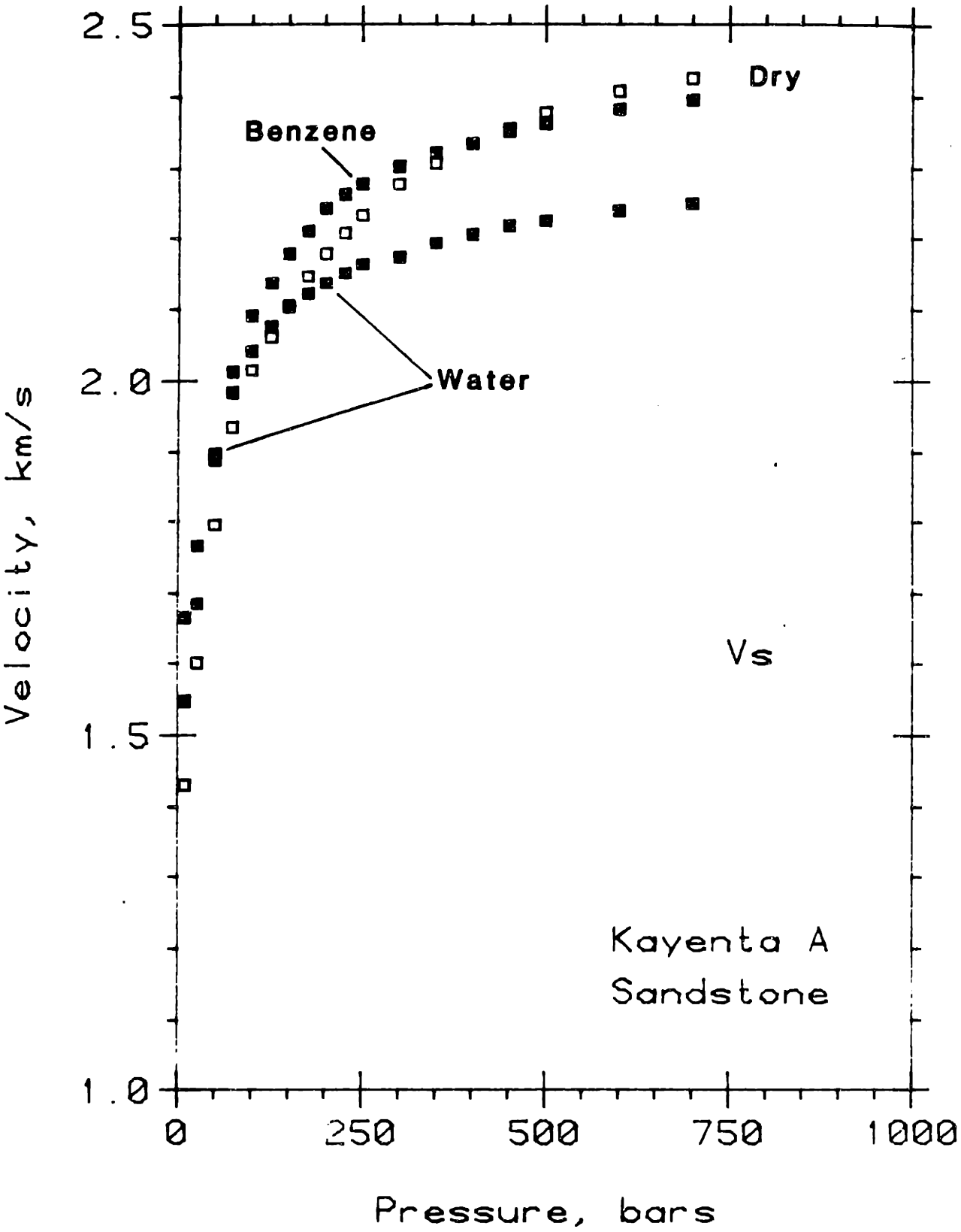


Figure 5-23. S-wave velocities for Kayenta sandstone versus differential pressure for dry (open squares; 20 $\mu$m Hg vacuum), benzene (labelled solid squares; 100 bars pore pressure), and distilled water (labelled solid squares; 100 bars pore pressure) saturations. Propagation direction perpendicular to bedding.

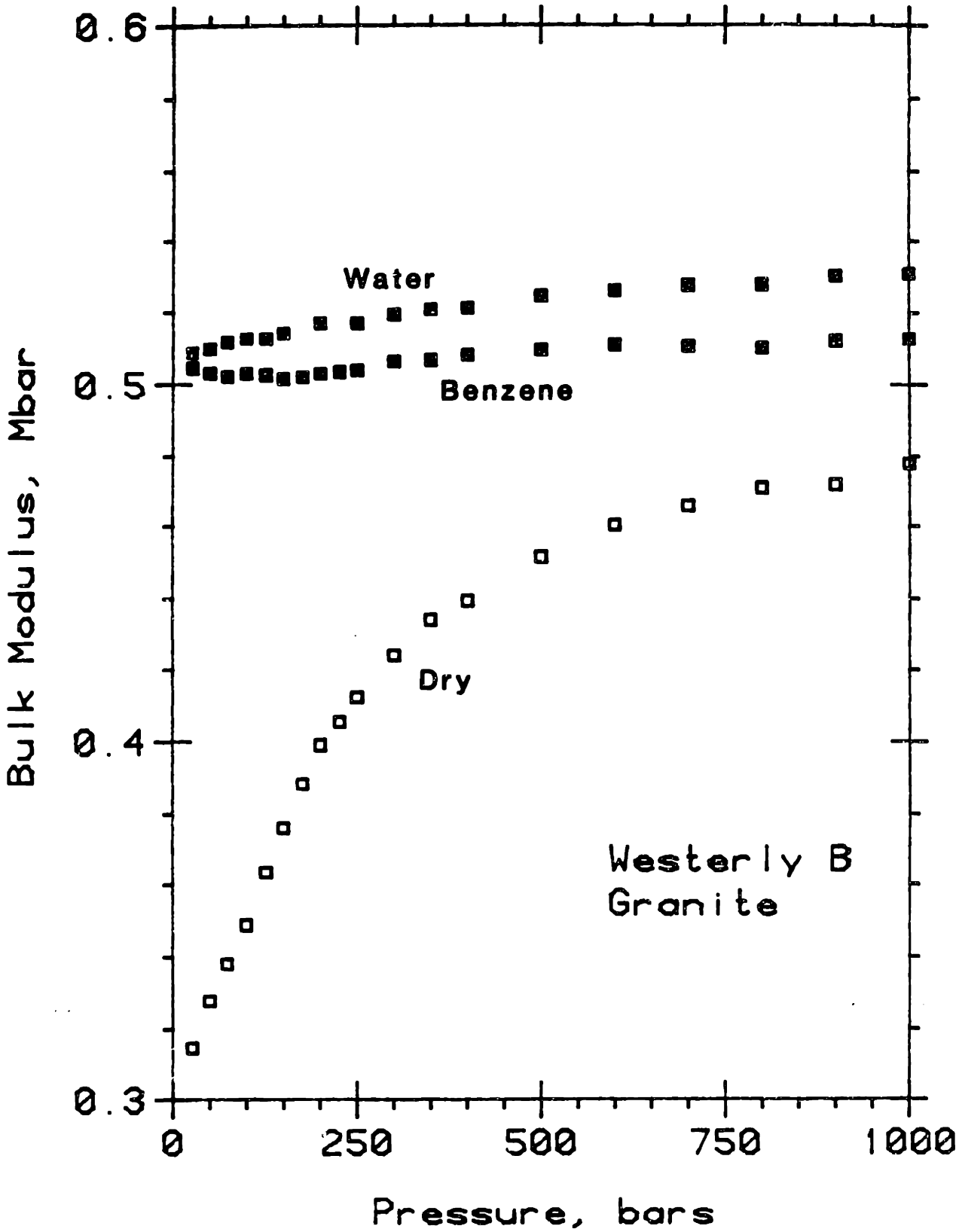


Figure 5-24. Vacuum dry, benzene-, and water-saturated bulk moduli for Westerly granite as a function of differential pressure.

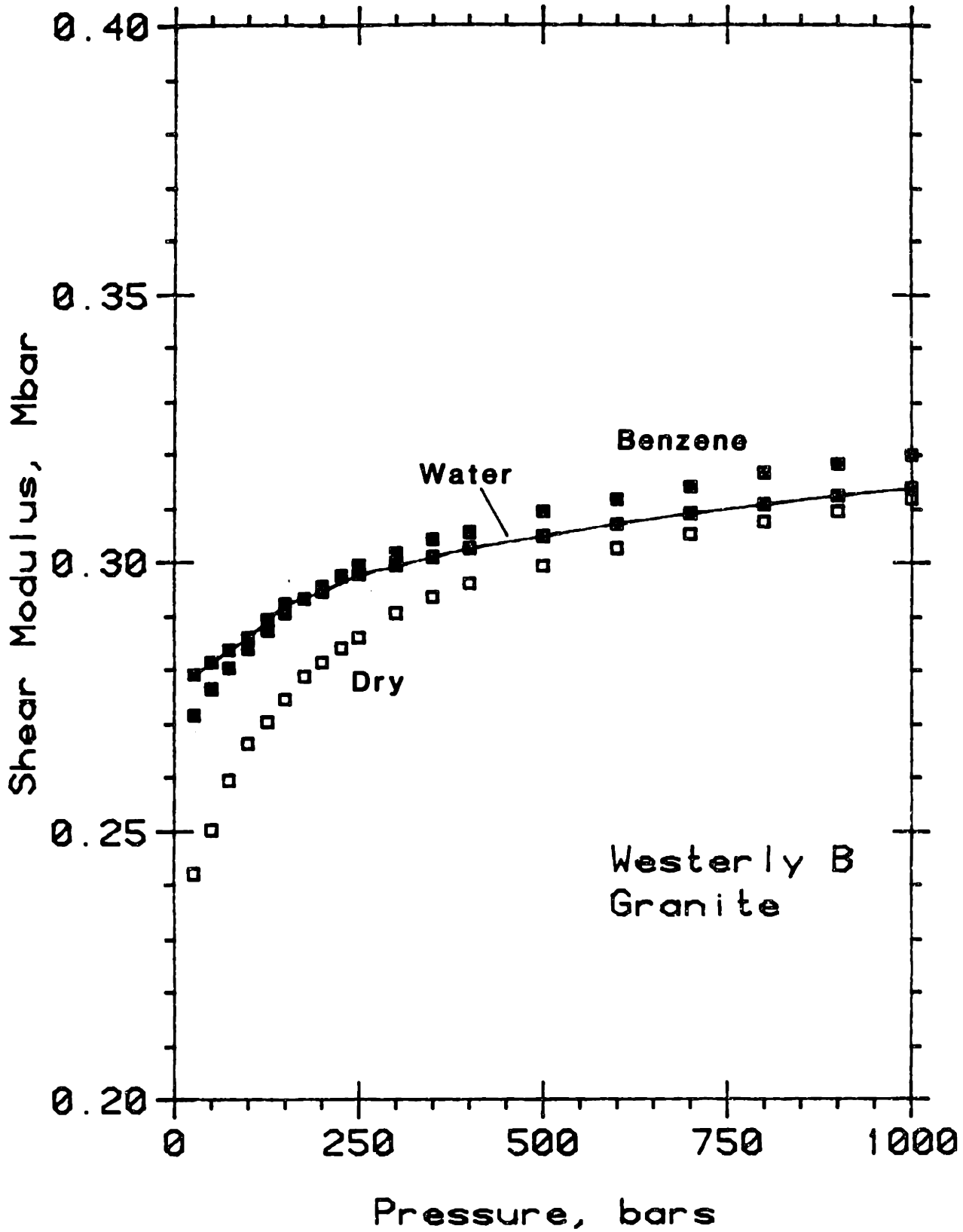


Figure 5-25. Vacuum dry, benzene-, and water-saturated shear moduli for Westerly granite as a function of differential pressure.

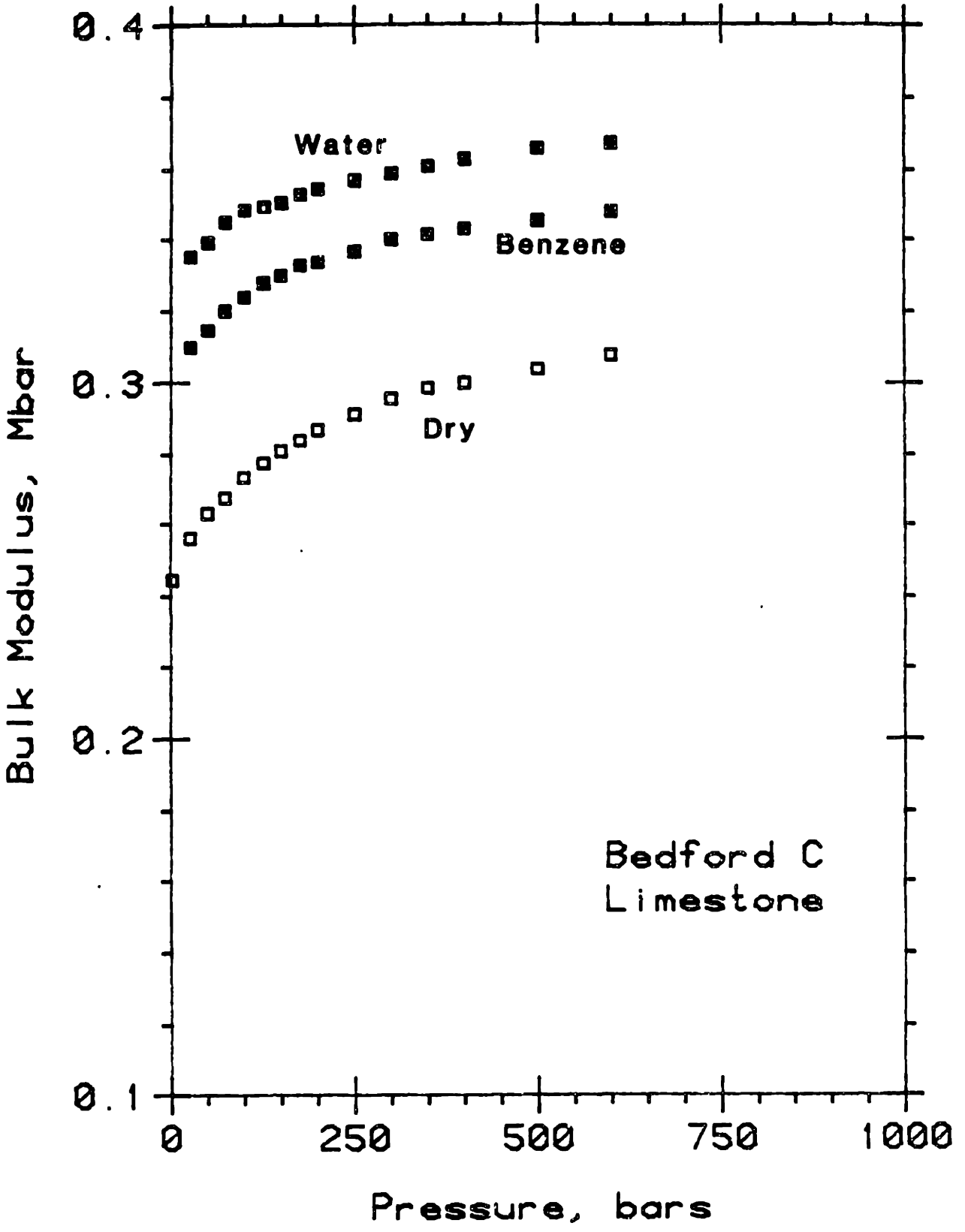


Figure 5-26. Vacuum dry, benzene-, and water-saturated bulk moduli for Bedford limestone as a function of differential pressure.

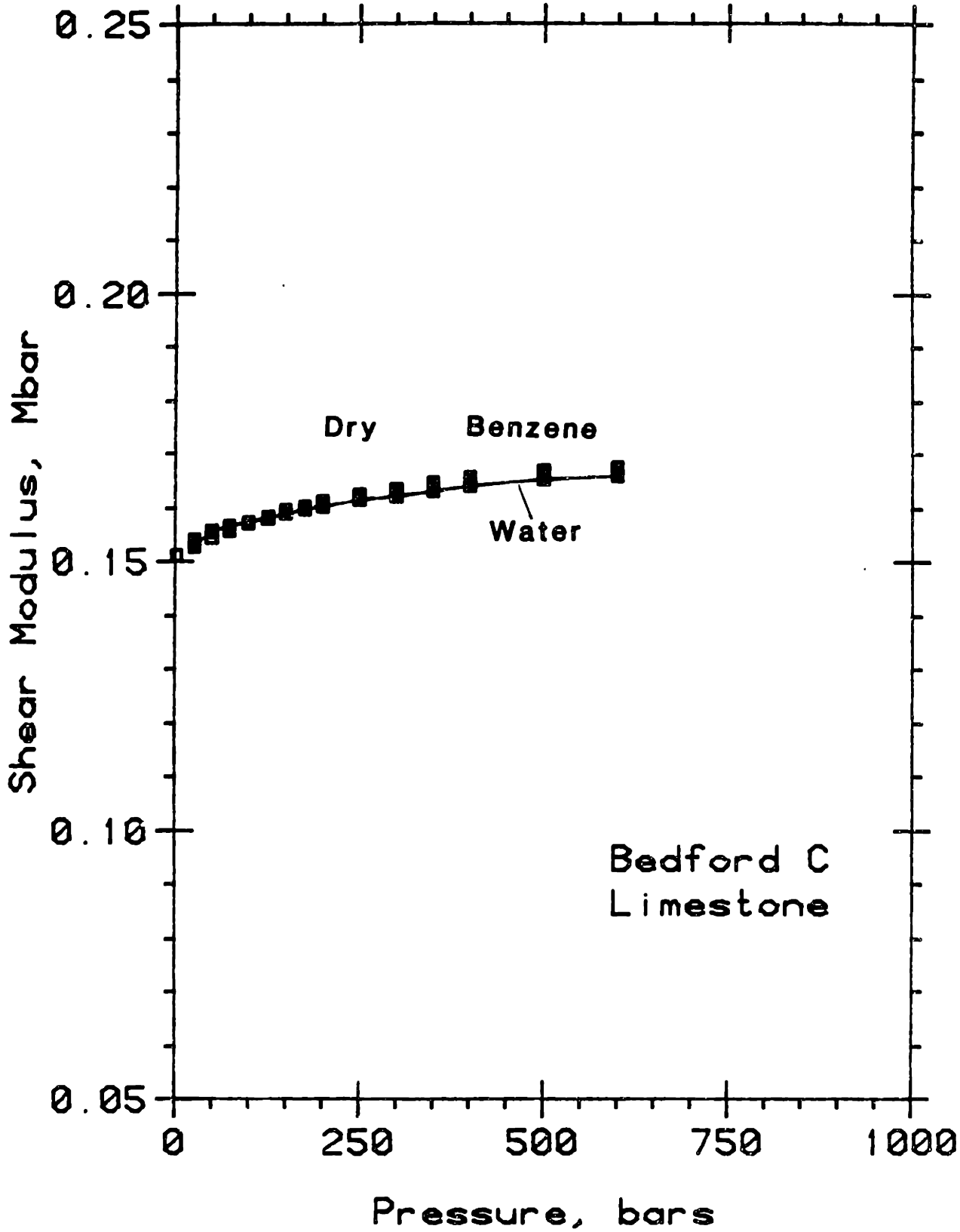


Figure 5-27. Vacuum dry, benzene-, and water-saturated shear moduli for Bedford limestone as a function of differential pressure.

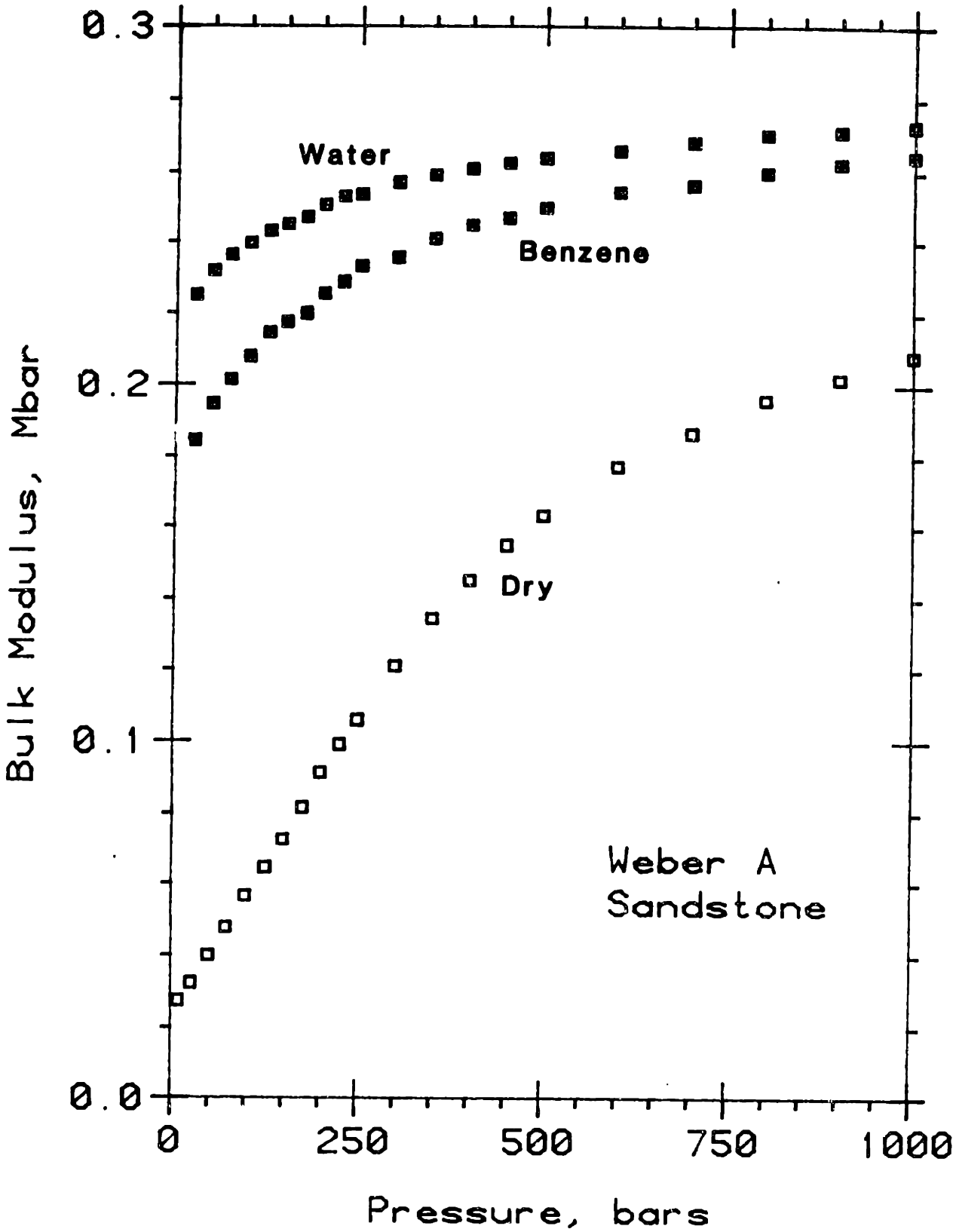


Figure 5-28. Vacuum dry, benzene-, and water-saturated bulk moduli for Weber sandstone as a function of differential pressure.

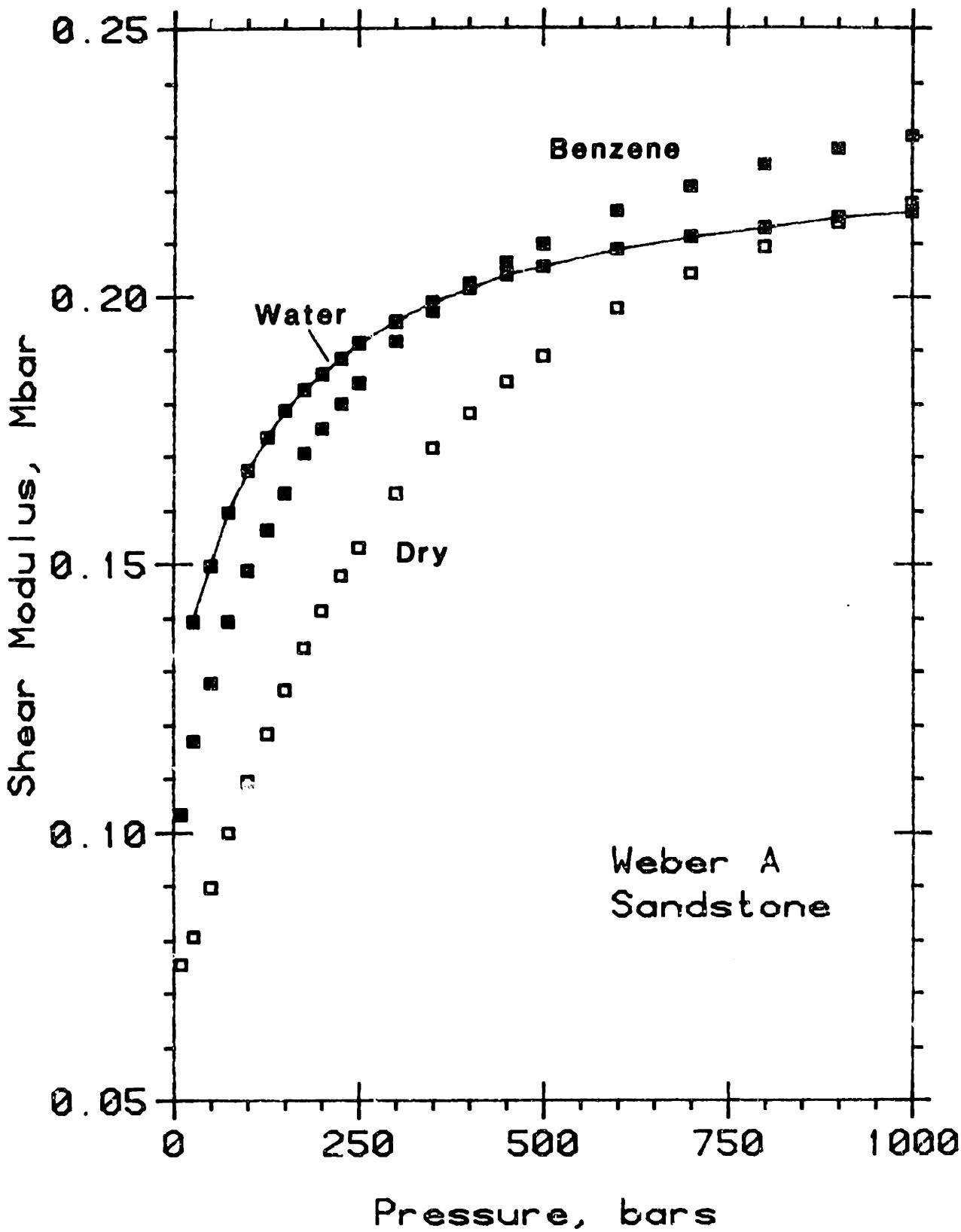


Figure 5-29. Vacuum dry, benzene-, and water-saturated shear moduli for Weber sandstone as a function of differential pressure.

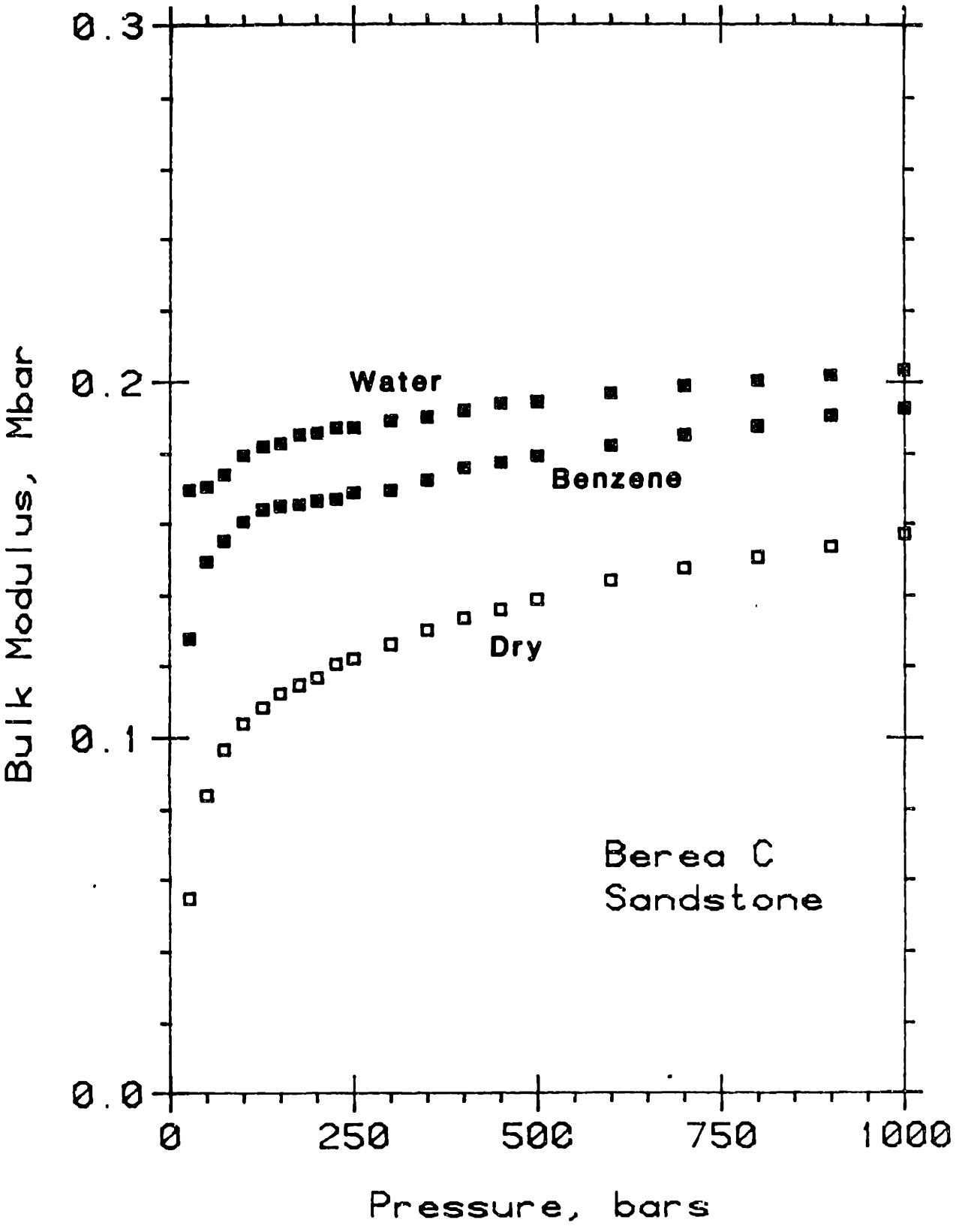


Figure 5-30. Vacuum dry, benzene-, and water-saturated bulk moduli for Berea sandstone as a function of differential pressure.

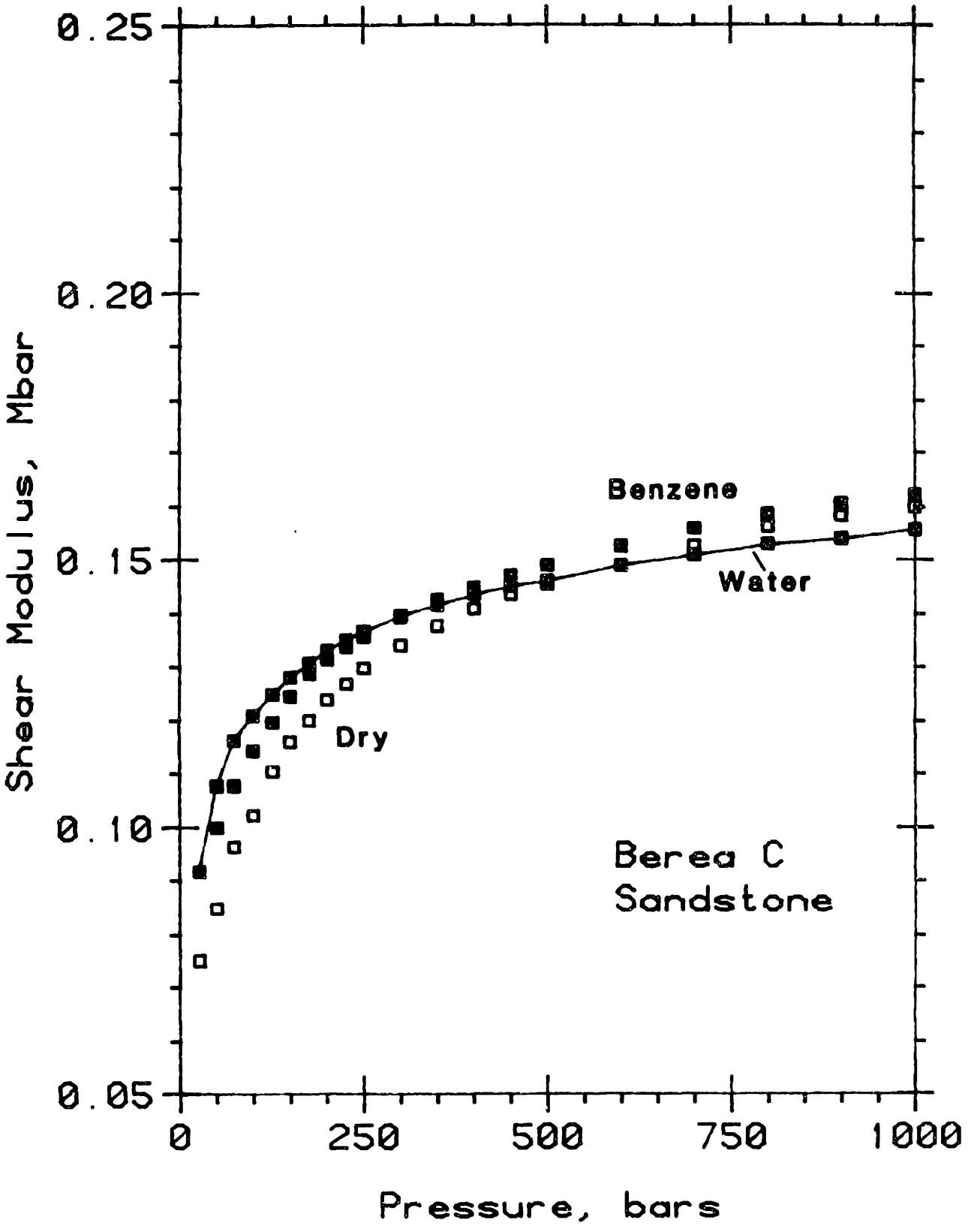


Figure 5-31. Vacuum dry, benzene-, and water-saturated shear moduli for Berea sandstone as a function of differential pressure.

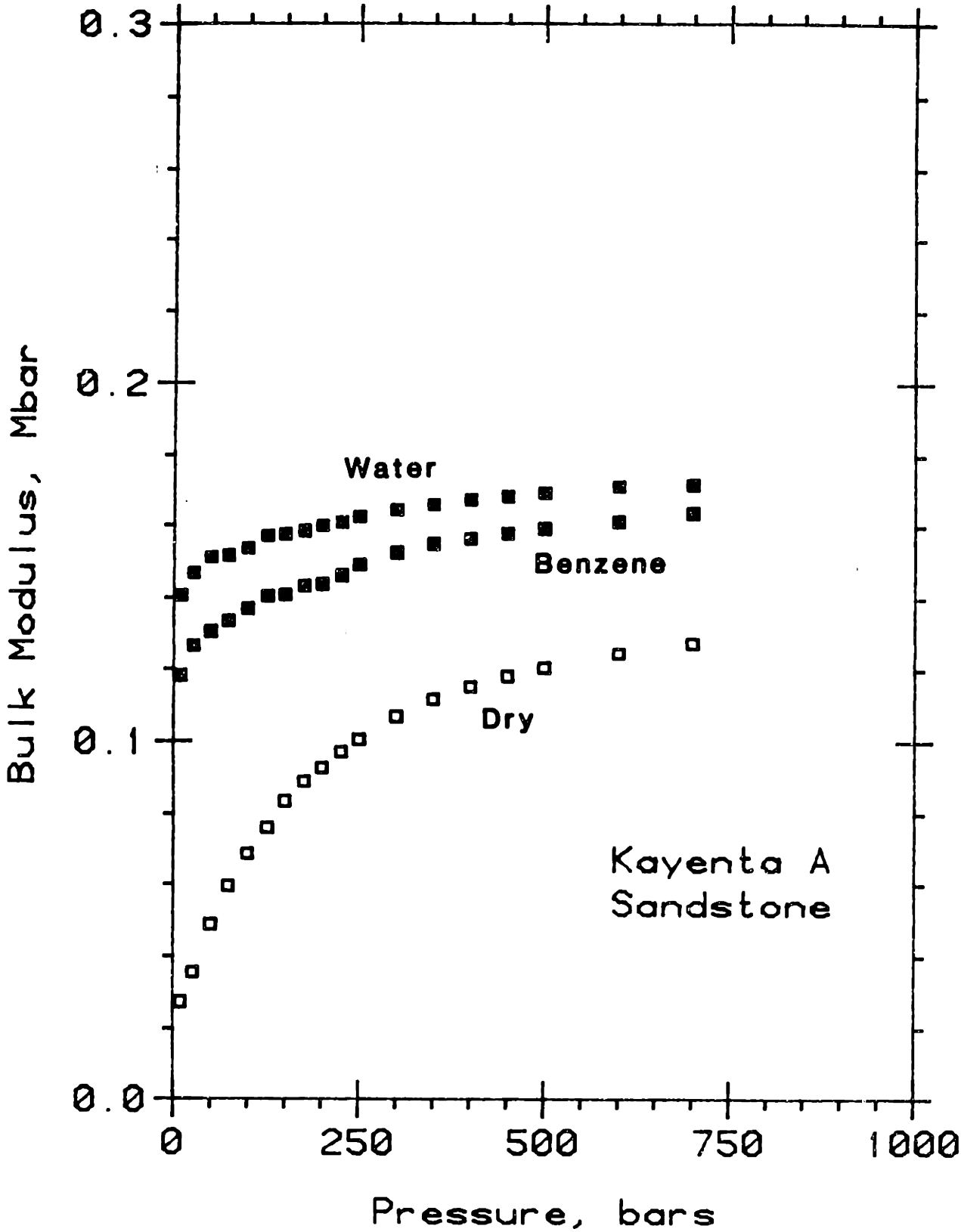


Figure 5-32. Vacuum dry, benzene-, and water-saturated bulk moduli for Kayenta sandstone as a function of differential pressure.

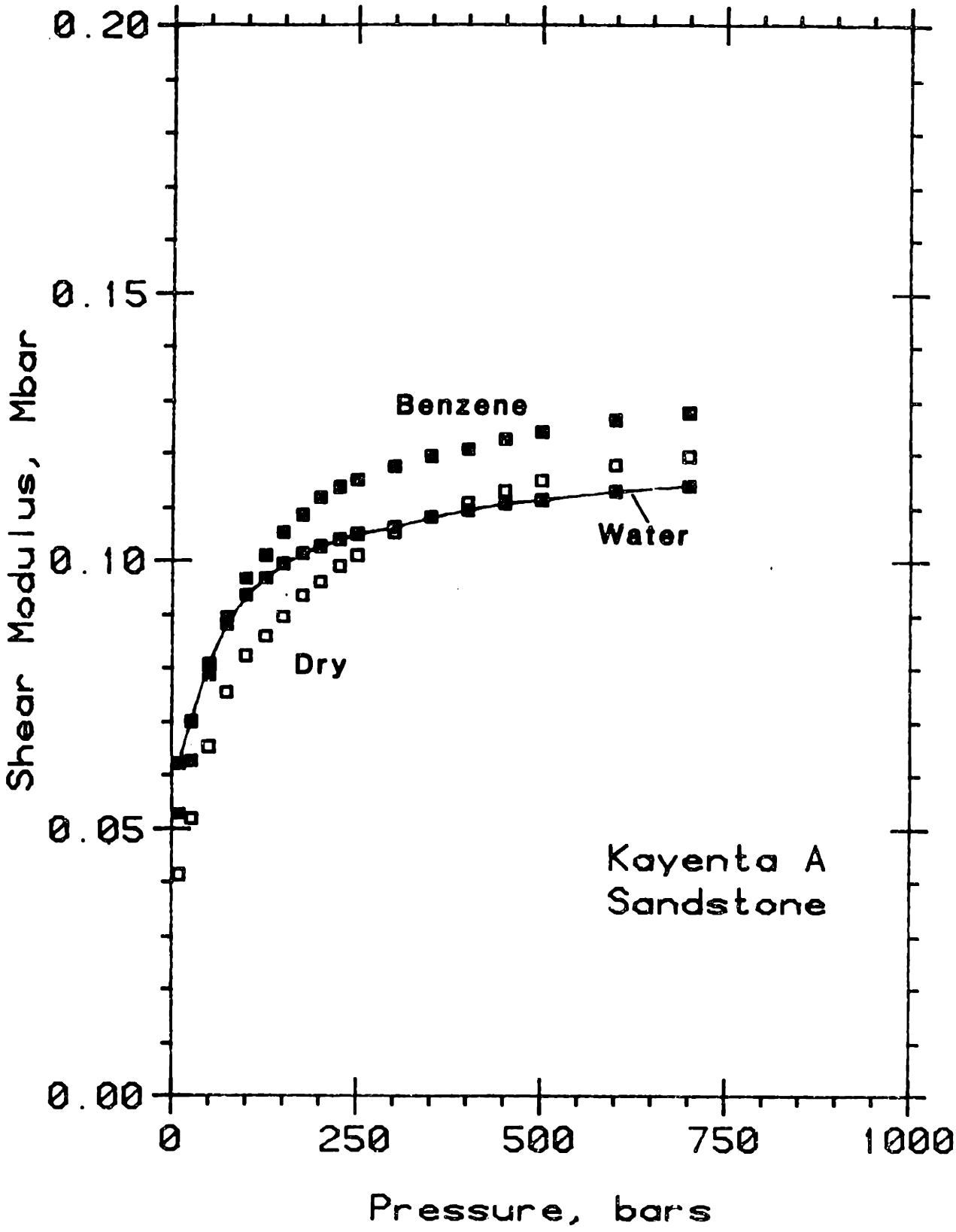


Figure 5-33. Vacuum dry, benzene-, and water-saturated shear moduli for Kayenta sandstone as a function of differential pressure.

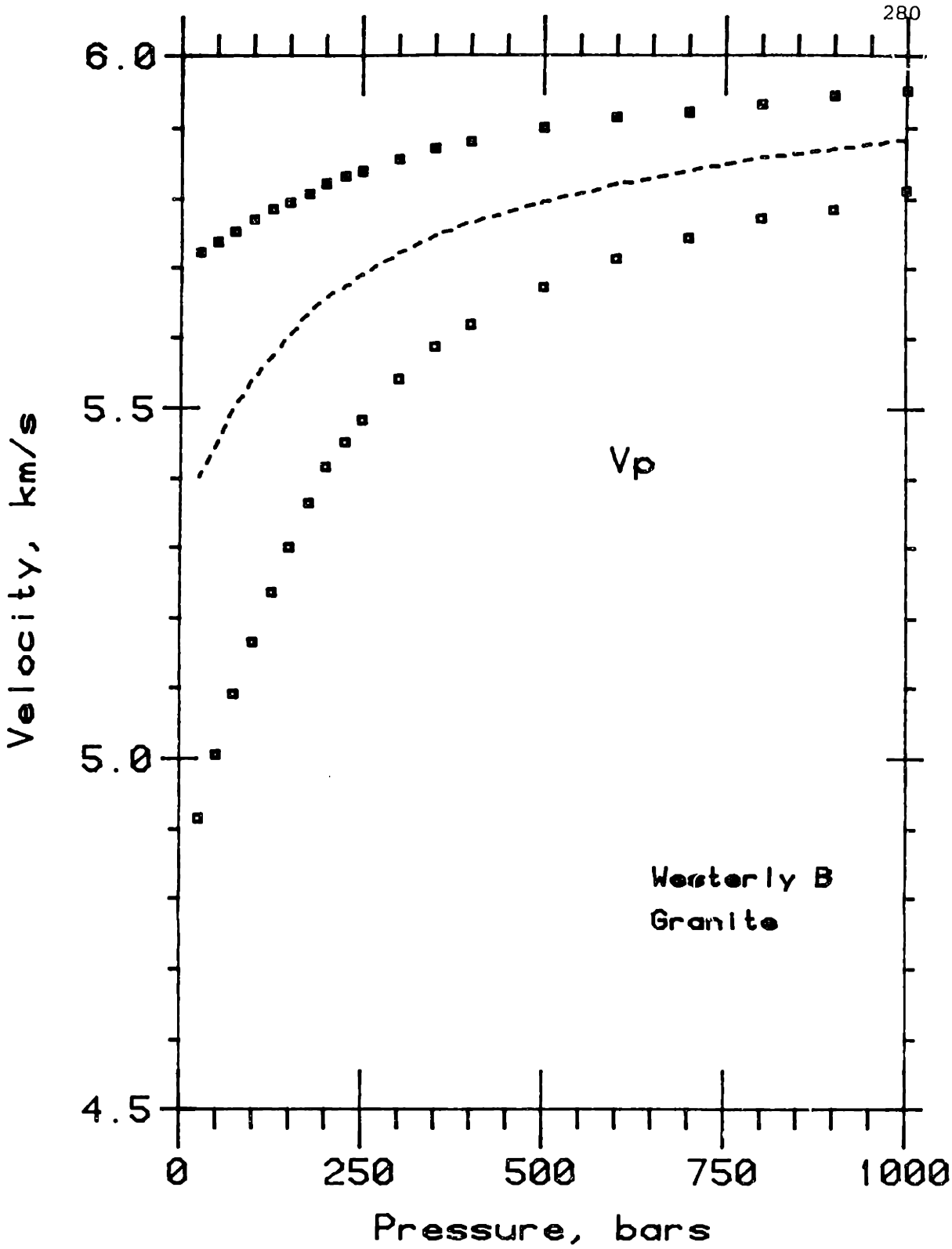


Figure 5-34. P-wave velocities for Westerly granite versus differential pressure for dry (open squares; 20 $\mu$m Hg vacuum) and benzene (solid squares; 100 bars pore pressure) saturations. Dashed line represents saturated P-wave velocities predicted from dry velocities (dry bulk and shear moduli) using Gassmann's equation for effective bulk modulus and the saturated bulk density.

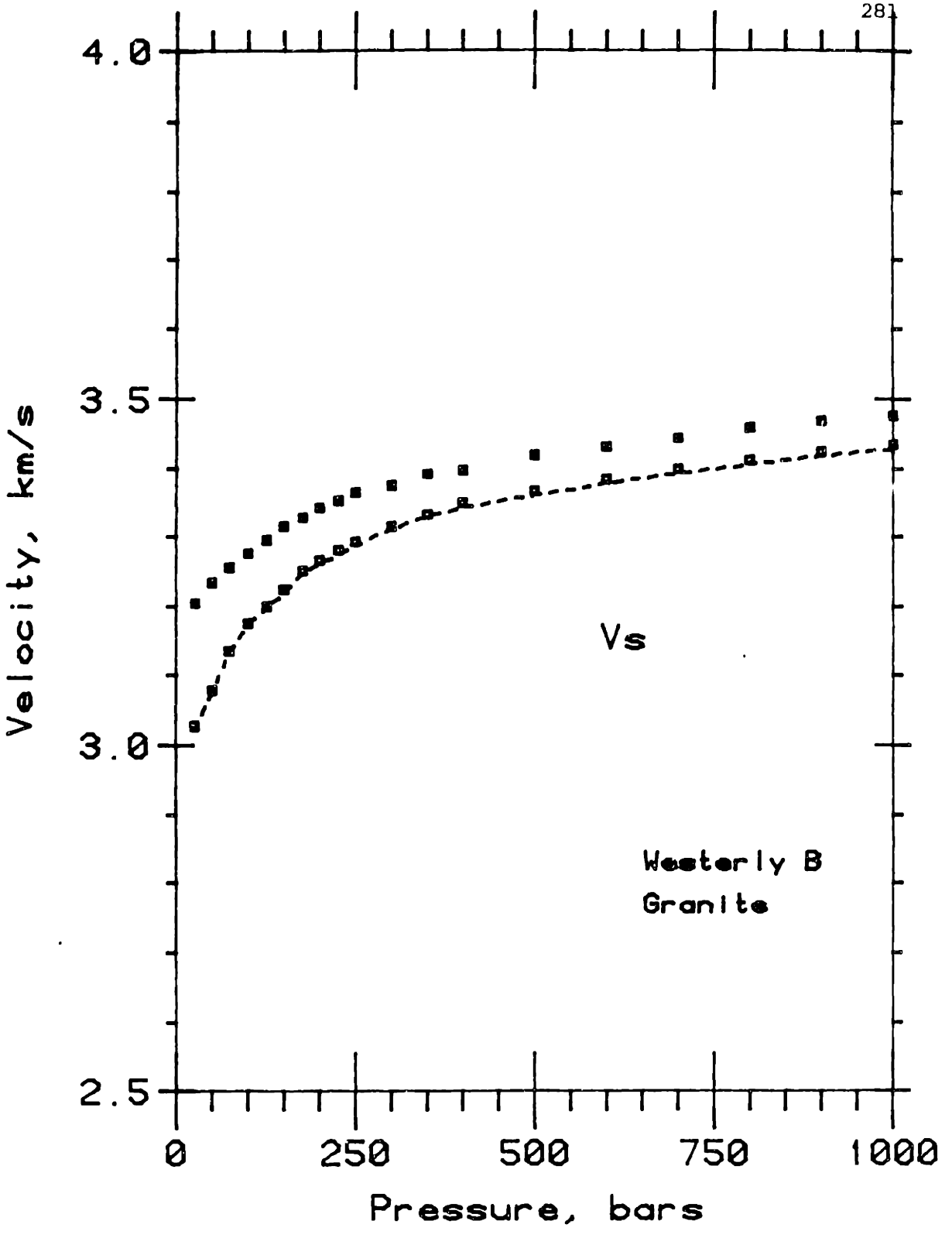


Figure 5-35. S-wave velocities for Westerly granite versus differential pressure for dry (open squares; 20 $\mu$m Hg vacuum) and benzene (solid squares; 100 bars pore pressure) saturations. Dashed line represents saturated S-wave velocities predicted from dry velocities (dry shear moduli) using the saturated bulk density.

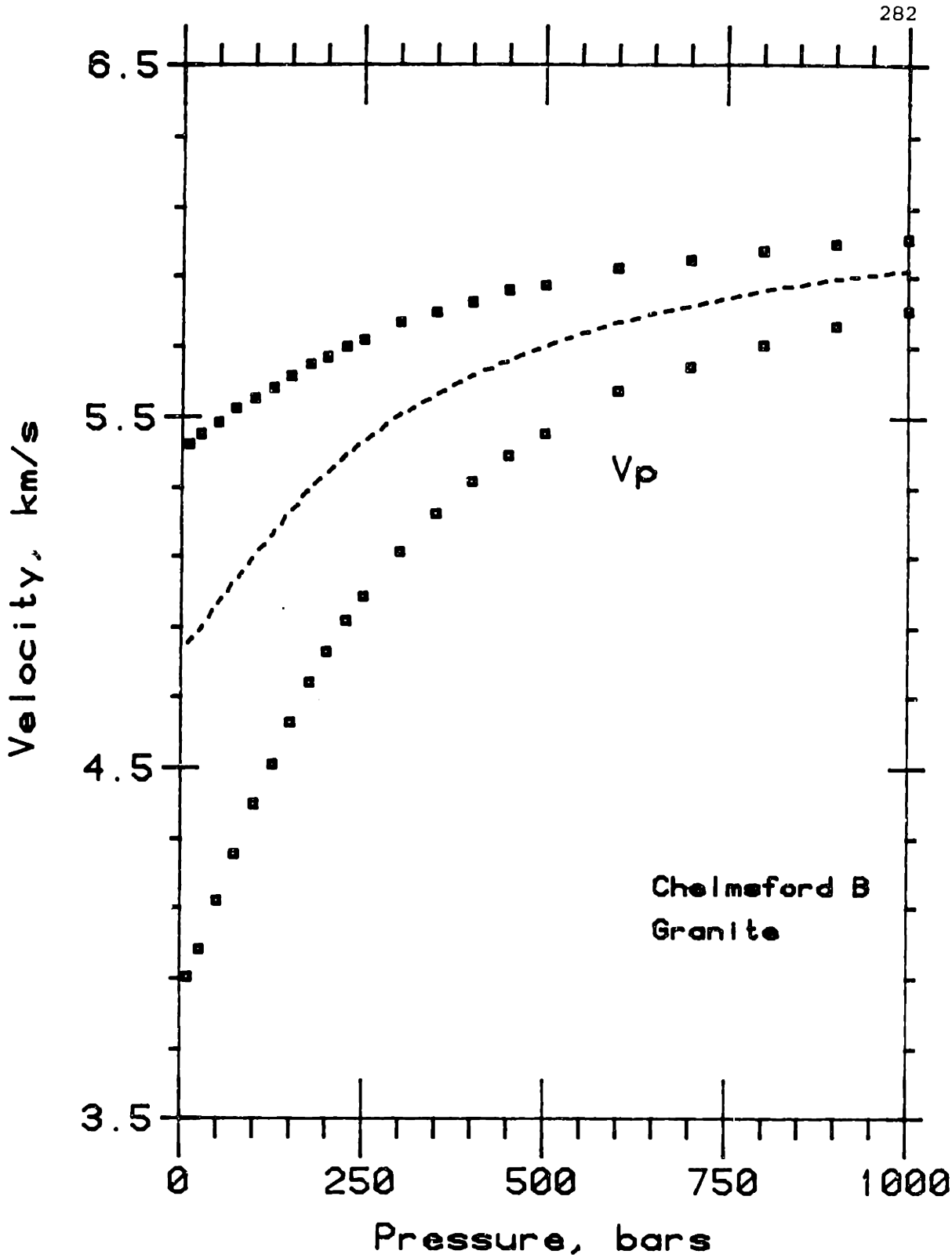


Figure 5-36. P-wave velocities for Chelmsford granite versus differential pressure for dry (open squares; 20 $\mu$m Hg vacuum) and benzene (solid squares; 100 bars pore pressure) saturations. Dashed line represents saturated P-wave velocities predicted from dry velocities (dry bulk and shear moduli) using Gassmann's equation for effective bulk modulus and the saturated bulk density.

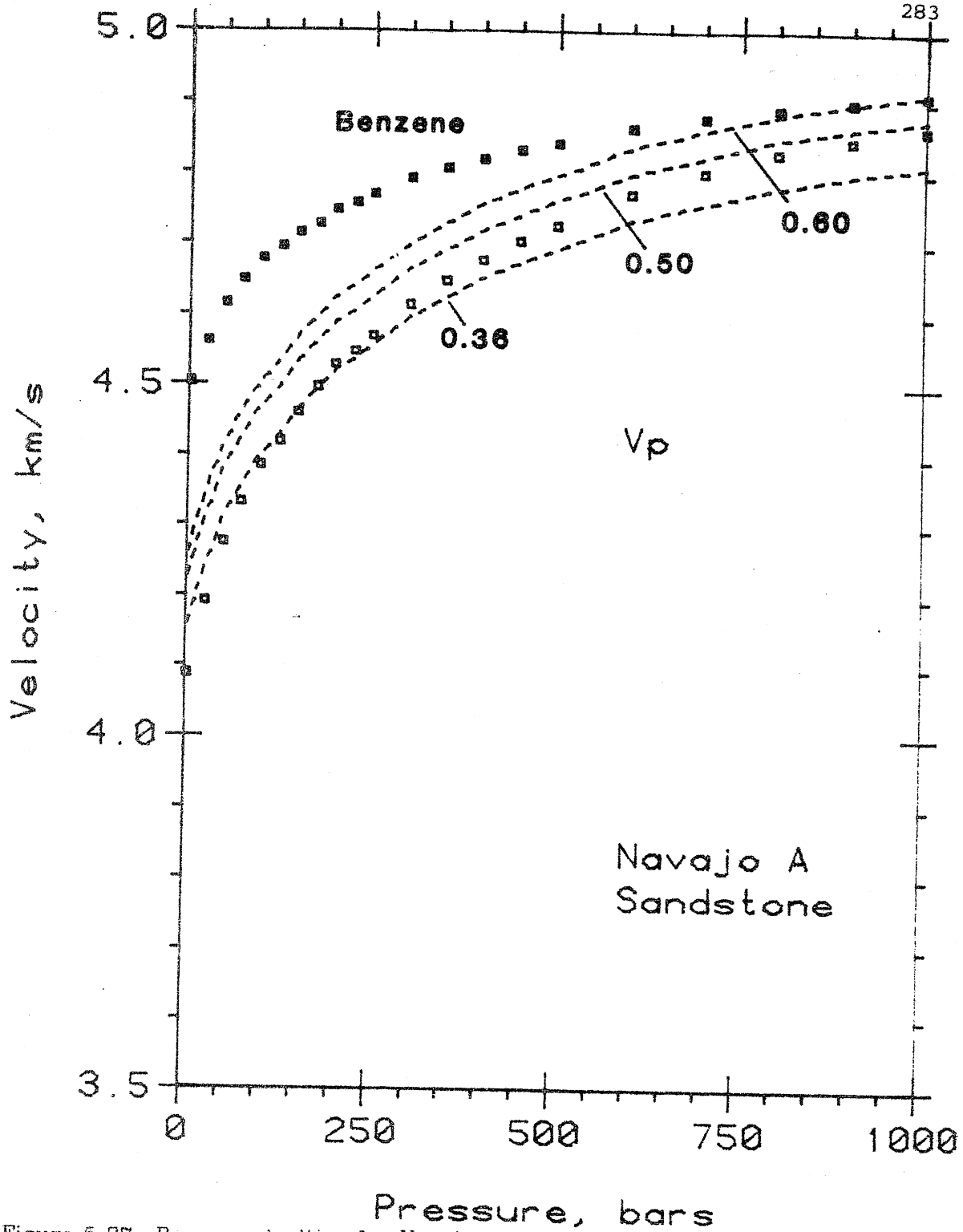


Figure 5-37. P-wave velocities for Navajo sandstone versus differential pressure for dry (open squares; 20 $\mu$m Hg vacuum) and benzene (solid squares; 100 bars pore pressure) saturations. Dashed lines represent saturated P-wave velocities predicted from dry velocities (dry bulk and shear moduli) using Gassmann's equation for effective bulk modulus and the saturated bulk density. Different dashed lines correspond to different intrinsic bulk moduli, $K_s$, in units of Mb, as indicated; $K_s$=0.36 Mb was measured in an unjacketed stress-strain test.

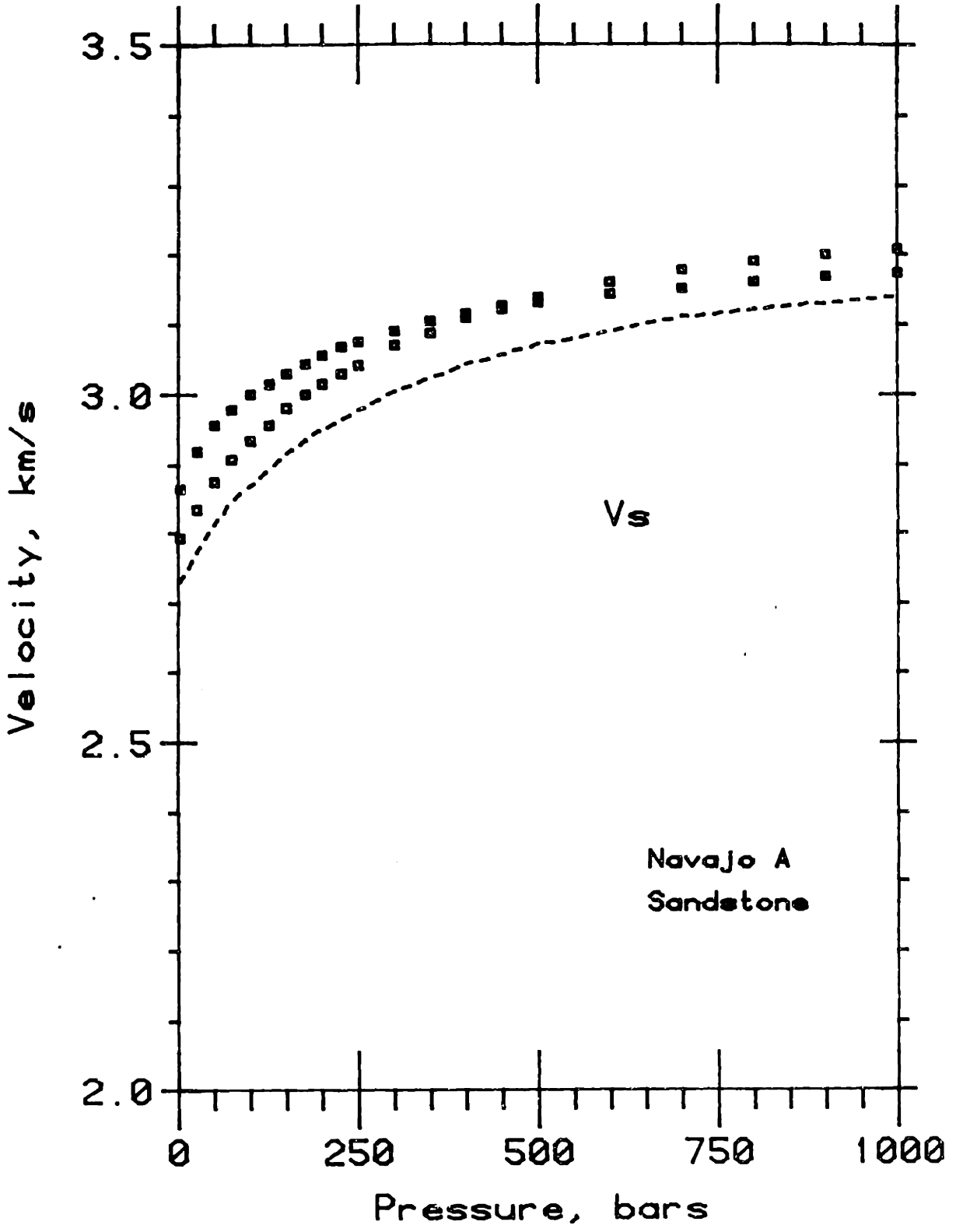


Figure 5-38. S-wave velocities for Navajo sandstone versus differential pressure for dry (open squares; 20 $\mu$m Hg vacuum) and benzene (solid squares; 100 bars pore pressure) saturations. Dashed line represents saturated S-wave velocities predicted from dry velocities (dry shear moduli) using the saturated bulk density.

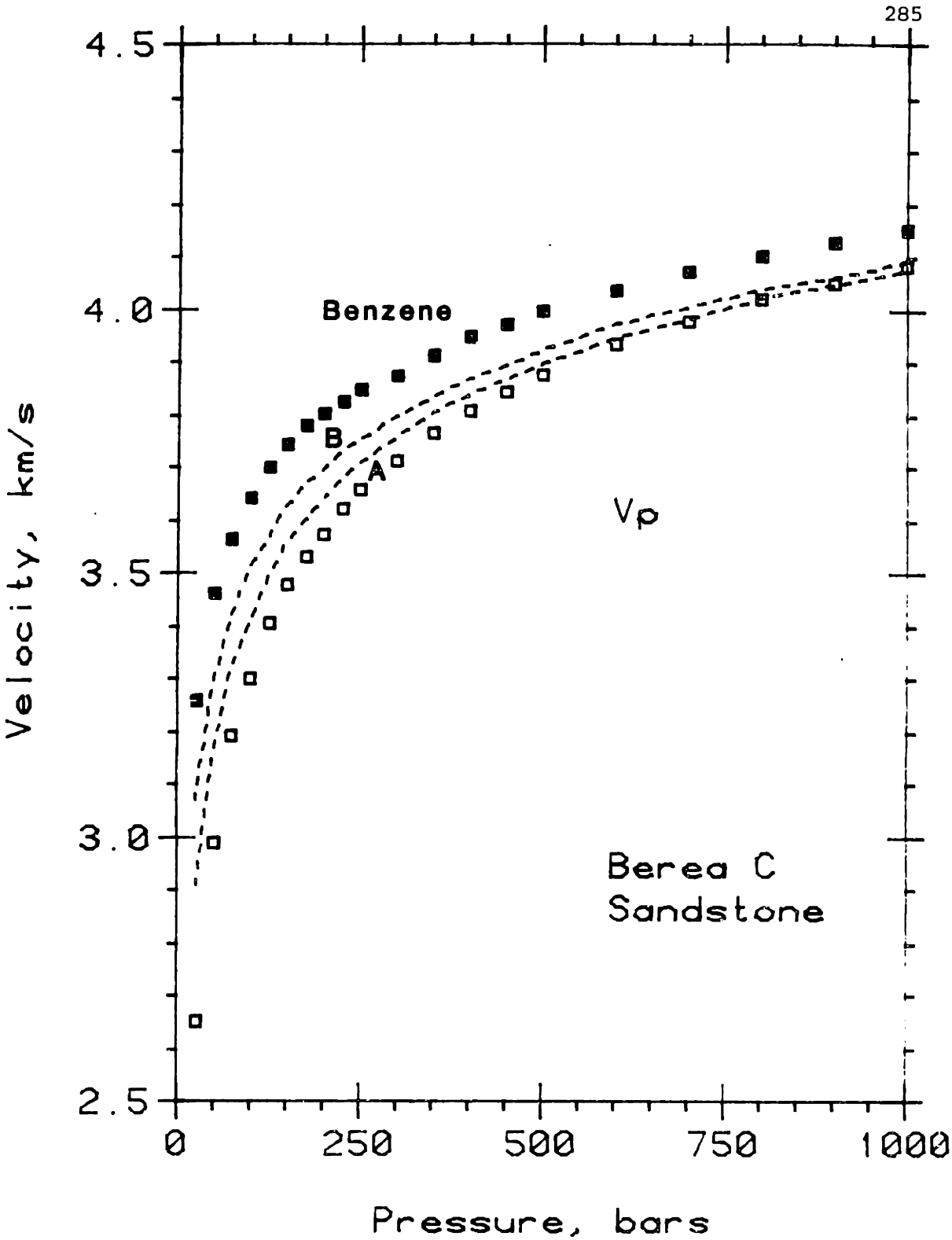


Figure 5-39. P-wave velocities for Berea sandstone versus differential pressure for dry (open squares; 20 $\mu$m Hg vacuum) and benzene (solid squares; 100 bars pore pressure) saturations. Dashed lines represent saturated P-wave velocities predicted from: A) dry velocities (dry bulk and shear moduli), and B) dry and saturated velocities (dry bulk moduli and benzene saturated shear moduli) using Gassmann's equation for effective bulk modulus and the saturated bulk density.

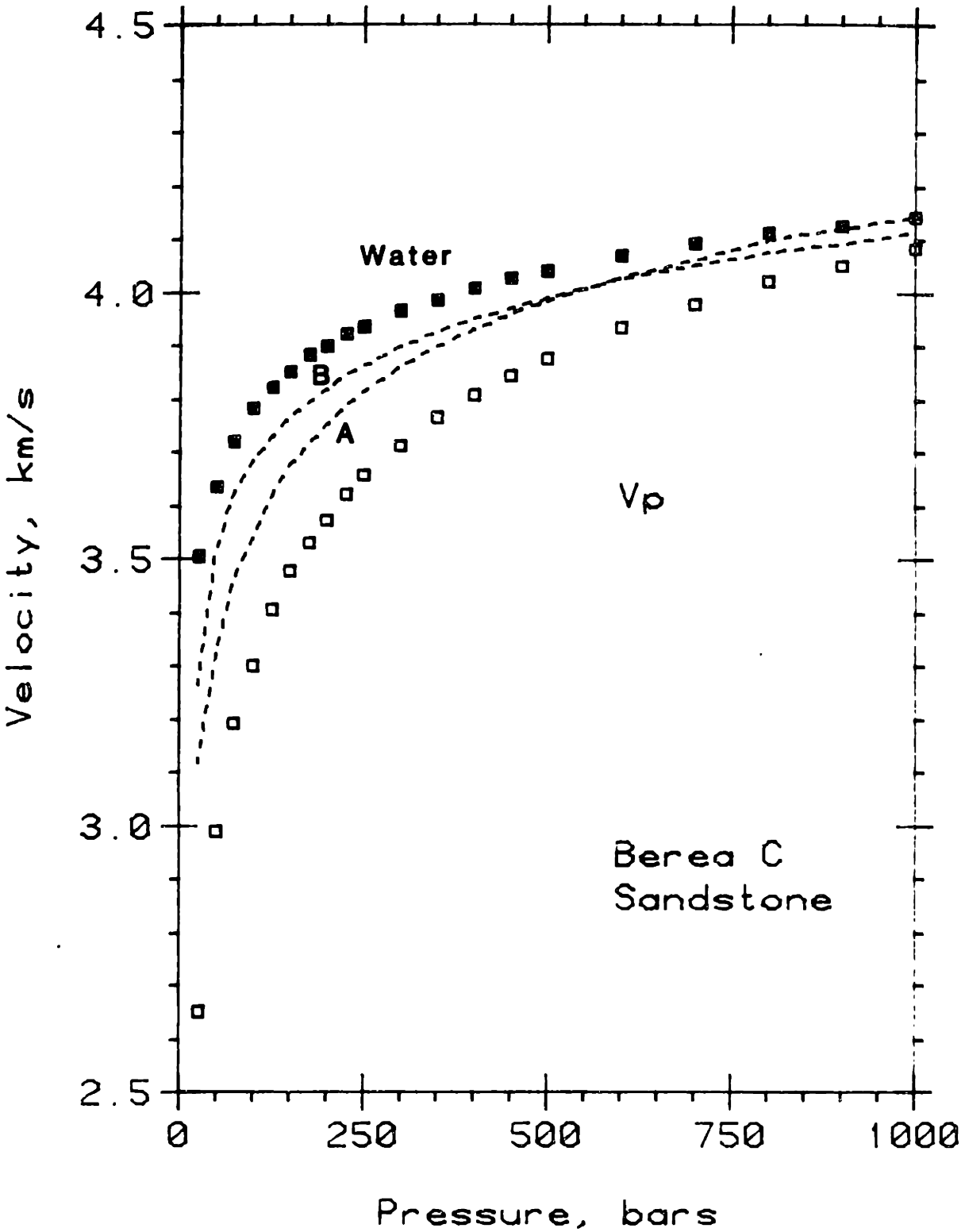


Figure 5-40. P-wave velocities for Berea sandstone versus differential pressure for dry (open squares; 20 $\mu$m Hg vacuum) and water (solid squares; 100 bars pore pressure) saturations. Dashed lines represent saturated P-wave velocities predicted from: A) dry velocities (dry bulk and shear moduli), and B) dry and saturated velocities (dry bulk moduli and water saturated shear moduli) using Gassmann's equation for effective bulk modulus and the saturated bulk density.

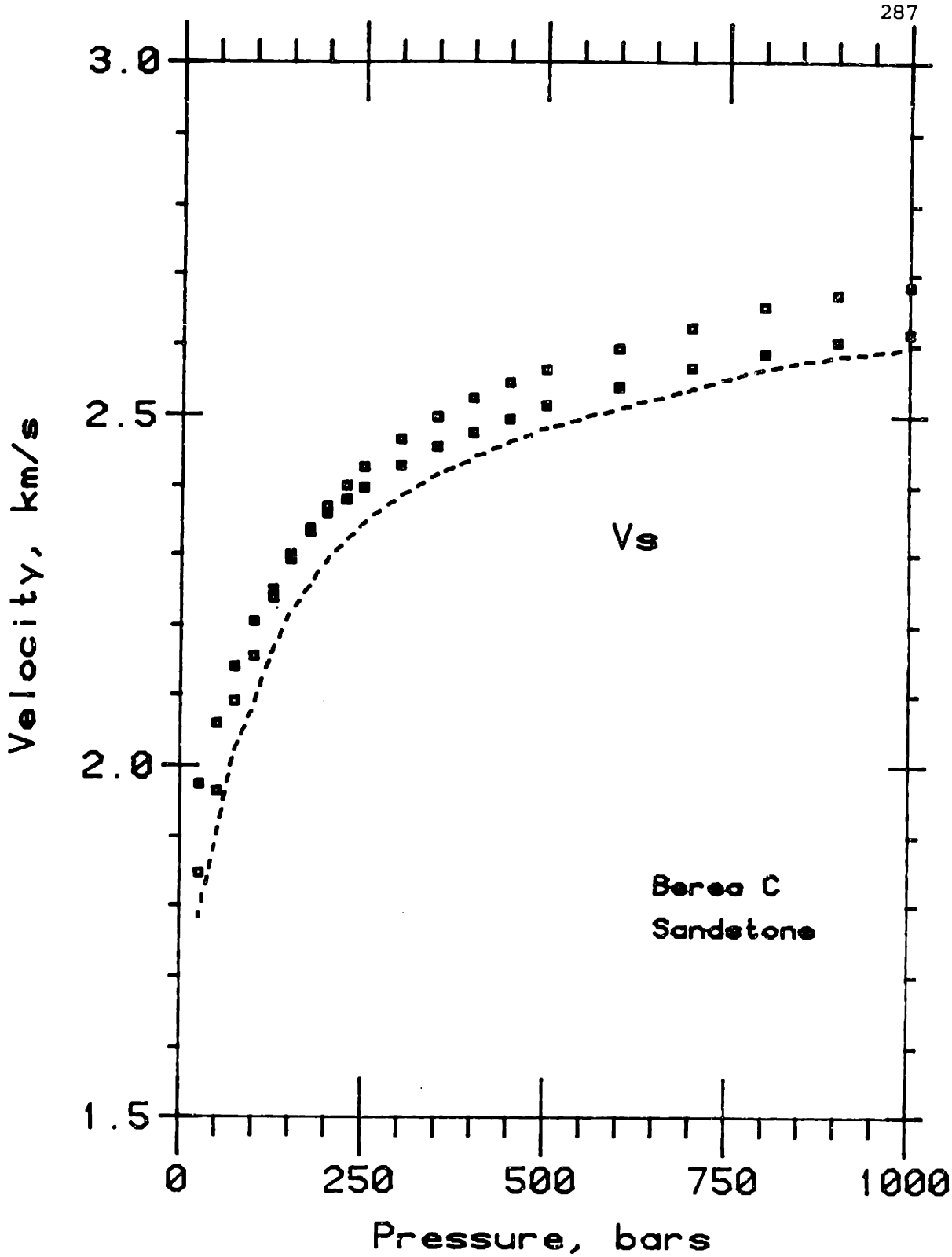


Figure 5-41. S-wave velocities for Berea sandstone versus differential pressure for dry (open squares; 20 $\mu$m Hg vacuum) and benzene (solid squares; 100 bars pore pressure) saturations. Dashed line represents saturated S-wave velocities predicted from dry velocities (dry shear moduli) using the saturated bulk density.

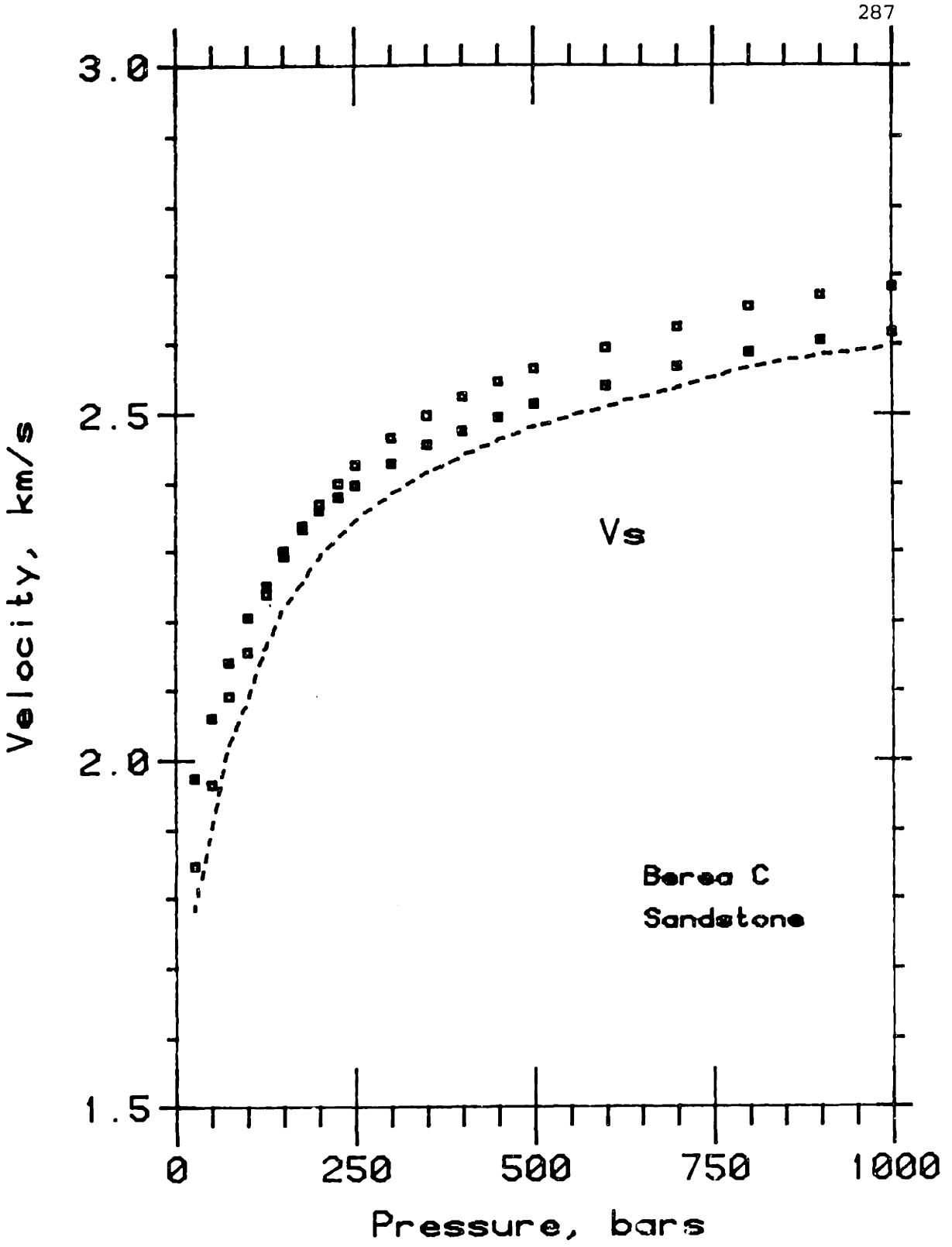


Figure 5-41. S-wave velocities for Berea sandstone versus differential pressure for dry (open squares; 20 $\mu$m Hg vacuum) and benzene (solid squares; 100 bars pore pressure) saturations. Dashed line represents saturated S-wave velocities predicted from dry velocities (dry shear moduli) using the saturated bulk density.

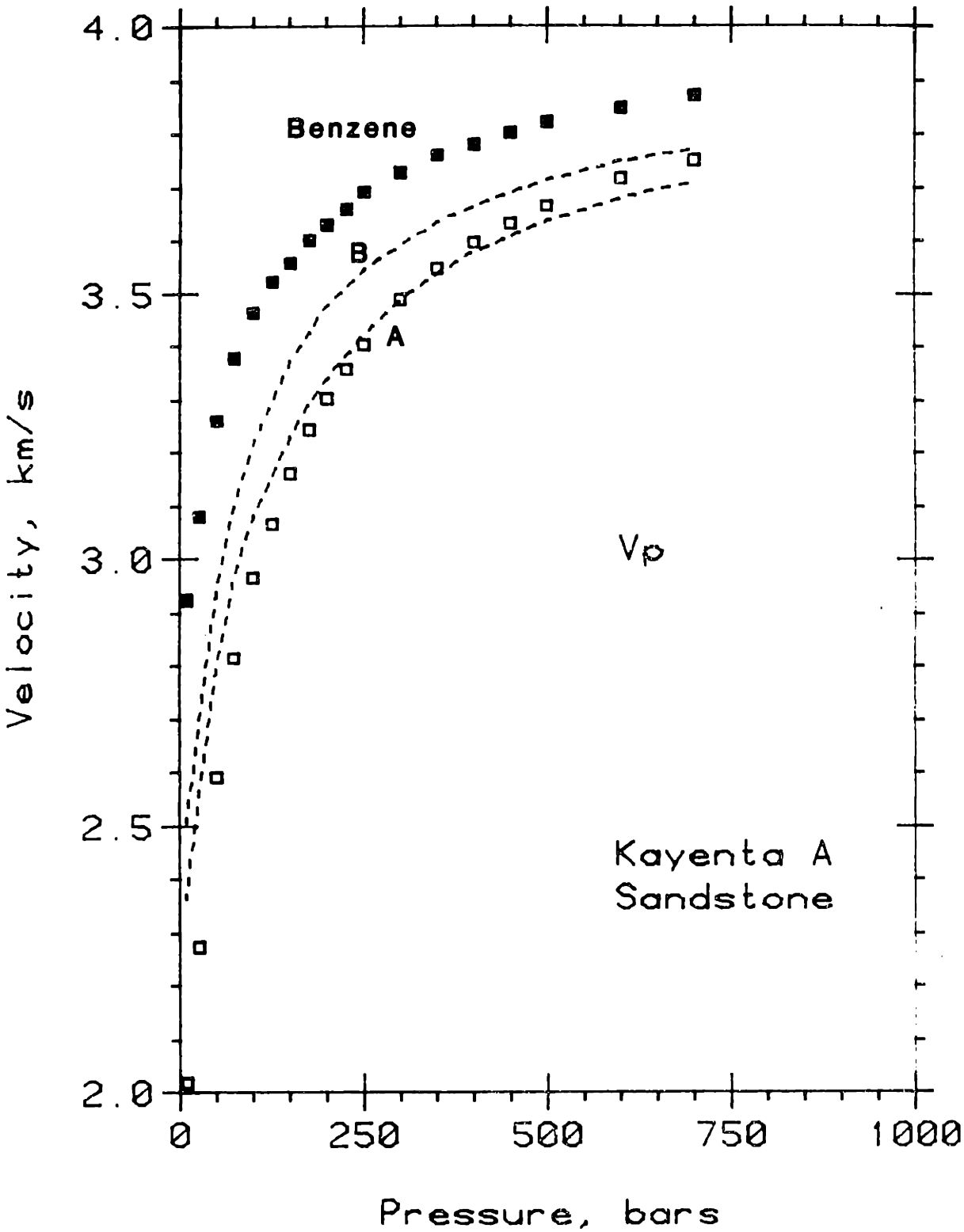


Figure 5-42. P-wave velocities for Kayenta sandstone versus differential pressure for dry (open squares; 20 $\mu$m Hg vacuum) and benzene (solid squares; 100 bars pore pressure) saturations. Dashed lines represent saturated P-wave velocities predicted from: A) dry velocities (dry bulk and shear moduli), and B) dry and saturated velocities (dry bulk moduli and saturated shear moduli) using Gassmann's equation for effective bulk modulus and the saturated bulk density.

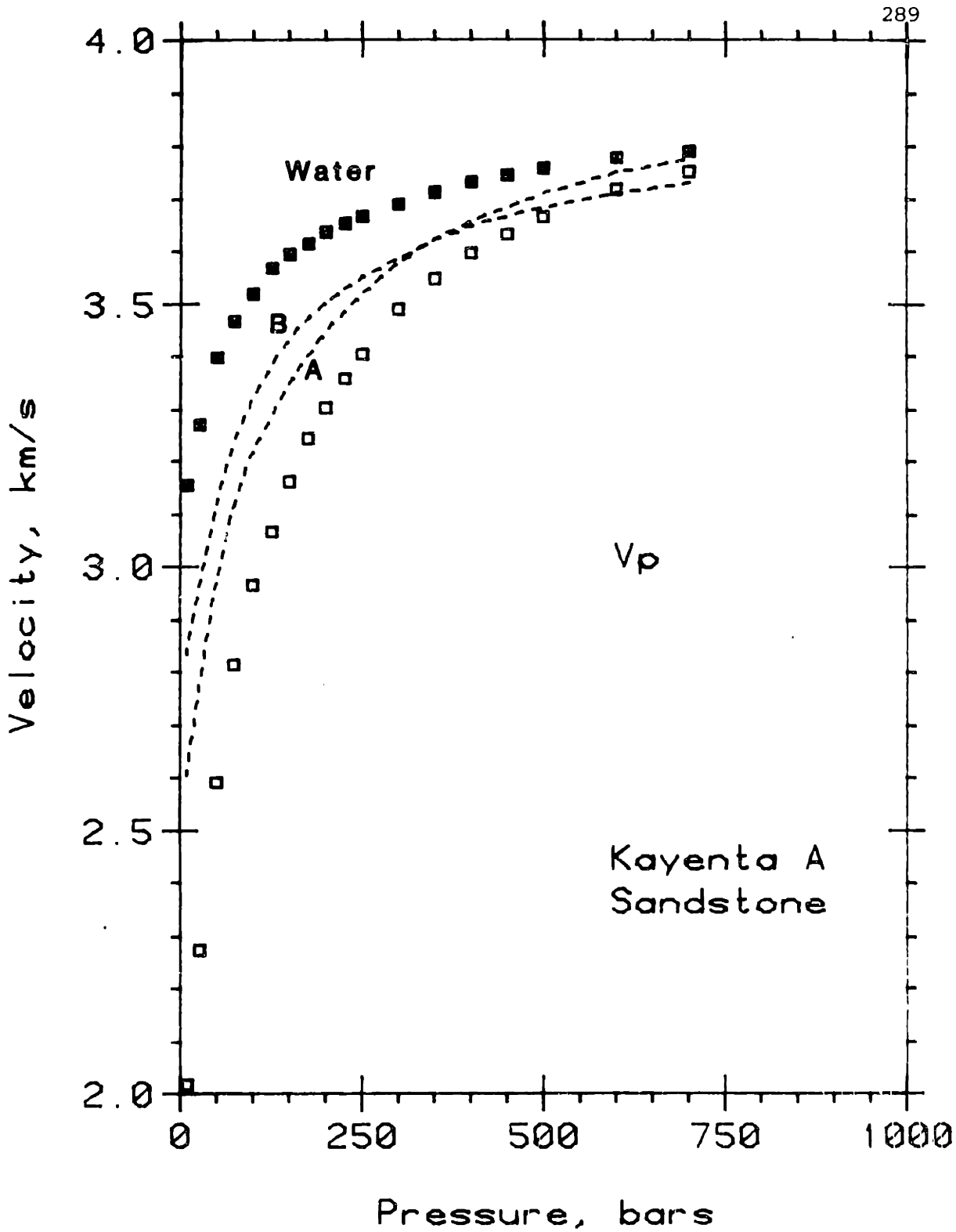


Figure 5-43. P-wave velocities for Kayenta sandstone versus differential pressure for dry (open squares; 20 $\mu$m Hg vacuum) and water (solid squares; 100 bars pore pressure) saturations. Dashed lines represent saturated P-wave velocities predicted from: A) dry velocities (dry bulk and shear moduli), and B) dry and saturated velocities (dry bulk moduli and saturated shear moduli) using Gassmann's equation for effective bulk modulus and the saturated bulk density.

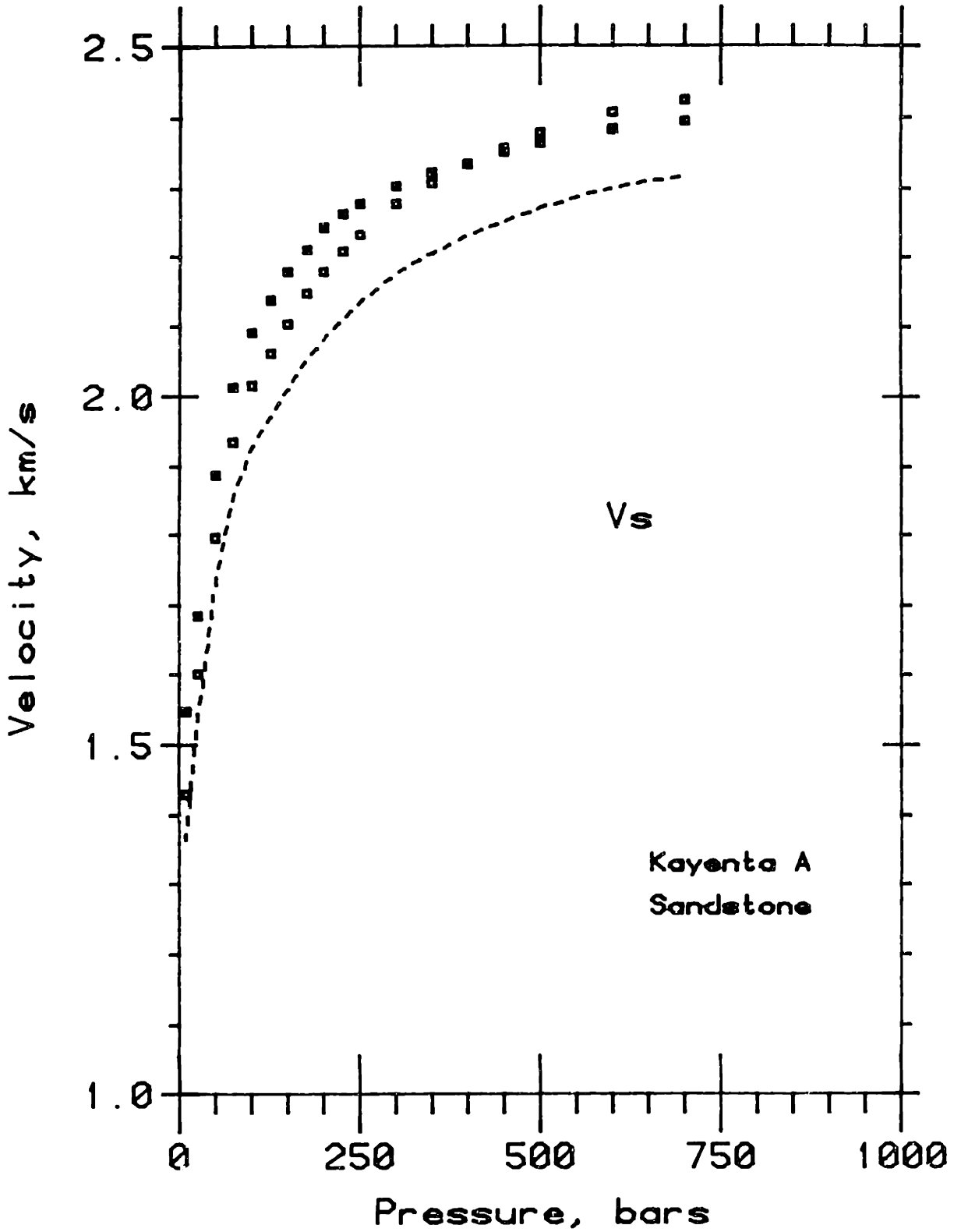


Figure 5-44. S-wave velocities for Kayenta sandstone versus differential pressure for dry (open squares; 20 $\mu$m Hg vacuum) and benzene (solid squares; 100 bars pore pressure) saturations. Dashed line represents saturated velocities predicted from dry velocities using the saturated bulk density.

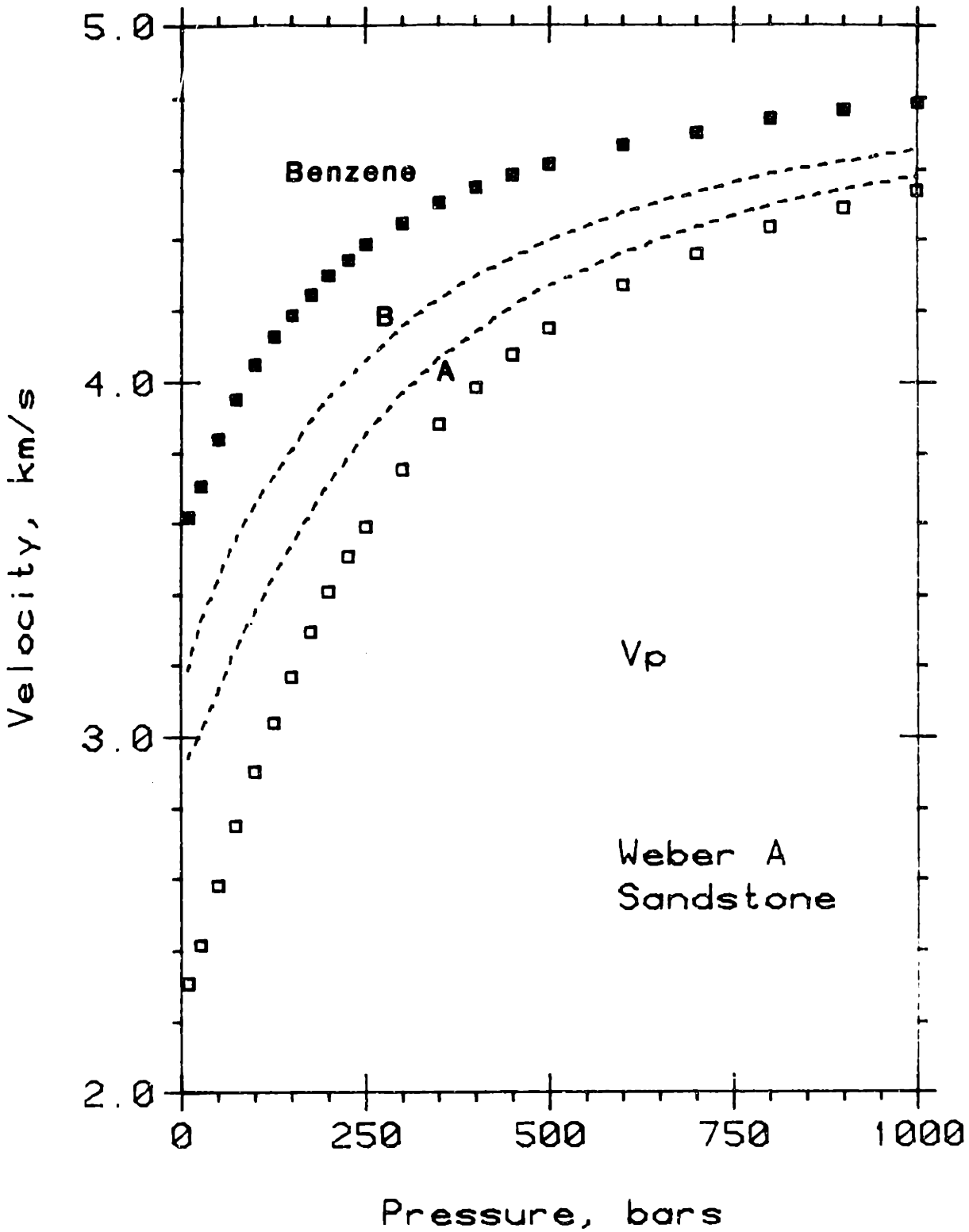


Figure 5-45. P-wave velocities for Weber sandstone versus differential pressure for dry (open squares; 20 $\mu$m Hg vacuum) and benzene (solid squares; 100 bars pore pressure) saturations. Dashed lines represent saturated P-wave velocities predicted from: A) dry velocities (dry bulk and shear moduli), and B) dry and saturated velocities (dry bulk moduli and saturated shear moduli) using Gassmann's equation for effective bulk modulus and the saturated bulk density.

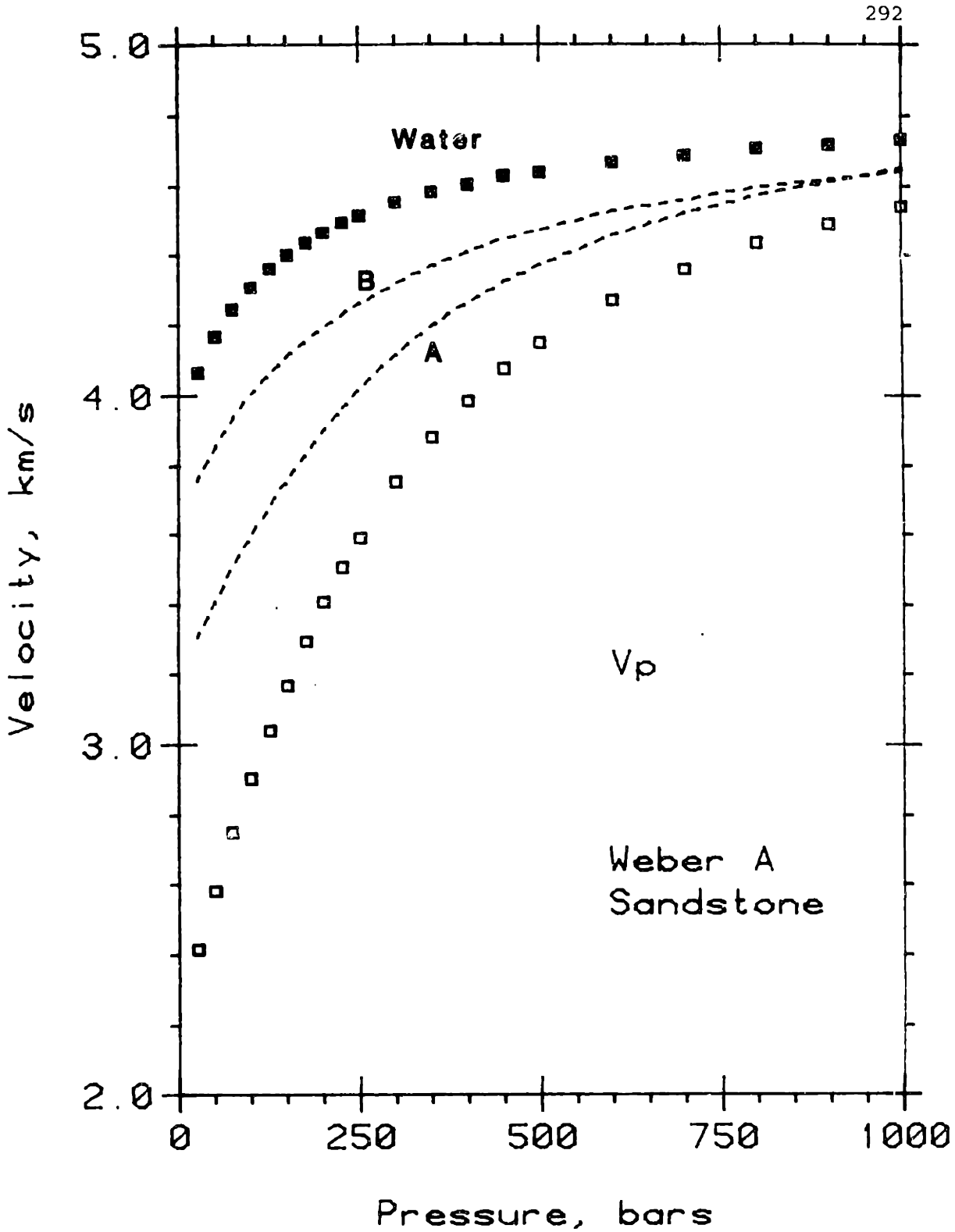


Figure 5-46. P-wave velocities for Weber sandstone versus differential pressure for dry (open squares; 20 $\mu$m Hg vacuum) and water (solid squares; 100 bars pore pressure) saturations. Dashed lines represent saturated P-wave velocities predicted from: A) dry velocities (dry bulk and shear moduli), and B) dry and saturated velocities (dry bulk moduli and saturated shear moduli) using Gassmann's equation for effective bulk modulus and the saturated bulk density.

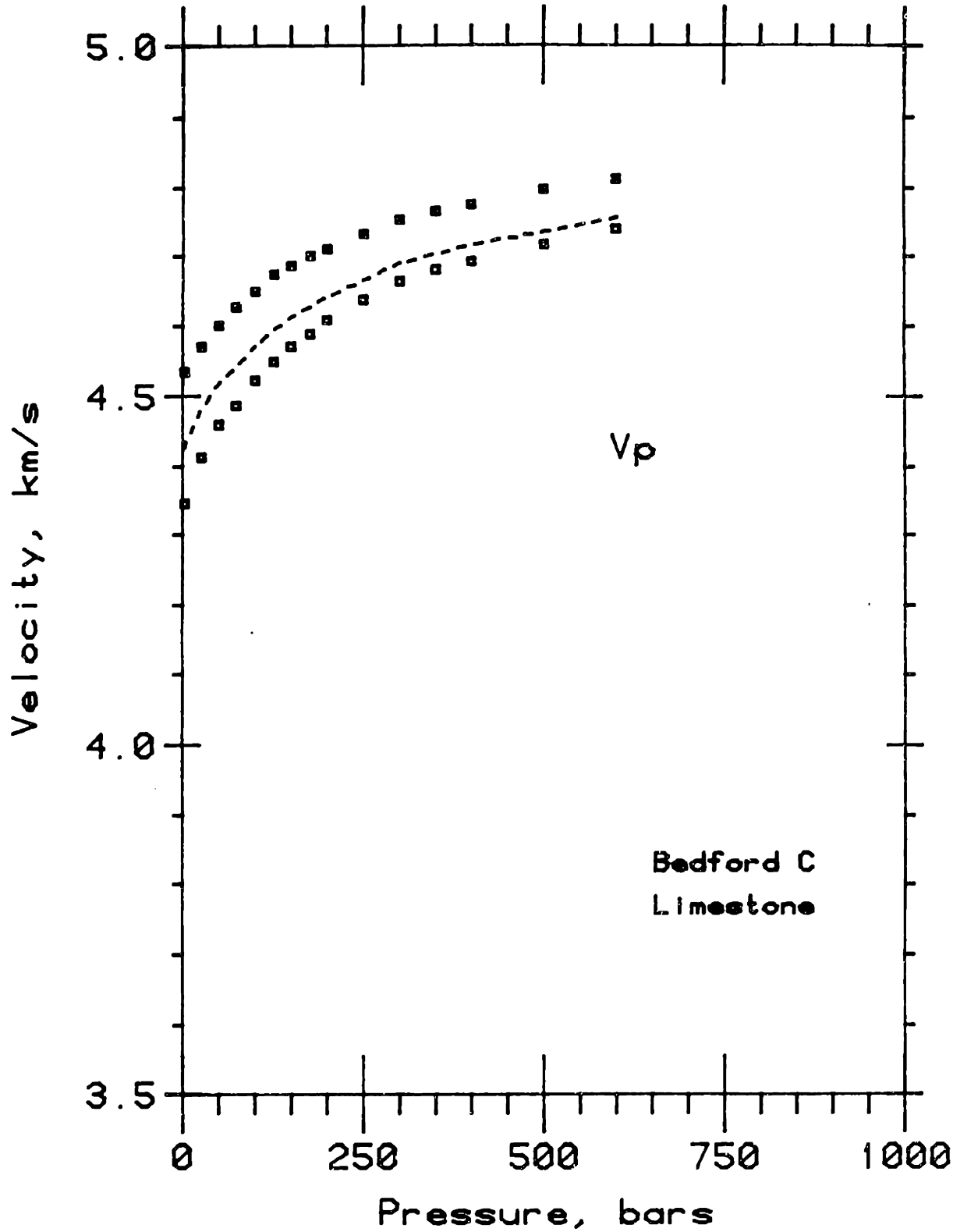


Figure 5-47. P-wave velocities for Bedford limestone versus differential pressure for dry (open squares; 20 $\mu$m Hg vacuum) and benzene (solid squares; 100 bars pore pressure) saturations. Dashed line represents saturated velocities predicted from dry velocities using Gassmann's equation for effective bulk modulus and the saturated bulk density.

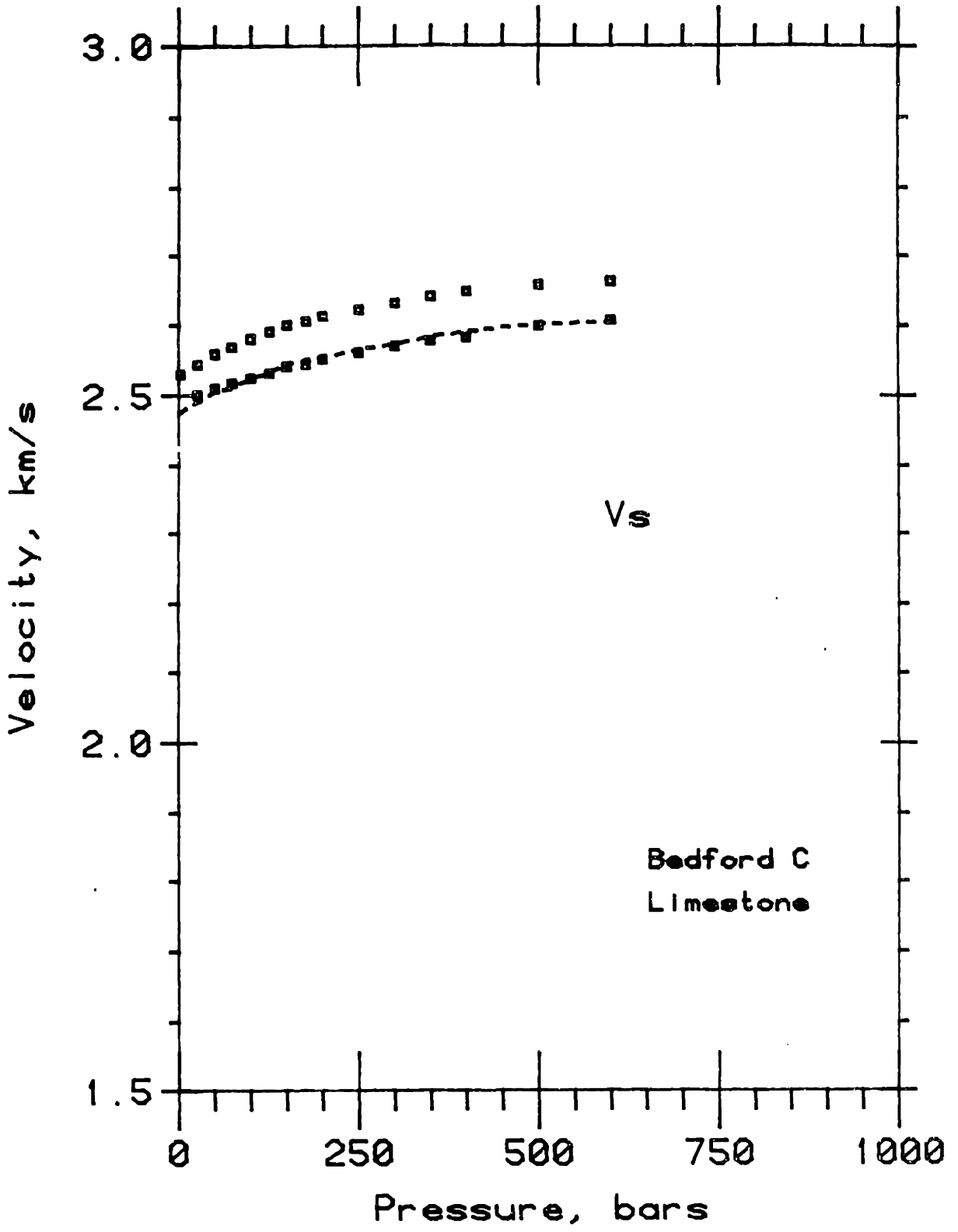


Figure 5-48. S-wave velocities for Bedford limestone versus differential pressure for dry (open squares; 20 $\mu$m Hg vacuum) and benzene (solid squares; 100 bars pore pressure) saturations. Dashed line represents saturated velocities predicted from dry velocities using the saturated bulk density.

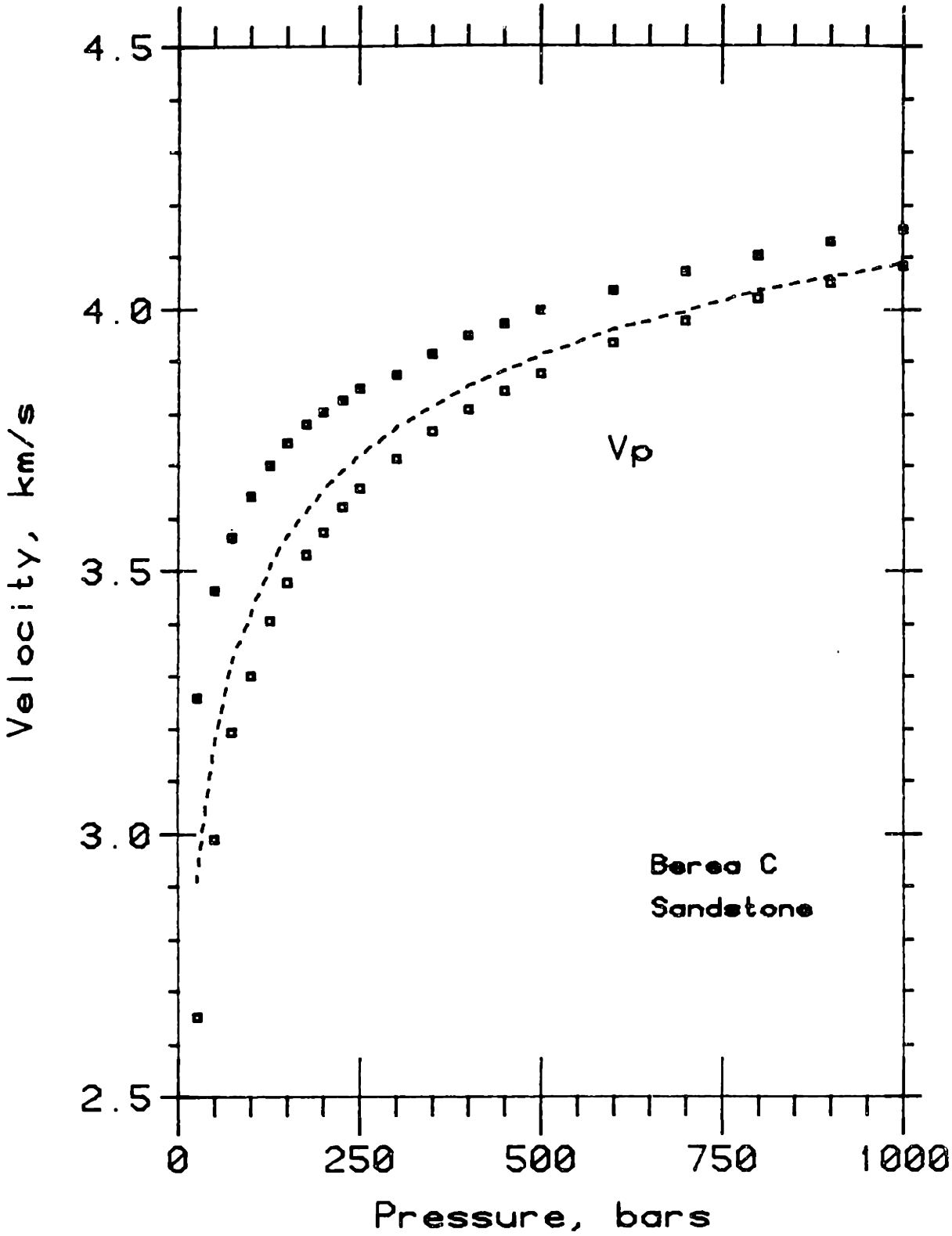


Figure 5-49. P-wave velocities for Berea sandstone versus differential pressure for dry (open squares; 20 $\mu$m Hg vacuum) and benzene (solid squares; 100 bars pore pressure) saturations. Dashed line represents saturated velocities predicted from dry velocities using the Biot inertial formulations with a geometrical factor $\alpha$=4.4.

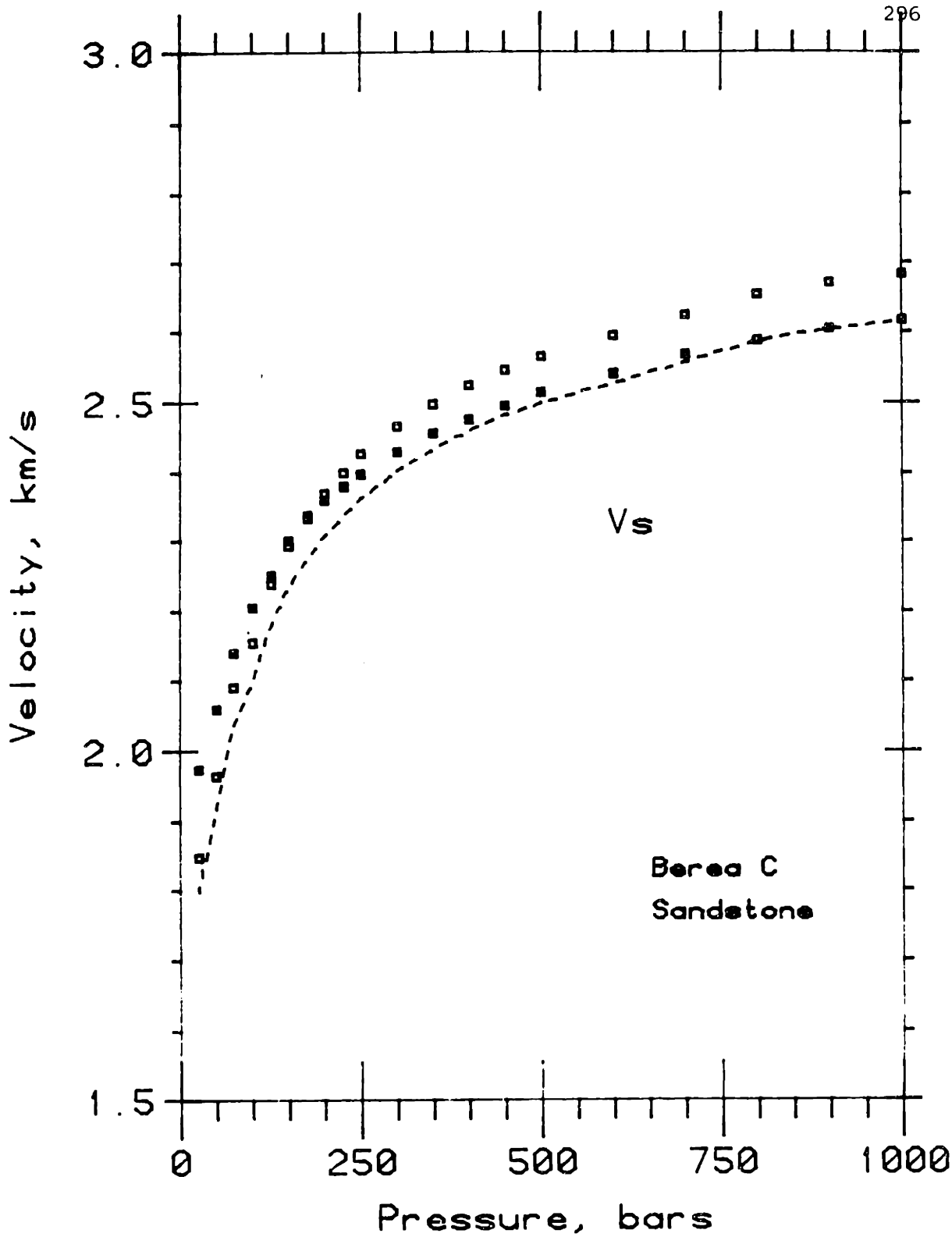


Figure 5-50. S-wave velocities for Berea sandstone versus differential pressure for dry (open squares; 20 $\mu$m Hg vacuum) and benzene (solid squares; 100 bars pore pressure) saturations. Dashed line represents saturated velocities predicted from dry velocities using the Biot inertial formulations with a geometrical factor $\alpha$=4.4.

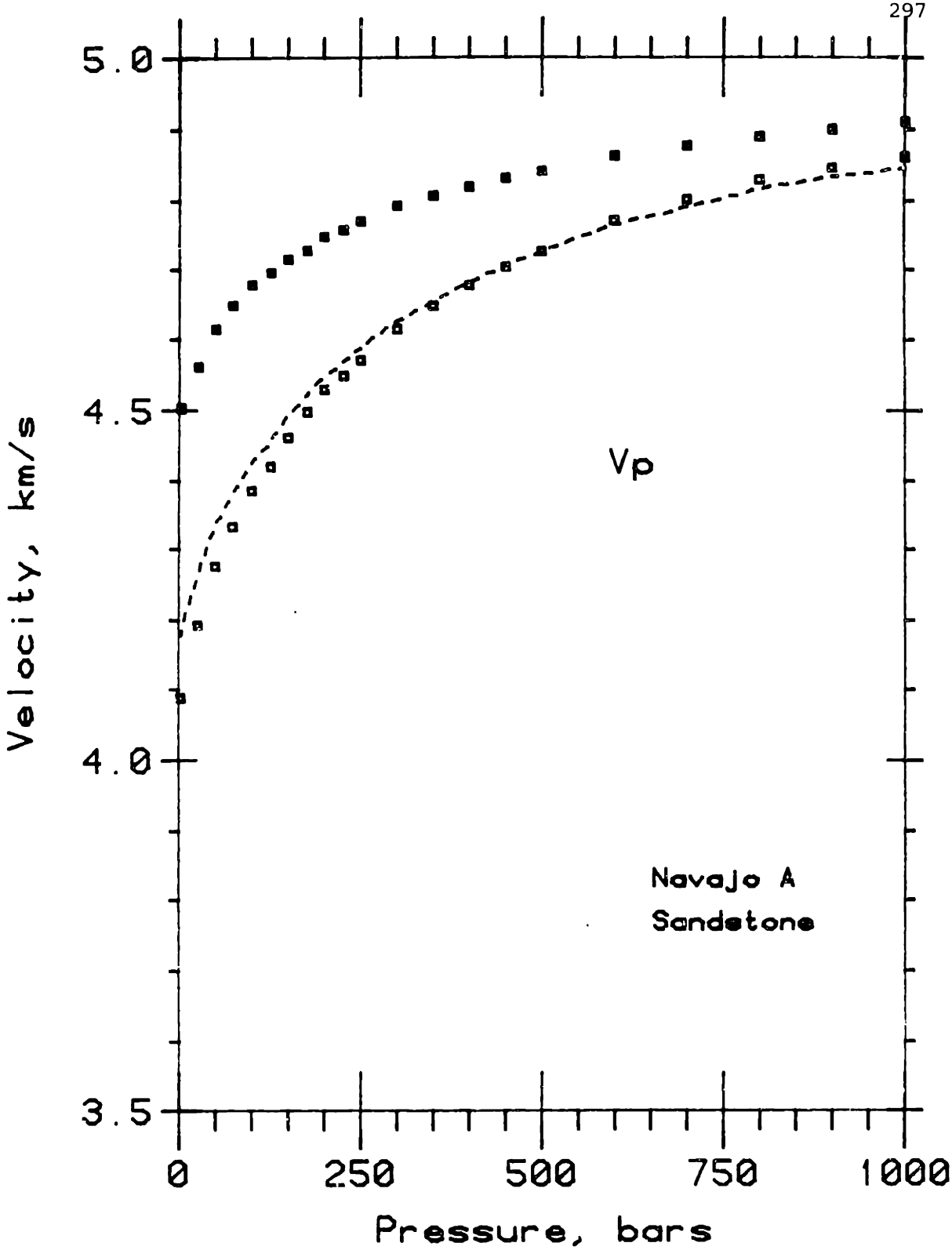


Figure 5-51. P-wave velocities for Navajo sandstone versus differential pressure for dry (open squares; 20 $\mu$m Hg vacuum) and benzene (solid squares; 100 bars pore pressure) saturations. Dashed line represents saturated velocities predicted from dry velocities using the Biot inertial formulations with a geometrical factor $\alpha$=2.1.

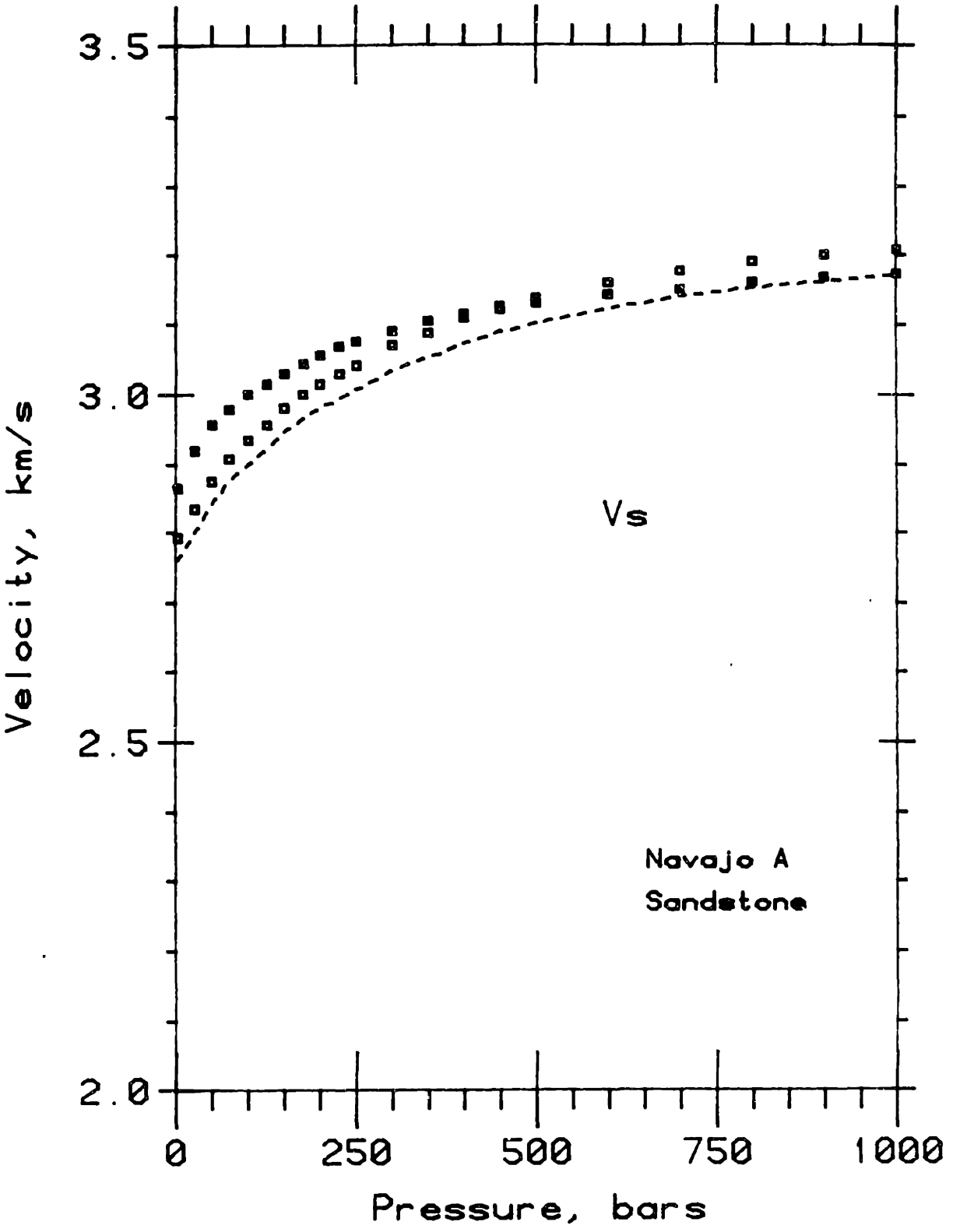


Figure 5-52. S-wave velocities for Navajo sandstone versus differential pressure for dry (open squares; 20 $\mu$m Hg vacuum) and benzene (solid squares; 100 bars pore pressure) saturations. Dashed line represents saturated velocities predicted from dry velocities using the Biot inertial formulations with a geometrical factor $\alpha$=2.1.

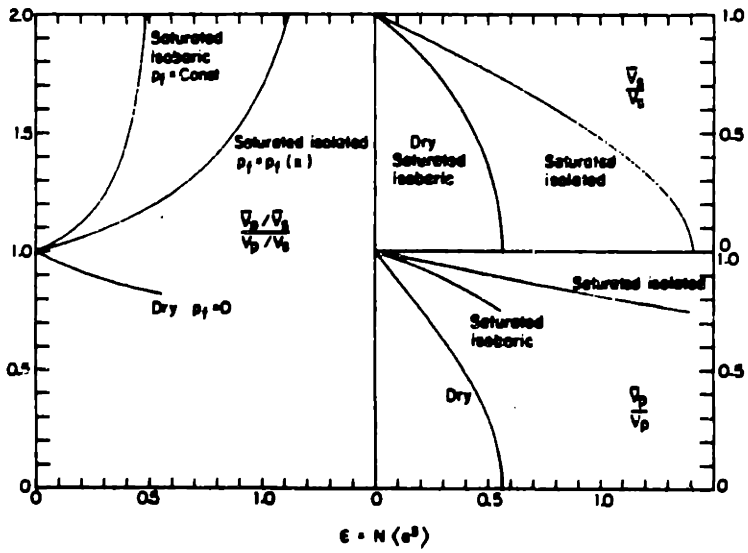


Figure 5-53. Normalized velocity ratios versus crack density parameter for dry and saturated cracks which are in communication (saturated isobaric) and which are not connected (saturated isolated). After O'Connell and Budiansky (1977).

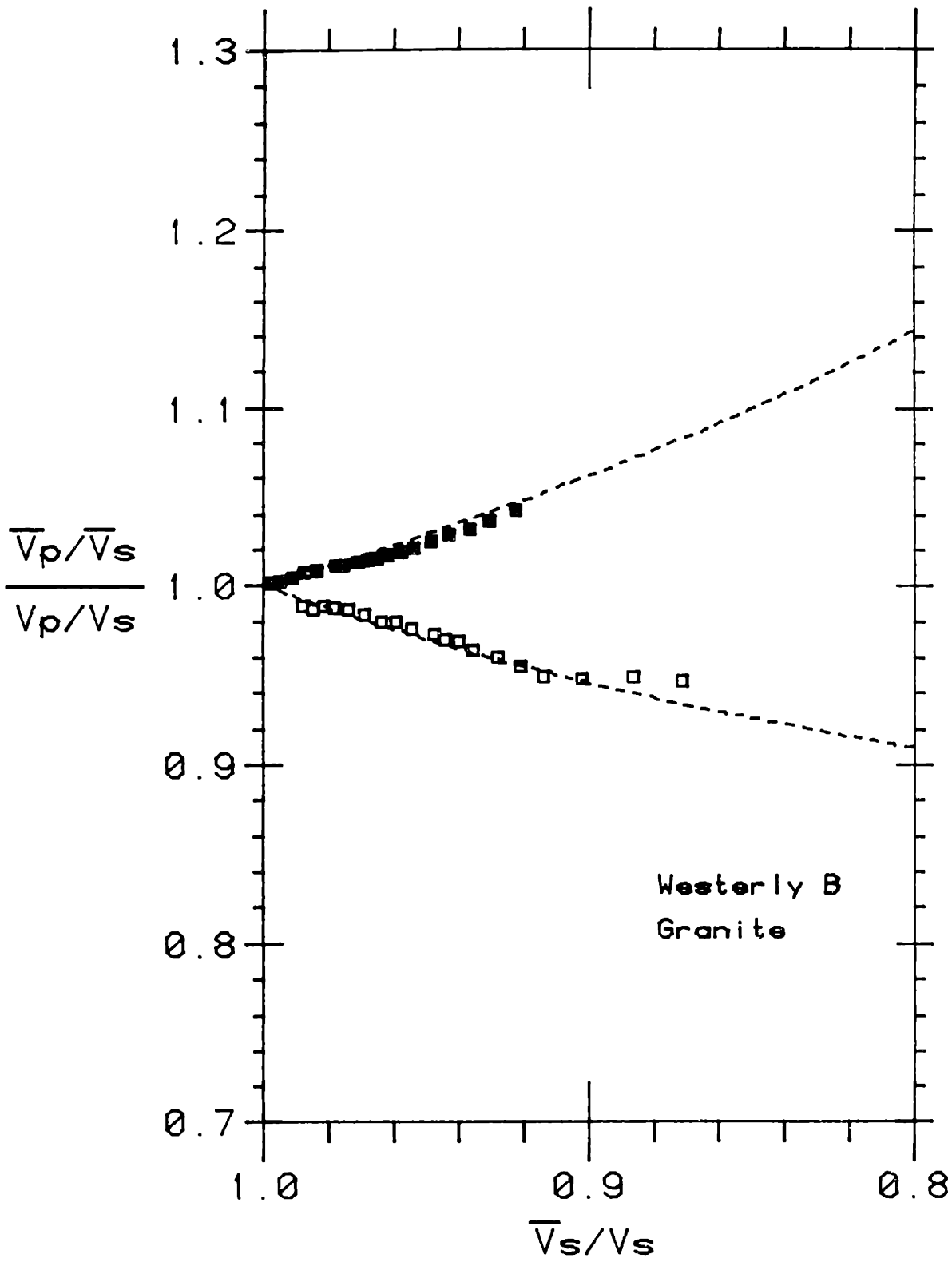


Figure 5-54. Normalized velocity ratio $(\bar{V}_p / \bar{V}_s)/(V_p / V_s)$ versus normalized S-wave velocity ratio $\bar{V}_s / V_s$ for Westerly granite. Solid and open squares are saturated and dry measured velocities, respectively. Normalizing velocities are highest velocities measured at 1 kbar. Upper and lower dashed lines are saturated isolated and dry velocity ratios calculated from the circular crack model of O'Connell and Budiansky (1974).

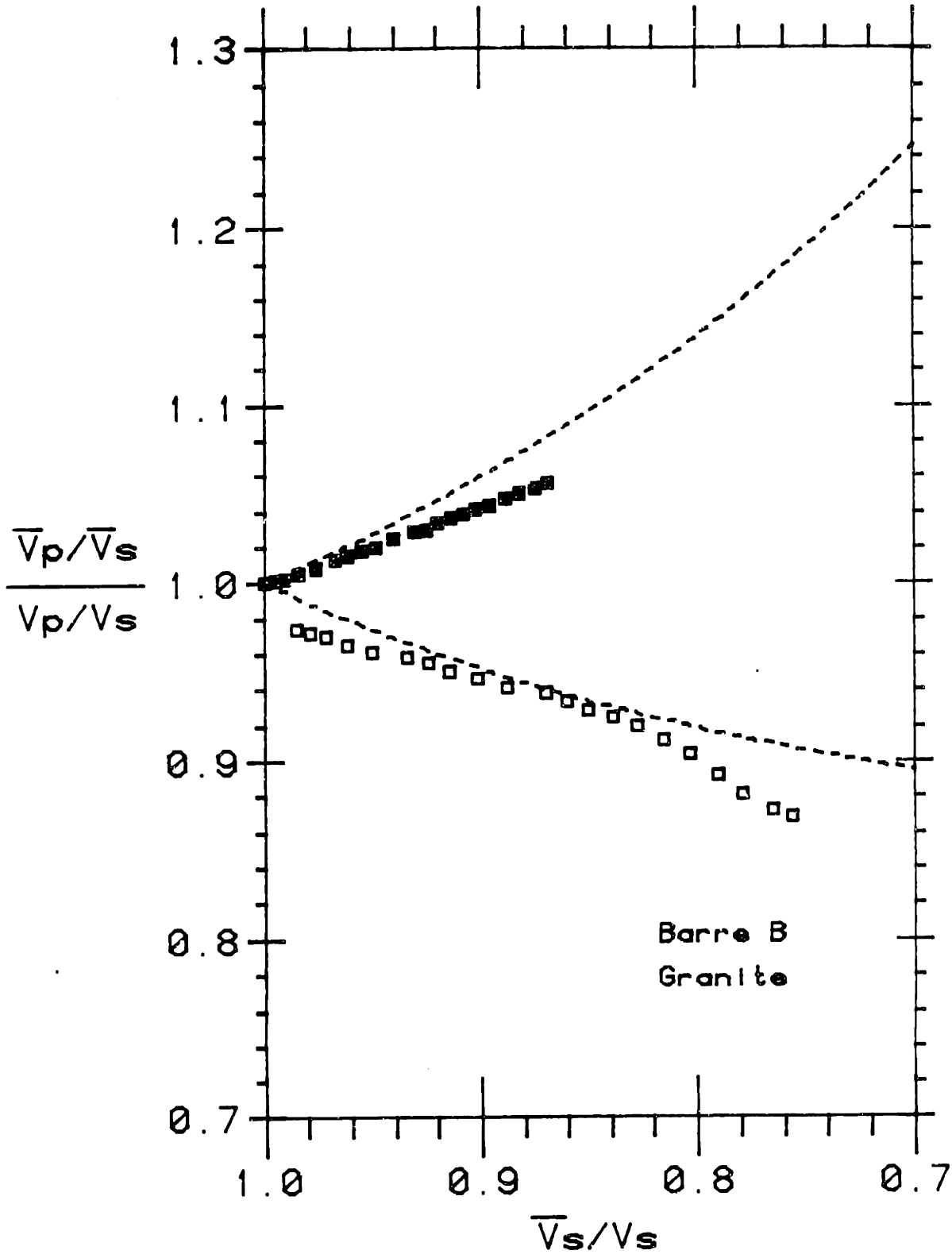


Figure 5-55. Velocity ratio plot similar to Figure 5-54 for Barre granite.

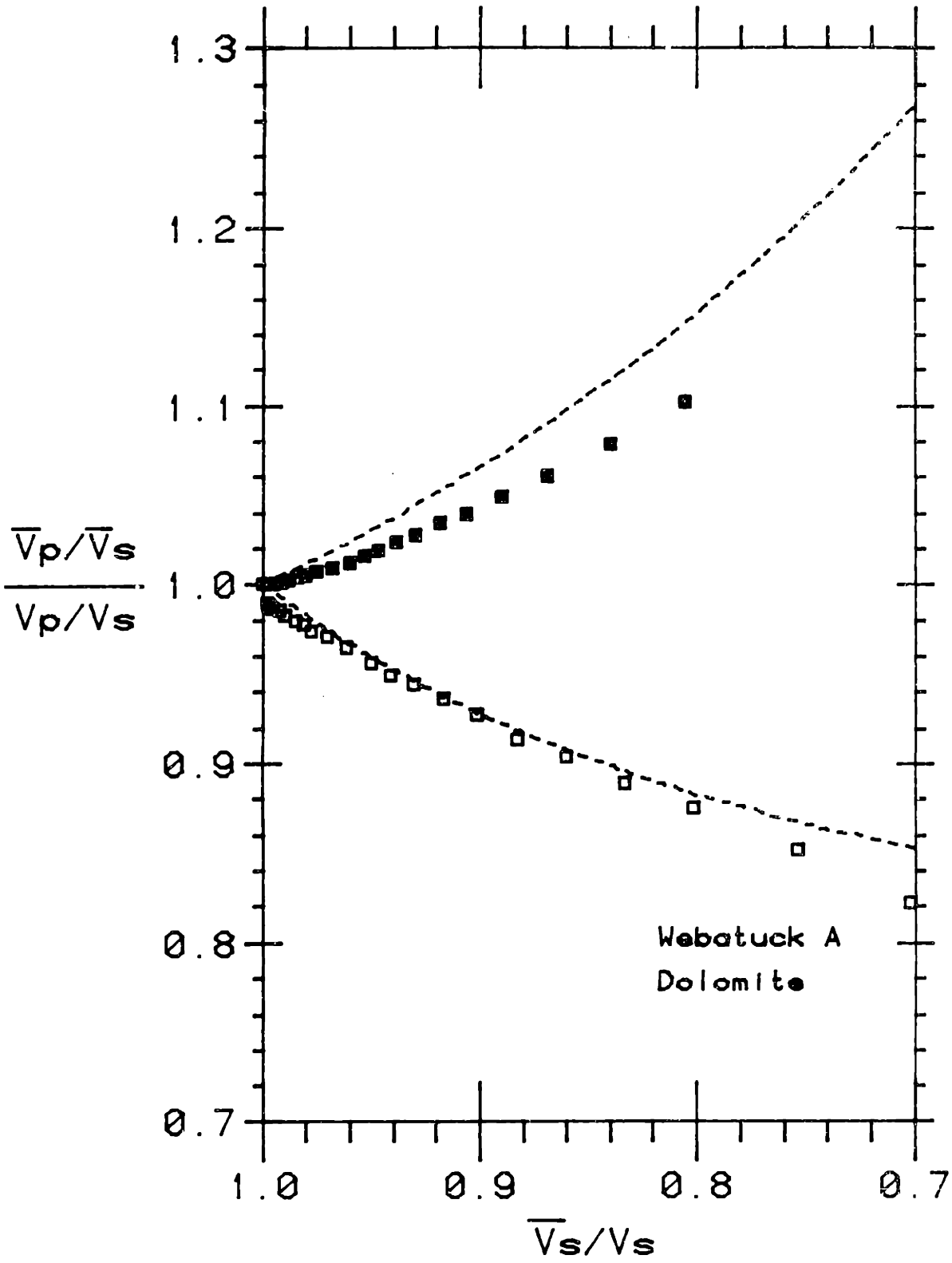


Figure 5-56. Velocity ratio plot similar to Figure 5-54 for Webatuck dolomite.

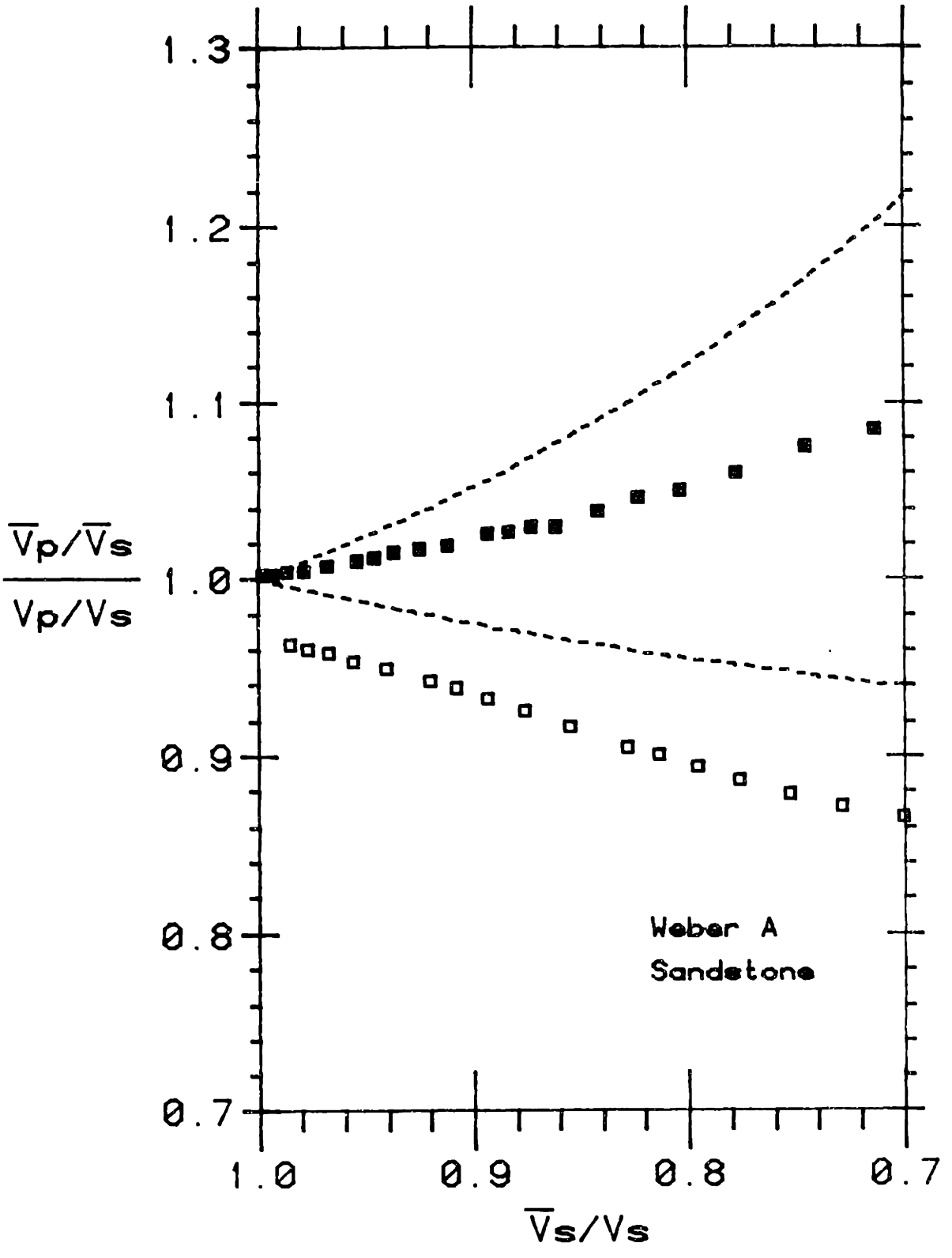


Figure 5-57. Velocity ratio plot similar to Figure 5-54 for Weber sandstone.

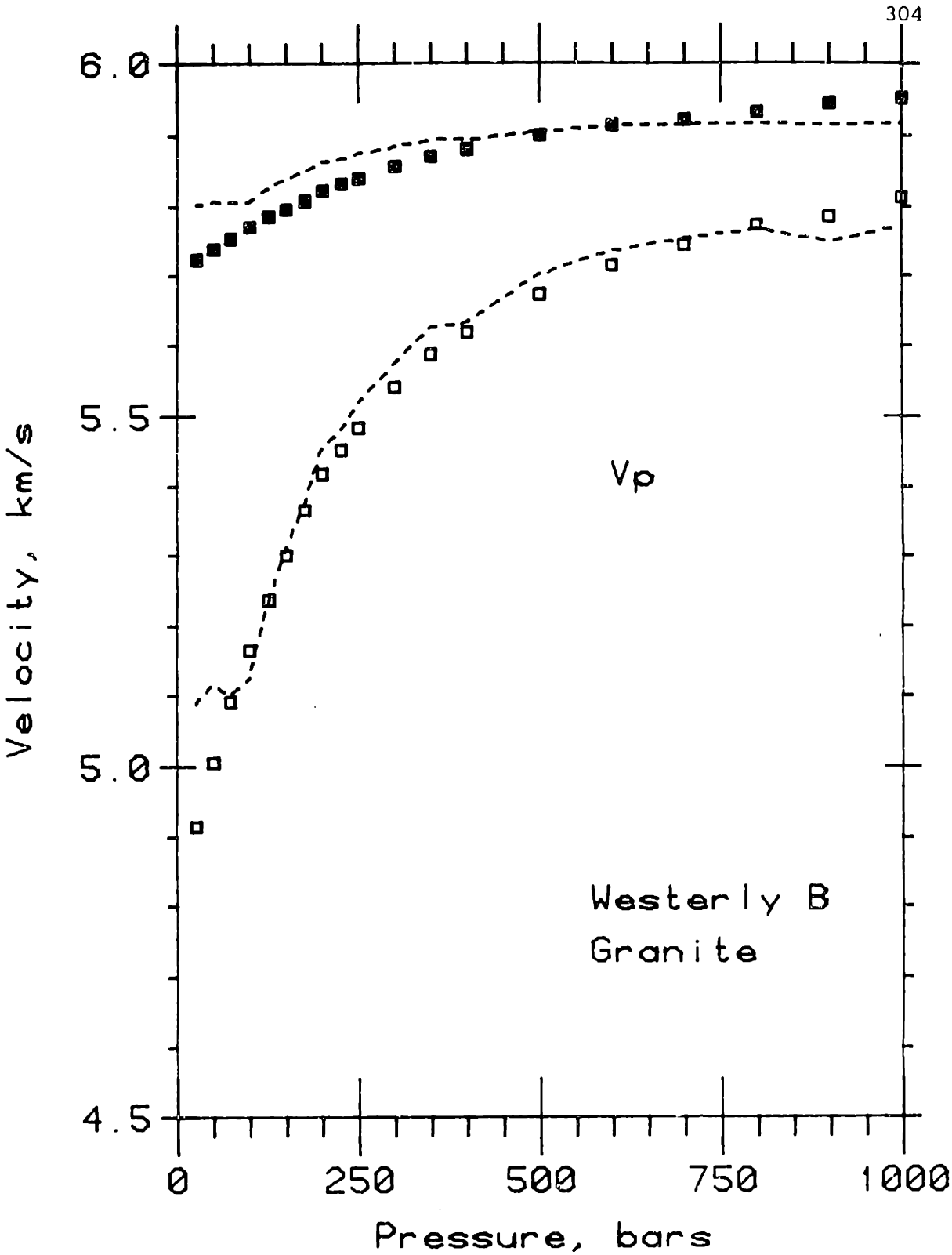


Figure 5-58. Measured dry and benzene saturated P-wave velocities for Westerly granite as a function of differential pressure and predicted dry and saturated velocities (dashed lines) based on circular crack model of O'Connell and Budiansky (1974).

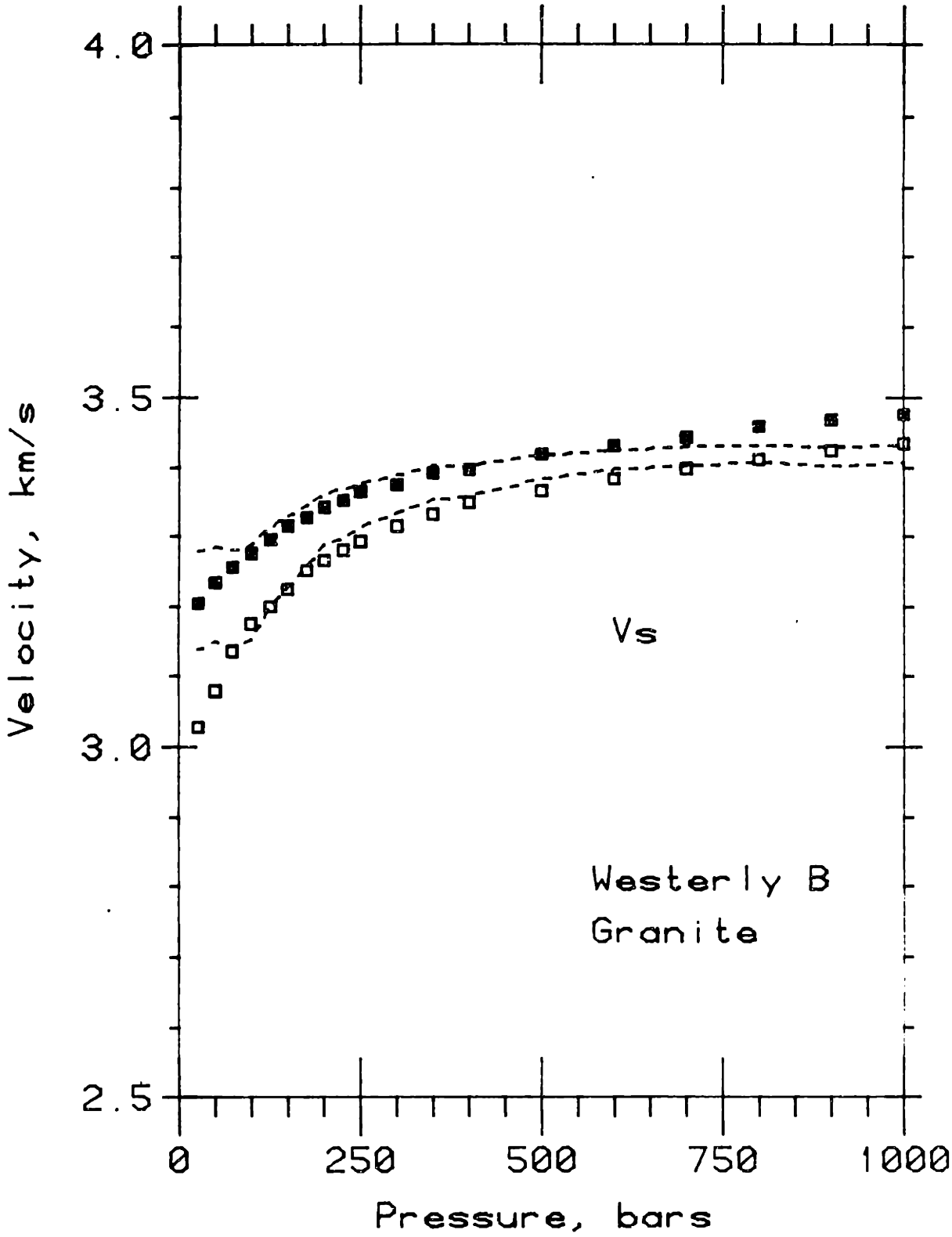


Figure 5-59. Measured dry and benzene saturated S-wave velocities for Westerly granite as a function of differential pressure and predicted dry and saturated velocities (dashed lines) based on circular crack model of O'Connell and Budiansky (1974).

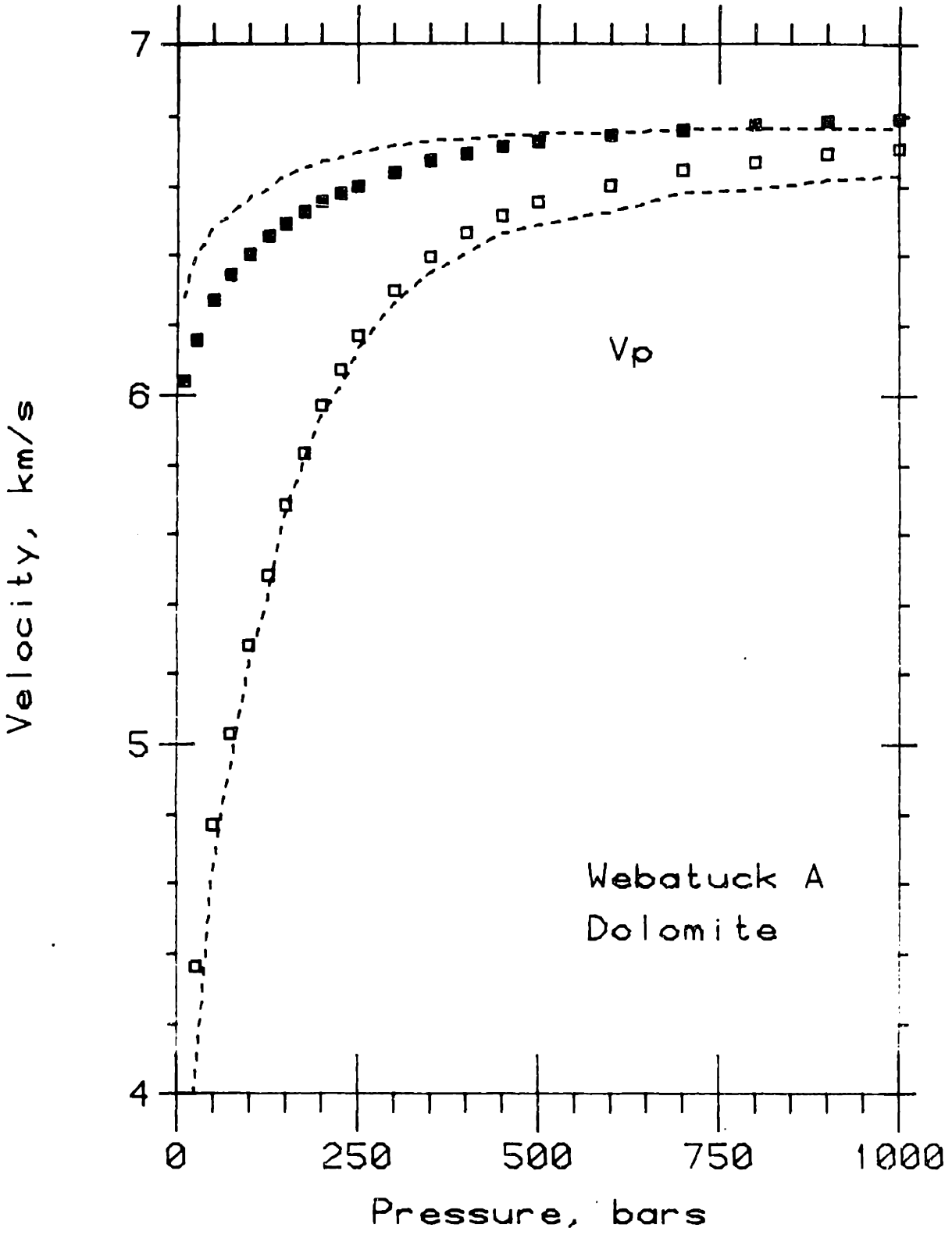


Figure 5-60. Measured dry and benzene saturated P-wave velocities for Webatuck dolomite as a function of differential pressure and predicted dry and saturated velocities (dashed lines) based on circular crack model of O'Connell and Budiansky (1974).

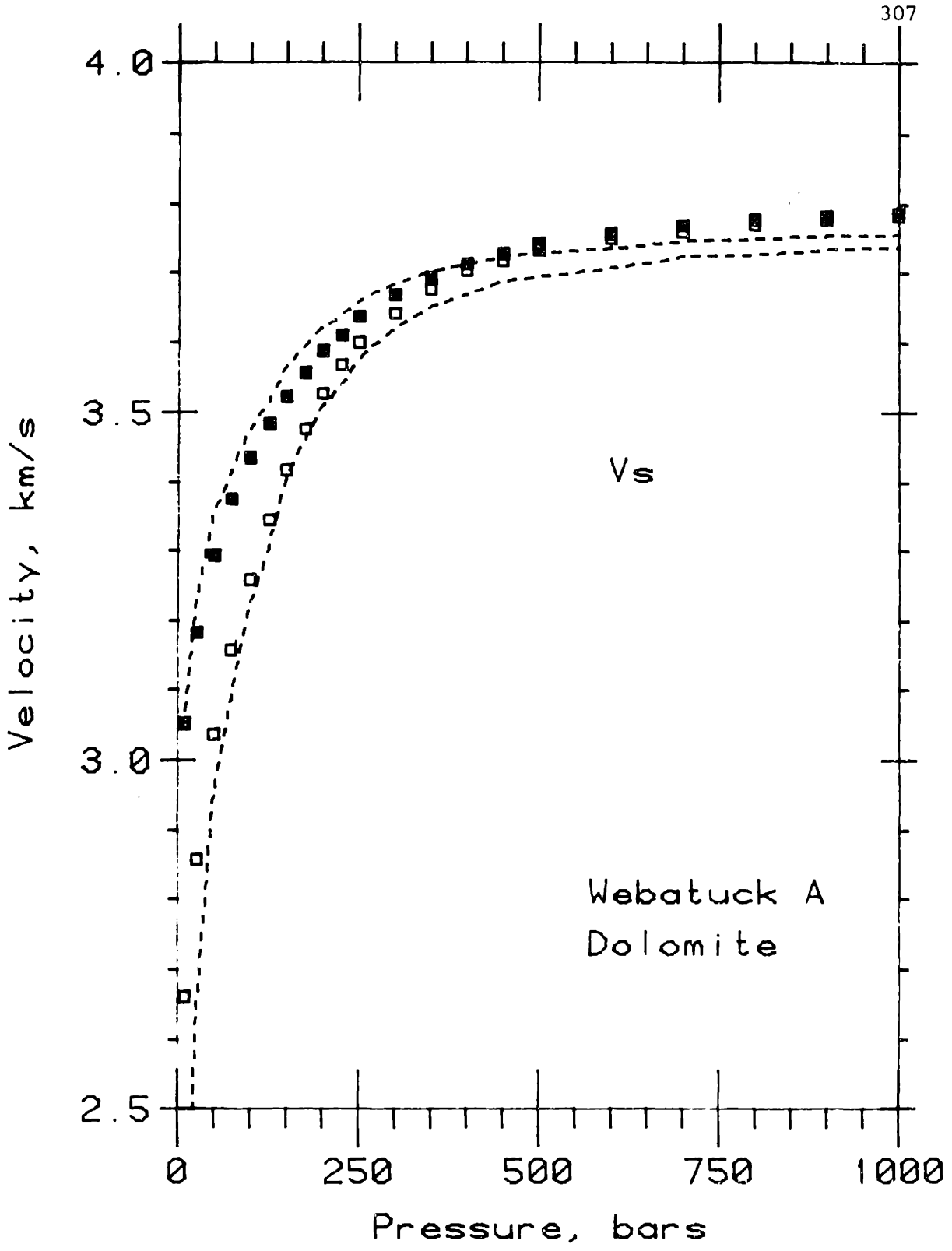


Figure 5-61. Measured dry and benzene saturated S-wave velocities for Webatuck dolomite as a function of differential pressure and predicted dry and saturated velocities (dashed lines) based on circular crack model of O'Connell and Budiansky (1974).

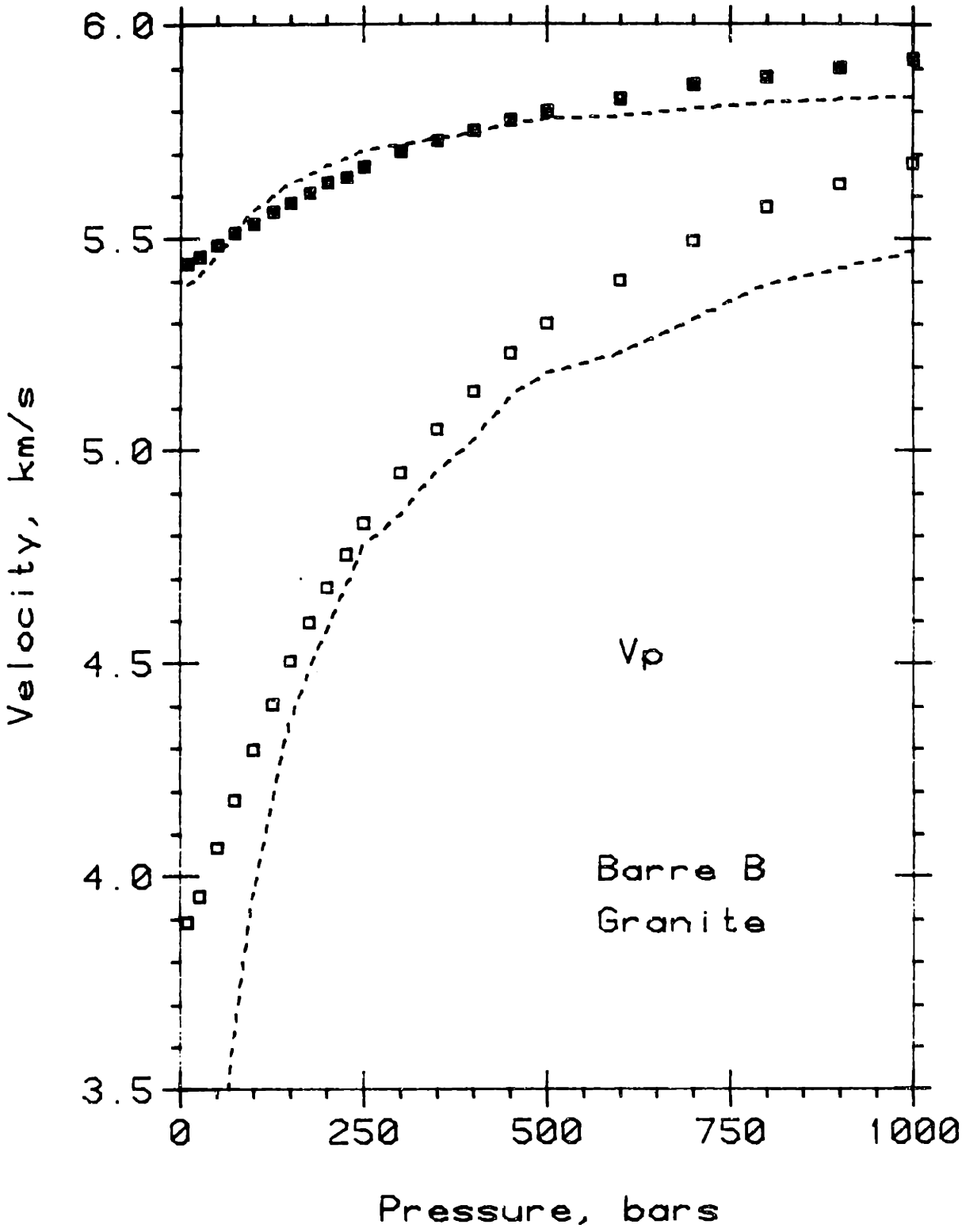


Figure 5-62. Measured dry and benzene saturated P-wave velocities for Barre granite as a function of differential pressure and predicted dry and saturated velocities (dashed lines) based on circular crack model of O'Connell and Budiansky (1974).

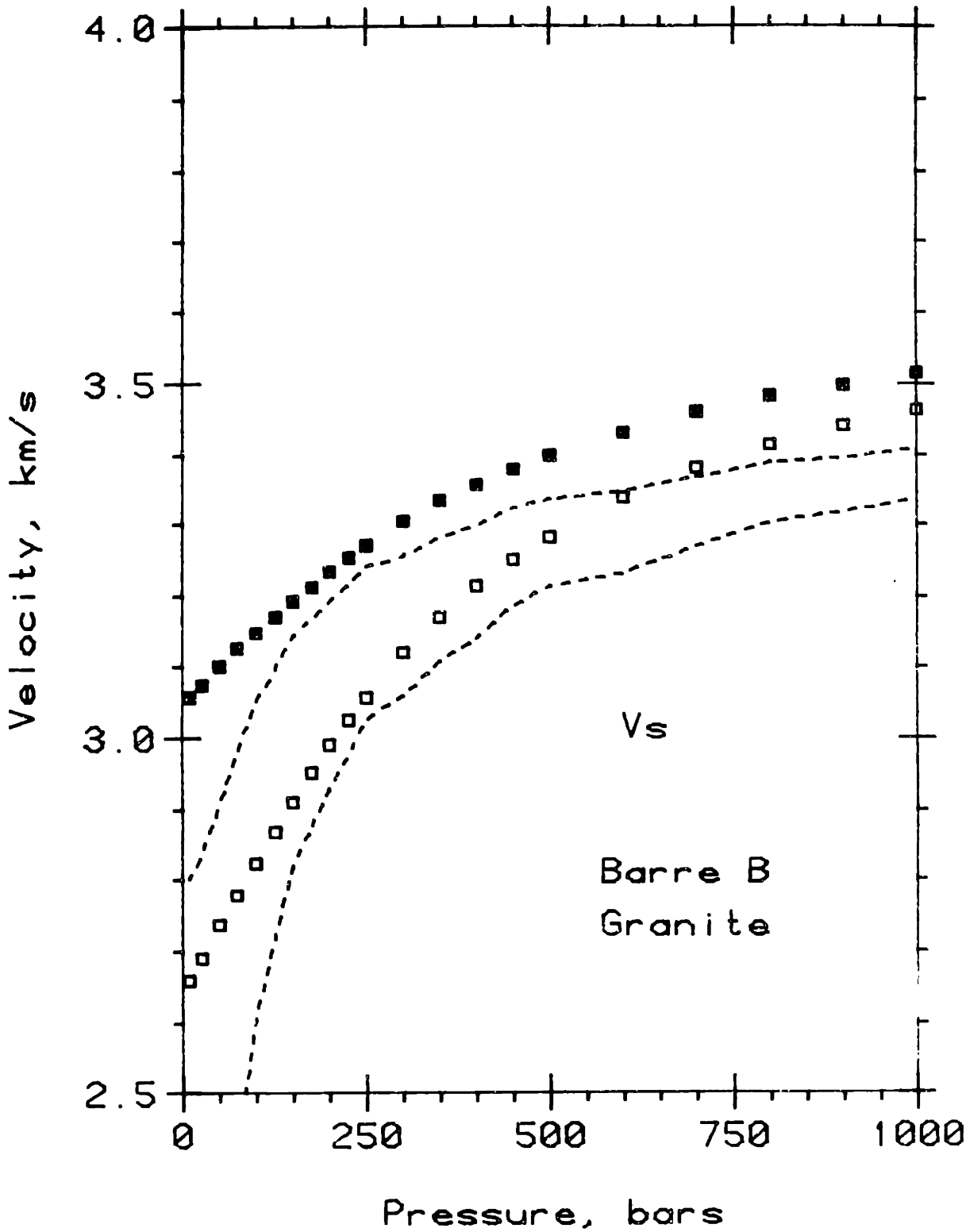


Figure 5-63. Measured dry and benzene saturated S-wave velocities for Barre granite as a function of differential pressure and predicted dry and saturated velocities (dashed lines) based on circular crack model of O'Connell and Budiansky (1974).

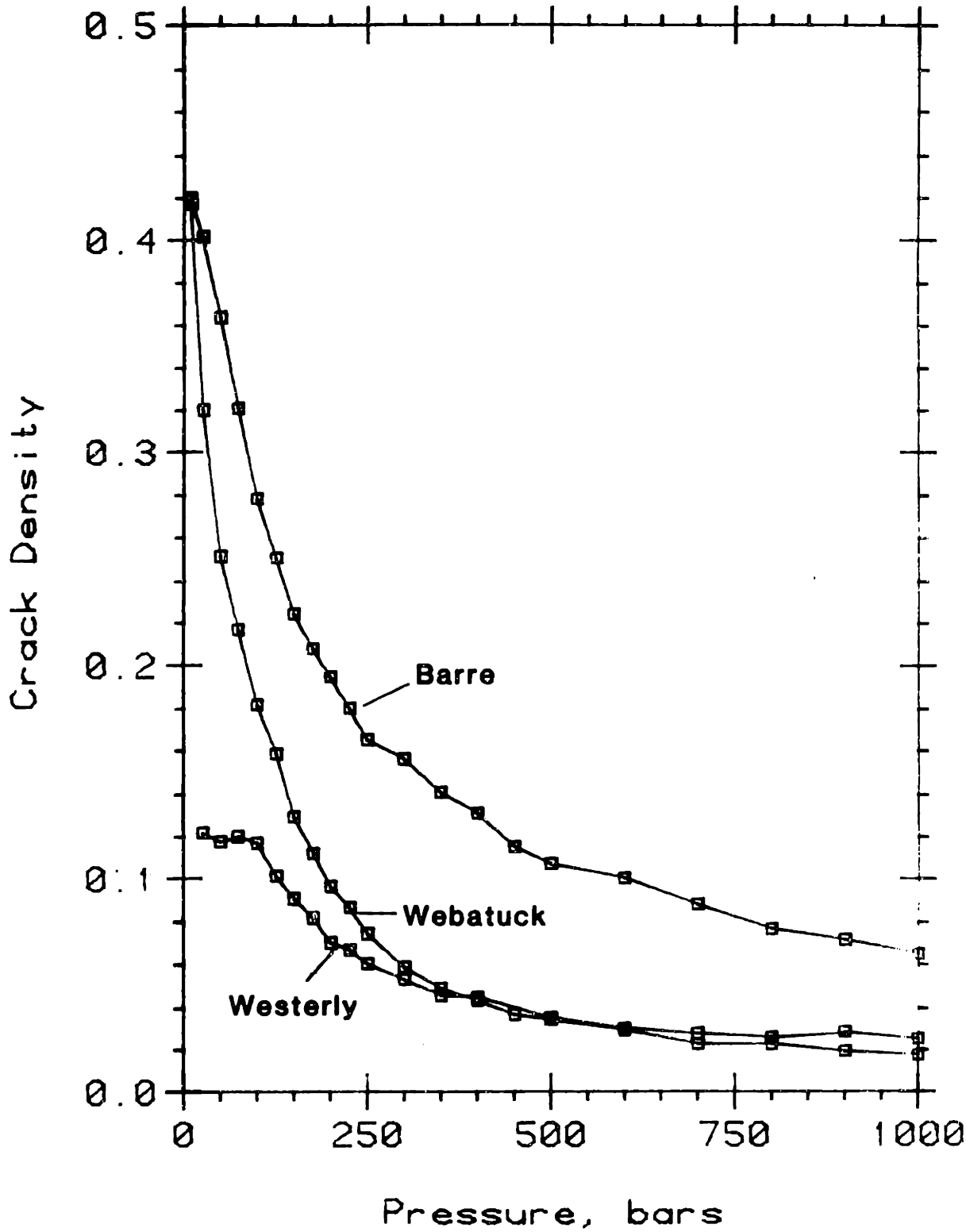


Figure 5-64. Crack density versus confining pressure for Westerly granite, Barre granite, and Webatuck dolomite calculated from measured dry velocities and the circular crack model of O'Connell and Budiansky (1974).

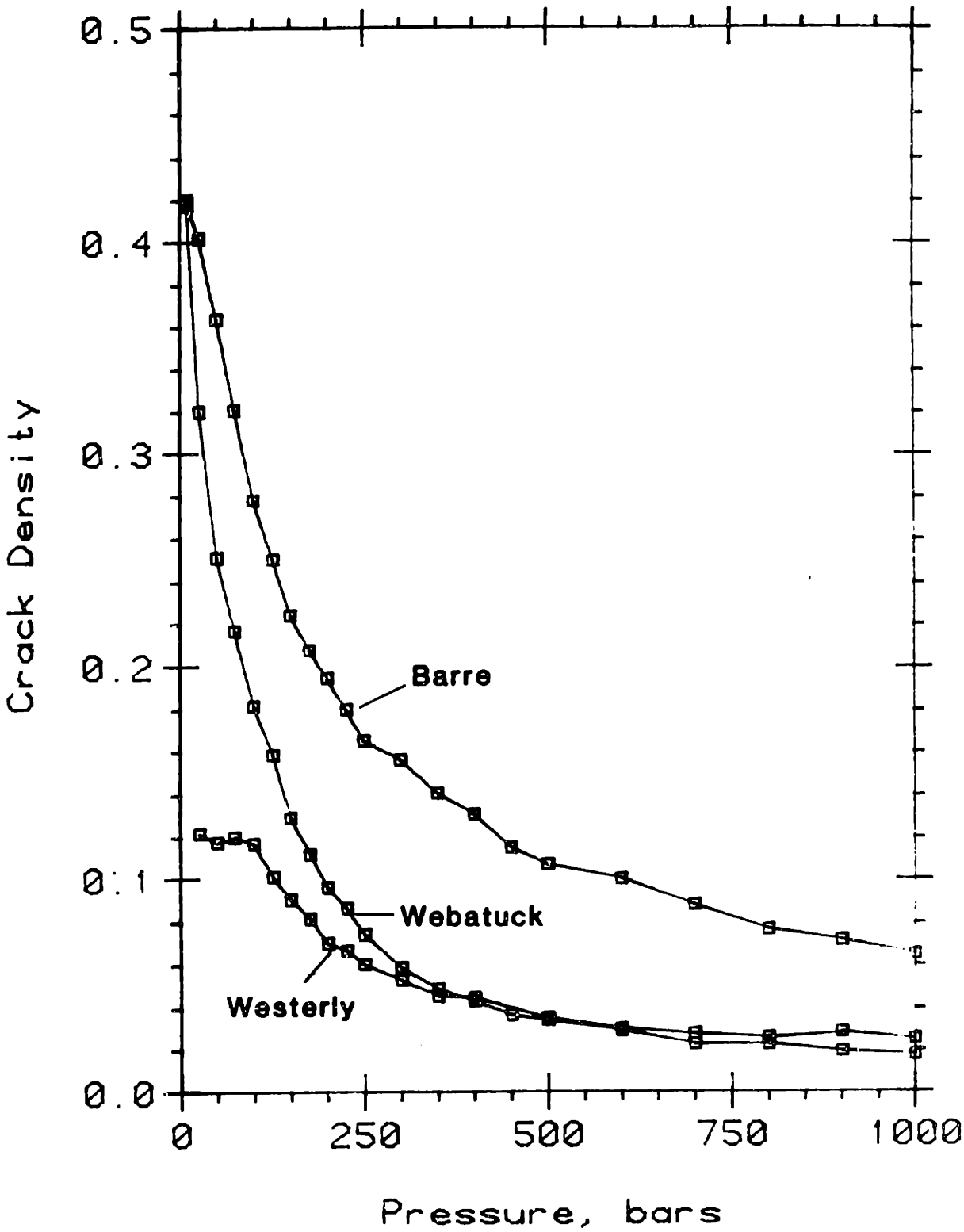


Figure 5-64. Crack density versus confining pressure for Westerly granite, Barre granite, and Webatuck dolomite calculated from measured dry velocities and the circular crack model of O'Connell and Budiansky (1974).

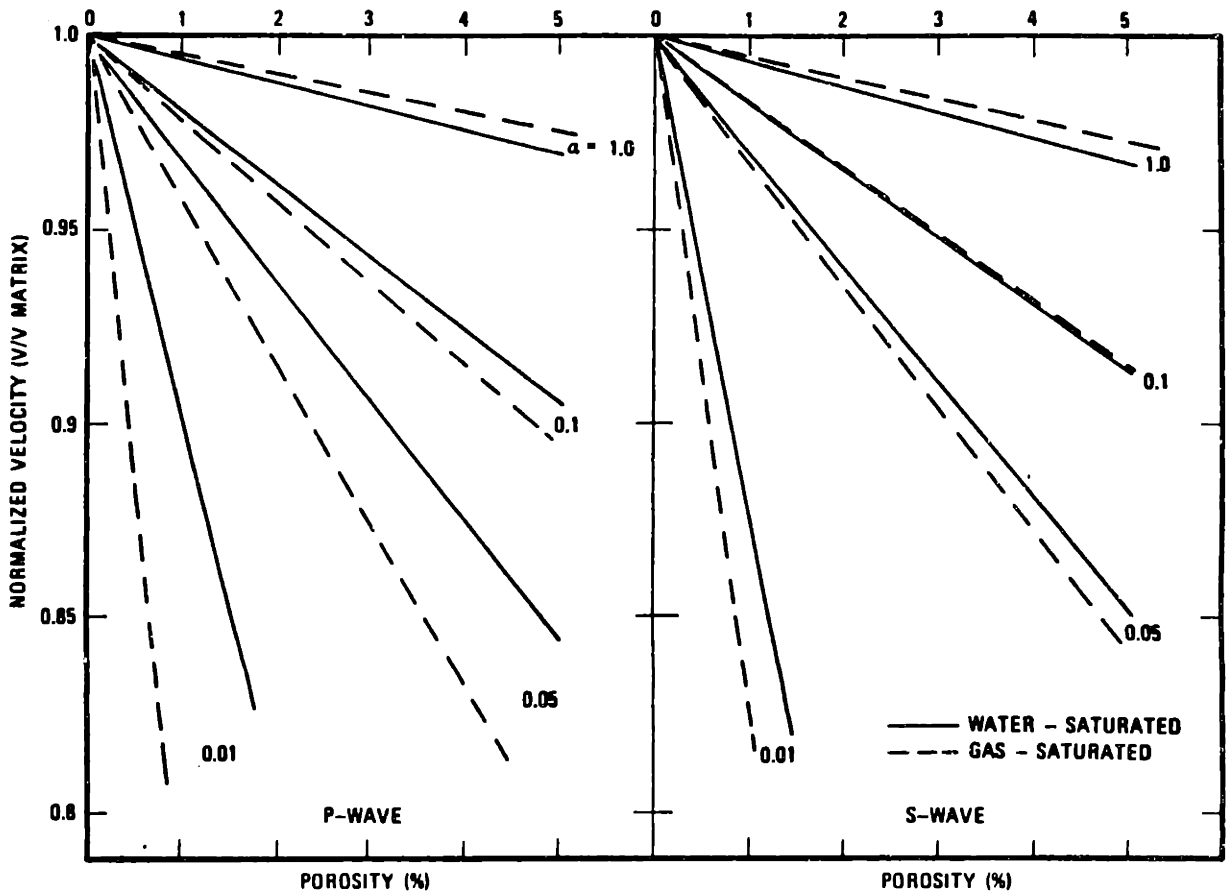


Figure 5-65. Normalized P- and S-wave velocities versus volume concentration of inclusions of different aspect ratios for water and gas saturated inclusions. After Toksöz *et al.* (1976).

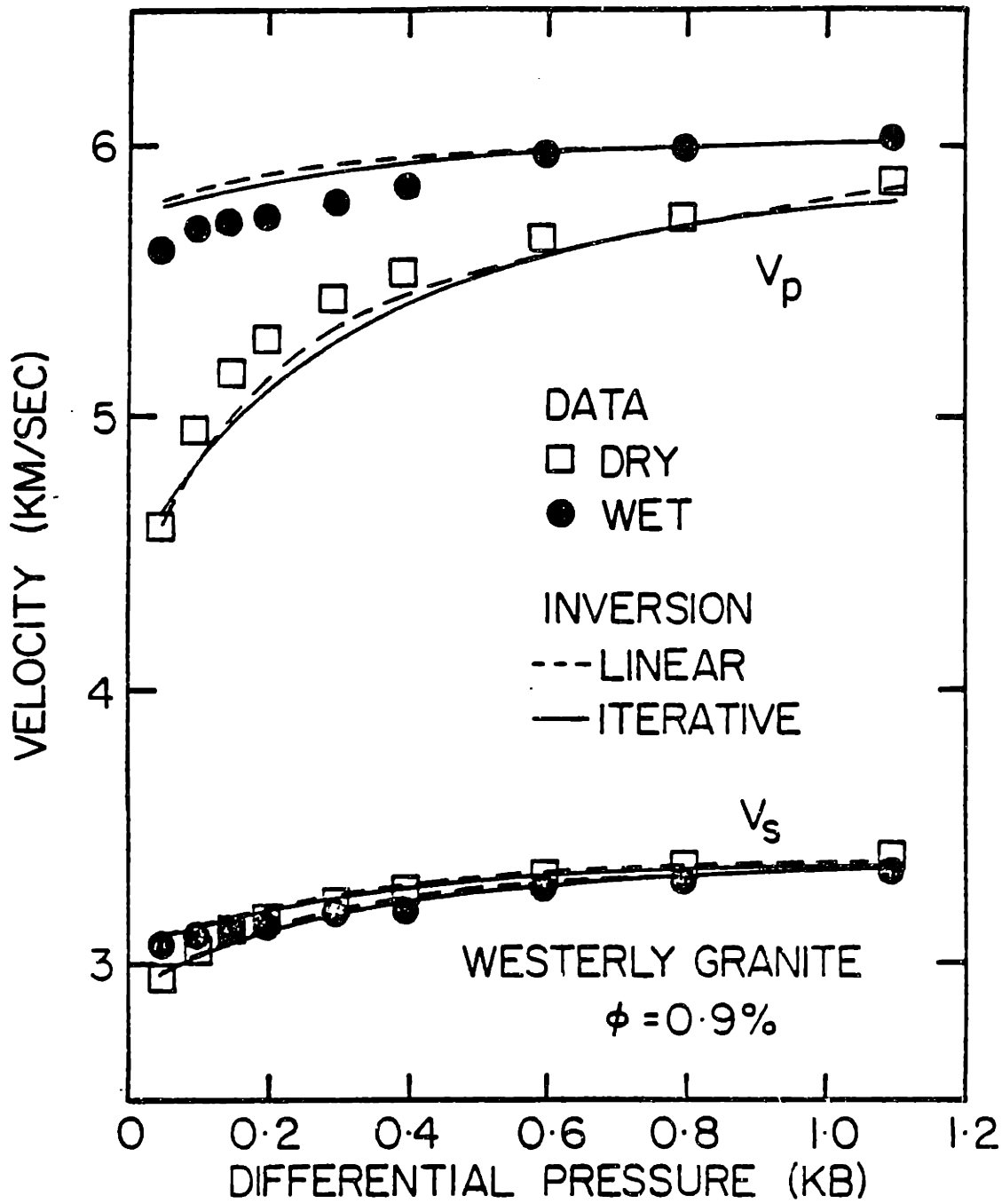


Figure 5-66. Measured dry and saturated P- and S-wave velocities for Westerly granite from Nur and Simmons (1969) with results of inversion for pore aspect ratio spectra by Cheng (1978) based on the model of Kuster and Toksöz (1974). After Cheng (1978).

# CHAPTER 6

## SUMMARY AND CONCLUSIONS

A comprehensive set of rock physical properties and their dependence on confining pressure, pore fluid pressure, and different fluid saturations have been presented in this thesis. Given the diversity of these properties, and the independence of the various chapters, results from each chapter are summarized separately.

Chapter 2. The bulk or linear strain response of rocks to combinations of confining and pore pressures can be predicted from 1) the jacketed and drained stress-strain relation, and 2) the unjacketed stress-strain relation. The jacketed bulk strain measures both strain of the intrinsic solid and that across all of the individual discontinuities; a calculated, jacketed bulk modulus reflects both the bulk modulus of the intrinsic solid and that of the discontinuities. The unjacketed bulk strain and unjacketed bulk modulus calculated from such strain is that of the intrinsic matrix material.

While an effective stress "law" for bulk strain can be defined by rearranging terms in the linear relations of Biot (1941, 1962) such a law has no practical significance or does it describe any fundamental decomposition of stresses between individual grains. If the purpose of such a definition is to predict the static strain response it is much easier to use jacketed and unjacketed strain data directly. The calculation of the bulk moduli necessary for the effective stress law are not necessary.

Direct measurement of jacketed and unjacketed strain allows for the calculation of porosity as a function of confining pressure by subtracting solid matrix strain from bulk volume strain.

Chapter 3. Elasticity considerations indicate that the difference between confining and pore pressures should determine the permeability of rocks. There are several exceptions due to hysteresis, inhomogenity, either because of variability in mineralogy or else because of anisotropy in individual mineral species, or else the presence of a secondary "hidden" phase within the pore space which has a different modulus than that of the overall solid. The permeability measurements of Chelmsford granite indicated that differential pressure determined permeability.

The main purpose of Chapter 3, however, was to investigate the anamalous pore pressure dependence in Berea sandstone previously observed. It was observed with saline solution pore fluid over the first cycle of confining and pore pressure variations. In succeeding cycles the effect diminished and disappeared. Identification of a compliant phase within the pore space is complicated by: 1) the water sensitivity of Berea sandstone, and 2) the presence of naturally occurring hydrocarbons in Berea sandstone. The water sensitivity follows that observed by Khilar and Fogler (1983) and was reflected by the decrease in permeability upon introduction of water in place of saline solution.

Chapter 4. The effect of confining and pore pressure on velocities in rocks was investigated in a manner similar to the way permeability was investigated in Chapter 3. Elasticity considerations of static strain indicate that pore shapes and porosity are governed by differential pressure, and since the intrinsic moduli of silicates are so large the increase in density with pressure at constant differential pressure is negligible. Consequently, velocities should be governed

by the differential pressure. In the experimental data, however, exceptions were found because of changing pore fluid properties with pressure. For velocity data, as opposed to permeability data, the effect of these pore fluid properties could not be isolated as the dynamic moduli are that of a mixed system. For those measurements where pore fluid properties were not a consideration it was found that differential pressure did determine velocity as could best be determined. When the pore fluid saturant is water, and and since the compressibility of water is low, differential pressure should nearly determine permeability, but this is only an approximation.

Chapter 5. The effect of saturation on P- and S-wave velocities was investigated by comparing vacuum-dry, benzene-, and water-saturated experimental velocities for a suite of rocks including granites, sandstones, a limestone, and a dolomite. Comparison of benzene- and water-saturated velocities and derived moduli indicates that water lowers the shear moduli at high pressures, particularly for the sandstones. This is not easily explained on the basis of the fluid properties (bulk modulus and density). Excluding this effect, a comparison of dry and saturated velocities and moduli indicate that both bulk and shear moduli are increased by the presence of water and benzene in the pore space . For all of the rocks benzene-saturated shear moduli were higher than dry except for the Bedford limestone, where dry and saturated shear moduli were apparently equal.

Several different models were examined to see if they could accout for the difference between dry and saturated velocities. Gassmann's equation for the effective bulk modulus of a fluid saturated porous solid was examined extensively and it was found that it did not predict saturated P-wave velocities in either the sandstone or granite data. In addition, assuming that dry and saturated shear moduli were equal and predicting a saturated S-wave velocity on the basis of bulk

saturated density underestimated S-wave velocities for all but the Bedford limestone sample. The Bedford limestone, because it has little compliant porosity and is nearly a linear solid, was predicted exactly from the fluid densities.

The Biot inertial effects (Biot, 1956a,b) were also examined and found to be almost negligible for both the low porosity rocks and the higher porosity sedimentary rocks.

The Budiansky and O'Connell crack model was used to model dry and saturated velocities for several of the low porosity granites and dolomite. Because the effect of saturation in these data is to increase S-wave velocities, however, the conclusion was made that it is the saturated isolated case which tends to agree with the data, and that the cracks which make up the cracked solids are appropriately modelled as being isolated.

# REFERENCES

Adams, L.H., and Williamson, E.D., 1923, The compressibility of minerals and rocks at high pressures: *J. Franklin Inst., 195*, 475-529.

Banthia, B.S., King, M.S., and Fatt, I., 1965, Ultrasonic shear-wave velocities in rocks subjected to simulated overburden pressure and internal pore pressure: *Geophysics, 30*, 117-121.

Biot, M.A., 1935, Le problème de la consolidation des atières argileuses sous une charge: *Ann. Soc. Sci. Bruxelles B55*, 110-113.

Biot, M.A., 1941, General theory of three-dimensional consolidation: *J. Appl. Phys., 12*, 155-164.

Biot, M.A., 1955, Theory of elasticity and consolidation for a porous anisotropic solid: *J. Appl. Phys., 26*, 182-185.

Biot, M.A., 1956, General solutions of the equations of elasticity and consolidation for a porous material: *J. Appl. Mech., 78*, 91-96.

Biot, M.A., 1956a, Theory of propagation of elastic waves in a fluid-saturated porous solid - I. Low frequency range: *J. Acoust. Soc. Am., 28*, 168-178.

Biot, M.A., 1956b, Theory of propagation of elastic waves in a fluid-saturated porous solid - II. Higher frequency range: *J. Acoust. Soc. Am., 28*, 179-191.

Biot, M.A., 1962a, Mechanics of deformation and acoustic propagation in porous media: J. Appl. Phys., 33, 1482-1498.

Biot, M.A., 1962b, Generalized theory of acoustic propagation in porous dissipative media: *J. Acoust. Soc. Am., 34*, 1254-1264.

Biot, M.A., 1965, *Mechanics of Incremental Deformations*, John Wiley, New York, 497pp.

Biot, M.A., 1972, Theory of finite deformations of porous solids: *Ind. Univ. Math. J., 21*, 597-620.

Biot, M.A., 1973, Nonlinear and semilinear rheology of porous solids: *J. Geophys. Res., 78*, 4924-4937.

Biot, M.A. and Willis, D.G., 1957, The elastic coefficients of the theory of consolidation: *J. Appl. Mech., 24*, 594-601.

Birch, F., 1966, Compressibility elastic constants: in *Handbook of Physical Constants, Geol. Soc. Am. Mem. 97*, 97-173.

Brace, W.F., 1964, Effect of pressure on electric-resistance strain gages: *Exp. Mech., 4*, 212-216.

Brace, W.F., 1965, Some new measurements of linear compressibility of rocks: *J. Geophys. Res., 70*, 391-398.

Brace, W.F., 1[illegible], Pore pressure in geophysics: *Amer. Geophys. Union Mono. 16*, 265-273.

Brace, W.F., 1980, Permeability of crystalline and argillaceous rocks: *Int. J. Rock Mech. Min. Sci. & Geomech. Abstr., 17*, 241-251.

Brace, W.F. and Martin, R.J., 1968, A test of the law of effective stress for crystalline rocks of low porosity: *Int. J. Rock Mech. Min. Sci., 5*, 415-426.

Brace, W.F., Walsh, J.B. and Frangos, W.T., 1968, Permeability of granite under high pressure: *J. Geophys. Res., 73*, 2225-2236.

Bridgman, P.W., 1923, The compressibility of thirty metals as a function of pressure and temperature: *Proc. Am. Acad., 58*, 166-242.

Brown, R.J.S. and Korringa, J., 1975, On the dependence of the elastic properties of a porous rock on the compressibility of the pore fluid: *Geophysics, 40*, 608-616.

Carpenter, C.B. and Spencer, G.B., 1940, Measurements of compressibility of consolidated oil-bearing sandstones: *R.I.3540, USBM.*

Carroll, M.M., 1979, An effective stress law for anisotropic elastic deformation: *J. Geophys. Res., 84*, 7510-7512.

Cheng, C.H., 1978, Seismic velocities in porous rocks: direct and inverse problems: PhD. thesis, M.I.T., Cambridge, Ma.

Cheng, C.H. and Johnston, D.H., 1981, Dynamic and Static Moduli: *Geophys. Res. Letters, 8*, 39-42.

Duffy, J., and Mindlin, R.D., Stress-strain relations and vibrations of a granular medium, 1957, *J. appl. Mech., 24* 585-593.

Fatt, I., 1958, The compressibility of sandstones at low to moderate pressures: *Bull. Am. Assoc. Pet. Geol., 42*, 1924-1957.

Fatt, I., 1959, The Biot-Willis elastic coefficients for a sandstone: *J. Appl. Mech., 26*, 296-297.

Gardner, H.F., Wyllie, M.R.J. and Droschak, D.M., 1965, Hysteresis in the velocity-pressure characteristics of rocks: *Geophysics, 30*, 111-116.

Garg, S.K. and Nur, A., 1973, Effective stress laws for fluid-saturated porous rocks: *J. Geophys. Res., 78*, 5911-5921.

Gassmann, F., 1951, Uber die elastizitat poroser medien: *Vierteljahrsschr Naturforsch. Ges. Zurich, 96*, 1-21.

Geertsma, J., 1957, The effect of fluid pressure decline on volumetric changes of porous rocks: *Trans. A.I.M.E., 210*, 331-340.

Handin, J., Hager, R.V., Jr., Friedman, M. and Feather, J.N., 1963, Experimental deformation of sedimentary rocks under confining pressure: Pore pressure tests: *Bull. Am. Ass. Petrol. Geol., 47*, 717-755.

Healy, J.H., Rubey, W.W., Griggs, D.T. and Raleigh, C.B., 1968, The Denver earthquakes: *Science, 161*, 1301-1310.

Hubbert, M.K. and Rubey, W.W., 1959, Role of fluid pressure in mechanics of overthrust faulting, 1, 2: *Bull. Geol. Soc. Am., 70*, 115-166.

Hubbert, M.K. and Rubey, W.W., 1960, Role of fluid pressure in mechanics of overthrust faulting: a reply: *Bull. Geol. Soc. Am., 71*, 611.

Hughes, D.S. and Cooke, C.E., 1953, The effect of pressure on the reduction of pore volume of consolidated sandstones: *Geophysics, 18*, 298-309.

Johnston, D.H., 1978, The attenuation of seismic waves in dry and saturated rocks: Ph.D. thesis, M.I.T., Cambridge, Ma.

Khilar, K.C., and Fogler, 1983, Water sensitivity of sandstones: J. Soc. Pet. Eng.,AIME, 55-64.

King, M.S., 1966, Wave velocities in rocks as a function of changes in overburden pressure and pore fluid saturants: *Geophysics, 31*, 50-73.

Knutson, C.F. and Bohor, B.F., 1963, Reservoir rock behavior under moderate confining pressure, *in* 5th Symposium on rock mechanics, Univ. Minnesota, MacMillan, New York, 627-659.

Korringa, J., Brown, R.J.S., Thompson, D.D., and Runge, R.J., 1979, Self-consistent

imbedding and the ellipsoidal model for porous rocks: *J. Geophys. Res.*, *84*, 5591-5598.

Land, L.S. and Dutton, S.P., 1978, Cementation of a Pennsylvanian deltaic sandstone: isotopic data: *J. Sed. Petrology*, *48*, 1167-1176.

Love, A.E.H., 1944, *A Treatise on the Mathematical Theory of Elasticity*, Dover, New York.

Mann, R.L. and Fatt, I., 1960, Effect of pore fluids on the elastic properties of sandstones: *Geophysics*, *25*, 433-444.

Mesri, G. and Olson, R.E., 1971, Mechanisms controlling the permeability of clays: *Clays and Clay Minerals*, *19*, 151-158.

Nur, A., 1969, *Effects of stress and fluid inclusions on wave propagation in rocks*: Ph.D. Thesis, M.I.T., Cambridge, Ma.

Nur, A., 1972, Dilatancy, pore fluids and premonitory variations of ts/tp travel times: *Bull. Seism. Soc. Am.*, *78*, 1217-1222.

Nur, A. and Booker, J.R., 1972, Aftershocks caused by pore fluid flow? *Science*, *175*, 885-887.

Nur, A. and Byerlee, J.D., 1971, An exact effective stress law for elastic deformation of rocks with fluids: *J. Geophys. Res.*, *76*, 6414-6419.

Nur, A. and Simmons, G., 1969, The effect of saturation on velocity in low porosity rocks: *Earth Planet. Sci. Lett.*, *7*, 183-193.

O'Connell, R.J. and Budiansky, B., 1974, Seismic velocities in dry and saturated cracked solids: *J. Geophys. Res.*, *79*, 5412-5426.

O'Connell, R.J. and Budiansky, B., 1977, Viscoelastic properties of fluid-saturated cracked solids: *J. Geophys. Res.*, *82*, 5719-5735.

Pepper, J.F., de Witt, W., Jr. and Demarest, D.F., 1954, Geology of the Bedford shale and Berea sandstone in the Appalachian basin: *U.S. Geol. Survey Prof. Paper 259*, 111pp.

Riepe, L., Sachs, W., and Schopper, J.R., 1983, Pressure effects on permeability: *Trans. Eighth European Formation Evaluation Symposium*, sponsored by Society of Professional Well Log Analysts, London Chapter, London, England, March 14-15, 1983.

Robin, P.,-Y.F., 1973, Note on effective pressure: *J. Geophys. Res.*, *78*, 2434-2437.

Robinson, L.H., Jr., 1959, The effect of pore and confining pressure on the failure process in sedimentary rock: *Colo. Sch. Mines Q.*, *54*, 177-199.

Rice, J.R., 1977, *Advances in Civil Engineering through Engineering Mechanics*, ASCE, New York, 295pp.

Rice, J.R., 1980, The mechanics of earthquake rupture: in *Physics of the Earth's Interiors* (Proceedings of the International School of Physics "Enrico Fermi", Soc. Italiana di Fisica, Bologna, Italy (printed by North Holland Publ. Co.), 1980, pp. 555-649.

Rice, J.R. and Cleary, M.P., 1976, Some basic stress diffusion solutions for fluid-saturated elastic porous media with compressible constituents: *Rev. Geophys. Space Phys.*, *14*, 227-241.

Schmoker, J.W., 1980, Organic content of Devonian shale in western Appalachian Basin: *AAPG Bull.*, *64*, 2156-2165.

Siegfried, R., and Simmons, G., 1978, Characterization of oriented cracks with differential strain analysis: *J. Geophy. Res.*, *83*, 1269-1278.

Simmons, G., Siegfried, R.W., and Feves, M., 1974, Differential strain analysis: a new method for examining cracks in rocks: *J. Geophy. Res.*, *79*, 4383-4385.

Simmons, G., Wilkens, R., Caruso, L., Wissler, T., and Miller, F., 1982, Physical properties and microstructures of a set of sandstones, and annual report to the Schlumberger-Doll Research Center.

Skempton, A.W., 1961, Effective stress in soils, concrete and rocks: in *Conf. on Pore Pressure and Suction in Soils*, *4-16*, Butterworth, London.

Sprunt, E.S., and Brace, W.F., 1974, Direct observation of microcavities in crystalline rocks: *Int. J. Rock Mech. Min. Sci. & Geomech. Abstr.*, *11*, 139-150.

Süklje, L., 1969, *Rheological Aspects of Soil Mechanics*, Interscience, New York, 123pp.

Terzaghi, K., 1923, Die Berechuung der durchlässigkeitsziffer des tones ans dem verlauf der hydrodynamischen spannungserscheinunger: *Sitz. Akad. Wissen. Wien Math-naturw Kl. Abt. IIa*, *132* 105-124.

Terzaghi, K., 1925, *Erdbaumechanik anf bodenphysikalischer Grundlage*, Leipzig.

Todd, T., 1973, Effect of cracks on elastic properties of low porosity rocks: Ph.D. thesis, M.I.T., Cambridge, Ma.

Toksöz, M.N., Cheng, C.H., and Timur, A., 1976, Velocities of seismic waves in porous rocks: *Geophysics*, *41*, 621-645.

Van der Knapp, W., 1959, Nonlinear behavior of elastic porous media: *Trans. Am. Inst. Min. Engr.*, *216*, 179-187.

Walls, J. and Nur, A., 1979, Pore pressure and confining pressure dependence of permeability in sandstone: paper presented at 7th Formation Evaluation Symposium of the Canadian Well Logging Society, Calgary, Alberta, Oct. 21-24, 1979, 7pp.

Walsh, J.B., 1965, The effect of cracks on the compressibility of rocks: *J. Geophys. Res.*, *70*, 381-389.

Walsh, J.B., and Brace, W.B., 1984, The effect of pressure on porosity and the transport properties of rock, manuscript in preparation.

Wyllie, M.R.J., Gregory, A.R. and Gardner, G.H.F., 1958, An experimental investigation of factors affecting elastic wave velocities in porous media: *Geophysics*, *23*, 459-493.

Zisman, W.A., 1933, Compressibility and anisotropy of rocks at and near the earth's surface: *Proc. Nat. Acad. Sci.*, *19*, 666-679.

Zoback, M.L., 1975, High pressure deformation and fluid flow in sandstone, granite, and granular materials: Ph.D. thesis, Stanford Univ., Palo Alto, Ca.

# APPENDIX A

## ADDITIONAL STRESS-STRAIN MEASUREMENTS, BULK MODULI, AND POROSITY CALCULATIONS

This appendix contains additional stress-strain data and calculations as a function of confining pressure for the rock samples after the first seven listed in Table 1 of Chapter 2. These include Solenhofen limestone, Vermont marble, Yule marble, Blair dolomite, Webatuck dolomite, Henderson augen gneiss, Pottsville sandstone, Boise Sandstone, Kayenta sandstone, Cedar City quartz diorite, and blue Westerly granite. The plots are arranged sequentially for each of the rock samples, with jacketed and unjacketed linear strain in the 'a' plot, jacketed and unjacketed bulk moduli and the value $\zeta$ in the 'b' plot, and porosity calculated from the jacketed and unjacketed strain in the 'c' plot. There is not a plot of porosity versus confining pressure for Blair dolomite since the initial porosity is nearly zero as can best be determined.

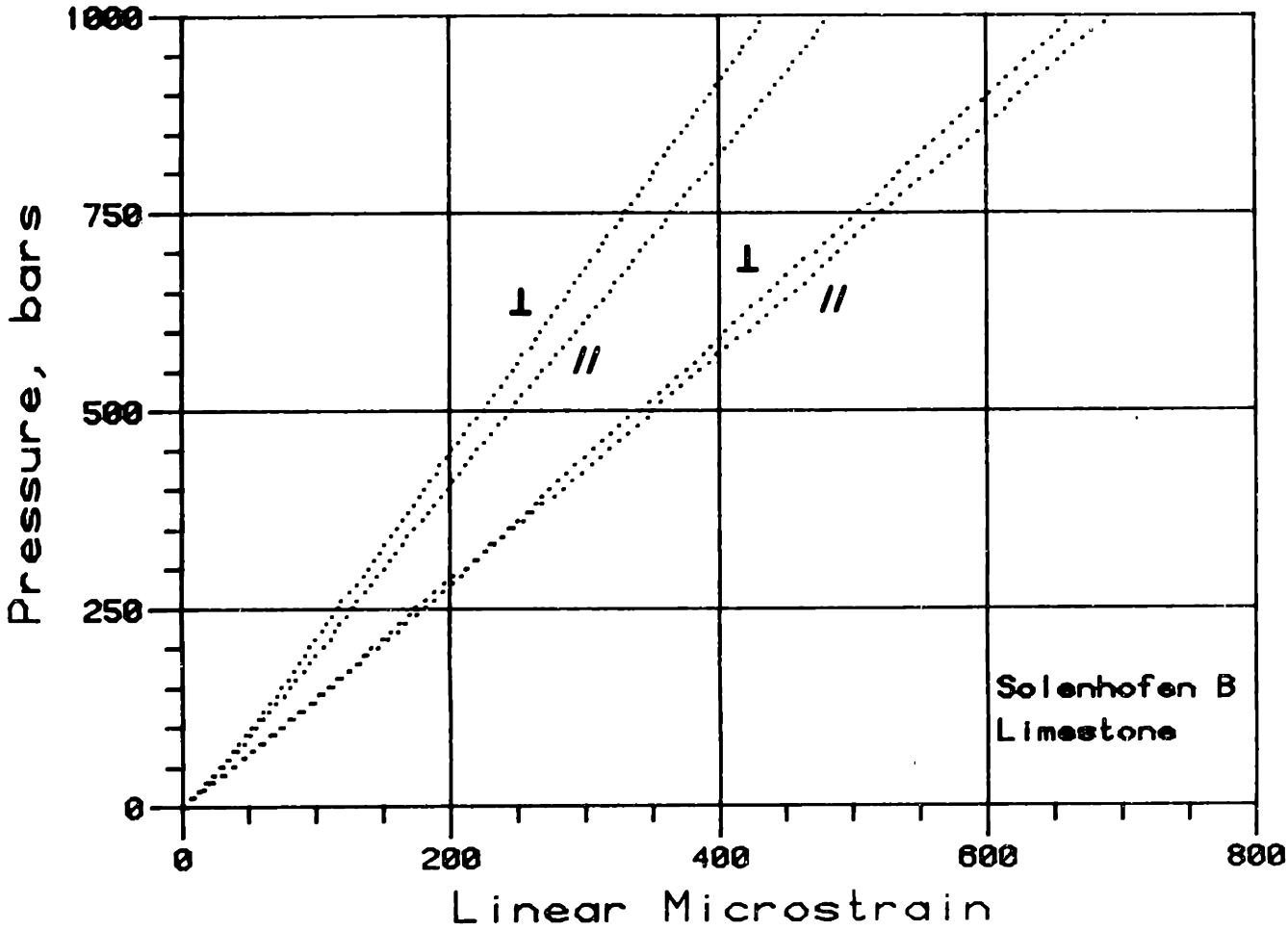


Figure A-1a. Unjacketed and jacketed linear stress-strain measurements for Solenhofen limestone. Symbols correspond to measurements parallel and perpendicular to planes of calcite concretions (bedding?).

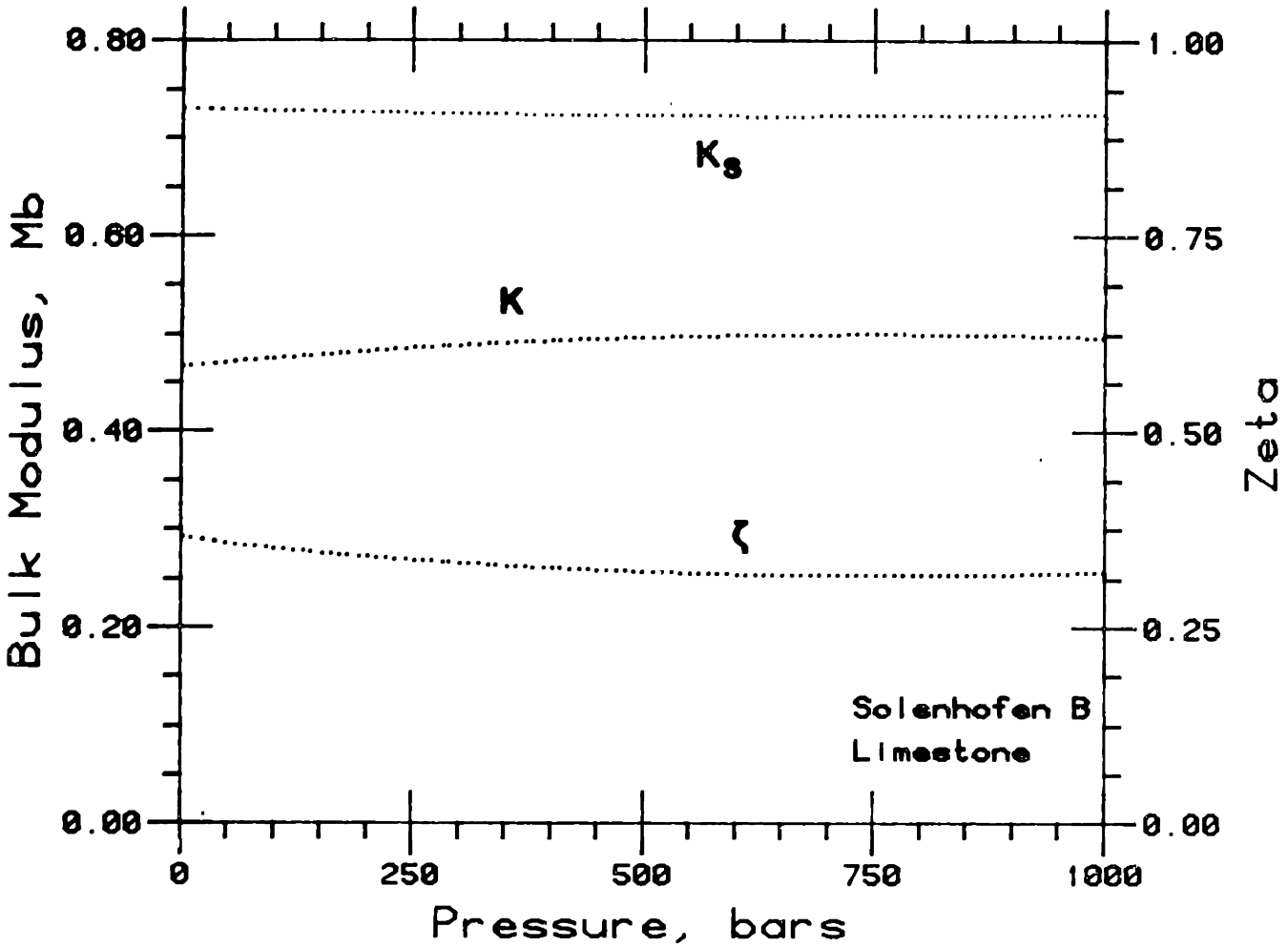


Figure A-1b. Jacketed bulk modulus $K$, unjacketed bulk modulus $K_s$, and $\zeta$ as a function of confining pressure for Solenhofen limestone.

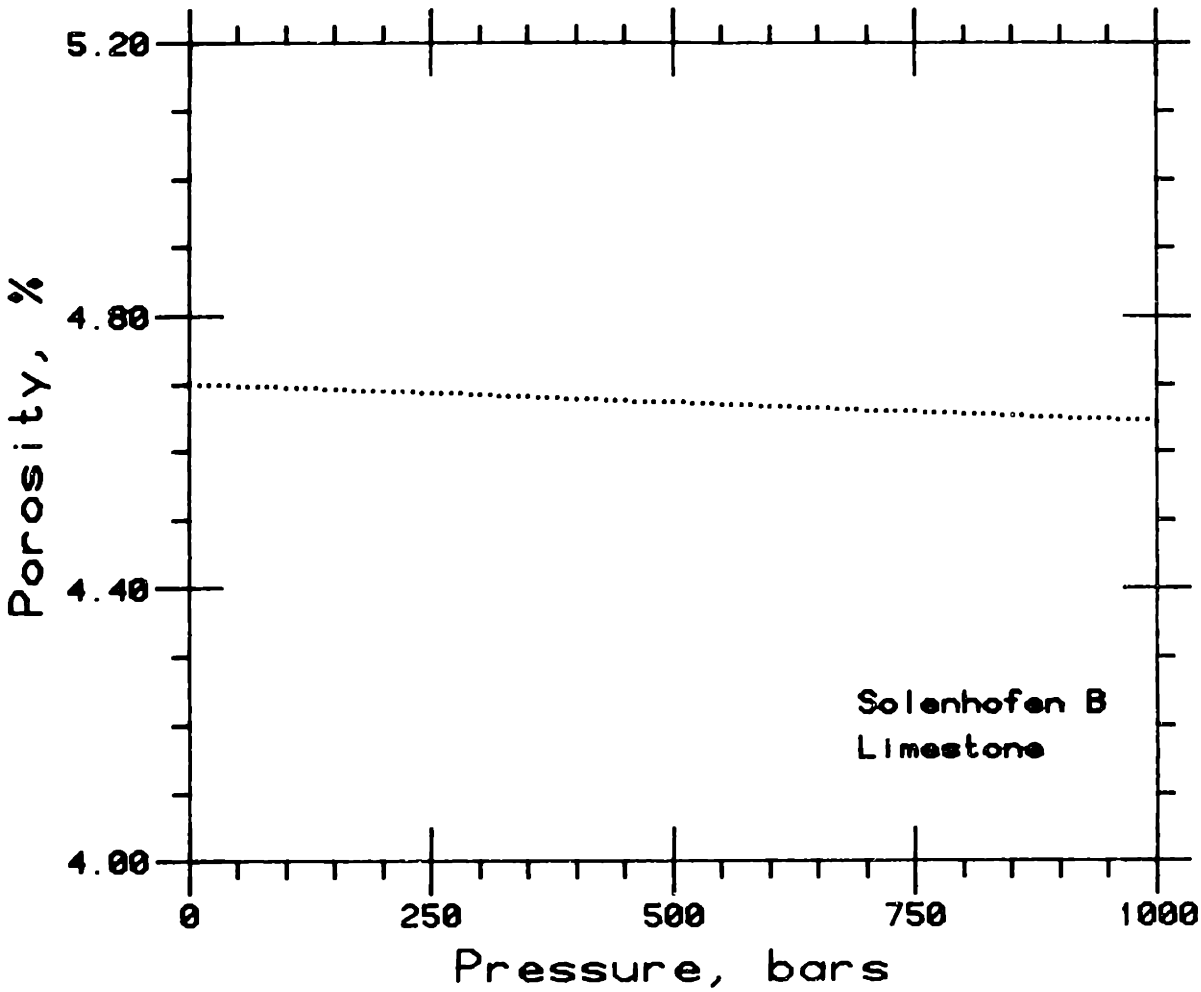


Figure A-1c. Porosity versus confining pressure for Solenhofen limestone calculated from jacketed and unjacketed volumetric strain measurements.

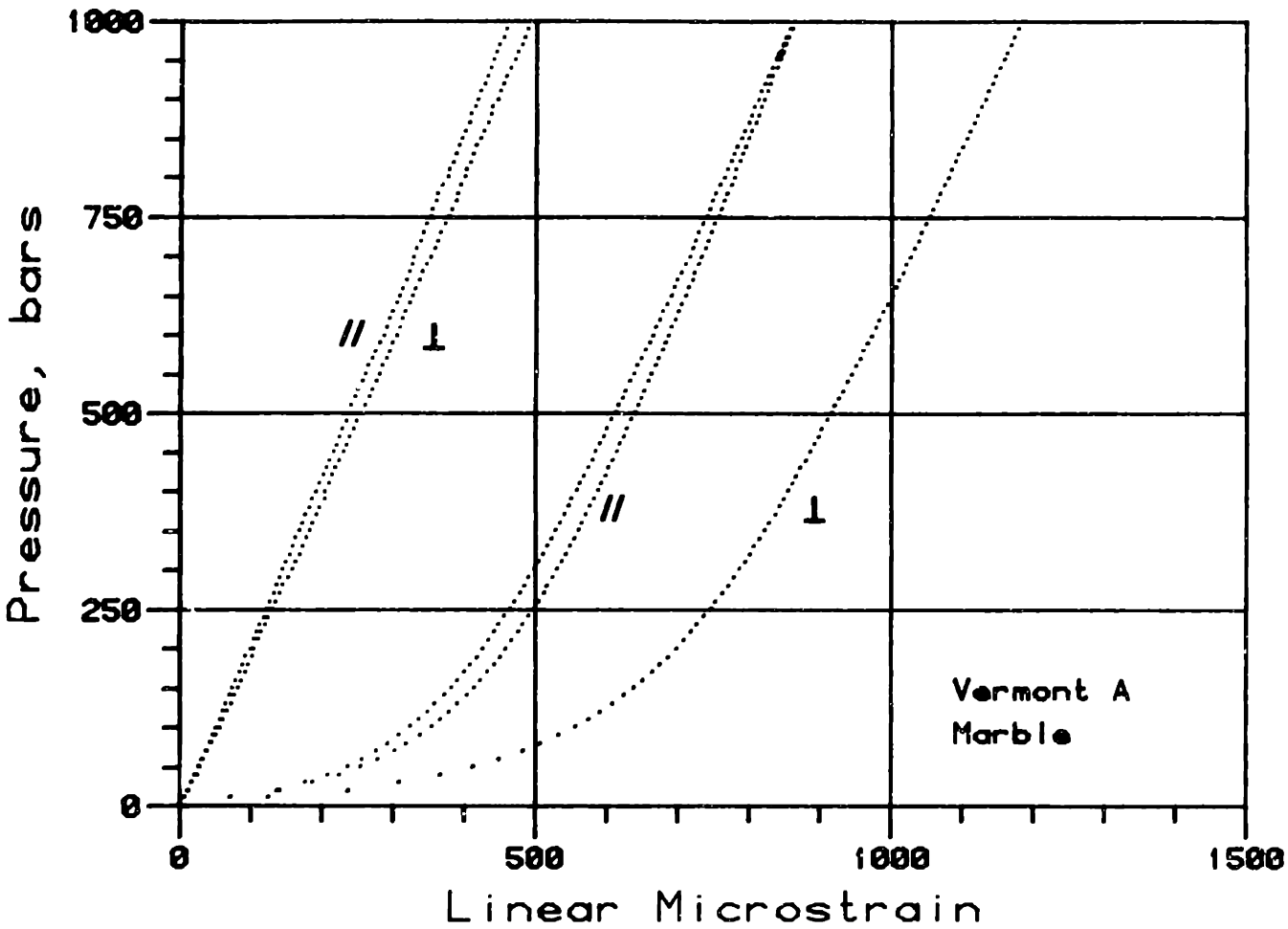


Figure A-2a. Unjacketed and jacketed linear stress-strain measurements for Vermont marble. Symbols correspond to measurements parallel and perpendicular to foliation planes; 2 gages parallel to foliation only for jacketed measurements.

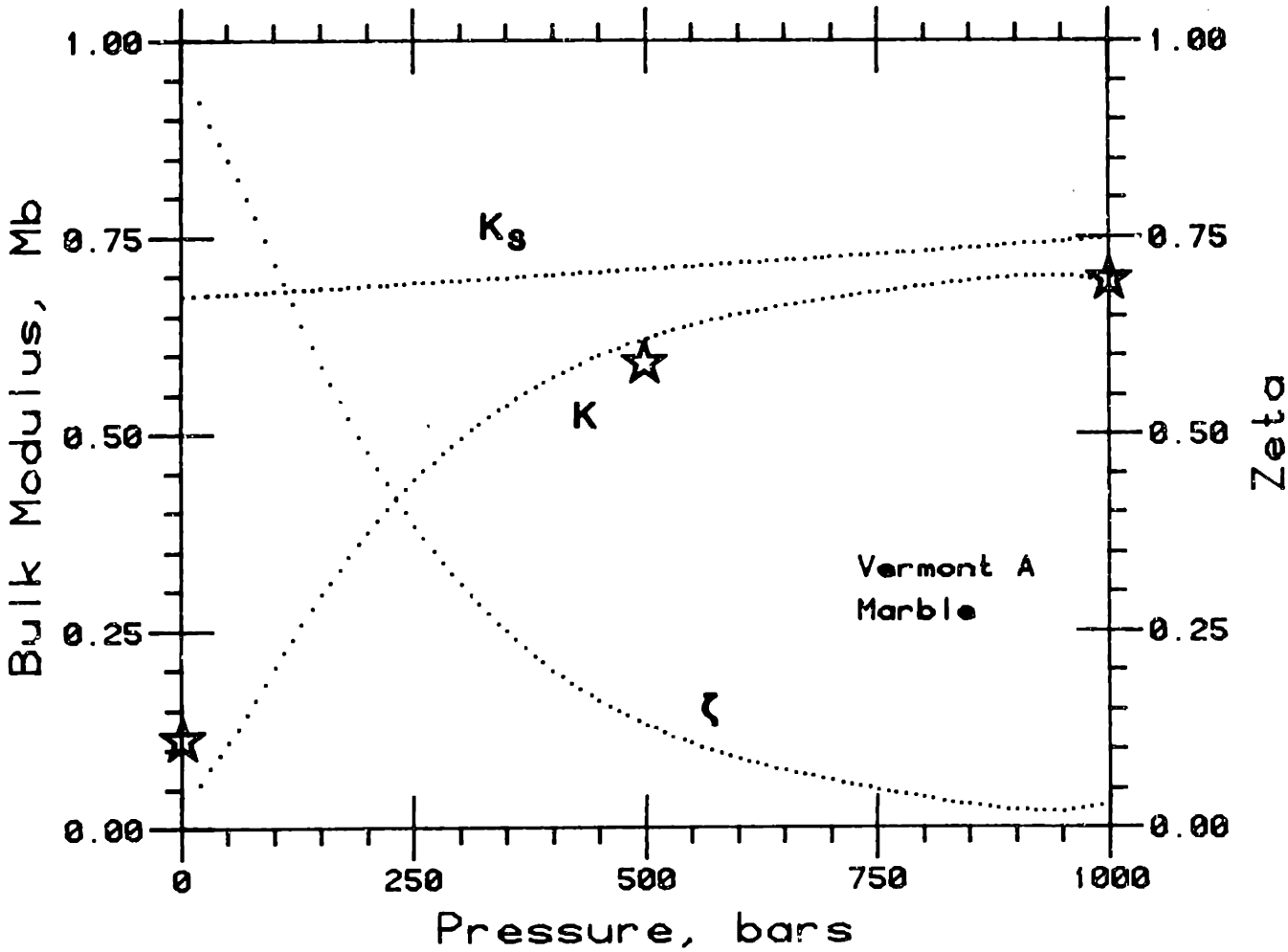


Figure A-2b. Jacketed bulk modulus $K$, unjacketed bulk modulus $K_s$, and $\zeta$ as a function of confining pressure for Vermont marble. Stars represent bulk moduli reported by Brace (1965).

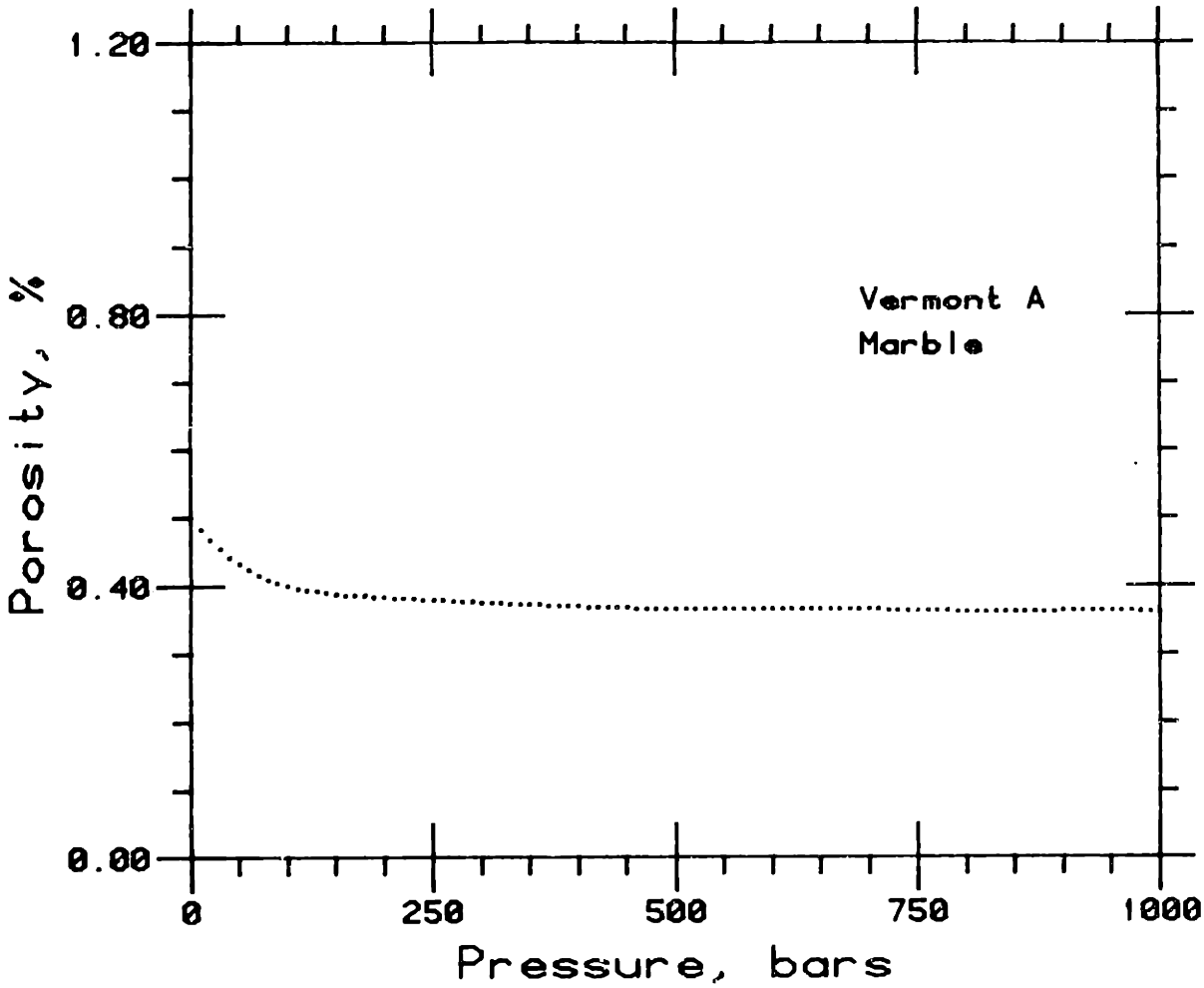


Figure A-2c. Porosity versus confining pressure for Vermont marble calculated from jacketed and unjacketed volumetric strain measurements.

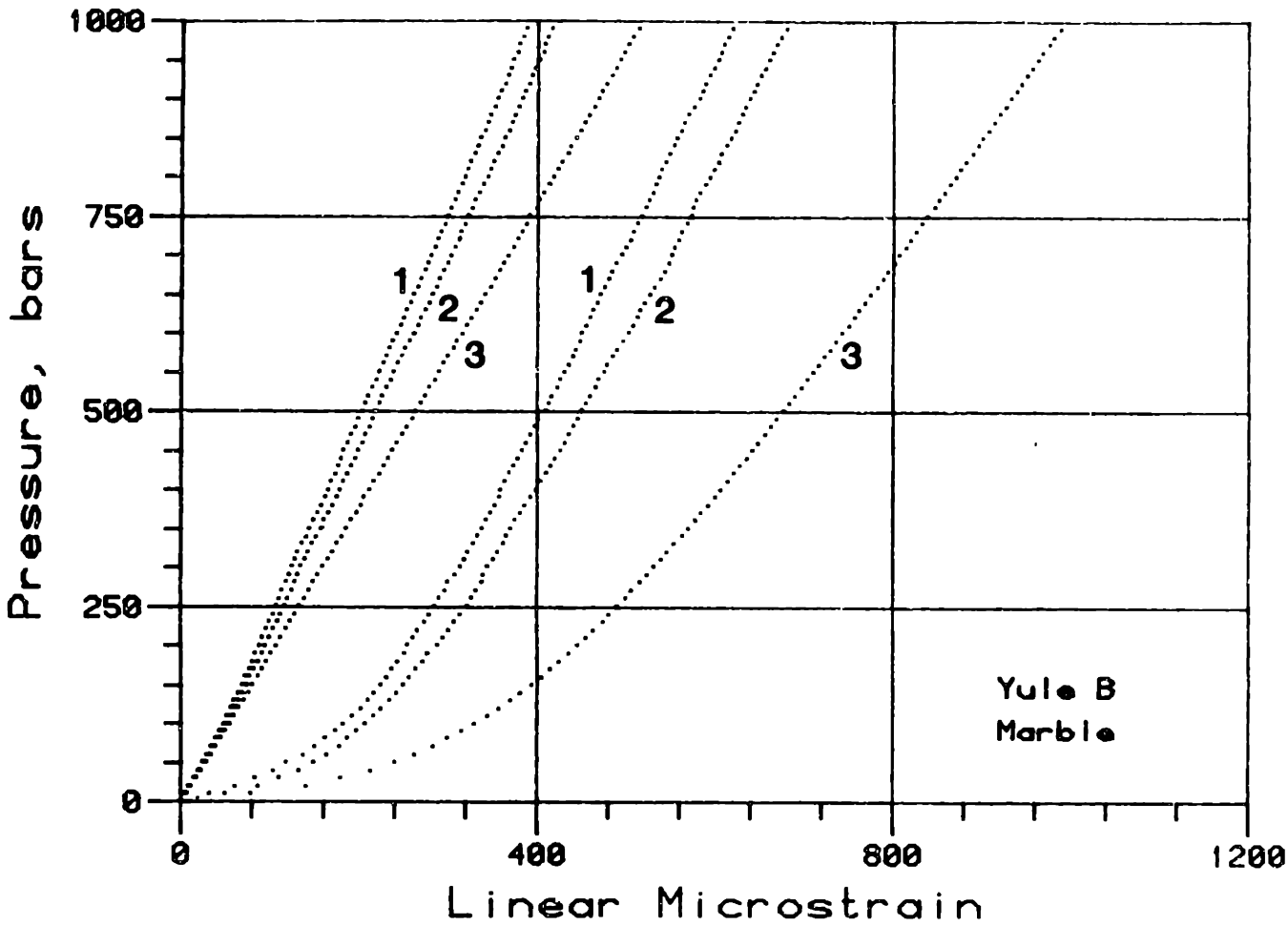


Figure A-3a. Unjacketed and jacketed linear stress-strain measurments for Yule marble. Numbers correspond to 3 directions; direction 3 is approximately perpendicular to foliation.

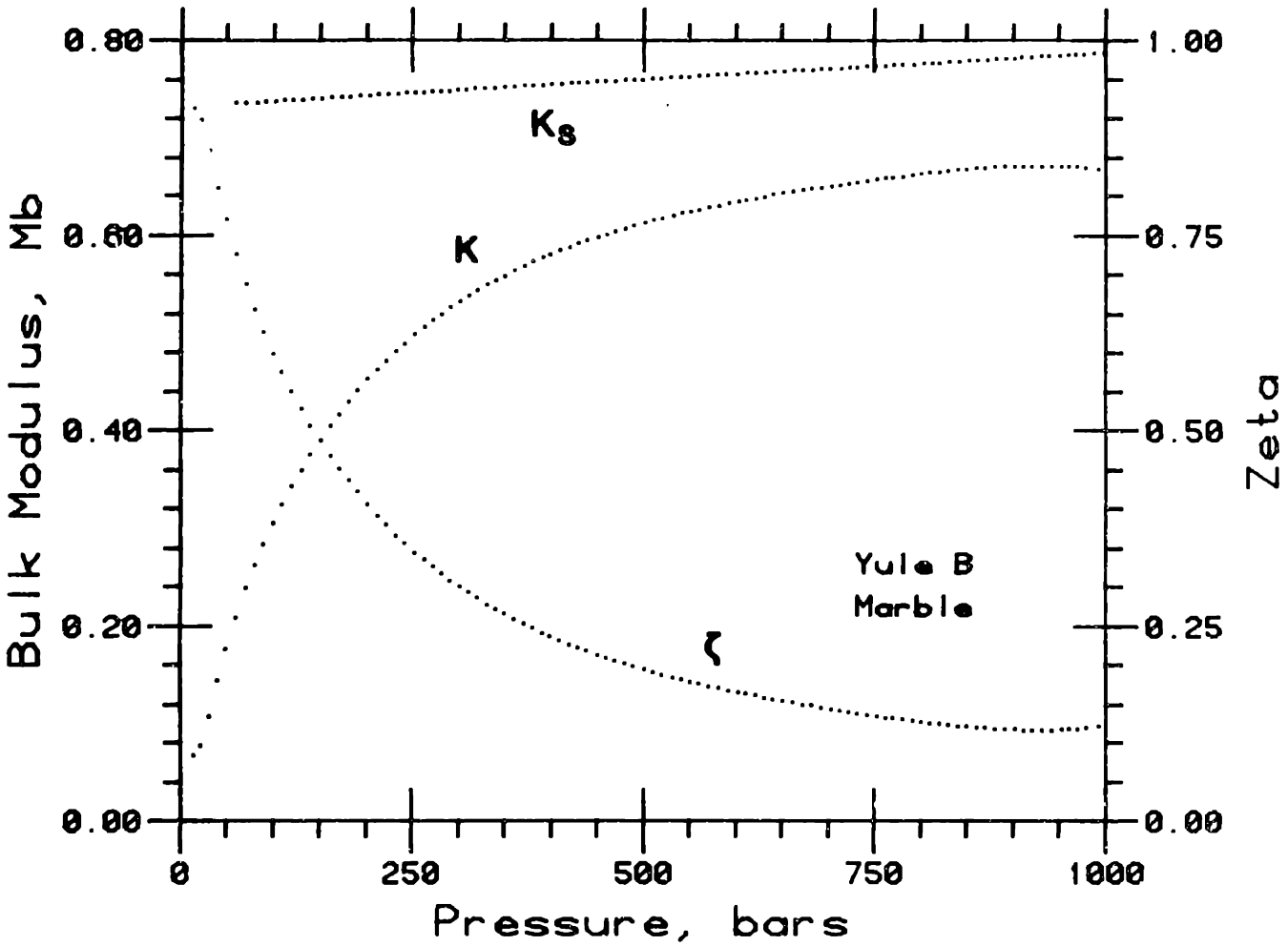


Figure A-3b. Jacketed bulk modulus $K$, unjacketed bulk modulus $K_s$, and $\zeta$ as a function of confining pressure for Yule marble.

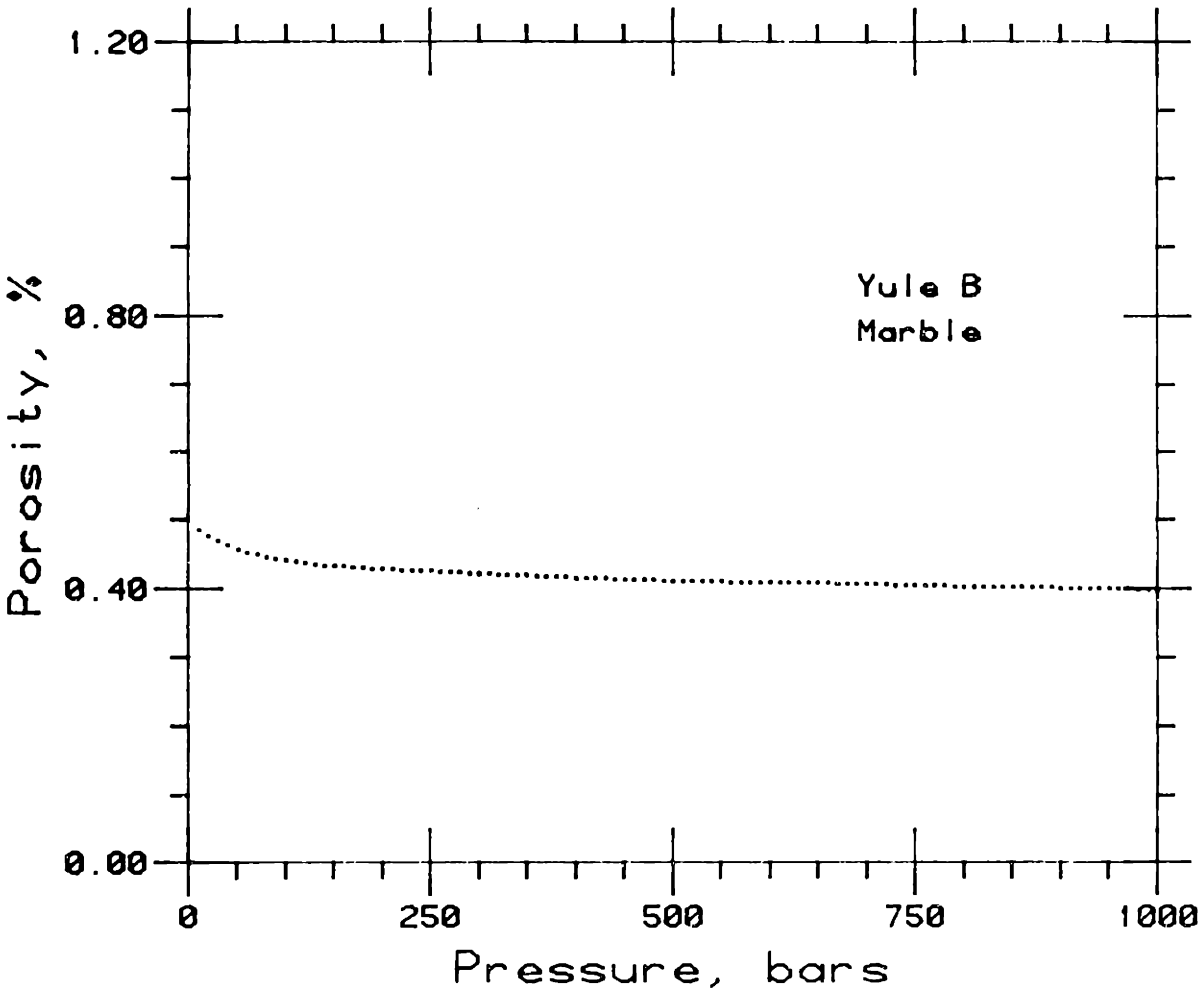


Figure A-3c. Porosity versus confining pressure for Yule marble calculated from jacketed and unjacketed volumetric strain measurements.

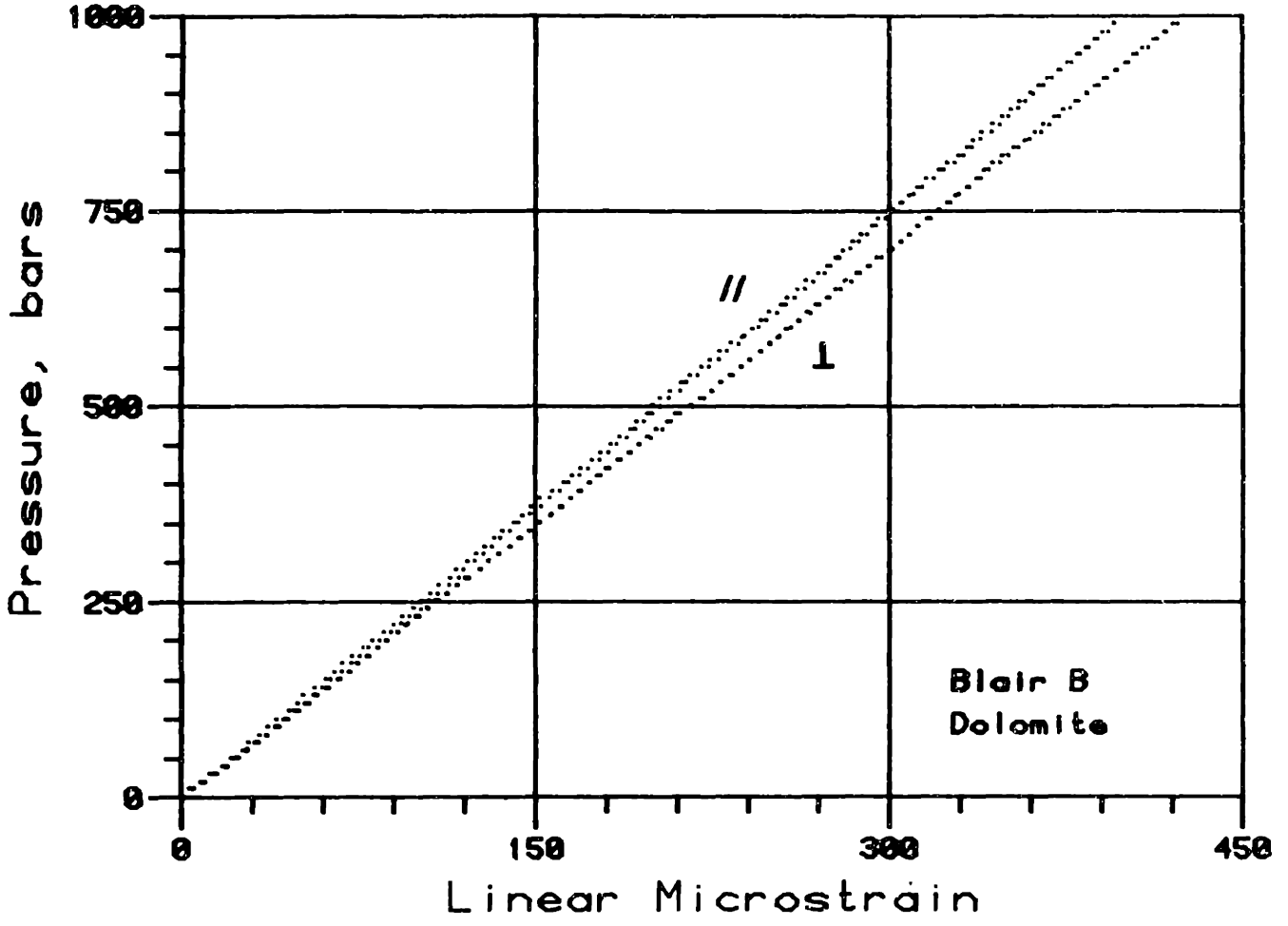


Figure A-4a. Unjacketed and jacketed linear stress-strain measurements for Blair dolomite.

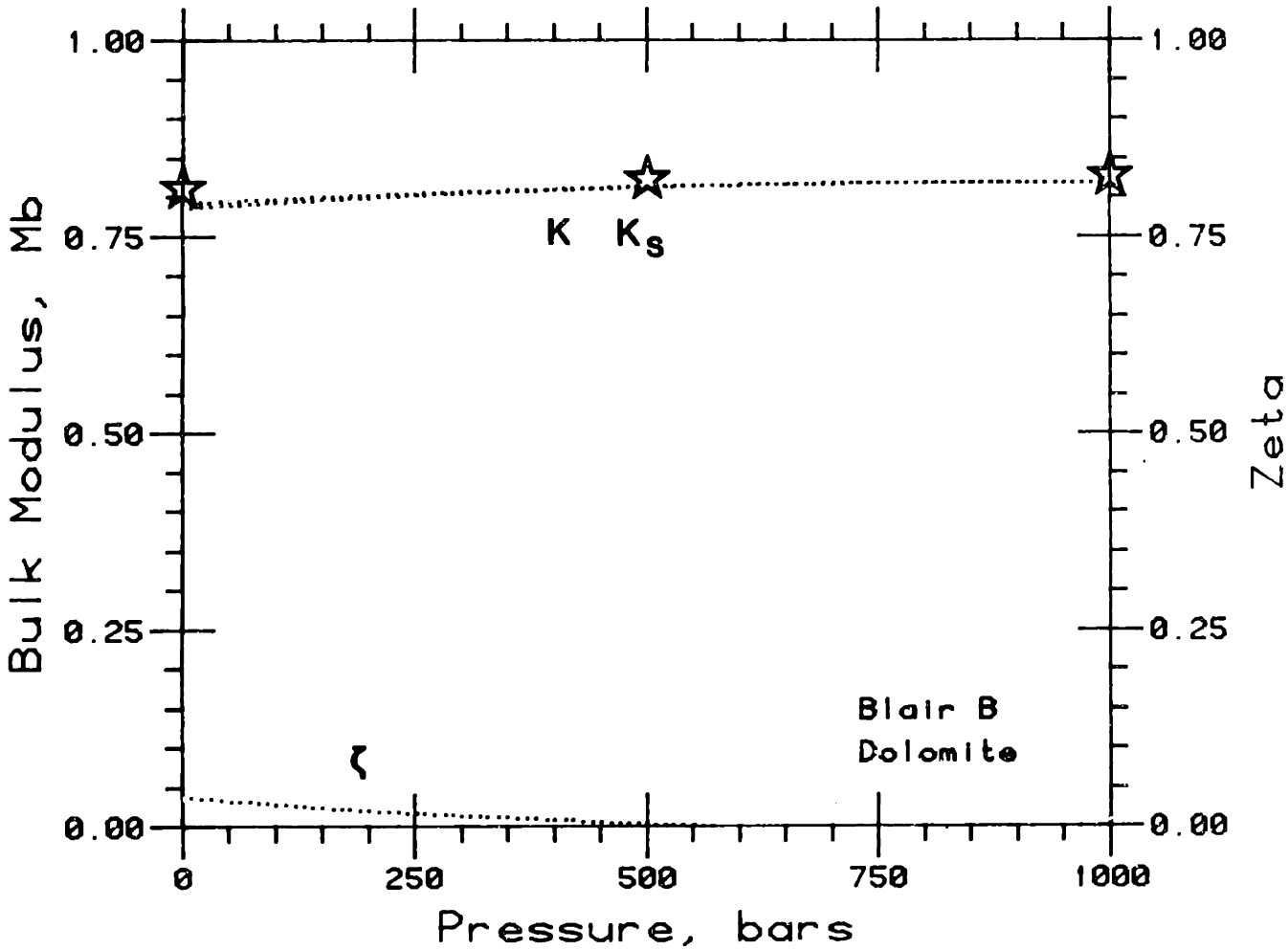


Figure A-4b. Jacketed bulk modulus $K$, unjacketed bulk modulus $K_s$, and $\zeta$ as a function of confining pressure for Blair dolomite. Stars represent bulk moduli reported by Brace (1965).

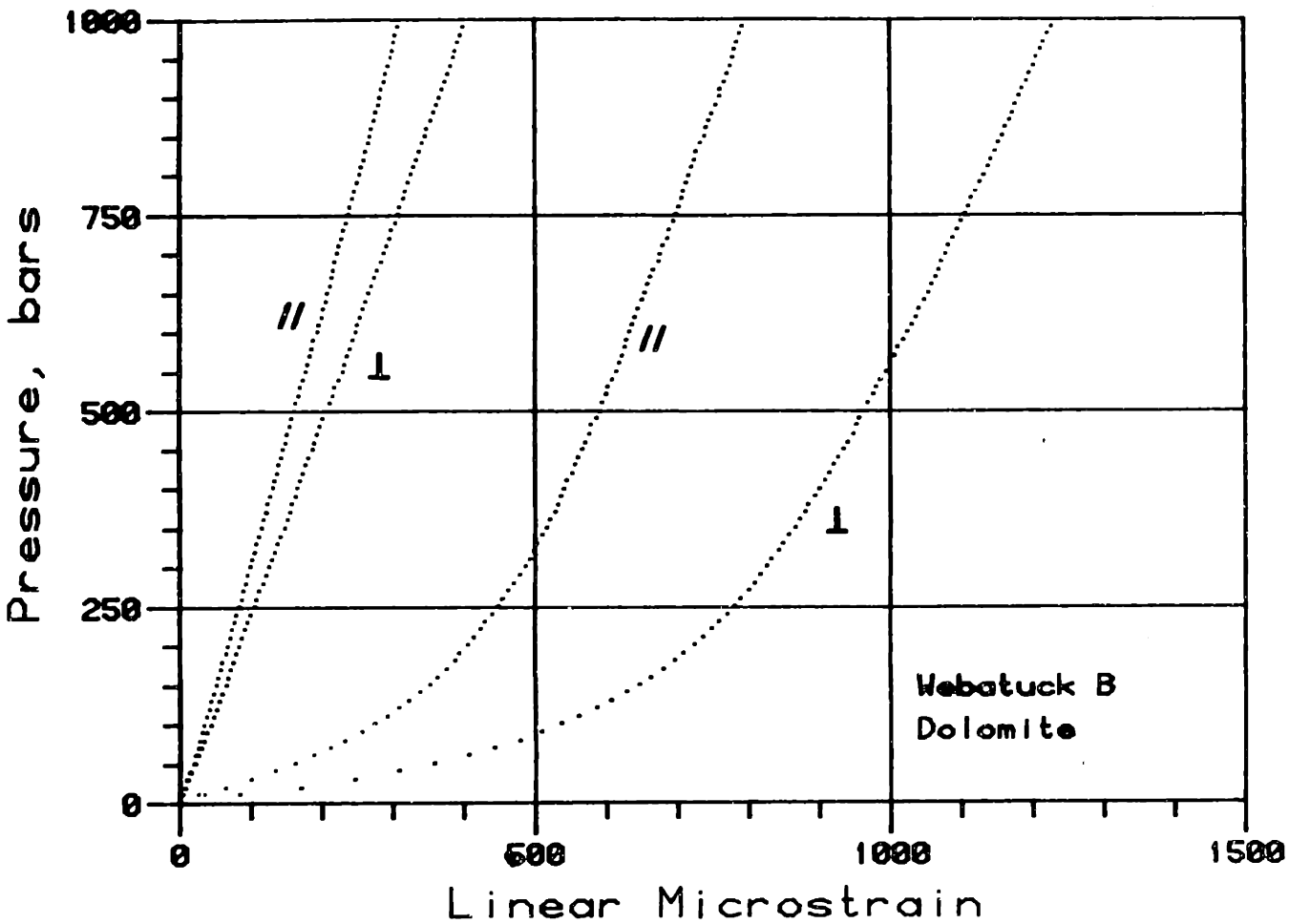


Figure A-5a. Unjacketed and jacketed linear stress-strain measurements for Webatuck dolomite. Symbols correspond to measurements parallel and perpendicular to foliation.

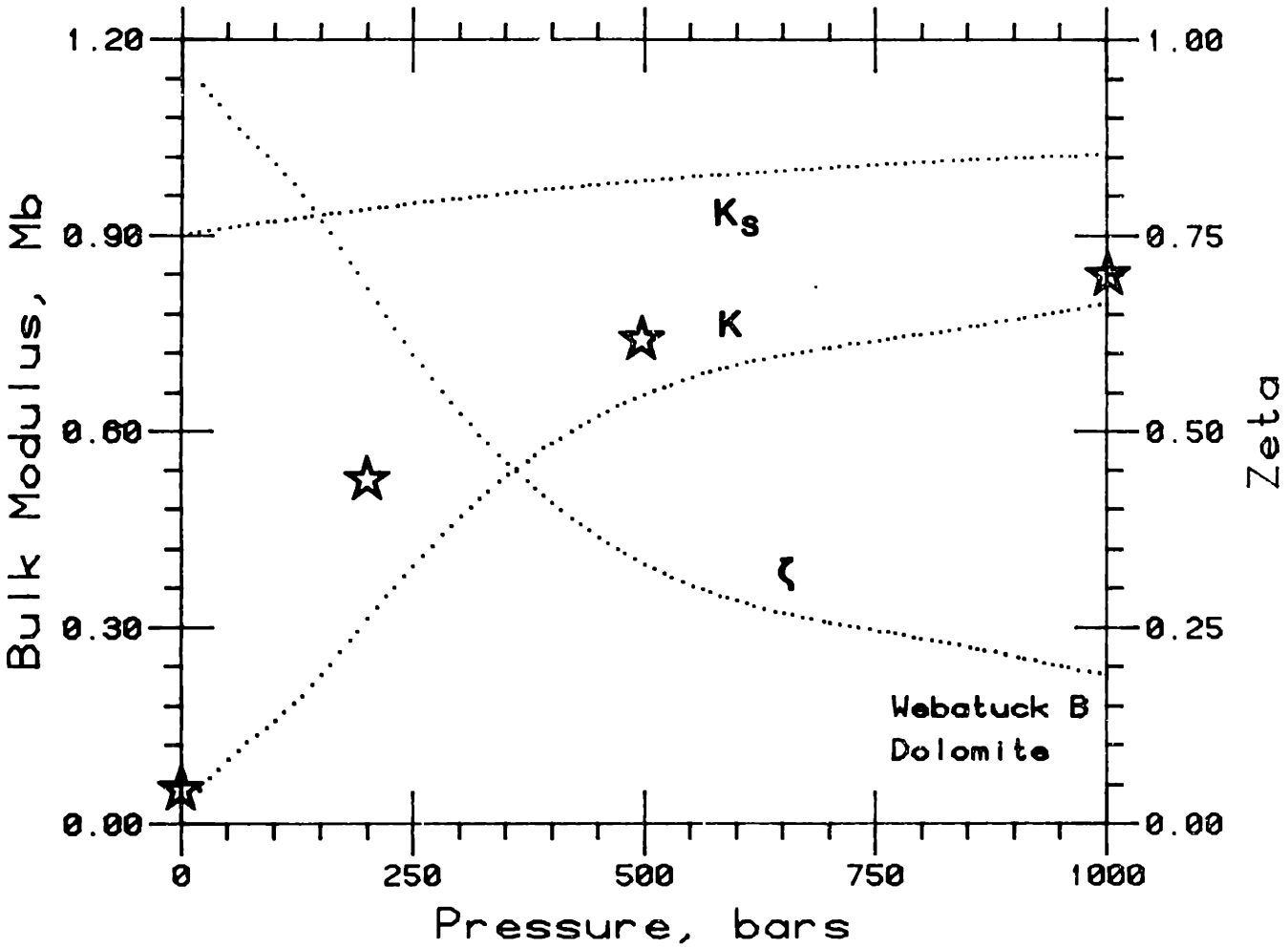


Figure A-5b. Jacketed bulk modulus $K$, unjacketed bulk modulus $K_s$, and $\zeta$ as a function of confining pressure for Webatuck dolomite. Stars represent bulk moduli reported by Brace (1965).

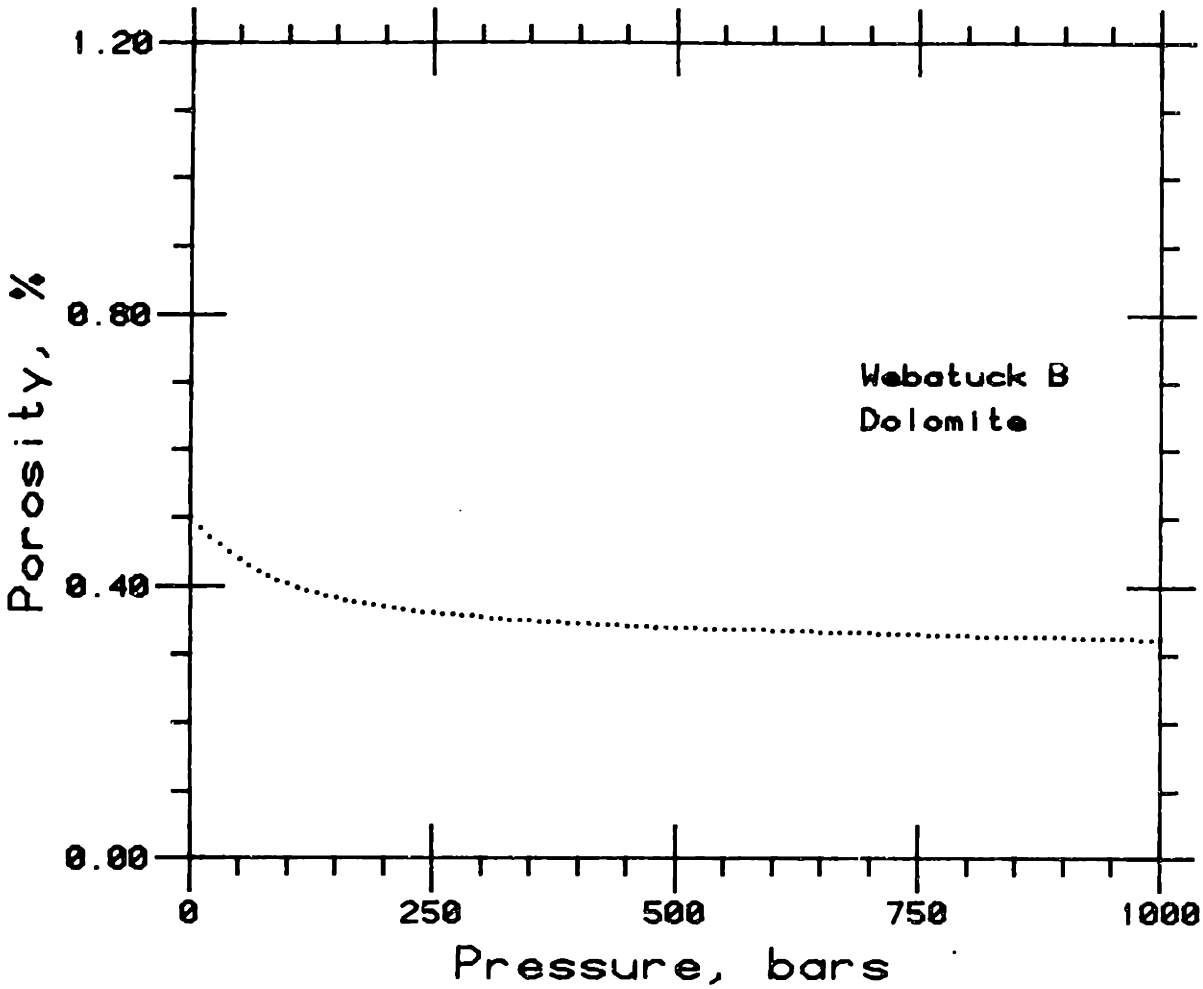


Figure A-5c. Porosity versus confining pressure for Webatuck dolomite calculated from jacketed and unjacketed volumetric strain measurements.

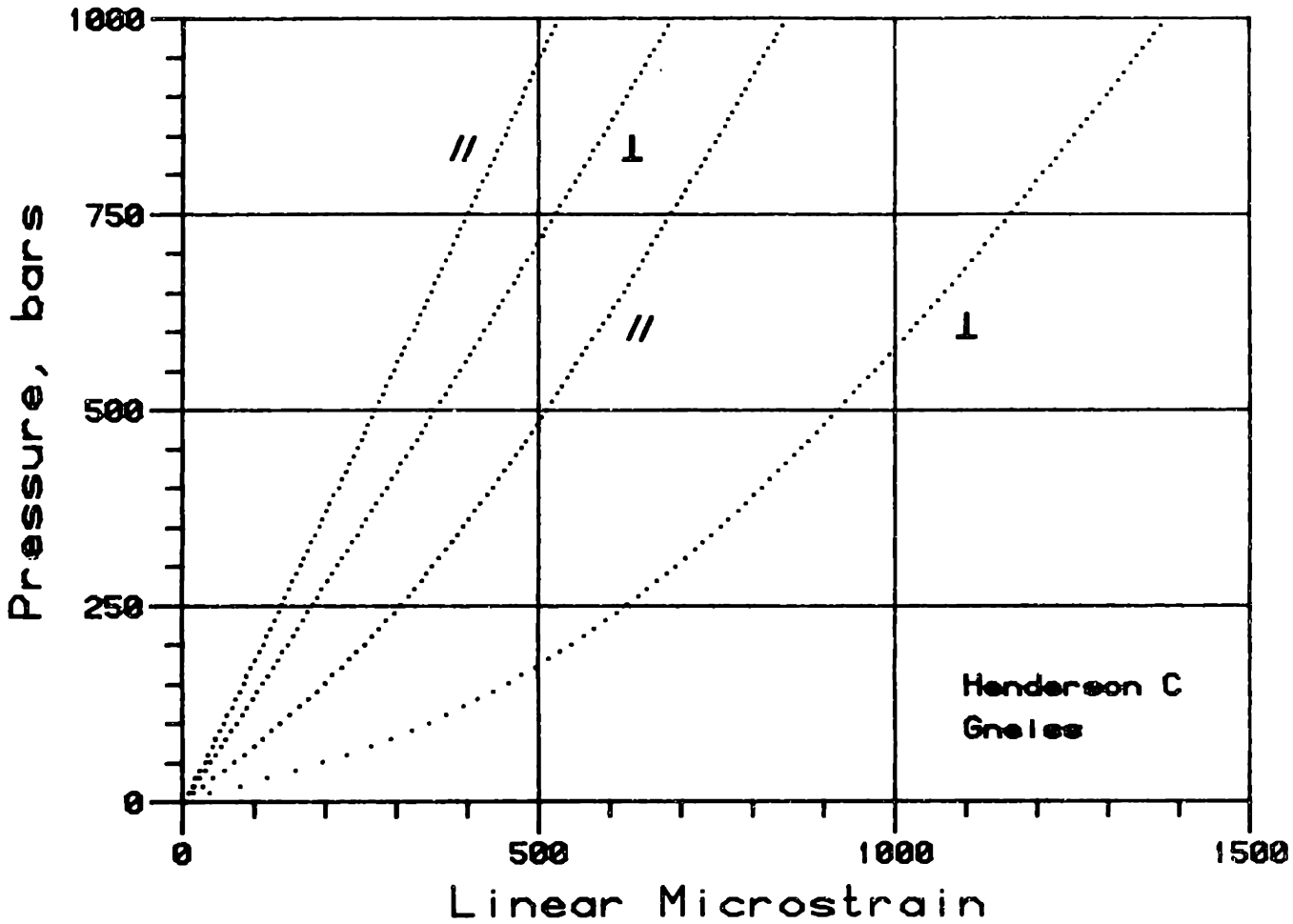


Figure A-6a. Unjacketed and jacketed linear stress-strain measurements for Henderson Augen gneiss. Symbols correspond to measurements parallel and perpendicular to foliation.

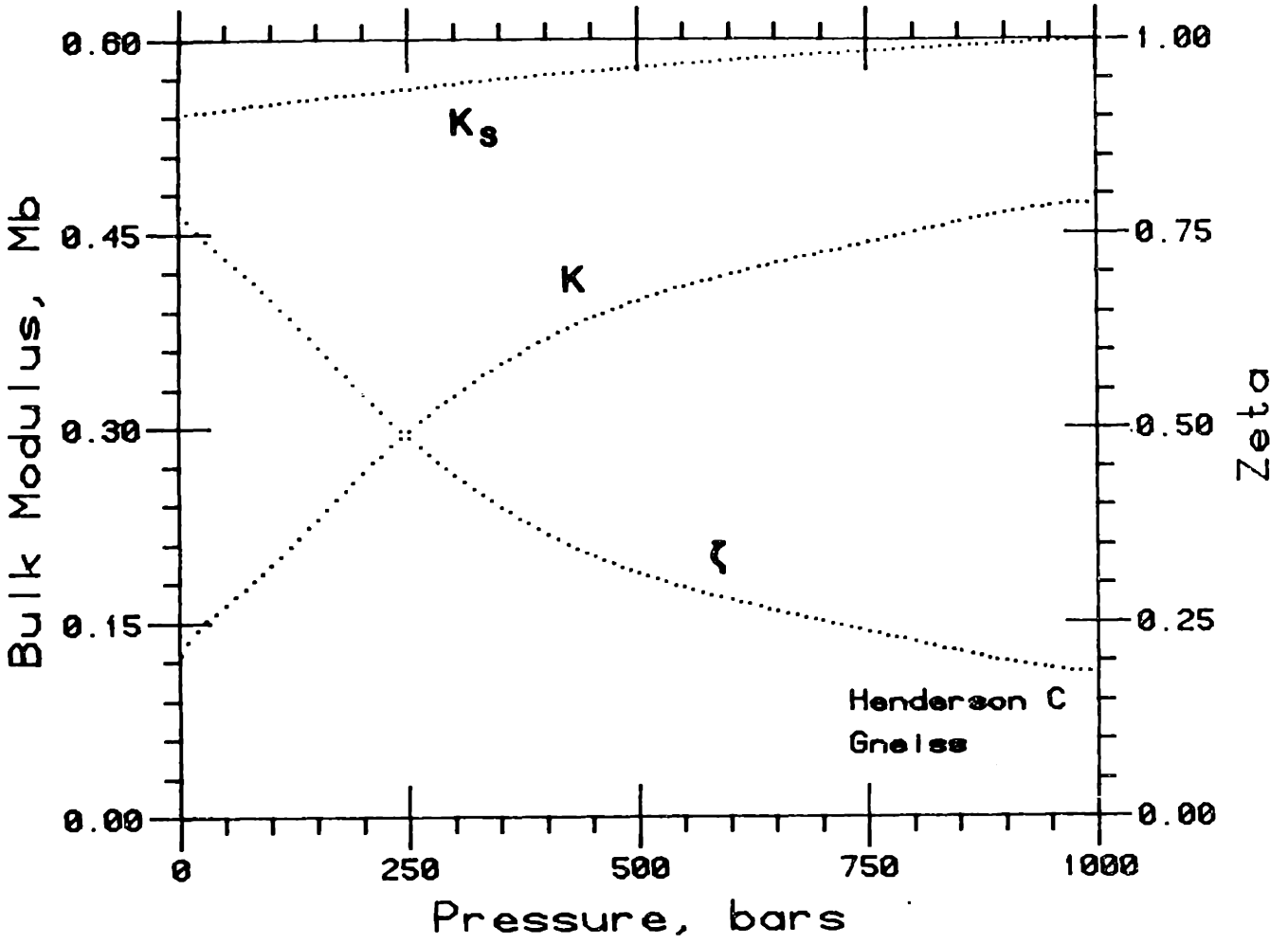


Figure A-6b. Jacketed bulk modulus $K$, unjacketed bulk modulus $K_s$, and $\zeta$ as a function of confining pressure for Henderson Augen gneiss.

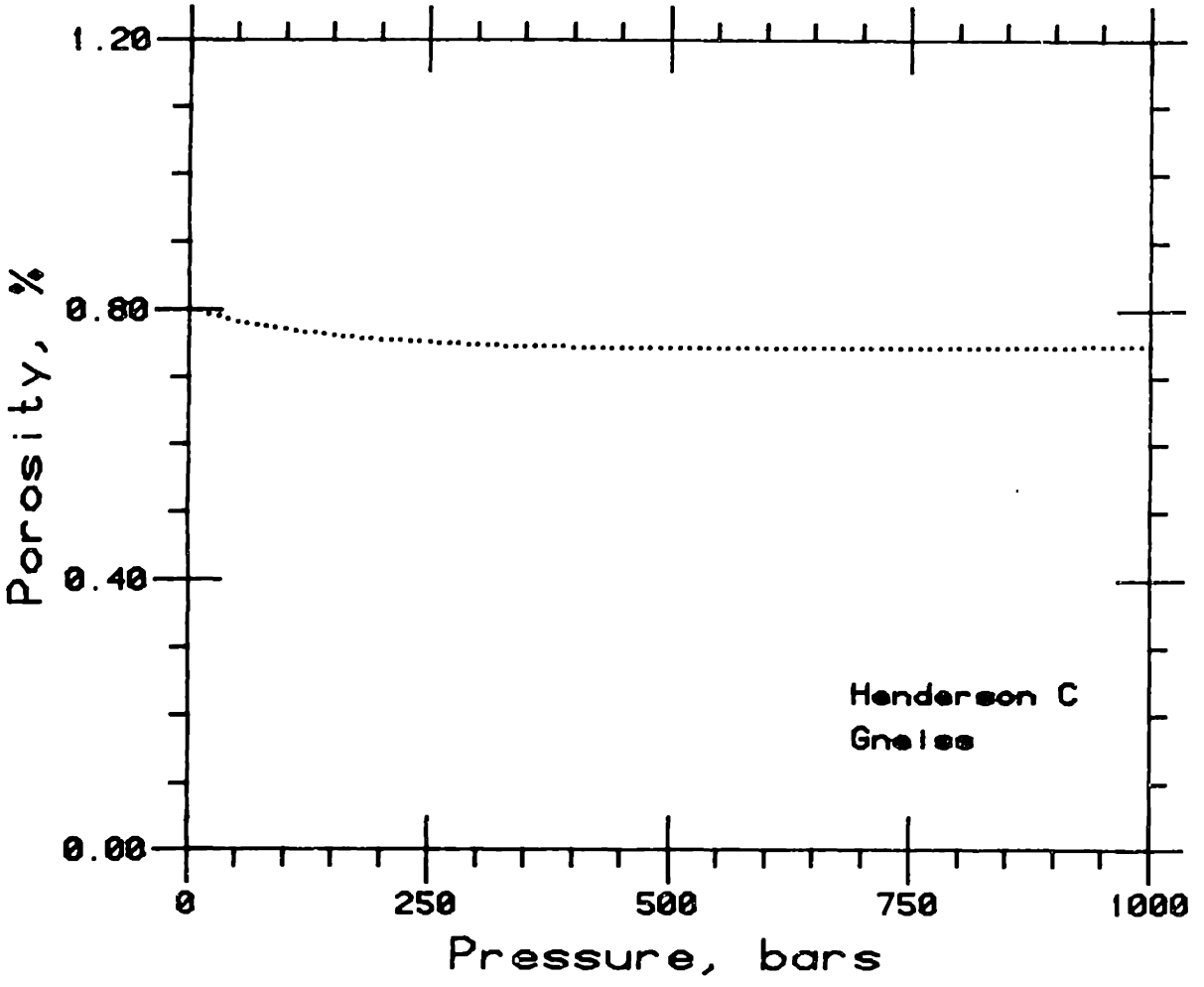


Figure A-6c. Porosity versus confining pressure for Henderson Augen gneiss calculated from jacketed and unjacketed volumetric strain measurements.

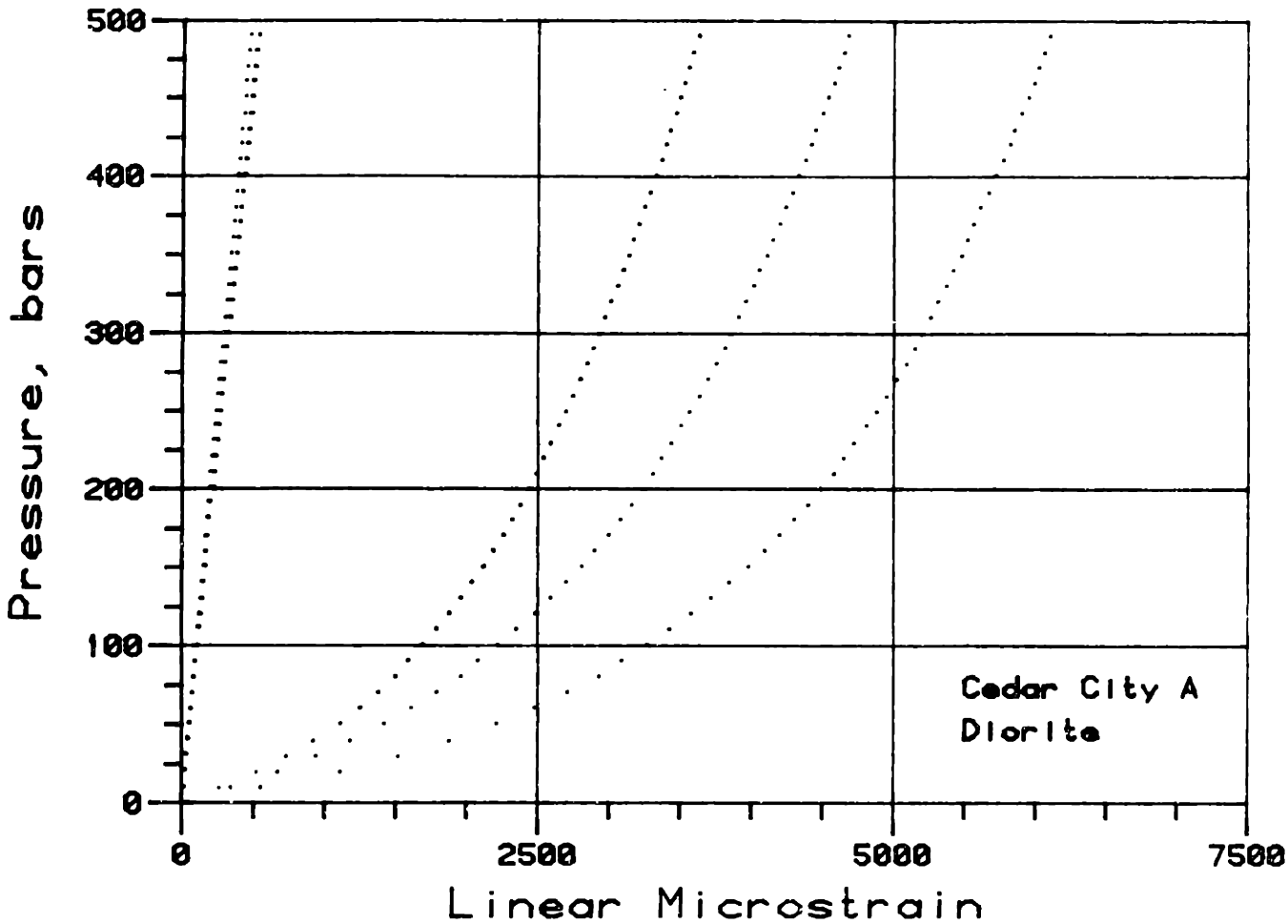


Figure A-7a. Unjacketed and jacketed linear stress-strain measurements for Cedar City quartz diorite.

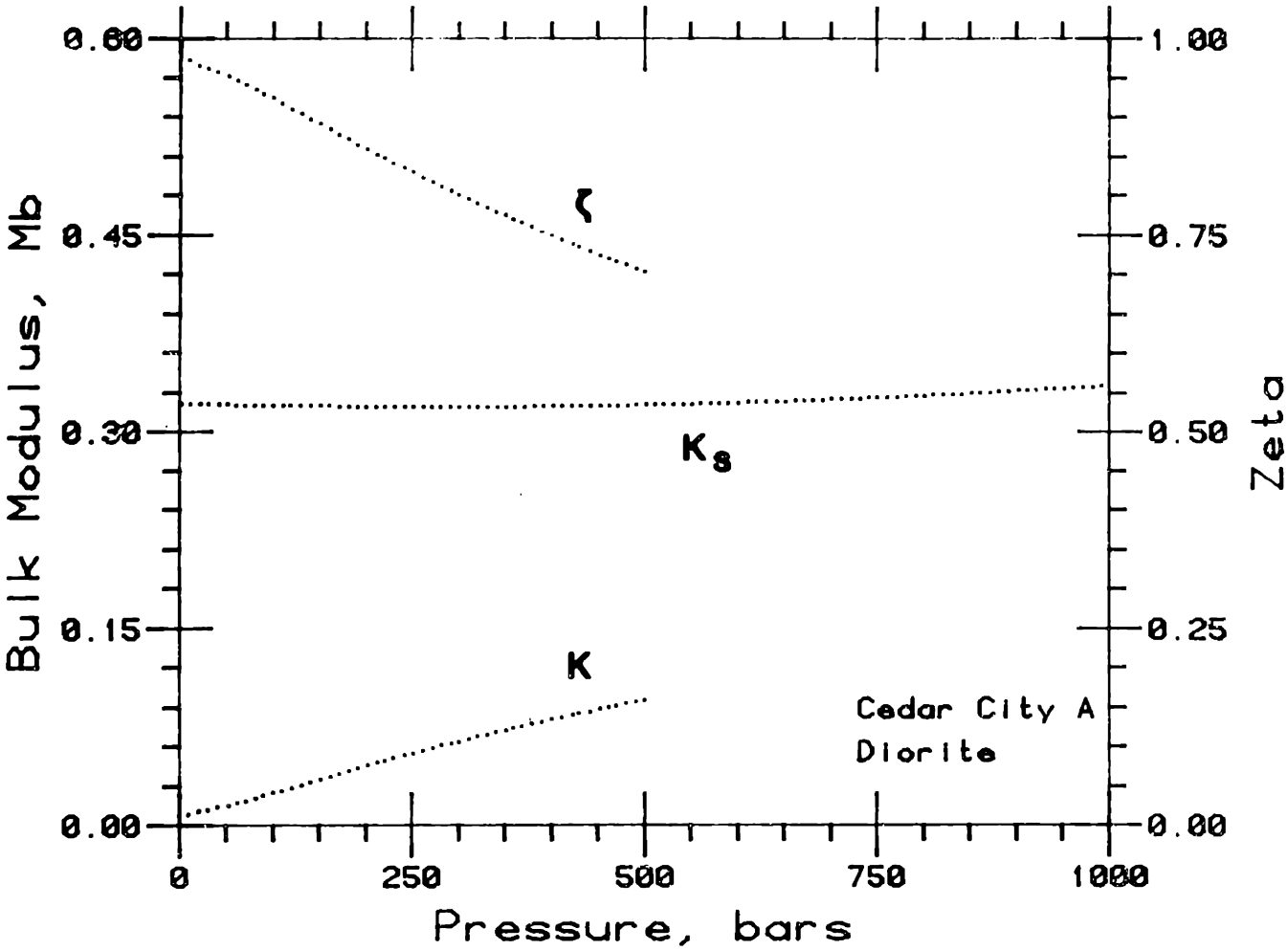


Figure A-7b. Jacketed bulk modulus $K$, unjacketed bulk modulus $K_s$, and $\zeta$ as a function of confining pressure for Cedar City quartz diorite.

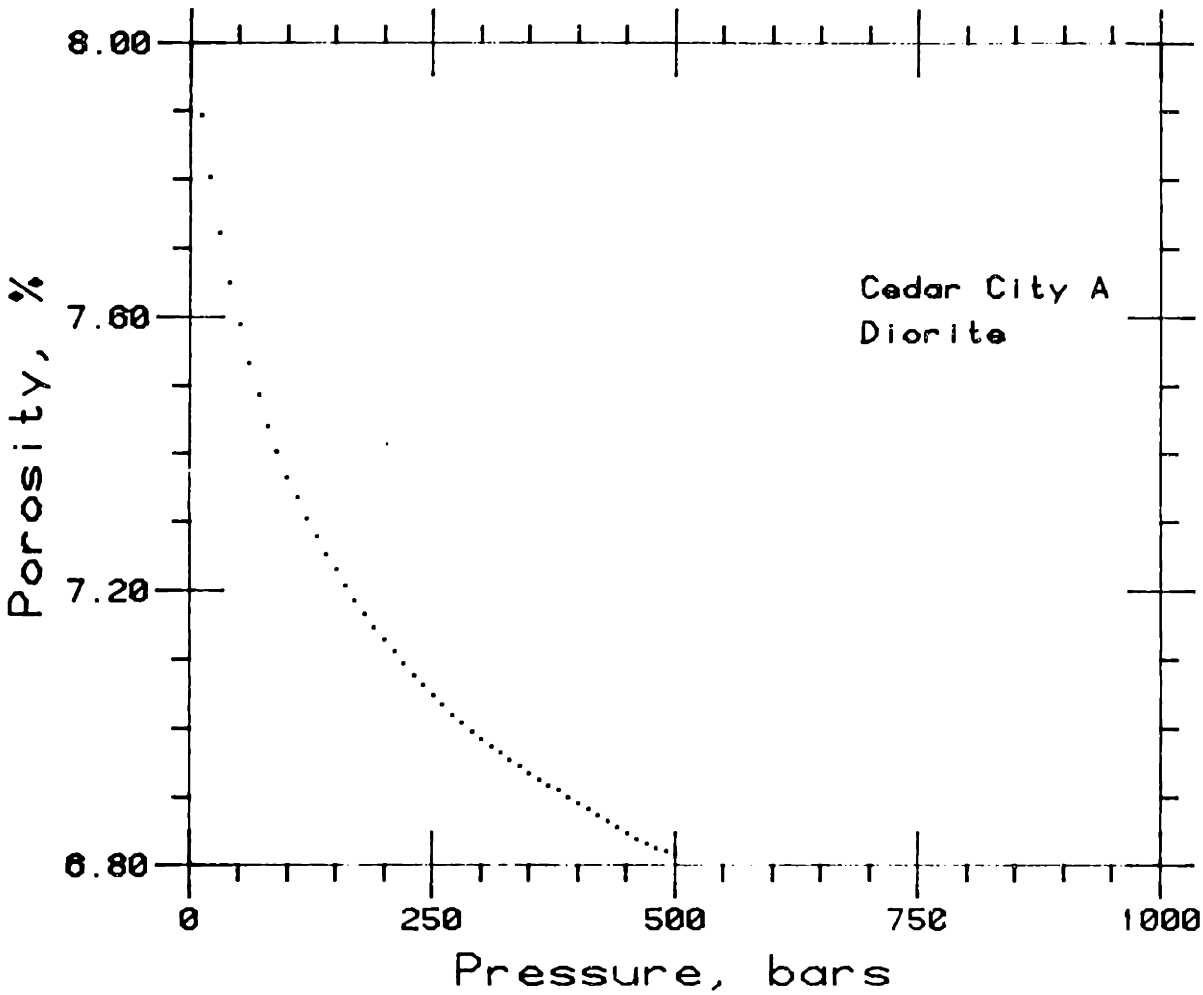


Figure A-7c. Porosity versus confining pressure for Cedar City quartz diorite calculated from jacketed and unjacketed volumetric strain measurements.

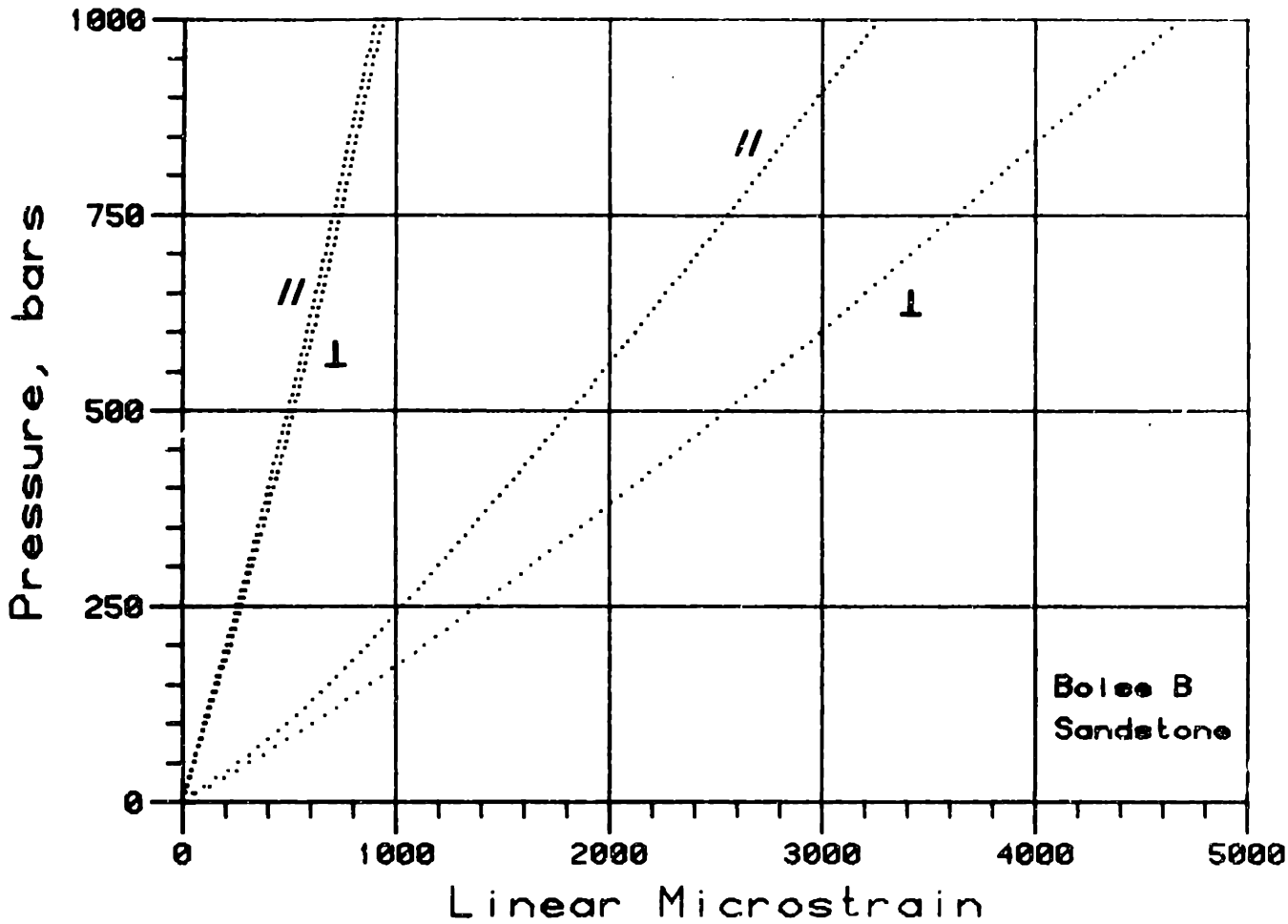


Figure A-8a. Unjacketed and jacketed linear stress-strain measurements for Boise sandstone. Symbols correspond to measurements parallel and perpendicular to bedding.

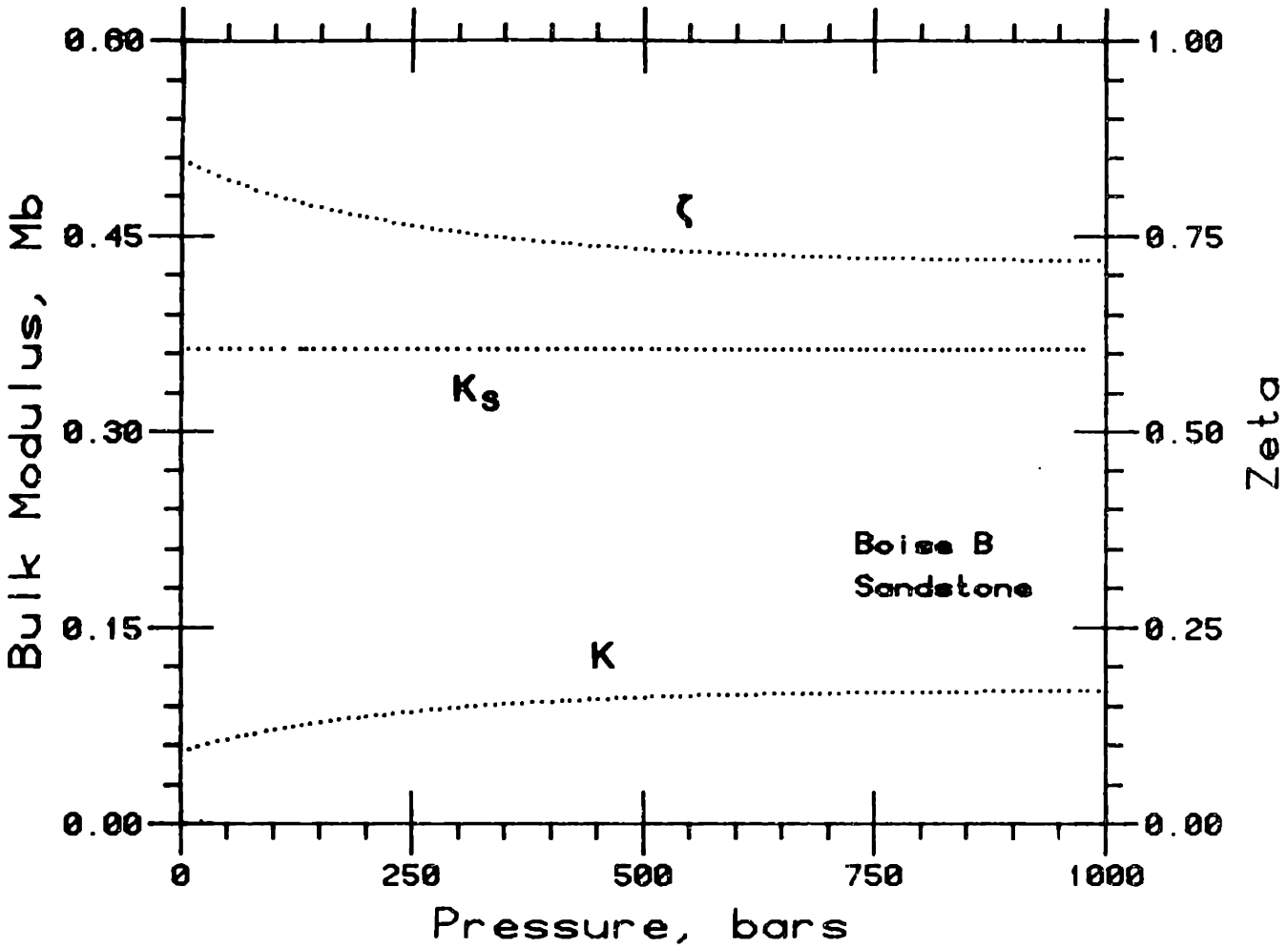


Figure A-8b. Jacketed bulk modulus $K$, unjacketed bulk modulus $K_s$, and $\zeta$ as a function of confining pressure for Boise sandstone.

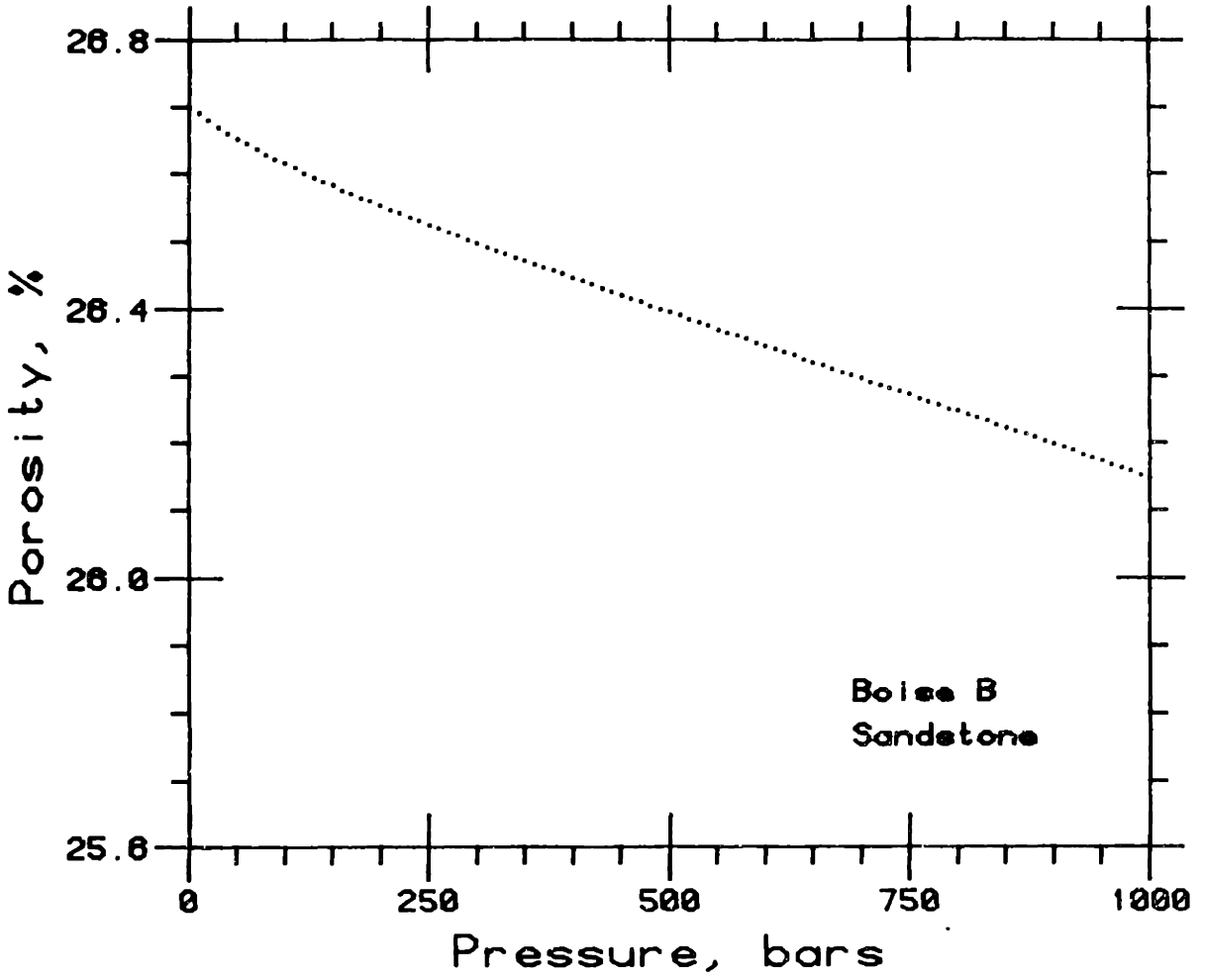


Figure A-8c. Porosity versus confining pressure for Boise sandstone calculated from jacketed and unjacketed volumetric strain measurements.

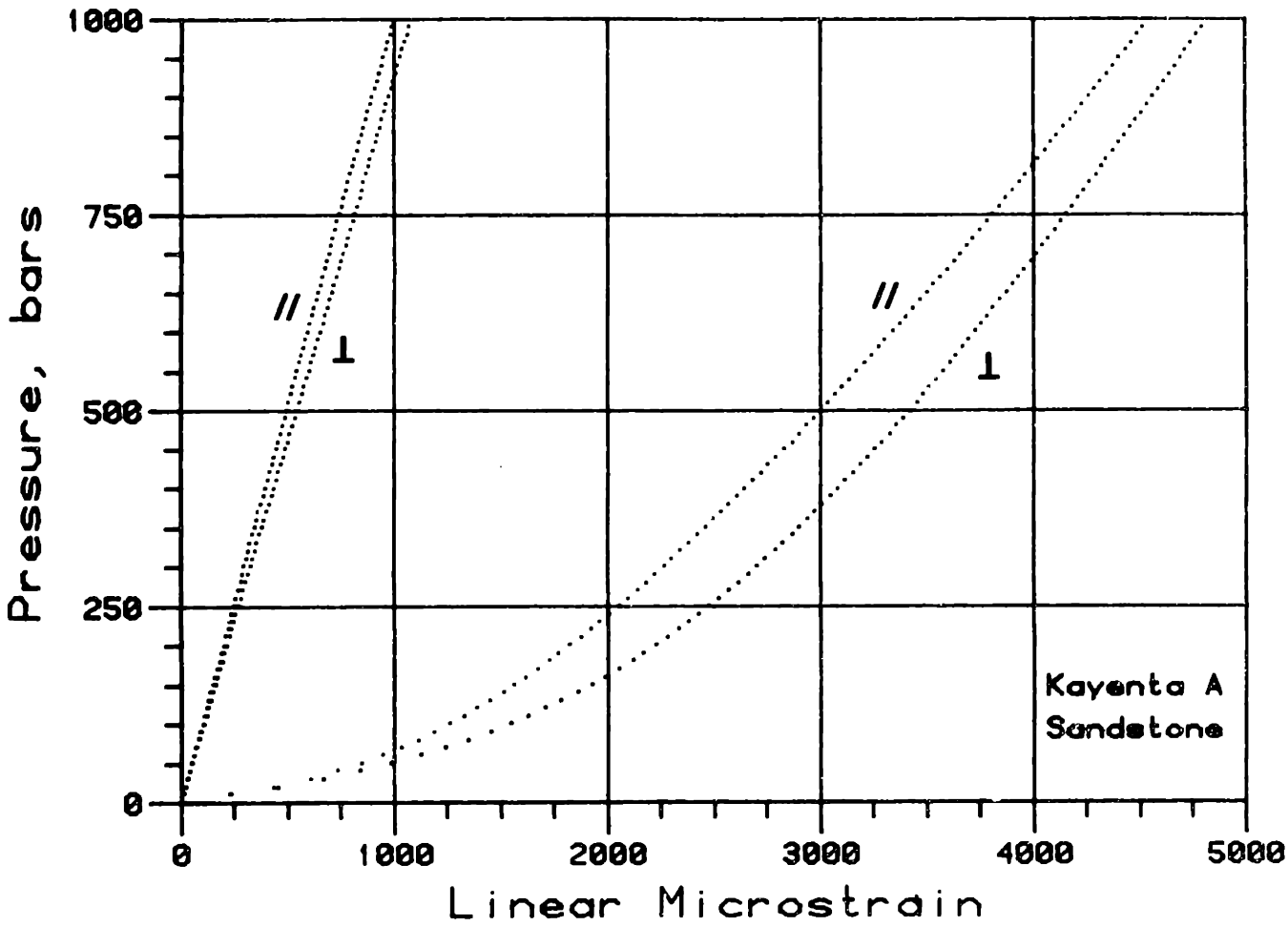


Figure A-9a. Unjacketed and jacketed linear stress-strain measurements for Kayenta sandstone. Symbols correspond to measurements parallel and perpendicular to apparent bedding.

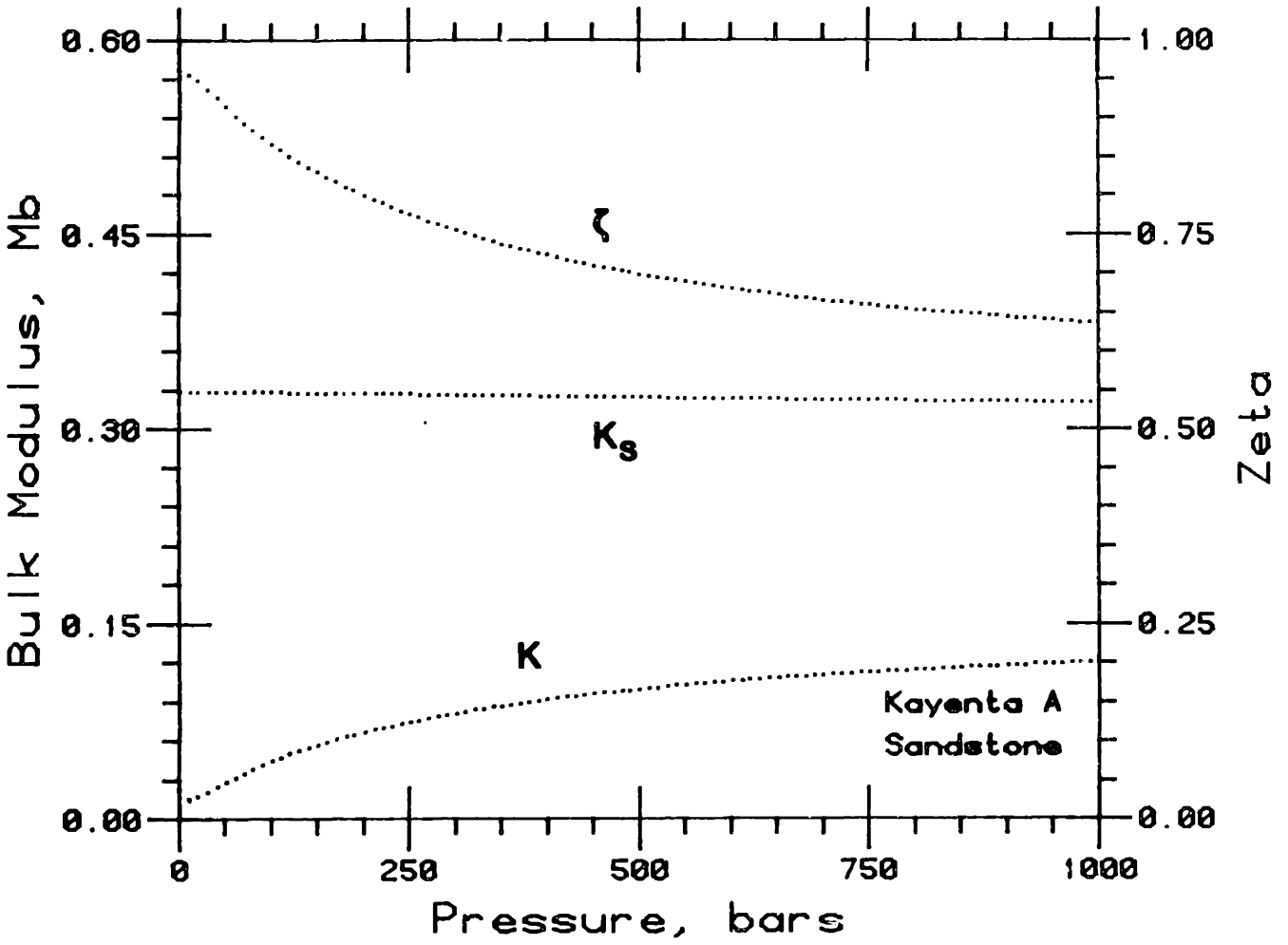


Figure A-9b. Jacketed bulk modulus $K$, unjacketed bulk modulus $K_s$, and $\zeta$ as a function of confining pressure for Kayenta sandstone.

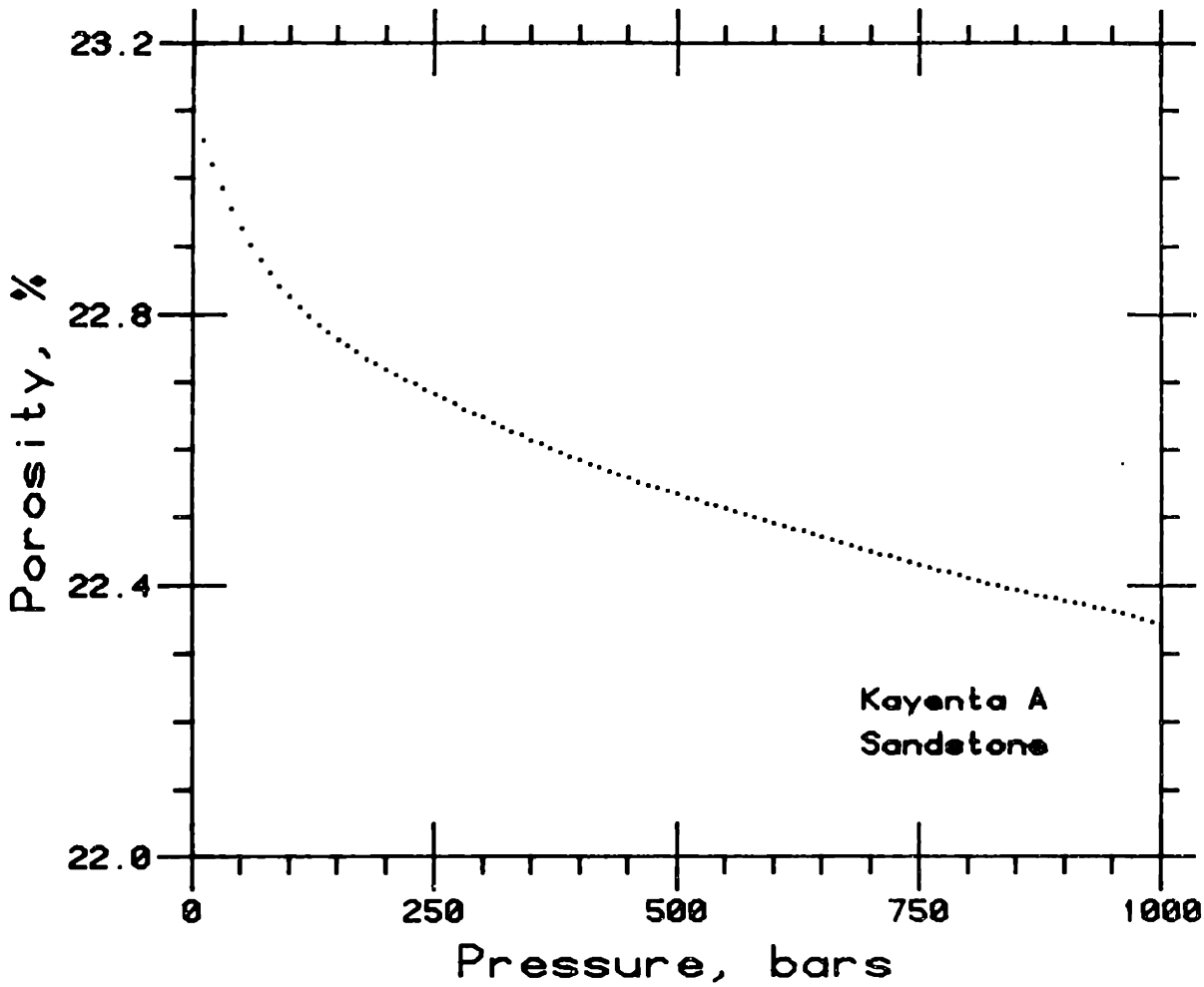


Figure A-9c. Porosity versus confining pressure for Kayenta sandstone calculated from jacketed and unjacketed volumetric strain measurements.

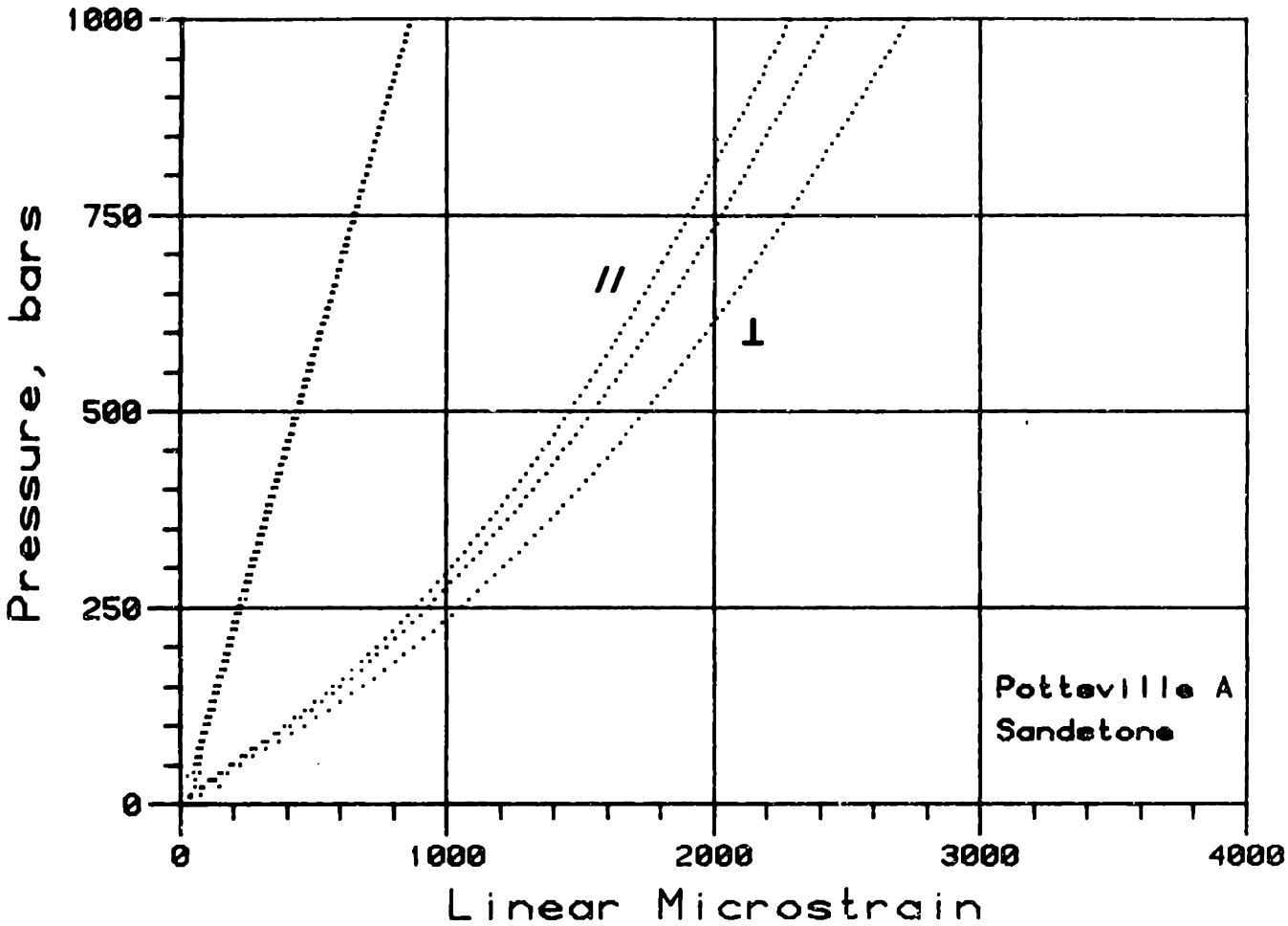


Figure A-10a. Unjacketed and jacketed linear stress-strain measurements for Pottsville sandstone. Symbols correspond to measurements parallel and perpendicular to bedding; only two gages used to measure unjacketed strain.

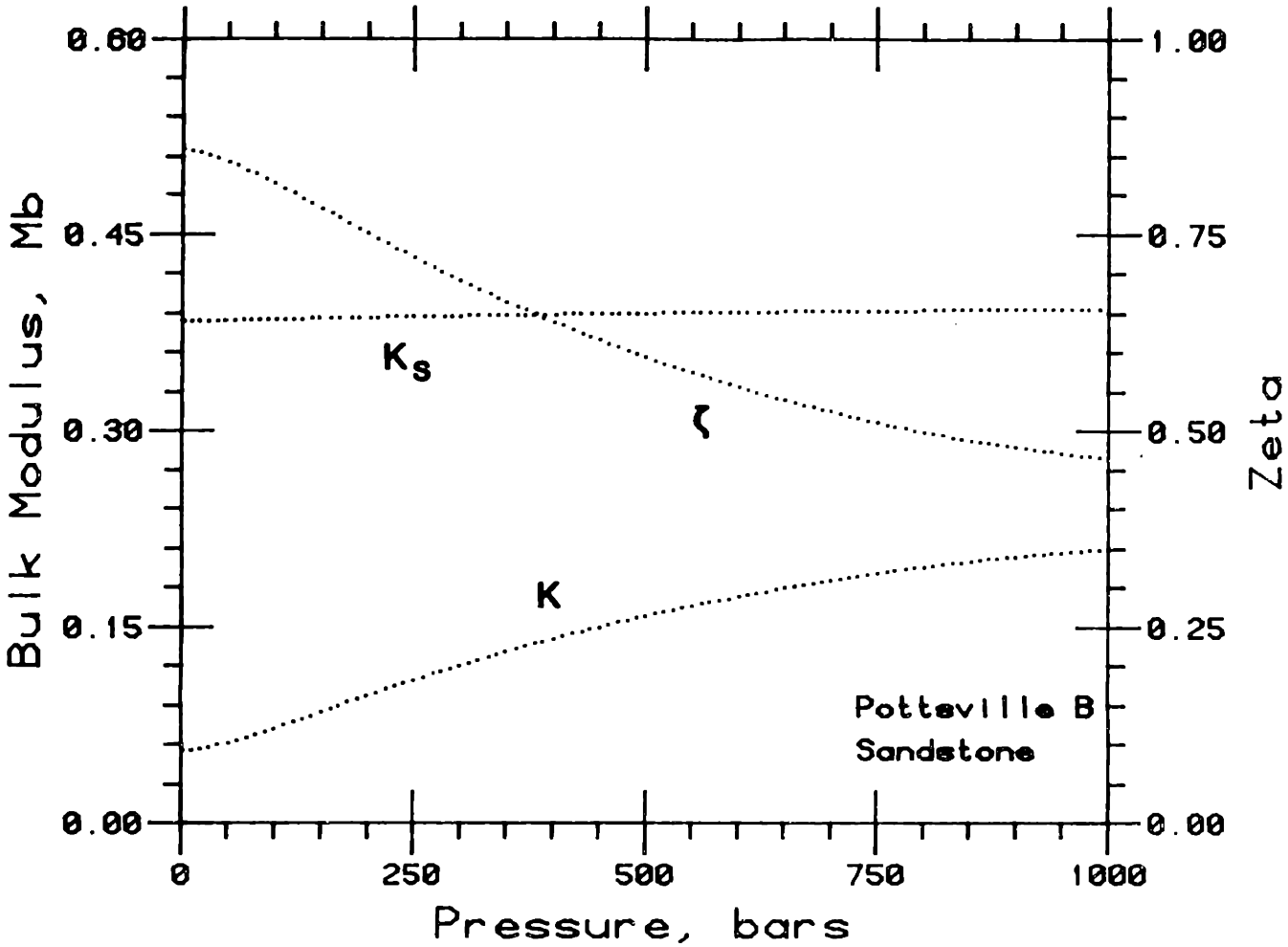


Figure A-10b. Jacketed bulk modulus $K$, unjacketed bulk modulus $K_s$, and $\zeta$ as a function of confining pressure for Pottsville sandstone.

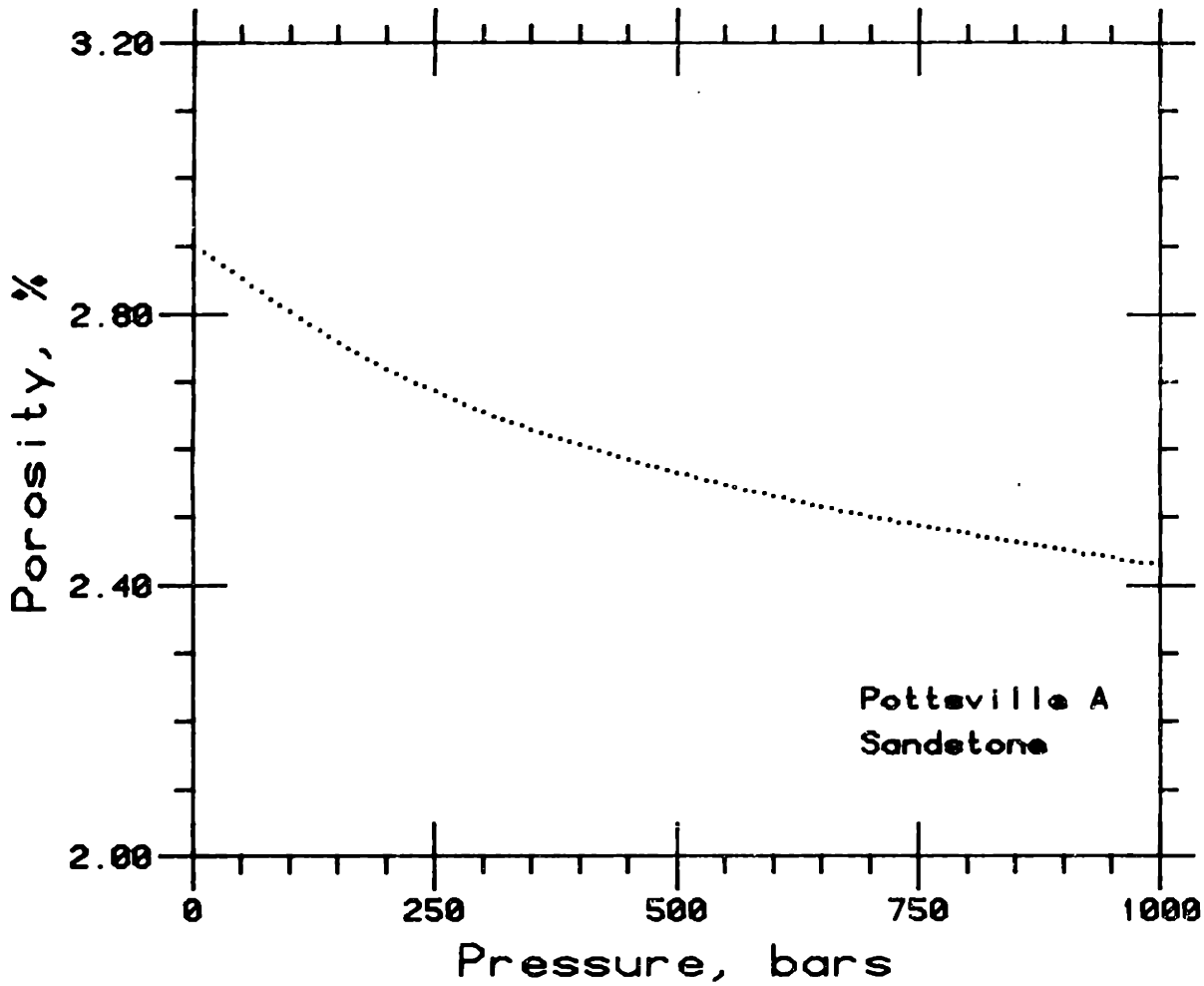


Figure A-10c. Porosity versus confining pressure for Pottsville sandstone calculated from jacketed and unjacketed stress-strain measurements.

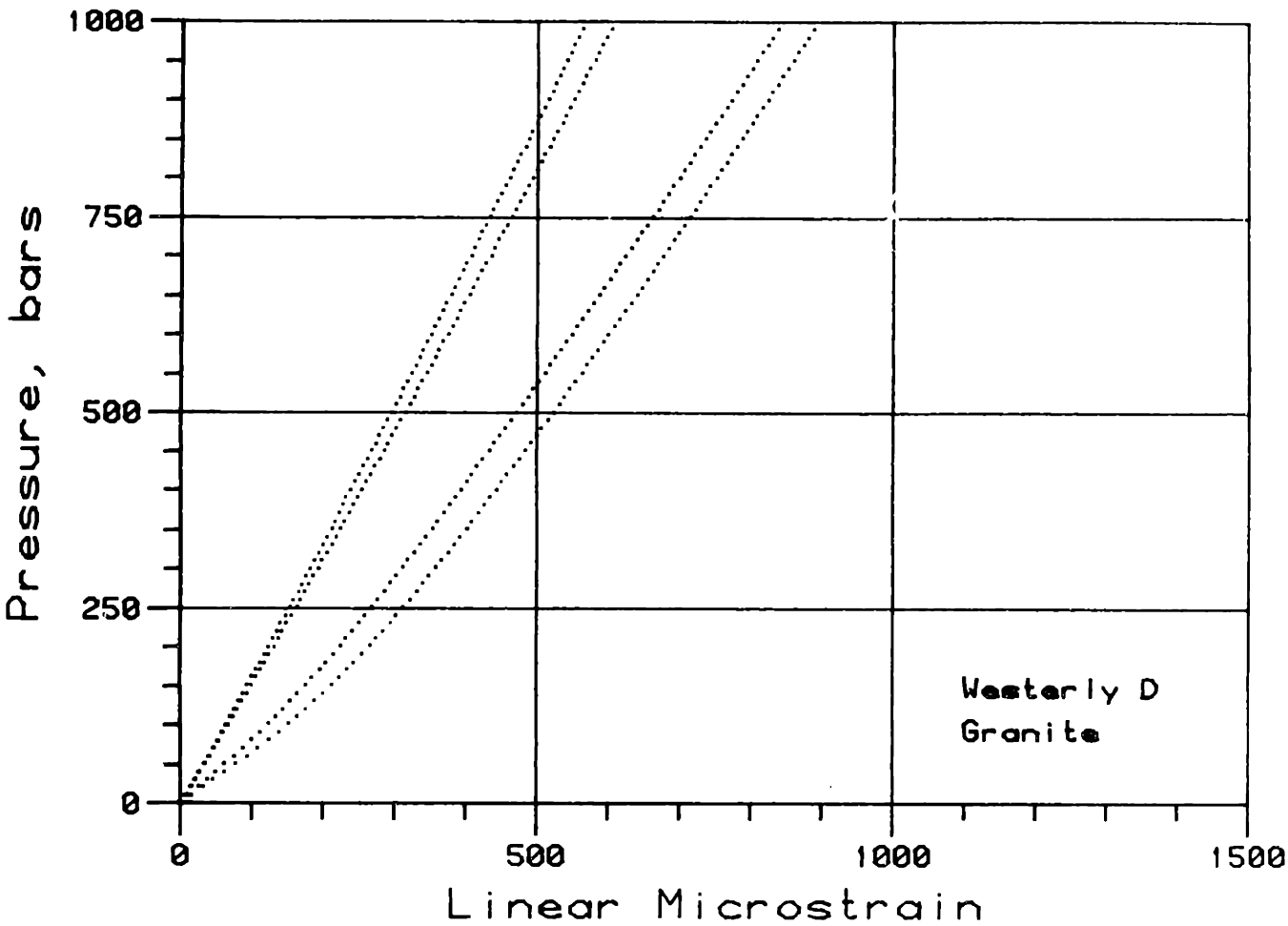


Figure A-11a. Unjacketed and jacketed linear stress-strain measurements for Westerly granite (blue) in two directions.

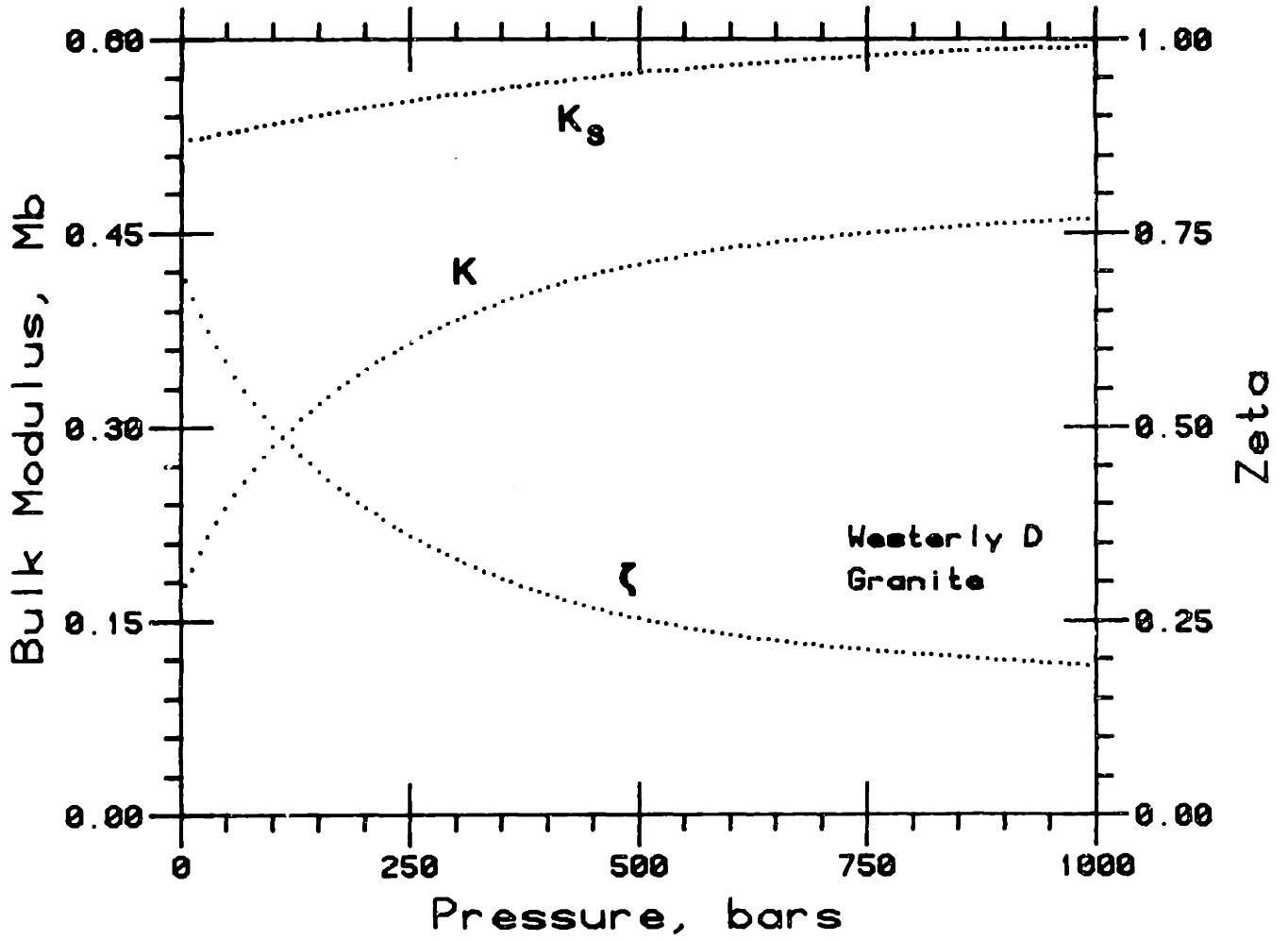


Figure A-11b. Jacketed bulk modulus $K$, unjacketed bulk modulus $K_s$, and $\zeta$ as a function of confining pressure for Westerly granite (blue).

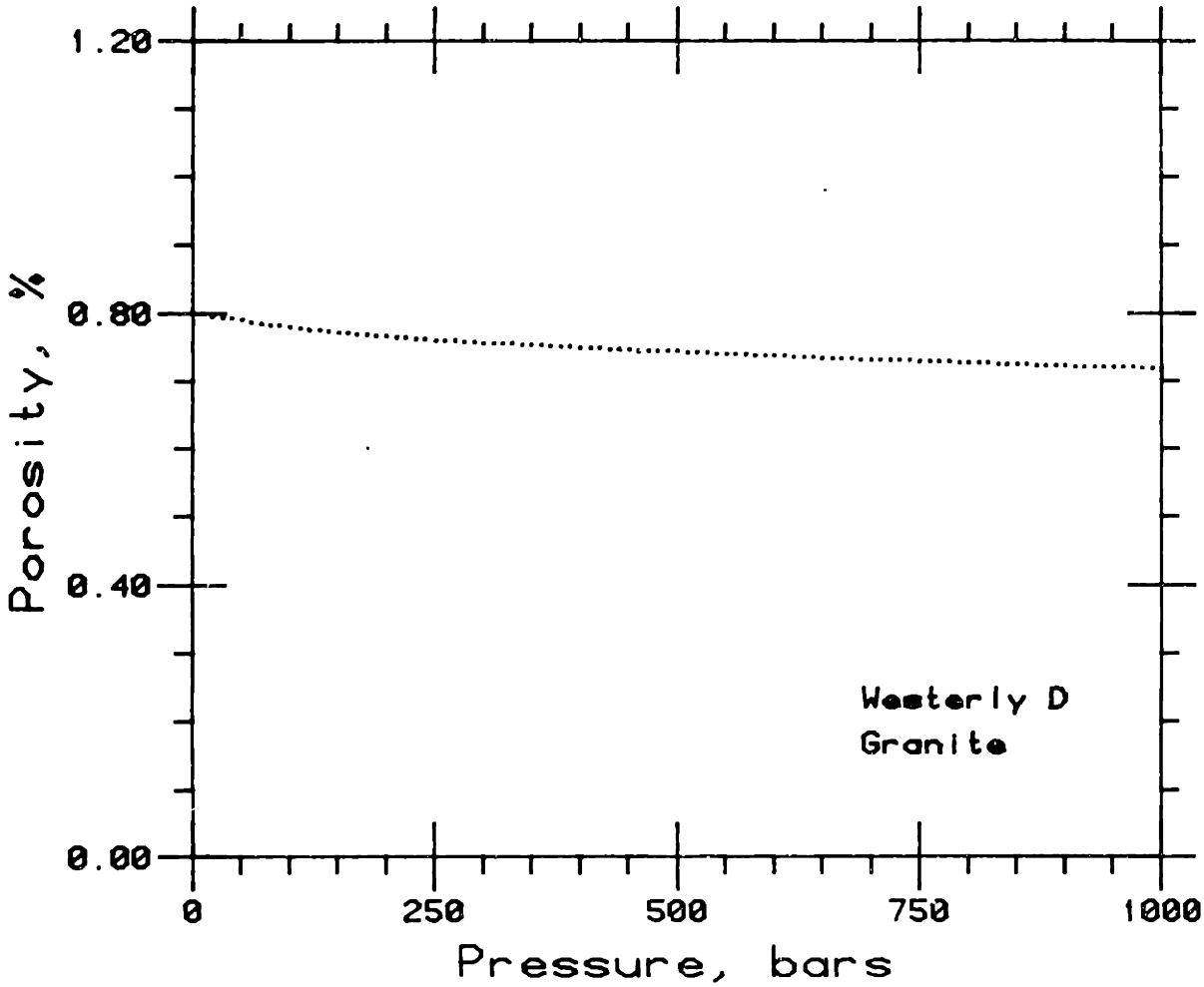


Figure A-11c. Porosity versus confining pressure for Westerly granite (blue) calculated from jacketed and unjacketed stress-strain measurements.

# APPENDIX B

## MATERIALS STUDIED

A short description is given for each of the rock samples used in this thesis. Table 1 at the end of Chapter 2 lists the dry bulk density, average grain size, and porosity for each of the samples and these data are not repeated here.

Weber sandstone. A dark brown colored, very fine-grained, moderately-sorted, subarkosic sandstone. Grains are subrounded. The sample was obtained from a core received from J. Byerlee's rock mechanics laboratory at the U.S.G.S., Menlo Park, California.

Navajo sandstone. A light straw colored, fine-grained, well-sorted orthoquartzite sandstone. From the upper member of the Navajo formation, as opposed to the lower member, which is red-colored and more porous (studied by Johnston, 1980). Mineralogy consists predominately of subrounded quartz grains (85%) with minor feldspar, chert, and siliceous rock fragments. Minor to moderate secondary quartz is the cementing material.

Berea sandstone. A light buff-gray colored, fine-grained, well-sorted, submature protoquartzite. Mineralogy consists of grains of rounded to subangular quartz, with calcite, siderite, micas, and fine-grained clays. Bedding is indicated by fine striations of dark brown oxidized minerals, probably siderite. Quartz grains are point to concave-convex. Cementing material is calcite, silica, and micas. Samples in this study were obtained from blocks collected at the Buckeye quarry, South Amherst, Ohio, Chevron Oil Field Research Company, and

J. Byerlee's laboratory at the U.S.G.S., Menlo Park, California. All reported measurements in this thesis are on material collected at the quarry; porosities for samples from the other sources are reported in Chapter 3. All samples are from the lower, massive sandstone, phase of Berea sandstone, as opposed to the upper, sheet sandstone, phase (Pepper *et al.*, 1954). Simmons *et al.* (1982) described the pore geometry of Berea sandstone as seen by the SEM in crack section and pore cast. Pore geometry is described as a network of intergranular and connective pores which are relatively uniform in size, with irregular intergranular pores smaller than individual grains and many connective pores as thin, curved planes. Khilar and Fogler (1983) give a mineralogical content for a typical Berea sandstone sample as 76% quartz, 9% feldspars, 1% calcite, 4% dolomite, 1% siderite, 7% kaolinite, 1% chlorite, and 1% illite/mica. Lene and Owen (1969) give the modal analysis of Berea sandstone at the Buckeye quarry as 76.4% quartz, 11.2% chert, 4.6% feldspars, 1.1% leucoxene, 0.4% zircon, 0.3% tourmaline, 0.4% muscovite, 0.4% chlorite, 2.6% siderite, and 2.5% calcite. Lene and Owen (1969) also give the grain-size parameters of Folk and Ward (1957): mean is 2.70 $\varphi$ (fine-grained), sorting is 0.61 $\varphi$ (moderately well sorted), skewness is 0.47 (strongly fine-skewed), and kurtosis is 2.05 (very leptokurtic). Tosaya and Nur (1983) report that clays are mixed illite-kaolinite on the basis of X-ray diffraction.

Kayenta sandstone. A light yellow colored, medium to coarse-grained, poorly consolidated arkosic sandstone. Mineralogy consists primarily of quartz grains with feldspar and calcite as the cementing material. Sample was aquired from the same 8" diameter core as used by Brace (1974) and Jones (1982). Modal analysis for a sample from this core by Brace (1974) is 52% quartz, 21% orthoclase, 20% calcite, and 7% microcline opaque lithic fragments.

Bedford limestone. A light tannish-gray colored, coarse-grained, poorly-sorted, well-cemented calcarenite, brecciated limestone, or coquina consisting of poorly sorted clastic calcite fossil debris. Crystalline calcite is the cementing material. Pore space is vuggy and irregularly scattered. Bedding is indicated by faint, broad laminations on a wetted surface. Sample was cored from a rock cube obtained from stock at the U.S. Bureau of Mines Twin Cities Mining Research Center, the properties of which are reported in Krech *et al.* (1974). Mineralogy is reported by the same to be 69% fossiliferous calcite (shells of gastropods, crinoid stems and calices) and 31% calcite cement.

Webatuck dolomite. A light grayish-white colored metamorphic foliated dolomite. Foliation is indicated by dark bands of dolomite and preferred orientation of dolomite minerals. Modal analysis from Brace (1965) is 99% dolomite. Sample taken from the same block of material as used by Brace (1964, 1965) and Nur (1969).

Westerly granite. Both a blue and red variety of Westerly granite were studied. The blue variety was collected at the Bonner Monument Co. in Westerly, R.I. The red variety was collected from W.F. Brace's laboratory at M.I.T. and was labelled "Avner." Mineralogies of the two varieties are indistinguishable. Both are fine-grained, equigranular, biotite granites of very uniform texture and grain size. Mineralogy consists of subhedral plagioclase and microcline feldspar, anhedral quartz, subhedral biotite and muscovite, and opaque accessory minerals. Modal analysis reported in Brace (1965) is 35.4% microcline, 31.4% plagioclase (17% anorthite), 27.5% quartz, 4.9% mica. Modal analysis reported in Siegfried and Simmons (1978) is 22.5% quartz, 30.7% potassium feldspar, 39.2% plagioclase (17% anorthite), 5.0% biotite, 0.7% muscovite, 0.7% opaques, 0.4% secondary minerals, and 0.8% others. Feves and Simmons (1976) compare the compositions of several samples of Westerly granite. Modal analysis reported in

Krech *et al.* (1974) for a light gray colored variety is 43% plagioclase, 22% microcline, 24.6% quartz, 6.9% biotite, 2.0% muscovite, 1.0% zicron, 0.9% magnetite.

Barre granite. A light gray medium- to fine-grained biotite granodiorite of very uniform texture. Mineralogy consists of subhedral plagioclase and microcline feldspar, anhedral quartz, subhedral biotite and muscovite, and opaque accessory minerals. Modal analysis reported by Birch (1960) is 37% plagioclase, 26% quartz, 25% potash feldspar (orthoclase), 9% biotite, 3% muscovite. Modal analysis reported by Krech *et al.* (1974) is 50% plagioclase, 22% quartz, 10% microcline, 8% biotite, 6% muscovite, and 4% opaque accessories.

Chelmsford granite. A light gray, medium-grained, weakly-schistose, quartz monzonite. Schistosity is defined by sub-parallel orientation of micas. Feldspar grains vary in size up to 5 mm, are occasionally zoned, and in combination with the micas give the rock a mottled appearance. Modal analysis from Todd (1973), and Simmons *et al.* (1975) for a sample of Chelmsford granite is 34.4% quartz, 36.3% microcline, 18.5% plagioclase, 8.1% muscovite, 0.9% biotite, 0.1% opaque, 0.4% chlorite, 0.6% epidote, 0.4% apatite, and tracesof zircon, carbonate, and garnet. Sample in this study was obtained from the Fletcher quarry in Chelmsford, Massachusetts.

Solenhofen limestone. A brownish-yellow colored, equigranular, aphanitic, lithographic limestone. Sample is streaked with subparallel, fine- to medium grained, discontinuous blotchy layers of lighter colored calcite. Sample is 99+% calcite. Sample is from Bavaria, Germany.

Vermont marble. A very pure (99+% calcite), white, foliated marble. Similar marble was studied by Brace (1965) and Birch (1960). Lensoidal calcite grains form a mosaic pattern. Sample obtained from quarry in Danby, Vermont.

Yule marble. A pure (99+% calcite), white, foliated marble. Sample is coarser-grained than the Vermont marble but shows similar oriented texture of lensoidal calcite grains. Sample obtained from quarry in Colorado.

Blair dolomite. Very fine-grained, massive, finely foliated dolomite with alternating bands of light and darker colored minerals. Porosity approches 0%. Sample from the same material as studied by Brace (1965), Brace and Martin (1968), and Simmons (1964). Analysis gave 85% dolomite, 6% calcite, and 9% insoluble residue. Sample is from Martinsburg, W. Virginia.

Henderson augen gneiss. A medium-grained, foliated, micaceous augen gneiss. Porphyroblasts of yellowish-pink plagioclase, 5 to 20 mm in diameter, partially oriented, in a groundmass of schistose muscovite and streaky segregated lenses of quartz and feldspar. Mineralogy approximately 25% quartz, 35% microcline, 20% plagioclase, and 20% mica, mostly muscovite. Sample obtained from Clark Hill Reservoir, South Carolina.

Cedar City quartz diorite. A light colored, medium-grained, partially decomposed quartz diorite. Mineralogy approximately 27% quartz, 50% feldspar, 8% amphibole, and 15% alteration products. Sample is highly altered; feldspars are altering to various clays (sericite and chlorite) which partially fill the porosity. Hornblende phenocrysts are present. Sample obtained from the same 6 inch core as used in the study by Walsh *et al.* (1970), who cited the location as the Air Force Weapons Laboratory test site at Cedar City, Utah.

Boise sandstone. A light grayish-yellow colored, medium to coarse-grained, poorly consolidated subarkosic sandstone with moderately sorted, subangular grains. Matrix grains are 35% quartz, 29% feldspar, and 6% lithic rock fragments. Intergranular material is secondary silica and clays (23%) and biotite (7%). Bedding indicated by subparallel orientation of micas.

Pottsville sandstone. A light brownish-gray colored, medium-grained, well-sorted orthoquarzite sandstone. Sample obtained from the same block as used by Brace and Martin (1968), from Spring City, Tenn. Modal analysis is given as 46% quartz, 41% orthoclase, 11% mica, and 2% oxides. Very faint bedding indicated by subparallel orientation of mica grains and occasional streaks of reddish-brown oxides.